RUSSIAN ACADEMY OF SCIENCES

National Geophysical Committee

RUSSIAN NATIONAL REPORT

Meteorology and Atmospheric Sciences

2015–2018

for the XXVII General Assembly
of the International Union of Geodesy and Geophysics
(Montreal, Canada, July 8–18, 2019)

МАКС ПРЕСС

Москва – 2019

УДК 55
ББК 26.2
Н35

DOI 10.29003/m662.978-5-317-06182-1

Editors:
Academician *I. I. Mokhov* (MASS Chairman);
Dr. *A. A. Krivolutsky* (MASS Scientific Secretary)

Russian National Report: Meteorology and Atmospheric Sciences: 2015–2018: for the XXVII General Assembly of the International Union of Geodesy and Geophysics (Montreal, Canada, July 8–18, 2019) / Ed.: I.I. Mokhov, A.A. Krivolutsky. – Moscow : MAKS Press, 2019. – 332 p.

ISBN 978-5-317-06182-1

This report of the Meteorology and Atmospheric Sciences Section (MASS) of the Russian National Geophysical Committee presents information on atmospheric research in 2015-2018 in Russia. It is based on reports of 10 National Commissions.

Key words: Russian National Report, Meteorology and Atmospheric Sciences. 2015-2018, atmospheric chemistry, atmospheric electricity, atmospheric radiation, climate, clouds and precipitation, dynamical meteorology, middle atmosphere, ozone, planetary atmospheres, polar meteorology.

Н35 **Национальный отчет России по метеорологии и атмосферным наукам в 2015–2018 гг.:** XXVII Генеральная Ассамблея Международного союза геодезии и геофизики: Монреаль, Канада, 8–18 июля 2019 г. / Ред.: И.И. Мохов, А.А. Криволуцкий. – Москва : МАКС Пресс, 2019. – 332 с.

ISBN 978-5-317-06182-1

В настоящем отчете Секции метеорологии и атмосферных наук Российского национального геофизического комитета представлена информация об исследованиях атмосферы в России в 2015–2018 гг., основанная на отчетах 10 национальных комиссий.

Ключевые слова: Российский национальный отчет, метеорология и атмосферные науки, 2015–2018, химия атмосферы, атмосферное электричество, атмосферное излучение, климат, облака и осадки, динамическая метеорология, средняя атмосфера, озон, планетные атмосферы, полярная метеорология.

УДК 55
ББК 26.2

Отчет Секции будет размещен на сайте
Национального Геофизического Комитета Российской Федерации:
ngc.gcras.ru

ISBN 978-5-317-06182-1

© National Geophysical Committee RAS, 2019
© Оформление. ООО «МАКС Пресс», 2019

Contents

Preface

This report of the Meteorology and Atmospheric Sciences Section (MASS) of the Russian National Geophysical Committee presents information on atmospheric research in 2015–2018 in Russia. It was prepared for the General Assembly of the International Union of Geodesy and Geophysics (IUGG) which includes the International Association of Meteorology and Atmospheric Sciences (IAMAS). This MASS report is based on reviews of 10 National Commissions:

1. Atmospheric Chemistry (Chairman I.K. Larin, Institute of Energy Problems and Chemical Physics of the Russian Academy of Sciences);
2. Atmospheric Electricity (Chairman V.N. Stasenko, State Research Center "Planeta");
3. Atmospheric Radiation (Chairman Yu.M. Timofeyev, St. Petersburg State University);
4. Climate (Chairman I.I. Mokhov, A.M. Obukhov Institute of Atmospheric Physics of the Russian Academy of Sciences, Lomonosov Moscow State University);
5. Clouds and Precipitation (Chairman N.A. Bezrukova, Central Aerological Observatory);
6. Dynamic Meteorology (Chairman M.V. Kurgansky, A.M. Obukhov Institute of Atmospheric Physics of the Russian Academy of Sciences);
7. Middle Atmosphere (Chairman A.A. Krivolutsky, Central Aerological Observatory);
8. Ozone (Chairman N.F. Elansky, A.M. Obukhov Institute of Atmospheric Physics of the Russian Academy of Sciences);
9. Planetary Atmospheres (Chairman O.I. Korablev, Space Research Institute of the Russian Academy of Sciences);
10. Polar Meteorology (Chairman A.I. Danilov, Arctic and Antarctic Research Institute).

Previous MASS report was published in 2015[*].

Igor I. Mokhov
MASS Chairman

---

[*] Russian National Report. Meteorology and Atmospheric Sciences. 2011–2014. Ed. by I.I. Mokhov and A.A. Krivolutsky. National Geophysical Committee RAS, MAKS Press, Moscow, 2015, 272 p.

Atmospheric Chemistry

I.K. Larin
Institute of Energy Problems of Chemical Physics RAS
ilarin@yandex.ru

A brief overview of the work of Russian scientists in the field of atmospheric chemistry in 2015–2018 years, including work on the chemistry of the troposphere, the chemistry of the ozone layer and on the role of chemistry in climate change is presented. Review has been prepared in the Commission on atmospheric chemistry and global pollution meteorology and atmospheric sciences section of the national Geophysics Committee.

Note first of all that in 2016 the work "Russian research in atmospheric chemistry in 2011–2014" was presented [1].

Chemistry of the troposphere

One of the important areas of research in this area is the study of elementary chemical reactions of atmospheric values, data about which are then used in mathematical models of the atmosphere. In this connection, mention should be made of work [2], in which using the resonant fluorescence method for registering active chemical reagents in a flow reactor, the rate constants of a homogeneous reaction of chlorine atoms with CH_3Br in the temperature range 298–358 K were measured: $kCl + CH_3Br = (1.3 \pm 0.1)\cdot 10^{-11}\exp(-976 \pm 91)/RT$ $molecule^{-1}cm^3s^{-1}$. In another paper [3], the same method in the temperature range of 295–368 K measured the rate constant for the reaction of chlorine atoms with CHF_2Br: $k_{Cl + CHF2BR} = (4.23 \pm 0.13)\cdot 10^{-12}\exp(-15.56 \pm 1.58)/RT$ $molecule^{-1}cm^3s^{-1}$ ($R = 8.314472E^{-03}$ kJ/mol K). Along with the method of resonant fluorescence, the mass spectral technique is used to study chemical reactions. In [4], using this method, the rate constant for the reaction of dichloroacetic acid with atomic fluorine was first calculated. In [5], the kinetics of the reaction of atomic fluorine with pyridine and 2-fluoroethanol was studied using competing reactions using molecular-beam mass spectrometry. The rate constant for the reaction of pyridine with atomic fluorine was determined for the first time, which was $k = (8.0 \pm 3.0)\cdot 10^{-10}$ $cm^3molecules^{-1}s^{-1}$. The main products of this reaction were established: pyridinyl and fluoropyridine. In this series it should be mentioned [6], in which the transformation of halogen-containing acids in the atmosphere was studied. A new method developed at the Institute of Chemical Physics RAN for analyzing these compounds revealed a detailed mechanism for the participation of these acids in the formation and growth of aero-

sols, and, in particular, to calculate the lifetime of difluoroacetic acid for different conditions. In this series, one can also mention the work [7], in which, on the basis of laboratory experiments, a qualitative scheme of chemical processes was proposed, describing the formation of gas and aerosol products of furfural photolysis. In addition to laboratory measurements, chemical reactions are also studied by calculation. Thus, in [8], using the quantum-mechanical calculations, the reaction of dicarbon in the $C_2(X^1\Sigma_G^+)$ state with the nitrogen molecule in the gas phase was studied with different orientations of reacting molecules in the collision complex: linear, perpendicular, and parallel. The latter is of the greatest interest, since in this case a system with a threshold energy of 37.2 kcal/mol passes through a state that turns into a highly vibrationally-excited cyan. The latter, in times of the order of 10^{-13}–10^{-14} s, splits into two radicals CN.

A significant place among the works on the study of the troposphere is occupied by work related to the modeling of tropospheric processes. Thus, in [9], the results of building statistical models of time series of atmospheric impurities (suspended particles less than 10 microns (PM_{10}), CO and NO_2) for a network of automated stations for monitoring air pollution in the Moscow metropolis are presented. Another paper [10] presents the results of modeling the transfer of ^{85}Kr in the atmosphere under the conditions of the ACURATE experiment using three transport models – FLEXPART, HYSPLIT, and models from the Nostradamus code. It was shown that using all three Lagrangian models, it is possible to qualitatively describe the ^{85}Kr concentration fields in the ACURATE experiment. In [11], comparisons of model forecasts by chemical transport models CHIMERE and COSMO-RU7-ART for surface air pollution with measurement data in Moscow in 2015 are presented. It is shown that the models, as a rule, somewhat underestimate the values of field data. Let us also name [12], in which the results of numerical simulations were compared using the WRF-CHEM model and aircraft sensing data. Important information about the chemical processes occurring in polluted urban air can be obtained from data on the chemical composition and acidity of urban precipitation. Such data (along with other atmospheric characteristics) are presented in the works of employees of the Meteorological Observatory of the Geographical Faculty of Moscow State University, presented in the monograph [13]. We also note the work [14], in which the analysis of precipitation in Moscow is carried out using isotopes. A significant number of works in the field of tropospheric chemistry was devoted to the monitoring of pollutants, including forest fire products, aerosols, as well as small components of the troposphere, such as ozone, carbon monoxide and dioxide, nitrogen dioxide, etc. [15–46]. As a “novelty” in the theory, we point out the work [47] whose authors attempted to establish a relationship between snow cover and ground-level ozone, although there are no any physical reasons for this connection.

Heterophase processes

Heterophase processes are of great importance for the understanding of ozonospheric chemistry. Recall that these processes have played a decisive role in the depletion of the ozone layer at the end of the 20th century and in the formation of the Antarctic and Arctic ozone holes. In recent years, new important results have been obtained in this area. Thus, in [48], a new mathematical model of the global transport of multicomponent gas impurities and aerosols and the formation of polar stratospheric clouds (PSO) in both hemispheres under conditions of the local polar winter are described. On the surface and in the volume of PSO particles, heterogeneous chemical reactions occur that affect the gas composition of the atmosphere, in particular, the content of chlorine and nitrogen-containing compounds involved in the destruction of ozone. In the work [49], two groups of aerosol particles were found in the surface air: "carbonate", including alkali carbonates (Na^+, K^+) and alkaline-earth (Mg_2^+, Ca_2^+) metals, and "ammonium", including mainly ammonium ions (NH_4^+) and anions of free atmospheric acids (HNO_3, H_2SO_4). The results obtained here show that the nature of the distribution of these anions among the groups of particles is sensitive to variations in relative air humidity (RH). According to these data, the formation channel in carbonate particles of sulphate anions, resulting from direct oxidation of sulfur dioxide captured from air, is reported. In [50], the reasons for the appearance of large concentrations of bicarbonates in Moscow precipitations, substantially exceeding the equilibrium level, are considered. In [51], the products of the monomolecular decomposition of the surface complex formed upon the capture of NO_2 by a coating of methane soot were studied. NO and HONO are registered as gas-phase capture products. At the same time, the NO product quantitatively corresponds to half of the spent NO_2 reagent. [52] investigated the capture of N_2O_5 on a carbon black coating at T = 255 and 298 K using a thermostated flow reactor with a movable insert and carbon black deposited on it, as well as a mass spectrometer with ionization by low-voltage electrons.

In [53], using the mathematical model of global transport of multicomponent gas impurities and aerosols, which was previously constructed by the authors, the concentrations in the atmosphere of sulfate aerosols and particles of polar stratospheric clouds in both hemispheres in winter were calculated. It was found that the key factor determining the type of aerosol particles forming in the atmosphere is the temperature distribution. [54] considered a wide range of issues related to nucleation, as well as with the processes of growth and dissociation of gas hydrates. Along with the mathematical models used to describe these processes, the results of their experimental studies are discussed. Separate

sections are devoted to the effect of self-preservation of gas hydrates, the manifestation in water hydration of the memory effect of water, the development of catalysts for the process of hydrate formation and the investigation of the effect of substances dissolved in the aqueous phase on it.

In [55], the data of field and laboratory observations of aerosol particles in the lower stratosphere were considered. The microphysics of their formation, the mechanisms of heterogeneous chemical reactions involving reservoir gases (HCl, $ClONO_2$, etc.), as well as their kinetic characteristics, are discussed. The work [56] considers the process of ice nucleation in the atmosphere, which occurs as a result of heterogeneous condensation of water vapor in the inhomogeneities of the surface of aerosol particles and subsequent heterogeneous crystallization of supercooled water clusters. It was established that the size, structure and composition of aerosol particles determine the thermal mode of crystallization. The work [57] deals with problems related to the assessment of the effect of sulfate aerosols on the formation of clouds over the sea in the middle troposphere, as well as the participation of these particles in the formation of polar stratospheric clouds in the lower stratosphere. It is shown that, without taking into account the effect of sulfate aerosols, the formation of clouds over the sea in the middle and upper troposphere is difficult. The results of numerical calculations of the distribution in the lower stratosphere of the concentrations of gaseous nitric and sulfuric acids, as well as the mass concentrations of these components in the particles of polar stratospheric clouds are given.

In [58], a description is given of the algorithm and the results of calculations of the dynamics of the destruction of stratospheric ozone in middle latitudes, taking into account the mechanism of halogen activation and particles of the Young layer. The contribution of heterophase reactions to the depletion of the ozone layer has been estimated and the need to take them into account when developing forecasts for ozone layer recovery in the 21st century has been substantiated. In [59], two types of polar stratospheric clouds (PSO) are considered: type Ia – formation of nitric acid trihydrate particles (NAT), and type Ib – formation of particles of a supercooled three-component H_2SO_4 / HNO_3 / H_2O solution in particles STS (supercooled ternary solutions). To model them, new equations have been proposed that describe the variability of components in the gas and condensed phases with regard to their thermodynamic properties. The formation of PSOs is considered together with the formation of sulfate aerosols in the upper troposphere and lower stratosphere, taking into account the chemical and kinetic transformation processes (photochemistry, nucleation, condensation / evaporation and coagulation). The formation of aerosol particles from supersaturated vapor was considered in [60] under the assumption that stable nuclei of a new phase contain two (dimers) or three (trimers) condensing vapor molecules.

In [61], a semiempirical method was developed for analyzing the mechanism of heterogeneous reactions, based on the Langmuir-Hinshelwood kinetic model, modified by the approximation of a two-exponential first-order decomposition. The method turned out to be very useful in describing the kinetics of photocatalytic oxidation in air on TiO_2 particles of a wide range of substances: ketones, organophosphorus compounds, alkyl sulfides, chlorinated hydrocarbons. The "aging" of the smoke aerosol during long-range transport, due in part to heterophase processes, is also considered in [62]. In [63], by numerical simulation, it was shown that the intensity of secondary organic aerosol formation (SOA) in smoke plumes from plant and peat fires under actual conditions can significantly depend on the size of the aerosol optical thickness, which determines the rate of photodissociation and the concentration of hydroxyl, on which in turn, the rate of generation of SOA as a result of the oxidation of semivolatile organic compounds depends.

The chemistry of the ozone layer

In this area in 2015–2018 a number of new results were obtained, both in the field of the theory of ozone layer and in the field of observations of its evolution, connected with the restoration of the total ozone content after its decrease at the end of the last century under the influence of anthropogenic factors. In the field of theory, we note the monograph [64], which examined in detail the ozonosphere mechanisms and processes, including the catalytic cycles of depletion of the stratospheric ozone, the formation of Antarctic and Arctic ozone holes, the effects of galactic cosmic rays on ozone and action of other natural and anthropogenic factors. In [65], the temporal boundaries of the ozone layer restoration in the latitudinal zones 0–85°, 0–30°, 30–60°, and 60–85° of the Northern Hemisphere in the XXI century were calculated. The calculations were performed using the interactive chemical-dynamically-radiative two-dimensional model of the middle atmosphere Socrates (altitude range of 0–120 km). For the initial data, the forecast scenarios of the IPCC (Intergovernmental Committee on Climate Change) greenhouse gas concentrations RCP 4.5 and RCP 6.0 were used for the calculations. It has been shown, in particular, that after recovery, the ozone layer will continue to grow and by the end of the 21st century will reach a stationary level that exceeds the "unperturbed" pre-freon level, which is no less an environmental threat than the depletion of the ozone layer at the end of the 20th century. The chemical composition of the middle atmosphere, including the troposphere, stratosphere, and mesosphere, and its change under the influence of mainly anthropogenic factors in the 21st century were considered in [66]. The main processes of the ozonosphere, including the processes of halogen activation, were examined in [67].

In [68], modern versions of the theory of chain processes of ozone layer destruction, including the author's version, are considered (for more details, see [61]). The contribution of O_x, HO_x, NO_x, ClO_x and BrO_x cycles to ozone depletion at the end of the 21st century at a latitude of 50 °N is calculated in [69] using the previously proposed algorithm for calculating the limiting stages of chain prolongatiom in ozonespheric cycles of stratospheric ozone depletion in different seasons of the year. A correct estimate of the atmospheric lifetime of odd oxygen was made for the first time in [70], taking into account its depletion in known catalytic cycles. It is shown that when the lifetime of odd oxygen becomes comparable or longer than the time of turbulent transport in height, it should be replaced with a combined lifetime that takes into account the effect of both photochemical and dynamic factors. In [71], the unsolved problems of middle atmosphere chemistry are considered, which include issues related to the atmospheric lifetime of the odd oxygen family Ox and its components, issues related to the lifetime components of the O_x, HO_x, NO_x, ClO_x and BrO_x families, with the calculation of the destruction rate of the odd oxygen in the catalytic cycles of O_x, HO_x, NO_x, ClO_x and BrO_x and the chain length of these cycles.

In connection with the gradual weakening of the effect on the ozone layer of anthropogenic factors, natural factors are beginning to attract increasing attention. Thus, in [72], the effect of planetary waves on the stability of the circumpolar vortex, the temperature of the polar stratosphere, and the content of ozone and other gases was modeled using the global climate model of the lower and middle atmosphere. The results of the numerical photochemical modeling of the impact of the most powerful proton flares of the Sun on the ozone layer of the polar regions of the Earth in the 23rd activity cycle are presented in [73]. The seasonal dependence of the ozone response to solar proton events was detected, and also the effect of long-term effects was obtained for the first time, the duration of which was about a year. In [74], the laws of sudden stratospheric warming (SSW) and their effect on the content of NO_2 and O_3 are considered. It is shown that SSW can lead to significant anomalies of the total content of NO_2, ozone, and the stratospheric temperature, and the sign of the anomalies may vary depending on the position of the observation point relative to the stratospheric vortex. Additional details regarding the NO_2 and O_3 anomalies associated with sudden stratospheric warmings in 2010 and 2011 are reported in [75, 76]. The effect of precipitating energetic particles on the ozone layer and climate is considered in [77]. It is shown that energetic electrons have the main influence on the long-term variability of the ozone layer. In a similar way, the increase in the atmospheric NO_2 content after the solar proton event in October 2003 is described in [78].

In [79], topical problems of studying ultraviolet radiation and the ozone layer are considered. It was shown, in particular, that the anomaly of the ozone layer in the Arctic, record for all the years of observation, in the spring of 2011, when elevated levels of ultraviolet radiation were noted even in Moscow, confirmed the need for further research in this area. The effect of solar activity on the ozone layer was studied in [80]. The results of model calculations showed that, in addition to increasing the spectral flux in the absorption bands of molecular oxygen, leading to an increase in the ozone content, changes in the flux at long wavelengths are also significant for the composition and temperature of the atmosphere.

Of great interest are works in which the direct effect of dynamic factors on the ozone layer is demonstrated. Such works include publication [81], which demonstrates the formation of an ozone mini-hole as a result of the prolonged blocking action of the anticyclone over the European territory of Russia in the summer of 2010. The analogous paper [82] analyzed the anomalies of ozone, water vapor and temperature associated with the relatively short spring event of atmospheric blocking and the anomalously long summer block over European Russia in 2010. The connection of water vapor and ozone in the atmosphere over the European part of Russia with the North Atlantic Oscillation in the summer of 2010 is discussed in [83]. In [84], the effect of the quasi-two-year cyclicity of the equatorial stratospheric wind on the total NO_2, ozone, and stratospheric temperature is considered.

Long-term observations of atmospheric components are also of considerable interest. In this connection, let us point out the work [85], in which the data of observations of the total NO_2 content conducted since 1990 are reported, and these data are obtained from measurements of the vertical NO_2 profile, which is not measured anywhere else in the world. In conclusion, a review of the work on the influence of natural factors on the ozonosphere is given in [86], which describes the CHARM (CHemical Atmospheric Researh Model) global numerical model and gives the results of three-dimensional numerical modeling of the ozone distribution and other small gas components of the Earth's atmosphere in the 0–90 km and their changes under the action of UV radiation from the Sun, as well as due to the destruction of ozone in the polar regions by high-energy particles of cosmic origin. The last work in this series is the work [87] on the stratosphere-troposphere exchange, which can also be attributed to natural factors. As for anthropogenic factors, then, as reported in [88], the increase in the content of hydrogen chloride (derived from anthropogenic chlorofluorocarbons) is currently stopping.

Chemical aspects of climate change

Work in this area was related to climate theory, climate change prediction, greenhouse gas monitoring and related issues. One of the important questions of climate theory is the question of the reasons for its change. Paper [89] discusses the delay in changes in the CO_2 content from changes in the surface temperature observed in the Pleistocene, which is considered to be an argument against the anthropogenic causes of modern global warming. In [89] it is shown that changes in the CO_2 content can both be late or outpace the temperature changes, which is determined by the type of external influence on the system, and that these advances do not contradict the conclusion that the anthropogenic factor plays a key role in modern climate change. In [90], a slightly different point of view is expressed, according to which temperature changes from the early 1970s to the mid-1990s and the pause in warming that replaced it are almost entirely due to variations in large-scale circulation described by the North Atlantic, Pacific-North American and Scandinavian fluctuations. Another point of view, about the possible influence on the climate of past solar activity, is expressed in [91] (the conclusion was made on the change in the width of the annual growth of fossil rings of fossilized trees). This idea develops in [92] (for the last 2000 years) and [93] (for the XXth century). In [94], the authors compared the variations in the concentration of carbon dioxide in the atmosphere and the average global surface air temperature over the past 50 years. It turned out that at the inter-annual scale variations of CO_2, lagged behind the corresponding temperature variations, however, CO_2 was the leader in the 1980–1990s, which the authors considered to be a sign that at that time man influenced the climate. In fact, no any conclusions can be drawn from such analysis, bearing in mind that the relaxation time of the climate system is many hundreds of years.

In [95], the variability of zonal trends in near-surface temperature for the period 1979–2012 is analyzed using ensemble calculations with the atmospheric general circulation (MOCA) model with identical prescribed conditions at the lower boundary of the atmosphere and different initial conditions. In [96], results are presented that characterize the ability of modern global and regional climate models not only to assess the risk of general trends of changes, but also to predict qualitatively new regional effects. [97] analyzes the capabilities of an ensemble of modern global climate models when reproducing the observed evolution of surface temperature on land in the Arctic, including the spatial correspondence of model calculations and observational data. In [98], changes in the temperature of the Earth's surface in 1850–2014 are analyzed using seven historical calculations performed with the INM-CM5 climate model. The global warming slowdown in 2000–2014 can be reproduced due to a more accurate

setting of the solar constant change scenario in the CMIP6 protocols. The most probable endogenous (internal) and exogenous (external) factors that can cause changes in the Earth's climate with periods ranging from a few to hundreds of thousands of years are considered in [99].

In [100], the results of using a nonparametric regression analysis method (quantile regression) to estimate changes in surface air temperature in different climatically quasi-homogeneous regions of Russia based on the daily resolution of 517 meteorological stations are given. In [101], on the basis of paleoclimatic data, projections of natural trends of global mean annual temperature and precipitation up to 3000 were developed. In [102], five paleoclimatic reconstructions for the extratropical zone of the Northern Hemisphere were decomposed into quasi-periodic components by spectral analysis. Based on the identified quasi-periodicities, a climatic forecast for the extratropical zone of the Northern Hemisphere has been constructed, showing that the warm climate currently observed will generally remain for 500 years, but in the XXII century. will begin to acquire a pronounced tendency to a gradual cooling.

In [103] using a single-layer atmospheric radiation model using data from the SRB archive (Surface Radiation Budget) for 1984–2007 an estimate was obtained of the change in the temperature distribution of the earth's surface with a general increase in the atmospheric albedo by 1%: on average over the globe, the surface temperature decreases by 1°C. The spectra of the outgoing thermal IR radiation measured by the SI-1 Fourier spectrometer in 1977 and 1979 were compared in [104]. from the satellites Meteor-28 and -29, with the data of calculations on the basis of the modern radiation code LBLRTM and data of the radio sounding of the atmosphere. In the majority of cases, the average differences between measurements and calculations do not exceed 2 mW / ($m^2 \times sr \times cm^{-1}$) in the spectral region 660–1600 cm^{-1}. In [105], a new version of the FIRE-ARMS software was described, supplemented by the vector VLIDORT radiation transfer model, which allows simulating the thermal radiation of the Earth leaving the space and the solar radiation reflected from the surface in the near-IR range taking into account multiple light scattering.

Progress estimates of climate change in Russian regions are considered in [106]. The problem is solved by conducting mass (50 members) ensemble calculations using the high-resolution (25 km horizontally) climate model systems developed at the Voeikov Main Geophysical Observatory. [107] considered possible approaches to overcoming the climate crisis – a rapid decrease in anthropogenic CO_2 emissions, the removal of an excess amount of CO_2 from the atmosphere and a targeted change in the balance of incoming solar radiation. It is concluded that since the middle of the XXI century. humanity will be forced

to use all three approaches to prevent the dangerous excess of the average global temperature. In [108] it is argued that with the help of modern climate models it is impossible to develop scenarios of climate change for the next decades. A scenario based on real features of global temperature variations is proposed, according to which in the coming decades not only the temperature stabilization that has been going on for 15 years, but also some cooling can be possible. [109] addresses the issue of the effects of emissions from Russian civil aviation in 2000–2012. on the climate. It is shown that the effect is insignificant. [110] discusses the impact of volcanic activity on the temperature of the surface air layer. It is shown that volcanic eruptions can lead to a global decrease in surface air temperature by 0.5–20°C per year, following the eruption, which can result in a long cooling. [111] discusses regional aspects of climate modeling and its changes, and [112] discusses anomalies and trends in current climate change.

Considerable attention has been paid in recent years to monitoring greenhouse gases and aerosols as well as to the study of gas hydrates and their properties. These data are presented in [113–129]. We conclude this review with the work [130], which quantifies the contribution of the radiative forcing of greenhouse gases and the Atlantic multi-ten-year oscillation to the trends of global near-surface temperature and near-surface temperature in different latitudinal zones.

References

1. Larin I.K. Russian investigations in atmospheric chemistry in 2011–2014. Izvestiya, Atmos. Oceanic Phys. (2016) V. 52. No. 3. P. 167–174.

2. Larin I.K., Spasskii A.I., Trofimova E.M. Measurement of the rate constant for the reaction of chlorine atoms with CH_3Br in the temperature range of 298–358 K by the method of resonant fluorescence of chlorine atoms. Kinetica i Cataliz (2018) P. 59. No. 1. P. 13–21. (rus.)

3. Larin I.K., Spasskii A.I., Trofimova E.M. Measurement of the rate constant for the reaction of chlorine atoms with CHF_2Br by the method of resonant fluorescence of chlorine atoms. Kinetica I Catalz (2016) V. 57. No. 3. P. 308–312. (rus.)

4. Vasilyev E.S., Syromyatnikov A.G., Shartava D.K., Karpov G.V., Morozov I.I. Mass spectrometric study of dichloroacetic acid. Chemical Safety (2018) V. 2. No. 1. P. 206–212. (rus.)

5. Volkov N.D., Morozov I.I., Vasiliev E.S. Kinetics of the reaction of fluorine atoms with pyridine. Chemical Safety (2018) V. 2. No. 2. P. 151–157. (rus.)

6. Morozov I.I., Vasilyev E.S., Karpov G.V., Butkovskaya N.I. Transformation of halogen-containing molecules in the atmosphere. Theses of the International Conference Dedicated to the Centenary of the Birth of Academician Alexander Mikhailovich Obukhov, May 16–18, 2018, M .: Fizmatkniga, 2018, P. 153. (rus.)

7. Dubtsov S.N., Dultseva G.G., Plokhotnichenko M.E., Koshlyakov P. V., Kobzeva T.V. Investigation of the kinetics of photolysis and photochemical formation of furfural. Optika atmosphery i okeana (2017) V. 30. No. 6. P. 476–480. (rus.)

8. Kolbanovsky Yu.A., Borisov Yu.A. Quantum-mechanical calculations of the mechanism of the reaction of dicarbene C2 ($X1\sum_{G}^{+}$) with molecular nitrogen. Khimicheskaja fizika (2015) V. 34. No. 2. P. 9–15. (rus.)

9. Demchenko P. F., Ginzburg A.S., Aleksandrov G.G., Vereskov A.I., Gorchakov G.I., Zavlishin N.N., Zakharova P. V., Lezina E.A., Yudin N.I. Statistical modeling of average daily pollutant concentrations in the atmosphere of the Moscow metropolis using the multiple regression method. Meteorologiya i gidrologiya (2015) No. 10. P. 31–43. (rus.)

10. Rubinshtein K.G., Safronov A.N., Pripachkin D.A., Ignatov R.Yu., Emelina S.V., Nabokova E.V., Kurbatova M.M., Blagodatskikh D.V., Arutyunyan R.V., Sorokovikova O.S., Semenov V.N. Comparison of the results of models of the transfer of 85Kr in the atmosphere with data from the natural experiment ACURATE. Meteorologiya i Gidrologiya (2017) No. 3. P. 41–57. (rus.)

11. Shalygina I.Yu., Nakhaev M.I., Kuznetsova I.N., Berezin E.V., Konovalov I.B., Blinov D.V., Kirsanov A.A. Comparison of surface concentration concentrations calculated using chemical transport models pollutants with measurement data in the Moscow region // Optika Atmosphery i Okeana (2017) V. 30. No. 1. P. 53–59. (rus.)

12. Antokhin P.N., Gorchakov A.V., Kolker A.B., Penenko A.V. Comparison of the results of calculations of the chemical transport model of WRF-CHEM with the data of aircraft measurements in the city of Norilsk. Optika Atmosphery i Okeana (2018) V. 31. No. 4. P. 282–287. (rus.)

13. Lokoshchenko M.A., Zhdanova E.Yu., Bogdanovich A.Yu., Gorbarenko E.V., Perepyolkin V.G. at all. Ecological and climatic characteristics of the atmosphere of Moscow in 2017 according to the Meteorological Observatory of the Moscow State University. Ed. by M.A. Lokoschenko. M .: MAX Press (2018) P. 239. ISBN 978-5-317-05987-3. (rus.)

14. Chizhova Yu.N., Eremina I.D., Budantseva N.A., Surkova G.V., Vasilchuk Yu.K. The use of the isotopic method in the assessment of precipitation in Moscow. Gigiena i Sanitariya (2017) V. 9. No. 8. P. 737–743. (rus.)

15. Elansky N.F., Kuznetsov R.D., Verevkin Ya.M., Prnomarev N.A., Rakitin V.S., Shilkin A.V., Semutnikova E.G., Zakharova P.V. Temporal variability of the concentration of pollutants in the atmosphere of Moscow and the assessment of their emissions. Theses of the International Conference Dedicated to the Centenary of the Birth of Academician Alexander Mikhailovich Obukhov, May 16–18, 2018, Moscow: Fizmatknig (2018) P. 10. (rus.)

16. Gorchakov G.I., Semutnikova E.G., Karpov A.V., Kuznetsov G.A. Moscow smoky haze in October 2014. Variations of the gas components of atmospheric pollution. Optika Atmosphery i Okeana (2017) Vol. 30. No. 6. P. 481–488. (rus.)

17. Gubanova D.P. , Belikov I.B., Elansky N.F., Skorokhod A.I., Chubarova N.E. Variability of surface concentration of PM2.5 aerosols in Moscow according to observations at the Meteorological Observatory of Moscow State University. Optika Atmosphery i Okeana (2017) V. 30. No. 12. P. 1033–1042. (rus.)

18. Kopeikin V.M., Emilenko A.S., Isakov A.A., Loskutova O.V., Ponomareva T.Ya. Variability of black and submicron aerosols in the Moscow region in 2014–2016. Optika Atmosphery i Okeana (2018) V. 31. No. 1. P. 5–10. (rus.)

19. Arshinov M.Yu., Belan B.D., Voronetskaya N.G., Golovko A.K., Davydov D.K., Kozlov A.S., Pevneva G.S., Simonenkov D.V., Fofonov A.B. Organic aerosol in the atmosphere of Siberia and the Arctic Part 1. Geographical features and temporal dynamics. Optika Atmosphery i Okeana (2017) V. 30. No. 8. P. 716–722. (rus.)

20. Arshinov M.Yu., Belan B.D., Voronetskaya N.G., Golovko A.K., Davydov D.K., Kozlov A.S., Pevneva G.S., Simonenkov D.V., Fofonov A.B. Organic aerosol in the atmosphere of Siberia and the Arctic Part 2. Vertical distribution. Optika Atmosphery i Okeana (2017) V. 30. No. 9. P. 733–739. (rus.)

21. Arshinov M.Yu., Belan B.D., Voronetskaya N.G., Golovko A.K., Davydov D.K., Kozlov A.S., Pevneva G.S., Simonenkov D.V., Fofonov A.B. Organic aerosol in the atmosphere of Siberia and the Arctic Part 3. Forest Fire Products. Optika Atmosphery i Okeana (2017) V. 30. No. 9. P. 740–749. (rus.)

22. Semutnikova E.G., Gorchakov G.I., Sitnov S.A., Kopeikin V.M., Karpov A.V., Gorchakova I.A., Ponomareva T.Ya., Isakov A.A., Gushchin R A., Datsenko O. I., Kurbatov G.A., Kuznetsov G.A. Siberian Smoky Haze over the European Territory of Russia in July 2016. Atmospheric pollution and radiation effects. Optika Atmosphery i Okeana (2017) V. 30. No. 11. P. 962–970. (rus.)

23. Antokhina O.Yu., Antokhin P.N., Arshinova V.G., Arshinov M.Yu., Belan B.D., Belan S.B., Davydov D.K., Ivlev G.A., Kozlov A.V., Nederlec P. ., Paris Jean-Daniel, Rasskazchikova, T.M., Savkin D.E., Simonenko. D., Sklyadneva T.K., Tolmachev G.N., Fofanov A.V. Vertical distribution of gas and aerosol impurities of air over the Russian Arctic sector. Optika Atmosphery i Okeana (2017) Vol. 30. No. 12. P. 1043–1052. (rus.)

24. Emilenko A.S., Sviridenkov M.A., Kopeikin V.M., Genchen Van. Long-term variability of atmospheric pollution with black carbon in the Beijing region in autumn periods. Optika Atmosphery i Okeana (2017) Vol. 30. No. 6. P. 497–501. (rus.)

25. Lokoshchenko M.A., Elansky N.F., Trifonova A.V., Belikov I.B., Skorokhod A.I. About limiting levels of air pollution in Moscow. Vestnik of Moscow University. Serija 5: Geographiya (2016) No. 4. P. 29–39. (rus.)

26. Kotelnikov S.N., Stepanov E.V., Chelibanov V.P. Spatio-temporal variability of ground-level ozone content in St. Petersburg, Kirov region and Crimea in, 2011–2012. Optika Atmosphery i Okeana (2016) Vol. 29. No. 12. P. 1086–1089. (rus.)

27. Panov A.V., Prokushkin A.S., Bryukhanov A.V., Korets M.A., Ponomarev E.I., Sidenko N.V., Zrazhevskaya G.K., Tiokhina A.V., Andrea M.O. An complex approach to assessing the emission of carbon-containing gases from forest fires in Siberia // Meteorologija i gidrologija (2018) No. 5. P. 30–38. (rus.)

28. Yanchenko N.I., Kotova E.I. Sources of fluorine in atmospheric precipitation in the city of Bratsk. Meteorologiya i Gidrologiya (2018) No. 5. P. 108–112. (rus.)

29. Zayakhanov A.S., Zhamsueva G.S., TsydypovV.V., Balzhanov T.S. Daily dynamics of ozone and other small gas impurities in the coastal zone of Lake Baikal (Boyarsky station). Meteorologiya i Gidrologiya (2017) No. 8. P. 85–92. (rus.)

30. Boyarsky A.N., Arabov A.Y., Golitsyn G.S., Gruzdev A.N., Elansky N.F., Elokhov A.S., Mokhov I.I., Savinnykh V.V., Senik I.A., Timazhev A.V. Variations of total nitrogen dioxide in the atmosphere in the North Caucasus. Meteorologiya i Gidrologiya (2016) No. 2. P. 29–44. (rus.)

31. Timokhina A.V., Prokushkin A.S., Onuchin A.A., Panov A.V., Kofman G.B., Verkhovets S.V., Heimann M. The long-term trend of CO_2 concentration in the atmosphere of the Arctic over central Siberia. Meteorologiya i Gidrologiya (2015) No. 3. P. 58–64. (rus.)

32. Romanchuk A.Yu., Kalmykov S.N., Kersting A., Zavarin M. Behavior of plutonium in the environment. Uspekhi Khimii (2016) № 9. P. 995–1010. (rus.)

33. Berezina, E.V., Moiseenko K.B., Skorokhod A.I., Elansky N.F., Belikov I.B. Aromatic volatile organic compounds and their role in the formation of surface ozone in Russia. Doklady Earth Sciences (2017) V. 474. No. 3. P. 356–360. (rus.)

34. Kozhevnikov V.N., Elansky N.F., Moiseenko K.B. Variations in the content of ozone and nitrogen dioxide in the field of orographic waves over the nearpolar Urals. Doklady Earth Sciences (2017) V. 475. No. 6. P. 691–696. (rus.)

35. Golitsyn G.S., Grechko E.I., Genchen Van, Pusay Van, Jola A.V., Emilenko A.S., Kopeikin V.M., Rakitin V.S., Safronov A.N., Fokeyeva E.V. Study of atmospheric pollution in Moscow and Beijing with carbon monoxide and aerosol. Izvestiya, Atmospheric and Oceanic Physics (2015) V. 51. No. 1. P. 8–19. (rus.)

36. Elansky N.F., Lokoshchenko M.A., Trifonova A.V., Belikov I.B., Skorokhod A.I. On the content of minor gas impurities in the near surface layer over Moscow. Izvestiya, Atmospheric and Oceanic Physics (2015) V. 51. No. 1. P. 39–45. (rus.)

37. Virolainen Ya.A., Timofeev Yu.M., Poberovskiy A.V, Kirner O., Höpfner M. Content of chlorine nitrate in the atmosphere over St. Petersburg. Izvestiya, Atmospheric and Oceanic Physics (2015) V. 51. No. 1. P. 60–68. (rus.)

38. Smyshlyaev S.P. , Mareev E.A., Galin V.Ya., Blakitnaya P. A. Modeling the effect of methane emissions from arctic gas hydrates on regional changes in the composition of the lower atmosphere. Izvestiya, Atmospheric and Oceanic Physics (2015) V. 51. No. 4. P. 472–483. (rus.)

39. Shtabkin Yu.A., Moiseenko K.B., Skorokhod A.I,, Vasilyeva A.V., Khaimann M. Sources and variations of tropospheric CO in Central Siberia: numerical experiments and observations on the high-altitude mast ZOTTO. Izvestiya, Atmospheric and Oceanic Physics (2016) V. 52. № 1. P. 51–63. (rus.)

40. Vetrov V.A., Kuzovkin V.V., Manzon D.A. Acidity of precipitation and deposition of sulfur and nitrogen on the territory of the Russian Federation according to the monitoring of the chemical composition of the snow cover. Meteorologiya i Gidrologiya (2015) No. 10. P. 44–53. (rus.)

41. Kashin F.V., Arefyev V.N., Sizov N.I., Akimenko R.M., Upenek L.B. The background component of carbon dioxide in the surface air (Obninsk monitoring station). Izvestiya, Atmospheric and Oceanic Physics (2016) V. 52. No. 3. P. 1–7. (rus.)

42. Sitnov S.A., Mokhov I.I., Jola A.V. The total content of carbon monoxide in the atmosphere over the Russian regions by satellite data. Izvestiya, Atmospheric and Oceanic Physics (2017) V. 53. No. 1. P. 38–55. (rus.)

43. Ionov D.V., Poberovskiy A.V. Integral emission of nitrogen oxides from the territory of St. Petersburg according to mobile measurements and numerical simulation. Izvestiya, Atmospheric and Oceanic Physics (2017) V. 53. No. 2. P. 232–241. (rus.)

44. Sitnov S.A., Mokhov I.I., Gorchakov G.I., Jola A.V. Smoky haze on the European part of Russia in the summer of 2016: connection with forest fires in Siberia and anomalies of atmospheric circulation. Meteorologiya i Gidrologiya (2017) No. 8. P. 50–63. (rus.)

45. Sitnov S.A., Mokhov I.I. Weekly cycles of formaldehyde and nitrogen dioxide in the atmosphere over Northern Eurasia: Anthropogenic or natural? Proc. SPIE (2017) V. 10466. No. 104665T. P. 1–11. doi: 10.1117/12.2287151.

46. Sitnov S.A., Mokhov I.I. Formaldehyde and nitrogen dioxide in the atmosphere during summer weather extremes and wildfires in European Russia in 2010 and Western Siberia in 2012. Intern. J. Remote Sensing (2017) V. 38. Issue 14. P. 4086–4106.

47. Belan B.D., Savkin D.E., Tolmachev G.N. Investigation of the relation of snow cover and ozone concentration in the surface air layer near the city of Tomsk. Optika Atmosphery i Okeana (2018) Vol. 31. No. 8. P. 665–669. (rus.)

48. Aloyan A.E., Ermakov A.N., Arutyunyan V.O. Aerosol in the troposphere and lower stratosphere. Theses of the International Conference Dedicated to the Centenary of the Birth of Academician Alexander Mikhailovich Obukhov, May 16–18, 2018, M.: Fizmatknig, 2018, P. 108. (rus.)

49. Ermakov A.N., Aloyan A.E., Arutyunyan V.O. Carbonate particles of aerosol in the urban atmosphere and their chemical transformations (using the example of Irkutsk). Theses of the International Conference Dedicated to the Centenary of the Birth of Academician Alexander Mikhailovich Obukhov, May 16–18, 2018, M .: Fizmatknig, 2018, P. 135. (rus.)

50. Eremina I.D., Aloyan A.E., Arutyunyan V.O., Larin I.K., Chubarova N.E., Ermakov A.N. Hydrocarbonates in precipitation in Moscow: monitoring data and their analysis. Izvestiya, Atmospheric and Oceanic Physics (2017) V. 53. № 3. P. 379–388. (rus.)

51. Zelenov V.V., Aparina E.V., Kashtanov S.A., Shardakova E.V. Study of the initial capture of NO_2 on a coating of methane soot. Khimicheskaya Fizika (2015) T. 34. № 3. P. 87–96. (rus.)

52. Zelenov V.V., Aparina E.V., Kashtanov S.A., Shardakova E.V. Kinetics of capture of N_2O_5 on a coating of methane soot. Khimicheskaya Fizika (2016) V. 35. № 4. P. 78–91. (rus.)

53. Aloyan A.E., Ermakov A.N., Arutyunyan V.O. Aerosol in the upper troposphere and lower stratospkrk. Sulfate particles in the northern latitudes. Optika Atmosphery i Okeana (2018) Vol. 31. No. 2. P. 136–142. (rus.)

54. Manakov A.Yu., Penkov N.V., Rodionova T.V., Nesterov A.N., Fesenko ml. E.E. Kinetics of the formation and dissociation of gas hydrates. Uspekhi Khimii (2017) V. 86. № 9. P. 845–869. (rus.)

55. Aloyan A.E., Ermakov A.N., Arutyunyan V.O. The mechanism and kinetics of formation and transport of aerosol particles in the lower stratosphere. J. Fizicheskoy Khimii (2018) V. 92. No. 3. P. 483–488. (rus.)

56. Golubev V.N. The role of aerosol particles in the formation of atmospheric ice. Meteorologiya i Gidrologiya (2015) No. 12. P. 19–28. (rus.)

57. Aloyan A.E., Ermakov A.N., Arutyunyan V.O. The role of sulfate in the formation of clouds over the sea. Izvestiya, Atmospheric and Oceanic Physics (2016) V. 52. No. 4. P. 402–415. (rus.)

58. Larin I.K., Aloyan A.E., Eomakov A.N. Chlorine activation of the lower stratosphere in mid-latitudes: influence on the ozone layer. Khimicheskaya Fizika (2016) V. 35. No. 9. P. 76–80. (rus.)

59. Aloyan A.E., Ermakov A.N., Arutyunyan V.O. Modeling the formation of polar stratospheric clouds taking into account kinetic and heterogeneous processes. Izvestiya, Atmospheric and Oceanic Physics (2015) V. 51. No. 3. P. 276–286. (rus.)

60. Lushnikov A.A., Zagainov V.A., Lyubovtseva Yu.S. The initial stage of aerosol formation from supersaturated vapors. J. Fizicheskoi Khimii (2018) V. 92. No. 3. P. 501–507. (rus.)

61. Kumpanenko I.V., Roshmn A.V., Ivanova A.A., Zelenina E.I., Volochenko T.S., Panin E.O. Heterogeneous photocatalytic oxidation of polluting substances in air on TIO2 particles. Khimicheskaja Fizika (2018) V. 37. № 2. P. 25–34. (rus.)

62. Gorchakov G.I., Smtnov S.A., Semutnikova E.G. "Aging" of smoke aerosol with long-distance transport. Theses of the International Conference Dedicated to the Centenary of the Birth of Academician Alexander Mikhailovich Obukhov, May 16–18, 2018, M .: Fizmatkniga (2018) P. 127. (rus.)

63. Konovalov I.B., Berezina E.V., Bekyann M. Effect of photochemical self-action of carbon-containing aerosol: natural fires. Izvestiya, Atmospheric and Oceanic Physics (2016) V. 52. No. 3. P. 300–308. (rus.)

64. Larin I.K. Chemical physics of the ozone layer. M .: RAN (2018) P. 212.

65. Larin I.K. On the restoration of the ozone layer in the Northern Hemisphere in the XXI century. Khimicheskaya Fizika (2015) V. 34. No. 1. P. 80–86. (rus.)

66. Larin I.K. The chemical composition of the middle atmosphere and its change in the XXI century. Khimicheskaya Fizika (2018) V. 37. No. 11. P. 88–92. (rus.)

67. Ermakov A.N., Larin I.K. Chemical physics of the ozone layerю Istoriна Nauki i Tekhniki (2017) No. 3. P. 90–100. (rus.)

68. Larin I.K. On the theory of chain processes of the ozonosphere. Theses of the International Conference Dedicated to the Centenary of the Birth of Academician Alexander Mikhailovich Obukhov, May 16–18, 2018, M .: Fizmatkniga (2018) P. 149. (rus.)

69. Larin I.K. On the contribution of O_X, HO_X, NO_X, ClO_X, and BrO_X cycles to the destruction of stratospheric ozone in the 21st century. Khimicheskaya Fizika (2017) V. 36. No. 1. P. 90–96. (rus.)

70. Larin I.K. Odd oxygen and its atmospheric lifetime. Khimicheskaya Fizika (2017) V. 36. No. 3. P. 87–91. (rus.)

71. Larin I.K. On the unsolved problems of the chemistry of the middle atmosphere. Khimicheskaya Fizika (2018) V. 37, No. 8, P. 79–82. (rus.)

72. Smyshlyaev S.P. , Pogoreltsev A.I., Galin V.Ya., Drobashevskaya E.A. Influence of wave activity on the gas composition of the stratosphere of polar regions. Geomagnetizm i Aeronomiya (2016) V. 56. No. 1, pP. 102–116. (rus.)

73. Krivolutsky A.A., Vyushkova T.Yu., Mironova I.A. Changes in the chemical composition in the polar regions of the Earth after proton flares on the Sun (three-dimensional modeling). Geomagnetizm i Aeronomiya (2017) V. 57. No. 2, P. 173–194. (rus.)

74. Gruzdev A.N., Ageeva V.Yu., Elokhov A.S., Mokhov I.I. Statistical patterns of sudden stratospheric warming and their influence on the content of NO_2 and O_3. Theses of the International Conference Dedicated to the Centenary of the Birth of Academician Alexander Mikhailovich Obukhov, May 16–18, 2018, M.: Fizmatkniga (2018) P. 70. (rus.)

75. Gruzdev A.N., Kropotkina E.P. , Solomonov S.V., Elokhov A.S. Winter-spring anomalies of the O3 and NO2 content in the stratosphere over the Moscow region in 2010 and 2011. Izvestiya, Atmospheric and Oceanic Physics (2017) V. 53. No. 2. P. 223–308. (rus.)

76. Gruzdev A.N., Kropotkina E.P. , Solomonov S.V., Elokhov A.S. Anomalies of ozone and nitrogen dioxide in the stratosphere over the Moscow region as a manifestation of the dynamics of the stratospheric polar vortex. Doklady Earth Sciences (2016) V. 468. No. 4. P. 451–454. (rus.)

77. Rozanov E.V. Influence of precipitating energetic particles on the ozone layer and climate. Khimicheskaya Fizika (2018) V. 37. No. 8. P. 73–78. (rus.)

78. Ageeva V.Yu., Gruzdev A.N., Elokhov A.S. Increase in the stratospheric content of NO_2 according to the results of ground-based observations after the solar proton event in October 2003. Doklady Earth Sciences (2018) V. 479. No. 6. P. 688–691. (rus.)

79. Chubarova N.E., Zhdanova E.Yu., Hattatov V.U., Vargin P. N. Current problems of studying ultraviolet radiation and the ozone layer. Vestnik Akademii Nauk (2016) V. 86. No. 9. P. 839–846. (rus.)

80. Smyshlyaev S.P., Galin V.Ya., Blakitnaya P.A., Lemishchenko A.K. Study of the sensitivity of the composition and temperature of the stratosphere to the variability of the spectral fluxes of solar radiation caused by the 11-year solar cycle. Izvestiya, Atmospheric and Oceanic Physics (2016) V. 52. No. 1. P. 19–36. (rus.)

81. Sitnov S.A., Mokhov I.I. Formation of the ozone "mini-hole" under conditions of a prolonged blocking anticyclone in the atmosphere over the European territory of Russia in the summer of 2010. Doklady Earth Sciences (2015) V. 460. No. 1. P. 74–78. (rus.)

82. Sitnov S.A., Mokhov I.I., Lupo A.R. Ozone, water vapor, and temperature anomalies associated with atmospheric blocking events over Eastern Europe in spring – summer 2010. Atmos. Environ. (2017) V. 164. P. 180–194.

83. Sitnov S.A., Mokhov I.I., Bezverkhny V.A. Analysis of the characteristics of the relationship of total ozone and water vapor over the European part of Russia with the North Atlantic Oscillation in the summer of 2010. Optika Atmosphery i Okeana (2016) V. 29. No. 6. P. 457–461. (rus.)

84. Ageeva V.Yu., Gruzdev A.N. Seasonal features of the quasi-biennial variations of the stratospheric content of NO_2 according to the results of ground-based measurements. Izvestiya, Atmospheric and Oceanic Physics (2017) V. 53. No. 1. P. 74–85. (rus.)

85. Gruzdev A.N., Elokhov A.S. The perennial sounding of the stratospheric content of NO_2 at the Zvenigorod scientific research station of the A.M. Obukhov Institute of Atmospheric Physics RAS. Theses of the International Conference Dedicated to the Centenary of the Birth of Academician Alexander Mikhailovich Obukhov, May 16–18, 2018, M.: Fizmatkniga (2018) P. 131. (rus.)

86. Krivolutsky A.A., Vyushkova T.Yu., Cherepanova L.A., Kukoleva A.A., Repnev A.I., Banin M.V. Three-dimensional global photochemical model CHARM. Taking into account the contribution of solar activity. Geomagnetizm i Aeronomiya (2015) V. 55. No. 1. P. 64–93. (rus.)

87. Ivanov A.R. Stratosphere-troposphere exchange and its some features in extratropical latitudes. Meteorologiya i Gidrologiya (2016) No. 3. P. 22–45. (rus.)

88. Timofeev Yu.M., Prlyakov A.V., Poberovskiy A.V. The increase in the content of hydrochloride in the atmosphere of the Northern Hemisphere stops. Doklady Earth Sciences (2016) V. 470. No. 3. P. 344–346. (rus.)

89. Muryshev K.E., Eliseev A.V., Mokhov I.I., Timazhev A. Mutual delay between temperature changes and atmospheric carbon dioxide in a simple joint climate and carbon cycle model. Doklady Earth Sciences (2015) V. 463. No. 6. P. 708–712. (rus.)

90. Popova V.V., Matskovsky V.V., Mikhailov A.Yu. Modern land climate changes in the extratropical zone of the Northern Hemisphere. Vestnik Moskovskogo Universiteta. Series 5: Geographiya (2018) No. 1. P. 3–13. (rus.)

91. Dergachev V.A., Raspopov O.M., Tyasto M.I., Dmitriev P.B., Ismagilov V.S., Blagoveshchenskaya E.E. The manifestation of cyclic solar activity in the paleoclimatic

parameters ~ 100–150 million years ago. Geomagnetizm i Aeronomiya (2015) V. 55. No. 5. P. 579–586. (rus.)

92. Dergachev V.A. Earth's paleoclimate and solar activity. Geomagnetizm i Aeronomiya (2017) V. 57. No. 5. P. 567–571. (rus.)

93. Zherebtsov G.A., Kovalenko V.A., Kirichenko K.E. The role of solar activity in the observed climate change of the twentieth century. Geomagnetizm i Aeronomiya (2017) V. 57. No. 6. P. 687–695. (rus.)

94. Vakulenko N.V., Kotlyakov V.M., Sonechkin D.M. On the relationship between anthropogenic growth of carbon dioxide concentration and modern warming. Doklady Earth Sciences (2017) V. 477. No. 1. P. 87–91. (rus.)

95. Demchenko P.F., Semenov V.A. Estimation of the uncertainty of climatic trends of the near-surface temperature associated with the internal dynamics of the atmosphere. Doklady Earth Sciences (2017) V. 476. No. 3. P. 339–342. (rus.)

96. Mokhov I.I. Assessment of the ability of modern climate models to adequately assess the risk of possible regional anomalies and trends of change. Doklady of Earth Sciences (2018) V. 479. No. 4. P. 452–455. (rus.)

97. Sporyshev P.V., Kattsov V.M., Gulev S.K. Changes in surface temperature in the Arctic: the accuracy of model reproduction and a probabilistic forecast for the near future. Doklady Earth Sciences. 2018. T. 479. No. 5. S. 569–573. (rus.)

98. Volodin E., Gritsun A. About the nature of the slowdown of global warming at the beginning of the XXI century. Doklady Earth Sciences (2018) V. 482. No. 3. P. 315–318. (rus.)

99. Khlystov A.I., Klige R.K., Simkin, V.S. Global warming and its possible causes. Zemlya i Vselennaya (2018) No. 1. P. 60–70. (rus.)

100. Sterin A.M., Timofeev A.A. On the assessment of trends in surface air temperature for the territory of Russia by the method of quantile regression. Meteorologiya i Gidrologiya (2016) No. 6. P. 17–30. (rus.)

101. Vetrov V.A., Borisova O.K., Velichko A.A. Experience of perspective assessment of the main parameters of the regional climate up to 3000. Meteorologiya i gidrologiya (2016) No. 5. P. 12–31. (rus.)

102. Babich V.V., Darin A.V., Kalugin I.A., Smolyaninova L.G. Using periodic natural processes for climate prediction of extratropical latitudes of the Northern Hemisphere for the next 500 years. Meteorologiya i Gidrologiya (2016) No. 9. P. 5–15. (rus.)

103. Korneva I.A., Semenov S.M. Sensitivity of the temperature of the earth's surface to changes in the albedo of the atmosphere; Evaluation of the radiation effect. Meteorologiya i gidrologiya (2016) No. 5. P. 5–11. (rus.)

104. Polyakov A.V., Golovin Yu.M., Deler V., Ertel D., Shpenkuh D. Comparison of the spectra of the outgoing thermal IR-radiation of dDifferent years. Issledovanija Zemli iz Kosmosa (2018) No. 5. P. 65–72. (rus.)

105. Zadvornykh I.V., Gribanov K.G., Zakharov V.I., Imasu R. Software for modeling the transfer of thermal and near-IR radiation in the atmosphere with multiple scattering taken into account. Optika Atmosphery i Okeana (2017) V. 30. No. 2. P. 128–133. (rus.)

106. Kattsov V.M., Shkolnik I.M., Efimov S.V. Prospective estimates of climate change in the Russian regions: the implementation in the physical and probabilistic spaces. Meteorologiya i Gidrologiya (2017) No. 7. P. 68–80. (rus.)

107. Ryaboshapko A.G., Revokatova A.P. The potential role of negative carbon dioxide in solving the climate problem. Meteorologiya i Gidrologiya (2015) No. 7. P. 18–36. (rus.)

108. Vakulenko N.V., Nigmatulin R.I., Sonechkin D.M. On the issue of global climate change. Meteorologiya i gidrologiya (2015) No. 9. P. 89–97. (rus.)

109. Dmitrieva T.M., Grabar V.A. Aviation emissions of Russian civil aviation when performing domestic flights in 2000–2012. and integral assessment of their impact on the climate system. Meteorologiya i Gidrologiya (2017) No. 8. P. 76–84. (rus.)

110. Ekba Ya.A., Akhsalba A.K., Leyedev S.A., Bedanokov M.K. The impact of volcanic activity on the temperature of the surface layer of the air. Theses of the International Conference Dedicated to the Centenary of the Birth of Academician Alexander Mikhailovich Obukhov, May 16–18, 2018, M.: Fizmatkniga (2018) P. 99. (rus.)

111. Lykosov V.N. Regional aspects of climate modeling and its changes. Theses of the International Conference Dedicated to the Centenary of the Birth of Academician Alexander Mikhailovich Obukhov, May 16–18, 2018, M.: Fizmatkniga (2018) P. 14. (rus.)

112. Mokhov I.I. Modern climate change: anomalies and trends. Theses of the International Conference Dedicated to the Centenary of the Birth of Academician Alexander Mikhailovich Obukhov, May 16–18, 2018, M .: Fizmatkniga (2018) P. 15. (rus.)

113. Denisov S.N., Eliseev A.V., Mokhov I.I., Arzhanov M.M. Model estimates of global and regional methane emissions to the atmosphere by wet ecosystems. Izvestiya, Atmospheric and Oceanic Physics (2015) V. 51. № 5. P. 543–549. (rus.)

114. Arzhanov MM, Mokhov I.I., Denisov S.N. The impact of regional climate change on the stability of relict gas hydrates. Doklady Earth Sciences (2016) V. 468. No. 5. P. 572–574. (rus.)

115. Arzhanov M.M., Mokhov I.I., Denisov S.N. Destabilization of relict gas hydrates with observed regional climate change. Arctica: Ecologiya i Economika. 2016. No. 4. P. 46–51. (rus.)

116. Sitnov S.A., Mokhov I.I., Jola A.V. The total content of carbon monoxide in the atmosphere over the Russian regions by satellite data. Izvestiya, Atmospheric and Oceanic Physics (2017) V. 53. No. 1. P. 38–55. (rus.)

117. Sitnov S.A., Mokhov I.I., Jola A.V. Variations of carbon monoxide in the atmosphere under blocking conditions over the European territory of Russia in the summer of 2010 (according to AIRS). Optika Atmosphery i Okeana (2017) V. 30. No. 3. P. 214–221. (rus.)

118. Arzhanov M.M., Mokhov I.I. Estimates of the degree of stability of continental relict methanhydrates in the Holocene optimum and under current climatic conditions. Doklady Earth Sciences (2017) V. 476. No. 4. S. 456–460. (rus.)

119. Sitnov S.A., Mokhov I.I. Anomalies of methane content in the atmosphere over northern Eurasia in the summer of 2016. Doklady Earth Sciences (2018) V. 480. No. 2. P. 223–228. (rus.)

120. Arzhanov M.M., Malakhov V.V., Mokhov I.I. The conditions of formation and dissociation of methane hydrates over the past 130 thousand years according to model calculations. Doklady Earth Sciences (2018) V.480. No. 6. P. 725–729. (rus.)

121. Arshinov M.Yu., Belan B.D., Davydov D.K., Krasnov O.A., Macsutov S., Machida T., Sasakawa M., Fofanov A.V. Features of the vertical distribution of carbon dioxide over the south of western Siberia in the summer period. Optika Atmosphery i Okeana (2018) V. 31. No. 8. P. 670–681. (rus.)

122. Zadvornykh I.V., Gribanov KG, Zakharov V.I., Imasu R. Method for determining the vertical profile of methane from atmospheric spectra measured simultaneously in the thermal and near-IR ranges. Optika Atmosphery i Okeana (2018) V. 31. No. 12. P. 962–967. (rus.)

123. Nasrtdinov I.M., Zhuravleva TB, Chesnokova T.Yu. Estimates of direct radiation effects of background and smoke aerosol in the infrared region of the spectrum for summer conditions of Siberia. Optika Atmosphery i Okeana (2018) V. 31. No. 2. P. 121–127. (rus.)

124. Vinogradova A.A., Vasilyeva A.V. Black carbon in the air of northern regions of Russia: sources, spatial and temporal variations. Optika Atmosphery i Okeana (2017) V. 30. No. 6. P. 467–475. (rus.)

125. Rakitin V.S., Yelansky N.F., Pankratova N.V., Skorokhod A.I., Jola A.V., Shtabkin Yu.A., Van Pusay, Van Genchen, Vasilyeva A.V., Makarova M .V., Grechko E.I. Investigation of trends in total CO and CH_4 content over Eurasia based on the analysis of ground-based and orbital spectroscopic measurements. Optika Atmosphery i Okeana (2017) V. 30. No. 6. P. 449–456. (rus.)

126. Antokhin P. N., Antokhina O.Yu., Arshinov M.Yu., Belan B.D., Davydov D.K., Sklyadneva T.K., Fofanov A.V., Sasakawa M., Machida T. Influence atmospheric blocking in western Siberia for changes in methane concentration in the summer period. Optika Atmosphery i Okeana (2017) V. 30. No. 5. P. 393–403. (rus.)

127. Glagolev M.V., Ilyasov D.V., Terentyeva I.E., Sabrekov A.F., Krasnov O.A., Maksyutov Sh.Sh. Flows of methane and carbon dioxide in the marshy forests of the southern and middle taiga of western Siberia. Optika Atmosphery i Okeana (2017) V. 30. No. 4. P. 301–309. (rus.)

128. Gorchakov G.I., Karpov A.V., Vasilyev A.V., Gorchakova I.A. Brown and black carbon in smogs of megacities. Optika Atmosphery i Okeana (2017) V. 30. No. 1. P. 5–11. (rus.)

129. Skorokhod A.I., Pankratova N.V., Belikov I.B., Rakitin V.S., Shtabkin Yu.A., Thompson R. Study of Atmospheric Methane Sources in the Arctic. Theses of the International Conference on the Centenary of the Day Birth of Academician Alexander Mikhailovich Obukhov, May 16–18, 2018, M.: Fizmatkniga (2018) P. 168. (rus.)

130. Mokhov I.I., Smirnov D.A. Contribution of radiation effects of greenhouse gases and Atlantic multi-ten-year oscillation to trends in surface temperature. Meteorologiya i Gidrologiya (2018) No. 9. P. 5–13. (rus.)

Atmospheric Electricity

E.A. Mareev, V.N. Stasenko, M.V. Shatalina, S.O. Dement'eva,
A.A. Evtushenko, N.N. Slyunyaev, E.K. Svechnikova
Institute of Applied Physics RAS
Planeta Research Center for Space Hydrometeorology

Introduction

This work presents a review of Russian studies in the field of atmospheric electricity in 2015–2018. has been and remains one of the fundamental problems of atmospheric physics that hasbeen drawing attention for many years. In recent years, many areas of good weather electricity physics, the processes of clouds electrization and the formation of their electrical structure, the study of the relationship of thunderstorm activity with other dangerous weather phenomena continue to develop. Experimental studies of atmospheric electricity, conducted in scientific centers of Russia, make a significant contribution to the improvement of theoretical and numerical models of various electrical processes in the atmosphere, as well as models of the global electrical circuit. New data were obtained in the field of lightning physics, including new results on the structure of leader and streamer discharges. Much attention is paid to the study of high-energy processes, such as X-ray and gamma outbreaks during thunderstorms. Research continues on lightning activity from space using microsatellites designed for this purpose. Of particular note is the great attention paid to the laboratory study of atmospheric discharges of various types. In more detail the main results in each of the areas are given in the relevant sections of this article.

Fair weather electricity

In recent years, the active study of good weather electricity has continued in Russia. There is a heightened interest in the processes occurring in the convective atmospheric boundary layer need for fundamental research of the formation of clouds and electrical effects associated with industrial and natural aerosols.

Long-term observations of the atmospheric electric field reveal the main features of daily and seasonal variations [1], study the effect of convection on electrical conductivity in the surface layer [2], estimate the effect of aerosol and radioactive pollution of the atmosphere [3], experimentally investigate the variability of vertical atmospheric electric currents in the surface layer [4].

According to the results of the analysis of long-term observations of the atmospheric electric field in Yakutsk, it has been established that the diurnal variation has two maxima in the spring, summer and autumn months, while in the winter months the diurnal variation has one maximum and one minimum. The seasonal variation of the average monthly field strength values has maximums in the spring and autumn months and minimums that occur in the summer and winter months. In the variations of the average monthly values of the electric field strength over a five-year period, there is a tendency to reduce the amplitude of seasonal variations in the field strength and the total values of the field strength [1].

Based on the monitoring data of the electrical quantities of the surface layer of the atmosphere, conducted in Tomsk in 2006–2017, their slow variations related to the passage of cumulonimbus clouds and associated atmospheric phenomena in warm and cold periods of the year were investigated. A statistical analysis of slow variations in the electric field potential gradient was performed. It is shown that the distribution of the total duration of slow variations in the potential gradient is described by a power distribution [5].

In [6], using the results of field observations, regularities were found in the daily dynamics of the scaling and energy characteristics of the aeroelectric field in various states of the surface atmosphere. It is shown that short-period aeroelectric pulsations in the frequency range Δf = 0.001–1 Hz have the property of self-similarity and the fractal dimension D = 1.1–1.8. Plots with intermittency were found at time intervals characterized by a change in the stratification of the atmospheric boundary layer. It is shown that the intermittency of the aeroelectric field is characterized by multifractality with a spectral width that is significantly different from zero, the non-Gaussianity of the field increment distribution, a change in spectral density indices from -2.3 to -4 for Δf = 0.01–1 Hz. In [6], using the results of field observations, regularities were found in the daily dynamics of the scaling and energy characteristics of the aeroelectric field in various states of the surface atmosphere. It is shown that short-period aeroelectric pulsations in the frequency range Δf = 0.001–1 Hz have the property of self-similarity and the fractal dimension D = 1.1–1.8. Plots with intermittency were found at time intervals characterized by a change in the stratification of the atmospheric boundary layer. It is shown that the intermittency of the aeroelectric field is characterized by multifractality with a spectral width that is significantly different from zero, the non-Gaussianity of the field increment distribution, a change in spectral density indices from -2.3 to -4 for Δf = 0.01–1 Hz.

Studies of the effect of solar activity on the variations of the electric field in the surface layer of the atmosphere have been carried out. Based on atmospheric-electrical observations in the high-altitude conditions of the Elbrus region, the

Forbush effect manifests itself in variations of the electric field. The relationship of the electric field with solar and geomagnetic activity was studied [7].

Much attention is paid to the development of theoretical and numerical models for the formation of the structure of the electrode layer in the surface atmosphere, in particular, the effects of aerosols and convection on the conductivity of the surface layer. In [8], on the basis of the analysis of the results of field observations and numerical modeling, it was established that the development of convection in the atmospheric boundary layer leads to a decrease in electrical conductivity near the surface of the earth. It is shown that the enhancement of turbulence generation associated with convection, accompanied by an increase in turbulent kinetic energy and dispersion of vertical velocity fluctuations, contributes to more intensive vertical mixing of radon and radioactive daughter products. The variability of the electrical conductivity and the strength of the aeroelectric field, determined by radon emission, air ionization, charge separation on electrical conductivity inhomogeneities, turbulent transport of radioactive elements and bulk electric charges, were estimated [2].

In [9–11], the electrodynamic model of a horizontally uniform aerosol-free surface layer was considered, consisting of balance equations for positive and negative light aero ions and the Poisson equation. Analytical expressions were obtained for stationary distributions of concentrations of air ions, electric field and electric charge density in the approximations of the classical and turbulent electrode effect [9]. It has been established that the height of the classical electrode layer in an atmosphere free of an aerosol is about 10 m, and its structure is mainly determined by the electric field. When the electric field is amplified, the height of the electrode layer and, consequently, the scale of distribution of electrical quantities increase. During the transition to the turbulent regime in the surface atmosphere, the height of the electrode layer increases and reaches several tens of meters [10]. The height of the turbulent electrode layer is determined by both the electric field and the degree of turbulent mixing. Amplification of the external electric field weakens the effects of turbulence. The distributions of the electrical characteristics of the surface layer are obtained depending on the concentrations of aerosol particles in the atmosphere and the degree of turbulent mixing [11].

Global electric circuit

The idea of the global electric circuit (GEC) plays a fundamental role in the studies of atmospheric electricity since it combines all electrical processes occurring in the atmosphere within a single concept. In recent years, the interest in studying the GEC has been gradually increasing.

A great attention is presently given to the numerical modeling of the GEC. Usually the input of GEC models consists of the distributions of the conductivity and source current density (representing charge separation inside thunderstorms and electrified shower clouds), hence the parameterization of these quantities is the most important part of every GEC model. In [12] a new parameterization of conductivity at different stages of the solar cycle has been suggested and used to estimate the variation of GEC parameters due to large-scale conductivity changes associated with solar activity. The problem of parameterizing source current corresponding to electrified clouds of different types has been considered in [13], while in [14] an attempt has been made to introduce additional source currents of a seismigenic nature. The problem of agreement of theoretical predictions of GEC parameters with observations has been discussed in [15].

Much more general problems regarding the equations of the GEC, involving ionospheric generators and anisotropic conductivity, have been analyzed from a mathematical perspective in [16]. The authors have shown that both quasi-stationary and steady-state problems describing the GEC with various boundary conditions are well-posed and convenient for implementation in numerical models. Further analysis of different boundary conditions at the upper atmospheric boundary has been carried out in [17], along with the estimates of perturbations generated by a thunderstorm at its magnetic-conjugate point. In [18] the implementation of voltage-source thunderstorms in numerical GEC models has been considered, which is particularly important for the problem of theoretical explanation of GEC variation on the scale of 11-year solar cycles [12]. The role of the Earth's orography in GEC analysis has been discussed in [19].

Another important direction of research is the interaction of the GEC with ionospheric and lithospheric processes. The penetration of non-stationary ionospheric electric fields to the lower atmosphere has been analysed in [20]. The related problem of modelling the electric field penetration from ground to the ionosphere has been considered in [21, 22]. The electric fields at ionospheric heights produced by thunderstorm generators have been estimated in [23]. The problem of lithosphere–ionosphere coupling, especially in the context of earthquakes, has been analyzed and discussed in [24, 25].

Electric processes in clouds

Description, modeling and observations of the electric processes in clouds are an important component of the atmospheric electricity research. The study of the electric processes in clouds covers a wide range of tasks, including theoretical and experimental study of the development and evolution of convective

systems, modeling and forecasting of the thunderstorms development, searching for correlations between the observed meteorological data and the registered lightning activity.

The forecast of thunderstorm events using numerical mesoscale models is one of the most important practical applications for modeling of the electric processes in clouds. The paper [26] presents statistical estimates of 26 indexes of atmospheric instability, widely used in world practice for forecasting of thunderstorm activity. A new index taking into account the vertical component of wind speed is also proposed for thunderstorm forecast. The modern methods for thunderstorms forecasting using numerical models are also discussed in [27]. The performed analysis of the possibility of using the LPI for prediction of the lightning flashes occurrence has shown a number of drawbacks that leads to decrease of the accuracy of the forecast based on the use of indirect indexes. Thus, a new algorithm for prediction of the lightning activity based on direct electric field calculation was proposed. The characteristic values of electrical parameters obtained using the developed parametrization showed a good correlation with the data of field measurements of the electric field and potentials in thunderclouds. The paper [28] presents the results of a study of a powerful thunderstorm on June 1–2, 2015 in the Nizhny Novgorod region using a WRF numerical model and the developed in [Дементьева С.О., Ильин Н.В., Мареев Е.А., Расчет электрического поля и индекса молниевой активности в моделях прогноза погоды, Известия Российской академии наук. Физика атмосферы и океана. 2015. Т. 51. № 2. С. 210] parameterization of the electric processes. A good agreement between the results of the simulation of radar reflectivity and meteorological radar data and the correspondence of the calculated electric parameters to the data of the electric field registration are shown. A model of the cumulonimbus electrification using the prediction results of the numerical mesoscale model WRF-ARW as input data is presented in [29]. Prediction of the electric field parameters in the atmosphere with the use of this model and comparison of the prediction results with the observed thunderstorms were carried out. Also a study of the effects of thunderstorms in the Black Sea basin on the chemical composition of the atmosphere was made in [30]. It was shown that temperature field changes associated with thunderstorm activity are higher in the continental part of the region than above the water surface.

Conducting the joint studies on the formation and electrification of thunderclouds by means of field observations and numerical simulation is also an important task. The paper [31] is devoted to the joint analysis of the instrumental observations of the lightning detection system LS8000, meteorological radars, electric field sensors and the results of numerical modeling of the electric parameters of powerful convective clouds with the use of the three-dimensional

model developed in the High-Mountain Geophysical Institute, which revealed the distinguishing features of the influence of electric processes on the formation of microstructural characteristics of convective clouds and precipitation. An analysis of simultaneous radiolocation, radiometric (using the SEVIRI radiometer installed on the Meteosat satellite) and radio direction finding measurements was performed to identify the relationship of the electric discharges characteristics with the parameters of cumulonimbus clouds during its development in the North Caucasus [32]. A correlation between the scale of the heterogeneity of the radiation temperature field of the cloud and the electric discharges frequency, as well as an increase of the electric discharges frequency with increasing precipitation intensity, reaching the maximum value at precipitation intensity of about 70 mm/h, were revealed.

The analysis of observations data of the development of a powerful thunderstorm with hail performed with the use of the radar MRL-5 and the lightning detection system LS8000 showed the presence of a link between the total lightning current in the LF range and the lightning frequency in the LF and VHF ranges [33]. According to the measurement data, the total charge transferred by negative discharges from the cloud to the ground was 387 C, the average charge value per one lightning is 0.44 C. To investigate a powerful thunderstorm over Pyatigorsk on May 29, 2012, accompanied by strong hail, a three-dimensional non-stationary model of a convective cloud was used [34]. The obtained values of cloud characteristics allowed us to analyze the evolution of the precipitation field and charge structure during cloud development. The experimental and theoretical study of the electrification processes in intense flows of dust, sand or snow, including effects associated with turbulent mixing of particles, are of particular interest among studies of atmospheric electric processes. For carring out experimental measurements of fluctuations of electric current of saltation, concentration of salting sand particles, and turbulent pulsations of wind speed, an instrumental complex, which made it possible to perform simultaneous measurements of these parameters in a deserted area in Kalmykia, was created [35]. These measurements made it possible to obtain the distribution of the specific charge of salting sand perticles for the first time. The average value of the specific charge was 48.5 μC/kg and varied from 10 to 150 μC/kg. The laws of transformation of statistical characteristics of variations of such parameters as wind speed, sand concentration, density of the electric current of saltation, caused by non-linear processes in wind-sand flow were also established. The high-speed video recording of a wind-sand flow, that was carried out in [36] made it possible to detect quasi-horizontal trajectories of sand in the lower millimeter layer of saltation, that became the basis of the wind profile model under stationary saltation conditions.

In addition, in 2017–2018 much attention was paid to the study of the influence of turbulence on the electrification of particles in the atmosphere. A theoretical study of the contribution of turbulence to the electrification of thunderclouds, snowstorms, and dust storms was carried out, and a model of the large-scale electric field generation in a weakly conducting medium containing two types of particles charged during collisions was proposed in [37]. It was found that the influence of turbulence differs significantly in the case of inductive and non-inductive mechanisms of charge separation. However, turbulence initiates an additional growth of the large-scale electric field for both mechanisms in the considered systems, which is a significant effect especially in the case of an electric field close to the breakdown value. A more detailed study of the influence of turbulence on the electrification of thunderclouds is presented in [38, 39]. Analytical estimates of changes of the thundercloud electric parameters caused by turbulent effects, for various characteristics of turbulence and hydrometeors, were used in these works to improve the parameterization of the electric processes and the numerical simulation of thunderstorm events. A detailed comparison of the results of numerical simulation of thunderstorm events with and without taking into account turbulent effects made it possible to reveal a number of characteristic features in changing the distributions of the electric parameters of a thundercloud.

Physics of lightning

In recent years, active experimental and theoretical studies in the field of lightning physics have continued. Thus, at the site of the Integrated High-Voltage Stand of the All-Russian Research Institute of VEI (Istra), experiments on the initiation of ascending and descending leaders continued during the development of a long spark using a high-voltage impulse voltage generator, as well as using an artificial charged cloud of water aerosol [40]. With the help of a unique high-voltage equipment (pulse voltage generator up to 6 MV) and a high-speed camera with an exposure of 0.2 ns, detailed images of streamer flashes of positive and negative leaders of a long spark were obtained for the first time [41].

The similarity of the shape and structure of streamer flashes of the leaders of both polarities was found, in contrast to the idea of their difference that existed until now. A similarity in the shape of the channel of a jump of a positive leader with channels of long streamers was found, which made it possible to put forward a hypothesis about the formation of a jump of a positive leader in a streamer channel, in contrast to a jump of a negative leader formed in the process of growth of a spatial leader [42]. Also, for the first time, detailed optical and IR images of the contact area of the positive and negative leaders and the

end-to-end phase were obtained based on model experiments using a negative charged cloud. It was established that the rates of positive and negative leaders within the common streamer zone coincide and increase with increasing current strength. The results obtained are important for solving the fundamental problems of the dynamics of the main stage of lightning [43]. The possibility of electric discharges initiated by a crossbow bolt (projectile) moving in an electric field of a cloud of negatively charged water droplets was first demonstrated in [44].

The works [45–48] present the results of experimental studies of the formation of ascending leaders from lightning conductor models and protected objects under the effect of an artificial thundercloud of negative polarity. Identified two options for the development of an upward leader: continuous and with a stop in between. It is established that the average value of the current of the ascending leader for the case of continuous development of the leader in the interval is 1.4 times greater than for the case where the leader stops. It was found that the counter-descending leader from the artificial thundercloud as a whole deviates from the vertical more than the ascending leader from the lightning-conductor or object model [45]. The significant influence of the shape and size of the lightning conductor models and objects on the probability of their being hit by a discharge from the cloud is shown. The optimal sizes of rod and cable lightning rods were determined, which ensure that the ascending leaders start ahead from them in comparison with the formation of ascending leaders from the protected objects. Analysis of some experimental data showed that high frequencies (up to several hundred MHz) in the spectrum of signals recorded by antennas appear in cases when a powerful streamer corona is formed from a part of the main discharge channel near the boundaries of the charged and often correspond to the cloudy part of the discharge formation [46]. It has been experimentally shown that groups of large hydrometeors of various shapes significantly increase the probability of initiating a channel discharge between an artificial thunderstorm cell and the ground, especially with a positive cloud polarity [47, 48]. The results can be used in the development of a method of purposeful artificial initiation of lightning between a thundercloud and the ground.

The fundamental problems of lightning physics and recent advances in instrumental (primarily satellite) recording of discharge phenomena in the atmosphere are also actively discussed [49]. The formation of plasma formations in the thundercloud with the parameters necessary for the initiation and development of a lightning discharge is considered to be a nonequilibrium phase transition induced by electrostatic noise [50]. Within the framework of the new three-dimensional model of lightning development, including bidirectional distribu-

tion of the discharge, its dynamic probabilistic branching and the possibility of simultaneous growth and / or decay of peripheral branches, and also taking into account for the first time the evolution of conductivity, longitudinal electric field and current of discharge channels, the dominant influence of the lower layer of positive charge is demonstrated on the typology and dynamics of a lightning discharge in a thundercloud [51].

For the first time, a consistent theoretical model has been proposed that can explain the close-to-lognormal distributions of peak currents in cloud-to-ground lightning discharges, which are observed when measuring currents of natural and trigger lightning [52]. According to the model, the distribution of peak currents of the first and subsequent components of lightning flashes are not strictly lognormal, but close to those in a certain range of values. In the area of extremely high peak currents (of the order of and more than 100 kA), the distribution can differ significantly from lognormal, which is important to consider when solving lightning protection tasks.

Particular attention is paid to the study of such a relatively recently discovered phenomenon, as a compact intracloud discharge in a thundercloud. In work [53] a hypothesis is developed according to which a compact intracloud discharge is a consequence of the development of avalanches of relativistic high-energy runaway electrons, initiated by a wide atmospheric shower, and breakdown on runaway electrons. A numerical simulation of the development of a positive streamer around charged water droplets at atmospheric pressure, typical for the height of a thundercloud and in various background fields, droplet sizes and charges, was carried out [54].

In [55,56] a new fractal model of a compact intracloud discharge was proposed a, which considers it as the result of the interaction of two (or more) bipolar streamer structures that form in a strong large-scale electric field of a thunderstorm cloud. It is shown that a single bipolar streamer structure as it develops accumulates near its ends significant electrical charges of a different sign. The features of electromagnetic radiation of a compact intracloud discharge are investigated within the framework of the proposed model. It is shown that high-frequency radiation at the preliminary stage of a compact discharge is negligible compared to radiation at the main stage. It was also found that at the preliminary stage of the discharge a burst of high-frequency radiation correlates well with the maximum pulse of the low-frequency electric field, and the spectrum of high-frequency radiation has a power-law appearance with an indicator lying in the interval from -2 to -1.

The scheme of wildfires climate model of the Institute of Atmospheric Physics them. A.M. Obukhova RAS (KM IFA RAS) expanded to include the effect of lightning activity and population density on the frequency of fires and the suppression of fires [57]. Using the IFA RAS CM, numerical experiments

were performed in accordance with the conditions of the CMIP5 climate model comparison project (Coupled Models Intercomparison Project, phase 5). The frequency of lightning flashes was set in accordance with LIS / OTD satellite data. As a result of the calculations, it turned out that anthropogenic fires play a dominant role in the occurrence of wildfires, with the exception of regions of subpolar latitudes and to a lesser extent tropical and subtropical regions. Taking into account the connection of the number of fires with lightning activity and population density in the model enhances the influence of the characteristics of natural fires on climate change in the tropics and subtropics compared with the version of the IMA RAS CM without taking into account the influence of ignition sources on the large-scale characteristics of natural fires.

High altitude discharges

The study of high-altitude discharges by Russian scientists continues quite actively. Satellite observations, laboratory and numerical simulations are conducted. Study of the initiation of sprites was done in [58]. Spherical plasma inhomogeneity located at mesospheric altitudes in the quasi-electrostatic field of a thundercloud is considered as a possible reason for the formation of a sprite. Assuming that the conductivity of the plasma formation is controlled by the processes of impact ionization and the attachment of electrons to neutral molecules, a simple semi-analytical model of ionization instability is developed in a quasi-electrostatic field. A numerical radially symmetric self-consistent model of the sprite at altitudes from 60 to 90 km was proposed in the work [59]. The perturbations of the concentration of ions, electrons, neutral particles and the intensity of photon emission at the heights of the mesosphere for the sprite at night were analyzed. It is shown that due to the rapid displacement of the electric field in the upper part of the diffuse area of the sprite, a toroidal structure of the electric field and the radiation of the sprite is observed. At altitudes of 83–87 km, the electron concentration decreases, which is associated with the increasing role of dissociative attachment to molecular oxygen, which significantly reduces the conductivity at these altitudes. The effect of thunderstorm activity on plasma-chemical processes in the air at altitudes of 95–100 km was considered [60]. It is shown that the electric fields of clouds charged unipolarly after lightning discharges lead to an increase in the concentration of electrons at these altitudes, which should lead to a noticeable increase in positioning errors of global satellite systems.

A series of articles is devoted to the launch of the Chibis-M microsatellite into orbit, a universal transport and starting device for launching microsatellites with a mass of 40–50 kg has been developed; for the first time, a scheme has

been developed to increase the height of the orbit of the Progress cargo vehicle for launching the microsatellite into orbit after it has completed the main task of delivering cargo to the ISS, which provided a significant economic effect; developed a full-featured microsatellite-complex; test cycles and the spacecraft flight control scheme were worked out [61–63]. Prospects for studying using satellites low-frequency electromagnetic fields generated by both conventional lightning in the troposphere and stratospheric and mesospheric electrical discharges such as sprite and blue jet are analyzed in [64] determines the sensitivity levels of devices necessary for recording various effects of discharges on the atmosphere. The results of observations obtained from the Vernov satellite, in comparison with the data from the "University-Tatiana-1, 2" satellites, are analyzed in [65]. Laboratory modeling of high-altitude discharges is carried out by two Russian groups. An installation for experimental research of high-voltage discharges in a gas with a pressure gradient [66] was created at the Institute of Applied Physics of the Russian Academy of Sciences. The possibility of using for modeling high-altitude discharges using an apocampic discharge is discussed in a number of papers [67, 68].

High-energy phenomena in the Earth's atmosphere

The study of high-energy phenomena in the atmosphere of the Earth is a young and rapidly developing branch of atmospheric physics, closely related to the study of altitude discharges. The phenomena of the emergence of energetic elementary particle fluxes in thunderclouds are divided into two classes, the relationship of which remains a controversial issue: terrestrial gamma ray flashes (TGFs) and thunderstorm ground enhancements (TGEs).

In order to gain new information about TGFs, the research team of the Institute of Nuclear Physics and the Cosmic Research Institute of the Russian Academy of Sciences used the RELEC equipment complex on the Vernov satellite. The device is equipped with a set of scintillation detectors, including four identical X-ray and gamma-radiation detectors with a working energy range from 10 keV to 3 MeV, with a total area of ~500 cm2. The monitoring information from the satellite is transmitted every second. Registration time of each gamma-quantum or electron is recorded with an accuracy of ~15 μs. The processing of data from the Vernov satellite led to the compilation of a catalog of TGFs published in [69]. The TGFs included in the catalog have a characteristic duration of ~400 μs, for which event 10–40 gamma quanta are recorded. For each gamma-ray burst the time profiles, spectral characteristics, and geographic location are given, as well as the result of comparison with the readings of other instruments installed on the Vernov satellite. A candidate for TGF, registered in the circumpolar region above Antarctica, is discussed.

The development of data processing methods for energetic events in the Earth's atmosphere is reflected in the publication [70], which sets out the results of a comprehensive study of the archived observational data of the SPI gamma spectrometer accumulated over 7 years of operation of the INTEGRAL observatory. The problems of processing arrays of observational data of the experiment, including the search algorithm and the method of automatic classification of detected events (gamma-ray flashes of both terrestrial and cosmic origin) based on a set of criteria, were separately discussed.

In [71], the location of the geographic areas of TGF excess and deficiency was compared with the location of areas of increased concentration of tropospheric impurities. As a measure of tropospheric pollution, data from the OMI tool (KNMI / NASA) on the nitrogen dioxide content of NO_2 in the troposphere was used. It is shown that the content of NO_2 in the "deficiency zones" of TGF is twice as high as the corresponding value in the "excess zones" of TGF. An additional analysis of the distribution of NO_2 concentrations around TGF locations with high spatial resolution based on radio data WWLLN showed the absence of features in the distribution of NO_2 on a scale of tens of kilometers characteristic of urban agglomerations.

The state of world research in the field of energetic particles fluxes originating in thunderclouds and recorded by ground-based detectors (TGEs) is determined by the activities carried out at the Aragats Research Station. A huge array of observational data on energetic atmospheric phenomena was analyzed in [72–75] the brief results of which are as follows. It is shown that almost always TGE is interrupted after a lightning flash that occurred in the same thundercloud, a detailed review of the characteristics of TGEs and lightning discharges interrupting them are described in [74]. An analysis of the spectrum of particles recorded by ground-based detectors showed that immediately after a lightning flash the high-energy part of the TGE radiation disappears. The decrease in the flux density of energetic particles from a thundercloud on a millisecond scale coincides with a lightning flash.

The key issue of atmospheric physics – the problem of initiating a lightning discharge – is fueled by new evidence obtained from TGEs observations. The time resolution of the applied equipment allowed us to relate the dynamics of the energetic particles flux from the redistribution of charges inside the thundercloud. Based on the consideration of relativistic runaway electron avalanche model, it is confirmed that the development of the TGE in a thundercloud favors the initiation of a cloud-to-ground negative lightning discharge [73]. Theoretical aspects of the physics of energetic particle fluxes from thunderclouds are discussed in [75], where a sufficiency of relativistic feedback mechanism (proposed by Dwyer) for explanation of the observational data is claimed.

Several years of experimental work on the study of variations in secondary cosmic ray particles during thunderstorms carried out at the facility "Kover" of the BNO INR RAS, allow the researches to assum the possibility of runaway breakdown in the atmosphere in the near-threshold mode [76, 77]. Breakdown is characterized by the presence of an electric field in the stratosphere with a potential difference of ~100 MV [77]. Runaway electrons that generate gamma quanta with energies up to 30 MeV multiply in an avalanche field. A more well-known analogue of the proposed discharge is a glow discharge. In [76], the transition of a discharge to an independent state is considered by means of "cyclic generation" of braking photons. The breakdown region of the type under discussion, most likely formed in the stratosphere between the top charge of a thunderstorm cloud and the ionosphere, should be accompanied by luminescence and disturb the electric and magnetic fields with a characteristic time of several minutes, which is the basis of the principle of detection of the discharge from measurement data. A correlation has been established between continuous luminescence of thunderclouds and anomalous disturbance of secondary particles of cosmic rays recorded at ground level. The case of the interruption of global micropulsations of the geomagnetic field as a result of the runaway electron breakdown in the near-threshold regime is described [76].The interaction of a thunderstorm front with precipitation of protons into the atmosphere from the Earth's radiation belt, due to seismic activity, was reported. The influence of seismic activity on the glow of the night sky was discussed separately [77].

Measurements of energetic particle flux conducted the Tien Shan Station have resulted in new information on extensive air showers and energetic radiation from lightning discharges [78–80]. The energy spectrum of particles of an extensive air shower in the range of 10^{14}–10^{17} eV was studied. It is shown that high-energy lightning discharge radiation is observed within ten seconds after the flash; gamma radiation, energetic electrons and neutrons were simultaneously detected [79]. The time series of the neutron flux generated by atmospheric discharges were obtained using detectors located on the Earth surface, as well as underground [78, 80]. A substantial part of neutrons is emitted in a short time immediately after discharge (200–400 μs). The magnitude of the time interval suggests that neutrons are mainly generated in a dense medium (presumably in the soil).

Observations at the Tien Shan high-altitude station made it possible to simultaneously register radiation in the radio frequency (0.1–30 MHz), infrared (610–800 nm), ultraviolet (240–380 nm) and soft X-ray (0.1–4 MeV) ranges [80]. The next step in the study of thunderstorm processes at Tian Shan Station was the registration of optical, radio and gamma radiation emitted during the bright lightning discharge stage. During the 2016 season, several hundred

bursts of optical radiation were recorded due to night lightning of ~30 thunderstorm events; at a distance of 3–10 km from the source. The importance of observing lightning discharges in a wide range of energies is demonstrated for checking and comparing the results of various theoretical models of atmospheric discharges, of which the so-called "dark discharge" ("dark lightning") is of particular interest. "Dark discharge" is one of the possible consequences of the relativistic runaway electron avalanche model. A clarification of the relationship between the energetic particles flux and lightning discharges, as well as possible conditions for the development of a "dark discharge" is the direction of future research based on a data ensemble on energetic events existing due to observations at the high-mountain stations of Aragats and Tian Shan.

High-energy atmospheric phenomena like TGF are often accompanied by radio emission, similar to lightning discharges, which can lead to the indistinguishability of TGF and lightning discharges by the WWLLN network. Studies of radio emission from thunderstorms conducted in the Nizhny Novgorod region showed that radio emission is concentrated in time intervals on the order of fractions of a microsecond with a gap of several microseconds between pulses, and does not show a smooth increase [81]. Radio emission is recorded not only during lightning discharges, but also in the intervals between them.

A significant part of the data on energetic events in the atmosphere results from the observations of neutron fluxes one of the main components of secondary cosmic rays. Preliminary results of the neutron flux analysis were obtained by means of complex of instruments created at the Institute of Physics and Energy of the Siberian Branch of the Russian Academy of Sciences [82]. Synchronous recording of neutron flux variations, electric field strength and electromagnetic radiation during lightning discharges is performed. The intensity of the neutron flux during lightnings in the vicinity of Yakutsk is measured using SNM-15 counters (in and without lead shells) with a resolution of 10 μs. The records obtained in the winter of 2013–2014 are also taken into account. The analysis also concerns variations of electric field and neutron intensity during snowstorms in Tiksi, in which powerful snow charges were observed with strong winds with speeds up to 60 m s^{-1}. It was shown that for the event of the considered type the electric field intensity can change direction to the opposite, reaching values of 90 kV m^{-1}, which is not accompanied by electric discharges and neutron bursts.

Data on neutron flux amplifications during thunderstorms have also been successfully applied to the study of thunderstorm nuclear reactions [83]. The assumption has been tested, whether the enhancement of the neutron flux could occur due to photonuclear reactions due to bremsstrahlung gamma-quanta of runaway electron avalanche that can develop in a thunderstorm electric field.

The importance of distinguishing the response of detectors to neutrons, electrons and gamma quanta is discussed.

Estimates of the contribution of thunderstorms to variations in the content of atmospheric radiocarbon 14C, widely used for dating of archaeological artifacts and works of art, were made in [84]. It is shown that the measured values of the flux of thunderstorm neutrons per discharge of lightning in areas with strong thunderstorm activity provide a local rate of radiocarbon production time, comparable to the accumulation of cosmic radiation. A previously unknown natural source not only of 14C radiocarbon, but also other isotopes in the atmosphere, such as 13N, 15N, 15O, 17O, 13C, was discovered.

Interrated methods for thunderstorm investigation

Regional researches of an electric field of the atmosphere have the considerable practical interest as variations of its strength characterize processes of an electrization upon development of the local weather phenomena, and also give information on regional features of functioning of the Global atmospheric electric circuit. Actual data on influence of the dangerous weather phenomena (rainfall, thunderstorms, etc.) and large-scale factors (cyclonic processes, solar and terrestrial relationship, etc.) on daily and seasonal changes of atmospheric electric field in regions aren't enough today.

Papers [31, 85] presented the results of the pilot studies of electric characteristics of thunderstorm by comparison of remote sensing data for clouds (the Doppler DMRL-C weather radar with cross-polarization signal processing) and lightning discharges (lightning detection system LS 8000), electric field strength measurements in a ground layer of the atmosphere (EFM550) and results of numerical modeling (NM) of deep convection clouds in the North Caucasus region are discussed. For the purpose of identification of a role of the storm phenomena in daily variations of the field gradient of the atmosphere synchronously with the field it was recorded the total lightning activity in the region.

The 3D non-stationary model with detailed description of the hydrothermodynamic, microphysical, and electric processes has been used for numerical simulations of the convective cloud formation under unstable atmospheric stratification and background wind. The microphysical unit of the model describes nucleation, condensation, coagulation among the droplets, sublimation, accretion, and freezing of droplets, cloud-particle deposition in the gravity field, particle transfer by air flows, as well as the cloud-particle interaction under the influence of the electric field of the cloud.

The model calculates the volume charges in the cloud, electrostatic potential, which is created by these charges, as well as the horizontal and vertical

components of the cloud-field intensity. The simulated radar reflectivity of the model cloud at wavelengths 3.2 and 10 cm are also compared with the actual radar observations of clouds. To analyze the model output, software for 3D visualization of the data has been developed for studying the cloud structure. By calculating the electric parameters of a cloud, it was assumed that formation and accumulation of the electric charges in the cloud is a result of the droplet freezing and accretion, i.e., interaction between the droplets and crystals.

Numerical experiments with and without allowance for the electric coagulation of the cloud particles were carried out. Comparative analyses of these two cases shows that the precipitation-particle growth time in deep convective clouds is significantly (by 20-30%) reduced because of the electric coagulation.

The results of calculations on the basis of the 3D model show that these processes in convective clouds interfere with each other, i.e., interact. This nonlinear interaction is rather complicated and plays an important role in the cloud microstructure formation. To verify numerical simulation of deep convection clouds, actual data on such weather hazards as lightning, hail, excessive precipitation, damaging wind will be used.

Besides, the model allows researchers to receive a missing set of dynamic, hydro-thermodynamic and microphysical characteristics in any point of a cloud and its environmental space for interpretation of results of observations. Three-dimensional visualization of parameters of convective clouds provides more reliable and effective interpretation of numerical and experimental data.

Paper [32] presents the interrelation of characteristics of electric discharges with parameters of developing hailstorm near Pyatigorsk (North Caucasus area) on May 29, 2012. That day the large hail of 2–3 cm size dropped out. Hail layer thickness on the ground was about 20 cm. For the analysis the data of the S-band MRL-5 radar, radiometric measurements of SEVIRI “Meteosat-8” satellite, and LS8000 lightning data were used. According to remote sensing data the first incloud discharge (IC) appeared at rather small radar reflectivity of 29 DBZ before rainfall on the ground. The first cloud – to – ground (C-G) discharge appeared 11 min lately, when cloud reflectivity reached 42 DBZ, and cloud top temperature – 36°C. The lightning discharges intensity in a cloud mature stage was 448 for IC and 23 for CG. During the maximum development of a cloud the intensity of rainfall exceeded 50 mm/h. Cloud top temperature was –59°C. Rainfall intensity growth was accompanied by increased total number of lightning discharges which maximized near 70 mm/h. It indicates that precipitation have the considerable impact on the lightning flash activity. Studying of regional features of deep convection cloud development by the integrated multi wavelength active and passive systems (weather radars, lightning sensors, microwave radiometers, automated meteorological stations) and results of

the simultaneous numerical cloud modeling has the great scientific and practical value.

Paper [86] presents the results of 5 years thunderstorm activity investigation aimed at density of lightning discharges in different regions of Northern Asia. These parameters – density of lightning discharges and corresponding currents are necessary for more effective lightning protection. The lack of the regular satellite and land observations in this region made it necessary of the WWLLN (World Wide Lightning Location Network) data application. The effectiveness of lightning flash detection by this system in 2012 averaged about 15% for CG and more than 30% for lightning with current peak value above 100 kA. According to authors the average density of lightning discharges revealed gradual increase for this period and the number of IC prevailed over CG. Here it should be noted that the probability of detection of IC by WWLLN network is rather small. In the Central Yakutia the share of CG lightning consisted of 40–60% for the summer period. When averaging location of thunderstorms on the area on a grid 0.25×0.25° the local maxima of thunderstorm activity forced by relief were found.

Paper [87] presents the analysis of changes of convective cloud characteristics, intensity and an amount of precipitation in the Leningrad Region upon their merging according to data of the DMRL-C radar, SEVIRI radiometer, lightning detection system Alves, network of Pluvio2 200 rain recorders and also by results of NM by means of non stationary 1,5 D convective cloud model. At merge the time course of the studied characteristics of clouds considerably changed: cloud top heights grew by 2 km, reflectivity maxima increased by 10 DBZ, the intensity and stream of rainfall increased approximately twice that is confirmed also by measurements of rain recorders. The same effect is supported with results of NM. The fact of number of lightning discharges increase was also confirmed with the Alves system.

Paper [26] presents comparative quality analysis for thunderstorm forecast based on 26 indexes of atmospheric instability, including test of the new index considered the speed of upflow. For validation of forecasts the WWLLN data were used. It was shown that it is necessary to attract the integrated methods of observation for thunderstorms, hail, heavy rains to further perfection of storm warning methods.

Papers [28, 88] present results of regional thunderstorm characteristics investigation. Data confirmed essential dependence of lightning activity over the area type. So, the lightning rate over the megalopolis was on average 46% more, than that over the low-populated territory what confirms the existence of city effect. At the same time the lightning rate over the dense forest area was about 2.4 times more, than that over farming zone.

Paper [89] presents the results of modeling the impact of aerosol air pollution on characteristics of deep convection cloud, its electric structure and precipitation. Aerosol impurity affects dynamic, microphysical and electric characteristics of a cloud: sharply increased the total number of ice crystals and hail embrio (approximately in 5 and 2 times respectively), maximal intensity of rainfall increased by 1.4 times and its amount – by 1.8 times. The increased concentration of natural aerosol with ice-forming properties altered the charge spatial distribution in a cloud and created its inverse electric structure.

Conclusions

In recent years, the studies of atmospheric electricity in the Russian Federation have received a new impetus to development. A wide range of experimental and theoretical studies of good weather electricity and the effects of atmospheric ions and aerosols on it has been carried out. Experimental and theoretical studies of the global electrical circuit, including the use of climate and climate-climate models. A set of experimental studies in the field of lightning physics and lightning protection has been carried out, including using unique laboratory stands and a natural stand of the All Russia Electrotechnical Institute in in Istra. In a number of Russian regions, studies of climatology of atmospheric electrical phenomena, regional meteorological features of thunderstorms, improvement of modeling methods and forecasting of thunderstorm phenomena are successfully continuing. Numerous laboratory experiments have been carried out to study the characteristics of the development of lightning discharges, both cloud-to-earth and earth-ionosphere. The Chibis-M microsatellite was put into orbit, the main task of which is to investigate discharge phenomena in the upper atmosphere. The results of observations obtained from the Vernov satellite are analyzed. Measurements of the surface fluxes of energetic particles produced at the Tien Shan station have resulted in new information on extensive air showers and energetic radiation from lightning discharges.

Over the past 3 years, conferences devoted to the problems of atmospheric electricity have been successfully held: the V and VI International Conference on Lightning Protection (St. Petersburg, 2016 and 2018), the Second and Third All-Russian Conference “Global Electrical Circuit” (Borok, Yaroslavl Region, 2015 and 2017). Russian scientists (12 people, including 11 representatives of institutions of the Russian Academy of Sciences) took an active part in the XVI International Conference on Atmospheric Electricity (ICAE2018, Nara, Japan, June 2018), which is held every 4 years and is the main international forum on atmospheric electricity.

References

1. Kozlov V.I., Karimov R.R. Variations of the atmospheric electric field from observations in Yakutsk, Science Education, 2016. No 2, P. 58–65. (in Russian)

2. Anisimov S.V., Galichenko S.V., Mareev E.A. Electrodynamic properties and height of atmospheric convective boundary layer, Atmos. Res., 2017. V. 194, P. 119–129.

3. Redin A.A., Kupovykh G.V., Kudrinskaya T.V., Grivtsov V.V. Atmospheric-electrical observations as a method to control the technogenic impact on the atmosphere, Technospheric Safety Technologies 2017, No 1, P. 271–277. (in Russian)

4. Panchishkina I.N., Petrova G.G., Petrov A.I. Experimental studies of the processes of vertical charge transfer in the surface atmosphere, Geomagnetism and Aeronomy, 2017. V. 57, No 3, P. 376–381. (in Russian)

5. Pustovalov P.M., Nagorskiy K.N. Comparative analysis of electric state of surface air layer during passage of cumulonimbus clouds in warm and cold seasons, Atmospheric and Oceanic Optics, 2018. V. 31, No 6, P. 685–689.

6. S.V. Anisimov, N.M. Shikhova, Fractal properties of aeroelectric pulsations, Geophysical studies, 2015. V. 16, No 4, P. 41–58. (in Russian)

7. Kudrinskaya T.V., Kupovy G.V., Redin A.A. Effect of solar activity on electric field variations in the surface layer of the atmosphere, Izvestiya Vysshikh Uchebnykh Zavedenii. Physics, 2016. V. 59, No. 12–3, P. 217–221. (in Russian)

8. Anisimov S.V., Galichenko S.V. Radon transport formation of the electric state of the atmospheric boundary layer, Fundamental Applied Hydrophysics, 2016. V. 9, No 4, P. 7–14. (in Russian)

9. Klovo A.G., Kupovykh G.V., Svidelsky S.S., Sklyarov N.E. Investigations of the Structure of the Electrode Layer in the Surface Atmosphere, News of Higher Educational Institutions. North Caucasus region. Series: Natural Sciences, 2018, No 1, P. 88–95.

10. Kupovykh G.V., Klovo A.G., Timoshenko D.V., Svidelsky S.S. Approximate analytical solution of the problem of the electrodynamic state of the surface atmosphere under conditions of aerosol pollution, Izvestiya Vysshikh Uchebnykh Zavedenii. North Caucasus region. Series: Natural Sciences, 2018. No 2, P. 84–89. (in Russian)

11. Morozov V.N., Kupovykh G.V., Redin A.A., Kudrinskaya T.V. Unsteady physical and mathematical modeling of electrical processes in the surface layer of the atmosphere taking into account submicron aerosol particles, Proceedings of the Voeikov Main Geophysical Observatory, 2017. No 584, P. 36–56. (in Russian)

12. Slyunyaev N.N., Mareev E.A., Zhidkov A.A. On the variation of the ionospheric potential due to large-scale radioactivity enhancement and solar activity, J. Geophys. Res.: SpacPhys., 2015. V. 120, No. 8, P. 7060–7082.

13. Slyunyaev N.N., Zhidkov A.A. On parameterization of the global electric circuit generators, Radiophysics and Quantum Electronics, 2016. V. 59, No. 3, P. 199–216.

14. Namgaladze A.A., Karpov M.I. Conduction current, external electric current in the global electric circuit, Chemical Physics, 2015. V. 34, No. 10, P. 8–11. (in Russian)

15. Morozov V.N., Sokolenko L.G., Zainetdinov B.G. Global atmospheric circuit: Theoretical models, experimental data, Proc. of the Voeikov Main Geophysical Observatory, 2018, No. 589, P. 98–113. (in Russian)

16. Kalinin A.V., Slyunyaev N.N. Initial-boundary value problems for the equations of the global atmospheric electric circuit, J. Math. Anal. Appl., 2017. V. 450, No 1, P. 112–136.

17. Denisova N.A., Kalinin A.V. Influence of the choice of boundary conditions on the electric field distribution in models of the global electric circuit, Izvestiya Vuzov. Radiofizika,V. 61, No 10, P. 831–842, 2018. (in Russian)

18. Slyunyaev N.N., Kalinin A.V., Mareev E.A. Thunderstorm generators operating as voltage sources in global electric circuit models, J. Atmos. Solar-Terrestrial Phys., 2019. V. 183, P. 99–109.

19. Denisenko V.V. Yakubailik O.E. Allowance for the relief when calculating the resistance of a global atmospheric conductor, Solar-Terr. Phys., 2015. V. 1, No 1, P. 104–108. (in Russian)

20. Morozov V.N. Penetration of non-stationary ionospheric electric fields into the lower atmosphere in the global electrical circuit model, Geomagnetism and Aeronomy, 2018. V. 58, No. 1, P. 119–124 (in Russian)

21. Denisenko V.V., Nesterov S.A., Boudjada M.Y., Lammer H. A mathematical model of quasistationary electric field penetration from ground to the ionosphere with inclined magnetic field, J. Atmos. Solar-Terr. Phys., 2018. V. 179, P. 527–537.

22. Denisenko V.V. Evaluation of the electric field strength penetrating from the surface of the earth into the ionosphere, Chemical Physics, 2015. V. 34, No 10, P. 44–50 (in Russian).

23. Denisenko V.V., Rycroft M.J., Harrison R.G. Mathematical simulation of the ionospheric electric field as a part of the global electric circuit, Surv. Geophys., 2019. V. 40, No 1, P. 1–35.

24. Pulinets S.A., Uzunov D.P., Karelin A.V., Davidenko D.V. Physical bases of the generation of short-term earthquake precursors. Complex model of geophysical processes in the lithosphere–atmosphere–ionosphere–magnetosphere system initiated by ionization, Geomagnetism and Aeronomy, 2015. V. 55, No 4, P. 540–558. (in Russian)

25. Denisenko V.V., Boudjada M.Y., Lammer H. Propagation of Seismogenic Electric Currents Through the Earth's Atmosphere, J. Geophys. Res.: Space Phys., 2018. V. 123, No. 5, P. 4290–4297.

26. Gubenko I.M., Rubinstein K.G. Analysis of the results of calculations of thunderstorm activity using atmospheric instability indices according to the data of the WRF-ARW numerical model, Meteorology and Hydrology, 2015, No. 1, P. 27–37. (in Russian).

27. Dementieva S.O., Ilin N.V., Mareev E.A. Calculation of the electric field of the index of lightning activity in models of weather forecast, Izvestiya Rossiyskoy akademii nauk. Fizika atmosfery okeana, V. 51, No 2, c. 210, 2015. (in Russian)

28. Shatalina M.V., Dementieva S.O., Mareev E.A. Monitoring Modeling Thunderstorm Events in the Nizhny Novgorod Region: Intense Thunderstorm June 1-2, 2015, Meteorology and Hydrology, V. 81–87, No 11, P. 81–87, 2016. (in Russian)

29. Gubenko I.M., Rubinstein K.G. Thunderstorm Activity Forecast Using the Cumulifiers Cloud Electrification Model, Meteorology and hydrology, No 2, P. 5–19, 2017. (in Russian)

30. Kolomeets L.I., Smyshlyaev S.P. Direct inverse effects between thunderstorm activity, temperature, atmospheric composition on a regional scale: sensitive tests with WRF-CHEM, Proceedings of the Voeikov Main Geophysical Observatory, No 585, P. 187–211, 2017. (in Russian)

31. Adzhiev A.Kh., Stasenko V.N., Shapovalov V.A., Shapovalov A.V. Atmospheric electric field intensity, thunderstorm phenomena in the North Caucasus, Meteorology and Hydrology, No 3, P. 46–54, 2016 (in Russian)

32. Sinkevich A.A., Mikhailovsky Yu.P., Dovgalyuk Yu.A., Veremey N.E., Bogdanov E.V., Adzhiev A.Kh., Malkarova A.M., Abshaev A.M. Development Studies a thunder-hail cloud. Part 1. Cloud development, formation of electrical discharges, Meteorology Hydrology, 2016 V. 9, No 27–40. (in Russian)

33. Mikhailovsky Yu.P., Sinkevich A.A., P. S.D., Gopalakrishnan V., Dovgalyuk Yu.A., Veremey N.E., Bogdanov E.V., Kurov A.B., Adzhiev A.H., Malkarova A.M., Abshaev A.M. Research on the development of a thunder-gradus cloud. Part 2. Analysis of methods for predicting the diagnosis of the electric state of clouds, Meteorology, and Hydrology, No 6, P. 31–45, 2017. (in Russian)

34. Sinkevich A.A., Dovgalyuk Yu.A., Veremey N.E., Kurov A.B., Mikhailovsky Yu.P., Bogdanov E.V., Toropova M.L., Ignatiev A.A., Adzhiev A.Kh., Malkarova A.M., Abshaev A.M., Gopalakrishnan V., Murugavell P., Pavar S.D. Research on the development of a thunder-gradus cloud. Part 3. Numerical modeling of cloud evolution, Meteorology and Hydrology, No 8, P. 18–28, 2017. (in Russian)

35. Gorchakov G.I., Kopeikin V.M., Karpov A.V., Titov A.A., Buntov D.V., Kuznetsov G.A., Gushchin R.A., Dazenko O.I., Kurbatov G.A., Seregin A.O., Sokolov A.V. Variations in the specific charge of saltating sand in a windsand flux over a desertified areaVariations in the specific charge of saltating sand in a windsand flux over a desertified area, Atmospheric and Oceanic Optics, 2016. V. 29, No 3, P. 244–251. (in Russian)

36. Gorchakov G.I., Karpov A.V., Kopeikin V.M., Sokolov A.V., Buntov D.V. Influence of the Saffman force, the lifting force of the electric force on the transport of particles in the wind-sandy stream, Doklady Earth Sci., 2016. V. 467, No 3, P. 336. (in Russian)

37. Mareev E.A. Dementyeva S.O. The role of turbulence in thunderstorm, snowstorm, and dust storm electrification, J. Geophys. Res. Atmos., V. 122, No 13, P. 6976–6988, 2017.

38. Dementieva S.O. Mareev E.A. Modeling electrical parameters of thunderstorms with regard to turbulent effects, Izvestiya Vuzov. Radiophysics, V. 61, No 8–9, P. 633–644, 2018. (in Russian)

39. Dementieva S.O., Mareev E.A. On the Contribution of Turbulence to the Electrification of Thunderstorm Clouds, Izvestiya Rossiyskoy akademii nauk. Izvestiya, Atmos. Oceanic Phys., V. 54, No 1, P. 28–35, 2018. (in Russian)

40. Kostinskiy A.Y., Syssoev V.S., Bogatov N.A., Mareev E.A., Andreev M.G., Makalsky L.M., Sukharevsky D.I., Rakov V.A. Observation of a new class of electric discharges within artificial clouds of charged water droplets and its implication for lightning initiation within thunderclouds, Geophys. Res. Lett., 2015. V. 42, No 19, P. 8165–8171.

41. Rakov V.A., Mareev E.A., Tran M.D., Zhu Y., Bogatov N.A., Kostinskiy A.Y., Syssoev V.S., Lyu W. High-Speed Optical Imaging of Lightning and Sparks: Some Recent Results, IEEJ Trans. Power Energy, V. 138, No 5, P. 321–326.

42. Kostinskiy A.Y., Syssoev V.S., Bogatov N.A., Mareev E.A., Andreev M.G., Bulatov M.U., Sukharevsky D.I., Rakov V.A. Abrupt elongation (stepping) of negative and positive leaders culminating in an intense corona streamer burst: Observations in long sparks and implications for lightning, J. Geophys. Res. Atmos., 2018. V. 123, No 10, P. 5360–5375.

43. Kostinskiy A.Y., Syssoev V.S., Bogatov N.A., Mareev E.A., Andreev M.G., Bulatov M.U., Makal'sky L.M., Sukharevsky D.I., Rakov V.A. Observations of the connection of positive and negative leaders in meter-scale electric discharges generated by clouds of negatively charged water droplets, J. Geophys. Res. Atmos., 2016.V. 121, No 16, P. 9756–9766.

44. Kostinskiy A.Y., Syssoev V.S., Mareev E.A., Rakov V.A., Andreev M.G., Bogatov N.A., Makal'sky L.M., Sukharevsky D.I., Aleshchenko A.S., Kuznetsov V.E., Shatalina M.V. Electric discharges produced by clouds of charged water droplets in the presence of moving conducting object, J. Atmos. Solar-Terrestrial Phys., 2015. V. 135, P. 36–41.

45. Temnikov A.G., Orlov A.V., Chernensky L.L., Belova O.S., Gerastanok T.K., Gundareva S.V. Study of the mechanisms of formation of jointly developing ascending leaders as a stage of a lightning strike on the ground Objects, Bulletin of the Moscow Energy Institute, 2015. No. 5, P. 58–64. (in Russian)

46. Temnikov A.G., Orlov A.V., Chernensky L.L., Belova O.S., Gerastanok T.K., Zimin A.S. Investigation of systems for determining the point of impact of lightning discharge parameters using artificial thunderstorm clouds, Bulletin of the Moscow Energy Institute, 2015. V. 6, No 80–86. (in Russian)

47. Temnikov A.G., Chernensky L.L., Orlov A.V., Lysov N.Yu., Zhuravkova D.S., Belova O.S., Gerastanok T.K. Use of artificial thunderstorm cells for research problems of initiating lightning between the thunderstorm cloud of the Earth, Proc. Rus. Acad. Sci. Power Engineering, 2017. No. 2, P. 48–61. (in Russian)

48. Temnikov A.G., Chernensky L.L., Orlov A.V., Lysov N.Yu., Belova O.S., Kivshar T.K., Zhuravkova D.S. Physical modeling of the formation of repeated shocks negative lightning using artificial thunderstorm cells, Lett. J. Techn. Phys., 2018. V. 44, No. 17, P. 57–64. (in Russian)

49. Iudin D.I., Davydenko S.S., Gotlib V.M., Dolgonosov M.S., Zeleny L.M. Lightning physics: New approaches to modeling the perspective of satellite observations, Adv. Phys. Sci., 2018. V. 188 , No. 8, P. 850–864. (in Russian).

50. Iudin D.I., Iudin F.D., Hayakawa M. Modeling the radio emission of an intracloud lightning discharge, Izvestiya Vuzov. Radiofizika, 2015. V. 58, No. 3, P. 187–199. (in Russian)

51. Iudin D.I., Rakov V.A., Mareev E.A., Iudin F.D., Syssoev A.A., Davydenko S.S. Advanced numerical model of lightning development: Application to studying the role of LPCR in determining lightning type, J. Geophys. Res. Atmos., 2017. V. 122, No. 12, P. 6416–6430.

52. Slyunyaev N.N., Mareev E.A., Rakov V.A., Golitsyn G.S. Statistical distributions of lightning peak currents: Why do they appear to be lognormal? J. Geophys. Res. Atmos., 2018. V. 123, No. 10, P. 5070–5089.

53. Babich L.P., Bochkov E.I., Kutsyk I.M. Numerical simulation of a compact intracloud discharge of an electromagnetic pulse generated by it, Doklady Earth Sci., 2015, V. 462, No. 4, P. 471–474. (in Russian)

54. Babich L.P., Bochkov E.I., Kutsyk I.M., Neubert T. Numerical simulation of positive streamer development in thundercloud field enhanced near raindrops, Lett. J. Experiment. Theor. Phys., 2016. V. 103, No 7–8, P. 510–515. (in Russian)

55. Iudin D.I., Davydenko S.S. Fractal model of a compact intracloud discharge. I. Features of the structure and evolution, Radiophysics and Quantum Electronics, 2015, V. 58, No 7. P 477–496.

56. Davydenko S.S., Iudin D.I. Fractal model of a compact intracloud discharge. II. Specific features of electromagnetic emission, Radiophysics and Quantum Electronics, 2016. V. 59, No 7, P. 560–575.

57. Eliseev A.V., Mokhov I.I., Chernokulsky A.V. The influence of lightning activity of anthropogenic factors on the large-scale characteristics of wildfires, Izvestiya Rossiyskoy akademii nauk Izvestiya, Atmos. Oceanic Phys., 2017. V. 53, No 1, P. 3–14, 2017.

58. Surkov V.V. Hayakawa M. Semi-analytical models of the formation of sprites from plasma inhomogeneities, Geomagnetism and Aeronomy, 2016. V. 56, No 6, P. 763–771 (in Russian)

59. Evtushenko A.A., Kuterin F.A., Self-consistent model of a night sprite, Radiophysics and Quantum Electronics, 2017, V. 59, No 12. P. 962–971.

60. Ardelyan N.V., Bychkov V.L., Golubkov G.V., Golubkov M.G., Kosmachevsky K.V. Effect of thunderstorm activity on the parameters of air plasma in the ionosphere, Chemical Physics, 2018. V. 37, No 7, P. 59–64 (in Russian)

61. Zelenyy L.M., Klimov S.I., Angarov V.N., Nazarov V.N., Rodin V.G., Sukhanov A.., Batanov O.V., Gotlib V.M., Kalyuzhny A.V., Karedin V.N., Kozlov V.M., Kozlov I.V., Eismont N.A., Ledkov A.A., Novikov D.I., Korepanov V.E., Bodnar L., Segedi P., Ferenc C., Papkov A.P. Chibis-M microsatellite project. Experience in Creating Implementation, Mechanics, Computer Science Management, 2015. V. 7, No 4, P. 91–118. (in Russian)

62. Zelenyy L.M., Klimov S.I., Angarov V.N., Rodin V.G., Nazarov V.N., Sukhanov A., Batanov O.V., Gotlib V.M., Kalyuzhny A.V., Karedin V.N., Kozlov V.M., Kozlov I.V., Eismont N.A., Ledkov A.A., Novikov D.I., Korepanov V.E., Bodnar L., Segedi P., Ferenc C., Papkov A.P. Microsatellite Space Experiment on the Russian segment of the International Space Station, Space Technology Technique, 2015. No. 3, P. 26–37. (in Russian)

63. Klimov S.I., Angarov V.N., Gotlib V.M., Dolgonosov M.S., Kalyuzhny A.V., Kozlov V.M., Nazarov V.N., Novikov D.I., Rodin V.G. Specific features of space research on microsatellite platforms integrated into the infrastructure of the Russian segment of the ISS, Izvestiya Vysshikh Uchebnykh Zavedenii. Instrument making, 2016. V. 59, No. 6, P. 435–442. (in Russian)

64. Mozgov K.S., Nosikova N.S., Rensky S.I., Surkov V.V., Klimov S.I., Pilipenko V.A., Shuvalov V.A., Yakovlev A.A. Impact research thunderstorm activity on near-earth space, Cosmonautics, Rocket Science, 2018. No. 5, P. 148–161. (in Russian)

65. Klimov P.A., Garipov G.K., Khrenov B.A., Morozenko V.S., Barinova V.O., Bogomolov V.V., Kaznacheyeva M.I., Panasyuk M.A., Saleev K.Yu., Svertilov S.I. Transient Atmospheric Phenomena Based on Measurements on the Vernov Satellite, Earth Study from Space, 2017. No. 3, P. 65–75. (in Russian)

66. Strikovsky A.A., Evtushenko A.V., Gushchin M.E., Korobkov S.V., Kostrov A.V. Pulsed high-voltage discharge in air with a pressure gradient, Plasma Physics, 2017. V. 43, No. 10, P. 866–873. (in Russian)

67. Tarasenko V.F., Sosnin E.A., Skakun V.S. Panarin V.A., Demonstration in the laboratory of analogues of red sprites of blue jets observed in atmospheric discharges,

Izvestiya Vysshikh Uchebnykh Zavedenii. Physics, 2017. V. 60, No. 10–2, P. 95–98. (in Russian)

68. Sosnin E.A., Panarin V.A., Skakun V.S., Tarasenko V.F. Blue jets and starters laboratory modeling by underpressure apokamp, Atmospheric and Oceanic Optics, 2016. V. 29, No. 10, P. 855–858. (in Russian)

69. Bogomolov V.V., Panasyuk M.I., Svertilov S.I., Bogomolov A.V., Garipov G.K., Iyudin A.F., Klimov P.A., Klimov S.I., Mishieva T.M., Minaev P.Yu., Morozenko V.S., Morozov O.V., Pozanenko A.S., Prokhorov A.V., Rotkel H. Observation of gamma-ray bursts of terrestrial origin in the space experiment RELEC on satellite Vernov, Space Exploration, 2017. V. 55, No. 3, P. 169–178. (in Russian)

70. Minaev P.Yu., Pozanenko A.S. Short transient gamma events in the SPI / INTEGRAL Experiment: Search, classification, interpretation, Proc. of the XIX Intern. Analytics Conf., data management in data intensive areas (DAMDID/ RCDL'2017), 10–13 October, 2017.

71. Chernenko A.M. On the relationship of gamma-ray flashes of terrestrial origin (TGF) with the distribution of impurities in the troposphere, Theses of the Fifteenth All-Russian Open Conf. Modern Problems of Remote Sensing of the Earth from Space, Space Research Institute, Moscow, 2017. (in Russian)

72. Chilingarian A., Chilingaryan S., Reymers A. Atmospheric discharges and particle fluxes, J. Geophys. Res.: Space Phys., 2015. V. 120, No. 7, P. 5845–5853.

73. Chilingarian A., Hovsepyan G., Kozliner L. Extensive air showers, lightning, and thunderstorm ground enhancements, Astropart. Phys., 2016. V. 82, P. 21–35.

74. Chilingarian A., Khanikyants Y., Mareev E., Pokhsraryan D., Rakov V.A., Soghomonyan S. Types of lightning discharges that abruptly terminate enhanced fluxes of energetic radiation and particles observed at ground level, J. Geophys. Res.: Atmos., 2017. V. 122, No. 14, P. 7582–7599.

75. A. Chilingaryan, On models based on the concept of "runaway" electrons used to explain high-energy phenomena in the atmosphere, News of the Russian Academy of Sciences, Physical Series, Izvestiya RAN, Seriya Fizicheskaya, 2018. V. 81, P. 254–257. (in Russian)

76. Kanonidi K.Kh., Lidvanskii A.S., Khaerdinov M.N., Khaerdinov N.S. Variations of cosmic rays during thunderstorms new geophysical effects, Izvestiya RAN, Ser. Fizicheskaya, 2015, V. 79, No. 5, P. 733. (in Russian)

77. Kanonidi K.Kh., Kurenya A.N., Lidvansky A.S., Khaerdinov M.N., Khaerdinov N.S. Storm effects according to a comprehensive study of variations of secondary cosmic-ray particles, Izvestiya RAN, Seriya Fizicheskaya, 2017. V. 81, No. 2, P. 242–245. (in Russian)

78. Ryabov V.A., Almenova A.M., Antonova V.P., Beisembayev R.U., Bezshapov S.P., Borisov A.S., Chubenko A.P., Dalkarov O.D., Gurevich A.V., Karashtin A.N., Kryakynova O.N., Mitko G.G., Mukhamedshin R.A., Mukhashev A.M., Nam R.A., Nikolaevsky N.F., Pavlyuchenko V.P., Piscal V.V., Ptitsyn M.O., Puchkov V.S., Saduev N.O., Sadykov T.K., Salikhov N.M., Shaulov S.B., Shepetov A.L., Shlyugaev Y.V., Stepanov A.V., Thu W.M., Vildanova L.I., Vildanova M.I., Zastrozhnova N.N., Zukhov V.V., Zybin K.P. Modern status of the Tien-Shan cosmic ray station, EPJ Web Conf., V. 145, P. 12001. 2017.

79. Gurevich A.V., Almenova A.M., Antonova V.P., Chubenko A.P., Karashtin A.N., Kryakunova O.N., Lutsenko V.Y., Mitko G.G., Ptitsyn M.O., Piscal V.V., Ryabov V.A., Salikhov N.M., Sadykov T.K., Shepetov A.L., Shlyugaev Y.V., Thu W.M., Vil'danova L.I., Zastrozhnova N.N., Zybin K.P. Observations of high-energy radiation during thunderstorms at Tien-Shan, Phys. Rev. D, 2016. V. 94, No 2, P. 023003.

80. Gurevich A.V., Garipov G.K., Almenova A.M., Antonova V.P., Chubenko A.P., Kalikulov O.A., Karashtin A.N., Kryakunova O.N., Lutsenko V.Y., Mitko G.G., Mukashev K.M., Nam R.A., Nikolaevsky N.F., Osedlo V.I., Panasyuk M.I., Ptitsyn M.O., Piscal V.V., Ryabov V.A., Saduev N.O., Sadykov T.K., Saleev K.Y., Salikhov N.M., Shepetov A.L., Shlyugaev Y.V., Svertilov S.I., Vil'danova L.I., Zastrozhnova N.N., Zhantaev Z.S., Zhilchenko K.S., Zhukov V.V., Zybin K.P. Simultaneous observation of lightning emission in different wave ranges of electromagnetic spectrum in Tien Shan mountains, Atmos. Res., 2018. V. 211, P. 73–84.

81. Karashtin A.N., Shlyugaev Y.V., Bulatov A.A., Karashtina O.S., Kuterin F.A., Mikryukov P.A. Sub-microsecond radio emission from thunderclouds, Proc. VI Intern. Conf. on Atmospheric Electricity, 17–22 June 2018, Nara city, Nara, Japan, P. P-06-22.

82. Kozlov V.I., Mullayarov V.A., Starodubtsev A.A., Toropov A.A. Registration of neutrons during a thunderstorm with a resolution of 10 μs in Yakutsk, Izvestiya RAN, Ser. Fizicheskaya, 2015. V. 79, No 5, P. 751–753.

83. Babich L.P. Radiocarbon production by Tpthunderstorms, Geophys. Res. Lett., 2017. V. 44, № 21. P. 11191–11200.

84. Babich L.P. Thunderous nuclear reactions, Nature. 2017. V. 551, № 7681. P. 443–444.

85. Adzhiev A.Kh., Stasenko V.N., Shapovalov A.V., Shapovalov V.A. Atmospheric electric field strength and thunderstorms in the North Caucasus. Meteorologia i Gidrologia, 2016, № 3, P. 46–54. (in Russian)

86. Tarabukina L.D., Kozlov V.I., Karimov R.R., Mullayarov V.A. Spatial pattern of lightnings in North Asia. Meteorologia i Gidrologia, 2017, № 2, P. 20–29 (in Russian).

87. Sin'kevich A.A., Popov V.B., Tarabukin I.A. et al. Changes in characteristics of convective clouds and precipitation during cloud merging. Meteorologia i Gidrologia, 2018, № 8, P. 19–32. (in Russian)

88. Bulatov A.A., Kuterin F.A., Shlyugaev Yu.V. Regional passive lightning detection network in the Nizhny Novgorod oblast. Meteorologia i Gidrologia, 2017, № 6, P. 113–121. (in Russian)

89. Veremei N.E., Dovgalyuk Yu.A., Gopalakrishnan V. Numerical modeling of the effects of severe aerosol pollution of the atmosphere on the dynamics of cumulonimbus cloud charge structure. Meteorologia i Gidrologia, 2015, № 12, P. 5–18 (in Russian)

Atmospheric Radiation

Yu.M Timofeyev and E.M. Shulgina
St. Petersburg State University,
e-mail:y.timofeev@spbu.ru

On the basis of materials provided by V.P. Budak (Moscow Power-Engineering Institute (MPEI)); A.A. Cheremisin (Siberian Federal University (SFU)); T.Yu. Chesnokova, M.V. Panchenko, T.K. Sklyadneva (Zuev Institute of Atmospheric Optics SB RAS (IAO SB RAS)); N.E. Chubarova (Lomonosov Moscow State University (MSU)); G.I. Gorchakov (Obukhov Institute of Atmospheric Physics (IAP RAS)); A.F. Neryshev (Scientific and Production Association "Typhoon" (Typhoon)); O.M. Nikolaeva (Keldysh Institute of Applied Mathematics RAS (IAM RAS)); S.B. Rozanov (Lebedev Physical Institute RAS (LPI RAS)); A.B. Uspensky (Scientific Research Center for Space Hydrometeorology "Planeta" (Planeta)).

During 2015–2018 the Russian Radiation Commission in cooperation with interested departments and institutions hold two International Symposia on Atmospheric Radiation and Dynamics (ISARD-2015, ISARD-2017). At these conferences most actual problems of atmospheric physics (radiation transfer, radiative climatology, greenhouse gases, clouds, aerosols and radiation forcing, remote measurement methods, new observation data) were discussed. In this review, 5 directions of studies covering the complete spectrum of investigations in atmospheric radiation are given.

Radiation Transfer

Numerous investigations in this line are dedicated to developing methods and algorithms for solving the radiation transfer equation in various mediums and for different measurement geometries and to applying the developed methods to various problems of atmospheric optics.

In the paper [Mikhailov et al., 2018] the comparative efficiency of different algorithms of statistical modeling of the polarized radiation transfer process is studied for the problem with the molecular matrix of scattering. The initial-boundary value problem for the non-stationary radiative transfer equation in a system of semitransparent bodies with the conditions of diffuse reflection and refraction of radiation is considered in the paper (Amosov, 2018). The unique solvability of the problem with boundary and initial data in the complete scale of Lebesgue spaces is established and estimates for solutions are obtained. The work (Ambos and Mikhailov, 2018) considers the radiation transfer through

random media of three different types. The radiative transfer is simulated numerically and statistically with the same one-dimensional distributions and correlation radii. In the paper (Ambos et al., 2017) a Monte Carlo algorithm admitting parallelization is constructed for estimating the probability moments of the spectral radius of the operator of the integral equation describing the transfer of particles with multiplication in a random medium. A randomized homogenization method is developed on the base of the theory of small perturbations and diffusive approximation. In (Aristova et al., 2017) the Lebesgue averaging method is applied to the numerical simulation of the radiative transfer equation. Monte Carlo simulation of backward scattering of polarized optical radiation has been performed in the time and frequency representations based on the description of radiation transport in terms of the Bethe–Salpeter equation (Kuzmin, 2017).

In (Kim and Prokhorov, 2018) a Cauchy problem for the time-dependent radiative transfer equation in a three-dimensional multicomponent medium with generalized matching conditions describing Fresnel reflection and refraction at the interface of the media is considered. The unique solvability of the problem is proven, a Monte Carlo method for solving the initial-boundary value problem is developed, and computational experiments for different implementations of the algorithm are conducted. The Cauchy problem for the non-stationary radiative transfer equation with generalized matching conditions that describes the diffuse reflection and refraction on the interface is studied in paper (Prokhorov et al., 2017). The solvability of the initial-boundary value problem is proved. Some stabilization conditions for the non-stationary solution are obtained. The paper (Budak et al., 2017) is devoted to the further development of small-angle modification of the spherical harmonics method. It has been shown that the quasi-diffusion approximation does not depend on the symmetry of the problem and, therefore, can be generalized to the case of an arbitrary geometry of the medium.

A number of studies are devoted to developing and improving the software for radiation transfer computations. The paper (Korkin et al., 2017) describes a new free program SORD for calculating the polarized radiation transfer (Fortran 90/95, ftp://maiac.gsfc.nasa.gov/pub/skorkin). The SORD numerically simulates the propagation of monochromatic solar radiation in a plane-parallel atmosphere over a reflecting surface using the successive scattering approximation method. The FIRE-ARMS program is added by the model of polarized radiation transfer VLIDORT. This version allows simulating the outgoing thermal IR radiation from the Earth and solar shortwave IR radiation reflected from the surface, taking into account the multiple scattering. Such simulation is compared with the spectra measured by satellite spectrometers GOSAT in a cloudless atmosphere over Western Siberia (Zadvornykh et al., 2017). The pa-

per (Russkova and Zhuravleva, 2017) refers to a series of works aimed at increasing the computational power of radiation codes realizing the Monte Carlo statistical method.

A huge role in the simulation of atmospheric radiation transfer plays the accuracy of the spectroscopic information on the absorption lines of atmospheric gases. To assess the accuracy of this information, the simulation of atmospheric spectra of solar radiation in strong absorption bands of methane and carbon dioxide and the comparison of modeled spectra with the spectra measured by the ground-based Fourier infrared spectrometer Bruker IFS 125M at the Ural atmospheric station in Kourovka for a large set of atmospheric conditions in 2013–2017 were performed. It has been shown that the total columns of these gases, retrieved using different versions of the popular spectroscopic databases HITRAN [https://www.cfa.harvard.edu/hitran/], GEISA [http://www.pole-ether.fr] and GOSAT and CDSD absorption lines banks (Nikitin et al., 2015; Tashkun et al., 2015) may vary significantly (from 1% for CO_2 to 4% for CH_4) (Chesnokova et al., 2015; 2016). A similar comparison was made for water vapour (Chesnokova et al., 2016a). The parameters of the CH_4 and H_2O line shapes, taking into account the effect of the Dike line narrowing in the near IR range for conditions close to atmospheric, were determined from the laboratory spectra measured by the Fourier spectrometer that improved the accuracy of atmospheric transmittance simulation (Petrova et al., 2017). The simulation of ascending and descending solar and thermal radiation fluxes with different models of continuous water vapor absorption for meteorological conditions typical for the summer of middle latitudes in the presence of Cirrus clouds of various powers has been carried out. The sensitivity of the atmospheric radiation balance and the radiation forcing of clouds to models of continuous water vapor absorption is estimated (Firsov et al., 2015, 2018).

In a number of studies methods for solving the radiation transfer equation in the context of atmospheric and underlying surface remote sensing are improved, models for retrieving the radiation-significant characteristics are developed. The paper (Falaleeva and Fomin, 2017) discusses the possibility for obtaining more information from atmospheric IR spectroscopic sounding by increasing the instrumental spectral resolution and using polarization measurements of solar and thermal radiation. The shortcomings of modern methods of molecular absorption spectra calculation in both strict (linear) and fast (based on k-distributions) models of atmospheric radiation transfer are shown. In (Vasilyev et al., 2017) dependences of solar radiation characteristics on optical models of the earth's atmosphere are investigated. Software used for homogeneous atmosphere models implements four methods of transfer theory: the single scattering approximation, the Eddington method, the Monte Carlo method,

and the asymptotic method. Simple linear approximations of the flux dependence on the parameters of the atmosphere and the Sun zenith angle are proposed.

In (Levashova et al., 2018) a three-dimensional model for obtaining spatial structures of photosynthetically active radiation reflected and absorbed by inhomogeneous forest cover with a multi-species structure is presented. Shabanov and Gastellu-Etchegorry (2018) has shown that the three-dimensional distribution of forest cover affects the radiation regime and the determination of its biophysical parameters. The algorithm based on the developed model allows determining the proportion of different tree species in the mixed forest from the measured coefficients of radiation reflection by the forest cover. In (Zinkov et al., 2018) the problem of seabottom reconstruction in the fluctuating ocean when the coefficients of seabootom and ocean's surface scattering are known is considered. A theoretical justification of the new method for measuring the emissivity of a rough underlying surface without absolute calibration of the radiometer is carried out (Sterlyadkin et al., 2018). This method can be applied not only to the ocean surface, but also to any rough surface, ice, agricultural plantings, and vegetation. The problem of retrieving the Lambert land surface albedo using the reflected brightness coefficients is considered, the modeled study of the accuracy of the algorithm for retrieving the albedo is executed (Nikolaeva, 2016, 2016a). The analytical representation for reflectance dependence on gas absorption sections has been obtained and the efficient algorithm to gas absorption effects elimination in reflectance is constructed (Nikolaeva, 2018).

Radiative Climatology

The research work in the frames of this topic has been carried out in several directions: the monitoring of components of radiation budget (RB); the study of RB climatic trends near a surface; the development of software for simulating the radiation characteristics in different atmospheric conditions and the analysis of radiative effects.

In Zuev Institute of Atmospheric Optics (IOA) SB RAS, the long-term monitoring of the total and UV solar radiation in Tomsk and the Tomsk region, and also in certain regions of Western Siberia is carried out. The results of the study of changes in the total solar radiation, cloudiness, sunshine duration, and surface air temperature in Tomsk for the period 1996–2016 are presented. It is shown that the decrease in the total solar radiation and sunshine duration and, vice versa, the increase in the surface air temperature and total and inferior cloud amount are observed. The analysis of synoptic processes observed in the Tomsk region from 1993 to 2016 showed that the difference between the recurrence of cyclones and anticyclones has significantly decreased in the Tomsk

region over the past decade. There is a tendency to reduce the invasion of Arctic air masses and to increase of the inflow of subtropical and tropical air to the region (Sklyadneva et al., 2018).

The work on the creation of software-algorithmic complex MATHART (**M**onte C**A**rlo Codes for **TH**ree-Dimension**Al R**adiative **T**ransfer), designed to calculate the radiation characteristics in different atmospheric conditions (clear sky, continuous and broken clouds) is continued. In the period 2015–2018, new statistical algorithms were implemented to calculate the spectral-angular characteristics of downward and outgoing solar and thermal radiation in (i) separate realizations of spatial inhomogeneous clouds and (ii) averaged over the ensemble of cloud fields (Zhuravleva and Nasrtdinov, 2018). The simulation of radiation characteristics is performed taking into account the sphericity of the atmosphere, multiple scattering and absorption by cloud, aerosol particles and air molecules, emission (in the IR range), as well as reflection from the underlying surface. The Poisson model of broken clouds was used to construct the realizations of mesoscale cloud fields; the clouds were approximated by overturned truncated paraboloids of rotation.

On the basis of the developed software, the regularities of the formation of brightness fields of ascending and descending solar radiation in spatially inhomogeneous clouds were investigated (Zhuravleva et al., 2017; Zhuravleva and Nasrtdinov, 2018). The developed algorithms were also used to estimate the effect of non-Lambertiance of the underlying surface on the angular characteristics of the field of reflected solar radiation in a cloudless atmosphere and under continuous clouds (Russkova and Zhuravleva, 2018). Application possibilities of the developed software for solving the inverse problems of atmospheric optics using the ground photometric observations are shown: the influence of stratification of aerosol optical characteristics on the sky brightness in the solar vertical is analyzed (Russkova et al., 2016), possible deviations of the optical thickness retrieved using standard AERONET network algorithm under crystal clouds are considered (Smirnov et al., 2018).

In Lomonosov Moscow State University, a complex of works on studying the UV radiation has been performed. The seasonal and inter-annual variability of the total UV radiation in the 300–380 nm range (Q380) in Moscow for the period 1968–2014 was investigated and the influence of clouds on its values was estimated (Nezval and Chubarova, 2017). The distinct long-period changes in erythemal UV radiation (Qer) characterized by a pronounced decrease at the end of the 1970s and a statistically significant positive trend of more than 5%/10 years since 1979 over the territory of the Moscow region according to the measurements and reconstruction model has been revealed. The positive trend is shown to be associated mainly with a decrease in the effective cloud

amount and total ozone content (TOC). The simulation experiments using the INM-RSHU chemistry climate model (CCM) for several scenarios with and without anthropogenic factors have revealed that the variations in the anthropogenic emissions of halogens have the most significant impact on the TOC and Qer variability. Among natural factors, noticeable effects are observed due to volcanic aerosol (Chubarova et al., 2018).

A new method for calculating the altitude UV dependence is proposed for different types of biologically active UV radiation (erythemally weighted, vitamin-D-weighted and cataract-weighted types). The parameterization takes into account the altitude dependence of molecular number density, ozone content, aerosol and spatial surface albedo. Calculations of high-altitude UV effects using the proposed method are consistent with the results of accurate modeling of the 8-stream DISORT model with a correlation coefficient > 0.996. Using the proposed parameterization implemented in the on-line UV tool (http://momsu.ru/uv/) for Northern Eurasia over the PEEX domain, the altitude UV increase and its possible effects on human health considering different skin types and various open body fraction for January and April conditions in the Alpine region were analyzed (Chubarova et al., 2016).

Aerosol and Radiation Forcing

Extensive laboratory and field measurements of aerosol parameters, the modeling and evaluation of aerosol impact on the radiative characteristics of the atmosphere are the main directions of study in this area.

Systematic laboratory studies of aerosol scattering and absorbing properties, its condensation activity and smoke optical and radiation properties are conducted in IOA SB RAS (Popovicheva et al., 2015, 2016, 2016a; Kozlov et al., 2016). The spatial and temporal variability of aerosol characteristics in the sea, polar regions and the Asian part of Russia is studied on the basis of expeditionary studies. In the paper (Sakerin et al., 2017) the results of 12-year aerosol studies along the route of Russian Antarctic expeditions in the Eastern Atlantic and Southern ocean are summarized. Statistical generalization and the zoning of the aerosol physical and chemical characteristics in the East Atlantic are given in (Sakerin et al., 2018). The results of studies of the physical and chemical composition of atmospheric aerosol in the expedition conducted in the winter of 2015/2016 along the route of the Indian-Atlantic expedition are discussed (Sakerin et al., 2017a). In (Kopeikin et al., 2018) the variability of soot and submicron aerosol in the Moscow region in 2014–2016 is analyzed. The results of measuring the aerosol optical thickness of the atmosphere (AOT), regularities of its spatial and temporal variability in the polar regions and in the Asian part of Russia are presented in papers (Sakerin et al., 2015; Sakerin et al.,

2018a; Tomasi et al., 2015; Kabanov and Sakerin, 2016). The atmospheric aerosol properties have been studied at the Moscow State University Meteorological Observatory (Moscow MSU MO) within the framework of the AERONET program over the 2001–2014 period. Statistically significant negative trends in annual AOT for UV and mid-visible spectral range have been revealed both for average and 50% quantile values (Chubarova et al., 2016a). The outcome of the complex experiment on studying microphysical, chemical and optical properties of aerosol particles is discussed, the contribution of atmospheric aerosol to the Earth's radiation budget is estimated (Matvienko et al., 2015).

A large number of studies are dedicated to developing the aerosol models and to evaluating the radiation effects of aerosol, large-scale smoke and dust removal into the atmosphere. Methods for the aerosol remote sensing and models for parameterizing the aerosol parameters have been constantly developed and improved. The effects of different aerosol climatologies in the COSMO mesoscale atmospheric model using long-term aerosol measurements and the accurate global solar irradiance observations at ground at the MSU MO (Russia) and Lindenberg Observatory (Germany) in clear sky conditions have been estimated. The differences are maximal during winter months (Chubarova et al., 2018a). The impact of brown carbon on the absorption spectra of the smoke aerosol and the aerosol in smog of megacities were analyzed (Gorchakov et al., 2016; 2017; 2017a).

Panchenko and Zhuravleva (2015) presented a brief overview of studies on the problems of retrieving the vertical profiles of microphysical and optical characteristics of tropospheric aerosols and their subsequent application in radiation calculations. A generalized empirical model of aerosol optical characteristics for the lower 5-kilometer atmospheric layer in the visible and near IR ranges for Western Siberia was created by Panchenko et al. (2018). In studies (Panchenko et al., 2016; Zhuravleva et al., 2018) model experiments have been carried out to estimate the radiation and temperature effects of aerosol and the dynamics of the vertical structure of solar radiation absorption in the background and smoky conditions of the Siberian atmosphere. It is shown that the deficit of daily values of total solar radiation at the underlying surface due to the appearance of an optically dense smoke layer, compared with background conditions is more than 13 MJ/m^2. Using the original Monte Carlo algorithm and OPAC models for typical summer conditions and smoke haze conditions of 2012 in the Siberian region, the direct radiation effects of background and smoke aerosol in the IR spectral region is estimated (Nasrtdinov et al., 2018).

The study of radiation effects of large-scale smoke on the territory of Northern Eurasia has been performed. The large-scale smoke pollution of the European territory of Russia (ETR) and adjoining areas in July 2017, caused by

long-range transport from forest-fire areas in Siberia has been characterized. The mass of the smoke aerosol and its radiation effects, including aerosol radiation forcing at the upper and lower atmospheric boundaries over ETR are estimated (Semoutnikova et al., 2018). The aerosol longwave radiative forcing of the atmosphere and heating rate of the near-surface aerosol layer are estimated for the extreme smoke conditions in the Moscow region in summer 2010 (Gorchakova et al., 2018). Based on the measurements at the AERONET station (Ilorin, Nigeria), quantitative estimates of radiation and temperature effects of dust aerosol during the intensive sand storm in the Sahara Desert from January 28 to February 6, 2000, are obtained (Gorchakova et al., 2015).

A series of studies on the transport of volcanic aerosol in the stratosphere after volcanic eruptions in the active volcanic period 2007–2011 has been completed based on data of the inter-regional lidar network of Siberia and the Far East (Cheremisin et al., 2017). The appearance of polar stratospheric clouds over Tomsk was recorded (Cheremisin et al., 2016).

Remote Sensing of the Atmosphere

At the Atmospheric Physics Department of SPbSU a variety of experimental and simulation studies of ozone and essential climate variables of the atmosphere have been constantly conducted, namely:

1. Ground-based investigations of ozone temporal variations using measurements in Peterhof (59.88°n, 29.83°e, 20 m above sea level) of direct solar infrared radiation spectra with a high spectral resolution (Fourier-spectrometer Bruker IFS 125HR). These studies are carried out for both the total ozone content and the ozone content in separate atmospheric layers (usually 4 layers).

2. Numerical simulation of spatial-temporal ozone variations using modern three-dimensional numerical models of atmospheric composition (together with Russian State Hydrometeorological University (RSHU)) and comparisons of experimental and modeled data.

3.The study of minor gas contents using ground-based Bruker IFS 125HR measurements in Peterhof. Such regular complex measurements of the total content of ~25 essential climate-affecting gases are carried out on the territory of the Russian Federation for the first time (Timofeev et al., 2016).

As a result:

– new information on elements of the ozone vertical distribution is obtained (Virolainen et al., 2015);

– temporal variations and trends in the content of various climate-affecting gases are analyzed (Cherepova et al., 2018; Polyakov et al., 2018; Timofeyev et al., 2016; Virolainen et al., 2015a; Wang et al., 2018; Rakitin et al., 2017, 2018; Vigouroux et al., 2018);

– the measurements of the contents of essential climate-affecting gases are compared with the results of numerical simulation (Virolainen et al., 2016, 2017, 2018; Timofeyev et al., 2017, 2018; Smyshlyaev et al., 2017; Shved et al., 2018);

– the intensity of emissions of a number of trace gases is determined (Makarova et al., 2018; Ionov and Poberovskii, 2017);

– the comparison of different remote methods for measuring the atmospheric gas composition is carried out and their errors are determined (Berezin et al., 2016, 2016a, 2017; Virolainen et al., 2016a, 2017a, 2017b; Ionov et al., 2017);

– methodical aspects of the interpretation of ground-based measurements are analyzed (Polyakov et al., 2015; Makarova et al., 2016; Virolainen, 2018; Ionov et al., 2015);

– satellite measurements by various instruments are validated (Berezin et al., 2016b).

The studies of NO_2 content in Peterhof and St. Petersburg using DOAS methodology (Ionov et al., 2017a) and the ground-based MW sensing of the atmosphere (Kostsov, 2015; Kostsov et al., 2016, 2018; Bochkovsky et al., 2016) are continued.

Multiyear observational data (obtained at the mobile railroad laboratory in the course of the 1995–2010 TROICA experiments) on the composition and state of the atmosphere were used to study the features of both spatial and temporal variations in the contents of trace gases in the surface air layer over Russian cities (Elansky et al., 2016). The results of the 2002–2012 continuous once-a-minute measurements of the surface air composition over Moscow are discussed and reliable regularities in both diurnal and annual variations in the contents of the five trace gases O_3, NO, NO_2, CO, and SO_2 are studied in detail by Elansky et al. (2015). The specific features in the long-term variations in the aerosol and black carbon surface concentrations, and carbon monoxide (CO) total column in 1992–2012 in Beijing and Moscow are discussed in (Golitsyn et al., 2015).

The results of sensing the atmospheric gas and aerosol composition with the Optik Tu-134 aircraft laboratory along the flight route Novosibirsk-Tomsk-Mirny-Yakutsk-Bratsk-Novosibirsk in the period from 31 July to 1 August 2012 are presented in (Antokhin et al., 2018). The maximal concentrations of CO_2, CH_4, and CO over fire zones are estimated.

New transportable microwave spectrometer-ozonemeter MOS-4 with increased sensitivity was put into regular operation at Lebedev Physical Institute (LPI) RAS. In 2014–2017 investigations of the night mesospheric ozone were successfully done with the instrument, and since March 2017 the MOS-4 was used for ground-based monitoring of the stratospheric ozone over Moscow

(Rozanov et al., 2016, 2017). Ground-based microwave monitoring of the stratospheric ozone over Moscow was continued at LPI in cold seasons of 2014–2015, 2015–2016, and 2016–2017 (the monitoring was started in 1996). Noticeable interannual differences in ozone variations closely connected with peculiarities of dynamics and temperature of the stratosphere are discovered (Solomonov et al., 2017). Positive and negative anomalies in contents of ozone and nitrogen dioxide in the stratosphere of the Northern hemisphere in winter-spring months of 2010 and 2011 were studied in cooperation with IAP RAS (Gruzdev et al., 2016, 2017).

Interpretation of Satellite Measurements

Studies in a wide range of modern problems of remote (satellite) sensing of the atmosphere and the underlying surface are conducted by specialists of the Ministry of Education, Roshydromet, Russian Academy of Science, Roscosmos and cover the following areas:

– satellite instruments, calibration and validation of satellite data and information products;

– retrieval of the characteristics of the atmosphere and the underlying surface from satellite measurements in different spectral ranges;

– use of satellite measurement data and information products to study various processes and phenomena in the atmosphere, ocean and land.

Most of the developments are focused on the analysis and use of information from existing and future meteorological satellites and earth observation satellites (domestic and foreign). The launch of the new polar-orbital and geostationary meteorological satellites of Meteor-M, Electro-L series (Meteor-M No. 2 – 2014, Electro-L No. 2 – 2015) led to the restoration of the Russian group of hydrometeorological satellites (Asmus et al., 2017). The inclusion the hyperspectral infrared atmospheric sounder IKFS-2, the microwave scanner/atmospheric sounder MTVZA-GY, as well as multi-channel scanning imager-radiometers MSU-MR, MSU-GS in the payload of these satellites stimulated the development of works on atmospheric remote sensing in Russian scientific organizations. Studies on the calibration and validation of satellite data and information products, as well as on the use of satellite sensing results in various applications, have been intensified.

Considerable attention was paid to the calibration (intercalibration) of the satellite instruments listed above, as well as to the validation of satellite measurements. The papers (Uspensky et al., 2017, 2017a) describe the method of external (absolute) calibration and validation of the measurement data of the microwave scanner/sounder MTVZA-GY, as well as the results of the method application to the data in atmospheric sensing channels. The improved method

of the external calibration of MTVZA-GY data in atmospheric sensing channels and the correction of displacements (which is necessary for effective assimilation of satellite measurement data in numerical weather forecast schemes) is considered in (Gayfulin et al., 2018, 2018a).

The paper (Polyakov et al., 2017) is devoted to the IKFS-2 description and gives the results of flight tests confirming the performance of the equipment and achievement of the specified technical characteristics (spectral resolution, sensitivity, level of radiometric calibration error). Error estimates and control of the IKFS-2 radiometric calibration are performed by the comparison with the SEVIRI/Meteosat measurement data (Zavelevich et al., 2018).

The method and results of inter-calibration of MSU-MR and AVHRR/NOAA short-wave channels are discussed in (Filei et al., 2018). In (Kiseleva et al., 2016), the inter-calibration of IR channels of the MSU-GS radiometer-imager and the AIRS/EOS-Aqua IR probe is considered. An improved procedure for the inter-calibration of IR channels of MSU-GS and SEVIRI/Meteosat is presented by Rublev et al. (2018). This procedure can be used to inter-calibrate IR channels of radiometer-imagers installed on adjacent geostationary weather satellites. Results of intercalibration of short-wave channels of MSU-GS and VIIRS/SNP° are discussed in (Filei et al., 2018a).

Studies directed to developing the methods for the interpretation and use of data from Meteor-M and Electro-L satellites are continued at the SRB "Planeta" and SPbSU. A number of works are dedicated to the analysis of data and results of IKFS-2 operation. The description of the method and technology for obtaining the remote temperature sensing data from IKFS-2 measurements, as well as the validation of the results are given in (Asmus et al., 2017a; Polyakov et al., 2017, 2018a). The validation of measurements of vertical temperature profiles by the IRFS-2 was based on the comparison with data of aerological sounding and NCEP GFS analysis. In the procedure of retrieving the temperature sounding data, the software for fast radiative calculations developed for modeling the IKFS-2 data was used (Rusin et al., 2015).

A new technique for retrieving the total ozone from IKFS-2 measurements was developed and validated by the comparison with independent satellite and ground-based data. Regular monitoring of the ozonesphere made it possible to detect and study the ozone mini-hole in the subarctic regions of Siberia in the winter of 2016 (Garkusha et al., 2017, 2018). The new method allowed to study in detail the temporal variations of ozone content during the formation of ozone mini-holes over the territory of Russia and to determine the main mechanisms of their formation in the winter and spring of 2015–2016 using the numerical simulation (Timofeyev et al., 2018).

The development of methods and technologies for automatic classification of measurement data from scanning radiometers-imagers onboard polar-orbital and geostationary meteorological satellites to determine the parameters of cloudiness and precipitation is continued in SRB "Planeta" (Volkova and Uspensky, 2016; Volkova, 2018). In (Volkova, 2017) for the first time IAS-MR data from "Meteor-M" № 2 (along with AVHRR, SEVIRI data) were used for these purposes.

A number of papers are dedicated to the satellite monitoring of the atmosphere and the comparison of satellite measurements with ground-based observations. The results of the space monitoring of natural fires during the period 2010–2014 to estimate the areas destroyed by fire, volumes of the emissions of greenhouse gases, and fine particulate aerosols over the entire territory of Russia and its individual regions are presented in (Bondur and Ginzburg, 2016). Russkova and Zenkova (2018a) estimated the spatial and temporal variability of the NO_2 content in the troposphere of Western Siberia using data of OMI spectrometer located on the Aura satellite. The overview of Zabolotskikh (2017), papers (Zabolotskikh and Chapron, 2016, 2017; Reul et al., 2017) are dedicated to contemporary methods for retrieving the integrated atmospheric characteristics using satellite passive microwave monitoring. In the paper (Rakitin et al., 2015) a significant amount of satellite and ground-based data on the CO, CO_2, and CH_4 total contents for 2010–2013 was collected, classified, and analyzed. Transition relations between satellite and ground-based data on the content of the impurities at different measuring sites (NDACC/ GAW and OIAP RAS stations) with different spatial and temporal resolutions have been found. In the paper (Rokotyan et al., 2015) a series of relative CO_2 and CH_4 concentrations in the atmospheric column retrieved from ground-based high-resolution Fourier-transform measurements of atmospheric transmittance in the near infrared range (4000–10 000 cm^{-1}) recorded at the Ural Atmospheric Station in 2012–2013 is compared with GOSAT measurements. In (Korshunov and Zubachev, 2018; Zubachev et al., 2018) results of lidar measurements of altitude profiles of ozone concentration over Obninsk during period 2012–2016 at the 12–35 km altitude range are presented. Measurement data are compared with the Aura MLS/OMI satellite measurements and ground-based measurements of total ozone by Brewer spectrophotometer. Comparison of ground and satellite monitoring of aerosol optical thickness of the atmosphere in Russia is performed in (Plakhina et al., 2018).

At Scientific and Production Association (SPA) "Typhoon" ground-based and satellite observations were used to analyse the spatial and temporal variability of total ozone and a number of meteorological parameters of the lower and middle atmosphere. Phase relations between time series were investigated by spectral, cross-wavelet and composite analysis. In general, the comparison of phase ratios has shown that variations in the total ozone content and atmos-

pheric parameters are characterized by shorter period variability than variations in solar activity (Visheratin et al., 2017; Visheratin, 2016, 2017; Visheratin and Kalashnik, 2018). The spatial and temporal variability of the main characteristics of jet streams of the upper troposphere of the Northern and Southern hemispheres, their relationship with climatic parameters and large-scale atmospheric phenomena were studied using measurements of European geostationary meteorological satellites for the ten-year period of 2007–2016 (Kalashnik et al., 2017; Nerushev et al., 2018).

Data from Russian and foreign satellites (SEVIRI/Meteosat, AVHRR/NOAA, ASCAT/Metop) are also applied to retrieving the parameters of the underlying surface and to comparing the results with independent measurements. The use of ASCAT/Metop scatterometer data for monitoring the near-surface soil moisture is discussed in (Bykov et al., 2017). Improved methods and algorithms for assessing the soil temperature and emissivity and air temperature at the surface of the vegetation cover based on AVHRR/NOAA, SEVIRI/Meteosat data are proposed in (Volkova and Uspensky, 2016a). Validation of the results of satellite monitoring of land surface temperature is considered in (Uspenskii et al., 2015). Results of monitoring the arable land in Russia using multiyear time series of MODIS data and the LAGMA classification technique are presented in (Bartalev et al., 2016). A number of papers are dedicated to the results of satellite monitoring of snow and ice cover characteristics (Bukharov, 2015, 2016, 2017; Tikhonov et al, 2016; Raev et al., 2015; Mitnik et al., 2016; Zabolotskikh et al., 2016).

The joint studies on the use of remote sensing data on the characteristics of the underlying surface in modeling the components of water and heat balances continued at Water Problems Institute of RAS and SRB “Planeta”. The method has been developed to evaluate water and heat balance components for vegetation covered area of regional scale based on the refined physical-mathematical model of vertical water and heat exchange between land surface and atmosphere (Land Surface Model, LSM) for vegetation season adapted to satellite information on land surface and meteorological conditions (Muzylev et al., 2018).

One of the most important fields of application of data of IR and microwave sounders (IKFS-2, MTVZA-GY) is their assimilation in the schemes of numerical weather forecast. The results of the use of MTVZA-GY measurements (in six temperature-sensitive channels) in the data assimilation system of the Russian Hydrometeorological Center are presented in (Gayfulin et al., 2017). It is demonstrated that the assimilation of these data significantly improves the accuracy of short-range weather forecasts in the Southern Hemisphere. The effect of the use of MTVZA-GY data in the Northern Hemisphere is neutral.

References

1. Ambos A.Y., G. Lotova, G. Mikhailov, 2017: New Monte Carlo algorithms for investigation of criticality fluctuations in the particle scattering process with multiplication in stochastic media. Rus. Journ. Num. Analysis Math. Model. V. 32, No 3. P. 165–172.

2. Ambos A.Y., G.A. Mikhailov, 2018: Numerically statistical simulation of the intensity field of the radiation transmitted through a random medium. Rus. Journ. Num. Analysis Math. Model. V. 33, No 3. P. 161–171.

3. Amosov A.A., 2018: Initial-boundary value problem for the nonstationary radiative transfer equation with diffuse reflection and refraction conditions. Journ. Math. Sci. V. 235, No 2. P. 117–137.

4. Antokhin P.N., Arshinova V.G., Arshinov M.Y. et al., 2018: Distribution of trace gases and aerosols in the troposphere over Siberia during wildfires of summer 2012. J. Geoph. Res.: Atmospheres. V. 123, No 4. P. 2285–2297.

5. Aristova E.N., M.N. Gertsev, A.V. Shilkov, 2017: Lebesgue averaging method in serial computations of atmospheric radiation // Comp. Math. Math. Phys. V. 57, No 6. P. 1022–1035.

6. Asmus V.V., V.N. Stasenko, A.B. Uspenskii et al., 2017: Development of the space observation system and geophysical monitoring system in Roshydromet. Rus. Met. Hydr. V. 42, No 7. P. 442–451.

7. Asmus V.V., Yu.M. Timofeyev, A.V. Polyakov et al. 2017a: Atmospheric temperature sounding with the Fourier spectrometer. Izv., Atm. Ocean. Physics. V. 53, No 4. P. 428–432.

8. Bartalev S. A., D.E. Plotnikov, E.A. Loupian, 2016: Mapping of arable land in Russia using multiyear time series of MODIS data and the LAGMA classification technique. Rem. Sens. Let. V. 7, No 3. P. 269−278.

9. Berezin I.A., Ya.A. Virolainen, Yu.M. Timofeyev, and A.V. Poberovskii, 2016: The comparison of IR and MW ground-based measurements of total precipitable water. Izv., Atm. Ocean. Physics. V. 52, No 3. P. 253–256.

10. Berezin I.A., Yu.M. Timofeyev, Ya.A. Virolainen, and K.A. Volkova, 2016a: Comparison of ground-based microwave measurements of precipitable water vapor with radiosounding data. Atm. Ocean. Opt. V. 29, No 3. P. 274–281.

11. Berezin I.A., Yu.M. Timofeyev, Ya.A. Virolainen et al., 2016b: The influence of spatial matching on the results of the comparison of integrated water vapor ground-based and satellite measurements. Sovremennye problemy distantsionnogo zondirovaniya Zemli iz kosmosa. V. 13, No 4. P. 149–156.

12. Berezin I.A., Yu.M. Timofeyev, Ya.A. Virolainen et al. 2017: Error analysis of integrated water vapor measured by CIMEL photometer. Izv., Atm. Ocean. Physics. V. 53, No 1. P. 58–64.

13. Bochkovsky D.A., Virolainen Ya.A., Kulikov Yu.Yu. et al., 2016: Ground-based microwave monitoring of middle-atmosphere ozone over Peterhof and Tomsk during stratospheric warming in the winter of 2013–2014. Radioph. Quant. El. V. 59, No 4. P. 270–277.

14. Bondur V.G., A.S. Ginzburg, 2016: Emission of carbon-bearing gases and aerosols from natural fires on the territory of Russia based on space monitoring. Dokl. Earth Sci. V. 466, No 2. C. 148–152.

15. Budak V.P., V.S. Zheltov, A.V. Lubenchenko, K.S. Freidlin, O.V. Shagalov, 2017: A fast and accurate synthetic iteration-based algorithm for numerical simulation of radiative transfer in a turbid medium. Atmos. Ocean. Opt. V. 30, No 1. P. 70–78.

16. Bukharov M.V., 2015: Identification of the properties of the arctic and antarctic ice cover from the MTVZA-GYA microwave radiometer data. Rus. Met. Hydr. V. 40, No 7. P. 470–476.

17. Bukharov M.V., 2016: Studying the effects of vortices flowing around seamounts on ice properties from satellite microwave data. Rus. Met. Hydr. V. 41, No 10. P. 698–705.

18. Bukharov M.V., 2017: Semidiurnal frequency of the fields of the arctic ice rarefaction and compression from the MTVZA-GYA satellite radiometer data. Rus. Met. Hydr. V. 42, No 1. P. 46–53.

19. Bykov P.L., V.A. Gordin, L.L. Tarasova, E.V. Vasilenko, 2017: The statistical structure of the field of surface soil layer moisture from ground-based and satellite observations. Rus. Met. Hydr. V. 42, No 6. P. 403–414.

20. Cheremisin A.A., Marichev V.N., Novikov P.V. et al., 2016: Analysis of polar stratospheric cloud observations at Tomsk in January 2016. Proc. SPIE. V. 10035. 22nd International Symposium Atmospheric and Ocean Optics: Atmospheric Physics, Tomsk, Russian Federation. doi:10.1117/12.2248748.

21. Cheremisin A.A., P.V. Novikov, V.N. Marichev, A.N. Pavlov, 2017: Interpretation of the lidar observations of volcanic aerosol over Tomsk and Vladivostok in the summer 2011 by trajectory method. Proc. SPIE 10466, 23rd International Symposium on Atmospheric and Ocean Optics: Atmospheric Physics, 10466 76 (30 November 2017); doi: 10.1117/12.2292543.

22. Cherepova M.V., S.P. Smyshlyaev, M.V. Makarova et al., 2018: A study of the column methane short-term variability in the atmosphere on a regional scale. Izv., Atm. Ocean. Physics. V. 54, No 5. P. 558–569.

23. Chesnokova T.Y., A.V. Chentsov, N.V. Rokotyan, V.I. Zakharov, 2015: Retrieval of content of greenhouse gases from atmospheric spectra of solar radiation with the use of different spectroscopic data on absorption lines. Atmos. Ocean. Opt. 2015. V. 28. No 5. P. 469–475.

24. Chesnokova T.Yu., A.V. Chentsov, N.V. Rokotyan, V.I. Zakharov, 2016: Impact of difference in absorption line parameters in spectroscopic databases on CO_2 and CH_4 atmospheric content retrievals. J. Mol. Spectr. V. 327. P.171–179.

25. Chesnokova T.Y., A.V. Chentsov, K.M. Firsov, 2016a: Atmospheric radiative transfer simulation in water vapor total content retrievals using different spectroscopic databanks of H_2O absorption line parameters. Atm. Ocean. Opt. V. 29, No 2. P. 119–126.

26. Chubarova N., Y. Zhdanova, Y. Nezval, 2016: A new parameterization of the UV irradiance altitude dependence for clear-sky conditions and its application in the online UV tool over northern Eurasia. Atm. Chem. Phys. V. 16. P. 11867–11881.

27. Chubarova N., A. Poliukhov, I. Gorlova, 2016a: Long-term variability of aerosol optical thickness in Eastern Europe over 2001–2014 according to the measurements at the Moscow MSU MO AERONET site with additional cloud and NO_2 correction. Atm. Meas. Techn. V. 9, No. 2. P. 313–334.

28. Chubarova N.E., A.S. Pastukhova, V.Y. Galin, S.P. Smyshlyaev, 2018: Long-term variability of UV irradiance in the Moscow region according to measurement and modeling data. Izvestiya, Atmos. Oceanic Phys. V. 54, No 2. P. 139–146.

29. Chubarova N., A. Poliukhov, M. Shatunova et al., 2018a: Clear-sky radiative and temperature effects of different aerosol climatologies in the COSMO model. Geography, Environment, Sustainability. V. 11, No. 1. P. 74–84.

30. Elansky N.F., I.B. Belikov, A.I. Skorokhod et al., 2015: On contents of trace gases in the atmospheric surface layer over Moscow. Izv., Atm. Ocean. Physics. V. 51, No 1. P. 30–41.

31. Elansky N.F., O.V. Lavrova, A.I. Skorokhod, I.B. Belikov, 2016: Trace gases in the atmosphere over Russian cities. Atm. Envir. V. 143, P. 108–119.

32. Falaleeva V.A., B.A. Fomin, 2017: Overcoming spectroscopic challenges in direct problems of satellite sounding of the atmosphere. Atmos. Ocean. Opt. V. 30, No 1. P. 1–6.

33. Filei A., A. Rublev, A. Zaitsev, 2018: Radiometric inter-calibration of MSU-MR shortwave channels on-board Meteor-M No. 2 relative to AVHRR on-board Metop-A. GSICS Quart. Newsletter. V. 12, No 1. P. 11–13.

34. Filei A., A. Rublev, Yu. Kiseleva, A. Zaitsev, 2018a: Radiometric inter-calibration between MSU-GS and VIIRS shortwave channels. GSICS Quart. Newsletter. V. 12, No 1. P. 13–15.

35. Firsov K.M., T.Y. Chesnokova, E.V. Bobrov, 2015: The role of the water vapor continuum absorption in near ground long-wave radiation processes of the Lower Volga region. Atmos. Ocean. Opt. V. 28, No 1. P. 1–8.

36. Firsov K.M., T.Yu. Chesnokova, A.A. Razmolov, A.V. Chentsov, 2018: Contribution of the water vapor continuum absorption to shortwave solar fluxes in the earth's atmosphere with cirrus cloudiness. Atmos. Ocean. Opt. V. 31, No 1. P. 1–8.

37. Garkusha A.S., A.V. Polyakov, Yu.M. Timofeev, Ya.A. Virolainen, 2017: Determination of the total ozone content from data of satellite IR Fourier-spectrometer. Izv., Atm. Ocean. Physics. V. 53, No 4. P. 493–501.

38. Garkusha A.S., A.V. Polyakov, Yu.M. Timofeev et al., 2018: Determination of the total ozone content in cloudy conditions based on data from the IKFS-2 spectrometer onboard the Meteor-M no. 2 satellite. Izv., Atm. Ocean. V. 54, No 9. P. 1230–1234.

39. Gayfulin D.R., M.D. Tsyrulnikov, P.I. Svirenko et al., 2017: The usage of MTVZA-GYA satellite microwave radiometer observations in the data assimilation system of the Hydrometcenter of Russia. Rus. Met. Hydr. V. 42, No 9. P. 564–573.

40. Gayfulin D., M. Tsyrulnikov, A. Uspensky, 2018: Post-launch assessment and adaptive correction for atmospheric sounding channels of the satellite microwave radiometer MTVZA-GY. Pure Appl. Geoph. V. 175, No 10. P. 3653–3670.

41. Gayfulin D., M. Tsyrulnikov, A. Uspensky, 2018a: Assessment and recalibration of Meteor-M N2 microwave imager/sounder MTVZA-GY data in atmospheric sounding channels. GSICS Quart. Newsletter. V. 12, No 1. P. 6–8.

42. Golitsyn G.S., E.I. Grechko, A.V. Dzhola et al., 2015: Studying the pollution of Moscow and Beijing atmospheres with carbon monoxide and aerosol. Izv., Atm. Ocean. Physics. V. 51, No 1. P. 1–11.

43. Gorchakov G.I., A.V. Vasil'ev, S.K. Verichev et al., 2016: Fine-dispersed brown coal in a smoke-filled atmosphere. Dokl. Earth Sci. V. 471, No. 1. P. 1158–1163.

44. Gorchakov G.I., A.V. Karpov, N.D. Pankratova et al., 2017: Brown carbon and soot in the smoky atmosphere in boreal forest fires. Izv. Atm. Ocean. Phys. V. 53, No 9. P. 875–884.

45. Gorchakov G.I., A.V. Karpov, A.V. Vasiliev, A.I. Gorchakova, 2017a: Brown and black coal in the megalopolis smog. Atm. Ocean. Opt. V. 30, No. 3. P. 248–254.

46. Gorchakova I.A., I.I. Mokhov, A.N. Rublev, 2015: Radiation and temperature effects of the intensive injection of dust aerosol into the atmosphere. Izv., Atmos. Ocean. Phys. V. 51, No 2. P. 113–126.

47. Gorchakova I.A., I.I. Mokhov, P.P. Anikin, A.S. Emilenko, 2018: Radiative and thermal impacts of smoke aerosol longwave absorption during fires in the Moscow region in summer 2010. Izv., Atmos. Ocean. Phys. V. 54, No. 2. P. 154–161.

48. Gruzdev A.N., E.P. Kropotkina, S.V. Solomonov, A.S. Elokhov, 2016: Anomalies of the ozone and nitrogen dioxide contents in the stratosphere over Moscow region as a manifestation of the dynamics of the stratospheric polar vortex. Dokl. Earth Sci. V. 468, No. 4. P. 602–606.

49. Gruzdev A.N., E.P. Kropotkina, S.V. Solomonov, A.S. Elokhov, 2017: Winter-spring anomalies in stratospheric O_3 and NO_2 contents over the Moscow region in 2010 and 2011. Izv., Atm. Ocean. Physics. V. 53, No. 2. P. 195–203.

50. Ionov D.V., A.V. Poberovskii, 2017: Integral emission of nitrogen oxides from the territory of St. Petersburg based on the data of mobile measurements and numerical simulation results. Izv., Atm. Ocean. Physics. V. 53, No 2. P. 204–212.

51. Ionov D.V., Yu.M. Timofeyev, and A. V. Poberovskii, 2015: Spectroscopic measurements of O_3 and NO_2 atmospheric content: Correction of ground-based method and comparison with satellite Data. Atm. Ocean. Opt. V. 28, No 6. P. 526–532.

52. Ionov D.V., V.V. Kalinnikov, Yu.M. Timofeyev et al., 2017: Comparison of radiophysical and optical infrared ground-based methods for measuring integrated content of atmospheric water vapor in atmosphere. Radiophys. Quantum El. V. 60, No 4. P. 300–308.

53. Ionov D.V., A.V. Poberovskii, V.V. Ionov, 2017a: Spectroscopic remote sensing of NO_2 levels in urban air. J. Appl. Spectrosc. V. 84, No 1. P. 109–113.

54. Kabanov D.M., S.M. Sakerin, 2016: Comparison of assessment techniques of fine and coarse component aerosol optical depth of the atmosphere from measurement in the visible spectrum. SPIE Proc.V. 10035. Part 1. 1003 3D [10035-46].

55. Kalashnik M.V., A.F. Nerushev, and R.V. Ivangorodsky, 2017: Characteristic scales and horizontal asymmetry of jet streams in the Earth's atmosphere. Izv., Atm. Ocean. Physics. V. 53, No 2. P. 156–163.

56. Kim A., I.V. Prokhorov, 2018: Theoretical and numerical analysis of an initial-boundary value problem for the radiative transfer equation with Fresnel matching conditions. Comp. Math. Math. Physics. V. 58, No 5. P. 735–749.

57. Kiseleva Y.V., A.V. Kuharsky, A.N. Rublev et al., 2016: Data inter-calibration technique for infrared channels of the Elektro-l/MSU-GS imager with the Airs infrared sounder data. Izv., Atm. Ocean. Phys. V. 52, No 9. P. 1181–1190.

58. Kopeikin V.M., A.S. Emilenko, A.A. Isakov et al., 2018: Variability of soot and fine aerosol in the Moscow region in 2014–2016. Atm. Ocean. Opt. V. 31, No. 2. 3. P. 243–249.

59. Korkin S., A. Lyapustin, A. Sinyuk, B. Holben, A. Kokhanovsky, 2017: Vector radiative transfer code SORD: Performance analysis and quick start guide. J. Quant. Spectrosc. Radiat. Transf. V. 200. P. 295–310.

60. Korshunov V.A., D.S. Zubachev, 2018: Temporal variations in the vertical distribution of stratospheric ozone over Obninsk from lidar data**.** Rus. Met. Hydr. V. 43, No 3. P. 168–177.

61. Kostsov V.S., 2015: Retrieving cloudy atmosphere parameters from RPG-HATPRO radiometer data. Izv., Atm. Ocean. Physics. V. 51, No 2. P. 156–166.

62. Kostsov V.S. Yu.M. Timofeyev, N.A. Zaitsev et al., 2016: Application of the information approach to the analysis of two-year microwave observations of the atmosphere by the RPG-HATPRO radiometer at St. Petersburg University. Int. J. Rem. Sens. V. 37, No 14. P. 3346–3364.

63. Kostsov V.S., D.V. Ionov, E.Yu. Biryukov, N.A. Zaitsev, 2018: Cross-validation of two liquid water path retrieval algorithms applied to ground based microwave radiation measurements by RPG HATPRO instrument types. Int. J. Rem. Sensing. V. 39, No 5. P. 1321–1342.

64. Kozlov V.S., V.P. Shmargunov, M.V. Panchenko et al., 2016: Seasonal variability of the Black Carbon size distribution in the atmospheric aerosol. Rus. Phys. Journal. 2016. V. 58, No 12. P. 1804–1810.

65. Kuzmin V.L., 2017: Simulation of polarized optical radiation transport in time and frequency representations. J. Experimental and Theoretical Physics. V. 125, No 4. P. 579–586.

66. Levashova N., D. Lukyanenko, Y. Mukhartova, A. Olchev, 2018: Application of a three-dimensional radiative transfer model to retrieve the species composition of a mixed forest stand from canopy reflected radiation. Remote Sensing. V. 10, No 10. P. 1661.

67. Makarova M.V., A.V. Poberovskii, F. Hase et al., 2016: Determination of the characteristics of ground-based IR spectral instrumentation for environmental monitoring of the atmosphere. J. Appl. Spectroscopy. V. 83, Vo 3. P. 429–436.

68. Makarova M.V., D.K. Arabadzhyan, S.Ch. Foka et al., 2018: Estimation of nocturnal area fluxes of carbon cycle gases in Saint Petersburg suburbs. Rus. Met. Hydrol. V. 43, No 7. P. 449–455.

69. Matvienko G.G., B.D. Belan, M.V. Panchenko et al., 2015: The complex experiment to study the microphysical, chemical and optical properties of aerosol particles and evaluate the contribution of atmospheric aerosols in the earth radiative balance of the atmosphere and ocean. IPU. Technique. 8, 4507–4520.

70. Mikhailov G.A., S.M. Prigarin, S.A. Rozhenko, 2018: Comparative analysis of vector algorithms for statistical modelling of polarized radiative transfer process. Rus. Journ. Num. Analysis Math. Model. V. 33, No 4. P. 253–263.

71. Mitnik L.M., M.L. Mitnik, A.V. Vykochko A.V., 2016: Sea surface wind and sea ice in the Barents sea using microwave sensing data from Meteor-M N1 and GCOM-W1 satellites in January–March 2013. Izv., Atm. Ocean. Physics. V. 52, No 9. P. 1041−1050.

72. Muzylev E.L., Z.P. Startseva, A.B. Uspensky, E.V. Volkova, 2018: Modeling water and heat balance components for large agricultural region utilizing information from meteorological satellites. Water Resources. Vol. 45, No 5. P. 672–684.

73. Nasrtdinov I.M., T.B. Zhuravleva, T.Yu. Chesnokova, 2018: Evaluation of direct radiation effects of background and smoke aerosol in the IR spectral region for summer conditions of Siberia. Atm. Ocean. Opt. V. 31, No. 3. P. 317–323.

74. Nerushev A.F., K.N. Visheratin, and R.V. Ivangorodsky, 2018: Spatiotemporal variability of high-altitude jet streams from satellite measurements. Izv., Atm. Ocea. Physics. V. 54, No 9. P. 1076–1088.

75. Nezval' E. I., N. E. Chubarova, 2017: Long-term variability of UVR radiation in the spectral range of 300–380 nm. Rus. Met. Hydrology. V. 42, No. 11. P. 693–699.

76. Nikitin A.V., O.M. Lyulin, S.N. Mikhailenko, V.I. Perevalov et al., 2015: GOSAT-2014 methane spectral line list. J. Quant. Spectrosc. Radiat. Transf. 2015. V. 154. P. 63–71.

77. Nikolaeva O.V., 2016: A new algorithm of retrieving the surface albedo by satellite remote sensing data. Atmos. Ocean. Opt. V. 29, No 4. P. 342–347.

78. Nikolaeva O.V., 2016a: Studying the accuracy of the algorithm for retrieving the surface albedo with high spatial resolution from a fragment of a satellite image. Atm. Ocean. Opt. V. 29, No 6. P. 526–532.

79. Nikolaeva O.V., 2018: Algorithm for eliminating gas absorption effects on hyperspectral remote sensing data. Computer Optics. V. 42, No 2. P. 328–337.

80. Panchenko M.V., T.B. Zhuravleva, 2015: Vertical profiles of optical and microphysical characteristics of tropospheric aerosol based on the results of aviation measurements. Light Scattering Surveys 10. Ed. Kokhanovsky, A. 2015. P. 199–234. SPRINGER–PRAXIS.

81. Panchenko M.V., T.B. Zhuravleva, V.S. Kozlov et al., 2016: Estimation of aerosol radiation effects under background and smoke-haze atmospheric conditions over Siberia from empirical data. Rus. Met. Hydrology. V. 41, No. 2. P.104–111.

82. Panchenko M.V., S.A. Terpugova, V.V. Pol'kin et al., 2018: Simulation of radiation important parameters of aerosol in the troposphere of Siberia on the basis of empirical data. Atmosphere. V. 9, No. 11. P. 414–430.

83. Petrova T.M., A.M. Solodov, A.P. Shcherbakov, V.M. Deichuli, et al., 2017: Parameters of broadening of water molecule absorption lines by argon derived using different line profile models. Atmos. Ocean. Opt. V. 30, No 2. P. 123–128.

84. Plakhina I.N., N.V. Pankratova, E.L. Makhotkina, 2018: Comparison of ground and satellite monitoring of aerosol optical thickness of the atmosphere in Russia. Sovremennye problemy distantsionnogo zondirovaniya Zemli iz kosmosa. V. 15, No 2. P. 225–234.

85. Polyakov A.V., Yu.M. Timofeev, A.V. Poberovsky, Ya.A. Virolainen, 2015: Consideration of high surface concentrations of hydrochloric acid vapors in ground-based spectroscopic measurements. Atm. Ocean. Opt. V. 28, No 03. P. 240–244.

86. Polyakov A.V., Yu.M. Timofeyev, Ya.A. Virolainen et al. 2017: Satellite atmospheric sounder IRFS-2. 1. Analysis of outgoing radiation spectra measurements. Izv., Atm. Ocean. Physics. V. 53, No. 9. P. 1185–1191.

87. Polyakov A.V., Yu.M. Timofeev, Ya.A. Virolainen et al., 2018: Ground-based measurements of the total column of freons in the atmosphere near St. Petersburg (2009–2017). Izv., Atmos. Ocean. Phys. V. 54, No 5. P. 487–494.

88. Polyakov A.V., Yu.M. Timofeyev, A.B. Uspensky, A.V. Kukharsky, 2018a: The satellite atmospheric sounder IRFS-2: 2. Validation of the temperature sounding of the atmosphere. Izv., Atmos. Ocean. Physics. V. 54, No 9. P. 1340–1347.

89. Popovicheva O.B., V.S. Kozlov, G. Engling et al., 2015: Small-scale study of Siberian biomass burning: I. Smoke microstructure. Aerosol and Air Quality Research. V. 14. P. 1392–1401.

90. Popovicheva O.B., V.S. Kozlov, R.F. Rakhimov et al., 2016: Optical-Microphysical and Physical-Chemical Characteristics of Siberian Biomass Burning: Experiments in Aerosol Chamber. Atm. Ocean. Opt. V. 29, No. 6. P. 492–500.

91. Popovicheva O.B., N.M. Persiantseva, M.A. Timofeev et al., 2016a: Small-scale study of siberian biomass burning: ii. smoke hygroscopicity. Aerosol and Air Quality Research. V. 16, No 7. P. 1558–1568.

92. Prokhorov I.V., A.A. Sushchenko, A. Kim, 2017: Initial boundary value problem for the radiative transfer equation with diffusion matching conditions. J. Appl. Indus. Math. V. 11, No 1. P. 115–124.

93. Raev M.D., E.A. Sharkov, V.V. Tikhonov, 2015: Peculiarities of stochastic regime of arctic ice cover time evolution over 1987–2014 from microwave satellite sounding on the basis of NASA team 2 algorithm. Izv., Atm. Ocean. Physics. V. 51, No 9. P. 929−934.

94. Rakitin V.S., Yu.A. Shtabkin, N.F. Elansky et al., 2015: Comparison results of satellite and ground-based spectroscopic measurements of CO, CH_4, and CO_2 total contents. Atm. Ocean. Opt. 2015. V. 28, No 6. P. 533–542.

95. Rakitin V.S., N.F. Elansky, N.V. Pankratova et al., 2017: Study of trends of total CO and CH_4 contents over Eurasia through analysis of ground-based and satellite spectroscopic measurements. Atm. Ocean. Opt. V. 30, No 6. P. 517–526.

96. Rakitin V.S., N.F. Elansky, P. Wang et al., 2018: Changes in trends of atmospheric composition over urban and background regions of Eurasia: Estimates based on spectroscopic observations. Geography. Environment. Sustainability. V. 11, No 2. P. 84–96.

97. Reul N., B. Chapron, A. Mouche, 2017: A new generation of tropical cyclone size measurements from space. Bull. Am. Met. Soc. V. 98, No 22. C. 2367–2385.

98. Rokotyan N.V., R. Imasu, V. I. Zakharov et al., 2015: The amplitude of the CO_2 seasonal cycle in the atmosphere of the Ural region retrieved from ground-based and satellite near-IR measurements. Atm. Ocean. Opt., V. 28, No 1. P. 49–55.

99. Rozanov S.B., A.S. Zavgorodniy, A.N. Ignat'ev, 2016: Technique of time-frequency analysis of a series of measurements of the radiation spectra of night mesospheric ozone in the millimetric wavelength range. Meas. Techn. V. 59, No. 8. P. 870–877.

100. Rozanov S.B., A.S. Zavgorodniy, A.N. Ignatyev, A.N. Lukin, 2017: Variations in microwave radiation of the nighttime mesospheric ozone over Moscow. Rad. Quant. El. V. 59, No. 8–9, P. 741–753.

101. Rublev A.N., E.V. Gorbarenko, V.V. Golomolzin et al., 2018: Inter-calibration of infrared channels of geostationary meteorological satellite imagers. Front. Environ. Sci., 27 November 2018, https://doi.org/10.3389/fenvs.2018.00142

102. Rusin E., V. Pyatkin, A. Kozlov et al., 2015: Fast Radiative Transfer Model for hyperspectral Meteor-M data simulation. GSICS Quart. Newsletter. V. 9, No 3. P. 5–7.

103. Russkova T.V., M.A. Sviridenkov , T.B. Zhuravleva, 2016: On the effect of stratification of atmospheric optical characteristics on the sky radiance in the solar principal plane. Atmos. Ocean. Opt. V. 29, No 2. P. 175–185.

104. Russkova T.V., T.B. Zhuravleva, 2017. Optimization of sequential code for simulation of solar radiative transfer in a vertically heterogeneous environment. Atmos. Ocean. Opt. V. 30, No 2. P. 169–175.

105. Russkova T., T. Zhuravleva, 2018: Top-of-atmosphere reflectance over homogeneous Lambertian and non-Lambertian surfaces. Appl. Optics. V. 57, No 22. P. 6345–6357.

106. Russkova T.V., P.N. Zenkova, 2018a: Nitrogen dioxide content in the troposphere of Western Siberia according to satellite observations. Spatio-temporal variability. Sovremennye problemy distantsionnogo zondirovaniya Zemli iz kosmosa. V. 15, No 7. P. 221–235.

107. Sakerin S.M., A.A. Bobrikov, O.A. Bukin et al., 2015: On measurements of aerosol-gas composition of the atmosphere during two expeditions in 2013 along Northern Sea Route. Atmos. Chem. Phys. V. 15, No. 21. P. 12413–12443.

108. Sakerin S.M., D.M. Kabanov, V.V. Polkin et al., 2017: Variations in aerosol optical and microphysical characteristics along the route of Russian Antarctic expeditions in the East Atlantic. Atm. Ocean. Opt. V. 30, No. 1. P. 89–102.

109. Sakerin S.M., L.P. Golobokova, D.M. Kabanov et al., 2017a: Spatiotemporal variations in aerosol characteristics along the route of the Indian-Atlantic expedition onboard the research vessel Akademik Nikolaj Strakhov. Atm. Ocean. Opt. V. 30, No. 3. 4. P. 349–359.

110. Sakerin S.M., L.P. Golobokova, D.M. Kabanov et al. 2018: Zonal distribution of aerosol physicochemical characteristics in the Eastern Atlantic. Atmos. Ocean. Opt. V. 31, No. 5. P. 492–501.

111. Sakerin S.M., D.M. Kabanov, V.F. Radionov et al., 2018a: Generalization of results of atmospheric aerosol optical depth measurements on Spitsbergen Archipelago in 2011–2016. Atm. Ocean. Opt. V. 31, No. 2. P. 163–170.

112. Semoutnikova E.G., G.I. Gorchakov, S.A. Sitnov et al., 2018: Siberian smoke haze over European territory of Russia in July 2016: Atmospheric pollution and radioactive effects // Atm. Ocean. Opt. V. 31, No. 2. P. 171–180.

113. Shabanov N., J.-P. Gastellu-Etchegorry, 2018: The stochastic Beer–Lambert–Bouguer law for discontinuous vegetation canopies. J. Quant. Spectrosc. Radiat. Transf. V. 214. P. 18–32.

114. Shved G.M., Ya.A. Virolainen, Yu.M. Timofeyev et al. 2018: Ozone temporal variability in the Subarctic region: Comparison of satellite measurements with numerical simulations. Izv., Atm. Ocean. Physics. V. 54, No 1. P. 32–38.

115. Sklyadneva T.K., T.M. Rasskazchikova, V. Arshinova, 2018: Changes in the synoptic regime of Tomsk over the period of 1993–2016. SPIE Proc. V. 10833. 108337G.

116. Smirnov A., T.B. Zhuravleva, M. Segal-Rosenheimer, B.N. Holben, 2018: Limitations of AERONET SDA product in presence of cirrus clouds. J. Quant. Spectrosc. Radiat. Transf. V. 206. P. 338–341.

117. Smyshlyaev S.P., Ya.A. Virolainen, M.A. Motsakov et al. 2017: Interannual and seasonal variations in ozone in different atmospheric layers over St. Petersburg based on observational data and numerical modeling. Izv., Atm. Ocean. Physics. V. 53, No 3. P. 301–315.

118. Solomonov S.V., E.P. Kropotkina, S.B. Rozanov et al., 2017: Influence of strong sudden stratospheric warmings on ozone in the middle stratosphere according to millimeter wave observations. Geom. Aeronomy. V. 57, No 3. P. 361–368.

119. Sterlyadkin V.V., D.S. Sazonov, A.V. Kuzmin, E.A. Sharkov, 2018: Ground radiometric measurements of the sea surface effective emissivity without absolute calibration. Sovremennye Problemy Distantsionnogo Zondirovaniya Zemli iz Kosmosa. V. 15, No 2. P. 29–41.

120. Tashkun S.A., V.I. Perevalov, R.R. Gamache, J. Lamouroux, 2015: CDSD-296, high resolution carbon dioxide spectroscopic databank: Version for atmospheric applications. J. Quant. Spectrosc. Radiat. Transf. 2015. V.152. P. 45–73.

121. Tikhonov V.V., M.D. Raev, E.A. Sharkov et al., 2016: Satellite microwave radiometry of sea ice of Polar Regions: a review. Izv., Atmos. Ocean. Phys. V. 52, No 9. P. 1012−1030.

122. Timofeev Yu., Ya. Virolainen, M. Makarova et al., 2016: Ground-based spectroscopic measurements of atmospheric gas composition near St. Petersburg (Russia). J. Mol. Spectr. V. 323. P. 2–14.

123. Timofeyev Yu.M., A.V. Polyakov, A.V. Poberovsky, 2016: HCl content has ceased to increase in the atmosphere of the Northern Hemisphere // Dokl. Earth Sci. V. 470, No 1. P. 994–996.

124. Timofeyev Yu.M., Ya.A. Virolainen, S.P. Smyshlyaev, and M.A. Motsakov, 2017: Ozone over St. Petersburg: Comparison of experimental data and numerical simulation. Atmos. Ocean. Opt. V. 30, No 3. P. 263–268.

125. Timofeyev Y.M., S.P. Smyshlyaev, Y.A. Virolainen et al., 2018: Case study of ozone anomalies over northern Russia in the 2015/2016 winter: Measurements and numerical modeling. Ann. Geophys. V. 36, No 6. P. 1495–1505.

126. Tomasi C., A.A. Kokhanovsky, A. Lupi et al., 2015: Aerosol remote sensing in polar regions. Earth-Science Reviews. V. 140. P. 108–157.

127. Uspenskii A.B., A.V. Kukharskii, S.A. Uspenskii, 2015: Validation of the results of the satellite monitoring of land surface temperature. Rus. Met. Hydr. V. 40, No 2. P. 131–140.

128. Uspensky A.B., V.V. Asmus, A.A. Kozlov et al., 2017: Absolute calibration of the MTVZA-GY microwave radiometer atmospheric sounding channels. Izv., Atm. Ocean. Physics. V. 53, No. 9. P. 1192–1204.

129. Uspensky A.B., E.K. Kramchaninova, V.S. Koscov et al., 2017a: Development of the calibration/validation system for microwave radiometer MTVZA-GYa observations from Meteor-M No. 2 satellite. Sovremennye problemy distantsionnogo zondirovaniya Zemli iz kosmosa. V. 14, No. 4. P. 27–35.

130. Vasilyev A.V., I.N. Melnikova, S.S. Novikov, 2017: Influence of atmospheric optical parameters on the characteristics of solar radiation. Sovremennye Problemy Distantsionnogo Zondirovaniya Zemli iz Kosmosa. V. 14, No 5. P. 285–299.

131. Vigouroux C., C.A. Bauer Aquino, M. Bauwens et al., 2018: NDACC harmonized formaldehyde time-series from 21 FTIR stations covering a wide range of column abundances. Atmos. Meas. Tech. V. 11. P. 5049–5073.

132. Virolainen Ya.A., 2018: Methodical aspects of the determination of carbon dioxide in atmosphere using FTIR spectroscopy. J. Appl. Spectr. V. 85, No 3. P. 462–469.

133. Virolainen Ya.A., Yu.M. Timofeyev, A.V. Poberovskii et al., 2015: Evaluation of ozone content in different atmospheric layers using ground-based Fourier Transform Spectrometry. Izv., Atmos. Ocean. Physics. V. 51, No 2. P. 167–176.

134. Virolainen Ya.A., Yu.M. Timofeyev, A.V. Poberovskii et al., 2015a: Chlorine nitrate in the atmosphere over St. Petersburg. Izv., Atmos. Ocean. Physics. V. 51, No 1. P. 49–56.

135. Virolainen Ya.A., Yu.M. Timofeyev, A.V. Polyakov et al. 2016: Comparing data obtained from ground-based measurements of the total contents of O_3, HNO_3, HCl, and NO_2 and from their numerical simulation. Izv., Atmos. Ocean. Physics. V. 52, No 1. P. 57–65.

136. Virolainen Ya., Yu. Timofeyev, I. Berezin et al., 2016a: Atmospheric integrated water vapour measured by IR and MW techniques at the Peterhof site (Saint Petersburg, Russia). Int. J. Rem. Sens. V. 37, No 16. P. 3771–3785.

137. Virolainen Ya.A., Yu.M. Timofeyev, S.P. Smyshlyaev et al., 2017: Study of ozone layer variability near St. Petersburg on the basis of SBUV satellite measurements and numerical simulation (2000–2014). Izv., Atm. Ocean. Physics. V. 53, No 9. P. 911–917.

138. Virolainen Y.A., Y.M. Timofeyev, V.S. Kostsov et al., 2017a: Quality assessment of integrated water vapour measurements at St. Petersburg site, Russia: FTIR vs. MW and GPS techniques. Atmos. Meas. Tech. V. 10. P. 4521–4536.

139. Virolainen Ya.A., Yu.M. Timofeyev, A.V. Poberovskii et al. 2017b: Empirical assessment of errors in total ozone measurements with different instruments and methods. Atmos. Ocean. Opt. V. 30, No 4. P. 382–388.

140. Virolainen Ya.A., Yu.M. Timofeev, I.A. Berezin et al., 2018: Validation of atmospheric numerical models based on satellite measurements of ozone columns. Rus. Meteorol. Hydrol. V. 43, No 3. P. 161–167.

141. Visheratin K.N., 2016: Quasidecadal variations in total ozone content, wind velocity, temperature, and geopotential height over the Arosa station (Switzerland). Izv., Atmos. Ocean. Phys. V. 52, No 1. P. 66–73.

142. Visheratin K.N., 2017: Spatio-temporal variability of the phase of total ozone quasi-decennial oscillations. Izv., Atmos. Ocean. Phys. V. 53, No 9. P. 904–910.

143. Visheratin K.N., A.F. Nerushev, M.D. Orozaliev et al., 2017: Temporal variability of total ozone in the Asian region inferred from ground-based and satellite measurement data // Izv., Atmos. Ocean. Phys. V. 53, No 9. P. 894–903.

144. Visheratin K.N., M.V. Kalashnik, 2018: Quasidecadal variations of lower stratosphere meteorological parameters and total ozone global fields based on satellite data // Izv., Atmos. Ocean. Phys. V. 54, No 9. P. 1068–1075.

145. Volkova E.V. and A.B. Uspensky, 2016: Detection and assessment of cloud cover and precipitation parameters using data of scanning radiometers of polar-orbiting and geostationary meteorological satellites. Izv., Atmos. Ocean. Phys. Vol. 52, No 9. P. 1096–1108.

146. Volkova E.V., S.A. Uspensky, 2016a: Land surface, land air and effective temperature estimation for territories of Southern European Russia based on satellite data. Sovremennye problemy distantsionnogo zondirovaniya Zemli iz kosmosa. Vol. 13, No. 5. P. 291–303.

147. Volkova E.V., 2017: Detection and assessment of cloud cover and precipitation parameters using data from MSU-MR radiometer of the polar-orbiting Meteor-M No. 2 for the European territory of Russia. Sovremennye problemy distantsionnogo zondirovaniya Zemli iz kosmosa. V. 14, No 5. P. 300–320.

148. Volkova E.V., 2018: Retrieval of cloud microphysical properties from satellite observations. Sovremennye problemy distantsionnogo zondirovaniya Zemli iz kosmosa. V. 15, No 4. P. 265–279.

149. Wang P., N.F. Elansky, Yu.M. Timofeev et al. 2018: Long-term trends of carbon monoxide total columnar amount in urban areas and background regions: Ground- and satellite-based spectroscopic measurements. Adv. Atmos. Sci. V. 35, No. 7. P. 785–795.

150. Zabolotskikh E.V., 2017: Contemporary methods for retrieving the integrated atmospheric water-vapor content and the total cloud liquid-water content. Izv., Atmos. Ocean. Phys. V. 53, No 3. C. 294–300.

151. Zabolotskikh E.V., B. Chapron, 2016: Neural network-based method for the estimation of the rain rate over oceans by measurements of the satellite radiometer AMSR2. Izv., Atmos. Ocean. Phys. V. 52, No 1. C. 82–88.

152. Zabolotskikh E.V., B. Chapron, 2017: Improvements in atmospheric water vapor content retrievals over open oceans from satellite passive microwave radiometers. IEEE J. Sel. Topics in Appl. Earth Obs. Rem. Sens. V. 10, No 7. C. 3125–3133.

153. Zabolotskikh E.V., I.A. Gurvich, B. Chapron, 2016: Polar lows over the Eastern part of the Eurasian Arctic: The sea-ice retreat consequence. IEEE Geoscience and Remote Sensing Letters. V. 13, No 10. P. 1492−1496.

154. Zadvornykh I.V., K.G. Gribanov, V.I. Zakharov, R. Imasu, 2017: Radiative transfer code for the thermal and near-infrared regions with multiple scattering. Atmos. Ocean. Opt. V. 30, No 4. P. 305–310.

155. Zavelevich F., D. Kozlov, I. Kozlov et al., 2018: IKFS-2 radiometric calibration stability in different spectral bands. GSICS Quart. Newsletter. V. 12, No 1. P. 4–6.

156. Zhuravleva T., I. Nasrtdinov, 2018: Simulation of bidirectional reflectance in broken clouds: from individual realization to averaging over an ensemble of cloud fields. Remote Sensing. V. 10, No 9. P. 1342.

157. Zhuravleva T.B., I.M. Nasrtdinov, T.V. Russkova, 2017: Influence of 3D cloud effects on spatial-angular characteristics of the reflected solar radiation field. Atmos. Ocean. Opt. V. 30, No 1. P. 103–110.

158. Zhuravleva T.B., M.V. Panchenko, V.S. Kozlov V.S. et al., 2018: Model estimates of dynamics of the vertical structure of solar absorption and temperature effects under background conditions and in extremely smoke-laden atmosphere according to data of aircraft observations. Atmos. Ocean. Opt. V. 31, No. 1. P. 25–30.

159. Zinkov S.Y., A.A. Sushchenko, K.V. Sushchenko, 2018: Analysis of surface and volume scattering in the problem of seabottom sounding. Siberian Electronic Mathematical Reports. V. 15. P. 1361–1377.

160. Zubachev D. S., V.A. Korshunov, N.B. Tereb, 2018: Concentration of stratospheric ozone derived from lidar, satellite, and surface observations. Rus. Meteorol. Hydrol. V. 43, No. 7. P. 488–493.

Climate

I.I. Mokhov
A.M. Obukhov Institute of Atmospheric Physics,
Russian Academy of Sciences
Lomonosov Moscow State University
mokhov@ifaran.ru

This review presents information about Russian studies of climate and its changes (published in 2015–2019). Significant part of key results of climate change studies with analysis of impacts for Russia during last years is given in [1–264]. Previous similar review was published in [1, 2]. Annual reviews of key climatic regional features in Russia are published every year with a regular information on climate studies in the bulletin "Climate Change" (http://meteorf.ru).

Climate and its changes from observations, reanalyses and paleoreconstructions

Results of climate studies based on observations, reanalyses data and paleoreconstructions are presented in [1–120]. Significant climate changes associated with strong weather-climate anomalies have been noted during last years in various regions. In Russia, as a northern country, the warming is much faster than for the Earth as a whole. In recent decades, the rate of the surface warming in Russia in general was twice and half higher than for the globe. In some regions it was several times larger. According to Roshydromet data (http://www.meteorf.ru) the trend of the annual-mean surface air temperature for Russia as a whole for the period 1976–2018 was equal to 0.47°C/(10 years). Such a rapid warming in Russia is accompanied by considerable interannual variability. The obtained linear trend is associated with 50% of the variance of surface air temperature for Russia as a whole.

An important area of research is related with extreme climate events and their changes [3–6, 13, 14, 20, 34–37, 40, 44, 45, 51–53, 63, 64, 67, 94–104, 110]. Recent decades are characterized by significant climate changes that are noticeably manifested in the frequency and intensity of extreme regional events. On the background of general warming, an increase in climate variability is observed. In 2012–2017 the number of anomalous meteorological phenomena in Russian regions was almost three times higher than that in 1998–2002, and in 2017 there were almost 4 times more of those than in 2000 (http://www.meteorf.ru/). The highest frequency of extreme events (especially those related to hydrological processes) is observed during the warmer months

of the year. By examining extreme events of recent decades, it can be assumed that the risk of extreme regional conditions similar to those observed in spring 2017 and 2018 in Moscow region with squalls of wind with storm and hurricane strength, is significant for the Russian regions. It should be noted, that the dangerous phenomena over the past two decades have been more intense and destructive than before.

Strongest climate anomalies and changes have been noted in Arctic and subarctic regions, which are characterized by high variability and sensitivity to various natural and anthropogenic forcings [21–32, 56, 60–62, 81, 82, 88–91, 106]. Regional increase in the surface temperature is accompanied by fast reduction of sea ice and significant changes of snow cover. In the Arctic regions, changes in the carbon cycle, including the methane cycle, associated with climate changes, are of special importance [9, 10, 81, 82, 89, 90]. New geophysical features (craters in permafrost) have been noted during last five years as a response to significant warming of north regions in the cryolithozone [32, 60, 61] (see also [121–123]). Such features can be indicators of critical changes for the regional stability of contemporary permafrost and methane hydrates [121–123].

Significant risks for the population and the environment associated with modern climate changes are caused by an increase in the frequency and intensity of extreme weather and climate events (http://www.meteorf.ru/), including those of convective nature: showers, thunderstorms, squalls, and tornadoes. There is a weakening of the static stability of the troposphere above midlatitude lands of the Northern Hemisphere, which can lead to intensification of convective processes. In particular, convective cloud cover and repeated rainfall have been observed in the regions of Northern Eurasia. The strongest regional climate anomalies are related to the long-term (up to a month or more) blockings in the troposphere of middle latitudes [35, 36]. The anomalous 2010 summer heat wave in the European part of Russia, record 2013 Amur flood, and cold winters during last decades in Eurasia and North America are associated with atmospheric blockings.

Significant contribution to regional and global-scale climate variations is associated with various cyclic and quasi-cyclic processes in the Earth climate system on different temporal scales. Noticeable contribution is associated with quasi-cyclic processes and phenomena like Quasi-Biennial Oscillation (QBO), the El-Niño / Southern Oscillation (ENSO), the Atlantic Equatorial Mode (AEM), the North Atlantic Oscillation (NAO), the Arctic Oscillation (AO), the Atlantic Multidecadal Oscillation (AMO), the Pacific Decadal Oscillation (PDO) and others [11, 14, 41, 42, 44, 52, 53, 72–77, 109, 116–118]. Climate effects of solar variability (of the 11-year solar cycle, in particular) are estimated in [48, 54, 119].

Analysis of historical data and paleoreconstructions advance our understanding of the role of different climatic mechanisms [38, 39, 56–58, 69, 107, 108, 111, 114].

The climatic anomalies of recent years testify not only to an increase in the risk of extreme regional events, but also to the manifestation of new phenomena that characterize reaching a certain critical level of the changes taking place. For example, in recent years, the formation of craters on Yamal (for the first time in 2014) and adjacent regions [32, 60, 61] has been revealed (see also [121–123]).

Climate theory and climate system modeling

Different topics of climate theory and climate system modeling are considered in [6, 7, 11, 14, 120–201]. Models of different complexity from conceptual models to the most detailed coupled models of general circulation (global and regional) are used for simulations of the global climate system and its changes. The development of climate model is associated with the more detailed spatio-temporal model resolution, taking into account new subsystems, additional phenomena and climate processes, more adequate simulations of interaction between different components of the climate system. New estimates of climatic effects have been obtained with the use of new parameterizations and specially developed algorithms for description of comprehensive climate processes. Significant development is associated with the Earth system models as an extention of the concept of climate models [1, 2, 7]. Earth system models include, in particular, interation with the natural carbon cycle.

Results of simulations with 3D chemical transport model in [147] for the situation in European Russia during the 2010 Russian heat wave with wildfires show that the intensity of formation of secondary organicaerosols in smoke plumes caused by vegetation and peat fires under real conditions can significantly depend on the aerosol optical thickness. The aerosol optical thickness determines the photodissociation rate and hydroxyl radical concentration, which in turn determines the rate of secondary organic aerosols generation as a result of oxidation of semi-volatile organic compounds.These results indicate that it is important to allow for this effect in studies focused on the analysis and prediction of air pollution due to wildfires, as well as climate and weather studies, whose results may depend on the assumptions about the content and properties of atmospheric carbon-containing aerosol (see also [148]).

In [181] simulations of current climate have been carried out with the use MGO regional model (with horizontal resolution 25 km) for extended region, including significant part of the Northern Eurasia and part of the Arctic. This

model version is planned to be used for ensemble climate change simulations with the IPCC scenarios.

Climate and Earth system models development requires an adequate simulation of processes in different atmospheric layers, including the upper atmosphere layers and their interaction with processes in the lower atmosphere. In particular, it is necessary to simulate adequately processes in the ionosphere [150–152]. New INM RAS atmospheric general circulation model, which includes troposphere, stratosphere, mesosphere, and the lower thermosphere, as well as the lower ionospheric regions (INMAIM) is resented in [152]. A new general circulation model is based on the atmospheric part of the INM climatic model INMCM with the addinion of the middle atmosphere and lower ionosphere description up to 130 km altitudes. A new algorithm for radiative processes simulations is used. For the lower ionosphere a plasma chemistry model was developed.

Causal climatic relationships are discussed in [166, 167] (see also [76, 77, 112]). Simulations with climate models of different complexity show that the phase shift between changes in global air surface temperature and atmospheric CO_2 content in general does not characterize causal relationships in the earth system [166, 167]. In particular, the sign of this shift depends on the time scale of the non-greenhouse radiative forcing.

For adequate interpretation of paleoreconstructions with the use of long-term climate simulations it is necessary to develop corresponding ice sheet models [2, 7, 171–173, 185]. Simple model of the global climate system using scaled equations of ice-sheet thermodynamics to combine them with a linear equation describing changes in climate temperature was presented in [185]. This model is a nonlinear dynamical system incorporating three variables: area of glaciation, ice-sheet basal temperature, and characteristic temperature of outside-of-glacier climate. When it is astronomically forced, depending on the values of the parameters involved, the system is capable of producing different modes of rhythmicity, some of which are consistent with paleoclimate records of the early and late Pleistocene.

Significant topic is related with modeling of potential effects of methane hydrates associated with climate warming and permafrost degradation [121–124, 136]. In [121–123], the formation of craters on Yamal and adjacent regions was associated with the decomposition of shallow-bed methanhydrates with gas emissions into the atmosphere in regions of permafrost with ongoing warming. According to model simulations under [121–123], the formation of shallow methane hydrates was possible high pressure of the ice sheet existing in the marked regions tens of thousands years ago. The fact that craters like the one in Yamal are currently being formed suggests that modern climate warming

can be not only comparable to the warming of the Holocene optimum about 6 thousand years ago, but also surpass it, at least at the regional scale. Assessments of crater formation in North America regions were also made in [121].

Russian climate models, parameterizations and algorithms are used in different international programs, initiatives and projects, including international comparisons of climate models and their blocks: CMIP6, CORDEX (Arc-CORDEX), NEFI, FAMOS, IMILAST, ISIMIP, PEEX and others.

Global and regional climate change simulations with assessment of natural and athropogenic contribution

Global and regional climate change simulations with an assessment of natural and athropogenic contribution, in particular for Russian regions, are presented in [197–219].

Very rapid climate changes, especially sea ice extent changes, are observed and simulated in arctic and subarctic regions. In particular, projections for the surface air temperature in the Arctic through the 21st century using an ensemble of CMIP5 climate models are analyzed in [208]. The projections are presented for 3 scenarios of radiative forcing: RCP2.6, RCP4.5 and RCP8.5. A comparison is undertaken with CMIP3 projections under SRES scenarios.

Climate models project further general decrease of the Arctic sea ice extent in the 21st century. According to model projections the navigation in the Arctic Ocean should be more accessible. The best models are able to adequately reproduce not only regional features of climatic regimes, but also their current variability and trends [162]. This is evidenced, in particular, in the results of model estimates of changes in the navigation period for the Northern Sea Route obtained in [210–213] compared with the satellite data for the last decades. Moreover, according to the obtained model estimates considering general warming and an increase in the navigation period on the Northern Sea Route in the 21st century, with sufficiently large interannual variability in the coming decades in the first half of the century, one can expect weakening of the growth trend of the navigation period duration and even local manifestations of its decrease.

Characteristics of cyclones (frequency, intensity and size) and their changes in the Arctic region in a warmer climate have been analyzed with the use of the HIRHAM regional climate model simulations with SRES-A1B anthropogenic scenario for the twenty first century [202]. The focus was on cyclones for the warm and cold seasons. Potential future changes in cyclone characteristics at the end of the twenty first century have been analyzed. According to the model simulations, the frequency of cyclones is increasing in warm seasons and de-

creasing in cold seasons for a warmer climate in the twenty first century, but these changes are statistically insignificant. Noticeable changes were detected for the intensity and size of cyclones for the both seasons. Significant increase was found for the frequency of weak cyclones during cold season. Further, a general increase in the frequency of small cyclones was simulated in cold seasons, while its frequency decreases in warm seasons.

An increase in the risk of tornadogenesis under general warming can be expected. Due to the intensification of convective processes, a tendency for the growth of convective clouds, in particular for Northern Eurasia, and for the frequency of rainfall is noted. In [203], the estimates of the tornado risk growth in the North Eurasian regions based on reanalysis data for the last decades were obtained. Appropriate estimates were obtained for possible climate changes in the 21st century from simulations with the ensemble of global climate models [203]. The increase in the frequency of conditions contributing to the tornadogenesis in the North Eurasian regions is revealed. The most significant increase was obtained for the Far East and the Black Sea region. Extremely high sea surface temperatures [161] contribute to the formation of powerful convective processes with extreme precipitation. For instance, the record flooding in the Amur River basin in 2013 was associated with the extremely high surface temperature of the Pacific Ocean.

Estimates of changes in the blocking characteristics (including the amount, duration, and frequency) in different regions of the Northern Hemisphere from model simulations of possible climate changes are presented in [214]. The results of analysis of distribution functions and their variations for characteristics of atmospheric blockings in the European–Atlantic region including the European part of Russia are presented in detail. The analysis is based on simulations with different climate models under various RCP scenarios of anthropogenic forcings for the 21st century.

Model estimates of regional hydrological changes under global warming are presented in [204, 206, 215, 216, 218, 219]. Detailed estimates of future changes in the hydrological extremes across river network on the interval 1990–1999 to 2050–2059 of northern Eurasia using a high-resolution system of regional atmospheric and hydrological models were obtained in [219]. Modeling ensemble consisted of 30 members differing in the atmospheric initial and ocean boundary conditions. Large ensemble size, along with reasonably high modeling resolution, allows one to efficiently sample natural climate variability and increase our ability to predict future changes in the hydrological extremes. It has been shown that the annual maximum river discharge can almost double by the mid-XXI century in the outlets of major Siberian rivers. In the western regions, there is a weak signal in the river discharge and flood hazard, hardly discernible above climate variability. A contribution of natural climate variabil-

ity at different temporal scales to the uncertainty of ensemble prediction is discussed. The analysis shows that there expected considerable changes in the extreme river discharge probability at locations of the key hydropower facilities.

Climate change impacts and problems of adaptation and mitigation

Different problems associated with the impacts of climate changes and with the problems of adaptation and mitigation taking into account current tendencies in the world economy and power engineering are analyzed in [1–5, 8, 10, 12, 13, 15, 220–264]. In particular, the problems related to the optimal adaptation of the Russian economy to hazardous effects of climate changes and hydrometeorological security are discussed.

In Russia, bases for the adaptation of natural and socio-economic systems are formed and developed both as part of international agreements and protocols (in particular, in the context of the UN Framework Convention on Climate Change, the Paris Agreement, the UN Convention to Combat Desertification, the UN Convention on Biological Diversity, The Sustainable Development Goals for the period up to 2030), and within the framework of national strategic programs (in particular, in the framework of the Climate Doctrine of the Russian Federation, the Comprehensive Plan for implementation; environmental strategies bezopasnostina period up to 2025, etc.) [3, 8, 235, 252]). The system of climate and environmental pollution monitoring in Russia and specific indicators to assess the effectiveness of adaptation measures are discussed in [252]. In [8], projected scenarios of climate change and their impact on agriculture and forestry are analyzed. An assessment is made of current trends and risks of degradation of soil and land resources of Russia, possible mechanisms and means of regulating carbon balance in agriculture and forestry, as well as measures for adaptation of farming and forest management systems and technologies to climate changes.

Inter-disciplinary studies socio-economic, demogrphic and ecological and climatic problems in megapolises are discussed in [15]. Special attention is paid to the climate of megacities, bioclimatic indicators, heat and cold waves, risk minimization and adaptation (see also [12]). The pronounced negative effect on human health have heat waves [3]. Problems of the Russian population health in conditions of changing climate are considered also in [250, 251, 253, 254].

The key point of the widely debated problem of global warming is the question of maximum permissible changes. It is necessary to develop objective criteria for estimating both global and regional climate changes and permissible

risks [2–5]. The global targets of the 2°C and 1.5°C global warming above the pre-industrial level in the connection with the corresponding IPCC Report [4] are considered in [5]. According to [4] the warming excess of 1.5°C leads to significant negative consequences for natural and socio-economic systems. The corresponding restrictions are associated with significant investments. Estimates of maximum permissible risks, in particular for Russia, are discussed in [3].

Different topics of the problem of the climate change mitigation are discussed in [221–223, 258–261]. In particular, a long-term projections of the costs and effects associated with the implementation of additional energy efficiency policies in Russian buildings are considered in [223]. According to [223], more than a third part of primary energy consumption is associated with buildings in Russia, and with this is associated significant potential for energy conservation. Ten different policy scenarios for improving energy efficiency are considered with a conclusion that it is possible to reduce the fossil fuel consumption of buildings by more than half, while doubling their area and size by 2050. Additional benefits are considered, such as reduced greenhouse gas emissions and air pollution, employment growth, improved living conditions, and reduced costs for both residents and the public sector. The costs and economic effects of the energy efficiency measures and policies are assessed, and it is shown that Russia's new growth model must focus on making the economy more efficient, including more energy efficient.

Problems of climate stabilization by using geoengineering methods are considered in [258–261] with the analysis of model simulations with aerosol injections in the stratosphere.

In [220] results of ClimPACT application for impact analysis of changing climate conditions on thermal and nuclear power plants operation in different Russian regions are discussed. Statistical software ClimPACT ClimPACT was developed by WMO CCl Expert Team on climate risk and sector-specific climate indices. It wasconcluded that the obtained results can be used in the context of climate risk management in the energy sector (see also [243]).

An adequate consideration for the carbon balance of Russian boreal forests, wetlands and other terrestrial ecosystems is necessary for a more detailed and comprehensive analysis with quantative estimates of the carbon cycle influence in the Earth's climate system [2]. Such quantitative estimates for different time horizons are necessary for adequate projections in relation to the Paris Agreement (an agreement within the United Nations Framework Convention on Climate Change, dealing with greenhouse-gas-emissions mitigation, adaptation, and finance). In connection with the Paris Agreement, a national climate change adaptation plan is developed.

As a whole, the necessity of change of many criteria of risk assessments and potential benefits associated with climate change should be considered, and

possible changes and their consequences should be strategically evaluated, including taking into account the increased probability of extreme regional conditions.

References

1. Russian National Report: Meteorology and Atmospheric Sciences (2011–2014). Moscow, MAKS Press, 2015, 272 p.

2. Mokhov I.I. Russian climate studies in 2011–2014. Izvestiya, Atmos. Oceanic Phys., 2017, **53** (5), 550–563.

3. Report on Climate Risks in the Russian Federation. St. Petersburg, MGO, 2017, 106 pp. (in Russian)

4. IPCC, 2018. Global Warming of 1.5°C. An IPCC Special Report on the impacts of global warming of 1.5°C above pre-industrial levels and related global greenhouse gas emission pathways, in the context of strengthening the global response to the threat of climate change, sustainable development, and efforts to eradicate poverty. V. Masson-Delmotte, P. Zhai, H. O. Pörtner, et al. (eds.). (http://report.ipcc.ch/sr15/)

5. Gladilshchikova A.A., Dmitrieva T.M., Semenov S.M. Global warming of 1.5°C: A Special Report of the Intergovernmental Panel on Climate Change. Fund. Appl. Clim., 2018, 4, 5–18. (in Russian)

6. Turbulence, Atmosphere and Climate Dynamics. Ed. by G.S. Golitsyn, I.I. Mokhov, S.N. Kulichkov, M.V. Kurgansky, I.A. Repina, O.G. Chkhetiani. Moscow, Fizmatkniga, 2018, 586 pp. (in Russian)

7. Mathematical Modeling of the Earth System. Volodin V.M. et al. Ed. by Iakovlev N.G. Moscow, MAKS Press, 2016, 328 p. (in Russian)

8. Global Climate and Soil Cover of Russia: Assessment of Risks and Environmental and Economic Consequences of Land Degradation. Adaptive Systems and Environmental Management Technologies (Agriculture and Forestry). National Report. Ed. by A.I. Bedritsky. Moscow, Soil Sci. Inst., GEOS, 2018, 357 pp. (in Russian)

9. Semenov S.M., Govor I.L., Uvarova N.E. The Role of Methane in the Modern Climate Change. Moscow, 106 p. (in Russian)

10. Monitoring of Greenhouse Gas Flows in Natural Ecosystems. Ed. by D.G. Zamolodchikov, D.V. Karelin, M.L. Gitarsky, V.G. Blinov. Saratov, Amirit, 2017, 279 p. (in Russian)

11. Polonsky A.B. Oceans, Global Warming Hiatus and Regional Climate Change. Lambert Acad. Publ., Saarbrucken, 2015, 192 pp.

12. Climate of Moscow in Conditions of Global Warming. Ed. By A.V. Kislov. Moscow, IMU, 2017, 288 p. (in Russian)

13. Groisman P.Ya., Shugart H.H., Kicklighter D., Henebry G., Tchebakova N., Maksyutov Sh., Monier E., Gutman G., Gulev S., Qi J., Prishchepov A., Kukavskaya E., Porfiriev B., Shiklomanov A., Loboda T., Shiklomanov N., Nghiem S., Bergen K., J. Albrechtová J., Chen J., Shahgedanova M., Shvidenko A., Speranskaya N., Soja A., deBeurs K., Bulygina O., McCarty J., Zhuang Q., Zolina O. and the NEFI Science Plan Preparation Team. Northern Eurasia Future Initiative (NEFI): facing the challenges and pathways of global change in the twenty-first century. Progr. Earth Planet. Sci., 2017, **4** (41), doi: 10.1186/s40645-017-0154-5.

14. Intense Atmospheric Vortices and Their Dynamics. I.I. Mokhov, M.V. Kurgansky, O.G. Chkhetiani (eds.). Moscow, GEOS, 2018, 482 p.

15. Man in the City: The Experience of Interdisciplinary Research. Ed. by B.A. Revich, O.V. Kuznetsova. Moscow, LENAND, 2018, 640 p. (in Russian)

16. Alduchov O.A., Chernykh I.V. Methods of Analysis and Interpretation of the Atmosphere Radiosonde Observations Data. V. 3. Humidity and Temperature in the Atmosphere: Statistics. Obninsk, ARRIHMI-WDC, 2015, 494. (in Russian)

17. Brasseur G., Lynch A., Cazenave A., Mata M.M., Visbeck M., Belcher S., Hesselbjerg Christensen J., Cleugh H., Güingla R.M., Kang I.-S., Kattsov V., Kimoto M., Hong Liao, Nobre C., Peter T., Renwick J., Sorooshian S., Yanda P. World Climate Research Programme Strategic Plan 2019–2028. WCRP Publ. No. 1/2019. 2018. 17 pp.

18. Groisman P.Y., Gutman G., Shugart H.H., Gulev S.K., Qi J., Maksyutov Sh. 10 years of NEESPI accomplishments and future plans highlighted at synthesis workshop. GEWEX News, 2015, **25** (3), 10–12.

19. Kulmala M., Lappalainen H.K., Petaja T., Kerminen V.-M., Viisanen Y., Matvienko G., Melnikov V., Baklanov A., Bondur V., Kasimov N., Zilitinkevich S. Pan-Eurasian Experiment (PEEX) Program: Grand challenges in the Arctic-boreal context. Geogr. Environ. Sustainabil. 2016, **9** (2), 5–18.

20. Nesterov E.S. Extreme Cyclones in the Atlantic-European Region. Moscow, Russ. Hydrometeocenter, 2018, 104 pp. (in Russian)

21. Overland J., Walsh J., Kattsov V., Barber D., Box J.E., Brown R., Mård J., Olsen M.S., Romanovsky V. SWIPA 2017 Synthesis: summary and implications of findings / In: Snow, Water, Ice and Permafrost in the Arctic (SWIPA). AMAP. Oslo, Norway, 2017, 257–268.

22. Shakhova N.E., Sergienko V.I., Semiletov I.P. Carbon Cycle in the East Arctic Seas at the turn of the 20th and 21st centuries. 2. Methane: Results of First Studies (1994–2010). Vladivostok, Dalnauka, 2018, 240 p.

23. Alekseev G.V., Aleksandrov E.I., Glok N.I., Ivanov N.E., Smolyanitsky V.M., Kharlanenkova N.E., Yulin A.V. Arctic sea ice cover in connection with climate change. Izvestiya, Atmos. Oceanic Phys., 2015, **51** (9), 889–902.

24. Alekseev G.V., Bolshiyanov D.Y., Radionov V.F., Frolov S.V. 95 years of climate and cryosphere studies of the Arctic in the Arctic and Antarctic Research Institute. Led i Sneg (Ice and Snow), 2015, **55** (4), 127–140. (in Russian)

25. Alekseev G., Glok N., Smirnov A. On assessment of the relationship between changes of sea ice extent and climate in the Arctic. Intern. J. Climatol., 2015, doi:10.1002/joc.4550.

26. Alekseev G.V., Glok N.I., Smirnov A.V., Vyazilova A.E. The influence of the North Atlantic on climate variations in the Barents Sea and their predictability. Russ. Meteorol. Hydrol., 2016, **41** (8), 544–558.

27. Alekseev G.V., Kuzmina S.I., Glok N.I., Vyazilova A.E., Ivanov N.E., Smirnov A.V. The influence of the Atlantic on warming and shrinking sea ice cover in the Arctic. Led I Sneg (Ice and Snow), 2017, **57** (3), 381–390. (in Russian)

28. Alekseev G.V., Kuzmina S.I., Urazgildeeva A.V., Bobylev L.P. Influence of atmospheric heat and moisture transfers on the increase of warming in the Arctic during the winter period. Fund. Appl. Climatol., 2016, **1**, 43–63. (in Russian)

29. Alekseev G.V., Radionov V.F., Smolyanitsky V.M., Filchuk K.V. Results and prospects of the climate studies and climate service in the Arctic. Arctic and Antarctic Research, 2018, **64** (3), 262–269. (in Russian)

30. Alexeev V.A., Walsh J.E., Ivanov V.V., Semenov V.A., Smirnov A.V. Warming in the Nordic Seas, North Atlantic storms and thinning Arctic sea ice. Env. Res. Lett., 2017, 12. 084011, doi: 10.1088/1748-9326/aa7a1d.

31. Anisimov O.A., Kokorev V.A. Comparative analysis of land, marine, and satellite observations of methane in the lower atmosphere in the Russian Arctic under conditions of climate change Izvestiya, Atmos. Oceanic Phys., 2015, **51** (9), 979–991.

32. Bogoyavlensky V.I. Gas-hydrodynamics in the Arctic craters of gas blowout. Arctic: Ecol. Econ., 2018, 1(29), 48–55. (in Russian)

33. Borzenkova I.I. History of sea ice in the Arctic basin: Lessons from the past for future. Led i Sneg (Ice and Snow), 2016, 56 (2), 221–234. (in Russian)

34. Bokuchava D.D., Semenov V.A. Analysis of surface air temperature anomalies in the Northern Hemisphere in the 20th century using observational and reanalysis data. Fund. Appl. Climatol., 2018, 1, 28–51. (in Russian)

35. Antokhina O. Yu., Antokhin P. N., Zorkal'tseva O. S., Devyatova E.V. Atmospheric blockings in Western Siberia. Part 1. Detection features, objective criteria, and their comparison**.** Russ. Meteorol. Hydrol., 2017, **42 (**10), 644–652.

36. Antokhina O.Y., Antokhin P.N., Devyatova E.V., Martynova Y.V. Atmospheric blockings in Western Siberia. Part 2. Long-term Variations in blocking frequency and their relation with climatic variability over Asia. Russ. Meteorol. Hydrol., 2018, **43** (3), 143–151.

37. Bardin M.Yu., Platova T.V., Samokhina O.F. Specific features of variability of cyclone activity in Northern extratropics associated with leading atmospheric circulation modes in Atlantic-European sector. Fund. Appl. Climatol., 2015, 2, 14–40. (in Russian)

38. Borzenkova I., Zorito E., Borisova O., Kalnina L., Kisieliene D., Koff T., Kuznetsov D., Lemdahl G., Sapelko T., Stancikaite M., Subetto D. Climate change during the Holocene (past 12,000 years). In: Second Assessment of Climate Change for the Baltic Sea basin. Regional Climate Studies. 2015, 25–49.

39. Borzenkova I., Zhiltsova O.K., Sapelko T.V. Cold period in the Northern Europe in the past (about 8200 years ago): analysis of empirical data and possible causes. Led I Sneg (Ice and Snow), 2017, **57** (1), 117–132.

40. Bulygina O.N., Arzhanova N.M, Groisman P.Ya. Icing conditions over Northern Eurasia in changing climate. Environ. Res. Lett., 2015, **10**, 025003. doi:10.1088/1748-9326/10/2/025003.

41. Byshev V.I., Neiman V.G., Anisimov M.V., Gusev A.V., Serykh I.V., Sidorova A.N., Figurkin A.L., Anisimov I.M., Anisimov I.M. Multi-Decadal Oscillations of the ocean active upper-layer heat content. Pure Appl. Geophys., 2017, **174** (7), 2863–2878.

42. Byshev V.I., Neiman V.G., Romanov,Y.A., Serykh I.V., Sonechkin D.M. Statistical significance and climatic role of the global atmospheric oscillation. Oceanol., 2016, **56** (2), 165–171.

43. Chen J.L., Pekker, T., Wilson C.R., Tapley B.D., Kostianoy A.G., Cretaux J.F., Safarov E.S. Long-term Caspian Sea level change. Geophys. Res. Lett., 2017, **44** (13), 6993–7001.

44. Cherenkova E.A., Bardin M.Yu., Zolotokrylin A.N. The statistics of precipitation and droughts during opposite phases of the quasi-biennial oscillation of atmospheric processes and its relation to the yield in the European part of Russia. Russ. Meteorol. Hydrol., 2015, **40** (3), 18–169.

45. Chernokulsky A.V., Esau I., Bulygina O.N., Davy R., Mokhov I.I., Outten S., Semenov A.V. Climatology and interannual variability of cloudiness in the Atlantic Arctic from surface observations since the late nineteenth century. J. Climate, 2017, **30**, 2103–2120.

46. Chernokulsky A.V., Kozlov F.A., Zolina O.G., Bulygina O.N., Semenov V.A. Climatology of precipitation of different genesis in Northern Eurasia. Russ. Meteorol. Hydrol., 2018, **43** (7), 425–435.

47. Chernokulsky A.V., Kurgansky M.V., Zakharchenko D.I., Mokhov I.I. Genesis environments and characteristics of the severe tornado in the South Urals on August 29, 2014. Russ. Meteorol. Hydrol., 2015, **40** (12), 794–799.

48. Eliseev A.V., Mokhov I.I. Extra-terrestrial factors' influence on climate: Possible mechanisms and modeling results. Fund. Appl. Climatol., 2015, 1, 119–132. (in Russian)

49. Frolov A.V., Georgievsky V.Y. Changes in water resources under conditions of climate warming and their impact on water inflow to Russian large reservoirs. Russ. Meteorol. Hydrol., 2018, **43** (6), 390–396.

50. Gang C., Zhou W., Wang Z., Chen Y., Li J., Chen J., Qi J., Odeh I., Groisman P.Y. Comparative assessment of grassland NPP dynamics in response to climate change in China, North America, Europe and Australia from 1981 to 2010. J. Agron. Crop Sci., 2015, **201** (1), 57–68.

51. Groisman P.Ya., Bulygina O.N., Yin X., Vose R.S., Gulev S.K., Hanssen-Bauer I., Førland E. Recent changes in the frequency of freezing precipitation in North America and Northern Eurasia. Environ. Res. Lett., 2016, **11**, 045007.

52. Mokhov I.I., Timazhev A.V. Assessment of the predictability of climate anomalies in connection with El Nino phenomena. Doklady Earth Sci., 2015, **464** (2), 1089–1093.

53. Mokhov I.I., Timazhev A.V. Assessing the probability of El Nino-related weather and climate anomalies in Russian regions. Russ. Meteorol. Hydrol., 2017, **42** (10), 635–643.

54. Gruzdev A.N. Variations in the temperature and circulation of the atmosphere during the 11-year cycle of solar activity derived from the ERA-Interim reanalysis data. Izvestiya, Atmos. Oceanic Phys., 2017, **53** (4), 441–448.

55. Guryanov V.V., Eliseev A.V., Mokhov I.I., Perevedentsev Yu.P. Wave activity and its changes in the troposphere and stratosphere of the Northern Hemisphere in winters of 1979–2016. Izvestiya, Atmos. Oceanic Phys., 2018, **54** (2), 114–126.

56. Jakobsson M., Nilsson J., Anderson L., Backman J., Bjork G., Cronin T.M., Kirchner N., Koshurnikov A., Mayer L., Noormets R., O'Regan M., Stranne C., Ananiev R., Barrientos Macho N., Cherniykh D., Coxall H., Eriksson B., Flodén T., Gemery L., Gustafsson Ö., Jerram K., Johansson C., Khortov A., Mohammad R., Semiletov I. Evidence for an ice shelf covering the central Arctic Ocean during the penultimate glaciations. Nature Comm., 2016, **7**, 10365, 1–10.

57. Kislov A. On the interpretation of century-millennium-scale variations of the Black Sea level during the first quarter of the Holocene. Quatern. Intern. 2016. http://dx.doi.org/10.1016/j.quaint.2016.09.008

58. Kislov A.V. The interpretation of secular Caspian Sea level records during the Holocene. Quatern, Intern., 2016, **409 A**, 39–43.

59. Kislov A.V. Secular variability of the Caspian Sea level. Russ. Meteorol. Hydrol., 2018, **43** (10), 679–685.

60. Kizyakov A.I., Sonyushkin A.V., Leibman M.O., Zimin M.V., Khomutov A.V. Geomorphological conditions of the gas-emission crater and its dynamics in Central Yamal. Kriosfera Zemli, 2015, **XIX** (2), 15–25. (in Russian)

61. Kizyakov A., Zimin M., Sonyushkin A., Dvornikov Yu., Khomutov A., Leibman M. Comparison of gas emission crater geomorphodynamics on Yamal and Gydan peninsulas (Russia), based on repeat very-high-resolution stereopairs. Remote Sens., 2017, 9, 1023, doi:10.3390/rs9101023

62. Kotlyakov V.M., Velichko A.A., Glazovsky A.F., Tumskii V.E. The past and present day Arctic cryosphere. Herald Russ. Acad. Sci., 2015, **85** (3), 251–259.

63. Kotlyakov V.M., Glazovsky A.F., Moskalevsky M.Yu. Dynamics of the ice mass in Antarctica in the time of warming. Led i Sneg (Ice and Snow), 2017, **57** (2), 149–169. (in Russian)

64. Kotlyakov V.M., Muravev A.Ya., Nikitin S.A., Nosenko G.A., Rototaeva O.V., Khromova T.E., Chernova L.P. Glacier revival and advances in the period of global warming. Doklady Earth Sci., 2018, 481 (2), 1113–1118.

65. Krokhin V.V., Fil A.Y., Veryatin V.Y. Long-term variations in the frequency of typhoons and their connection with various formation factors. Russ. Meteorol. Hydrol., 2017, **42** (12), 766–774.

66. Liu X., Tang Q., Zhang X., Groisman P. et al. Spatially distinct effects of preceding precipitation on heat stress over eastern China. Environ. Res. Lett., 2017, **12**, 103780, doi: http://iopscience.iop.org/article/10.1088/1748-9326/aa88f8/meta

67. Loginov S.V., Eliseev A.V., Mokhov I.I. Impact of non-Gaussian statistics of atmospheric variables on extreme intramonth anomalies. Izvestiya, Atmos. Oceanic Phys., 2017, **53** (3), 269–278.

68. Lokoshchenko M.A., Korneva I.A., Kochin A.V., A.Z. Dubovetsky A.Z., Novitsky M.A., Razin P.Ye. Vertical extension of the urban heat island above Moscow. Doklady Earth Sci., 2016, **466** (10), 70–74.

69. Luterbacher J., Werner J.P., Smerdon J.E., Fernandez-Donado L., Gonzalez-Rouco F.J., Barriopedro D., Ljungqvist F.C., Buntgen U., Zorita E., Wagner S., Esper J., McCarroll D., Toreti A., Frank D., Jungclaus J.H., Barriendos M., Bertolin C.,Bothe O., Brazdil R., Camuffo D., Dobrovolny P., Gagen M., Garica-Bustamante E., Ge Q., Gomez-Navarro J.J., Guiot J., Hao Z., Hegerl G.C., Holmgren K., Klimenko V.V., Martin-Chivelet J., Pfister, C., Roberts N., Schindler A., Schurer, A., Solomina O., von Gunten L., Wahl E., Wanner H., Wetter O., Xoplaki E., Yuan N., Zanchettin, D., Zhang H., Zerefos C. European summer temperatures since Roman times. Environ. Res. Lett., 2016, 11 (2), 024001, doi: 10.1088/1748–9326/11/2/024001.

70. Makhotkina E.L., Plahina I.N., A. Makhotkin A.N. The transparency of the atmosphere in Russia: changes in the last 40 years. Proc. MGO, 2015, 579, 162–177. (in Russian)

71. Mescherskaya A.V., Golod M.P. Catalogues anomality winters for Russion territory. Proc. MGO, 2015, 579, 129–161. (in Russian)

72. Mokhov I.I., Smirnov D.A. Estimating the coupling between variations in the Atlantic Multidecadal Oscillation and the El Nino/Southern Oscillation. Izvestiya, Atmos. Oceanic Phys., 2015, **51** (5), 472–481.

73. Mokhov I.I., Smirnov D.A. Relation between the variations in the global surface temperature, El Nino/La Nina phenomena, and the Atlantic Multidecadal Oscillation. Doklady Earth Sci., 2016, **467** (2), 384–388.

74. Mokhov I.I., Smirnov D.A. The trivariate seasonal analysis of couplings between El Nino, North Atlantic Oscillation, and Indian monsoon. Russ. Meteorol. Hydrol., 2016, **41** (11–12), 798–807.

75. Mokhov I.I., Smirnov D.A. Estimates of the mutual influence of variations in the sea surface temperature in tropical latitudes of the Pacific, Atlantic, and Indian Oceans from long-period data series. Izvestiya, Atmos. Oceanic Phys., 2017, **53** (6), 613–623.

76. Mokhov I.I., Smirnov D.A. Estimating the contributions of the Atlantic Multidecadal Oscillation and variations in the atmospheric concentration of greenhouse gases to surface air temperature trends from observations. Doklady Earth Sci., 2018, **480** (1), 602–606.

77. Mokhov I.I., Smirnov D.A. Contribution of greenhouse gas radiative forcing and Atlantic Multidecadal Oscillation to surface air temperature trends. Russ. Meteorol. Hydrol., 2018, **43** (9), 557–564.

78. Monier E., Kicklighter D., Sokolov A., Zhuang Q., Sokolik I., Lawford R., Kappas M., Paltsev S., Groisman P. A review of and perspectives on global change modeling for Northern Eurasia. Environ. Res. Lett., 2017, **12,** 083001. http://iopscience.iop.org/article/10.1088/1748–9326/aa7aae/meta.

79. Perevedentsev Yu.P., Shantalinskii K.M. Changes in the near-surface air temperature of the Northern Hemisphere during the period of 1850–2014. Uch. Zap. Kaz. Univ. Ser. Est. Nauki, 2015, 157 (3), 8–19. (in Russian)

80. Perevedentsev Yu.P.,Shantalinskiy K.M. Dynamics of the tropo- and stratosphere anf modern climate changes. Fund. Appl. Climatol., 2015, 1, 211–231. (in Russian)

81. Pipko I.I., Pugach S.P., Semiletov I.P. Assessment of the CO2 fluxes between the ocean and the atmosphere in the eastern part of the Laptev Sea in the ice-free period. Doklady Earth Sci., 2016, 467 (2), 398–401.

82. Pipko I.I., Pugach S.P., Semiletov I.P., Anderson L.G., Shakhova N.E., Gustafsson Ö., Repina I.A., Spivak E.A., Charkin A.N., Salyuk A.N., Shcherbakova K.P., Panova E.V., Dudarev O.V. The spatial and interannual dynamics of the surface water carbonate system and air–sea CO2 fluxes in the outer shelf and slope of the Eurasian Arctic Ocean. Ocean Sci., 2017, **13**, 997–1016.

83. Popova V.V. Present-day changes in climate in the north of Eurasia as a manifestation of variation of the large-scale atmospheric circulation. Fund. Appl. Climatol., 2018, 1, 84–111. (in Russian)

84. Popova V.V., Shiryaeva A.V., Morozova P.A. Changes in the snow depth characteristics in the territory of Russia in 1950–2013: The regional features and connection with the global warming. Kriosfera Zemli, 2018, 22 (4), 65–75. (in Russian)

85. Popova V.V., Matskovsky V.V., Mikhailov A.Yu. Recent climate change over the terrestrial part of extra-tropical Northern Hemisphere zone. Moscow Univ. Bull., Ser. 5, Geogr., 2018, 1, 3–13.

86. Privalsky V., Yushkov V. Getting it right matters: Climate spectra and their estimation. Pure Appl. Geophys., 2018, 175 (8), 3085–3096.

87. Reid Ph.C., Hari R.E., Beaugrand G., Livingstone D.M., Marty C., Straile D., Barichivich J., Goberville E., Adrian R., Aono Y., Brown R., Foster J., Groisman P., Helaouet P., Hsu H.-H., Kirby R., Knight J., Kraberg A., Li J., Lo T.-T., Myneni R.B., North R.P., Pounds J.A., Sparks T., Stubi R., Tian Y., Wiltshire K.H., Xiao D., Zhu Z. Global impacts of the 1980s regime shift. Glob. Change Biol., 2016, **22**, 682–703.

88. Semenov E.K., Sokolikhina N.N., Tudrii K.O. Synoptic mechanisms of winter warming in the Arctic. Russ. Meteorol. Hydrol., 2015, **40** (9), 576–583.

Shakhova N., Semiletov I., Sergienko V., Lobkovsky L., Yusupov V., Salyuk A., Salomatin A., Chernykh D., Kosmach D., Panteleev G., Nicolsky D., Samarkin V., Joye S., Charkin A., Dudarev O., Meluzov A., Gustafsson O. The East Siberian Arctic Shelf: towards further assessment of permafrost-related methane fluxes and role of sea ice. Phil Trans. Roy. Soc. A – Math. Phys. Engin. Sci., 2015, **373** (2052), 20140451.

Shakhova N., Semiletov I., Gustafsson O., Sergienko V., Lobkovsky L., Dudarev O., Tumskoy V., Grigoriev M., Maruzov A., Salyuk A., Ananiev R., Koshurnikov A., Kosmach D., Charkin A., Dmitrievsky N., Karnauch V., Gunar A., Meluzov A., Chernykh D. Current rates and mechanisms of subsea permafrost degradation in the East Siberian Arctic Shelf. Nature Comm., 2017, **8**, 15872.

89. Sherstyukov A.B., Sherstyukov B.G. Spatial features and new trends in thermal conditions of soil and depth of its seasonal thawing in the permafrost zone. Russ. Meteorol. Hydrol., 2015, 40 (2), 73–78.

90. Shiryaeva A.V., Shiryaev M.V., Semenov V.A. Changes in the duration of stable cold and warm seasons at the beginning of the 21st century in Russia. Doklady Earth Sci., 2018, 481 (1), 934–938.

91. Sidorenkov N.S. Long-term oscillations in surface temperature: Role of cloudiness factor. Fund. Appl. Clim., 2015, **2**, 93–102.

92. Shukurov K.A., Semenov V.A. Characteristics of winter surface air temperature anomalies in Moscow in 1970–2016 under conditions of reduced sea ice area in the Barents Sea. Izvestiya, Atmos. Oceanic Phys., 2018, **54** (1), 10–24.

93. Sitnov S.A., Mokhov I.I. Ozone mini-hole formation under prolonged blocking anticyclone conditions in the atmosphere over European Russia in Summer 2010. Doklady Earth Sci., 2015, **460** (1), 41–45.

94. Sitnov S.A., Mokhov I.I. Satellite-derived peculiarities of total ozone field under atmospheric blocking conditions over the European part of Russia in summer 2010. Russ. Meteorol. Hydrol., 2016, **41** (1), 28–36.

95. Sitnov S.A., Mokhov I.I. Anomalous transboundary transport of the products of biomass burning from North American wildfires to Northern Eurasia. Doklady Earth Sci., 2017, **475** (1), 832–835.

96. Sitnov S.A., Mokhov I.I. Formaldehyde and nitrogen dioxide in the atmosphere during summer weather extremes and wildfires in European Russia in 2010 and Western Siberia in 2012. Intern. J. Remote Sensing, 2017, **38** (14), 4086–4106.

97. Sitnov S.A., Mokhov I.I. Anomalies in the atmospheric methane content over Northern Eurasia in the summer of 2016. Doklady Earth Sci., 2018, **480** (1), 637–641.

98. Sitnov S.A., Mokhov I.I., Bezverkhny V.A. Connections of precipitable water vapor and total ozone anomalies over European Russia with the North Atlantic Oscillation: Specific features of summer 2010. Izvestiya, Atmos. Oceanic Phys., 2017, **53** (9), 885–893.

99. Sitnov S.A., Mokhov I.I., Dzhola A.V. Total content of carbon monoxide in the atmosphere over Russian regions according to satellite data. Izvestiya, Atmos. Oceanic Phys., 2017, **53** (1), 32–48.

100. Sitnov S.A., Mokhov I.I., Gorchakov G.I. The Link between smoke blanketing of European Russia in summer 2016, Siberian wildfires and anomalies of large-scale atmospheric circulation. Doklady Earth Sci., 2017, **472** (2), 190–195.

101. Sitnov S.A., Mokhov I.I., Gorchakov G.I., Dzhola A.V. Smoke haze over the European part of Russia in the summer of 2016: A link to wildfires in Siberia and atmospheric circulation anomalies. Russ. Meteorol. Hydrol., 2018, **42** (8), 518–528.

102. Sitnov S.A., Mokhov I.I., Lupo A.R. Ozone, water vapor, and temperature anomalies associated with atmospheric blocking events over Eastern Europe in spring – summer 2010. Atmos. Environ., 2017, **164**, 180–194.

103. Smirnov D.A., Mokhov I.I. Relating Granger causality to long-term causal effects. Phys. Rev. E. 2015, **92** (4), 042138.

104. Smith D.M., Screen J.C., Deser C., Cohen J., Fyfe J.C., García-Serrano J., Jung T., Kattsov V., Matei D., Msadek R., Peings Y., Sigmond M., Ukita J., Yoon J.-H., Zhang X. The Polar Amplification Model Intercomparison Project (PAMIP) contribution to CMIP6: investigating the causes and consequences of polar amplification. Geosci. Model Dev. Discuss., 2018, https://doi.org/10.5194/gmd-2018-82.

105. Solomina O.N., Bradley R.S., Hodgson D.A., Ivy-Ochs S., Jomelli V., MackintoshA.N., Nesje A., Owen L.A., Wanner H., Wiles G., Young N.E. Holocene glacier fluctuations. Quatern. Sci. Rev. 2015, **111**, 9–34.

106. Solomina O.N., Bradley R.S., Jomelli V., Geirsdottir A., Kaufman D.S., Koch J., Mckay N.P., Masiokas M., Miller G., Nesje A., Nicolussi K., Owen L.A., Putnam A.E., Wanner H., Wiles G., Yang B. Glacier fluctuations during the past 2000 years. Quatern. Sci. Rev. 2016, **149**, 61–90.

107. Stepanov V.N. A plausible reason for changes in El Niño parameters in the 2000s. Russ. Meteorol. Hydrol., 2016, **41** (11–12), 747–759.

108. Titkova T.B., Cherenkova E.A., Semenov V.A. Regional features of changes in winter extreme temperatures and precipitation in Russia in 1970–2015. Led i Sneg (Ice and Snow), 2018, **58** (4), 486–497. (in Russian)

109. Valukenko N.V., Sonechkin D.M., Kotlyakov V.M. Is climate predictable on a geological time scale? Doklady Earth Sci., 2015, **460** (1), 68–72.

110. Vakulenko N.V., Sonechkin D.M., Kotlyakov V.M. The connection between the growth of anthropogenic carbon dioxide in the atmosphere and the current climate warming. Doklady Earth Sci., 2017, **477** (1), 1307–1310.

111. Voskresenskaya E., Bardin M., Kovalenko O. Climate variability of winter anticyclones in the Mediterranean-Black Sea region. Quatern. Intern. 2016, **409 A**, 70–74.

112. Yanko-Hombach V., Kislov A. Late Pleistocene – Holocene sea-level dynamics in the Caspian and Black Seas: Data synthesis and Paradoxical interpretations. Quatern. Intern., 2017, https://doi.org/10.1016/j.quaint.2017.11.030

113. Zahn M., Akperov M., Rinke A., Feser F., Mokhov I.I. Trends of cyclone characteristics in the Arctic and their patterns from different re-analysis data. J. Geophys. Res. – Atmos., 2018, **123** (5), 2537–2551.

114. Zheleznova I.V., Gushchina D.Yu. Hadley and Walker circulation anomalies associated with the two types of El Niño. Russ. Meteorol. Hydrol., 2017, **42** (10), 625–634.

115. Zheleznova I.V., Gushchina D.Yu. The response of global atmospheric circulation to two types of El Nino. Russ. Meteorol. Hydrol., 2015, **40** (3), 170–179.

116. Zheleznova I.V., Gushchina D.Yu. Circulation anomalies in the atmospheric centers of action during the Eastern Pacific and Central Pacific El Nino. Russ. Meteorol. Hydrol., 2016, **41** (11–12), 760–769.

117. Zherebtsov G.A., Kovalenko V.A., Kirichenko K.E. The role of solar activity in observed climate changes in the 20th century. Geomagnet. Aeron., 2017, 57 (6), 637–644.

118. Mokhov I.I. Contemporary climate changes in the Arctic. Herald Russ. Acad. Sci., 2015, 85 (3), 265–271.

119. Arzhanov M.M., Mokhov I.I. Stability of continental relic methane hydrates for the holocene climatic optimum and for contemporary conditions. Doklady Earth Sci., 2017, **476** (2), 1163–1167.

120. Arzhanov M.M., Mokhov I.I., Denisov S.N. Impact of regional climatic change on the stability of relic gas hydrates. Doklady Earth Sci., 2016, **468** (2), 616–618.

121. Arzhanov M.M., Mokhov I.I., Denisov S.N. Destabilization of relict methane hydrates with observed changes of regional climate. Arctic: Ecol. Econ., 2016, 4, 46–51. (in Russian).

122. Arzhanov M.M., Malakhova V.V., Mokhov I.I. Simulation of the conditions for the formation and dissociation of methane hydrate over the last 130 000 years. Doklady Earth Sci., 2018, **480** (2), 826–830.

123. Akperov M., Rinke A., Mokhov I., Matthes H., Semenov V. and the Arctic Cordex Team. Cyclone activity in the Arctic from an ensemble of regional climate models (Arctic CORDEX). J. Geophys. Res. – Atmos., 2018, **123** (5), 2537–2554.

124. Anisimov O.A., Kokorev V., Zhiltcova Y. Arctic ecosystems and their services under changing climate: Predictive-modeling assessment. Geogr. Rev., 2016, **107** (1), 108–124.

125. Bohn T.J., Melton J.R., Ito A., Kleinen T., Spahni R., Stocker B.D., Zhang B., Zhu X., Schroeder R., Glagolev M.V., Maksyutov S., Brovkin V., Chen G., Denisov S.N., Eliseev A.V., Gallego-Sala A., McDonald K.C., Rawlins M.A., Riley W.J., Subin Z.M., Tian H., Zhuang Q., Kaplan J.O. WETCHIMP-WSL: intercomparison of wetland methane emissions models over West Siberia. Biogeosci., 2015, **12** (11), 3321–3349.

126. Dallmeyer A., Claussen M., Fischer N., Haberkorn K., Wagner S., Pfeiffer M., Jin L., Khon V., Wang Y., Herzschuh U. The evolution of sub-monsoon systems in the Afro-Asian monsoon region during the Holocene – comparison of different transient climate model simulations. Clim. Past, 2015, **11**, 305–326.

127. Dallmeyer A., Claussen M., Ni J., Cao X., Wang Y., Fischer N., Pfeiffer M., Jin L., Khon V., Wagner S., Haberkorn K., Herzschuh U. Biome changes in Asia since the mid-Holocene – an analysis of different transient Earth system model simulations. Clim. Past, 2017, **13**, 107–134.

128. Demchenko P.F., Ginzburg A.S. Influence of feedbacks in the climate–energetics system on the intensity of an urban heat island. Izvestiya, Atmos. Oceanic Phys., 2018, **54** (4), 313-321.

129. Demchenko P.F., Semenov V.A. Estimation of uncertainty in surface air temperature climatic trends related to the internal dynamics of the atmosphere. Doklady Earth Sci., 2017, **476** (3), 339–342.

130. Denisov S.N., Eliseev A.V., Mokhov I.I., Arzhanov M.M. Model estimates of global and regional atmospheric methane emissions of wetland ecosystems. Izvestiya, Atmos. Oceanic Phys., 2015, **51** (5), 482–487.

131. Dymnikov V.P., Lykossov V.N., Volodin E.M. Mathematical simulation of Earth system dynamics. Izvestiya, Atmos. Oceanic Phys., 2015, **51** (3), 227–240.

132. Eliseev A.V. Influence of sulfur compounds on the terrestrial carbon cycle. Izvestiya, Atmos. Oceanic Phys., 2015, **51** (6), 599–608.

133. Eliseev A.V. Impact of tropospheric sulphate aerosols on the terrestrial carbon cycle. Glob. Planet. Change, 2015, **124**, 30–40.

134. Eliseev A.V. Global CO_2 cycle: Main processes and interactions with climate. Fund. Appl. Climatol., 2017, 4, 9–31. (in Russian)

135. Eliseev A.V. The methane cycle: A review. Fund. Appl. Climatol., 2018, 1, 52–70. (in Russian)

136. Eliseev A.V., Malakhova V.V., Arzhanov M.M., Golubeva E.N., Denisov S.N., Mokhov I.I. Changes in the boundaries of the permafrost layer and the methane hydrate stability zone on the Eurasian Arctic shelf, 1950–2100. Doklady Earth Sci., 2015, **465** (2), 1283–1288.

137. Eliseev A.V., Mokhov I.I., Chernokulsky A.V. The influence of lightning activity and anthropogenic factors on large-scale characteristics of natural fires. Izvestiya, Atmos. Oceanic Phys., 2017, **53** (1), 1–11.

138. Gavrilov A., Mukhin D., Loskutov E., Feigin A., Kurths J., Volodin E. Method for reconstraction nonlinear modes with adaptive structure from multidimensional data. Chaos, 2016, 26 (12), 123101, doi:10.1063/1.4968852.

139. Gulev S.K., Latif M. Ocean science: The origins of a climate oscillation. Nature, 2015, **521** (7553), 428–430.

140. Jennings R.P., Singarayer J., Stone E.J., Krebs-Kanzow U., Khon V., Nisancioglu K.H., Pfeiffer M., Zhang X., Parker A., Parton A., Groucutt H.S., White T.S., Drake N.A., Petraglia M.D. The greening of Arabia: Multiple opportunities for human occupation of the Arabian Peninsula during the Late Pleistocene inferred from an ensemble of climate model simulations. Quatern. Intern., 2015, **382**, 181–199.

141. Jin L., Schneider B., Park W., Latif M., Khon V., Zhang X. The spatial-temporal patterns of Asian summer monsoon precipitation in response to Holocene insolation change: a model-data synthesis. Quatern. Sci. Rev., 2014, **85**, 47–62.

142. Karol I.L., Kiselev A.A. Radiative and temperature indices (metrics) of modern anthropogenic climate changes. Proc. MGO, 2017, 587, 79–97. (in Russian)

143. Kattsov V.M., Pavlova T.V. Arctic in the context of the climate science “grand challenges”. Proc. MGO, 2015, 579, 66–78. (in Russian)

144. Khon V.C., Schneider B., Latif M., Park W., Wengel C. Evolution of eastern equatorial Pacific seasonal and interannual variability in response to orbital forcing during the Holocene and Eemian from model simulations. Geophys. Res. Lett., 2018, 45, 9843–9851.

145. Klimenko M.V., Bessarab F.S., Sukhodolov T.V., Klimenko V.V., Koren'kov Yu.N., Zakharenkova I.E., Chirik N.V., Vasil'ev P.A., Kulyamin D.V., Shmidt Kh., Funke B., Rozanov E.V. Ionospheric effects of the sudden stratospheric warming in 2009: Results of simulation with the first version of the EAGLE model. Russ. J. Phys. Chem. B, 2018, **12** (4), 760–770.

146. Koenigk T., Gao Y., Gastineau G., Keenlyside N., Nakamura T., Ogawa F., Orsolini Y., Semenov V., Suo L., Tian T., Wang T., Wettstein J.J., Yang S. Impact of Arctic sea ice variations on winter temperature anomalies in northern hemispheric land areas. Clim. Dyn., 2018, doi: 10.1007/s00382-018-4305-1.

147. Konovalov I. B., Beekmann M., Berezin E.V., Petetin H., Mielonen T., Kuznetsova I.N., Andreae M.O. The role of semi-volatile organic compounds in the mesoscale evolution of biomass burning aerosol: a modeling case study of the 2010 mega-fire event in Russia. Atmos. Chem. Phys., 2015, 15, 13269–13297.

148. Konovalov I.B., Berezin E.V., Beekmann M. Effect of photochemical self-action of carbon-containing aerosol: Naturally occurring fires. Izvestiya, Atmos. Oceanic Phys., 2016, **52** (3), 263–270.

149. Krupchatnikov V.N., Platov G.A., Golubeva E.N., Fomenko A.A., Klevtsova Y.Y., Lykosov V.N. Some results of studies in the area of numerical weather prediction and climate theory in Siberia. Russ. Meteorol. Hydrol., 2018, **43** (11), 713–721.

150. Kulyamin D.V., Dymnikov V.P. Modeling of the lower ionosphere climate. Izvestiya, Atmos. Oceanic Phys., 2015, **51** (3), 272–291.

151. Kulyamin D.V., Dymnikov V.P. Numerical modelling of coupled neutral atmospheric general circulation and ionosphere D region. Russ. J. Numer. An. Math. Modell., 2016, **31** (3), 159–171.

152. Kulyamin D.V., Volodin E.M. INM RAS coupled atmosphere-ionosphere general circulation model INMAIM (0–130 km). Russ. J. Numer. An. Math. Modell., 2018, **33** (6), 351–357.

153. Kurgansky M.V. On one estimate of the boundary of the Rossby regime zone in the atmosphere. Izvestiya, Atmos. Oceanic Phys., 2018, **54** (3), 257–264.

154. Latif M., Semenov V.A., Park W. Super El Niños in response to global warming in the Kiel climate model. Clim. Change, 2015, **132** (4), 489–500.

155. Malakhova V.V., Eliseev A.V. The role of heat transfer time scale in the evolution of the subsea permafrost and associated methane hydrates stability zone during glacial cycles. Glob. Planet. Change, 2017, **157**, 18–25.

156. Malakhova V.V., Eliseev A.V. Influence of rift zones and thermokarst lakes on the formation of subaqueous permafrost and the stability zone of methane hydrates of the Laptev Sea shelf in the Pleistocene. Led i Sneg (Ice and Snow), 2018, **58** (2), 231–242. (in Russian)

157. Matveeva T., Gushchina D., Dewitte B. The seasonal relationship between intraseasonal tropical variability and ENSO in CMIP5. Geosci. Model Develop., 2018, **11** (6), 2373–2392.

158. Meleshko V.P., Johannessen O.M., Baidin A.V., Pavlova T.V., Govorkova V.A. Arctic amplification: does it impact the polar jet stream? Tellus A – Dyn. Meteorol. Oceanogr., 2016, **68**, 32330. https://doi.org/10.3402/tellusa.v68.32330

159. Meleshko V.P., Kattsov V.M., Baidin A.V., Pavlova T.V., Govorkova V.A. Expected change of hydrologic cycle in Northern Eurasia due to disappearance of multi-year sea ice in the Arctic Ocean. Russ. Meteorol. Hydrol., 2016, **41** (11–12), 735–746.

160. Meleshko V.P., Kattsov V.M., Mirvis V.M., Baidin A.V., Pavlova T.V., Govorkova V.A. Is there a link between Arctic sea ice loss and increasing frequency of extremely cold winters in Eurasia and North America? Synthesis of current research. Russ. Meteorol. Hydrol., 2018, **43** (11), 743–755.

161. Meredith E.P., Semenov V.A., Maraun D., Park W., Chernokulsky A.V. Crucial role of Black Sea warming in amplifying the 2012 Krymsk precipitation extreme. Nature Geosci., 2015, 8, 615–620.

162. Mokhov I.I. Assessment of the ability of contemporary climate models to assess adequately the risk of possible regional anomalies and trends. Doklady Earth Sci., 2018, **479** (2), 482–485.

163. Mokhov I.I., Semenov A.I., Volodin E.M., Dembitskaya M.A. Changes of cooling near mesopause under global warming from observations and model simulations. Izvestiya, Atmos. Oceanic Phys., 2017, **53** (4), 383–391.

164. Mokhov I.I., Semenov V.A. Weather and climate anomalies in Russian regions related to global climate change. Russ. Meteorol. Hydrol., 2016, **41** (2), 84–92.

165. Mukhin D., Loskutov E., Mukhina A., Feigin A., Zalapin I., Ghil M. Predicting critical transitions in ENSO models. Part I: Methodology and simple models with memory. J. Clim., 2015, **28**, 1940–1961.

166. Mukhin D., Kondrashov D., Loskutov E., Gavrilov A., Feigin A., Ghil M. Predicting critical transitions in ENSO models. Part II: Methodology and simple models with memory. J. Clim., 2015, **28**, 1962–1976.

167. Muryshev K.E., Eliseev A.V., Mokhov I.I., Timazhev A.V. A lag between temperature and atmospheric CO2 concentration based on a simple coupled model of climate and the carbon cycle. Doklady Earth Sci., 2015, **463** (2), 863–867.

168. Muryshev K.E., Eliseev A.V., Mokhov I.I., Timazhev A.V. Lead-lag relationships between global mean temperature and the atmospheric CO2 content in dependence of the type and time scale of the forcing. Glob. Planet. Change, 2017, **148**, 29–41.

169. Nasonova O.N., Gusev Ye.M., Volodin E.M. et al. Application of the land surface model SWAP and global climate model INMCM4.0 for projecting runoff of Northern Russian rivers. 1. Historical simulations. Water Res., 2018, **45** (2), 73–84.

170. Privalsky V., Yushkov V. ENSO influence upon global temperature in nature and in CMIP5 simulations. Atmos. Sci. Lett., 2015, **16** (3), 240–245.

171. Petrov D.A. On the influence of fluctuations of coefficient linear feedback in a simple energy balance climate model on the frequency spectrum of averaged temperature. Izvestiya, Atmos. Oceanic Phys., 2017, **53** (5), 472–481.

172. Rybak O.O., Volodin E.M., Morozova P.A. Reconstruction of climate of the Eemian Interglacial using an Earth System Model. Part 1. Set–up of numerical experiments and model fields of surface air temperature and precipitation sums. Russ. Meteorol. Hydrol., 2018, **43** (6), 357–365.

173. Rybak O.O., Volodin E.M., Morozova P.A. Reconstruction of climate of the Eemian interglacial using an Earth system model. Part 2. The response of the Greenland ice sheet to climate change. Russ. Meteorol. Hydrol., 2018, **43** (6), 366–371.

174. Rybak O.O., Volodin E.M., Morozova P.A., Huybrechts P. Equilibrium state of the Greenland ice sheet in the Earth System Model. Russ. Meteorol. Hydrol., 2018, **43** (2), 63–71.

175. Segschneider J., Schneider B., Khon V. Climate and marine biogeochemistry during the Holocene from transient model simulations. Biogeosci., 2018, **15**, 3243–3266.

176. Semenov V.A. Oscillations of present-day climate associated with feedbacks in atmosphere-Arctic ice-ocean system. Fund. Appl. Climatol., 2015, 1, 232–248. (in Russian)

177. Semenov V.A. Link between anomalously cold winters in Russia and sea-ice decline in the Barents Sea. Izvestiya, Atmos. Oceanic Phys., 2016, **52** (3), 225–233.

178. Semenov V.A., Chernokulsky A.V., Solomina O.N. Influence of long-period oscillations on the development of droughts in Northern Eurasia. Doklady Earth Sci., 2016, **471** (1), 1217–1220.

179. Semenov V.A., Latif M. Nonlinear winter atmospheric circulation response to Arctic sea ice concentration anomalies for different periods during 1966–2012. Environ. Res. Lett., 2015, **10**, 054020, doi:10.1088/1748-9326/10/5/054020.

180. Semenov V.A. Martin T., Behrens L.K., Latif M., Astafieva E.S. Arctic sea ice area changes in CMIP3 and CMIP5 climate models' ensembles. Led I Sneg (Ice and Snow), 2017, **57** (1), 77–107. (in Russian)

181. Semmler T., Stulic L., Jung T., Tilinina N., Campos C., Gulev S., Koracin D. Seasonal atmospheric responses to reduced Arctic sea ice in an ensemble of coupled model simulations. J. Clim., 2016, **29** (16), 5893–5913.

182. Shkolnik I.M., Efimov S.V. A new generation regional climate model for northern Eurasia. Proc. MGO, 2015, 576, 201–211. (in Russian)

183. Alexandrov G.A., Brovkin V.A., Kleinen T. The influence of climate on peatland extent in Western Siberia since the Last Glacial Maximum. Sci. Rep., 2016, **6**, 24784, doi:10.1038/srep24784

184. Sporyshev P.V., Kattsov V.M., Gulev S.K. Changes in surface temperature in the Arctic: Accuracy of model reproduction and probabilistic prediction for the near future. Doklady Earth Sci., 2018, **479** (2), 503–506.

185. Varentsov M., Konstantinov P., Baklanov A., Esau I., Miles V., Davy R. Anthropogenic and natural drivers of a strong winter urban heat island in a typical Arctic city. Atmos. Chem. Phys., 2018, **18**, 17573–17587.

186. Vargin P.N., Kostrykin S.V., Volodin E.M. Analysis of simulation of stratosphere-troposphere dynamical coupling with the INM-CM5 climate model. Russ. Meteorol. Hydrol., 2018, **43** (11), 780–786.

187. Vargin P.N., Volodin E.M. Analysis of the reproduction of dynamic processes in the stratosphere using the climate model of the Institute of Numerical Mathematics, Russian Academy of Sciences. Izvestiya, Atmos. Oceanic Phys., 2016, **52** (1), 1–15.

188. Verbitsky M.Y., Crucifix M., Volobuev D.M. A theory of Pleistocene glacial rhythmicity. Earth Syst. Dyn., 2018, **9** (3), 1025–1043.

189. Vigasin A.A., Mokhov I.I. Greenhouse effect in planetary atmospheres caused by molecular symmetry breaking in intermolecular interactions. Izvestiya, Atmos. Oceanic Phys., 2017, **53** (2), 164–173.

190. Volodin E.M. Influence of methane sources in Northern Hemisphere high latitudes on the interhemispheric asymmetry of its atmospheric concentration and climate. Izvestiya, Atmos. Oceanic Phys., 2015, **51** (3), 251–258.

191. Volodin E. The nature of 60-year oscillations of the Arctic climate according to the data of the INM RAS climate model. Russ. J. Numer. Anal. Math. Modell., 2018, 33 (6), 359–366.

192. Volodin E., Gritsoun A. Simulation of observed climate changes in 1850–2014 with climate model INM-CM5. Earth Syst. Dyn., 2018, 9, 1235–1242.

193. Volodin E.M., Kostrykin S.V. The aerosol module in the INM RAS climate model. Russ. Meteorol. Hydrol., 2016, **41** (8), 519–528.

194. Volodin E.M., Mortikov E.V., Kostrykin S.V., Galin V.Y., Lykosov V.N., Gritsun A.S., Diansky N.A., Gusev A.V., Yakovlev N.G. Simulation of the modern climate using the INM-CM climate model. . Izvestiya, Atmos. Oceanic Phys., 2017, **53** (2), 142–155.

195. Volodin E.M., Mortikov E.V., Kostrykin S.V., Galin V.Y., Lykosov V.N., Gritsun A.S., Diansky N.A., Gusev A.V., Yakovlev N.G. Simulation of the present-day climate with the climate model INMCM5. Clim. Dyn., 2017, **49** (11–12), 3715–3734.

196. Volodin E.M., Mortikov E.V., Kostrykin S.V., Galin V.Y., Lykosov V.N., Gritsun A.S., Diansky N.A., Gusev A.V., Iakovlev N.G. Simulation of the modern climate using the INM-CM climate model. Russ. J. Numer. An. Math. Modell., 2018, **33** (6), 367–374.

197. Volodin E.M.,Tarasevich M.A. Simulation of climate and weather extreme indices with the INM-CM5 climate model. Russ. Meteorol. Hydrol., 2018, **43** (11), 756–762.

198. Volosciuk C., Maraun D., Semenov V.A., Tilinina N., Gulev S.K., Latif M. Rising Meditterranean sea surface temperatures amplify extreme summer precipitation in Central Europe. Nature Sci. Rep., 2016, **6**, 32450, doi:10.1038/srep32450.

199. Vorobyeva V.V., Volodin E.M. Investigation of the structure and predictability of the first mode of stratospheric variability based on the INM RAS climate model. Russ. Meteorol. Hydrol., 2018, **43** (11), 737–742.

200. Akperov M., Mokhov I., Rinke A., Dethloff K., Matthes H. Cyclones and their possible changes in the Arctic by the end of the twenty first century from regional climate model simulations. Theor. Appl. Climatol., 2015, **122** (1–2), 85–96.

201. Chernokulsky A.V., Kurgansky M.V., Mokhov I.I. Analysis of changes in tornadogenesis conditions over Northern Eurasia based on a simple index of atmospheric convective instability. Doklady Earth Sci., 2017, **477** (2), 1504–1509.

202. Dobrovolsky S.G., Tatarinovich E.V., Yushkov V.P. Runoff of major Russian rivers and its variability from the data of CMIP-5 climate models. Russ. Meteorol. Hydrol., 2016, 12, 44–62. (in Russian)

203. Eliseev A.V., Semenov V.A. Arctic climate changes in the 21st century: Ensemble model estimates accounting for realism in present-day climate simulation. Doklady Earth Sci., 2016, 471 (1), 1183–1187.

204. Dobrovolsky S.G. Incorporating natural changes in global climate in very-long-range forecasting of river runoff. Water Resources, 2018, **45** (4), 437–446.

205. Gelfan A.N., Kalugin A.S., Motovilov Y.G. Assessing Amur water regime variations in the XXI century with two methods used to specify climate projections in river runoff formation model. Water Resources, 2018, **45** (3), 307–317.

206. Kattsov V.M., Pavlova T.V. Expected Arctic surface air temperature changes through the 21st century: projections with ensembles of global climate models (CMIP5 and CMIP3). Proc. MGO, 2015, 579, 7–21. (in Russian)

207. Khon V.C., Mokhov I.I., Semenov V.A. Transit navigation through Northern Sea Route from satellite data and CMIP5 simulations. Environ. Res. Lett., 2017, **12** (2). 024010.

208. Kibanova O.V., Eliseev A.V., Mokhov I.I., Khon V.C. Variations in the duration of the navigation period along the Northern Sea Route in the 21st century based on simulations with an ensemble of climatic models: Bayesian estimates. Doklady Earth Sci., 2018, **481** (1), 907–911.

209. Kattsov V.M., Shkolnik I.M., Efimov S.V. Climate change projections in Russian regions: The detailing in physical and probability spaces. Russ. Meteorol. Hydrol., 2017, **42** (7), 452–460.

210. Mokhov I.I., Khon V.Ch. The duration of the navigation period and changes for the Northern Sea Route: model estimates. Arctic: Ecology and Economy, 2015, 2 (18), 88–95. (in Russian)

211. Mokhov I.I., Khon V.Ch., Prokof'eva M.A. New model estimates of changes in the duration of the navigation period for the Northern Sea Route in the 21st century. Doklady Earth Sci., 2016, **468** (2), 641–645.

212. Mokhov I.I., Timazhev A.V. Model assessment of possible changes of atmospheric blockings in the Northern Hemisphere under RCP scenarios of anthropogenic forcings. Doklady Earth Sci., 2015, **460** (1), 63–67.

213. Moreido V.M., Kalugin A.S. Assessing possible changes in Selenga River water regime in the XXI century based on a runoff formation model. Water Resources, 2017, **44** (3), 390–398.

214. Nasonova O.N., Gusev Ye.M., Volodin E.M. et al. Application of the land surface model SWAP and global climate model INMCM4.0 for projecting runoff of Northern Russian rivers. 2. Projections and their uncertainties. Water Res. 2018, **45** (2), 85–92.

215. Panin G.N., Diansky N.A., Solomonova I.V., Gusev A.V., Vyruchalkina T.Yu. Assessment of climatic changes in the Arctic in the 21st century based on the combined forecast. Arctic: Ecology and Economy, 2017, 2 (26), 35–52. (in Russian)

216. Pavlova T.V., Kattsov V.M. Expected Arctic precipitation and evaporation changes through the 21st century: projections with an ensemble of global climate models (CMIP5). Proc. MGO, 2015, 579, 22–36. (in Russian)

217. Shkolnik I., Pavlova T., Efimov S., Zhuravlev S. Future changes in peak river flows across northern Eurasia as inferred from an ensemble of regional climate projections under the IPCC RCP8.5 scenario. Climate Dyn., 2018, **50** (1–2), 215–230.

218. Akenteva E., M., Tyusov G.A. ClimPACT software usability for assessment of climate conditions impact on energy generation (in terms of thermal and nuclear power plants operation). Proc. MGO. 2015. Vol. 578. P. 86−100.

219. Bashmakov I.A. World energy: Myths of the past and lessons of the future. Voprosy Ekonomiki, 2018, 4, 49–75. (in Russian)

220. Bashmakov I. Economics of the constants" and long cycles of energy prices dynamics. Voprosy Ekonomiki, 2016, 7, 36–63. (in Russian)

221. Bashmakov I. Improving the energy efficiency of Russian buildings. Probl. Econ. Trans. 2016, **58** (11–12), 1096–1128.

222. Bedritskii A.I., Korshunov A.A., Shaimardanov M.Z. The Impact of severe hydrometeorological events on the sustainable development of the Russian economy. Russ. Meteorol. Hydrol., 2017, 7, 59–67. (in Russian)

223. Chen Y.Z., Mu S.J., Sun Zh.G., Gang C.C., Li J.L., Podarian J., Groisman P.Y., Chen J., Li S.W. Grassland carbon sequestration ability in China: A new perspective from terrestrial aridity zones. Rangeland Ecol. Manag., 2016, **69**, 84–94.

224. Bukvareva E., Grunewald K., Bobylev S., Zamolodchikov D., Zimenko A., Bastian O. The current state of knowledge of ecosystems and ecosystem services in Russia: A status report. AMBIO, 2015, **44** (6), 491–507.

225. Bukvareva E., Zamolodchikov D., Kraev G., Grunewald K., Narykov A. Supplied, demanded and consumed ecosystem services: prospects for national assessment in Russia. Ecological Indicators, 2017, 78, 351–360.

226. Fan P., Chen J., Ouyang Z., Groisman P., Loboda T., Gutman G., Prishchepov A., Kvashnina Anna., Messina J., Moore N., Myint S., Qi J. Urbanization and sustainability under transitional economies: A synthesis for Asian Russia. Environ. Res. Lett., 2018, **13**, 095007 https://doi.org/10.1088/1748–9326/aadbf8

227. Flato G., Ananicheva M., Antonov E., Atkinson D., Brown R., Hamilton L., Harwood L., Jia G., Kattsov V., Kivva K., Muir M., Outridge P., Overland J., Rong R., Steiner N., Stern G., Walsh J., Wang X. Regional drivers and projections of regional change. In: Adaptation Actions for a Changing Arctic: Perspectives from the Bering-Chukchi-Beaufort Region. AMAP. Oslo, Norway. 2017. P. 89–124.

228. Groisman P., Bulygina O., Henebry G, Speranskaya N., Shiklomanov A., Chen Y., Tchebakova N., Parfenova E., Tilinina N., Zolina O., Dufour A., Chen J., John R., Fan P., Mátyás C., Yesserkepova I., Kaipov I. Dry land belt of Northern Eurasia: Contemporary environmental changes and their consequences. Environ. Res. Lett**.,** 2018, **13**, 115008.

229. Gang C., Wang Z., Zhou W., Chen Y., Li J., Chen J., Qi J., Odeh I., Groisman P.Y. Assessing the spatiotemporal dynamic of global grassland water use efficiency in response to climate change from 2000 to 2013. J. Agron. Crop Sci., 2016, **202** (5), 343–354.

230. Genikhovich E., Gracheva I., Rumyantsev D., Yakovleva E., Kattsov V., Shkolnik I., Efimov S. Model estimation of the ecological loading sensitivity to climate changes over the territory of Russia. Proceedings of MGO. 2016. V. 583. P. 85–98. (in Russian)

231. Ginzburg A.S., Demchenko P.F. Air temperature and energy consumption feedbacks within urbanized areas. Izvestiya, Atmos. Oceanic Phys., 2017, **53** (5), 487–494.

232. Gauthier S., Kuuluvainen T., Shvidenko A.Z., Schepaschenko D.G. Boreal forests and global changes. Sustainable Forestry, 2016, 2 (48), 2–7. (in Russian)

233. Kattsov V.M., Porfiriev B.N. Adaptation of Russia to climate change: a concept of the national plan. Proc. MGO, 2017, 586, 7–20. (in Russian)

234. Khlebnikova E.I., Kattsov V.M., Pikaleva A.A., Shkolnik I.M. Assessment of climate change impacts on the economic development of the Russian Arctic in the 21st century. Russ. Meteorol. Hydrol., 2018, **43** (6), 347–356.

235. Khlebnikova E.I., Sall I.A. Cold temperature extremes in Russia and risks of critical temperature Impacts on infrastructure facilities. Russ. Meteorol. Hydrol., 2018, **43** (6), 372–378.

236. Klimenko V.V. Klimenko A.V., Tereshin A.G. Test of developing long-term forecasts of world energy impact on the earth's atmosphere. Izvestiya, Atmos. Oceanic Phys., 2015, **51** (2), 138–147.

237. Klimenko V.V., Fedotova E.V., Tereshin A.G. Vulnerability of the Russian power industry to the climate change. Energy, 2018, **142**, 1010–1022.

238. Klimenko V.V., Tereshin A.G., Kasilova E.V. Moscow: A natural testing area for strong warming impact assessment. Doklady Phys., 2017, **62** (11), 527–531.

239. Klimenko, V.V., Ginzburg A.S., Demchenko P.F., Tereshin A.G., Belova I.N., Kasilova E.V. Impact of urbanization and climate warming on energy consumption in large cities. Doklady Phys., 2016, **61** (10), 521–525.

240. Klimenko V.V., Mikushina O.V., Tereshin A.G. The 2015 Paris climate conference: A turning point in the world's energy history. Doklady Phys., 2016, **61** (6), 301–304.

241. Kobysheva N.V., Akentieva E.M., Galyuk L.P. Climatic Risks and Adaptation to the Climate Change and Variability in the Technical Field. St. Petersburg, Publ. House "Kirillitsa", 2015, 214 p. (in Russian)

242. Koroleva T.S., Konstantinov A.V., Shunkina E.A. Threats and socio-economic impacts of climate change for the forest sector. Proc. SPFRI, 2015, 3, 55–71. (in Russian)

243. Korzukhin M.D., Korotkov V.N. Modification of the ROBUL model for accounting the carbon balance of Russian forests. Fund. Appl. Climatol., 2018, 3 (3), 30–53. (in Russian)

244. Makarov I.A., Chen H., Paltsev S.V. Impacts of Paris Agreement on Russian economy. Questions of Economy, 2018, 4, 76–94 (in Russian).

245. Pavlova V.N., Varcheva S.E. Estimating the level of territory vulnerability and climate-related risk of significant grain crop failure in grain-producing regions of Russia. Russ. Meteorol. Hydrol., 2017, **42** (8), 510–517.

246. Porfiriev B.N., Voronina S.A., Semikashev V.V., Terentiev N.E., Eliseev D.O., Naumova Yu.V. Climate change impact on economic growth and specific sectors' development of the Russian Arctic. Arctic: Ecology and Economy. 2017, 4 (28), 4–16. (in Russian)

247. Qi J., Xin X., John R., Groisman P., Chen J. Understanding livestock production and sustainability of grassland ecosystems in the Asian dryland belt. Ecol. Proc., 2017, **6** (22), 10 pp., doi: 10.1186/s13717-017-0087-3.

248. Revich B.A., Shaposhnikov D.A., Podolnaya M.A., Khorkova T.L., Kvasha E.A. Heat waves in southern cities of European Russia as a risk factor for premature mortality. Stud. Russ. Econ. Develop., 2015, **26** (2), 142–150.

249. Revich B.A., Shaposhnikov D.A. Cold waves in southern cities of European Russia and premature mortality. Stud. Russ. Econ. Develop., 2016, **27** (2), 210–215.

250. Romanovskaya A.A. Needs and ways to develop adaptation monitoring. Problems of Ecological Monitoring and Ecosystem Modelling, 2018, **XXIX** (1), 107–126. (in Russian)

251. Shaposhnikov D., Revich B. Toward meta-analysis of impacts of heat and cold waves on mortality in Russian North. Urban Clim., 2016, **15**, 16–24.

252. Shartova N., Shaposhnikov D., Konstantinov P., Revich B. Cardiovascular mortality during heat waves in temperate climate: an association with bioclimatic indices. Intern. J. Environ. Health Res., 2018, **28** (5), 522–534.

253. Shkolnik I.M. Projected climate change impacts on the operation of power engineering facilities in Russia. Russ. Meteorol. Hydrol., 2017, **42** (12), 775–782.

254. Sinyak Y.V. Impact of climate risks on the development rate and pattern of the Russian fuel and energy complex in the first half of thew XXI century. The Energy Policy, 2016, 3, 31–42. (in Russian)

255. Soja A., Groisman P.Y. Earth science and the integral climatic and socio-economic drivers of change across northern Eurasia: The NEESPI legacy and future direction. Environ. Res. Lett. 2018, **13**, 040401, doi: 10.1088/1748-99326/aab834

256. Soldatenko S.A. Weather and climate manipulation as an optimal control for adaptive dynamical systems. Complexity, 2017, 4615072, doi: 10.1155/2017/4615072

257. Soldatenko S.A., Yusupov R.M. Optimal control of aerosol emissions into the stratosphere to stabilize the Earth's climate. Izvestiya, Atmos. Oceanic Phys., 2018, **54** (1), 480–486.

258. Soldatenko S.A. Estimating the impact of artificially injected stratospheric aerosols on the global mean surface temperature in the 21th century. Clim., 2018, **6** (4), 85, doi:10.3390/cli6040085.

259. Soldatenko S.A., Alekseev G.V., Ivanov N.E., Vyazilova A.E., Kharlanenkova N.E. On climate risk assessment and vulnerability of natural and economic systems in the marine Arctic zone of the Russian Federation. Problems of the Arctic and Antarctic. 2018. T. 64. № 1. S. 55–70. (in Russian)

260. Surkova G.V., Krylov A.A. Changes in the hydrothermal climatic resources of the Arctic against the background of the warming of the 21st century. Arctic and Antarctic, 2017, 1, 47–61. (in Russian)

261. Trunov A.A. Deforestation in Russia and its contribution to the anthropogenic emission of carbon dioxide in 1990–2013. Russ. Meteorol. Hydrol., 2017, **42** (8), 529–537.

262. Tyusov G.A., Akentyeva E.M., Pavlova T.V., Shkolnik I.M. Projected climate change impacts on the operation of power engineering facilities in Russia. Russ. Meteorol. Hydrol., 2017, **42** (12), 775–782.

Clouds and Precipitation

N.A. Bezrukova[1], *A.V. Chernokulsky*[2]
[1] Central Aerological Observatory
bezrukova@cao-rhms.ru
[2] A.M. Obukhov Institute of Atmospheric Physics RAS
a.chernokulsky@ifaran.ru

Cloud physics. General cloud characteristics

Observation and investigation of different cloud types by different methods. Climatological issues of clouds and precipitation

The year 2017 marked a centenary of the first Russian atlas of clouds [1]. The Atlas was compiled by V.V. Kuznetsov and published at the then Main Physical Observatory (Main Geophysical Observatory at present). It included 50 color photos of basic cloud types, with 3 of them taken from a balloon, which was then quite an achievement. The explanatory text was accompanied by a morphological classification of clouds that included 5 classes (upper, middle, low, and daytime updraft clouds, and elevated fog). This atlas largely contributed to the knowledge of clouds and their morphological classification. It was of great use to observation activities. Later, the atlas was republished several times.

Clouds play an important role in climate formation and, at the same time, are an uncertainty factor in the current theoretical and numerical models. The main reason for that is the complicacy of cloud cover formation. The way clouds form, develop, and turn into thunderstorm clouds with hail, lightning is a kind of mystery that has remained unraveled for centuries. That is why popular science publications devoted to this enigma attract public attention. Increasingly more people become interested in the problem of climate change and processes in the atmosphere and clouds. Scientists, in their turn, strive to supply curious readers with most complete state-of-the-art information [2–3].

The general global estimates of the characteristics of clouds, which play a significant, but still insufficiently appreciated role in the formation of climate and tendencies of its changing, are also of interest to other fields of knowledge. Particularly, the studies [4–16] focus on cloud climatology and variability at global and regional scales.

A theoretical three-parameter bounded distribution for characterizing the probability density distributions of fractional total and low cloud cover over the global oceans is suggested [4].Both a continuous form of this distribution and its discrete counterpart were derived, which can be directly applied to cloud

cover reports. The distribution is applied to the cloud cover characteristics for the period 1950–2011, reported by voluntary observing ships, after filtering nighttime observations with poor lunar illumination. The suggested distribution demonstrates a high goodness of fit to the data and good skill in capturing probability distributions with different shapes. Seasonal climatologies of the distribution parameters are presented.

Climatologies of daytime and nighttime cloudiness based on various satellite data (AIRS-LMD, CERES, MODIS, CALIPSO-GOCCP, PATMOS-x) and surface observations are analyzed and compared [5] for the period 2003–2006. It was found that day-time cloudiness prevails over land and over the entire Northern Hemisphere, while night-time cloudiness prevails over the ocean and over the Southern Hemisphere.Moreover,the difference between cloudiness over land and over the ocean (and, consequently, over both hemispheres) is higher in the nighttime. A disagreement among the data is noted over the vast equatorial and high-mountain regions in Eurasia, Africa, South America, Australia, North Pacific and North Atlantic. It was shown that the time of observationscan affect the estimate of total cloudiness. Though, only day-time measurements lead to overestimation of cloudiness over land and underestimation over the ocean.

In [6–8], a vertical structure of the cloud field is evaluated. In [6], the cloud overlap parameter α was estimated, using remote sensing data. This parameter is a measure of the relative weight of maximum ($\alpha = 1$) and random ($\alpha = 0$) overlap, and can be used to diagnose the relative contribution of convective and stratiform cloudiness to the total cloud fraction. The parameter was calculated given MODIS and CERES data for the total cloud fraction and CALIPSO data for the vertical structure for 2007–2010 years. The global annual mean α is 0.36 (for CERES) and 0.26 (for MODIS), which points to the dominance of a random overlap. A maximum cloud overlap occurs in subtropical highs over the ocean and in subtropical and polar deserts over land. A random cloud overlap occurs in regions with large values of cloud fraction (e.g., ITCZ and midlatitudinal storm tracks). Midlatitude oceanic lows are characterized by negative values of α, mostly in summer. Presumably, an assumption of a minimum overlap of cloud layers should be used in these regions due to the strong baroclinic instability and horizontal shift of cloud layers.

During the period reported, the relevant studies were fulfilled [7] long-term estimates of the characteristics of vertical cloud layer distribution were obtained, which were calculated from atmospheric radio sounding measurements of humidity and temperature [7]. Using the global upper-air dataset CARDS (Comprehensive Aerolpgical Reference Dataset) for the period 1964–1998 for Russia, calculated were estimates for the parameters of temperature – humidity

stratification of the atmosphere from the ground up to 10 km revealing cloud layers and cloudless ones between them. It was shown that such stratification is characteristic of the 0-10 km layer considered. The average total thickness of all the cloud layers changes between 1200 and 3100 m. Separate cloud layers are 2-5 times as thin as cloudless ones, which is equally true of a 6-km and 1-km layer. The conclusions obtained, on the whole, confirm the previous estimates based on the data of 1957–1963 aircraft soundings (by L.S. Dubrovina, 1982). To specify the characteristic features of atmospheric stratification in space and time, geographic distributions of the mean values and root-mean-square deviations from the above parameters in January and July for a long-term period were constructed, and the amplitude of their changes was determined. The same authors did a similar work for the period 1964–2014 [8]. To specify the peculiarities of atmospheric stratification in space and time into cloud layers and cloudless ones between the clouds, mean monthly, seasonal, and annual values of the number of cloud layers as well as their root-mean-square deviations were calculated, and the amplitude of their changes determined.

The studies [9–16] are devoted to estimates of a regional climatology ofcloudiness (total, low, different morphological types). Cloud changes over Moscow Region [12] and Siberian regions [13–16] are thoroughly evaluated.

In [9], for the first time, a long-term climatology of cloudiness is presented for the Norwegian, Barents, and Kara Seas (NBK), based on visual surface observations from the end of the 19th century. A decrease of total cloud cover in the middle of the twentieth century and an increase in the last few decades were found at individual stations and for the NBK as a whole. In most cases, these changes are statistically significant, with the magnitudes exceeding the data uncertainty. The most pronounced trends are observed in autumn, when the largest changes in thesea ice concentration (SIC) occur. A significant long-term negative correlation between the cloud cover and SIC is revealed. An overall increase in the frequency of broken and scattered cloud conditions and a decrease in the frequency of overcast and cloudless conditions are found over open-water areas. These changes are statistically significant and likely to be connected with the long-term changes of the morphological types (an increase ofconvective and a decrease of stratiform cloud amounts).

In [10], the climatology of the total cloud cover over the Black, Caspian, and Aral Seas is evaluated based on surface and satellite observations as well asdata fromreanalysis. The differences among datasets are discussed and evaluated. Long-term meansand trends are established for surface observations. Particularly, a statistically significant positive trend is revealed for autumn.Opposite findings are obtained for the Black Sea, based on 1985–2009 satellite data for the area[11]. Specifically, adecrease of cloud amount isrecord-

ed.Additionally, the authors of the paper [11]found stronglypronounced four-year cycles and variations in antiphase with sea surfacetemperature.

Besides solving direct problems of atmospheric optics, of great importance is solving its inverse problems that would permit deriving atmospheric characteristics from instrumental measurements of standard meteorological parameters. Different forms and types of clouds have both specific and common features as concerns their optical thickness. Using the features such as "transparent – semitransparent – opaque", each cloud type can be described by its own specific influence on the intensity of solar radiation incident on the earth surface. The paper [17] proposes an approach to parameterization of cloud forms and types based on the analysis of their influence on the values of direct and scattered radiation.

Paper [18] based on radio sounding data discusses the main laws of space-time distribution of the total atmospheric moisture content over the territory of Eastern Siberia, depending on the season as well as on physiographic and circulation conditions. Estimates of the total moisture content in the atmosphere are obtained using the data of a large number of stations for a long observation period (10 years), up to 30 km, with high vertical resolution in the atmospheric boundary layer.

The GPS system using networks of dual-frequency receivers is largely employed during the last years in solving problems of sounding the ionosphere and troposphere. Of special interest is the estimation of atmospheric moisture content, which is important for the improvement of weather forecasts. Theintegral moisture content of the atmosphere is also analyzed in [19] using measurements of a phase delay of signals from the GPS satellites. Demonstrated are the results of the method operation, using the data of the North American network of the GPS receivers SOPAC. The accuracy of the method operation is assessed by comparing the obtained results with the data from the global and regional re-analyses.

The worsening of the weather and lowering of the lower cloud boundary affect the characteristics of a horizontal visibility range and vertical visibility. Estimation of the occurrence of such conditions is especially important for defining climatic conditions at airports. Suchestimation was carried out [20] based on the data from 41 airports in the Asian part of Russia and the neighboring countrieswere calculated from the data of airport observations for the period 2001–2014. Mean annual, seasonal and monthly distributions of the occurrences of different visibility values, as well as those depending on weather characteristics, were obtained for ≤ 300 m and ≤ 800 m. The above results were obtained for the territory considered for the first time ever. Datasets of airport observations for 2001–2014 were used. Lowvisibility at airports over the terri-

tory concerned is quite a rare phenomenon which continues for no longer than 2 hours in 60–90 % of all cases. Generally, meteorological visibility range in ≤ 50 m and 50–100 m gradations is associatedwiththe lower cloud boundary height < 90 m. However, even with these gradations of the lower cloud boundaryheight, the frequency of low meteorological visibility does not appear high. For most airports, threshold relative humidity values can be indicated; a decreased visibility never occurs at relative humidity values below this threshold. Thus, for meteorological visibility range ≤ 300 m, threshold values are most often 70–80%. In more than 50 % of all cases, a decreased visibility is associated with still conditions, low winds of varying directions, or wind speeds of 2–6 m/s.

The studies described in [21–60] focus on precipitation climatology and variability as well on the causes of the variability and changesobserved.

In [21–23], a probability distribution for extreme precipitation is proposed. An asymptotic model is proposed for distributing a maximal daily rainfall rate during wet periods given a negative binomial distribution of the duration of wet periods. The model has the form of a combination of Frechet distributions andcoincideswith the distribution of a positive degree of a random variable having Fisher–Snedecor distribution.Several methods are proposed for the estimation of the distribution parameters.The results of fitting this distribution to real data are presented, illustrating a high validity of the proposed model.

The variability of precipitation and evaporation over the ocean is estimated based on satellite data for the period 1988–2008 [24]. Moisture-exchange components for the entire World Ocean and for the North Atlantic Ocean within 30–60° N are calculated. Systematic errors in moisture-exchange components are revealed.

A method for discriminating among different types of precipitation is presented [25]. The method is based on surface observations of precipitation, the present and past weather, and morphological cloud types. The climatology of showery, non-showery, and drizzle precipitation in northern Eurasia is studied using the data of 529 Russian weather stations for the period 1966–2014. It is shown that showery precipitation prevails in northern Eurasia and, generally, demonstrates a higher temporal (monthly and diurnal) and spatial variability than non-showery precipitation,as does its intensity as well. The majority of showers are recorded in summer, whereas the largest monthly non-showery precipitation total is observed in autumn [25].

The studies presented in [26–31] focus on extreme precipitation characteristics and their changes. In [31], long-term changes in some characteristics of extreme precipitation in Russia in 1966–2012 are analyzed using daily data from rain gauges. Linear trends in the characteristics of absolute and relative

extremes as well as in the duration of wet and dry spells are found and quantified, using new and more robust metrics. In general, an increased intensity of extreme precipitation is observed in Russia, which may result in a growing risk of flooding. Simultaneously, a tendency of dry period lengthening is also revealed. This implies an increase in the probability of droughts. Hence, the frequencies of hazardous hydrological phenomena associated with both water excess and scarcity have increased substantially in recent decades [31]. Positive long-term trends in heavy precipitation events are also established in [27] where 99.9-percentile is assessed forstations in the European part of Russia, and in [28–29] where the concentration index is analyzed for the southern part of Russia. In [30], the features of extreme precipitation over the Antarctic station "Progress" are analyzed, with thorough evaluation of its causes (thermodynamic and dynamic). It was found that thermodynamic (non-circulation) processes account for 80% of the trend in extreme precipitation.

Frozen precipitation and icing conditions over northern midlatitudes as well as theirchanges during the last four decades are analyzed in [32–34]. It was found [32] that hoar frosts are observed in most parts of Russia, but icing only occurs in the European Russia and the Far East. On the Arctic coast of Russia, this phenomenon can even be observed in summer months. Statistically significant decreasing trends in the occurrence of icing and hoar frost events are found over most of Russia. An increasing trend in icing weights was found in the Atlantic Arctic region in autumn. Statistically significant negative trends in icing weights were found in the Pacific Arctic in winter and spring. In [33], the climatology and trends of daily freezing rain and freezing drizzle occurrences are analyzed for Russia, the United States, Canada, and Norway Regions with the highest frequency of freezing rains (from 3 to 8 days per year) were found in the northeastern quadrant of the conterminous United States and adjacent areas of southeastern Canada south of 50 °N and over the south and southwest parts of the Great East European Plain. The frequency of freezing drizzle exceeds the frequency of freezing rainin allthe areas. During the past decade, the frequency of freezing rain events somewhat decreased over the southeastern US, whilein North America, north of the Arctic Circle, it increased (1 day per year). Over Norway, freezing rain occurrences increased substantially, especially in the Norwegian Arctic. In the European Russia and Western Siberia, the frequency of freezing rain somewhat increased (except the southernmost steppe and arctic regions), while freezing drizzle frequency decreased over entire Russia [33].

Regional climatologies of precipitation as well its contemporary and projected changes are estimated in [35–45]. Particularly, in [45] projections of arctic precipitation in the 21st century are analyzed using an ensemble of CMIP5 climate models for three scenarios of radiative forcing (RCP2.6, RCP4.5 and

RCP8.5). Ageneral increase of arctic precipitation (up to 50%) is projected. A more aggressive scenario (RCP8.5) and more sensitive models (which showahigher increase of temperature) generally display a larger precipitation increase. In [44], large-scale indicators of intensive precipitation (aspecific pattern of pressure field andfrontal zone presence) for the coastal regions of the European sector of the Arctic and the Caucasus Black Sea coast are identified. It is demonstrated that in the 21st century, the frequency of conditions accompanying extreme precipitation events of afrontal origin will increase on the southern coast of the European part of Russia in summer and on the Arctic coast during the cold season [44].

The causes of precipitation changes and variability are evaluated and discussed in [46–60]. In [52], statistical relationships between precipitation and vector frontogenesis are estimated using the data of an objective analysis and observations at the stations in Europe and thewestofCentral Asia for 2005–2013. It is found that the vector of frontogenesis is a third important factor of precipitation generation following convective instability and atmospheric fronts. Rotational frontogenesis is the most efficient one among the vector frontogenesis characteristics for the discrimination between the cases of precipitation occurrence and non-occurrence (especially for heavy and very heavy precipitation) [52].

The urban influence on precipitation is evaluated in [58] on the example of the city of Moscow. High-resolution (1 km) numerical simulations for several summers were conducted using amesoscale atmospheric model with and withoutanurban canopy model. Urban-derived precipitation enhancement was revealed. Particularly, an increase in summer precipitation up to +25% over the city center and its leeward side was found when the urban canopy model was included into the mesoscale model.

In [53, 60], the role of theBlack and the Mediterranean Seawarming in amplifying precipitation extremes was highlighted and thoroughly evaluated based on ensemble sensitivity simulations with a global circulation model (1.53) or a convection-permitting atmospheric model [53]. In particular, it was establishedthat the warming of the Black Sea playeda crucial role inenhancing the Krymsk event of July, 2012 [53]. It was found that the enhancement of lower tropospheric instability due to the currentlywarmer Black Sea allows deep convection to be triggered, thusincreasing simulated precipitation by more than 300% relative to simulations with theSSTs characteristic of the early 1980s. A highly nonlinear precipitation response to the incremental SST increase suggests that the Black Sea has exceeded a regional threshold ofthe intensification of convective extremes.

Convection, convective cloud characteristics, and cloud water content

Convective processes and convective clouds, when sufficiently developed, are related with numerous hazardous weather phenomena. Convective clouds commonly receive great attention. Considering the local peculiarities of convection development, it is quite evident that apart from studying the common properties of convective processes, this mesoscale phenomenon has to be investigated on a regional scale as well. The obtained regional quantitative characteristics connected with local features are used to allow for convection in regional models and forecast regional weather hazards. The results of such investigations are applied to the development of specific forecasts for every branch of national economy, particularly, for aviation, transport, and power economy.

Publication [61] is devoted to the theory of convective jets and thermiques; the paper pays attention to their sources. The author points out that in traditional models of convection from isolated sources the results depend but little on the size of the sources – convective jets and thermiques "forget" the geometry of the sources quite soon. But, lately, some new problems have become topical, which address relatively large sources that may influence the results. The paper considers some generalizations of well-known integral models of jets and thermiques. Although these simplified patterns cannot compete with sophisticated numerical models in describing the spatial structure of flows, they are shown to satisfactorily retrieve most important numerical results (height, the time of assent of convective elements) and besides, make it possible to reveal evident physical laws and determine apparent dependences on the problem parameters.

In [62], a modeling study of an upward thermiquewas fulfilled. To calculate the parameters of an upward thermique, Pristly stability criterion was used. In the model, a critical size and height of the thermique ascent was calculated for given values of overheating at the earth surface, of the initial speed of ascent, and vertical temperature gradient. Reports from the International Science Conference "Innovation methods and means of investigation in the field of atmospheric physics, hydrometeorology, ecology, and climate change"aredevoted to the investigation of the influence of air speed divergence on the character of thermal convection [63] and to the practical work of calculating the parameters of cloud convection at the convection level, i.e., at the peak of convective process development [64].

Studies [65–73]are devoted to the investigation of the development of cumulonimbus and thunderstorm hail clouds, including the analysis of several case studies considered in a series of publications [65–67].

To reveal the relations between the characteristics of electric discharges and cumulonimbus cloud parameters in the course of the cloud development in

North Caucasus, the results of simultaneous radar, radiometer, and radio direction finding measurements are analyzed in [65]. The dependence of cloud electric activity on radar characteristics as well as on the characteristics obtained from the measurements using SEVIRI radiometer mounted on "Meteosat" platform is discussed. Electric discharges (inside clouds and outside lightning) were recorded during 1 h 40 min., with their maximal frequency of 448 discharges per minute. Also revealed are the relations between electric discharge characteristics, precipitation intensity, and the field of cloud radiation temperature. It is established that the frequency of discharges increases with increasing precipitation intensity and reaches its maximum at precipitation intensity of 70 mm/h. The authors constructed normalized autocorrelation functions of the field of radiation temperature development. A close correlation between the scale of the inhomogeneity of cloud radiation temperature field and the frequency of electric discharges was established.

In [66], the results of analyzing the data of thick thunderstorm hail cloud observations using the radar MRL-5 and thunderstorm finding system LS8000 are presented. The characteristics of cloud electric state obtained with the system LS8000 as well as their relation with radar cloud parameters and indirect electric cloud state criteria calculated on their basis are presented. The potentials of thunderstorm forecast by different thermodynamic hazard criteria are investigated. A close relation between the total lightning current in a low-frequency range and lightning frequency in low-frequency and very-high-frequency ranges is established. The total charge delivered by negative lightning discharges from a given cloud to the ground is calculated to be 387 Кл, with the mean charge value per lightning of – 0.44 Kl. Regression equations relating the radar criteria of thunderstorm hazard with lightning frequency are presented

In [67], in order to study the thunderstorm hail cloud that developed over Pyatigorsk on 29 May 2012 and caused extremely great hail damage, a 3D nonstationary convective cloud model is used. The values of cloud characteristics such as moisture and ice content as well as the speed of vertical movements, etc. are determined. The importance of wind changes with height to be allowed for is pointed out. The modeling results (for the calculation area of 20x20x80 km) are used to analyze the transformation of precipitation field and its charge structure during cloud development (unfortunately, the results of precipitation intensity calculation largely differ from the observed values). The modeling results led the authors to conclude that the 3D model constructed by the Main Geophysical Observatory with participation of the Central Aerological Observatory is an important tool to investigate the laws of moisture transformation in a cloud, especially under deep convection conditions, when the cloud repre-

sents a three-phase system. The development of such clouds is observed to result in the occurrence of hazardous weather phenomena such as shower rains, thunderstorms, hail, and squalls. Model calculations testify to the existence of an interrelation between the dynamic, microphysical, and electric cloud characteristics.

Investigations such as presented in papers [68–70] are also devoted to this direction. The latter publication discusses the results of studying the changes of cloud characteristics during their merging observed in St.Petersburg environs.14 cloud merging events during the warm periods of 2015 and 2016 were selected and analyzed. As a result, it was pointed out that the process of cloud merging leads to an increase of medians in the distribution of the following characteristics: the height of the of the upper cloud boundary, the height of maximal reflectivity, maximal reflectivity in an atmospheric column, maximal intensity of precipitation and precipitation flow, as well as to a decrease of cloud area.

Paper [71] studies the influence of the merging of convective clouds on their evolution, using a numerical non-stationary 3D model of a convective cloud with parameterized microphysics. Convective cloud evolution over India on 12.10.2015 is considered, and characteristics are presented for: 1. the evolution of a single cloud; 2. the evolution of two merging clouds. The results of the calculation indicate that the merging process significantly influences the evolution of the cloud formed upon the merging of separate clouds. In this cloud, the speed of an updraft, moisture content, and precipitation intensity increase, in contrast with a single cloud, which confirms the fact that the process of cloud merging leads to enhanced cloud convection and precipitation formation.

The work in this direction was described and generalized in the monograph “Cloud merging” [72].

Radar studies of the formation and development of hail cells in thick convective clouds were fulfilled [73]. They consisted in the accumulation of data on hail clouds through continuous radar observations for many hours. Examined were 314 hail cells, and time distributions of basic radar parameters were determined for each of them. The most informative time characteristics of the development of hail cells and the relation between them were singled out. Changes in the natural variability of hail cell volume were shown. An empirical dependence of a maximal hail cell volume on a maximal radar reflectivity of a hail cloud was obtained.

Convective clouds are responsible for atmospheric pressure variations and generate internal gravity waves. In [74], based on experimental data, a relationship between thunderstorm-related variations in atmospheric pressure at the land surface and those in tropospheric temperature was found. The propagation of internal gravity waves caused by atmospheric heating due to water-vapor

condensation during the formation of a convective cloud is simulated. The simulations show that the lifetime of these internal gravity waves may significantly exceed the lifetime of the cloud. The form of the disturbance of atmospheric pressure below a convective cloud is a sequence of minimal and maximal pressure variations with the maxima amplitude exceeding that of the minima.

Turbulence in convective clouds is studied in [75–77].

Paper [75] presents the results of the analysis of spectral turbulence characteristics (spectra and co-spectra) and moisture content parameters of convective clouds in a tropical zone, which were obtained in a complex aircraft experiment in Cuba. The co-spectra for vertical heat fluxes permit classifying convective clouds by stages of their and revealing the stages of cloud growth, stabilization and dissipation. The magnitude of cloud overheating relative to the ambient air is a parameter that determines the stage of cloud development. Interrelation between the integral characteristics of turbulence and moisture content (the mean values and functions of parameters) for different stages of convective cloud development is revealed. Recommendations for the application of data on the structure of air movements in intended weather modification are formulated, and a method of instrumental estimation of cloud suitability for intended modification aimed at precipitation enhancement is proposed.

In [76, 77], the role of turbulence in thunderstorm electrification isevaluatedfor the first time. A model of large-scale electric field generation in a weakly conducting medium containing two fractions of colliding hydrometeors is used. The calculation results are compared with experimental data. It is found that scenarios of electric-field generation and growth for inductive and non-inductive charging mechanisms are significantly different. The range of thundercloud parameters (conductivity and particle radii) for which the electric field grows exponentially in the case of inductive charging isestablished.

Paper [78] presents an overview of the laboratory studies of the mechanisms of electrifying cloud particles and precipitation in cumulonimbus clouds. The processes of charging graupel and hail are discussed: 1) upon their collision with cloud crystals and 2) upon supercooled drop destruction over the surface as a result of their bursting or spraying. The way these mechanisms act at different development phases is described. A pattern of particle charging parameterization for numerical simulation of cloud electrification is proposed. An electric field of convective clouds is also evaluated in [79, 80].

Regional peculiarities of convection development from the tropics to the Arctic are considered in many studies [81–110].

Particularly, in [81], the authors investigate the characteristics of deepconvective clouds in the tropical zone, using model downward transport and mixing of stratospheric air with air from the upper troposphere, which was ob-

served in a system with deep convection in a research flight during the SCOUT-O3 campaign. The WRF-ARW model with horizontal resolution of 333 m is used in order to study the downward transport. Simulation reproduces the system with deep convection, its timing, and height overshooting reasonably well as compared with radar and aircraft data. It is shown that passive tracers initialized at pre-storm times indicate a downward air transport from the stratosphere to the upper troposphere as well as an upward transport from the boundary layer into cloud anvils and overshooting tops.

Convective cloud development during cold-air outbreaks is studied in [82, 83].

In [82], a typical case of winter cold-air outbreak in the Black Sea region on 25 January 2010 is investigated based on the WRF numerical model simulations and satellite data on cloudiness, cloud top temperature, and specific humidity. According to both the modeling results and satellite data, a mixed convection over the sea occurred, but with the prevalence of cells playing the main part in the mixing in the atmospheric boundary layer. The model reproduces well the observed increase at the cloud top height over the sea with the distance from the coast and the horizontal size of cloud structures near the shore, which increased downwind. The main components of the convective kinetic energy balance in the atmospheric boundary layer are considered: energy generation due to pressure pulsations and the work of the buoyancy force, as well as energy decrease due to turbulent diffusion and convective advection. It is demonstrated how these quantities varied with height and the distance from the shore.

In [83], convective cloudiness in the Atlantic sector of the Arctic is considered as an atmospheric spatially self-organized convective field. Convective cloud development follows cold-air outbreaks into the areas with relatively warm surface. As a result, the physical and morphological characteristics of clouds, such as the type of convective clouds and their geographical localization, are interrelated. It is shown that marginal sea ice and coastal zones are the most frequently occupied by Cu hum and Cu med convective clouds which are organized in convective rolls. Simultaneously, open-water marine areas are occupied by Cu cong and Cb clouds which are organized in convective cells. Thus, the retreat of the sea-ice boundary may lead to an increase in the amount of convective clouds. An intercomparison of cloud statistics using the ISCCP satellite data and ground-based observations revealed inconsistency in the cloudiness trends in these data sources: convective cloudiness decreases in the ISCCP data and increases in the ground-based observation data.

Over northern Eurasia regions, regionally-focused studies mostly investigate hazardous weather events that are associated with atmospheric convective processes [84–110]. A variety of convective phenomena are investigated, discussed and reviewed: thunderstorms in [84, 85, 90, 93, 107, 110], squalls in

[84, 103, 104], tornadoes in [87, 88, 95–97, 100–102, 105, 108], and convective clusters in [86, 89, 98, 106, 109] that are associated with various events. In a number of papers, particular attention is paid to indices of convective instability that can adequately describe hazard and formation conditions of convective events [87, 91, 92, 99, 101].

A review of the state-of-the-art of squall studies is presented in [104] which analyzed squall formation conditions, diagnosing and forecasting, the current knowledge of the phenomenon, methods of its investigation and recording. Squalls are hazardous hydro-meteorological phenomena developing due to mesoscale atmospheric convection. Their influence is short-time, and they are local in space. Therefore, they are hard to record in real time by standard means, with the exception of using data from observational radar networks. With separately located radars, the event is often recorded upon its termination based on space remote sounding data. The accuracy of squall forecasting with the flowly available techniques is still insufficient, and there are practically no methods to predict catastrophic squalls. That is why squalls continue to be the subject of investigation all over the world. The development and upgrading of methods to predict squalls are under way.

In paper [99], peculiar features of strong convection development in the atmosphere of Western Siberia are investigated. Threshold values of a number of convective instability indices, with which major convective phenomena, such as thunderstorm, hail, and squall, form in the atmosphere of Western Siberia,are determined.In [91], the feasibility of using MODIS spectroradiometer database for the determination of atmospheric convective indices over Western Siberia is considered. Three indices computed from the satellite and radiosondedata are compared as instability characteristics. It is revealed that two indices, namely, LIFT and TOTL, correlate well. It is demonstrated that the results of MODIS sounding enable identifying the spatial position of deep convective cells and specifying short-term thunderstormforecast.

In [89], various data is used to diagnose a rare case of supercell transition to mesoscale convective cluster on 13 July 2016. The convective cluster moved through Belarus and the European part of Russia and brought about a variety of hazardous convective events, including thunderstorms, hail, squalls, and tornadoes. Different data sources were used to diagnose the cluster (satellite, radar, lightning location network, global forecast model). A possibility of finding a special signature of the cluster (‘hook echo’ from radar data, Cold-U/V signatures from satellite data) aimed at forecast improvement is discussed.

A technology of monitoring hazardous tornado(waterspout) situations was developed for the Black Sea area [95] aiming at weather data accumulation in an archive for the Black Sea water and coastal areas, with its subsequent usein de-

veloping a methodology of forecasting waterspouts in the region with its specific climate. The composition of data in the archive is similar to that in foreign archives. This technology is employed to display weather observations in real-time. The characteristics of waterspouts for the period 2014–2015 over the Black Sea are studied [96]. A so-called 'waterspout risk index' for the Black Sea coast is presented in [97]. The index is based on an empirically-derived combination of predictors including temperature differences between the surface and several atmospheric layers (1, 2, and 3 km), vertical vorticity potential (for different low-level layers), relative humidity, and wind shear (for different layers).

The study fulfilled in [108] presents a novel approach of tornado track identification in forested regions of Europe,using remote sensing data. The method is based on the identification of narrow and elongated areas such as forest disturbances obtained using Landsat satellite images and subsequent verification with high-resolution satellite images; it enables objective estimation (i.e., independent of population density and observational networks) of tornado climatology in forested regions. It is proposed to use a minimal F-scale tornado intensity estimated by Weibull distribution model, using information on tornado path lengths and widths. The method is applied to the forested regions of northeast Europe, where 110 tornado tracks were identified between the years 2000 and 2014, with 105 of them previously unreported. For some regions, tornado density estimates obtained by the new method are 2–3 times higher than the ones published before.

In [89], the 1984 Ivanovo tornado outbreakis evaluated as one of the most dramatic convective-related events in Europe. Based on Landsat images, tornado-induced forest disturbances are discovered, and the actual characteristics of tornadoes during the outbreak are retrieved. The occurrence of eight tornadoes during the outbreak is confirmed; their actual location, path width and length are determined. Other tornado occurrences during the outbreak are discussed. It is shown that the Ivanovo outbreak includes 8–13 tornadoes with F-scale rating mean ranges from 1.8 to 2.5 and has an adjusted Fujita length around 540 km, which makes the outbreak one of the strongest in Europe and places it within the upper quartile of U.S. outbreaks. The characteristics of certain tornadoes within the Ivanovo outbreak are exceptional for Russia.

Experimental operations, instruments, measurement and processing methods. Modeling cloud processes

Observations of clouds, both visual ones and in-situ and remote measurements, always incur problems of accuracy for different space and time scales. Due to the evident insufficiency of standard ground-based weather and upper-air observations, passive and active remote methods of sounding hydrometeors

have made progress in cloud and precipitation studies. Some problems, such as sensitivity of cloud and precipitation characteristics to dynamic and thermodynamic atmospheric processes, microphysical composition of cloud elements, the number and properties of condensation nuclei, etc. can be partly solved by mathematical modeling. For more detailed investigation of a fine cloud structure and validation of remote techniques and numerical modeling results, in situ observations in clouds are required.

In situ measurements in a cloud layer can be carried out using an aircraft platform equipped with measuring systems. In [81, 111–122], such aircraft-based in-situ measurements of cloud properties are evaluated.

In Russia, a new-generation aircraft weather laboratory was built on the basis of a commercial aircraft Yak-42D and put to practice in 2014. On board the aircraft is installed up-to-date instrumentation to measure temperature, pressure, air density and humidity, wind, and turbulence, as well as to study the microphysical structure of clouds and precipitation, gas and aerosol atmospheric composition, radiation, atmospheric electricity, radar characteristics of clouds, relief, radiation, heat-transfer characteristics of the earth surface, and radioactive contamination of the atmosphere and underlying surface. The potentials of the new aircraft lab were reported at the 16th International Conference on Clouds and Precipitation, July 30 – August 03, 2012, Leipzig, Germany [111].

In 2015, a paper on the measurements of flight navigation parameters and thermodynamic characteristics of the atmosphere, using instrumentation installed aboard the aircraft lab, Yak-42D “Roshydromet” was published [112].

During research flights, actinometric measurements are fulfilled, and studies of thermodynamic atmosphere characteristics, atmospheric gas and aerosol composition, microphysical characteristics of clouds and cloud-forming aerosol, radioactivity, and spectral characteristics of the underlying surface are carried out. The measurements obtained compose a single database.The specific features of the aircraft data collection system are described in paper [113, 114] where the actinometric system aboard the aircraft lab Yak-43D “Rosgidromet” to study radiation processes in the troposphere is described. Also presented are some results on radiation fluxes obtained during the flights over the arctic regions of Russia. The measurement data can be useful in validating radiation codes used in models of the general atmospheric circulation and in processing the data of the Earth’s remote sounding from satellite platforms.

The aircraft lab is also used to create favorable weather conditions in Moscow during mass festivities, which also contributes to the accumulation of atmospheric data and enhancement of weather modification experience. The air-

craft is equipped to fulfill cloud modification using liquid nitrogen and pyrotechnical flares with silver iodide.

With the use of the new aircraft instrumentation systems, the accuracy and quality characteristics of temperature and wind measurements in the atmosphere and clouds were investigated [115].

Paper [116] is devoted to the investigation of the characteristics of temperature and wind measurements based on the processing and analysis of the data obtained from board the new-generation aircraft lab. The thesis prepared by D.N. Zhivoglotov at the Central Aerological Observatory generalizes the characteristics obtained.

The characteristics of aerosol transport in Moscow area were studied based on the results of aircraft observations [117]. The aircraft laboratory is shown to be an effective tool in studies of the propagation of impurities in megacity areas. Background values and concentrations of aerosols in an impurity plume are estimated, with the latter exceeding the background values by a factor of 25. The mean spectra of the distribution of aerosol particles within the range of 0,066–1,7 μ at altitudes from 350 to 1080 m are presented, and the shape of the spectral curves is shown to independent of the measurement height.The highest values of the spectra intensity were found at 850 m. The values of the spectral densities of aerosol particle sizes were found to become nearly twice as low with the distance from the plume axis increased from 15 to 40 km.

Aircraft observations were used to investigate the influence of thermodynamic conditions in the atmosphere on the distribution of black carbon mass concentration [118].

Based on aircraft observations, the relation between the dynamic structure of convective clouds and their moisture content was investigated [75]. The paper presents the results of analyzing the spectral characteristics of turbulence (spectra and co-spectra) and moisture content parameters of convective clouds of a tropical zone, which were acquired as a result of a complex aircraft experiment at a weather observation site in Cuba (see the details in the Section "Convection").

The aircraft data on electrization are employed to verify numerical models of convective clouds [119].

Russian specialists from the Central Aerological Observatory participated in the measurement aircraft campaign of the international project StratoClim, which was conducted during the period 17.07–13.08.2017, over Bengali Bay area in Nepal in order to study the troposphere-stratosphere exchange in the region of Asian monsoons formation. Within the framework of the campaign, a measurement system on the basis of the Russian stratospheric aircraft M-55 "Geophysica" was employed, and the basic phase of the measurement cam-

paign was carried out, with the base at the airport of Katmandu, Nepal. The measurement system included instruments to measure thermodynamic parameters of the atmosphere, concentrations of ozone and water vapor: a fluorescent hygrometer to measure stratospheric humidity FLASH-M55, an aircraft chemiluminescence ozonometer FOZAN to measure stratospheric ozone concentration, and a thermodynamic system to measure temperature, pressure and wind speed. These instruments were developed at the Central Aerological Observatory and are part of the set of instrumentation participating in the measurement campaign of the project StratoClim. The hygrometer and the thermodynamic system were mounted under the aircraft wing in a special gondola, and the ozonometer inside the aircraft, on the eve of the transport flight of M-55 to Katmandu.

Throughout the period of the campaign, 8 measurement flights were fulfilled. The unique results on the state of water vapor, ozone, and thermodynamic parameters of the atmosphere along flight path as well as the result of preliminary data processing were presented at the working meeting of the project participants and included in the common database of the results. The Russian specialists as the project participants have an access to all the results obtained in the course of the campaign at http:.stratoclim.org/ . The outputs of the project were presented in the scientific publications [85, 120, 121].

Different aspects of remote sensing data on clouds and precipitation, including radar and lidar observations, are considered in [123–164].

The deployment of a network of new-generation radar systems DMRL-C on the territory of Russia to carry out observations of clouds, precipitation, and hazardous weather phenomena is under way. At present, 34 DMRL-C stations and also radars in Sochi, Minsk, and Gomel are in operation. Working stationsto display weather radar data have been organized at the Roshydromet SituationCenter and the Hydrometeorological Center of Russia, which receive information in a 10-min. regime: the upper cloud boundary, weather phenomena, and precipitation intensity (http:.meteorad.ru). 12DMRL-C systems have been adjusted already to fulfill weather observations. A methodological document on the operation of the new technical aid has been developed and introduced to practice: “User’s Guide on the Application of Doppler DMRL-C Weather Radar Data in Synoptic Practice” [123], and an instruction on the validation of radar observations is being developed [124]. The validation technique is adapted to the radar systems in operation on the ground-based observational network of Roshydromet.

The paper [102], using information provided by the new DMRL-C network, analyzes the probability of an advance warning of a tornado. A real tornado event that occurred in Bashkiria on 29 August 2014 was considered. To calculate the meteorological fields, the model WRV with a high space-time resolu-

tion was employed. The indices of convective instability were calculated. The feasibility of predicting the occurrence of conditions fraught with tornado formation 3 days in advance with an accuracy of up to several hours, and at a distance of 200 km, was proved based on considering convective indices. The recording and nowcasting of tornado events were demonstrated to be possible with the currently available radar data processing software. A possibility of a complex use of such information in creating a system of the monitoring and forecast of hazardous weather phenomena is under discussion. A technology to monitor tornado hazardous situations over the Black Sea area has been developed in [95].

The specific features of using the new radar information in weather forecast assessment are presented in the papers [125, 126]. Based on the actual observations of radar reflectivity, the intensity and total amount of precipitation and the upper cloud boundary are estimated, and weather phenomena forecasted. On the example of radar data assimilation at the Central Aerological observatory and weather nowcasting, up-to-date methods, mainly used abroad, to assess the quality of predicting precipitation intensity, precipitation totals, and weather forecast with high spatial resolution are considered. The system of assessment prepared is connected with the Web-Geo-Information System (WEB-GIS) "METEORAD" and makes it possible to compare a predicted field with a similar one using radar data. A forecast of precipitation characteristics is analyzed, and the atmospheric model WRF is assessed using radar data of the precipitation fields. In this connection, prior to calculating the indices of forecast quality, radar data are prepared in the WRF projection concerned, but with a higher spatial resolution.

Some other issues of radar observations and their utilization in weather forecast are examined in [127–133]. Particularly, a precipitation nowcasting system is overviewed in [132]. The system was developed at the Hydrometeorological Center of Russia on the basis of consecutive radar fields obtained in real-time from the Central Aerological Observatory, which are utilized in the STEPS statistical scheme (Short-Term Ensemble Prediction System). This scheme is constructed as a multiplicative cascade model, using an optical flow technology. The methods of the practical application of radar measurements in diagnosing certain characteristics of rainfall, hail, and squall, developed at the Hydrometcenter of Russia, are presented in [128, 129].

The application of laser sounding in determining cloud characteristics is discussed in [134–138]. In particular, in [134], the height of the lower cloud boundary is determined based on lidar observations; here are analyzed the currently available methods of solving the equation of laser sounding. A new method is proposed to process echo signals, which significantly decreases the

necessary number of pulses emitted by a laser meter, and thus simplifies obtaining output data, which is important for practical activity, especially under unfavorable weather conditions with precipitation.

Studies [139–151] presentalgorithms of cloud and precipitation detection as well as results of the determination of basic cloud characteristics using satellite observations.In [139], authors constructed a model of the texture of different types of cloud images (up to 25 types) by MODIS data with 250 m spatial resolution. A technique to form sets of image fragment with characteristic textures for different cloud types. Based on this technique, the database of statistical models of the texture features of different cloud types was compiled [142]. The MODIS images with 250-m spatial resolution for 27 cloud types served as input data. The images were analyzed based on texture features. The database suggested also includes information about cloud images (cloud type, date, time, weather station, satellite angle, solar angle) and permits automating the construction of a statistical model of texture signs for different cloud types.

The paper (1443.34) presents a method of the identification and classification of clouds in satellite images, with subsequent retrieval of quantitative characteristics. The method provides acquisition of numerical data sets in the form of the charts of cloud classes, height, and temperature of cloud upper boundary. In [145], a method for the identification of mesoscale clouds in satellite images is presented, which is based on the use of texture analysis and synthesis of three RGB-textural features.

Another method to obtain cloud cover and precipitation parameters based on satellite data was developed at the State Research Centre of Space Hydrometeorology “Planeta” [147–150]. In [150], a Specialized Complex of Programs (SCP) is introduced, which automatically, pixel-by-pixel, classifies the SEVIRI/Meteosat-10 and AVHRR/NOAA data to retrieve cloud, precipitation and weather hazard properties for day and night, all-year-round conditions above the land, water and snow/ice surfaces on the European territory of Russia, and automatically validates satellite estimates, using ground-based observations at meteorological stations, meteorological radar, and similar products of independent satellite systems.

Some other issues of wave propagation through cloud media are discussed in[152–157]. In [153], the role of three-dimensional inhomogeneity of rainfall fields in the formation of the field of their inherent radiation in a microwave range is revealed. Paper [157] presents the structure, functions, and characteristics of the RoshydrometLightning Location System.

Ground-based devices developed to study cloud and precipitation characteristics are presented in [163–169]. Based on the method of differential spectroscopy, an attempt was made to retrieve the characteristics of tropospheric clouds

[158]. In paper [159], it is proposed to solve a practical problem of the assessment of sky cloud cover extent and determination of cloud amount, based on panoramic images of the sky obtained with super-wide-angle lenses; paper [164] proposes to do this by determining the extent of the sky blue, while paper [163] presents the grayness rate index that is applied to panoramic all-sky images for cloud cover estimation. In [160–162], an optical rain gage to observe the parameters of falling raindrops is presented.

Some issues of using unmanned aerial vehicles in studies of atmospheric parameters, aerosol impurities, and clouds are evaluated in [165, 166].

Papers [167–187] are devoted to various aspects of cloud and precipitation modeling and forecasting.

The book "Mathematical modeling of the Earth's system"[167] includes a chapter by E.M. Volodin "Clouds and condensation" from the Section "Parameterization of processes of a sub-gridscale in the atmosphere". This collective monograph presents some of the results achieved at Marchuk Institute of Numerical Mathematics of the Russian Academy of Sciences in developing a numerical model of the Earth's system, which would satisfy up-to-date requirements and be in the vanguard of the world science and technology activity in this direction.

Some issues of precipitation simulation in general circulation models are examined in [168, 169]. In [168], the added value of convection-permitting models is explored based on a showcase example of coastal precipitation extremes. It was found that the increased local intensities of vertical motion and precipitation in the convection-permitting simulations play a crucial role in shaping a strongly nonlinear extreme precipitation response to SST increase, which is not evident when convection is parameterized (and precipitation intensity has a much more linear response to increasing SSTs). In [169], the influence of atmospheric model resolution on the representation of daily precipitation extremes is investigated. It is shown that the resolution affects both the representation of physical processes and the averaging of precipitation across grid boxes. The latter smooths out localized extreme events. In particular, in the summer tropical hemisphere, extreme precipitation is reduced by up to 30% due to the averaging effect, and a further 65% owing to a coarser representation of physical processes. Toward middle to high latitudes, the latter effect reduces to 20%; in the winter hemisphere it vanishes toward the poles. Coarser vertical resolution causes an equatorward shift of maximum extreme precipitation in the tropics.

Investigation of convection by a numerical modeling technique, using a 3D model jointly developed by several institutes of ROSHYDROMET, was analyzed in the publications [170] on the prospects of developing a numerical 3D

model of a convective cloud; [171] on the concept of developing a non-stationary 3D model of a concept of developing a non-stationary 3D model of a convective rain cloud under natural and deliberately modified conditions; [172] where a complete numerical non-stationary 3D model of a convective cloud is described, and a parameterized description of microphysical processes is given; also presented are the hydrodynamic and microphysical equations, a description of the initial and boundary conditions, as well as a numerical algorithm of solving the system of equations; and [173] on verification of the numerical models of convective clouds based on aircraft studies of electrification.

Paper [174] presents a three-dimensional numerical model of moist convection and formation of convective cloudiness in the atmosphere of the Arctic. The authors used the model of mixed clouds with an explicit description of liquid and ice phases with nonstationary equations for cloud-drop and ice-particle size distributions. The capability of the model to reproduce polar lows in the Arctic atmosphere is analyzed.

Papers [177–187] present some results on clouds and precipitation forecasting, including forecasts of thunderstorms [179, 180, 186], mesoscale convective systems [181], heavy snowfalls [177, 183, 184], and fog [187].

Tropospheric aerosol, cloud condensation nuclei, ice nuclei

Aerosols, their variability, characteristics, and role in cloud formation have received particular attention in many studies [188–315].

The role of aerosols as cloud condensation nuclei (CCN) and ice nuclei is studied in [188–196]. Using numerical modelling, the impact of sulfate aerosols on cloud formation over the sea is studied in [188]. The authors found that a significant source of condensation nuclei in the troposphere is the photochemical transformation of biogenic dimethyl sulfide (in addition to NaCl) and speculated that the absence of sulfate aerosols hinders cloud formation over the sea. In [189–191]the role of aerosol properties in drop crystallization process is assessed. Laboratory experiments show increase in freezing temperature due to the presence of sand, clay and soot particles in aerosol [190, 191].

Studies [192–196] are devotedto the analysis of the role of aerosol in convective cloud formation and development. Based on the data from Amazon Tall Tower Observatory [192], different regimes of convective cloud formation and microphysics over Amazon region were found depending on aerosol properties and meteorological conditions. It was demonstrated that CCN activation and droplet formation are mostly aerosol-limited under pristine conditions and updraft-limited under biomass burning conditions [192]. Based on numerical simulations, interaction of convective clouds in different regions with fire-related aer-

osols is investigated [193, 194]. For two case studies in Moscow and Leningrad regions it is shown that forest-fire-related aerosol pollution of the atmosphere led to a decreased intensity of rain and hail from the cloud [193]. At the same time, for case studies in Eastern Siberia it is established that soot and ash contribute to precipitation formation, which does not occur in a pristine atmosphere [194]. The influence of severe aerosol pollution on the charge structure of a cumulonimbus cloud is analyzed based on observations and modelling [195, 196].

Studies [197–204] focus on the evaluation of hygroscopic properties of aerosols in different regions. In particular, the characteristic range of hygroscopicity parameter k was measured for Aitken mode aerosol at a suburban area of St. Petersburg [198], for coarse and accumulation mode in central Siberia [199], and for Aitken and accumulation mode in central Amazon region [200]. In [197, 201, 202], biomass burning aerosol hygroscopicity, including the dependence on aerosol aging, was evaluated based on experiments in an aerosol chamber.

Other issues related to aerosols such as their modeling and observations, analysis of their optical and physical properties, chemical composition, origin (including wildfires), sedimentation rate, temperature effects, space-time variability (in many regions including Eurasia, Arctic, different parts of the World Ocean, etc.), transport, aging, and so on, are widely evaluated and discussed in [205–316].

Cloud microphysics

A number of studies are devoted to the analysis of cloud microphysics and precipitation chemistry [317–330].

The spatial structure of fog and raindrops is evaluated in laboratory and field experiments [317, 318]. Indicators of the spatial structural organization of fog droplets are found for the first time [317]. It is shown that an inter-drop distance increases with an increasing drop size. The mechanism of fog buoyancy increase during condensation growth of droplets is discussed and numerically validated [317]. The grouping of rain drops of the same size in certain regions of space was revealed during in situ measurements of an instantaneous structure as well as space and time distribution of rains [318]. It is shown that a lateral wind gust leads to the grouping of drops of different sizes in different layers. The clustering mechanism concerned can cause rapid formation of raindrops in clouds and must be accounted for in radar observations [318].

The optical properties of cloud ice crystals and their influence on radiation were studied by observation [319] and model simulation [320]. Particularly, in [319], the optical characteristics of irregular hexagonal ice columns are calculated based on lidar observations. It is shown that the logarithm of the scattering matrix can be linearly approximated well by the particle size logarithm.

This can significantly accelerate the calculations of the optical characteristics of clouds. It is found that the optical characteristics are in a good agreement with the lidar observations throughout the range of sizes calculated even at deformation angles of a few degrees.

The electric properties of water and ice are studied in [321], where a mechanism of water and ice electrization during evaporation (condensation) is proposed. It is shown that evaporation leads to the accumulation of protons and hydroxide ions on the phase front, while condensation leads to their depletion. The electric charge of spherical water drops is estimated at various radiuses of drops and electrical field gradient.

The chemical composition of precipitating raindrops is studied in a number of papers [321–330]. Particularly, studies [322–325] focus on the analysis of precipitation acidification. Based on snow samples analysis from the network of 570 Russian observation stations across Russia, the values of pH and the rate of nitrogen and sulfur fallout are analyzed for the 2000–2013 period [322]. The analysis revealed the absence of intense processes of atmospheric precipitation acidification in cold seasons. However, some local effects can be substantial; for instance, deicing salts may be involved into heterophase chemical reactions and lead to the appearance of hydrogen chloride in precipitation, which is found over Moscow [322].

In [326], the concentration of oxygen isotope ^{18}O in precipitation over Moscow was evaluated based on observational data. A statistically significant positive correlation was revealed between the oxygen isotopic composition of precipitation and surface air temperature. The analysis of back trajectories and weather charts demonstrated that the most isotopically light precipitation is typical of relatively cold air masses slowly moving over the continent during five days preceding precipitation. On the contrary, fast air transport from the Atlantic Ocean leads to the relatively constant values of $\delta^{18}O$ in precipitation.

Intended weather modification. Seeding agents and technical aids

Weather modification

Intended cloud modification aims at preventing or diminishing negative effects of the formation of clouds and precipitation as well as weakeninghazardous weather phenomena related with these processes. This refers to intended modification of rain clouds aimed at precipitation redistribution, preventive dispersal of fast growing cumulus clouds, prevention of agricultural hail damage and mitigation of draughts as well as deliberate dispersal of stratiform clouds and fogs.

In 2017, a collection of papers was published on the history of intended modification of meteorological processes in the USSR and later, over its former territory [331].It is devoted to the development and current achievements in the fundamental branch of hydro-meteorological research and practice – intended modification of meteorological processes aimed at mitigation hazardous weather phenomena. The publication discusses the formation and development of science and methodic basics, technology and unique material and technical weather modification resources. The papers refer to the materials of research and the outputs of weather modification practices at research institutes and specialized departments of the national hydro-meteorological service.

Recent climate changes pose a question as to what methods should be used to enhance precipitation. This general question is often discussed in popular science papers in terms of the feasibility of weather control, particularly, inducing precipitation, and thus solving the problem of fresh water deficit [332].

The work devoted to intended modification of cloud processes proceeds in several directions: first, investigation of clouds of various forms and their characteristics, including the characteristics and properties of cloud elements and precipitating hydrometeors; second, the development and testing of cloud seeding agents, as well as studying their efficiency, etc.Besides, guidance and methodological documents, directions and instructions on using and optimization of the methods developed are prepared. One more important aspect is the assessment of weather modification effects and the development of methods to assess cloud seeding efficiency.

In the Proceedings of the 2nd International science conference “Innovation methods and means of research in the field of atmospheric physics, hydrometeorology, ecology, and climate change”(Stavropol), included are reports on the experimental studies of changes in the characteristics of cumulonimbus clouds after their intended modification, on turbulence inside convective clouds and in cloud vicinity, as well as on experimental and numerical studies of the propagation of ice-generating agents in the boundary atmospheric layer upon interaction with ground aerosol generators [333–335].

The development of echnical aids for intended weather modification is done in different ways including theoretical work, laboratory experiments, numerical modeling, field observations using ground-based equipment and aircraft laboratories, and experimental work using all available remote instruments.

In 2015, reports were published on such activities [336, 337] including development of instruments and softwaremaking it possible to expand the scope of application of domestic cloud modification techniques aimed at precipitation increase and lower cost of such work due to the introduction of up-to-date mobile technical systems to practice.

Based on the processing of materials of aircraft atmospheric sounding from [338], considered is a feasibility of undulated and stratiform cloud dispersal over the northern European territories of Russia to provide hydrometeorological support of the Army's activity.

To obtain detailed information about wave clouds, the authors processed the data of aircraft atmospheric soundings from upper-air tables (over 3000 aircraft ascents over Arkhangelsk during the period 1953–1964).

It was established that airmass undulated clouds were mainly single-layered (over 80% within a year), liquid-water, supercooled ones, which is favorable for cloud dispersal operations. Frontal clouds do not seem to be promising positive dispersal effect due to their considerable stratification, complex phase structure, and significant vertical extension.

It was also shown that supercooled airmass undulated clouds suitable for intended dispersal most often occur during the cold half-year (84,5%), with a maximum in winter (93,9%). Frontal stratiform clouds without precipitation that are suitable for dispersal mainly occur in winter (no more than 50%).

The results obtained in the above work are of practical importance as they allow one, without fulfilling field experiments, to assess the suitability of clouds in certain areas for dispersal with chemical agents in the interests of hydrometeorological support of the Army activities in the northern European part of Russia.

Investigation of hail processes progress the best in the southern, North Caucasus region of Russia where they cause the largest damage.

The fundamental and research studies reported at the 2nd International conference "Innovation methods and means of research in the field of atmospheric physics, hydrometeorology, ecology, and climate change" were fulfilled at the High-mountain geophysical institute. The physical basics of hail prevention were stated in the report [339]; hail processes were discussed in the reports [340–342].

The efficiency of hail protection operationsremains vital for cloud seeding operations aimed at precipitation redistribution and is highly topical at conferences.In particular, the work fulfilled at Nomangan State University [343] discusses the results of agricultural hail protection in the countries of the former USSR that were highly physically and economically effective. However, the author point out that since the second half of the 1980's, despite the progress in seeding technology and technical aids achieved as well as considerable increase of cloud seeding area, the efficiency of hail protection at all the target sites remains the same (within 50 to 95%). The analysis fulfilled shows that this may be due to the sub-micron size of seeded particles, their consumption mainly by

the coagulation growth of natural hailstones, inaccuracy in determining the point of agent seeding, etc.

Draught mitigation activity consists in the development of a new experimental direction devoted to precipitation enhancement during periods most important for vegetation. This is vital for areas suffering from water deficit, e.g. steppe where vegetation period partly coincides with the period of atmospheric precipitation deficiency, During the last years, research in this direction has been given a new impulse due to the increasing occurrence of summer draughts not only in southern, but also in central regions of Russia against the background of climate warming. Considerable preparatory work was done to collect and analyze climatic data in the publication "Basic principles of organizing and operating the system of draught mitigation in the Russian Federation through intended precipitation enhancement (Beriuliev et al., 2013).

The activities in this direction are continuing. In 2018, a long-term task plan to enhance precipitation in steppe areas suffering from water deficit was compiled and submitted to the Government for approval.

A large weather modification work series is devoted to intended cloud and fog dissipation. The papers [344, 345] describe the 3D numerical model "FogSeeding" developed at the ATTEX Agency. The results of the numerical experiments in supercooled fog dispersal at motorways and in open pits are presented. These results can be used as initial data in solving the problems of protecting motorways and other infrastructure elements from fog.

Experimental weather modification is rather complicated and costly, while the assessment of its efficiency necessitates staging numerous series of such experiments to collect significant statistics. Impossibility of repeating such experimental series demands searching new ways of assessing weather modification efficiency, e.g. modeling. Thus, the monograph «Cu merging» [72, see paragraph 'Convection'] describes the results of modeling cloud development, mixing, entrainment, and finally, merging of neighboring clouds. These processes can largely affect the estimate of weather modification efficiency. It is shown that upon merging the height of the newly formed cloud somewhat increases, the convection and speed of the updraft grows, liquid water content, ice content and radar reflectivity as well as the intensity of precipitation from the cloud formed by merging increases by 30% during 20 minutes. The same effect was observed in several field experiments, and simultaneously numerical modeling was fulfilled. The cloud evolution during the field experiment was partly followed in the course of the numerical experiment; the differences were pointed out and discussed by the authors. As a result, several cloud merging mechanisms were revealed, but in general, the process of cloud merging leads to intensified convection, increased vertical movement speed, changing movement

direction, and higher probability of hazardous phenomena in clouds. The efficiency of cloud modification during the process of cloud merging, according to the authors, failed to be statistically significant, being not more than 5%: however, this does not mean that the modification activity was ineffective. Moreover, the use of mathematical statistics methods is considered to be insufficiently effective, while the number of experimental cases in which cloud modification efficiency can be estimated is 500–1000. Besides, other authors also point to a considerable number of such cases – 200–300 (Breed et al., 2014).

Development of 3-D models of cumulonimbus clouds and modeling intended cloud modification. A number of publications [346, 347] are devoted to the development of a 3D model of a cumulonimbus cloud for calculating the parameters of liquid and solid precipitation both naturally occurring and deliberately induced, based on the current parameterized non-stationary 3D model of a rain convective cloud. In a series of numerical experiments with a 3D model of a convective cloud deliberately modified using hygroscopic, ice-generating, and combined techniques, the estimates obtained show that a maximal increase of precipitation amount can be up to 20% with a combined cloud seeding technique employed. The paper describes a case of using the base blocks developed at the Main Geophysical Observatory for the numerical modeling of intended modification of a thunderstorm cumulonimbus cloud with ice-generating agents. Within the framework of constructing a 3D model of a cumulonimbus cloud, numerical modeling of a thunderstorm cumulonimbus cloud modification with hygroscopic agents was fulfilled.

References

1. Dovgalyuk Y.A., N.E. Veremei, A.A. Sin'kevich. A centenary of the first domestic atlas of clouds. Meteorologia i Gidrologia, 2017. No. 8, p. 118–119. (in Russian).

2. Makhmutov V.S.,E.N. Mochalov, Y.I. Stozhkov.Secrets of clouds. Khimiya I Zhizn' – XXI vek. 2016, No. 9, p. 2–5. (in Russian).

3. Chernokulsky A.V. Climate as a reflection of clouds. Nauka I Zhizn'. 2017, No. 10, p. 70–77 (in Russian).

4. Aleksandrova M., S.K. Gulev, K. Belyaev. Probability distribution for the visually observed fractional cloud cover over the ocean. J. Clim. 2018. V. 31, p. 3207–3232.

5. Chernokulsky A.V. Day and night cloudiness using satellite data from different sources. Izvestiya, Ser. Geograficheskaya. 2015. No. 6, p. 48–60. (in Russian).

6. Chernokulsky A.V., A.V. Eliseev. Climatology of cloud overlap parameter. Sovremennye Problemy Distancionnogo Zondirovaniya Zemli iz Kosmosa. 2017. V. 14, No. 1, p. 216–225. (in Russian).

7. Chernykh I.V., Aldukhov O.A. Estimating the number of cloud Layers through radiosonde data from Russian aerological stations for 1964–2014. Russ. Meteorol. Hydrol. 2018. V. 43, No. 3, p. 152–160.

8. Chernykh I.V., O.A. Aldukhov.Long-term estimates of parameters of the vertical distribution of cloud layers from atmospheric radiosounding data. Russ. Meteorol. Hydrol. 2016. V. 41. No. 4, p. 229–239.

9. Chernokulsky A.V., I.Esau, O.N.Bulygina, R. Davy, I.I. Mokhov, S. Outten, V.A. Semenov. Climatology and interannual variability of cloudiness in the Atlantic Arctic from surface observations since the late nineteenth century. J. Clim. 2017. V. 30, p. 2103–2120.

10. Calbó J., J. Badosa, J. González, L. Dmitrieva, V.Khan, A. Enríquez-Alonso, A. Sanchez-Lorenzo. Climatology and changes in cloud cover in the area of the Black, Caspian, and Aral seas (1991–2010): a comparison of surface observations with satellite and reanalysis products. Intern. J. Climatol. 2016. V. 36, p. 1428–1443.

11. Kubryakov A.A., M.V. Shokurov, S.V. Stanichnyi. Cloudiness over the Black Sea region in 1985–2009 from satellite data. Russ. Meteorol. Hydrol. 2016. V. 41. No. 10, p. 691–697.

12. Gorbarenko E.V., O.A. Shilovtseva, N.A. Bunina. Climatology of the cloud cover in Moscow.Trudy GGO, 2017. No. 585, p. 126–141 (in Russian).

13. Komarov V.S., G.G. Matvienko, S.N. Il'in, N.Ya. Lomakina. Estimate of local features of long-term variations in cloud cover over the territory of Siberia using results of its climatic zoning according to total and low-level cloud regimes. Atmos. Oceanic Optics. 2015. V. 28. No. 3, p. 265–272.

14. Komarov V.S., G.G. Matvienko, S.N. Il'in, N.Ya. Lomakina.Regional features of long-term changes in cloud cover in Siberian sector of Northern hemisphere for the last 45 years (1969–2013). Atmos. Oceanic Optics. 2015. V. 28. No. 2, p. 175–179.

15. Komarov V.S., G.G. Matvienko, S.N. Il'in, N.Ya. Lomakina. The effect of the modern changes in the low-level stratiform clouds on the temperature regime of surface atmospheric layer in Siberia. Atmos. Oceanic Optics. 2016. V. 29. No. 1, p. 79–83.

16. Komarov V.S., G.G. Matvienko, N.Ya. Lomakina, S.N. Il'in, A.V. Lavrinenko Statistical structure and long-term change of the lower stratiform clouds over Siberia as a base for meteorological support for solution of applied problems. Part 1.Statistics of lower stratiform clouds. Atmos. Oceanic Optics (Optika Atmosfery i Okeana). 2015. V. 28.No. 7, p.622–629 (in Russian).

17. Zuev, S.V., N.P. Krasnenko, E.S. Kartashova. Parameterization of cloud forms based on actinometric information. Atmospheric and Oceanic Optics. Atmospheric Physics: XXI Intern. Symp., Tomsk, 2015: Abstracts, p. 66 (in Russian).

18. Lomakina, N.Ya. Space-time distribution of the total atmospheric moisture content over the territory of Eastern Siberia. 23th Working Group "Aerosols of Siberia", Tomsk, 2016: Abstracts, p. 54 (in Russian).

19. Kunitsyn, V.E., I.A. Nesterov, N.A. Teryoshin. Analysis of atmospheric moisture content by the data of GPS receivers. Zhurnal Radioelektroniki. 2015. No. 6, p. 6 (in Russian).

20. Shakina, N.P., E.N. Skriptunova. The maincharacteristics of limited visibility conditions at airports of the Asian part of Russia and neighboring countries. Trudy Gidrometcentra Rossii. 2018. No.4 (370), p. 18–35 (in Russian).

21. Korolev V.Yu., A.K. Gorshenin.The probability distribution of extreme precipitation. Doklady Earth Sci. 2017. V. 477. No. 2, p. 1461–1466.

22. Korolev V.Yu., A.K. Gorshenin, S.K. Gulev, K.P. Belyaev, A.A. Grusho. Statistical analysis of precipitation events. AIP Conf. Proc. 2017. V. 1863. Article ID 090011, doi: 10.1063/1.4992276.

23. Gorshenin A.K., V.Yu. Korolev. Scale Mixtures of Frechet Distributions as Asymptotic Approximations of Extreme Precipitation. J. Math. Sci. 2018. V. 234. No. 6, p. 886–903.

24. Malinin V.N., S.M. Gordeeva. Variability of Evaporation and Precipitation over the Ocean from Satellite Data. Izvestiya, Atmospheric and Oceanic Physics. 2017. V. 53, No. 9, p. 934–944.

25. Chernokulsky A.V., Kozlov F.A., Semenov V.A., Zolina O.G., Bulygina O.N. Climatology of precipitation of different genesis in Northern Eurasia. Russ. Meteorol. Hydrol. 2018. V. 43. No. 7, p. 425–435.

26. Cheredko N.N., M.A. Volkova, G.G.Zhuravlev, L.A. Ogurtzov. Structure of extreme precipitation field in Western Siberia. Proceedings of SPIE, 21-st International Symposium Atmospheric and Ocean Optics: Atmospheric Physics, 2015. V. 9680, Article ID 968065, doi: 10.1117/12.2205500.

27. Shabanov P.A., T.A. Matveeva, M.Yu. Markina. Inter-annual variations of heavy precipitation events over European Russia. Fundamental'naya i Prikladnaya Klimatologiya. 2017. V. 4, p.106–123. (in Russian).

28. Vyshkvarkova E.V., E.N. Voskresenskaya. Changes of extreme precipitation in Southern Russia. IOP Conference Series: Earth Environmental Science. 2018. V. 107, Article ID 012044, doi: 10.1088/1755-1315/107/1/012044.

29. Vyshkvarkova E., E.N. Voskresenskaya, J. Martin-Videb. Spatial distribution of the daily precipitation concentration index in Southern Russia. Atmos. Res. 2018. V. 203, p. 36–43.

30. Yu L., Q. Yang, T. Vihma, S. Jagovkina, J. Liu, Q. Sun, Y. Li. Features of extreme precipitation at Progress Station, Antarctica. J. Clim. 2018. V. 31, p. 9087–9105.

31. Zolina O.G., O.N. Bulygina. Current climatic variability of extreme precipitation in Russia. Fundamental'naya i Prikladnaya Klimatologiya. 2016. V. 1, p. 84–103. (in Russian).

32. Bulygina O.N., N.M. Arzhanova, P.Ya. Groisman. Icing conditions over Northern Eurasia in changing climate. Environ. Res. Lett. 2015. V. 10. No. 2. Article ID 025003, doi: 10.1088/1748-9326/10/2/025003

33. Groisman P.Ya., O.N. Bulygina, X. Yin, R. Vose, S.K.Gulev, I. Hanssen-Bauer, E. Forland. Recent changes in the frequency of freezing precipitation in North America and Northern Eurasia.Environmental Research Letters. 2016. V. 11.No. 4. Article ID 045007, doi:10.1088/1748-9326/11/4/045007

34. Semenov E.K., N.N. Sokolikhina, I.I.Leonov, E.V. Sokolikhina. Atmospheric circulation over centre of European Russia during freezing precipitation event in December 2010. Meteorologiya i Gidrologiya. 2018. No. 5, p. 91–101 (in Russian).

35. Aleshina M.A., P.A.Toropov, V.A. Semenov. Temperature and humidity regime changes on the Black Sea Coast in 1982–2014. Russ. Meteorol. Hydrol. 2018. V. 43. No. 4, p. 235–244.

36. Ashabokov B.A., A.A. Tashilova, L.A. Kesheva, Z.A. Taubekova. Trends in precipitation parameters in the climate zones of southern Russia (1961–2011). Russ. Meteorol. Hydrol. 2017. V. 42. No. 3, p. 150–158.

37. Danova T.E., E.A. Grigorieva. Dynamics of atmospheric precipitation in the south of Far East based on component analysis. Geografiya i Prirodnye Resursy, 2015. No. 3, p. 146–154 (in Russian).

38. Evstigneev V.P., D.V.Mishin, L.P. Ostroumova. Calculation of precipitation layer as a water balance component of the Sea of Azov. Russ. Meteorol. Hydrol. 2018. V. 43. No. 8, p. 520–529.

39. Ignatov A.V., Osipova O.P., Balybina A.S. Spatial structure of the relationships of annual precipitation amounts in Siberia and Kazakhstan. Geography and Natural Resources, 2018. V. 39. No. 2, p. 148–152.

40. Ivanov V.A., A.V. Prusov, Sizov A.A. Anomalies of temperature and annual runoff of the Danube River in the wide range of solar variability scales. Russ. Meteorol. Hydrol. 2014. V. 39. No. 12, p. 832–837.

41. Speranskaya N.A., T.V. Fuksova. Long-term changes in the main components of Lake Khanka water regime. Russ. Meteorol. Hydrol. 2018. V. 43. No. 8, p. 530–538.

42. Suhova M.G., O.V. Zhuravleva. Dynamic of changes in air temperature and precipitation in the Intermountain Hollows of the Southeast and Central Altai. Izvestiya, Ser. Geograficheskaya, 2018. No. 6, p. 93–101. (in Russian).

43. Cherenkova E.A., V.A. Semenov, E.D. Babina, M.A. Aleshina, D.D. Bokuchava. Modern and projected changes of extreme summer precipitation in the Far East of Russia. Proceedings of SPIE, 24-th Intern. Symp. on Atmospheric and Ocean Optics: Atmospheric Physics. 2018. Vol. 10833, Article ID 108337A, doi: 10.1117/12.2503789.

44. Matveeva T.A., D.Y. Gushchina, O.G. Zolina. Large-scale indicators of extreme precipitation in coastal natural-economic zones of the European part of Russia. Russ. Meteorol. Hydrol. 2015. V. 40. No. 11, p. 722–730.

45. Pavlova T.V., V.M. Kattsov Expected Arctic precipitation and evaporation changes through the 21-st century: projections with an ensemble of global climate models (CMIP5). Trudy GGO. 2015. V. 579, p. 22–36 (in Russian).

46. Antokhina O.Yu., P.N. Antokhin, E.V. Devyatova, Yu.V. Martynova, V.I. Mordvinov. The main precipitation modes over Mongolia and southern part of Eastern Siberia in July. Optika Atmosfery i Okeana. 2018. V. 31. No. 6. p. 443–450. (in Russian).

47. Antokhina O.Yu., P.N. Antokhin, E.V. Devyatova, V.I. Mordvinov. Dynamic processes in the atmosphere determining summertime precipitation anomalies in the Western Siberia and Mongolia. Fundamental'naya i Prikladnaya Klimatologiya. 2018. V. 1, p. 10–27. (in Russian).

48. Cherenkova E.A. Seasonal precipitation in the East European Plain during the periods of warm and cool anomalies of the North Atlantic surface temperature. Izvestiya, Ser. Geograficheskaya, 2017. No. 5, p. 72–81. (in Russian).

49. Cherenkova E.A., M.Y. Bardin, A.N. Zolotokrylin. The statistics of precipitation and droughts during opposite phases of the quasi-biennial oscillation of atmospheric processes and its relation to the yield in the European part of Russia. Russ. Meteorol. Hydrol. 2015. V. 40. No. 3, p. 160–169.

50. Cherenkova E.A., V.A. Semenov.A link between winter precipitation in Europe and the Arctic Sea ice, sea surface temperature, and atmospheric circulation. Russ. Meteorol. Hydrol. 2017. V. 42, No. 4, p. 238–247.

51. Ignatov A.V., O.P. Osipova, A.S. Balybina. Patterns and stochastic models of the annual precipitation variability in Siberia. Proc. of SPIE, 23rd Intern. Symp. on Atmos. and Ocean Optics: Atmos. Physics, 2017. V. 10466. Art. ID 1046653, doi: 10.1117/12.2285015.

52. Komas'ko N.I., N.P. Shakina, E.N. Skriptunova, A.R. Ivanova. Vector frontogenesis as a factor of precipitation generation. Russ. Meteorol. Hydrol. 2015. V. 40. No. 9, p. 565–575.

53. Meredith E.P., V.A. Semenov, M. Douglas, W. Park, A.V. Chernokulsky. Crucial role of Black Sea warming in amplifying the 2012 Krymsk precipitation extreme. Nat. Geosci. 2015. V. 8, p. 615–619.

54. Mokhov I.I., A.V. Timazhev. Assessing the probability of El Niño-related weather and climate anomalies in Russian regions. Russ. Meteorol. Hydrol. 2017. V. 42. No. 10, p. 635–643.

55. Piao J., W. Chen, K. Wei, Y. Liu, H.-F. Graf, J-B. Ahn, A. Pogoreltsev. An abrupt rainfall decrease over the Asian inland plateau region around 1999 and the possible underlying mechanism. Adv. Atmos. Sci. 2017. V. 34. No. 4, p. 456–468.

56. Shukurov K.A., I.I. Mokhov. Potential sources of precipitation in Lake Baikal basin. Proceedings of SPIE, 23rd Intern. Symp. on Atmos. and Ocean Optics: Atmos. Physics, 2017. V. 10466, Article ID 104663T, doi: 10.1117/12.2287910.

57. Sukovatov K.Y., N.N. Bezuglova. Coherent oscillations of cold-season precipitation on the territory of the Ishim Plain and atmospheric circulation indices. Russ. Meteorol. Hydrol. 2015. V. 40. No. 1, p. 10–15.

58. Varentsov M., H. Wouters, V. Platonov, P. Konstantinov. Megacity-induced mesoclimatic effects in the lower atmosphere: A modeling study for multiple summers over Moscow, Russia. Atmosphere, 2018. V. 9. No. 2. Article ID 50, doi: 10.3390/atmos9020050.

59. Vasil'ev D.Yu., O.K. Babkov, E.S. Kochetkova, V.A. Semenov. Wavelet and cross-wavelet analysis of the sums of atmospheric precipitation and surface air temperature in European Russia. Izvestiya, Ser. Geograficheskaya. 2017. No. 6, p. 63–77. (in Russian).

60. Volosciuk C., D. Maraun, V.A. Semenov, N. Tilinina, S.K. Gulev, M. Latif. Rising Mediterranean Sea surface temperatures amplify extreme summer precipitation in Central Europe. Sci. Rep. 2016. V. 6. Article ID 32450, doi: 10.1038/srep32450.

61. Ingel L.Kh.On the theory of convective jets and thermals in the atmosphere. Izvestiya, Atmos. Oceanic Phys., 2016, Vol. 52, No. 6, p. 602–605,doi: 10.1134/S0001433816060062

62. Sukhov S.A., Z.M. Atabiyev, R.G. Zakinian. Estimation of an upward thermique parameters. North Caucasus Federal University. Estestvennyie i Tekhnicheskiye Nauki. 2017. No. 6 (108), p. 71–73 (in Russian).

63. Avanesian K.S., O.S. Yanovskaya, V.I. Volkova, R.G. Zakinian. Investigation of air speed divergence on the nature of warm convection. Proceedings of the 2nd Intern. Science Conf. "Innovation methods and means of investigation in the field of atmospheric physics, hydrometeorology, ecology, and climate change", Stavropol, 21–25 September 2015, p. 53–57 (in Russian).

64. Danilova N.E., A.I. Shevchenko, L.M. Kulagina.On the problem of calculating the parameters of cloud convection at convection level. Proceedings of the 2nd Intern. Science Conf. "Innovation methods and means of investigation in the field of atmospheric physics, hydrometeorology, ecology, and climate change", Stavropol, 21–25 September 2015, p. 217–219 (in Russian).

65. Sin'kevich A.A., Y.P. Mikhailovskii, Y.A. Dovgalyuk, N.E. Veremei, E.V. Bogdanov, A.K. Adzhiev, A.M. Abshaev, A.M. Malkarova. Investigation of development of thunderstorm with hail. Part 1. Cloud development and formation of electric discharges. Russ. Meteorol. Hydrol., 2016. V. 41. No. 9, p. 610–619.

66. Mikhailovskii Y.P., A.A. Sin'kevich, Y.A. Dovgalyuk, N.E. Veremei, E.V. Bogdanov, A.B. Kurov, S.D. Pawar, V. Gopalakrishnan, A.K. Adzhiev, A.M. Abshaev, A.M. Malkarova. Investigation of development of thunderstorm with hail. Part 2. Analisis of methods for the forecast and diagnosis of electrical properties of clouds. Russ. Meteorol. Hydrol., 2017. V. 42. No. 6, p. 377–387,.

67. Sin'kevich A.A., Y.A. Dovgalyuk, N.E. Veremei, A.B. Kurov, Y.P. Mikhailovskii, E.V. Bogdanov, M.L.Toropova, A.A. Ignat'ev, A.Kh. Adzhiev, A.M. Abshaev, A.M. Malkarova, V. Gopalakrishnan, P. Murugavel, S.D. Pawarr. Investigation of the development of thunderstorm with hail. Part 3. Numerical simulation of cloud evolution. Russ. Meteorol. Hydrol. 2017. V. 42. No. 8, p. 494–502.

68. Abshayev A.V., M.T. Abshayev, A.Kh. Adzhiyev, Ya.A. Sadykhov, A.B. Chochayev, A.A. Sin'kevich, Yu.P. Mikhailovsky. Analysis of the development and interaction of cells in thunderstorm hail clouds. Trudy GGO. 2017. No. 586, p. 93–116 (in Russian).

69. Sin'kevich A.A., V.B. Popov, I.A.Tarabukin, E.V. Dorofeev, Y.A. Dovgalyuk, N.E. Veremei, Y.P. Mikhailovskii,V.S. Snegurov, A.V. Snegurov. Changes in Cu characteristics precipitacion during Cu merging. Russ. Meteorol. Hydrol. 2018. V. 43. No. 8, p. 506–515.

70. Popov V.B., A.A. Sinkevich. Investigation of the merging of convective clouds in the northwest of Russia. Trudy GGO. 2017. No. 585, p. 39–55 (in Russian).

71. Dovgaluk Yu. A., N.E. Veremei, M.A. Zatevakhin, A.A. Ignatiev, V. Gopalakrishnan, Yu.P Mikhailovsky, P. Murugawel, S.D Pawar, A.A. Sinkevich, M.L. Toropova. Numerical simulation of cloud merging using a three-dimensional nonstationary model of cloud convection. Trudy GGO. 2017. No. 584, p.7–35 (in Russian).

72. Sinkevich A.A., Yu.A. Dovgaluk, N.E. Veremei, Yu.P. Michailovsky. The monograph "Cu merging". Ed. by E.L. Makhotkina. MGO. 2018. 280 p. (in Russian).

73. Inyukhin V.S., Makitov V.S., Kushchev S.A. Radar studies of formation and development of hail cores in severe convective clouds. Russ. Meteorol. Hydrol., 2017. V. 42. No. 7, p. 471–476.

74. Kshevetskii S.P., Kulichkov S.N. Effects that internal gravity waves from convective clouds have on atmospheric pressure and spatial temperature-disturbance distribution. Izvestia, Atmos. Oceanic Phys. 2015. V. 51. No. 1, p. 42–48.

75. Strunin A.M., Strunin M.A. Interrelation between the dynamic structure and water content of convective clouds based on aircraft observations. Russ. Meteorol. Hydrol. 2018. V. 43. No. 4, p. 227–234.

76. Mareev E.A., S.O. Dementyeva.The role of turbulence in thunderstorm, snowstorm, and dust storm electrification. J. Geophys. Res. Atmos. 2017. V. 122, p. 6976–6988.

77. Dementyeva S.O., Mareev E.A.On the Contribution of Turbulence to the Electrification of Thunderclouds. Izvestiya, Atmos. Oceanic Phys. 2018, V. 54. No. 1, p. 25–31.

78. Kashleva L.V., Yu.P.Mikhailovsky, V.Yu. Mikhailovsky. Charging mechanisms of cloud hydrometeors in thunderstorm clouds. Trudy RGGMU. 2016. No. 45, p.118–131 (in Russian).

79. Pustovalov K.N., Nagorskii P.M.The main types of electric field variations during the passage of cumulonimbus clouds of different genesis. OptikaAtmosfery I Okeana. 2016.V. 29. No. 8, p.647–653. (in Russian).

80. Pustovalov K.N., P.M. Nagorskiy. Comparative Analysis of Electric State of Surface Air Layer during Passage of Cumulonimbus Clouds in Warm and Cold Seasons. Atmos. Oceanic Optics. 2018. V. 31. No. 6, p. 685–689.

81. Frey, W., R. Schofield, P. Hoor, A. Ulanovsky, et al.The impact of overshooting deep convection on local transport and mixing in the tropical upper troposphere / lower stratosphere (UTLS). Atmospheric Chemistry and Physics, 2015. V. 15. No. 11, p. 6467–6486.

82. Iarovaia D.A., V.V. Efimov.Cloud Cells by Data of Satellite Measurements and Convective Energy Balance on Invasion of Cold Air into the Atmosphere over the Black Sea. Izvestiya, Atmospheric and Oceanic Physics, 2018. V. 54. No. 9, p. 1214–1222, doi: 10.1134/S000143381809044X

83. Esau I.N., A.V. Chernokulsky. Convective cloud fields in the Atlantic sector of the Arctic: Satellite and ground-based observations. Izvestiya, Atmospheric and Oceanic Physics, 2015.V. 51. No. 9, p. 1007–1020, doi:10.1134/S000143381509008X.

84. Adzhiev A.Kh., A.A. Adzhieva, Z.M Knyazeva., V.N. Stasenko. Spatial features of thunderstorm activity in the North Caucasus from meteorological and instrumental data. Russ. Meteorol. Hydrol. 2015. V. 40. No. 4, p. 253–258.

85. Adzhiev A.Kh., V.N. Stasenko, A.V. Shapovalov, V.A. Shapovalov. Atmospheric electric field strength and thunderstorms in the North Caucasus. Russ. Meteorol. Hydrol. 2016. V. 41, No. 3, p. 186–192.

86. Chernogubova Yu.Ya. Occurrence of hazardous convective weather phenomena at the Central Black Earth region and their forecasting. Trudy Gidrometcentra Rossii. 2015. No. 357, p. 125–145 (in Russian).

87. Chernokulsky A.V., M.V. Kurgansky, I.I. Mokhov. Analysis of changes in tornadogenesis conditions over Northern Eurasia based on a simple index of atmospheric convective instability. Doklady Earth Sci. 2017. V. 477. Part 2, p.1504–1509.

88. Chernokulsky A.V., M.V. Kurgansky, I.I. Mokhov, D.I. Zakharchenko. Genesis environments and characteristics of the severe tornado in the South Urals on August 29, 2014. Russ. Meteorol. Hydrol. 2015. V. 40. No. 12, p. 794–799.

89. Chernokulsky A.V., Shikhov A.N. 1984 Ivanovo tornado outbreak: determination of actual tornado tracks with satellite data. Atmos. Res. 2018. V. 207, p. 111–121.

90. Dovgaluk Yu.A., M.L. Toropova, N.E. Veremey. Research of characteristics of storm clouds and thunderstorm activity according to ground-based observations and numerical modeling (for example, the station of Saint-Petersburg). Trudy GGO. 2015. No. 576, p. 50–61 (in Russian).

91. GorbatenkoV.P., O.E. Nechepurenko, S.Y. Krechetova, M.Y. Belikova. The comparison of atmospheric instability indices retrieved from the data of radio sounding and MODIS spectroradiometer on thunderstorm days over West Siberia. Russ. Meteorol. Hydrol. 2015. V. 40. No. 5, p. 289–295.

92. Gorbatenko V.P., O.E. Nechepurenko, S.Yu. Krechetova, M.Yu. Belikova.The verification of atmospheric instability parameters recovered by spectroradiometer MODIS/ Terra with data from upper-air soundings. Optika Atmosfery i Okeana. 2016. V. 29. No. 7, p. 603–607. (in Russian).

93. Grischenko I.V., T.N. Rumina. Thunderstorms in the European North. Probable weather and climate threats and risks. Trudy GGO. 2015. No. 576, p. 92–101 (in Russian).

94. Kalinin N.A., A.V. Bykov, E.V. Pischalnikova, A.N. Shikhov. Analysis of conditions for the formation of strong squalls in the Perm region environments in using the ground-based data and numerical weather prediction data. Gidrometeorologicheskie Issledovaniya I Prognozy. 2018. No.2 (368), p. 7–26 (in Russian).

95. Kalmykova O.V., V.M. Shershakov. A technology of waterspout monitoring over the Russian part of the Black Sea. Russ. Meteorol. Hydrol. 2016. V. 41. No. 10, p. 728–734.

96. Kalmykova O.V., V.M. Shershakov. Common characteristics of waterspouts over the Russian Black Sea area during 2014–2015. Trudy GGO. 2016. No. 581, p. 165–175 (in Russian).

97. Kalmykova O.V., V.M. Shershakov. Waterspout Risk Index over the Russian Black Sea water area. Trudy GGO. 2017. No. 584, p.142–163 (in Russian).

98. Kuzhevskaya I.V., K.N. Pustovalov, A.A. Sharapova. Characteristics of convective clusters reconstructed from data obtained with ATOVS sensing tools. Fundamental'naya I Prikladnaya Klimatologiya. 2018. V. 2, p. 69–85. (in Russian).

99. Nechepurenko O.E., V.P. Gorbatenko, D.A. Konstantinova, V.V. Sevastyanov. Instability indices and their thresholds for the forecast of thunderstorms over Siberia. Gidrometeorologicheskie Issledovaniya I Prognozy. 2018. No.2 (368), p. 44–59 (in Russian).

100. Novitskii M.A., B.Y. Shmerlin, S.A. Petrichenko, L.A. Tereb, O.V. Kalmykova, Y.B. Pavlyukov, S.V. Makhnorylova, N.I. Serebryannik. The tornado in Bashkortostan: the potential of analyzing and forecasting tornado-risk conditions. Russ. Meteorol. Hydrol. 2016. V. 41. No. 10, p. 683–690.

101. Novitskii M.A., B.Y. Shmerlin, S.A. Petrichenko, L.A. Tereb, L.K. Kulizhnikova, O.V. Kalmykova. Using the indices of convective instability and meteorological parameters for analyzing the tornado-risk conditions in Obninsk on May 23, 2013. Russ. Meteorol. Hydrology. 2015. V. 40. No. 2, p. 79–84.

102. Novitskii M.A., B.Ya. Shmerlin, S.A. Petrichenko, L.A. Tereb, O.V. Kalmykova. Joint calculation of vertical velocity and convective indices in the WRF model for the analysis and forecasting of tornado-risk situations. Russ. Meteorol. Hydrol. 2018. V. 43. No. 9, p. 565–573.

103. Peskov B.E., Golubev A.D., Alekseeva A.A., Dmitrieva T.G. Analysis of conditions of the occurrence of a strong squall in the Kursk region on 3 April 2017. Trudy Gidrometcentra Rossii. 2016. No. 364, p. 93–103 (in Russian).

104. Pomortseva, A.A., N.A. Kalinin. Analytical review of the current status of studying squals: formation conditions, methods of diagnosis and prognosis. Geograficheskiy Vestnik. Perm State University. 2016. No. 3 (38), p. 90–104 (in Russian).

105. Romanskii S.O., E.M.Verbitskaya, S.V.Ageeva, D.P. Istomin.Tornado in the City of Blagoveshchensk on July 31, 2011. Russ. Meteorol. Hydrol. 2018.V. 43. No. 9, p. 574–580.

106. Shapovalov, M.A. Investigation of hazardous fast-developing convective processes in the North Caucasus region of the Russian Federation. Author's PhD thesis. High-Mountain Institute, Nalchik, 2015 (in Russian).

107. Shatalina M.V., O.S. Dementieva, E.A. Mareev. Observations and modelling of thunderstorm events in Nizhniy Novgorod region: intensive thunderstorm on 1–2 June 2015. Meteorologiya I Gidrologiya, 2016. No. 11, p. 81–87 (in Russian).

108. Shikhov A.N., A.V. Chernokulsky. A satellite-derived climatology of unreported tornadoes in forested regions of northeast Europe. Remote Sens. Environ. 2018. V. 204, p. 553–567.

109. Sprygin A.A., M.I. Prokharenya. Diagnosis and forecasting of convective structures accompanied by severe weather events based on model and remote sensing data over the territory of Belarus and central Russia. Gidrometeorologicheskie Issledovaniya I Prognozy. 2018. No. 3 (369), p. 6–22 (in Russian).

110. Tarabukina L.D., V.I. Kozlov, R.R. Karimov, V.A. Mullayarov. Spatial pattern of lightning strikes in North Asia. Russ. Meteorol. Hydrol. 2017. V. 42. No. 2, p. 88–94.

111. Borisov Y., V. Petrov, M. Strunin, V. Khattatov, B. Danelyan, A. Azarov, B. Fomin, V. Martanov, V. Stasenko, S. Vakulovskiy, A. Sinkevich, L. Sokolenko, B. Lepukhov. New Russian aircraft-laboratory Yak-42D «Atmosphere» for environmental research and cloud modification. 16th Intern. Conf. on Clouds and Precipitation. Abstract 184 (ICCP_2012_Programme/index.html). July 30 – August 03, 2012. Leipzig, Germany.

112. Zhivoglotov D.N., M.A. Strunin. Measurements of flight navigation parameters and thermodynamic characteristics of the atmosphere using the new-generation instrumentation of the aircraft laboratory Yak-42D "Rosgidromet". Proc. of the 2nd All-Russia Science Conf. "Ecology and Cosmos".A.F. Mozhaisky Military-Space Academy. St. Petersburg, 10–11.02.2015, p. 124–130.

113. Volkov V.V., N.V. Bazanin, G.E. Kolokutin, M.A. Strunin. Specific features of the data collection system aboard the aircraft laboratory Yak-42D "Rosgidromet" to study atmospheric processes. Pribory i Metody Eksperimenta, 2019 (in Russian).

114. Kolokutin, G.E., B.A. Fomin, V.V. Petrov. Actinometric sistem abroad the aircraft laboratory Yak-42D "Roshydromet" reseach aircraft. Russ. Meteorol. Hydrol. 2018. V. 43. No. 3, p. 203–208.

115. Zhivoglotov D.N. Characteristics of the quality of temperature and wind measurements in the atmosphere and clouds from board a new-generation aircraft laboratory. Proc. of the 2nd Intern. Science Conf. "Innovation methods and means of investigation in the field of atmospheric physics, hydrometeorology, ecology, and climate change", Stavropol, 21–25 September 2015, p. 85–87 (in Russian).

116. Zhivoglotov D.N. The results of investigations of the characteristics of temperature and wind measurements in the atmosphere from board a new-generation aircraft laboratory. Author's abstract of PhD thesis. MGO, Roshydromet, St.Petersburg. 2018, p. 25 (in Russian).

117. Bazanin N.V., V.V. Volkov, A.V. Ganshin, B.G. Danelian, D.N. Zhivoglotov, D.V. Kirin, N.O. Krutikov, E.A. Kukanova, A.N. Lukyanov, A.M. Strunin, M.A. Strunin. Aerosol transport characteristics a megacity area (Moscow) as obtaned by aircraft observations. 2015. "Problems of cloud physics. Atmospheric aerosol. Weather modificacion". (Coliection of papers to the memory of N.O. Plaude). Moscow. 2015, p. 89–117.

118. Zhivoglotov D.N., E.V. Zakharov, D.V. Kirin, N.O. Krutikov, A.M. Strunin, M.A. Strunin. Investigation of the influence of thermodynamic conditions in the atmosphere on the distribution of black carbon mass concentration. Intern. Conf. "Turbulence, dynamics of the atmosphere and climate" dedicated to A.M. Obukhov's Centenary, Moscow, 16–18 May 2018. Collection of abstracts, Moscow. Fizmatkniga. 2018, p. 136. (in Russian).

119. Mikhailovsky Yu.P. On verifying numerical models of convective clouds based on the results of aircraft studies of electrization. Proc. Main Geophys. Observatory. 2016. No. 580, p. 125–138 (in Russian).

120. Meyer J., C. Rolf, C. Schiller, N. Sitnikov, et al. Two decades of water vapor measurements with the FISH fluorescence hygrometer: a review. Atmos. Chem. Phys. 2015. V. 15. No. 14, p. 8521–8538.

121. Afchine A., C. Rolf, A. Costa, N. Spelten, M. Riese, B. Buchholz, V. Ebert, R. Heller, S. Kaufmann, A. Minikin, C. Voigt, M. Zöger, J. Smith, P. Lawson, A. Lykov, S. Khaykin, and M. Krämer. Ice particle sampling from aircraft – influence of the probing position on the ice water content. Atmos. Measurement Techn. 2018. V. 11, p. 4015–4031.

122. Torgunakov R.E., Mikhailovskiy Yu.P., Sinkevich A.A. Aircraft studies of the electric field strength and aircraft charge in convective clouds at the early stage of development. Trudy GGO, 2017. No. 587, p. 32–46 (in Russian).

123. User's Guide on the Application of Doppler DMRL-C Weather Radar Data in Synoptic Practice. No. 52. (http://meteorad.ru).

124. Methods of the validation of observations of the Doppler weather radar "DMRL". (http://meteorad.ru)

125. Pavlyukov Y.B., Luk'yanov A.N., Shestakova A.A., Shumilin A.A., Travov A.V., Zaripov R.B. The impact of radar data assimilation on atmosphere state analysis in the Moscow region. Russ. Meteorol. Hydrol. 2017. V. 42, No. 6, p. 357–368.

126. Zaripov R.B., Yu.B. Pavlyukov, A.A. Shumilin, A.V. Travov. Utilization of radar information in weather forecast estimation with high resolution. Gidrometeorologicheskiye Issledovaniya I Prognozy. 2018. No. 2 (368), p. 60–86. (in Russian).

127. Abshaev A.M., M.T. Abshaev, A.Kh. Gergokov, A.B. Chochaev, Zh.M. Gekkieva. Calibration methods for meteorological radars. Meteorologiya i Gidrologiya. 2017. No. 3, p. 114–121. (in Russian).

128. Alekseeva A.A., B.E. Peskov Estimate of maximum convective velocity, characteristics of convective precipitation and hail using radar measurements.Trudy Gidrometcentra Rossii. 2016. No. 360, p. 135–148. (in Russian).

129. Alekseeva A.A., E.V. Vasiliev, V.M. Bukharov. Forecast of strong squalls over European part of Russia and their identification with Doppler radars. Trudy Gidrometcentra Rossii. 2017. No. 363, p. 47–64. (in Russian).

130. Kapustin A.V., V.A. Kolbin, A.D. Kuznetsov, O.S. Seroukhova, T.E. Simakina. Estimation of duration and intensitivity of shelves on radar location characteristics of the cloudy. Trudy GGO. 2018. No. 589, p.114–124. (in Russian).

131. Kashleva L.V., N.D. Hu, Yu, p. Mikhailovskii. About control of convective clouds precipitation using radar parameters. Trudy GGO. 2017. No. 587, p. 105–115. (in Russian).

132. Murav'ev A.V., D.B. Kiktev, A.V. Smirnov. Operational precipitation nowcasting system based on radar data and verification results for the warm period of the year (May-September 2017). Gidrometeorologicheskie Issledovaniya i Prognozy. 2018. No. 1 (367), p. 6–38. (in Russian).

133. Zharashuev M.V., V.S. Makitov, A. Kh. Kagermazov, D.D. Kallie. The method of calibration of the locators, the network alert of storm. Trudy GGO, 2017. No. 586, p. 164–174 (in Russian).

134. Dyomin A.V., E.A. Selyodkina. Enhancing the reliability of receiving echo signal in determining the height of the lower cloud boundary. Navigatsiya i Gidrografiya, 2017. No. 47, p.85–92. (in Russian).

135. Konoshonkin A.V., N.V. Kustova, A.G. Borovoi, J. Reichardt Retrieving the fraction of quazi-horizontally oriented ice crystals from a Raman lidar and a ceilometer. Optika Atmosfery i Okeana, 2017. V. 30. No. 7, p. 552–557. (in Russian).

136. Vostretsov N.A. The probability density of fluctuations of focused laser beam scattered radiation in the surface air layer under rain, drizzle, fog. Optika Atmosfery i Okeana, 2018. V. 31. No. 1, p. 24–27. (in Russian).

137. Wang Z., Shishko V.A., Konoshonkin A.V., Kustova N.V., Borovoi A.G., Matvienko G.G., Xie C., Liu D., Wang Y. The study of cirrus clouds with the polarization lidar in the South-East China (Hefei). Atmospheric and Oceanic Optics, 2017. V. 30. No. 3, p. 234–235.

138. Zhakamikhov K.M., Abshaev A.M. Numerical simulation of scattered light polarization in a developing convective cloud for millimeter wavelengths .Russ. Meteorol. Hydrol., 2017. V. 42. No. 6, p. 369–376.

139. Astafurov V.G., K.V. Kur'yanovich, A.V. Skorokhodov. A statistical model for describing the texture of cloud cover images from satellite data.Russian Meteorology and Hydrology, 2017. V. 42. No. 4, p. 248–257.

140. Astafurov V.G., Skorokhodov A.V. Identification of atmospheric gravity waves cloud views above water surface by satellite imagery MODIS.Optika Atmosfery i Okeana, 2016. V. 29. No. 7, p. 579–584. (in Russian).

141. Astafurov V.G., A.V. Skorokhodov.Multi-layer cloud classification from MODIS data using neural network technology and fuzzy logic approach. Sovremennye Problemy Distancionnogo Zondirovaniya Zemli iz Kosmosa, 2015. V. 12. No. 6, p. 162–173. (in Russian).

142. Astafurov V.G., A.V. Skorokhodov, O.P. Musienko, K.V. Kur'yanovich. Statistical models of image texture and physical parameters of cloudiness during snow cover periods on the Russian Federation territory from MODIS data. Optika Atmosfery i Okeana, 2018.Vol. 31. No. 7, p. 537–541. (in Russian).

143. Chukin V.V., Melnikova I.N., Nguyen T.T., Nikulin V.N., Sadykova A.F., Chukina A.M. Diagnosis of ice nuclei in the clouds by the device SEVIRI. Sovremennye Problemy Distancionnogo Zondirovaniya Zemli iz Kosmosa, 2015. Vol. 12. No. 4, p. 133–142 (in Russian).

144. Kostornaya A.A., Saprykin E.I., Zakhvatov M.G., Tokareva Y.V. A method of cloud detection from satellite data.Russian Meteorology and Hydrology, 2017. V. 42. No. 12, p. 753–758.

145. Kuznetsov A.D., Serouhova O.S., Simakina T.E. Methods of identification mesoscale clouds on the satellite images.Trudy GGO, 2017. No. 585, p. 85–97 (in Russian).

146. Skorokhodov A.V., V.G. Astafurov. A method for determining types of weather fronts based on cloud classification results from MODIS satellite data. Sovremennye Problemy Distancionnogo Zondirovaniya Zemli iz Kosmosa, 2018. V. 15. No. 3, p. 209–216. (in Russian).

147. Volkova E.V. Detection and assessment of cloud cover and precipitation parameters using data from MSU-MR radiometer of the polar-orbiting Meteor-M No. 2 for

the European territory of Russia.Sovremennye Problemy Distancionnogo Zondirovaniya Zemli iz Kosmosa, 2017.V. 14. No. 5, p.300–320, doi: 10.21046/2070-7401-2017-14-5-300-320 (in Russian).

148. Volkova E.V. Retrieval of cloud microphysical properties from satellite observations.Sovremennye Problemy Distancionnogo Zondirovaniya Zemli iz Kosmosa, 2018. V. 15. No. 4, p.265–282, doi: 10.21046/2070-7401-2018-15-4-265-279 (in Russian).

149. Volkova E.V., A.B. Uspensky. Detection and assessment of cloud cover and precipitation parameters using data of scanning radiometers of polar–orbiting and geostationary meteorological satellites. Izvestiya, Atmospheric and Oceanic Physics, 2016. V. 52. No. 9, p. 1097–1109, doi: 10.1134/S0001433816090280

150. Volkova E.V., A.B. Uspensky, A.V. Kuharsky. Specialized complex of programs for retrieving and validating satellite estimates of cloud and precipitation. Sovremennye Problemy Distancionnogo Zondirovaniya Zemli iz Kosmosa, 2015. V. 12. No. 3, p. 7–26 (in Russian).

151. Zabolotskikh E.V. Contemporary methods for retrieving the integrated atmospheric water-vapor content and the total cloud liquid-water content. Izvestiya, Atmospheric and Oceanic Physics, 2017. V. 53.No. 3, p. 294–300.

152. Busygin V.P., L.R. Dmitrieva-Arrago, L.D. Krasnokutskaya, I.Y. Kuzmina. The influence of the cloud parameters on the optical signals of the lightnings that are registered from cosmic apparatuses, Trudy Gidrometcentra Rossii, 2016, No. 359, p. 73–89. (in Russian).

153. Ilyushin Y.A., B.G. Kutuza. Influence of a spatial structure of precipitates on polarization characteristics of the outgoing microwave radiation of the atmosphere. Izvestiya, Atmospheric and Oceanic Physics, 2016. V. 52. No. 1, p. 74–81.

154. Kostsov V.S. Retrieving cloudy atmosphere parameters from RPG-HATPRO radiometer data. Izvestiya, Atmospheric and Oceanic Physics, 2015. V. 51. No. 2, p. 156–166.

155. Linkova A.M., G.I. Khlopov. Retrieval of microstructure characteristics of liquid precipitation by active-passive remote sensing. Trudy GGO, 2015, No. 582, p. 62–80. (in Russian).

156. Melnikova I.N., Kuznetsov A.D., Serouhova O.S., Simakina T.E. Remote sensing of the optical parameters of clouds through the use of aircraft measurements of solar radiation in the visible and near infrared ranges. Trudy GGO, 2017, No. 585, p. 98–109 (in Russian).

157. Snegurov A.V., V.S. Snegurov. Lightning location system.Trudy GGO, 2017.No. 586, p. 117–140. (in Russian).

158. Chulichkov A.I., Andreev M.S., Golitsyn G.S., Elansky N.F., Medvedev A.P., Postylyakov O.V. On cloud bottom boundary determination by digital stereo photography from the Earth's surface.Atmospheric and Oceanic Optics, 2017. V. 30. No. 2, p. 184–190.

159. Galileisky V.P., A.I. Elizarov, D.V. Kokarev, A.M. Morozov. Detection of cloud elements in panoramic sky images. Optika Atmosfery I Okeana Fizika Atmosfery: XXI Intern. Symp., Tomsk, 2015. Abstracts, p. 46. (in Russian).

160. Kalchikhin V.V., A.A.Kobzev, V.A.Korol'kov, A.A. Tikhomirov. Determination of precipitation type using the results of optical measurements of the precipitation microstructure characteristics.Optika Atmosfery i Okeana, 2016. Vol. 29. No. 8, p. 654–657. (in Russian).

161. Kalchikhin V. V., A. A. Kobzev, V. A. Korol'kov, A. A. Tikhomirov. Determination of the rate of fall of rain drops in measurements of their parameters by an optical rain gauge. Measurement Techniques. 2017. V. 59. No. 11, p. 1175–1180.

162. Kalchikhin V.V., A.A. Kobzev, V.A. Korolkov, A.A. Tikhomirov. Results of optical precipitation gauge field tests. Atmospheric and Oceanic Optics. 2018. V. 31. No. 5, p. 545–547.

163. Krinitskiy M.A., A.V. Sinitsyn. Adaptive algorithm for cloud cover estimation from all-sky images over the sea.Oceanology. 2016. V. 56. No. 3, p. 315–319.

164. Zuev, S.V., V.A. Levikin. Determination of the total cloud amount number by the extent of the sky blue. 19th Working Group "Aerosols of Siberia", Tomsk, 2016: Abstracts, p. 82. (in Russian).

165. Sitnikov N.M., Yu.A. Borisov, I.I. Chekulaev, D.I. Efremov, D.V. Akmulin, V.I. Sitnikova, A.E. Ulanovskii. Returnable upper-air sonde based on unmanned or remotely-piloted aerial vehicles for atmospheric balloon sounding. Russ. Meteorol. Hydrol., 2014. V. 39. No. 9, p. 634–638. (in Engish)

166. Strashko O.V.,Kusnetzov I.E., Kachalkin A.Yu., Akmulin D.V., Gorelik A.G., Sitnikov N.M., Chekulaev I.I. Tecnology of unmanned aviation system application for solution of meteorological tasks.Aviakosmicheskoe priborostroenie."Nauchtehizdat", 2018. No.1, p. 42–51. (in Russian).

167. Volodin, E.M. Chapter "Clouds and condensation" in the monograph "Mathematical modeling of the Earth's system". The Marchuk Institute Numerical Mathematics, the Russian Academy of Sciences, Moscow, 2016, p. 85–91. (in Russian).

168. Meredith E.P., D. Maraun, V.A. Semenov, W. Park. Evidence for added value of convection-permitting models for studying changes in extreme precipitation. J. Geophys. Res.: Atmos., 2015. V. 120, p. 12500–12513.

169. Volosciuk C., D. Maraun, V.A. Semenov, W. Park. Extreme precipitation in an atmosphere general circulation model: Impact of horizontal and vertical model resolutions. J. Clim., 2015. V. 28, p. 1184–1205.

170. Dovgaluk, Yu. A., N.E. Veremei, S.A. Vladimirov, A.C. Drofa, M.A. Zatevakhin, A.A. Ignatiev, V.N. Morozov, R.S. Pastushkov, A.A. Sinkevich, A.V. Shapovalov. Perspectives of the further development of three-dimensional convective cloud model. Proc. of the Main Geophysical Observatory, 2016. No. 582, p. 202–213. (in Russian).

171. Dovgaluk Yu.A., N.E. Veremei, S.A. Vladimirov, A.C. Drofa, M.A. Zatevakhin, A.A. Ignatiev, V.N. Morozov, R.S. Pastushkov, A.A. Sinkevich, A.V. Shapovalov. The concept of development of numerical nonstationary three-dimentional model of precipitation forming convective cloud in natural conditions and during active modifications. Proc. of the Main Geophysical Observatory, 2016. No. 582, p. 7–44. (in Russian).

172. Veremei N.E., Yu.A, Dovgaluk, M.A. Zatevakhin, A.A. Ignatiev. V.N. Morozov, R.S. Pastushkov. A description of the basic numerical non-stationary model of a convective cloud. Proc. of the Main Geophysical Observatory, 2016. No. 582, p. 45–91. (in Russian).

173. Mikhailovsky Yu.P. On verifying numerical models of convective clouds based on the results of aircraft studies of electrization. Proc. of the Main Geophysical Observatory, 2016. No. 580, p.125–138. (in Russian).

174. Aloyan A.E., V.O. Arutyunyan, A.N. Ermakov. Mathematical modeling of convective cloudiness in polar regions. Optika Atmosfery i Okeana, 2017. V. 30. No. 3, p. 222–226. (in Russian).

175. Ashabokov B.A., A.H. Kagermazov, A.V. Shapovalov, V.A. Shapovalov. About one approach to formation of conditions at modeling of the convective clouds. Trudy GGO, 2016, No. 582, p. 159–173 (in Russian).

176. Shapovalov V.A. Numerical simulation of electrical processes in storm clouds. Trudy GGO, 2018. No. 588, p. 28–36. (in Russian).

177. Aniskina O.G., O.V. Volobueva, S.V. Mostamandi, N.A. Novikova, V.S. Ryabinin. Forecast of snowfall evaluations, arranged by using of WRF model in the northwest of the European Russia. Trudy GGO, 2017, No. 586, p. 175–190. (in Russian).

178. Gavrikov A.V. Estimating the reproduction quality of precipitation over the north Atlantic and influence of the hydrostatic approximation in the WRF–ARW atmospheric model. Oceanology, 2017. V. 57. No. 2, p. 232–238.

179. Gubenko I.M., Rubinshtein K.G. Thunderstorm activity forecasting based on the model of cumulonimbus cloud electrification. Russian Meteorology and Hydrology, 2017. V. 42. No. 2, p. 77–87.

180. Gubenko I.M., K.G. Rubinshtein. Analysis of the results of thunderstorm forecasting based on atmospheric instability indices using the WRF-ARW numerical model data. Russ. Meteorol. Hydrol. 2015. V. 40. No. 1, p. 16–24.

181. Kalinin N.A., A.N. Shikhov, A.V. Bykov. Forecasting mesoscale convective systems in the Urals using the WRF model and remote sensing data. Russ. Meteorol. Hydrol., 2017. V. 42. No. 1, p. 9–18.

182. Kulikova I.A., Kruglova E.N., Kiktev D.B., Sal'nikov V.G. Practical predictability of the standardized precipitation index on monthly and seasonal timescales. Russ. Meteorol. Hydrol., 2017. V. 42. No. 9, p. 582–593.

183. Pischalnikova E.V., N.A. Kalinin, A.N. Shikhov, A.V. Bykov. The success of a numerical forecast of heavy precipitation in the cold half-year for Perm region. Gidrometeorologicheskie Issledovaniya i Prognozy, 2018. No. 1(367), p. 135–145 (in Russian).

184. Pischalnikova E.V., N.A. Kalinin, A.L. Vetrov, A.N. Shikhov, E.M. Sviyazov, A.V. Bykov. Forecast of heavy and very heavy snowfall in the Urals based on the model WRF. Trudy Gidrometcentra Rossii, 2016. No. 359, p. 58–72 (in Russian).

185. Rusin I.N., M.A. Maddah, A.M. Ahund-Ali. Evaluation of WRF physical parameterizations in simulating heavy rainfall events in southwestern Iran. Trudy GGO, 2017. No. 586, p.191–204 (in Russian).

186. Tokarev V.M., M.Ya. Zdereva, N.A. Khluchina, L.P. Vorobyeva, N.A. Baboshina. Operational technology for thunderstorms forecasting in the Ural-Siberian region and test results.Gidrometeorologicheskie Issledovaniya i Prognozy, 2018. No. 2 (368), p. 27–43 (in Russian).

187. Zarochentsev G.A., Rubinstein K.G., Bychkova V.I., Ignatov R.Y., Yusupov Y.I. Comparison of several numerical methods for fog forecast. Optika Atmosfery i Okeana, 2018. V. 31. No. 12, p. 981–987. (in Russian).

188. Aloyan A.E., Arutyunyan V.O., Yermakov A.N. The role of sulfate aerosol in the formation of cloudiness over the sea. Izvestiya, Atmos. Oceanic Phys., 2016. V. 52. No. 4, p. 353–364.

189. Golubev V.N. A role of aerosol particles in atmospheric ice nucleation. Russ. Meteorol. Hydrol., 2015. V. 40. No. 12, p. 787–793.

190. Sinkevich A.A., Pawar S.D., Kurov A.B., Volkov N.N., Mikhailovskiy V.Yu., Veremey N.E., Gopalakrishnan V. An impact of natural aerosols on crystallization temperature of water drops. Trudy GGO, 2015. No. 576, p. 42–49 (in Russian).

191. Kurov A.B., Veremey N.E., Volkov N.N., Letenko D.G., Mikhailovskiy V. Yu., Sinkevich A.A. Impact of soot particles on crystallization of water drops. Trudy GGO, 2015. No. 579, p. 205–213 (in Russian).

192. Pöhlker M.L., Ditas F., Saturno J., Klimach T., Hrabě de Angelis I., Araùjo A.C., Brito J., Carbone S., Cheng Y., Chi X., Ditz R., Gunthe S.S., Holanda B.A., Kandler K., Kesselmeier J., Könemann T., Krüger O.O., Lavrič J.V., Martin S.T., Mikhailov E., Moran-Zuloaga D., Rizzo L.V., Rose D., Su H., Thalman R., Walter D., Wang J., Wolff S., Barbosa H.M. J., Artaxo P., Andreae M.O., Pöschl U., Pöhlker C. Long-term observations of cloud condensation nuclei over the Amazon rain forest – Part 2: Variability and characteristics of biomass burning, long-range transport, and pristine rain forest aerosols. Atmos. Chem. Phys., 2018. V. 18, p. 10289–1033.

193. Dovgaluk Yu. A., Veremey N.E., Toropova M.L., Sinkevich A.A., Kurov A.B., Volkov N.N., Ignatiev A.A. An impact of aerosol pollution of the atmosphere during forest fires on the evolution of convective clouds and precipitations associated with them. Trudy GGO, 2017. No. 585, p. 7–38. (in Russian).

194. Dovgalyuk Yu. A., Veremey N.E., Toropova M.L., Sinkevich A.A., Kurov A.B., Volkov N.N., Ignatiev A.A. Peculiarities of convective clouds and precipitation evolution during strong aerosol atmosphere pollution due to forest fires. Trudy GGO, 2018. No. 588, p. 7–27. (in Russian).

195. Veremei N.E., Dovgalyuk Y.A., Komarovskikh K.F., Sinkevich A.A., Gopalakrishnan V., Murugavel P., Pawar S.D. Studying the effects of severe aerosol pollution of the atmosphere on the dynamics of cumulonimbus cloud charge structure by numerical modeling. Russ. Meteorol. Hydrol., 2015. V. 40. No. 12, p. 777–786.

196. Sinkevich A.A., Pawar S.D., Veremei N.E., Dovgaluk Yu. A., Gopalakrishnan V., Mikhailovsky Yu, p., Murugavel P. Investigation of the changes of thunderstorm cloud electrical structure during high atmospheric pollution by aerosols. Trudy GGO, 2015, No. 578, p. 23–46. (in Russian).

197. Kozlov V.S., Rakhimov R.F., Shmargunov V.P. Variations in Condensation Properties of Mixed Smoke from Biomass Burning at Different Smoke Evolution Stages. Atmospheric and Oceanic Optics, 2018. V. 31. No. 1, p. 9–18.

198. Mikhailov E.F., Ivanova O.A., Vlasenko S.S., Nebos'ko E.Y., Ryshkevich T.I. Cloud condensation nuclei activity of the Aitken mode particles near St. Petersburg, Russia. Izvestiya, Atmos. Oceanic Phys., 2017. V. 53. No. 3, p. 326–333.

199. Mikhailov E.F., Mironov G.N., Pöhlker C., Chi X., Krüger M.L., Shiraiwa M., Förster J.-D., Pöschl U., Vlasenko S.S., Ryshkevich T.I., Weigand M., Kilcoyne A.L.D., Andreae M.O. Chemical composition, microstructure, and hygroscopic properties of aerosol particles at the Zotino Tall Tower Observatory (ZOTTO), Siberia, during a summer campaign. Atmos. Chem. Phys., 2015. V. 15, p. 8847–8869.

200. Pöhlker M.L., Pöhlker C., Ditas F., Klimach T., Hrabe de Angelis I., Araújo A., Brito J., Carbone S., Cheng Y., Chi X., Ditz R., Gunthe S. S., Kesselmeier J., Könemann T., Lavrič J.V., Martin S.T., Mikhailov E., Moran-Zuloaga D., Rose D., Saturno J., Su H., Thalman R., Walter D., Wang J., Wolff S., Barbosa H.M.J., Artaxo P., Andreae M.O., Pöschl U. Long-term observations of cloud condensation nuclei in the Amazon rain forest – Part 1: Aerosol size distribution, hygroscopicity, and new model parametrizations for CCN prediction. Atmos. Chem. Phys., 2016. V. 16, p. 15709–15740.

201. Popovicheva O.B., Persiantseva N.M., Timofeev M.A., Shonija N.K., Kozlov V.S. Small-Scale Study of Siberian Biomass Burning: II. Smoke Hygroscopicity. Aerosol and Air Quality Research, 2016. V. 16. No. 7, p. 1558–1568.

202. Popovicheva O.B., Kozlov V.S., Rakhimov R.F., Shmargunov V.P., Kireeva E.D., Persiantseva N.M., Timofeev M.A., Engling G., Eleftheriadis K., Diapouli E., Panchenko M.V., Zimmermann R., Schnelle-Kreis J. Optical-microphysical and physical-chemical characteristics of Siberian biomass burning: Experiments in aerosol chamber. Atmospheric and Oceanic Optics, 2016.Vol. 29. No. 6, p. 492–500.

203. Ryshkevich T.I., Mironov G.N., Mironova S.Y., Vlasenko S.S., Mikhailov E.F., Chi X., Andreae M.O. Comparative analysis of hygroscopic properties of atmospheric aerosols at ZOTTO Siberian background station during summer and winter campaigns of 2011. Izvestiya, Atmos. Oceanic Phys., 2015. V. 51. No. 5, p. 512–519.

204. Vlasenko S.S., Su H., Pöschl U., Andreea M.O., Mikhailov E.F. Tandem configuration of differential mobility and centrifugal particle mass analysers for investigating aerosol hygroscopic properties. Atmos. Measurement Techn., 2017. V. 10, p. 1269–1280.

205. Adushkin V.V., Chen B.B., Popel S.I., Weidler P.G., Friedrich F., Izvekova Yu.N. Properties and origin of small particles in the atmosphere of Central Asia. Doklady Earth Sci., 2016.V. 466. No. 2, p. 177–182.

206. Adushkin V.V., Chen B.B., Popel S.I., Weidler P.G., Imashev S.A., Losseva T.V., Sverdlik L.G., Friedrich F. Radiative forcing of aerosols in Central Asia. Doklady Earth Sci., 2015. V. 460. No. 2, p. 137–141.

207. Antokhin P.N., Arshinova V.G., Arshinov M.Yu., Belan B.D., Belan S.B., Voronetskaya N.G., Golovko A.K., Davydov D.K., Ivlev G.A., Kozlov A.V., Kozlov A.S., Malyshkin S.B., Pevneva G.S., Rasskazchikova T.M., Savkin D.E., Simonenkov D.V., Sklyadneva T.K., Tolmacheva G.N., Fofonov A.V. Organic aerosol in air of Siberia and the Arctic. Part 3. Forest fire porducts. Optika Atmosfery i Okeana, 2017. V. 30. No. 9, p. 740–749. (in Russian).

208. Antokhina O.Yu., Antokhin P.N., Arshinova V.G., Arshinov M.Yu., Belan B.D., Belan S.B., Davydov D.K., Ivlev G.A., Kozlov A.V., Nédélec P., Paris J.-D., Rasskazchikova T.M., Savkin D.E., Simonenkov D.V., Sklyadneva T.K., Tolmachev G.N., Fofonov A.V. Vertical Distributions of Gaseous and Aerosol Admixtures in Air over the Russian Arctic. Atmospheric and Oceanic Optics, 2018. V. 31. No. 3, p. 300–310.

209. Arkhipov V.A., Zharova I.K., Kozlov E.A., Tkachenko A.S. Prediction of ecological consequences of toxic aerosol clouds spreading in the fall areas of waste booster stages. Optika Atmosfery i Okeana, 2015. Vol. 28. No. 1, p. 89–93, (in Russian).

210. Arschinov M.Yu., Belan B.D., Voronetskaya N.G., Golovko A.K., Davydov D.K., Kozlov A.S., Malyshkin S.B., Pevneva G.S., Simonenkov D.V., Tolmachev G.N. Annual dynamics of aerosol organic components in the free atmosphere over South-Western Siberia.Atmospheric and Oceanic Optics, 2016. V. 29. No. 1, p. 1–4.

211. Arshinov M.Yu., Belan B.D., Belan S.B., Voronetskaya N.G., Golovko A.K., Davydov D.K., Ivlev G.A., Kozlov A.S., Malyshkin S.B., Pevneva G.S., Simonenkov D.V., Fofonov A.V. Organic aerosol in air of Siberia and the Arctic. Part 2.Vertical distribution. Optika Atmosfery i Okeana, 2017. V. 30. No. 9, p. 733–739. (in Russian).

212. Arshinov M.Yu., Belan B.D., Davydov D.K., Kozlov A.V., Kozlov A.S., Arshinova V.G. Nucleation bursts in the atmosphere over boreal zone in West Siberia. Part II. Formation and growth rates of nanoparticles. Optika atmosfery i okeana, 2015. No. 78, p. 730–737 (in Russian).

213. Arshinov M.Yu., Belan B.D., Voronetskaya N.G., Golovko A.K., Davydov D.K., Kozlov A.S., Pevneva G.S., Simonenkov D.V., Fofonov A.V. Organic aerosol in air of Siberia and the Arctic. Part 1.Geographic features and temporal dynamics.Optika Atmosfery i Okeana, 2017.V. 30. No. 8, p. 716–722. (in Russian).

214. Balin Yu.S., Klemasheva M.G., Kokhanenko G.P., Nasonov S.V., Novoselov M.M., Penner I.E. Lidar study of the vertical structure of aerosol fields in the atmosphere over Lake Baikal during forest fires. Optika Atmosfery i Okeana, 2016. V. 29. No. 8, p. 689–693 (in Russian).

215. Belan B.D., Buchelnikov V.S., Lysova V.F., Simonenkov D.V., Talovskaja A.V., Tentyukov M.P., Yazikov E.G. Estimation of the Effect of Meteorological and Orographic Conditions on Aerosol Contamination of the Snow Cover in the South of Tomsk Region. Atmospheric and Oceanic Optics, 2018. V. 31. No. 6, p. 656–664.

216. Belan B.D., Simonenkov D.V., Talovskaya A.V., Tentyukov M.V., Fofonov A.V., Yazikov E.G. Comparative estimation of the geochemical activity of the atmosphere based on the ratios of the compositions of different aerosol fractions in the surface air layer at the "Fonovaya" observatory: measurement campaign of autumn 2016. Optika Atmosfery i Okeana, 2017. V. 30. No. 9, p. 740–749. (in Russian).

217. Bondur V.G., Gordo K.A., Kladov V.L. Spacetime Distributions of Wildfire Areas and Emissions of Carbon-Containing Gases and Aerosols in Northern Eurasia according to Satellite-Monitoring Data. Izvestiya, Atmospheric and Oceanic Physics, 2017. V. 53. No. 9, p. 859–874.

218. Chubarova N.Ye., Poliukhov A.A., Gorlova I.D. Long-term variability of aerosol optical thickness in Eastern Europe over 2001–2014 according to the measurements at the Moscow MSU MO AERONET site with additional cloud and NO_2 correction. Atmos. Measurement Techn., 2016. V. 9, p. 313–334.

219. Emilenko A.S., Sviridenkov M.A., Kopeikin V.M., Wang G. Long-term variability of air pollution with black carbon in the region of Beijing in autumn periods. Atmospheric and Oceanic Optics, 2017. V. 30. No. 6, p. 550–554.

220. Golitsyn G.S., Grechko E.I., Dzhola A.V., Emilenko A.S., Kopeikin V.M., Rakitin V.S., Safronov A.N., Fokeeva E.V., Wang G., Wang P. Studying the pollution of Moscow and Beijing atmospheres with carbon monoxide and aerosol. Izvestiya, Atmos. Oceanic Phys., 2015. V. 51. No 1, p. 1–11.

221. Golobokova L.P., Polkin V.V., Onischuk N.A., Khuriganova O.I.1 Tikhomirov A.B., Terpugova S.A., Turchinovich U.S., Radionov V.F. Chemical composition of aerosol in the atmospheric surface layer of the East Antarctica coastal zone. Led i Sneg, 2016.V. 56. No. 2, p. 177–188 (in Russian).

222. Golovko V.V., Istomin V.L. Determination of the sedimentation rate of the pollen particles of anemophilous plants growing in Western Siberia.Optika Atmosfery i Okeana, 2017.V. 30. No. 9, p. 806–810. (in Russian).

223. Golovko V.V., Istomin V.L., Koutsenogii K.P. Determination of the sedimentation rate of weed pollen of both individual grains and their agglomerates.Optika Atmosfery i Okeana, 2015. V. 28. No. 7, p. 655–660. (in Russian).

224. Golovko V.V., Koutsenogii K.P., Istomin V.L. Number and mass concentrations of the pollen component of atmospheric aerosol measured near Novosibirsk during blossoming of arboreal plants.Optika Atmosfery i Okeana, 2015. V. 28. No. 6, p. 529–533. (in Russian).

225. Golovko V.V., Kutsenogii K.P., Istomin V.L. Determination of volume and density of pollen grains of anemohhyle plants in Novosibirsk region.Optika Atmosfery i Okeana, 2015. V. 28. No. 1, p. 86–88. (in Russian).

226. Gorbarenko E.V., Rublev A.N. Long-term changes in the aerosol optical thickness in Moscow and correction under strong atmospheric turbidity .Izvestiya, Atmos. Oceanic Phys., 2016. V. 52. No. 2, p. 188–195.

227. Gorchakov G.I., Sitnov S.A., Karpov A.V., Gorchakova I.A., Gushchin R.A., Datsenko O.I. Large-scale hazes over Eurasia in July 2016: Siberian smoke haze evolution. IOP Conference Series: Earth Environ. Sci., 2019. V. 231, article ID: 012019, doi: 10.1088/1755–1315/231/1/012019.

228. Gorchakov G.I., Golitsyn G.S., Sitnov S.A., Karpov A.V., Gorchakova I.A., Gushchin R.A., Datsenko O.I. Large-scale haze over Eurasia in July 2016. Doklady Earth Sci., 2018. V. 482. No. 1, p. 1212–1215.

229. Gorchakov G.I., Karpov A.V., Kuznetsov G.A., Buntov D.V. Quasiperiodic saltation in the windsand flux over desertified areas. Atmospheric and Oceanic Optics, 2016. V. 29. No. 6, p. 501–506.

230. Gorchakov G.I., Karpov A.V., Pankratova N.V., Semoutnikova E.G., Vasiliev A.V., Gorchakova I.A. Brown carbon and black carbon in the smoky atmosphere during boreal forest fires. Izvestiya, Atmos. Oceanic Phys., 2017. V. 53. No. 9, p. 875–884.

231. Gorchakov G.I., A.V. Karpov, A.V. Vasiliev, I.A. Gorchakova. Brown and black carbons in megacity smogs. Atmospheric and Oceanic Optics, 2017. V. 30. No. 3, p. 248–254.

232 Gorchakov G.I., Kopeikin V.M., Karpov A.V., Titov A.A., Buntov D.V., Kuznetsov G.A., Gushchin R.A., Dazenko O.I., Kurbatov G.A., Seregin A.O., Sokolov A.V. Variations in the specific charge of saltating sand in a windsand flux over a desertified area.Atmospheric and Oceanic Optics, 2016. V. 29. No. 3, p. 244–251.

233. Gorchakov G.I., Kopeikin V.M., Sitnov S.A., Semoutnikova E.G., Sviridenkov M.A., Karpov A.V.1, Lezina E.A., Emilenko A.S., Isakov A.A., Kuznetsov G.A., Ponomareva T.Ya. Moscow smoke haze in October 2014. Variations in the aerosol mass concentration. Atmospheric and Oceanic Optics, 2016. V. 29. No. 1, p. 5–11.

234. Gorchakov G.I., Sitnov S.A., Semoutnikova E.G., Kopeikin V.M., Karpov A.V., Gorchakova I.A., Pankratova N.V., Ponomareva T.Ya., Kuznetsov G.A., Loskutova O.V., Kozlovtseva E.A., Rodina K.V. Large-Scale Smoke Haze over the European Part of Russia and Belorus in July 2016. Izvestiya, Atmos. Oceanic Phys., 2018. V. 54. No. 9, p. 986–996.

235. Gorchakova I.A., Mokhov I.I., Anikin P.P., Emilenko A.S. Radiative and Thermal Impacts of Smoke Aerosol Longwave Absorption during Fires in the Moscow Region in Summer 2010. Izvestiya, Atmos. Oceanic Phys., 2018. V. 54. No. 2, p. 154–161.

236. Gorchakova I.A., Mokhov I.I., Rublev A.N. Radiation and temperature effects of the intensive injection of dust aerosol into the atmosphere. Izvestiya, Atmos. Oceanic Phys. 2015. V. 51. No 2, p. 113–126.

237. Gruzdev A.N., Isakov A.A. On the nature of long-period variations in mass concentration of near-ground aerosol. Atmospheric and Oceanic Optics, 2016. V. 29. No. 1, p. 73–78.

238. Gubanova D.P., Belikov I.B., Elansky N.F., Skorokhod A.I., Chubarova N.E. Variations in PM2.5 Surface Concentration in Moscow according to Observations at MSU Meteorological Observatory. Atmospheric and Oceanic Optics, 2018. V. 31. No. 3, p. 290–299.

239. Ignatov A.V., Osipova O.P., Balybina A.S. Spatial structure of the relationships of annual precipitation amounts in Siberia and Kazakhstan. Geography and Natural Resources, 2018. V. 39. No. 2, p. 148–152.

240. Ivlev L.S., Dovgaluk Ju. A. Geterogeneous processes of aerosols increase of the upper troposphere and stratosphere. Trudy GGO, 2015, No. 577, p. 65–105 (in Russian).

241. Kalinskaya D.V., Kabanov D.M., Latushkin A.A., Sakerin S.M. Atmospheric aerosol optical depth measurements in the Black sea region (2015–2016). Optika Atmosfery i Okeana, 2017. V. 30. No. 6, p.489–496 (in Russian).

242. Kalogridis A.-C., Popovicheva O.B., Engling G., Diapoulia E., Kawamura K., Tachibana E.,Ono K., Kozlov V.S., Eleftheriadis K. Smoke aerosol chemistry and aging of Siberian biomass burning emissions in a large aerosol chamber. Atmospheric Environment, 2018. V. 185, p. 15–28.

243. Kokhanenko G.P., Balin Yu.S., Klemasheva M.G., Penner I.E., Samoilova S.V., Terpugova S.A., Banakh V.A., Smalikho I.N., Falits A.V., Rasskazchikova T.M., Antokhin P.N., Arshinov M.Yu., Belan B.D., Belan S.B. Structure of aerosol fields of the atmospheric boundary layer according to aerosol and Doppler lidar data during passage of atmospheric fronts.Atmospheric and Oceanic Optics, 2017. V. 30. No. 1, p. 18–32.

244. Konovalov I.B., Beekmann M., Berezin E.V., Formenti P., Andreae M.O. Probing into the aging dynamics of biomass burning aerosol by using satellite measurements of aerosol optical depth and carbon monoxide.Atmospheric Chemistry and Physics, 2017. V. 17, p. 4513–4537.

245. Konovalov I.B., Beekmann M., Berezin E.V., Petetin H., Mielonen T., Kuznetsova I.N., Andreae M.O. The role of semi-volatile organic compounds in the mesoscale evolution of biomass burning aerosol: a modeling case study of the 2010 mega-fire event in Russia. Atmos. Chem. Phys., 2015. V. 15, p. 13269–13297.

246. Konovalov I.B., E.V.Berezin, M. Beekmann. Effect of photochemical self-action of carbon-containing aerosol: Wildfires.Izvestiya, Atmospheric and Oceanic Physics, 2016. Vol. 52. No. 3, p. 263–270, doi: 10.1134/S0001433816030063.

247. Konovalov I.B., Lvova D.A., Beekmann M. Estimation of the elemental to organic carbon ratio in biomass burning aerosol using AERONET retrievals. Atmosphere, 2017. V. 8. No. 7, article ID: 122, doi: 10.3390/atmos8070122.

248. Konovalov I.B., Lvova D.A., Beekmann M., Jethva H., Mikhailov E.F., Paris J.-D., Belan B.D., Kozlov V.S., Ciais P., Andreae M.O. Estimation of black carbon emissions from Siberian fires using satellite observations of absorption and extinction optical depths .Atmos. Chem. Phys., 2018. V. 18, p. 14889–14924.

249. Kopeikin V.M., Emilenko A.S., Isakov A.A., Loskutova O.V., Ponomareva T.Ya. Variability of soot and fine aerosol in the Moscow Region in 2014–2016. Atmospheric and Oceanic Optics. 2018, Vol. 31, No. 3, p. 243–249.

250. Lisitzin A.P., Lukashin V.N., Novigatsky A.N., Klyuvitkin A.A., Dara O.M., Politova N.V. Aerosols in the near-water surface layer of the Caspian Sea. Doklady Earth Sci., 2018.V. 478. No. 2, p. 268–273.

251. Lukashin V.N. Fluxes of aerosols to the sea surface in the North Atlantic. Oceanology, 2015, V. 55, No 6, p. 877–883.

252. Lukashin V.N., Klyuvitkin A.A., Bobrov V.A., Dara O.M., Shevchenko V.P. Chemical composition of the North Atlantic aerosols. Oceanology, 2018. V. 58. No. 5, p. 717–726.

253. Mikhailov E.F., Mironova S., Mironov G., Vlasenko S., Panov A., Chi X., Walter D., Carbone S., Artaxo P., Heimann M., Lavric J., Pöschl U., Andreae M.O. Long-term measurements (2010–2014) of carbonaceous aerosol and carbon monoxide at the Zotino Tall Tower Observatory (ZOTTO) in central Siberia. Atmos. Chem. Phys., 2017. V.17, p.14365–14392.

254. Mikhailov E.F., Mironova S.Y., Makarova M.V., Vlasenko S.S., Ryshkevich T.I., Panov A.V., Andreae M.O. Studying seasonal variations in carbonaceous aerosol particles in the atmosphere over central Siberia. Izvestiya, Atmos. Oceanic Phys., 2015. V. 51, No. 4, p. 423–430.

255. Moiseenko K.B., Malik N.A. Estimation of total discharges of volcanic ash using atmospheric-transport models. J. Volcanol. Seismol., 2015. V. 9, No. 1, p. 30–47.

256. Moiseenko K.B., N.A. Malik.Reconstruction of the ashfall at Bezymyanny volcano during the eruption of December 24, 2006 by using a mesoscale model of the atmospheric transport of ash particles. Izvestiya, Atmos. Oceanic Phys., 2015. V. 51. No. 6, p. 585–5968.

257. Morozov V.N. Influence of aerosol particles on the electrical state of the surface layer. Trudy GGO, 2016. No. 583, p. 162–181. (in Russian).

258. Nakhaev M.I., Berezin E.V., Shalygina I.Yu., Kuznetsova I.N., Konovalov I.B., Blinov D.V., Lezina E.A. Pilot calculations of PM 10 and CO concentrations with complex models CHIMERE and COSMO-Ru7. Optika Atmosfery i Okeana, 2015. V. 28. No. 6, p.569–578 (in Russian).

259. Nemirovskaya I.A., Lisitzin A.P., Novigatsky A.N., Redzhepova Z.U., Dara O.M. Concentrations and composition of aerosols and particulate matter in surface waters along the transatlantic section . Doklady Earth Sci., 2016. V. 469. No. 1, p. 680–685.

260. Panchenko M.V., Zhuravleva T.B., Kozlov V.S., Nasrtdinov I.M., Pol'kin V.V., Terpugova S.A., Chernov D.G. Estimation of Aerosol Radiation Effects under Background and Smoke-haze Atmospheric Conditions over Siberia from Empirical Data. Russ. Meteorol. Hydrol. 2016, V. 41, No. 2, p. 104–111.

261. Pankratova N.V., Plakhina I.N., Makhotkin A.N. Comparing of the data of terrestrial and satellite monitoring for aerosol optical thickness of the atmosphere over Russia . Trudy GGO, 2016. No. 583, p. 251–263 (in Russian).

262. Panov A.V., Timokhina A.V., Heintzenberg J., Birmili W., Seifert P., Chi X., Andreae M.O. Spatial distribution of atmospheric aerosols over the territory of Eurasia in middle and high latitudes .Geography and Natural Resources, 2015. Vol. 36. No. 1, p. 25–30.

263. Penenko A.V., Sorokovoy A.A., Sorokovaya K.E. Numerical model of bioaerosol transformation in the atmosphere.Atmospheric and Oceanic Optics. 2016, V. 29. No. 6, p. 570–574.

264. Plakhina I.N., N.V.Pankratova, E.L. Makhotkina. Comparison of ground and satellite monitoring of aerosol optical thickness of the atmosphere in Russia.Sovremennye Problemy Distancionnogo Zondirovaniya Zemli iz Kosmosa, 2018. V. 15, No. 2, p. 225–234, (in Russian).

265. Plakhina I.N., Pankratova N.V., Makhotkina E.L. Spatio-temporal variability of the aerosol optical thickness of the atmosphere in Primorye by terrestrial and satellite data. Trudy GGO, 2017. No. 587, p. 137–152 (in Russian).

266. Poddubnyi V.A., V.V. Pol'kin, S.M. Sakerin, L.P. Golobokova, A.P. Luhzetskaya, Yu.I.Markelov, E.S. Dubinkina,O.I. Khuriganova.Complex aerosol experiment at the Middle Urals. Part 1.Experimental conditions and results of photometric measurements.Optika Atmosfery i Okeana, 2016. V. 29. No. 12, p. 1003–1010 (in Russian).

267. Poddubnyi V.A., Pol'kin V.V., Sakerin S.M., Golobokova L.P., Luhzetskaya A.P., Markelov Yu.I., Dubinkina E.S., Khuriganova O.I. Complex aerosol experiment at the Middle Urals. Part 2.Aerosol characteristics in the near-ground atmospheric layer.Optika Atmosfery i Okeana, 2016. V. 29. No. 12, p. 1011–1022 (in Russian).

268. Popovicheva O.B., Evangeliou N. , Eleftheriadis K., Kalogridis A.C., Sitnikov N., Eckhardt S., Stohl A. Black Carbon Sources Constrained by Observations in the Russian High Arctic. Environmental Science and Technology, 2017. V. 51. No. 7, p. 3871–3879.

269. Popovicheva O.B., Irimiea C., Carpentier Y., Ortega I.K., Kireeva E.D., Shonija N.K., Schwarz J., Vojtíšek-Lom M, Focsa C. Chemical Composition of Diesel/Biodiesel Particulate Exhaust by FTIR Spectroscopy and Mass Spectrometry: Impact of Fuel and Driving Cycle. Aerosol and Air Quality Research. 2017. V. 17. No. 7, p. 1717–1734.

270. Popovicheva O.B., Kireeva E.D., Persiantseva N.M., Timofeev M.A., Kistler M., Shoniya N.K., Kopeikin V.M. Aerosol composition and microstructure in the smoky atmosphere of Moscow during the August 2010 extreme wildfires. Izvestiya, Atmos. Oceanic Phys., 2017. V. 53. No. 1, p. 49–57.

271. Popovicheva O.B., Makshtas A.P., Movchan V.V., Persiantseva N.M., Timofeev M.A., Sitnikov N.M. Aerosol component of the atmospheric surface layer according observations of the expedition «North-2015». Problemy Arktiki i Antarktiki, 2017. No. 4 (114), p. 57–65 (in Russian).

272. Prokof'eva T.V., V.A.Shishkov, A.V.Kiryushin, I.Yu. Kalushin. Properties of atmospheric solid Fallouts in roadside areas of Moscow. Izvestiya, Ser. Geograficheskaya, 2015. No. 3, p. 107–120 (in Russian).

273. Raputa V.F., Akhmatova N.P., Yaroslavtseva T.V. Reconstruction of aerosol fallout fields from a series of sources .Optika Atmosfery i Okeana, 2015. V. 28. No. 6, p. 564–568 (in Russian).

274. Raputa V.F., Simonenkov D.V., Belan B.D., Yaroslavtseva T.V. Numerical study of gas and aerosol impurity transfer and transformation processes in the plume of the Norilsk industrial region. Atmospheric and Oceanic Optics. 2018. V. 31. No. 5, p. 466–470.

275. Rusina E.N., V.F.Radionov, E.E. Sibir. SIBIR Monitoring of the aerosol component in the atmosphere at middle and high latitudes and over the world ocean. Problemy Arktiki i Antarktiki. 2016. No. 2 (108), p. 5–15 (in Russian).

276. Sakerin S.M., Golobokova L.P., Kabanov D.M., Kozlov V.S., Pol'kin V.V., Radionov V.F., Chernov D.G. Comparison of average aerosol characteristics in the neighboring Arctic regions .Optika Atmosfery i Okeana. 2018. V. 31. No. 8, p. 640–646. (in Russian).

277. Sakerin S.M., Golobokova L.P., Kabanov D.M., Pol'kin V.V., Radionov V.F. Zonal distribution of aerosol physicochemical characteristics in the Eastern Atlantic. Atmospheric and Oceanic Optics. 2018. V. 31. No. 5, p. 492–501.

278. Sakerin S.M., L.P. Golobokova, D.M. Kabanov, V.V. Pol'kin, Yu.S. Turchinovich, T.V. Khodzher, O.I. Khuriganova. Spatiotemporal variations in aerosol characteristics along the route of the Indian-Atlantic expedition onboard the research vessel Akademik Nikolaj Strakhov. Atmospheric and Oceanic Optics. 2017. V. 30. No. 4, p. 349–359.

279. Sakerin S.M., D.M. Kabanov. Spatiotemporal Variations in Atmospheric Aerosol Optical Depth along the Route of the 42nd Cruise of RV "Akademik Boris Petrov". Atmospheric and Oceanic Optics. 2018. V. 31. No. 3, p. 250–256.

280. Sakerin S.M., Kabanov D.M., Kozlov V.S., Pol'kin V.V., Radionov V.F., Chernov D.G. Comparative analysis of atmospheric aerosol in polar regions of the Northern and Southern hemispheres. Problemy Arktiki i Antarktiki. 2016. No. 1 (107), p. 73–83 (in Russian).

281. Sakerin S.M., Kabanov D.M., Polkin V.V., Radionov V.F., Holben B.N., Smirnov A. Variations in optical and microphysical characteristics of aerosol along the route of Russian Antarctic Expeditions in the East Atlantic. Atmospheric and Oceanic Optics. 2017. V. 30. No. 1, p. 89–102.

282. Sakerin S.M., D.M. Kabanov, V.F. Radionov, D.G.Chernov, Yu.S. Turchinovich, K.E. Lubo-Lesnichenko, A.N. Prakhov. Generalization of results of atmospheric aerosol optical depth measurements on Spitsbergen Archipelago in 2011–2016. Atmospheric and Oceanic Optics, 2018. V. 31. No. 2, p. 163–170.

283. Samoilova S.V., Balin Yu.S., Kokhanenko G.P., Penner I.E. Troposphere aerosol layers: homogeneity in the altitude distribution of the aerosol optical and microphysical characteristics. Optika Atmosfery i Okeana, 2016. V. 29. No. 12, p. 1043–1049 (in Russian).

284. Semoutnikova E.G., Gorchakov G.I., Sitnov S.A., Kopeikin V.M., Karpov A.V., Gorchakova I.A., Ponomareva T.Ya., Isakov A.A., Gushchin R.A., Datsenko O.I., Kurbatov G.A., Kuznetsov G.A. Siberian smoke haze over European territory of Russia in July 2016: Atmospheric pollution and radiative effects. Atmospheric and Oceanic Optics, 2018. V. 31. No. 2, p. 171–180.

285. Shevchenko V.P., D.P.Starodymova, A.A.Vinogradova, A.P.Lisitzin, V.I.Makarov, S.A.Popova, V.V.Sivonen, V.P. Sivonen.Elemental and organic carbon in atmospheric aerosols over the northwestern coast of Kandalaksha Bay of the White Sea. Doklady Earth Sci., 2015. V. 461. No. 1, p. 242–246.

286. Shukurov K.A., Shukurova L.M. Source regions of ammonium nitrate, ammonium sulfate, and natural silicates in the surface aerosols of Moscow oblast. Izvestiya, Atmos. Oceanic Phys., 2017. V. 53. No. 3, p. 316–325.

287 Sitnov S.A., Mokhov I.I. Anomalous transboundary transport of the products of biomass burning from North American wildfires to Northern Eurasia. Doklady Earth Sci. 2017. V. 475. No. 1, p. 832–835.

288. Sitnov S.A., Mokhov I.I., Gorchakov G.I. The link between smoke blanketing of European Russia in summer 2016, Siberian wildfires and anomalies of large-scale atmospheric circulation. Doklady Earth Sci., 2017. V. 472. No. 2, p. 190–195.

289. Sitnov S.A., Mokhov I.I., Gorchakov G.I., Dzhola A.V. Smoke haze over the European part of Russia in the summer of 2016: A link to wildfires in Siberia and atmospheric circulation anomalies. Russ. Meteorol. Hydrol., 2017. V. 42. No. 8, p. 518–528.

290. Sizov N.I., Akimenko R.M., Aref'ev V.N., Kashin F.V., Orozaliev M.D., Sinyakov V.P., Sorokina L.I. Variability of atmospheric aerosol optical depth over the Northern Tian Shan .Russ. Meteorol. Hydrol., 2015. V. 40. No. 3, p. 180–185.

291. Smirnov N.S., Korotkov V.N., Romanovskaya A.A. Black carbon emissions from wildfires on forest lands of the Russian Federation in 2007–2012. Russ. Meteorol. Hydrol., 2015. V. 40. No. 7, p. 435–442.

292. Sorokin A.A., Mal'kovskii S.I., Korolev S.P., Girina O.A., Romanova I.M., Lupyan E.A., Balashov I.V., Efremov V.Y., Kramareva L.S., Simonenko E.V. Satellite observations and numerical simulation results for the comprehensive analysis of ash cloud transport during the explosive eruptions of Kamchatka volcanoes. Russ. Meteorol. Hydrol., 2017. V. 42. No. 12, p. 759–765.

293. Starodymova D.P., Shevchenko V.P., Sivonen V.P., Sivonen V.V. Material and elemental composition of surface aerosols on the north-western coast of the Kandalaksha Bay of the White Sea. Atmospheric and Oceanic Optics, 2016. V. 29. No. 6, p. 507–511.

294. Stepkina M.Y., Kudryashova O.B., Antonnikova A.A., Muravlev E.V. Experimental study of the evolution of fine particles by methods of aerosol cloud generation .Optika Atmosfery i Okeana, 2018. V. 31. No. 6, p. 501–504. (in Russian).

295. Terpugova S.A., Zenkova P.N., Kabanov D.M., Pol'kin V.V., Golobokova L.P., Panchenko M.V., Sakerin S.M., Lisitzin A.P., Shevchenko V.P., Politova N.V., Kozlov V.S., Khodzher T.V., Shmargunov V.P., Chernov D.G. Results of the Study of Aerosol Characteristics in the Atmosphere of the Kara and Barents Seas in Summer and Autumn 2016 .Atmospheric and Oceanic Optics, 2018. V. 31. No. 5, p. 507–518.

296. Tomshin O.A., Solovyev V.S. Study of large-scale inhomogeneities of aerosol fields caused by forest fires in Siberia. Optika Atmosfery i Okeana. 2016, V. 29. No. 7, p. 598–602 (in Russian).

297. Troshkin D.N., Pavlov V.E. Statistical model of cloud optical thickness in specific Yamal areas using satellite-based data.Optika Atmosfery i Okeana, 2018. V. 31. No. 11, p. 876–880. (in Russian).

298. Uspensky A.A., Makhotkin A.N., Volberg N. Sh., Stepakov A.V. Aethalometer AE-33 use in atmospheric aerosol's research. Trudy GGO, 2016. No. 583, p. 209–226 (in Russian).

299. Vasiliev M.S., Nikolashkin S.V. Temperature effect of smoke aerosol in the summer season over the central part of Yakutia for the period 2004–2014.Optika Atmosfery i Okeana, 2015. Vol. 28. No. 12, p.1106–1111 (in Russian).

300. Veretennikov V.V. Interannual variations in aerosol microstructure parameters according to data of sun photometer measurements in Tomsk. Atmospheric and Oceanic Optics. 2017. V. 30. No. 6, p. 564–573.

301. Veretennikov V.V. Retrieval of microstructure parameters of coarse-mode aerosol using their regression relationships with spectral extinction of light in the IR.Atmospheric and Oceanic Optics, 2017. V. 30. No. 6, p. 555–563.

302. Veretennikov V.V., Men'shchikova S.S. Modified algorithm for reconstructing the aerosol microstructure from measurements of spectral light extinction on the basis of the hybrid model.Atmospheric and Oceanic Optics, 2016. V. 29. No. 1, p. 27–32.

303. Veretennikov V.V., Men'shchikova S.S., Uzhegov V.N. Variability of microstructure parameters of the near-surface aerosol in the summer period retrieved by inverting the spectral extinction measurements along a horizontal path in Tomsk. Part II. Volume concentration and mean radius of particles.Optika Atmosfery i Okeana, 2018. V. 31. No. 11, p. 867–875. (in Russian).

304. Vinogradova A.A., Smirnov N.S., Korotkov V.N. Anomalous wildfires in 2010 and 2012 on the territory of Russia and supply of black carbon to the Arctic.Atmospheric and Oceanic Optics, 2016. V. 29. No. 6, p. 545–550.

305. Vinogradova A.A., Smirnov N.S., Korotkov V.N., Romanovskaya A.A. Forest fires in Siberia and the Far East: Emissions and atmospheric transport of black carbon to the Arctic.Atmospheric and Oceanic Optics, 2015. V. 28. No 6, p. 566–574.

306. Vinogradova A.A., Titkova T.B., Ivanova Yu.A. Passages of anomalies in black carbon surface air concentration at Tiksi station, Yakutiya.Optika Atmosfery i Okeana, 2018. V. 31. No. 10, p. 837–844. (in Russian).

307. Vinogradova A.A., Vasileva A.V. Black carbon in air over northern regions of Russia: Sources and spatiotemporal variations.Atmospheric and Oceanic Optics, 2017. V. 30. No. 6, p. 533–541.

309. Volkova K.A., Poberovsky A.V., Timofeev Yu.M., Ionov D.V., Holben B.N., Smirnov A., Slutsker I. Aerosol optical characteristics retrieved from CIMEL Sun Photometer measurements (AERONET) near St. Petersburg. Atmospheric and Oceanic Optics, 2018. V. 31. No. 6, p. 635–641.

310. Volodin E.M., Kostrykin S.V. The aerosol module in the INM RAS climate model. Russ. Meteorol. Hydrol., 2016. V. 41. No. 8, p. 519–528.

311. Voronetskaya N.G., Pevneva G.S., Golovko A.K., Kozlov A.S., Arschinov M.Yu., Belan B.D., Simonenkov D.V., Tolmachev G.N. Spatial variability of aerosol organic component in the ground layer and in the free atmosphere. Optika Atmosfery i Okeana, 2015. V. 28. No. 9, p. 825–829 (in Russian).

312. Whiteman D.N, Pérez-Ramírez D., Veselovskii I., Colarco P., Bucharde V. Retrievals of aerosol microphysics from simulations of spaceborne multiwavelength lidar measurements. J. Quantitat. Spectrosc. Radiat. Transfer. 2018. Vol. 205, p. 27–39.

313. Yermakov A.N., Golobokova L.P., Netsvetaeva O.G., Khodzher T.V., Aloyan A.E., Arutyunyan V.O. On the Nature of Aerosol Particles in the Atmosphere of Irkutsk. Izvestiya, Atmos. Oceanic Phys., 2018. V. 54. No. 2, p. 162–172.

314. Zakharenko V.S., Daybova E.B. Composition and properties of the surface of aerosol microparticles produced from nonporosity zinc oxide in ambient air. Optika Atmosfery i Okeana, 2018. V. 31. No. 6, p. 481–484. (in Russian).

315. Zayakhanov A.S., Zhamsueva G.S., Sungrapova I.P., Tsydypov V.V. Features of Diurnal Variability of Ultrafine Aerosol in the Air of the Baikal Coastal Zone and Arid Zone of Mongolia. Atmospheric and Oceanic Optics, 2018. V. 31. No. 3, p. 257–262.

316. Zhdanova E. Yu., Chubarova N.E. Spatial variability of aerosol optical thickness on the territory of Moscow and Moscow Region by satellite and ground based data.Sovremennye Problemy Distancionnogo Zondirovaniya Zemli iz Kosmosa, 2018. V. 15. No. 7, p. 236–248. (in Russian).

317. Shavlov, A.V., I.V. Sokolov, V.L. Hazan, et al. Spatial structure of water fog. Doklady Earth Sci., 2015. V. 461. No. 2, p. 422–426.

318. Sterlyadkin V.V. Spatial selection and grouping of raindrops by size in wind gusts. Izvestiya. Atmos. Oceanic Phys., 2015. V. 51. No 6, p. 615–623.

319. Konoshonkin, A.V. Optical characteristics of irregular atmospheric ice columns. Atmospheric and Oceanic Optics, 2017. V. 30. No 6, p. 508–516.

320. Dmitrieva-Arrago L.R., Trubina M.A., Tolstykh, M.A. The role of cloud phase composition in shortwave and longwave radiation fluxes formation. Trudy Gidrometcentra Rossii, 2017. No. 363, p. 19–34. (in Russian).

321. Shavlov A.V., Dzhumadzhi V.A., Yakovenko A.A. Charge of drops of water at evaporation and condensation. Trudy GGO, 2017. No. 587, p. 56–78. (in Russian).

322. Vetrov V.A., Kuzovkin V.V., Manzon D.A. Precipitation acidity and fallout of nitrogen and sulfur on the territory of the Russian Federation from the data of monitoring the chemical composition of snow cover. Russ. Meteorol. Hydrol., 2015. V. 40. No. 10, p. 667–674.

323. Eremina I.D., N.E. Chubarova, A.E. Aloyan, V.O. Arutyunyan, I.K. Larin, A.N. Yermakov. Acidity and mineral composition of precipitation in Moscow: Influence of deicing salts. Izvestiya, Atmos. Oceanic Phys., 2015, V. 51. No. 6, p. 624–632.

324. Eremina, I.D., A.E. Aloyan, V.O. Arutyunyan, I.K. Larin, N.E.Chubarova, A.N. Yermakov. Hydrocarbonates in atmospheric precipitation of Moscow: Monitoring data and analysis. Izvestiya, Atmos. Oceanic Phys., 2017. V. 53. No. 3, p. 334–342.

325. Lavrukhin, Y.E., M.I. Dinu. Influence of radon on the acidification of atmospheric precipitation .Geochemistry Intern., 2017. V. 55. No. 1, p. 125–130.

326. Chizhova J.N., I.D. Eremina, N.A. Budantseva, G.V. Surkova, Y.K. Vasil'chuk. Concentration of ^{18}O in precipitation over Moscow in 2014. Russ. Meteorol. Hydrol., 2017. V. 42. No. 1, p. 54–63.

327. Kondrat'ev I.I., D.E. Mukha, A.G. Boldeskul, S.G.Yurchenko, T.N. Lutsenko. Chemical composition of precipitation and snow cover in the Primorsky krai. Russ. Meteorol. Hydrol. 2017. V. 42. No. 1, p. 64–70.

328. Semenets E.C. The method of determining a typical concentration of contaminants in precipitation (according to the chemical precipitation data of stations in St. Petersburg and Voeikovo). Trudy GGO, 2016. No. 583, p. 197–208. (in Russian).

329. Kalinskaya D.V., Varenik A.V., Papkova A.S. Phosphorus and silicon as markers of dust aerosol transfer over the Black Sea region. Sovremennye Problemy Distancionnogo Zondirovaniya Zemli iz Kosmosa, 2018. V. 15. No. 3, p. 217–225. (in Russian).

330. Yanchenko N.I., E.I. Kotova. Sources of fluorine in atmospheric precipitation in Bratsk.Meteorologiya i Gidrologiya. 2018. No. 5, p. 108–112 (in Russian).

331. Essays on the History of Weather Modification in the USSR and the Post-Soviet Territory. St-Petersburg, Russian State Hydrometeorological University (RSHMU), 2017. St. Petersburg. Fenix. 352 p. (in Russian).

332. Galechan G.A. Stimulation of precipitation. Nature (Russia). The Russian Academy of Sciences. No. 6. Published: Nauka (Moscow), 2015, p. 3–11. (in Russian).

333. Petrunin, A.M., V.P. Korneyev, B.P. Koloskov, A.V. Chastukhin, et al. Numerical and experimental studies of the propagation of ice-generating agent in the atmospheric boundary layer when interacting with ground-based aerosol generators. Proceed-

ings of the 2nd International science conference “Innovation methods and means of research in the field of atmospheric physics, hydrometeorology, ecology, and climate change.”Stavropol, 21–25 September, 2015, p. 105–110 (in Russian).

334. Sinkevich, A.A., T.V. Kraus, Yu.P. Mikhailovsky, A.B. Kurov. Investigation of changesin the characteristics of a cumulonimbus cloud upon its modification with remote aids.Proceedings of the 2nd International science conference “Innovation methods and means of research in the field of atmospheric physics, hydrometeorology, ecology, and climate change”. Stavropol, 21–25 September, p. 113–114 (in Russian).

335. Kalov, Kh.M., R.Kh. Kalov. Investigation of turbulence in convective clouds and near-cloud space.Proceedings of the 2nd International science conference with elements of a scientific school “Innovation methods and means of research in the field of atmospheric physics, hydrometeorology, ecology, and climate change”. Stavropol, 21–25 September, 2015, p. 88–92.

336. Abshaev A.M., M.T. Abshaev, V.A. Zorin, D.B. Kratirov et al. Automated antihail system “AS-Elia”. Proc. of the 2nd Intern. Sci. Conf. with Elements of a Sci. School “Innovation methods and means of research in the field of atmospheric physics, hydrometeorology, ecology, and climate change”. Stavropol, 21–25 September, 2015, p. 43–48.

337. Bychkov, A.A., A.M. Petrunin, A.V. Chastukhin. A mobile weather modification system aimed at intended precipitation enhancement. Proc. of A.F. Mozhaisky Military – Space Academy, 2016. No. 653, p. 67–70, 212. (in Russian).

338 Doronin,A.P., G.G. Shchukin, V.M. Petrochenko, O.I. Didyk, S.A. Shmalko. Assessment of the feasibility of undulated stratiform cloud dissipation in the interests of hydrometeorological support. Navigatsiya I Gidographiya, 2015. No.45, p. 6069 (in Russian).

339. Abshaev M.T., A.V. Malkarova. Physical basics of hail prevention, the results and prospects of development.Proceedings of the 2nd Intern. Sci. Conf. “Innovation methods and means of research in the field of atmospheric physics, hydrometeorology, ecology, and climate change”. Stavropol, 21–25 September, 2015, p. 7–15 (in Russian).

340. Ashabokov, B.A., L.M. Fedchenko, A.V. Shapovalov, V.A. Shapovalov. Development of a method controlling the formation of hail cloud microstructure. Proc. of the 2nd Intern. Sci. Conf. “Innovation methods and means of research in the field of atmospheric physics, hydrometeorology, ecology, and climate change”. Stavropol, 21–25 September, 2015, p. 208–211 (in Russian).

341. Kamalov B.A. Some uncertainties of modifying hail processes by cloud seeding. Proceedings of the 2nd Intern. Sci. Conf. “Innovation methods and means of research in the field of atmospheric physics, hydrometeorology, ecology, and climate change”. Stavropol, 21–25 September, 2015, p. 93–98 (in Russian).

342. Abshaev, M.T., I.V. Merkulova.A brief analysis of the quality of implementing hail protection technology. Proc. of the 2nd Intern. Sci. Conf “Innovation methods and means of research in the field of atmospheric physics, hydrometeorology, ecology, and climate change”. Stavropol, 21–25 September, 2015, p. 48–53 (in Russian).

343. Kamalov B.A.The problems of the CIS intended weather modification theory and practice. (Namangan State University). Meteorologiya i Gidrologiya, 2017. No. 4, p. 113–123 (in Russian).

344 Chastukhin A.V., N.S. Kim, A.M. Petrunin. Methodological aspects of the assessment of ice-generating efficiency of aircraft and ground-based generators. Proc. of the 2nd Intern. Sci. Conf. “Innovation methods and means of research in the field of atmospheric physics, hydrometeorology, ecology, and climate change”. Stavropol, 21–25 September 2015, p. 115–119 (in Russian).

345 Chastukhin, A.V., B.N. Sergeyev, A.A. Bychkov, A.M. Petrunin.The results of the numerical modeling of supercooled fog dispersal using three-dimensional numerical model «FogSeeding». Materials of the 4th All-Russia Science Conf. “The problems of military-application geophysics and natural environment control. St-Petersburg, 20–21 April 2016, p. 152–155 (in Russian).

346 Vladimirov, S.A. Numerical modeling with parameterization of the microphysical processes of intended modification of convective cloud precipitation. Proc. of the 2nd Intern. Sci. Conf. “Innovation methods and means of research in the field of atmospheric physics, hydrometeorology, ecology, and climate change”. Stavropol, 21–25 September 2015, p. 215–217 (in Russian).

347 Pastushkov, R.S. Algorithmization of the formation and evolution of liquid-drop and crystal phases for the numerical modeling of convective clouds and their modification with ice-generating aerosols. Proc. of the 2nd Intern. Sci. Conf. “Innovation methods and means of research in the field of atmospheric physics, hydrometeorology, ecology, and climate change”. Stavropol, 21–25 September, 2015, p. 25–28 (in Russian).

Dynamic Meteorology

M.V. Kurgansky[1], *V.N. Krupchatnikov*[2,3]
[1] A.M. Obukhov Institute of Atmospheric Physics,
Russian Academy of Sciences
kurgansk@ifaran.ru
[2] Siberian Regional Scientific Research
Hydrometeorological Institute
[3] Institute of Computational mathematics
and mathematical Geophysics,
Siberian Branch of Russian Academy of Sciences
vkrupchatnikov@yandex.ru

Introduction

Scientific work in the field of dynamical meteorology, which has been carried out by the Russian researchers in 2015–2018 and will be discussed in this review can conditionally be related to the following topics: "General dynamics of the atmosphere", "Large-scale processes and the weather forecast", "Mesoscale processes", "Small-scale motions and turbulence in the atmospheric boundary layer", "Dynamical interaction between lower, middle and high atmosphere", "Mathematical problems of climate and ecology". The review structure follows basically the previous review report over 2011–2014 (Kurgansky and Krupchatnikov, 2016).

General dynamics of the atmosphere

All-Russian conference with international participation "Turbulence, atmosphere and climate dynamics", dedicated to the centenary of the birth of Academician Alexander Mikhailovich Obukhov, took place from March 16 to 18, 2018 in Moscow. The conference discussed key issues related to one of the most relevant areas in the Earth sciences, namely the research in the field of atmospheric physics, climate and environment. Selected papers from the conference were published in the collection (Turbulence, Atmospheric and Climate Dynamics, 2018).

Under the auspices of the WMO World Weather Research Program in connection with the Olympic Games, a number of meteorological projects have been prepared and implemented since 2000, because the timely provision of high-quality weather forecasts is extremely important for organizers and participants of sporting events, especially outdoors. This allows meteorologists to

demonstrate new technologies for weather forecasting, taking advantage of the broad capabilities of the observation network in the Olympic Games area and comparing various weather forecasting systems. One of these projects (FROST-2014) was associated with the Winter Olympic and Paralympic Games in Sochi from February 7 to 23 and from March 7 to 16, 2014, respectively. The articles by Kiktev et al. (2015, 2017) present a general description of the project FROST-2014 and the results of its successful implementation. In particular, it was noted that for the meteorological support of the Winter Olympic Games in 2014, the observation network in the Sochi region was strengthened by more than 40 automatic meteorological stations, a Doppler radar with dual polarization, temperature and wind profilers, radars, etc., which allowed the use of Sochi booth for the development, testing and intercomparison of various technologies for forecasting the current weather and short-term numerical weather forecasting. The predictive products of the project FROST-2014 were used for operational meteorological services for Olympic events. The FROST-2014 system involved six current weather forecast systems (based on models, radar tracking and combined current weather forecasting systems), nine deterministic mesoscale numerical weather prediction models (with grid spacing down to 250 meters) and six ensemble forecasting systems (including two ones with explicitly simulated deep convection). The archive of winter meteorological observations and forecasts formed during the implementation of the FROST-2014 project is a valuable information resource for research on mesoscale predictability, as well as for the development and validation of current weather forecast systems and short-term forecast systems in a complex landscape. The new technologies obtained and also the exchange of experience and professional development contributed to the success of the Olympics and left a valuable legacy for further research.

During the reporting period, three monographs were published that relate to the dynamics of the atmosphere. In 2016, the MAKS Press Publishing House published a collective monograph “Mathematical modeling of the Earth system” (Volodin et al., 2016). The purpose of the authors was to present some of the results of work carried out at the G.I. Marchuk Institute of Computational Mathematics of the Russian Academy of Sciences to create a numerical model of the Earth system that meets modern requirements and is at the forefront of the worldwide scientific and technological activities in this research field. This model is used both to predict future climate change, and to study the effects of these changes on land and sea ecosystems, the chemical composition of the atmosphere, the earth's global electrical circuit, etc. The first chapter of this monograph entitled “Atmospheric Dynamics” is directly related to this review in its content. The “Atmospheric and Underlying Surface Interaction” section

of the second chapter of the book written by V.N. Lykosov has also a direct bearing on this review. In 2017, the Publishing House GEOS published the book "Dynamics of Wave and Exchange Processes in the Atmosphere" (Dynamics of Wave and Exchange Processes…, 2017), which presents the results of experimental, theoretical and model studies of the dynamics of wave and echange processes in the atmosphere performed in recent years in the A.M. Obukhov Institute of Atmospheric Physics of the Russian Academy of Sciences, including under the support of the Russian Foundation for Basic Research. The book addresses a wide range of issues: the interaction of the atmosphere with the underlying surface; development, propagation and interaction of waves, vortex structures and turbulence in the atmosphere from the surface layer to the lower thermosphere and the systematic influence of these processes on the results of remote sensing. In accordance with the topics covered, the book consists of four chapters: Atmospheric Turbulence, Atmospheric Boundary layer, Atmosphere and Ocean Interaction, Upper Atmosphere. The same Publishing House published the the book "Intense Atmospheric Vortices and their Dynamics" (Intense Atmospheric Vortices…, 2018), which presents the results of experimental, diagnostic, theoretical, and model studies of atmospheric vortices that have been performed in recent years in A.M. Obukhov Institute of Atmospheric Physics, with the support from the Russian Foundation for Basic Research. An attempt was made to present general analysis of the hierarchy of intense atmospheric vortices, ranging from circumpolar vortices and centers of action of the oceanic and continental scale to extratropical cyclones & anticyclones, including blocking anticyclones, tropical cyclones (hurricanes, typhoons), intense polar lows ("polar hurricanes"), and tornadoes.

The classic chapter of general dynamics of the atmosphere is the dynamics of large-scale atmospheric processes, including the theory of quasi-two-dimensional turbulence and the theory of dynamical systems.

In Dymnikov (2016) problems are considered in which the role of Casimirs in forming dynamics of the two-dimensional ideal incompressible fluid is basically studied; in particular, the conditions are formulated which arise in the stability problem of two-dimensional flows in the presence of Casimirs. Some general approaches to the construction of difference schemes for solving equations of two-dimensional fluid which possess the given Casimirs are considered.

In Perezhogin et al. (2017) the influence of numerical approximations on statistical characteristics of modelled two-dimensional turbulence sustained by a stochastic external forcing is studied. The ability of various finite-difference and semi-Lagrangian schemes to reproduce reliably the dual energy and enstrophy cascades for coarse spatial resolution is tested. It is also studied how the requirement of preserving invariants inherent to a two-dimensional ideal fluid

is important relative to numerical schemes. The results of calculations with high spatial resolution were taken as a reference solution. The choice of studied schemes was motivated by their use in atmosphere and ocean numerical models, in particular, in the Institute of Numerical Mathematics climate model (INMCM) and semi-Lagrangian absolute vorticity (SLAV) model of medium-range weather forecast. The importance of conservation laws of integral vorticity and enstrophy is revealed in the numerical experiments with a small-scale external forcing. Contrary to a viscous fluid at high Reynolds numbers, the equations of a two-dimensional ideal fluid have an infinite number of invariants, the presence of which complicates both its statistical description and the numerical modeling.

In Perezhogin and Dymnikov (2017a,b) equilibrium states of Arakawa approximations of a two-dimensional incompressible inviscid fluid are investigated in the case of high resolution 8192×8192. Comparison of these states with quasi-equilibrium states of a viscous fluid is made. Special attention is paid to the stepped shape of large coherent structures and to the presence of small vortices in final states. It is shown that the large-scale dynamics of Arakawa approximations is similar to the theoretical predictions for an ideal fluid. The possibility of application of the theory of Cesaro convergence (time averaging) for the solution of the problem of unsteadiness of final states and the problem of achievement of equilibrium states are considered.

In a paper by Dymnikov and Perezhogin (2018) published in the memorial issue of Izvestiya, Atmospheric and Oceanic Physics journal dedicated to the centenary of birth of A.M. Obukhov, statistical properties of different finite-dimensional approximations of two-dimensional ideal fluid equations are studied. A special class of approximations introduced by A.M. Obukhov (systems of hydrodynamic type) is considered. Vorticity distributions over area and quasi-equilibrium coherent structures are studied. These coherent structures are compared to structures occurring in a viscous fluid with random forcing.

Gritsun and Lucarini (2017) study the response of a simple quasi-geostrophic barotropic model of the atmosphere to various classes of perturbations affecting its forcing and its dissipation using the formalism of the Ruelle response theory. They investigate the geometry of such perturbations by constructing the covariant Lyapunov vectors of the unperturbed system and discover in one specific case – orographic forcing – a substantial projection of the forcing onto the stable directions of the flow. This results into a resonant response shaped as a Rossby-like wave that has no resemblance to the unforced variability in the same range of spatial and temporal scales. Such a climatic surprise corresponds to a violation of the fluctuation–dissipation theorem, in

agreement with the basic tenets of nonequilibrium statistical mechanics. The resonance can be attributed to a specific group of rarely visited unstable periodic orbits of the unperturbed system. The obtained results reinforce the idea of using basic methods of nonequilibrium statistical mechanics and highdimensional chaotic dynamical systems to approach the problem of understanding climate dynamics.

The nonlinear dynamics of long-wave perturbations of the inviscid Kolmogorov flow, which models periodically varying in the horizontal direction geophysical flows, either atmospheric motions or oceanic currents, is studied in (Kalashnik and Kurgansky, 2018). To describe this dynamics, the Galerkin method with basis functions representing the first three terms in the expansion of spatially periodic perturbations in the trigonometric series is used. The orthogonality conditions for these functions formulate a nonlinear system of partial differential equations for the expansion coefficients. Based on the asymptotic solutions of this system, a linear, quasilinear, and nonlinear stage of perturbation dynamics is identified. It is shown that the time-dependent growth of perturbations during the first two stages is succeeded by the stage of stable nonlinear oscillations. The corresponding oscillations are described by the oscillator equation containing a cubic nonlinearity, which is integrated in terms of elliptic functions. An analytical formula for the period of oscillations is obtained, which determines its dependence on the amplitude of the initial perturbation. Structural features of the field of the stream function of the perturbed flow are described, associated with the formation of closed vortex cells and meandering flow between them. As a supplement, an asymptotic analysis of nonlinear dynamics of long-wave perturbations superimposed on a damped by small viscosity Kolmogorov flow (very large, but finite Reynolds numbers) is made. It is strictly shown that all velocity components of the perturbed flow remain bounded in this case.

Enstrophy in a fluid relates to the dissipation tendency in a fluid that has use in studying turbulent flows. It also corresponds to vorticity as kinetic energy does to velocity. Earlier work showed that the integrated regional enstrophy (IRE) was related to the sum of the positive Lyapunov exponents. Lyapunov exponents are the characteristic exponent(s) of a dynamic system or a measure of the divergence/convergence of system trajectories that are initially close together. Relatively high values of IRE derived from an atmospheric flow field in the study of atmospheric blocking was identified with the onset/demise of blocking events, but also transitions of the large-scale flow in general. Kolmogorov – Sinai Entropy (KSE), also known as metric entropy, is related to the sum of the positive Lyapunov exponents as well. This quantity can be thought of as a measure of predictability (higher values, less predictability) and will be

non-zero for a chaotic system. Thus, the measure of IRE is related to KSE as well. The study by Jensen et al. (2017) shows that relatively low (high) values of IRE derived from atmospheric flows correspond to a more stable (transitioning) large-scale flow with a greater (lesser) degree of predictability and KSE. The transition is least predictable and should be associated with higher IRE and KSE.

The dynamic character of an enstrophy-based diagnostic, previously used in the study of atmospheric blocking, is examined by Jensen et al. (2018), in near-term future simulations from the Institut Pierre Simon Laplace Climate Model version 4 (IPSL-CM4) and version 5 (IPSL-CM5) climate models of the Northern Hemisphere flow for moderate climate change scenarios. Previous research has shown that integrated regional enstrophy (IE) increases during blocking onset and decay, which is a reflection of planetary-scale instability. In addition, IE has been shown previously to increase during flow regime transitions in general, even those not associated with blocking events. Here, a 31-year IE diagnostic time series is examined for changes in short term (5–40 days) planetary-scale variability that may correspond to flow regime changes in an increased carbon dioxide environment. The time-series analysis herein indicates that the IE diagnostic provides evidence for approximately 30–35 atmospheric flow regime transitions per year in a warmer climate, which is similar to that of the control run and the latest 30-year observed climate, as derived from reanalyses. This result has implications regarding the predictability of weather in a warmer world.

Atmospheric convection is a fundamentally important mechanism responsible for the generation of kinetic energy of atmospheric motion, and several papers are devoted to its study.

In Sukhanovskii et al. (2016a), convection over a localized heat source in a cylindrical layer was studied experimentally and numerically for fluids with different values of Prandtl number. A basic flow produced by a horizontal temperature gradient occupies the whole layer and leads to unstable temperature stratification over the heating area and the formation of a complex system of secondary flows. The main focus of the study was the spatial and temporal evolution of small-scale convective structures in the boundary layer of a basic flow. Transitions from transverse rolls to radial rolls and further to their superposition were found in experiment and numerical simulation. Various types of visualization revealed co-existence of different kinds of secondary flows. Complex convective patterns over the heating area are temporally periodic. The characteristic frequency of transverse rolls depends on Rayleigh number for a wide range of governing parameters.

An experimental study of the steady-state cyclonic vortex from an isolated heat source in a rotating fluid layer is described in Sukhanovskii et al. (2016b). The structure of the laboratory cyclonic vortex is similar to the typical structure of tropical cyclones from observational data and numerical modelling, including secondary flows in the boundary layer. Different constraints of the steady-state hurricane-like vortex were studied. The three main dimensional parameters that define the vortex structure for a fixed geometry – heat flux, rotation rate and viscosity – were varied independently. Characteristics of the steady-state cyclonic vortex were measured experimentally for different values of kinematic viscosity (from 5 to 25 cSt), rotation rate (from 0.04 to 0.17 rad s^{-1}) and heat flux (from 1 to 4.6 kW m^{-2}). The crucial importance for the vortex formation has angular momentum exchange in the viscous boundary layer. It was shown that viscosity is one of the main parameters that define the steady-state vortex structure. Increasing the kinematic viscosity may substantially suppress the cyclonic motion for fixed values of buoyancy flux and rotation rate. Strong competition between buoyancy and rotation provides the optimal ratio of the heat flux and rotation rate for achieving a cyclonic vortex of maximal intensity. It was found that relatively small variation of the rotation rate for the fluids with low kinematic viscosity may remarkably change the cyclonic vortex structure and intensity.

In Sukhanovskii et al. (2017b), the secondary flows of different types were studied in a boundary layer of cyclonic vortex over localized heater. Near the periphery of the heating area system of horizontal rolls oriented along the basic flow is formed. Thermal plumes which are originated between counter-rotating horizontal rolls are pushed to the centre by basic flow and create spiral bands. Both types of observed secondary flows (rolls and spiral bands) are of convective nature. Cyclonic vortex becomes unstable at low values of viscosity and fast rotation of the experimental model. The instability of the vortex is tightly connected with a structure of the radial inflow. For moderate values of rotational Reynolds number Re the radial flows consist of several branches which transport angular momentum to the centre of the model. When Re exceeds critical value (about 23) radial inflow changes its structure and appears as one wide branch which does not reach the centre. As a result, the vortex that slowly moves around the centre is formed instead of the vortex localized in the centre. Further increase of Re leads to chaotic state with several vortices which appears at different locations near the periphery of the heating area. The map of regimes with stable and unstable vortices is presented. The applicability of experimental results to the formation of large-scale atmospheric vortices is discussed.

In traditional theoretical models of convection from isolated sources, the results usually depend little on their sizes: convective jets and isolated thermals rapidly “forget” the source geometry. However, new problems in which the

sizes of a source are relatively large and can significantly influence results have recently become important. These are, for example, problems of the dynamics of intensive methane emissions of geologic origin. The paper by Ingel (2016) generalizes some well-known integral models of thermals and jets. Although these simple schemes cannot compete with complicated numerical models in describing the spatial structure of the currents, they are shown to be able to reproduce a number of important numerical results rather well (the height and time of the rise of convective elements) and, moreover, to find clear physical laws and determine explicit dependences on parameters of the problem.

In Ingel (2018d) the nonlinear integral model of a turbulent thermal is extended onto the case of the non-zero horizontal component of its motion relative to the medium (e.g., thermal floating-up in shear flow). In contrast to traditional models, the possibility of a heat source in the thermal is taken into account. For a piecewise constant vertical profile of the horizontal velocity of the medium, analytical solutions are obtained which describe different modes of dynamics of thermals. The nonlinear interaction between the horizontal and vertical components of thermal motion is studied because each of the components influences the rate of entrainment of the surrounding medium, i.e., the growth rate of the thermal size and, hence, its mobility. It is shown that the enhancement of the entrainment of the medium due to the interaction between the thermal and the cross flow can lead to a significant decrease in the mobility of the thermal.

Ingel (2018c) presents results of theoretical assessments referring to the convection that appears above a "cold spot" on a horizontal surface. Consideration is given to the case of thermal inhomogeneities with fairly large amplitude where one cannot restrict oneself to a linear approximation. An analog of the Rayleigh number proportional to the amplitude of the temperature deviation and to the cube of the horizontal scale of the thermal inhomogeneity is a dimensionless criterion. From simple physical considerations and the scaling analysis, the author has obtained explicit analytical expressions for the depth (height) of penetration of thermal perturbations into a medium and for the amplitudes of convection-velocity components. These results are in good agreement with the experimental data available in the literature. The Nusselt number is proportional to the analog of the Rayleigh number to power 1/5; here, from a comparison with the experimental results, it follows that the proportionality factor is of the order of unity. The influence of the convection in question on the transfer of a passive impurity has been determined.

The linear hydrodynamic instability of the spatially periodic system of updrafts and downdrafts in a stably stratified atmosphere is studied in Kalashnik and Kurgansky (2018). Such formulation of the problem is used to simulate the

cloud systems observed in the atmosphere, when the zones of up drafts correspond to clouds and those of downdrafts correspond to intercloud intervals. A rather unexpected conclusion was made that the consideration of turbulent viscosity and thermal conductivity of the at mo sphere as well as of radiative cooling leads to the in stability at the Richardson numbers exceeding the critical value of 1/8 for the nondissipative case.

The classical Rayleigh theory of convective instability of a viscous and heat conductive rotating atmospheric layer is generalized in Shmerlin et al. (2015) to the case of phase transitions of water vapor both for the precipitation convection (PC) and for the nonprecipitation (NPC) one. A principal difference is stated between moist convection and Rayleigh convection, on the one hand, and PC and NPC, on the other hand. In particular, the instability region on the plane of model parameters turned out to generally consist of two subregions, in one of which the localized axisymmetric disturbances with a tropical cyclone (hurricane) structure have the highest growth rate. In case of PC the ascending motions on the axis of symmetry correspond to such disturbances, in case of NPC a spontaneous growth of localized vortices both with ascending and descending motions on the axis is possible. Under other parameters values in case of PC spatially periodic cloud structures (convective rolls or closed cloud cells) have the highest growth rate and in case of NPC–mesoscale systems of convective rolls or mesoscale cloud clusters with annular cloud structures.

The problem of convective instability of an atmospheric layer containing finite horizontally domain filled with cloud medium is considered by Shmerlin and Shmerlin (2017). The exponentially increasing in time problem solutions are created. These solutions have the form either of solitary cloud rolls or of systems of convective cloud rolls localized in space. In case of axisymmetry their analogues are convective vortexes both with ascending and descending motions on the axis of symmetry as well as cloud clusters with annular convective structures. Depending on the anisotropy of the turbulent mixing vortices scale changes from the scale of a tornado to the scale of a tropical cyclone The solutions with descending motions on the axis can correspond to the formation of tonardo “trunk” or “the eye of the storm” in tropical cyclones.

Some papers were devoted to the study of intense convective atmospheric vortices: tropical cyclones, tornadoes and dust devils.

The paper by Sukhanovskii et al. (2018) presents laboratory model of tropical cyclone with controlled forcing and describes the technology to integrate a measurement system and a supercomputer. Procedures of real-time data acquisition, storing and processing, specifics of PIV and heating control systems integration are described. A series of experiments with laboratory analogue of tropical cyclone using feedback between velocity and a heating is carried out. It is found that imposed temperature difference defines the mean radial velocity

and intensity of the vortex. It is shown that the relationship between velocity and heat release is of crucial importance for the cyclonic vortex formation.

A numerical diagnosis of tropical cyclogenesis in a quiescent, rotating environment is presented in (Levina and Montgomery, 2015) to suggest an answer to the question "When Will Cyclogenesis Commence Given a Favorable Tropical Environment?". The author's research approach employs near-cloud-resolving numerical simulations to quantitatively analyze helical self-organization of moist-convective atmospheric turbulence. The simulations permit a diagnosis of cyclogenesis when the primary and secondary circulations in a forming hurricane vortex become linked by special convective coherent structures – Vortical Hot Towers (VHTs). The VHTs are argued to be intrinsic elements of the turbulent vortex dynamo in the tropical atmosphere of the Earth. It is discussed how the generated linkage makes the nascent vortex an integral helical system, supporting a positive feedback between the circulations. The feedback is sustained by only modest fluxes of latent heat from the underlying ocean, convective instability and vortical convection. The feedback indicates a release of potential energy that is converted into kinetic energy of developing large-scale helical vortex. Energy exchange between the primary and secondary circulation and their further mutual intensification is inferred from the numerical experiments.

Based on similarity arguments, Kurgansky (2015) proposed a simple fluid dynamic model of tornado-like vortices that, with account for "vortex breakdown" at a certain height above the ground, relates the maximal azimuthal velocity in the vortex, reachable near the ground surface, to the convective available potential energy (CAPE) stored in the environmental atmosphere under pre-tornado conditions. The relative proportion of the helicity (kinetic energy) destruction (dissipation) in the "vortex breakdown" zone and, accordingly, within the surface boundary layer beneath the vortex is evaluated. These considerations form the basis of the dynamic-statistical analysis of the relationship between the tornado intensity and the CAPE budget in the surrounding atmosphere.

Studies of dust devils, and their impact on society, are reviewed by Lorenz et al. (2016). Dust devils have been noted since antiquity, and have been documented in many countries, as well as on the planet Mars. As time-variable vortex entities, they have become a cultural motif. Three major stimuli of dust devil research are identified, nuclear testing, terrestrial climate studies, and perhaps most significantly, Mars research. Dust devils present an occasional safety hazard to light structures and have caused several deaths. Simple analytical models for the flow structure of dust devils in steady state, and a "thermophysical" scaling theory that explains how these flow structures are maintained are re-

viewed in Kurgansky et al. (2016). Then, results from high-resolution numerical simulations are used to provide insights into the structure of dust-devil-like vortices and study the impact of surface roughness on them. The article concludes with an overview of the influence of lofted dust on the flow structure of dust devils and a discussion of open questions. The papers by Lorenz et al. (2016) and Kurgansky et al. (2016) are reprinted in the book (Dust Devils, 2017).

A self-consistent hydrodynamic model for the solar heating-driven onset of a dust devil vortex is derived and analyzed by Horton et al (2016). The toroidal flows and vertical velocity fields are driven by an instability that arises from the inversion of the mass density stratification produced by solar heating of the sandy surface soil. The nonlinear dynamics in the primary temperature gradient-driven vertical airflows drives a secondary toroidal vortex flow through a parametric interaction in the nonlinear structures. While an external tangential shear flow may initiate energy transfer to the toroidal vortex flow, the nonlinear interactions dominate the transfer of vertical-radial flows into a fast toroidal flow. This secondary flow has a vertical vorticity, while the primary thermal gradient-driven flow produces the toroidal vorticity. Simulations for the complex nonlinear structure are carried out with the passive convection of sand as test particles. Triboelectric charging modeling of the dust is used to estimate the charging of the sand particles. Parameters for a Dust Devil laboratory experiment are proposed considering various working gases and dust particle parameters. The nonlinear dynamics of the toroidal flow driven by the temperature gradient is of generic interest for both neutral gases and plasmas. A new type of "explosively growing" vortex structure is investigated theoretically in the framework of ideal fluid hydrodynamics by Onishchenko et al. (2016). It is shown that dust-devil-like vortex structures may arise in convectively unstable atmospheric layers containing background vorticity. From an exact analytical vortex solution the vertical vorticity structure and toroidal speed are derived and analyzed. The assumption that vorticity isconstant with height leads to a solution that grows explosively when the flow is inviscid. The results shown are in agreement with observations and laboratory experiments.

Intense atmospheric vortices are characterized by non-zero helicity of the velocity field. The following papers were devoted to the study of the dynamic aspects of helicity, which also have a general hydrodynamic significance.

An overview on the helicity of the velocity field and the role played by this concept in modern research in the field of geophysical fluid dynamics and dynamic meteorology is given by Kurgansky (2017). Different (both previously known in the literature and first presented) formulations of the equation of helicity balance in atmospheric motions (including those with allowance for effects of air compressibility and Earth's rotation) are brought together. Equations and relationships are given which are valid in different approximations

accepted in dynamic meteorology: Boussinesq approximation, quasi-static approximation, and quasi-geostrophic approximation. Emphasis is placed on the analysis of helicity budget in large-scale quasi-geostrophic systems of motion; a formula for the helicity flux across the upper boundary of the nonlinear Ekman boundary layer is given, and this flux is shown to be exactly compensated for by the helicity destruction inside the Ekman boundary layer.

A numerical analysis of the process of helicity generation in the tropical atmosphere of the Earth was carried out by Levina et al. (2017). The study was performed based on post-processing of the US data of cloud-resolving numerical simulation of tropical cyclones obtained by using the model RAMS – Regional Atmospheric Modeling System (Montgomery et al., 2006). A mechanism is discussed that generates the vertical vorticity and helicity in the tropical atmosphere due to the interaction of cloud convection with vertical shear of horizontal velocity. In connection with the fact that in all known examples of large-scale instabilities found in helical turbulent media there exist excitation thresholds dependent on helicity magnitude, in this work, the close attention is paid to the influence of the initial conditions on helicity generation during the first hours of the experiments. Helical flow characteristics were calculated and compared for two numerical experiments, in one of which an initial weak large-scale vortex disturbance was specified in the middle troposphere while in the other, the initial vortex was absent. The discussion is offered for the influence on helicity generation of a local heating at low levels of the troposphere, which was applied during the initial 300 seconds of experiments in order to accelerate development of cloud convection. A process is considered of generation, by the local heating, of a single intense helical cloud structure – the vortical hot tower (VHT) that reached its maximal intensity within the first 1–2 hours. Quantitative analysis of helicity generation by the single VHT was carried out for two different scenarios.

In Teimurazov et al. (2017), convective flows from localized heater in a rotating layer were studied numerically in a three-dimensional non-stationary formulation. Distribution of helicity, its mean and fluctuating contributions were simulated for two specific regimes. In the first one the stable cyclonic vortex and intensive convective jet produce substantial amount of helicity near the axis of rotation. In the second one convective flow is more chaotic, cyclonic vortex appears at some distance from the center and as a result helicity is more dispersed in the lower layer of the fluid. Helicity in a described system is characterized by high level of pulsations. Spatial and temporal variations of helicity sources were analysed using equation for helicity balance. Time variations of viscous term and buoyancy term in helicity equation strongly exceed variations of other terms and the helicity time derivative. In a described system the buoy-

ancy term is a source of helicity and viscous term is a sink. It was found that they are in antiphase and compensate each other.

Experimental and numerical study of the steady-state cyclonic vortex from isolated heat source in a rotating fluid layer is described in Sukhanovskii et al. (2017a). The structure of laboratory cyclonic vortex is similar to the typical structure of tropical cyclones from observational data and numerical modelling including secondary flows in the boundary layer. Differential characteristics of the flow were studied by numerical simulation using CFD software FlowVision. Helicity distribution in a rotating fluid layer with localized heat source was analysed. Two mechanisms which play role in helicity generation are found. The first one is the strong correlation of cyclonic vortex and intensive upward motion in the central part of the vessel. The second one is due to large gradients of velocity on the periphery. The integral helicity in the considered case is substantial and its relative level is high.

Currently, there is a keen interest in a fundamental question on the possibility of a cyclone-anticyclone asymmetry, which is principally absent in the classical formulation, based on the Charney−Obukhov equation for the quasi-geostrophic potential vorticity.

The cyclone–anticyclone asymmetry is found in atmospheric and oceanic processes, laboratory experiments, and numerical calculations. This is manifested, in particular, in their different frequency. Mokhov et al. (2015) analyze the effects of cyclone–anticyclone asymmetry in the atmosphere of the extratropical latitudes of the Northern Hemisphere in different seasons depending on the size of the atmospheric vortices and their lifetime. The authors also obtained the results of comparative analysis for extratropical cyclones and anticyclones with the characteristic radius not exceeding 1500 km (less than the Obukhov radius for the barotropic atmosphere) and durations not longer than two weeks.

The manifestations of the cyclone-anticyclone asymmetry on the stability of rotating shear flows are investigated by Kalashnik et al. (2016) both theoretically and experimentally. The stability of certain classes of shear flows, namely, rotating tangential discontinuities and flows with a constant shear, is analyzed. The dependence of the disturbance growth rate on the sign and absolute value of the shear is determined. The three-dimensional disturbances leading to longitudinal flow modulations are shown to be most dangerous. The results of the observations of the cyclone-anticyclone asymmetry effect in the laboratory conditions are presented.

Wind-speed distributions in atmospheric upper air jet streams have a horizontal asymmetry: the wind shear on the northern (cyclonic) side of the jet is larger than that on the southern (anticyclonic) side. The paper by Kalashnik et al. (2017) suggests an explanation of this feature on the basis of the theory of

nonlinear geostrophic adjustment. Simple theoretical estimates are obtained for the asymmetry coefficient of the speed profile. It is shown that the asymmetry increases with the Rossby number (with a jet-stream velocity). Results of the statistical analysis of the horizontal asymmetry of jet streams from Earth's satellite measurements are described.

Considerable attention was drawn to the classical Eady model of baroclinic instability and to a variety of fluid dynamical problems which can be formulated and solved within the Eady model framework.

A nongeostrophic version of the classical problem of zonal flow instability with constant shear (the Eady problem) is considered by Kalashnik (2015a). The linearized set of dynamic equations for two-dimensional disturbances is reduced to a single wave-type second-order equation relative to modified pressure (a linear combination of pressure and stream function). Dynamic features of disturbances with zero potential vorticity are studied in the framework of the equations formulated. Asymptotic solutions of the spectral problem of hydrodynamic stability theory are derived. The initial-value problem at large Richardson numbers is considered using multiple-time-scale expansions. The solution to the problem is represented as the sum of fast (wave) and slow (quasi-geostrophic) components. In the unstable regime, the slow component describes baroclinic waves (cyclones and anticyclones) generated by inhomogeneous initial buoyancy (potential temperature) distributions at the boundaries.

The structure of baroclinic waves in a geostrophic flow with a constant vertical shear (Eady model) is very consistent with that of atmospheric vortex formations. The paper by Kalashnik (2015b) proposes an approach to describing the generation of these waves by initial perturbations of potential vorticity (PV). Within the framework of the suggested approach, the solution to the initial-value problem for a quasi-geostrophic form of the PV transport equation is represented as a sum of the wave and vortex components with zero and nonzero PV, respectively. A set of ordinary differential equations with the right-hand side dependent on the vertical PV distribution is formulated using Green functions for the amplitude of the wave component (amplitude of excited baroclinic waves). The solution provides a simple description of the resonant and quasi-resonant baroclinic-wave excitation effects under which the wave amplitude grows according to the linear or logarithmic laws. These types of excitation take place for singular and discontinuous initial PV distributions if the frequencies of the wave and vortex components coincide. Smooth distributions generate finite-amplitude waves.

Edge baroclinic waves are generated in a geostrophic flow with a vertical shear near a solid surface. Kalashnik et al. (2018) investigate a new class of baroclinic waves in flows with horizontal and vertical shears and a linear distri-

bution of potential vorticity. It is shown that taking account of the horizontal shear leads to the appearance of new features of wave dynamics. These include the nonmodal growth of energy in the initial stage of development, the time dependence of the vertical wave scale, and the possibility of generation of stationary or blocked waves. The horizontal shear makes the mechanism of generation of baroclinic waves by initial vortex perturbations more efficient. One important feature is associated with vortex paths, which are formed by the superposition of a baroclinic wave on the flow with horizontal shear.

In the Eady model of baroclinic instability, numerical methods of variational calculations are usually used to find optimal disturbances. In the work by Kalashnik and Chkhetiani (2018), a simple physical approach, which makes it possible to analytically determine the parameters of optimal disturbances, is proposed. This approach is based on the energy balance equation and explicit expressions for energy functionals, which follow from the representation of disturbances through the superposition of edge Rossby waves. The corresponding expressions are the functions of initial-disturbance parameters, and determining optimal parameters is reduced to studying these functions for an extremum in a standard way. The amplitudes of initial buoyancy distributions at atmospheric-layer boundaries and phase shifts between these distributions are used as parameters for disturbances with zero potential vorticity. An analytical formula for an optimal phase shift, which determines its dependence on wavenumber and optimization time, is obtained. It is also shown that optimal disturbances always have equal boundary amplitudes. The parameters of optimal disturbances are compared with those of growing normal modes. It is found that there is only one exponentially growing normal mode, which is an optimal disturbance. In this case, the wavenumber of this mode differs from that of a normal mode with maximum growth increment.

The quasi-geostrophic dynamics of disturbances of a flow with a vertical shear is described in Kalashnik (2018) by a transport equation for potential vorticity. Wave solutions of this equation are represented by edge baroclinic waves (modes in a discrete spectrum) and singular modes in a continuous spectrum. When frequencies of these modes coincide, the effect of resonant excitation occurs in which the amplitude of baroclinic waves increases linearly. This paper studies this effect in the presence of Ekman bottom friction. It is shown that friction suppresses linear wave growth and gives rise to baroclinic waves of finite amplitude.

There are also papers on the general dynamics of the atmosphere, which can conditionally be classified as “Miscellaneous”.

Ingel (2015a) derived an approximate analytical solution of the one-dimensional problem of steady oscillations of a rotating viscous fluid subjected

to harmonic-in-time shear stresses on the horizontal boundary. The solution demonstrates the resonance amplification of the oscillation amplitude and the depth of their penetration into the fluid as the excitation frequency approaches the inertial frequency. At latitudes ±30°, the frequency of diurnal variations in the atmosphere coincides with the inertial one; this may be associated with some resonance phenomena in the atmosphere and water bodies. In (Ingel, 2015b) the problem of a response from a stably stratified fluid to the action of vertically extended harmonic heat and momentum sources is solved analytically. Emphasis is placed on the high sensitivity of such fluids to actions with frequencies close to the buoyancy frequency.

Ingel (2018a) generalized a Prandtl slope flow model onto the case with a homogeneous stationary source of a heavy admixture that significantly changes the medium density. A stationary analytical solution for a velocity of arising flows, temperature deviations, and admixture distribution is obtained. The model describes, for example, some special features of the dynamics of a ground snowstorm above a slope surface. Paradoxical properties of the classical Prandtl solution for flows occurring in a semibounded liquid (gaseous) medium above an infinite homogeneously cooled/heated inclined plane are analyzed in Ingel (2018b). In particular, the maximum velocity of steady-state slope flow is independent, according to this solution, of the angle of inclination. Consequently, there is no transition to the limit case of zero angle where the cooling/heating is unlikely to give rise to homogeneous horizontal flows. It is shown that no paradoxes arise if buoyancy sources of infinite spatial scale are not considered, which act infinitely long. It follows from this results that, in particular, the solution of the problem for a semi-bounded medium above a homogeneously cooled surface in the gravity field is unstable to small deviations of this surface from horizontal.

It is known long ago that atmospheric processes lead to generation of the seismic signals. But for a long time seismologists considered them only as a noise. In the recent years, the additional motivations appeared for study of such signals. There are two different aspects: (1) seismic signals as a source of information (prompt recording of hazardous phenomena, monitoring, warning system, forecasting for very short periods); (2) dramatic effects: possible influence of atmospheric processes on a seismic activity. The article by Yaroshevich et al. (2014) presents some of the relevant results of the authors obtained in recent years.

The horizontal movement of inertial particles in the intense vortices, where the centrifugal force can be substantially higher than the gravity, is studied analytically by Ingel (2017). A similar problem was studied earlier for small

(Stokes) particles at low Reynolds numbers, which allow one to be limited to the linear resistance law. It is shown that the previous results to a great extent can be extrapolated onto the case of considerably heavier particles (e.g., water droplets with a diameter up to 1 mm at Reynolds numbers up to 10^3). The nonlinear nature of the resistance, i.e., its dependence on the particle velocity relative to the medium, should be taken into account for such particles. Some general laws are established for particle dynamics in vortex flows. In particular, their tangential velocity is close to the velocity of the medium, while the radial velocity is substantially lower (it is close on the order of magnitude to the geometric mean of the particle tangential velocity and the difference between the latter and the tangential velocity of the medium). The limits of applicability of the results are found, i.e., the restrictions on the size and mass/density of particles.

In Ingel and Makosko (2015) linear disturbances induced by gravity-field inhomogeneities in a horizontal stratified flow with a vertical shear are calculated analytically. In addition to being dependent on the amplitude of these inhomogeneities, disturbances depend strongly on their horizontal scales, background flow velocity, stratification, and Coriolis parameter. The most important governing dimensionless parameters are the Froude number (the ratio of inertial forces and buoyancy) and the Burger number (the ratio of the effect of rotation to the effect of stratification). The analytical solutions derived show that the influence of inhomogeneities of the gravitational field on atmospheric flows can be significant in some cases. Physical generation mechanisms of these disturbances are analyzed.

A theoretical problem of linear stationary disturbances of the background geostrophic flow of a stratified rotating medium (atmosphere) that are induced by inhomogeneities of the gravitational field is considered by Ingel and Makosko (2017). There is a common belief that such inhomogeneities may only somewhat deform (distort) the state of hydrostatic equilibrium, but cannot affect the dynamics of the flow in the atmosphere. Generally, the problem statement is different for the processes over a solid surface and a water surface, because a water surface (the lower boundary condition for the atmosphere) is deformed by inhomogeneities of the gravitational field. The problem of disturbances over a water surface has been considered in recent papers of the authors; in this paper, the results are developed and significantly revised. The emphasis is on disturbances over a flat horizontal surface, which were not examined before. From the analytical solutions, it follows that the influence of inhomogeneities of the gravitational field on the atmospheric flows may be significant in some cases.

One possible mechanism for the effect of gravity-field inhomogeneities (GFIs) on the atmosphere dynamics has been investigated theoretically by Ingel

and Makosko (2018). It is shown that the vertical heat exchange in an air layer in an inhomogeneous gravity field can disrupt the state of hydrostatic equilibrium and lead to the generation of vortex flows. Estimates of the amplitude of velocity perturbations are made on the basis of a linear stationary hydrodynamic model that takes planetary rotation into account. The magnitude of the horizontal component of the velocity can reach values on the order of the product of the buoyancy frequency and a geoid deviation from a uniform Earth ellipsoid. The amplitude of the emerging vertical motions, in addition to the parameters mentioned, also depends on the intensity of the turbulent exchange and horizontal scales of the inhomogeneities.

In Nigmatulin (2018), hydrodynamic and thermodynamic equations for the atmosphere are considered on the meteorological and climatic scales where the inertial forces are negligibly small in comparison with gravity. In this case, the inertia of the horizontal velocity and temperature has an effect. For such a vertically quasi-static flow, an equation for the vertical velocity distribution is obtained that is asymptotically exact in density, temperature, and horizontal velocity. A closed system of hydro- and thermodynamic equations is presented in which the pressure at each point is determined by the weight of the air column above this point. It is suggested that this system of equations should be used to calculate the climatic and meteorological processes in which the inertia of the horizontal velocity and the inertialess vertical velocity play an essential role.

The problem of the stability of an isolated jet flow and two counter-streaming jet flows in a rotating shallow-water layer is considered by Kalashnik and Chkhetiani (2016). These flows are described by exact solutions of the Charney–Obukhov equation with one or two discontinuities of the potential vorticity, respectively. The isolated jet flow is shown to be stable. For the system consisting of two jet flows the dependence of the characteristics of the unstable wave modes on a geometric parameter, namely, the ratio of the spacing between the jet axes to the deformation radius, is determined. On the basis of the contour dynamics method a weakly-nonlinear model of the longwave instability is developed.

The linear mechanism of generation of gravity waves by potential vorticity (PV) disturbances in flows with constant horizontal and vertical shears is studied by Kalashnik and Chkhetiani (2017). The case of the initial singular distribution of PV, in which the PV is localized in one coordinate and is periodic with respect to other coordinates, is considered. In a stratified rotating medium, such a distribution induces a vortex wave (continuous mode), the propagation of which is accompanied by the emission of gravity waves. To find the emission characteristics, a linearized system of dynamical equations is reduced to wave equations with sources that are proportional to the initial distributions of

PV. The asymptotic solutions of the equations are constructed for small Rossby numbers (horizontal shear) and large Richardson numbers (vertical shear). When passing through the inertial levels symmetrically located with respect to a vortex source, the behavior of the solutions for wave amplitudes radically changes. Directly in the vicinity of the source, the solutions are of monotonic character, corresponding to a quasi-geostrophic vortex wave. At long distances from the source, the solutions oscillate. The horizontal momentum flux and the Eliassen–Palm flux are estimated using asymptotic solutions. It is found that, within the indicated range of both Rossby and Richardson numbers, these fluxes are exponentially small: that is, the emission of waves is weak.

The question of the instability of internal gravity waves (IGWs) propagating at small angles to the vertical is re-visited in Kurgansky (2018). The case of an IGW of finite-amplitude propagating at a very small but finite angle to the vertical is considered. This angle serves as a small parameter in the problem, and the instability of such an IGW is investigated by using the Fourier method and the Sivashinsky integral relations. The analysis undertaken confirms the existence of short-wave instability for small IGW amplitudes and for an arbitrarily small value of their propagation angle to the vertical. For small viscosity and thermal conductivity of the fluid medium, the growth rate of the most unstable mode is proportional to the square of the amplitude of the IGW. The results obtained may be of interest for interpreting the results of observations and confirming the existence of turbulence in the middle atmosphere.

Some data on a high frequency infrasound recorded within a range of 2–16 Hz (voice of the sea) in the water area of the Black Sea are given in Perepelkin et al. (2015). Different parameters of the recorded infrasonic signal – the direction and phase velocity of arriving infrasonic waves, spectral composition, and coherence – have been studied. In the course of measurements, both wind and wave conditions in the water area of the Black Sea have been studied in detail. The collision of two atmospheric vortices was observed a few hours before the first arrivals of infrasonic waves, and the collision of differently directed sea waves was observed during infrasound recording. The direction of the arrivals of infrasonic waves coincides with the direction between the zone of collision of sea waves and the point of infrasound recording. The assumption was made that, in order to explain the observed infrasonic waves, it is necessary to use the mechanism responsible for the emission of infrasound into the atmosphere by standing surface wave formed due to the nonlinear interaction of surface waves propagating in opposite directions and to take into account the frequency filtering properties of both wind velocity and temperature stratifications of the atmosphere itself along the path of infrasound propagation. This assumption calls for additional verification.

Large-scale processes and the weather forecast

In recent years, the forecast quality of numerical weather prediction (NWP) models has steadily improved, mainly due to the possibility of increasing the resolution of the forecast models and the corresponding observational data assimilation system (DA), physical parametrizations and new high-performance computational methods. However, complex orography is still a problem for NWP models, mainly due to insufficient terrain resolution, but also due to physical parameterizations based on assumptions of horizontal homogeneity and flat terrain.

Assessment of the state of the environment from observational data is one of the most urgent tasks at present. The development of data assimilation (DA) methods for numerical weather prediction (NPP) models began with simple horizontal interpolation methods (Eliassen, 1954; Gandin, 1963) which gradually became three-dimensional and multi-element (Lorenc, 1981). Variational methods were developed to use the dynamics model in the DA process as early as the 1970s–1980s (Penenko and Obraztsov, 1976; Le Dimet and Talagrand, 1986) and is now being applied operatively. The various forms of Ensemble Kalman Filters (Evensen, 1994) that have emerged have begun to compete successfully with variational methods for DA in the atmosphere. Since each approach has its own unique advantages, scientists began to create hybrid combinations of these methods in order to take advantage of both. They are now becoming the main methods in DA for NWP in many operational forecast centers.

The data assimilation system requires a lot of observation data. In fact, there are two types of observations. The first type can be attributed to the usual observations (data from the network of synoptic stations (SYNOP), airborne sounding data, measurements from the buoys in the ocean, lidar measurements (LIDAR active sensing by laser beams from the earth's surface), radar measurements others). Today they are much less numerous than observations using remote sensing, which are carried out by instruments on satellites. However, routine observations are generally more accurate. In addition, they offer a direct assessment of the physical system data, in contrast to observations using remote sensing. For example, in 2014, 99% of the data processed at the European Center for Medium-Range Weather Forecasting (ECMWF) were satellite sensing data, but only 91.5% of the observations actually used in the analysis were remote sensing data (Bannister, 2017). From the point of view of data assimilation, satellite sounding has significantly improved the coverage of the globe, especially in the southern hemisphere covered mainly by oceans.

In recent years, the Kalman ensemble filter, in which the prediction error covariances are estimated using an ensemble of forecasts for perturbed initial fields, has become very popular.

In the article (Klimova, 2018) a variant of the Kalman stochastic ensemble filter is proposed, which is an ensemble smoothing algorithm, when ensemble smoothing is performed for the average value of the sample and then the perturbation ensemble is transformed. The proposed algorithm is stochastic. With the smoothing algorithm proposed in the article, model numerical experiments were carried out for a 1-dimensional model of transport and diffusion, in which the model parameter is estimated, namely, emission of a passive tracer. It should be noted that in problems of high dimensionality the ensemble Kalman filter (EnKF) is effective in use only with a small number of ensemble implementations.

Many of the modern DA methods are based on probabilistic methods that use the Bayesian approach. Tsyrulnikov and Rakitko (2017) proposed and tested a new ensemble filter that takes into account the uncertainty in the previous distribution. The filter is based on the conditional Gaussian state distribution taking into account the covariance matrices of the model error and the forecast error. The latter are treated as random matrices and are updated in the hierarchical Bayes scheme along with the state. It is assumed that the a priori distribution of the covariance matrices is the inverse of the Wishart distribution. The efficiency of the new filter has been tested in numerical experiments. Experiments have shown that using a new filter significantly improves the results compared to EnKF.

A generator of spatio-temporal pseudo-random Gaussian fields was proposed in (Tsyrulnikov and Gayfulin, 2017). The generator is designed to create disturbances that simulate the errors of numerical predictive models in geophysics. The generator was tested with the COSMO meteorological model as a source of additive space-time disturbance of prognostic fields.

The members of the ensemble of forecasts differ in the uncertainties of the initial conditions and in the uncertainties of the models themselves. The inclusion of stochastic schemes to represent model uncertainties allows us to improve the probabilistic estimates of the ensemble of forecasts by reducing the mean error over the ensemble. In the coming years, there will probably be a further increase in the use of ensemble methods in forecasting and assimilating observational data. This will increase the requirements for the methods used to disturb the prognostic model, especially in high-resolution models, in convectively-resolved models (1 km and lower grid resolution). Measurements of the parameters of the state of the atmosphere using instruments installed on the satellite began in the 1960s, but it was not until the 1990s that these observa-

tions began to contribute to the improvement of numerical weather forecasts. As is well known, data assimilation is a filtering processing, which uses known statistical properties of observation errors and a numerical model in which data are assimilated. It is also a process that corrects the state obtained using a numerical model using observations of the real state of the atmosphere.

This part is based on the well-known physical laws relating meteorological quantities (temperature, humidity, pressure, wind, etc.) with the observed ones. The effect of observations on the assimilation of data is determined by the sensitivity of a particular type of observation to a specific variable of the forecast model and the error of observation. In the case of satellite observations, most of the information is assimilated as measurement data of radiation in various wavelength ranges using radiometers and other instruments, these measurement data are sensitive to atmospheric temperature, humidity, gas concentrations, clouds and surface conditions. Given this, assessing the impact of satellite data can be quite complex.

Zaripov et al. (2016) address the problems of assimilation of observational data from satellite instruments AMSU-A and AIRS and evaluate the effect of their use in analyzing meteorological fields in Western Siberia. Experiments have shown that the DA system is functioning successfully; in winter, AMSU-A observational data somewhat improves the quality of the analysis and forecast fields; in the summer period, the effect of assimilation of satellite observations on the quality of forecasts is ambiguous.

Further development of the concept of environmental forecasting and design, implemented in the form of mathematical modeling technology was proposed in the articles (Penenko et al., 2015a,b, 2016, 2017). A feature of this concept is its focus on solving direct and inverse problems based on a variational principle in a formulation with weak constraints. The main provisions of the concept are presented on the example of joint models of hydrothermodynamics and atmospheric chemistry.

The dynamic downscaling method is applied when using atmospheric models in a limited area (LAM) for weather forecasting in a region or for modeling a regional climate with a higher resolution than a global model, which provides a regional climate model (RCM) with initial and boundary conditions, i.e. behaves as a steering (driving) global model. One distinct advantage of RCM application is its higher horizontal resolution, which enables the RCM to handle more realistically certain, critically important climate processes, such as clouds and land surface processes/features (e.g., topography), especially when RCM provides cloud-permitting resolutions to avoid the cumulus parameterization issues. Studies have shown that with more detailed information over mountain ranges and coastal regions, RCMs are capable of reproducing the formation of

mesoscale phenomena. The quality of RCM results also depends on the driving GCM information. For example, if the GCM misplaces storm tracks, there will be errors in the RCM's precipitation climatology (Wilby et al., 2009). Additionally, different RCMs contain distinct dynamical schemes and physical parameters, which means that RCMs driven by the same GCM can produce different results.

It is well known that the main problems of the development of systems for the numerical weather prediction, with the rapid growth of computing power and various types of observation systems, are associated with a number of key areas: these are parametrization of physical and chemical processes, analysis and estimation of forecast uncertainty using ensembles and preparation of consistent initial and boundary conditions for predictions using observational data, as well as the development of supercomputer technologies for high-resolution numerical predictions.

In the article (Bedritskii et al., 2017) the main stages are considered of the process of Roshydromet forecast technologies modernization that started in the 1990s, especially those related to the use of super computers for operational numerical weather prediction (NWP) and to the develop ment of supercomputer technologies for NWP with different lead times. Some outcomes of the modernization are presented.

The second stage of the work (2011–2014) on the implementation and development of the COSMO-Ru system of nonhydrostatic short-range weather forecasting is described in (Rivin et al., 2015). Demonstrated is how the research activities and ideas of G.I. Marchuk influenced modern methods for solving the systems of differential equations that describe atmospheric processes (in particular, the version of the Marchuk's splitting method is used to find the solution of the finite-difference analog of the system of differential equations in the COSMO-Ru model); it is shown how he contributed to the development of the methods of assimilation of meteorological information associated with the use of adjoint equations. Given is a brief description of the COSMO model of the atmosphere and soil active layer, the COSMO-Ru system, and research activities on this system development.

Vil'fand et al. (2017) presented description numerical chemical weather prediction model COSMO-ART, which is used in operational mode. The COSMO-Ru7-ART system is able to simulate adequately the values of concentration of impurities in the atmosphere. The system includes the module for estimating the emission of pollutants to the atmosphere from forest fires that was success fully tested on the case of forest fires occurred in the sum mer of 2010 for the European part of Russia. The accurate forecast of pollutant concentration has also a positive effect on the air temperature forecast due to taking into account the aerosol feedback on radiation.

The global hydrodynamic atmosphere model SL-AV is applied in (Tolstykh et al., 2015) for operational medium range weather forecast and as a component of the probabilistic long-range forecast system. The review of the previous development of the model is presented and the model features are noted. The existing model versions are described. The unified multi-scale version of the model is developed on the basis of these versions. This version is intended both for numertcal weather prediction and for modeling of climate changes. The numerical experiments on climate modeling with the developed multi-scale version are carried out according to the protocol of the international AMIP2 experiment. First results are pret ented. The pos tibiltty of application of the unified vertion of the SL-AV model for the met dium-range weather forecast, and, after some development, for modeling of climate changes is shown.

The article by Tolstykh et al., (2017) presents the new dynamical core SL-AV model. SL-AV (semi-Lagrangian, based on the absolute vorticity equation) is a global hydrostatic atmospheric model. Its latest version, SL-AV20, provides global operational medium-range weather forecast with 20 km resolution over Russia. The lower-resolution configurations of SLAV20 are being tested for seasonal prediction and climate modeling. Its main features are a vorticity-divergence formulation at the unstaggered grid, high-order finite-difference approximations, semi-Lagrangian semi-implicit discretization and the reduced latitude–longitude grid with variable resolution in latitude. The accuracy of SL-AV20 numerical solutions using a reduced lat–lon grid and the variable resolution in latitude is tested with two idealized test cases. Accuracy and stability of SL-AV20 in the presence of the orography forcing are tested using the mountain-induced Rossby wave test case. The results of all three tests are in good agreement with other published model solutions. It is shown that the use of the reduced grid does not significantly affect the accuracy up to the 25% reduction in the number of grid points with respect to the regular grid. Variable resolution in latitude allows us to improve the accuracy of a solution in the region of interest.

The impact of last model improvements on forecast quality is studied in the paper (Tolstykh et al., 2018). Development of the multiscale version of the global atmosphere model SL-AV required many improvements in the dynamical core, refinement of parameterization algorithms and complex tuning of the model. These modifications were initially included in the climate version of the model and recently incorporated into the version for medium-range numerical weather prediction. The increase in accuracy of model climate characteristics has led to the reduction of forecast errors. The comparison of quality for numerical forecasts starting from initial data of Hydrometcentre of Russia and ECMWF is carried out. The effect of replacing the initial data turned out to be comparable to the effect of multi-year works on model development. This

shows the importance and necessity of development and improvement for Hydrometcentre of Russia data assimilation system.

Systematic errors in forecast near-surface air temperature (SAT) still constitute a considerable problem for numerical weather prediction (NWP) at high latitudes. Numerous studies in the past have attempted to reduce this problem through recalibration of physical parameterization schemes and better approximation of the surface energy budget. The errors, however, remain despite notable improvements in the overall weather forecast performance. Esau et al. (2018) look at the problem from a different perspective. They analyze asymmetries in the SAT forecast errors. Their study reveals a statistical pattern of warm SAT biases under cold weather conditions and cold SAT biases under warm weather conditions. The largest errors were found in shallow atmospheric boundary layers (ABLs). The study attributes the problem to the modeled excessive ABL thickness in northern Eurasia (the NEFI region). The ABL thickness is considered as a scaling factor controlling the efficacy of the applied surface heating. Too thick an ABL damps the magnitude and agility of the SAT response. The study utilized the operational model SL-AV of the Russian Hydrometeorological Centre. Two turbulence schemes were evaluated in the northern European and western Siberian regions of Russia against observations from 73 meteorological stations. The pTKE (old) scheme is based on the local balance of the turbulence characteristics. The TOUCANS (new) scheme incorporated the total turbulence energy equations in an energy-flux balance approach. Neither scheme uses the ABL thickness as a prognostic parameter. The study reveals that the SAT errors are consistent with the damped response of temperature and reduced agility of temperature fluctuations in too thick ABLs. The TOUCANS scheme did not improve those features, probably because it links the turbulent fluxes and the ABL thickness. The SAT errors in shallow ABLs persist in the new scheme. The study emphasizes the need for a closer look at the ABL thickness in the NWP models.

The paper by Bart and Starchenko (2015) presents an approach to specify initial and boundary conditions from the output data of global model SLAV for mesoscale modelling of atmospheric processes in areas not covered by meteorological observations. From the data and the model equations for a homogeneous atmospheric boundary layer the meteorological and turbulent characteristics of the atmospheric boundary layer are calculated.

The results of calculation of meteorological parameters using a meteorological model, TSU-NM3, as well as prediction of some indices of atmospheric air pollution in the city of Tomsk obtained from a mesoscale photochemical model are presented in Starchenko et al. (2015). The calculation results are compared with observational data on the atmosphere and pollutants.

The paper by Starchenko and Danilkin (2015) presents a non-steady three-dimensional eddy-resolving model intended for the simulation of non-isothermal turbulent separation flows in street canyons. For a subgrid-scale turbulence parameterization, the Smagorinsky gradient model is used. The calculation results demonstrate the effects of pollutant source location, street canyon size, main stream velocity and wall temperature difference on air pollution in the canyon.

The paper by Sitnikov et al. (2015) presents the results of forecasting meteorological conditions that promote aircrafts icing in the atmospheric boundary layer; the forecasting results were obtained based on mesoscale meteorological model TSU-NM3. Godske formula which is based on the calculation of saturation temperature above ice, NCEP method, and statistical method of Hydrometeorological Centre of Russia were used as criteria of probability of aircraft icing during take-off or landing. Numeric forecast results were compared with physical observations made in the atmospheric boundary layer in October 2012 at the Tomsk airport. A good agreement obtained provided an opportunity to be certain about the above approach viability.

One of the most difficult problems of weather forecasting is the prediction of precipitation, especially convective precipitation. Convection is usually initiated in response to the formation of local convergence of flow at the lower boundary with temperature and humidity differences, which are often associated with horizontal gradients of sources of surface heating. Numerical simulation of convection is usually ineffective, even with high-resolution models, due to the chaotic nature of these sediments. This is especially critical in the watershed areas. Forecast errors can occur due to the parametrization of physical processes, the uncertainty of the initial state of the atmosphere, the nature of the heterogeneity of the earth's surface (inhomogeneity of soil moisture content, surface temperature, orography, etc.).

The method of calculating snow accumulation using the prediction of precipitation fields for the mesoscale numerical atmospheric model, the prediction results using the WRF model of two cases of heavy snowfall, noted on October 18 and 23, 2014 in the Urals, analysis of the results of modeling the formation and evolution of mesoscale convective systems (ISS), accompanied by dangerous weather phenomena over the territory of the Western Urals are presented in the papers (Kalinin et al., 2015, 2016, 2017), where obtained estimates of precipitation prediction are compared with the estimates of the global GFS NCEP model. The results indicate that, as applied to the process under consideration, both models have approximately the same accuracy of the predicted amount of precipitation.

Storm surge is one of the most serious threats in the coastal regions of the seas. Accurate and timely numerical forecasting of surges is a critical task for mitigating the effects of natural disasters.

In the paper by Fomin and Diansky (2018) study was conducted of the most extreme for the period of instrumental observations since 1881, surges in the Taganrog Bay, which took place on March 24, 2013 and September 24, 2014, to study the characteristics of their formation and identify the requirements for accurate reproduction of the atmospheric and marine circulation in the Azov Sea. For this purpose, two versions of the marine circulation model INMOM (Institute of Numerical Mathematics Ocean Model) with a spatial resolution of ~ 4 km and ~ 250 m were used. Two types of data were used to specify the atmospheric forcing over the Black Sea region: Era-Interim reanalysis and WRF (Weather Reasearch and Forecast Model) models with spatial resolution of 80 and 10 km respectively.

Large-scale extreme weather/climate events, such as an extraordinary heat wave in the summer of 2010 over the European part of Russia, continued attracting attention of researchers.

The peculiarities of blocking conditions and weather anomalies over the East European Plain in the summer of 2010 are considered in Kislov et al. (2017) using the EOF analysis and vorticity equation. The EOF analysis simulates the time series of the anticyclone as a whole using the principal modes of temporal variability. The vorticity equation is transformed into the specific form which enables assessing the contribution of different factors to the development and lasting existence of blocking conditions.

As an index of the general atmospheric circulation over the hemisphere, it is proposed in Kurgansky (2018) to calculate the hemisphere-area-averaged (poleward of the latitude 20°) product of the Coriolis parameter f by the wind velocity squared U^2 at the upper boundary of the planetary boundary layer. In practical calculations, data on the wind velocity at an isobaric level of 850 hPa were used. Control calculations for the 900 hPa level gave similar results. It is shown that the index introduced adequately characterizes the seasonal and interannual variability of the general atmospheric circulation over both hemispheres. It was also suggested that the observed index maxima during the Northern Hemisphere summer (July) are in a certain correlation with the "heat waves", in particular over Russia in 2010. This correlation can be explained by the fact that though long-term atmospheric blocking events that cause "heat waves" are characterized by low local values of fU^2, they are always accompanied by intensive cyclonic activity over the hemisphere, which both supports and feeds these blocking structures. Hence, in total, a higher value of this index is obtained.

Traditional research of various aspects of large-scale dynamics of the atmosphere was continued, including the study of a wide range of synoptic and climatically significant atmospheric processes on the Earth.

The El Niño Southern Oscillation (ENSO) amplitude is modulated at decadal timescales, which, over the last decades, has been related to the low-frequency changes in the frequency of occurrence of the two types of El Niño events, that is the Eastern Pacific (EP) and Central Pacific (CP) El Niños. Meanwhile ENSO is tightly linked to the intraseasonal tropical variability (ITV) that is generally enhanced prior to El Niño development and can act as a trigger of the event. In (Gushchina and Dewitte, 2018), the ITV/ENSO relationship was revisited taking into account changes in ENSO properties over the last six decades. The focus was on two main components of ITV, the Madden–Julian Oscillation (MJO) and convectively coupled equatorial Rossby waves (ER). It was shown that the ITV/ENSO relationship exhibits a decadal modulation that is not related in a straight-forward manner to the change in occurrence of El Niño types and Pacific decadal modes. However MJO predictive score related to EP El Niño is highly correlated to the Pacific decadal oscillation (PDO) with positive PDO phase being favorable for MJO contribution to ENSO development. The ER activity is enhanced prior to El Niño development over the whole period with a tendency to relate more to CP El Niño than to EP El Niño. The significant positive long-term trend of the ER predictive value is observed during last six decades. The statistics of the MJO and ER activity is consistent with the hypothesis that they can be considered a state-dependent noise for ENSO linked to distinct lower frequency climate modes.

Further in Matveeva et al. (2018) the relationship between ITV and ENSO was assessed based on models from the Coupled Model Intercomparison Project (CMIP) phase 5 (CMIP5) taking into account the so-called diversity of ENSO, that is, the existence of two types of events. As a first step, the models' skill in simulating ENSO diversity was assessed. The characteristics of the ITV are then documented revealing a large dispersion within an ensemble of 16 models. A total of 11 models exhibit some skill in simulating the key aspects of the ITV for ENSO: the total variance along the Equator, the seasonal cycle and the characteristics of the propagation along the Equator of the MJO and ER Five models that account realistically for both the two types of El Niño events and ITV characteristics are used for the further analysis of seasonal ITV-ENSO relationship. The results indicate a large dispersion among the models and an overall limited skill in accounting for the observed seasonal ITV-ENSO relationship. Implications of our results are discussed in light of recent studies on the forcing mechanism of ENSO diversity.

In Zahn et al. (2018), cyclones in the Arctic are detected and tracked in four different reanalysis data sets from 1981 to 2010. In great detail the spatial and seasonal patterns of changes are scrutinized with regards to their frequencies, depths, and sizes. The authors find common spatial patterns for their occurrences, with centers of main activity over the seas in winter, and more activity over land and over the North Pole in summer. The deep cyclones are more frequent in winter, and the number of weak cyclones peaks in summer. Overall, they find a good agreement of their tracking results across the different reanalyses. Regarding the frequency changes, they find strong decreases in the Barents Sea and along the Russian coast toward the North Pole and increases over most of the central Arctic Ocean and toward the Pacific in winter. Areas of increasing and decreasing frequencies are of similar size in winter. In summer there is a longish region of increase from the Laptev Sea toward Greenland, over the Canadian archipelago, and over some smaller regions west of Novaya Zemlya and over the Russia. The larger part of the Arctic experiences a frequency decrease. All the summer changes are found statistically unrelated to the winter patterns. In addition, the frequency changes are found unrelated to changes in cyclone depth and size. There is generally good agreement across the different reanalyses in the spatial patterns of the trend sign. However, the magnitudes of changes in a particular region may strongly differ across the data.

Characteristics of cyclones (frequency, intensity and size) and their changes in the Arctic region in a warmer climate have been analyzed in Akperov et al. (2015) with the use of the HIRHAM regional climate model simulations with SRES-A1B anthropogenic scenario for the twenty first century. The focus was on cyclones for the warm (April–September) and cold (October–March) seasons. The present-day cyclonic characteristics from HIRHAM simulations are in general agreement with those from ERA-40 reanalysis data. Differences noted for the frequency of cyclones are related with different spatial resolution in the model simulations and reanalysis data. Potential future changes in cyclone characteristics at the end of the twenty first century have been analyzed. According to the model simulations, the frequency of cyclones is increasing in warm seasons and decreasing in cold seasons for a warmer climate in the twenty first century, but these changes are statistically insignificant. Noticeable changes were detected for the intensity and size of cyclones for the both seasons. Significant increase was found for the frequency of weak cyclones during cold season. Further, a general increase in the frequency of small cyclones was calculated in cold seasons, while its frequency decreases in warm seasons.

The ability of state-of-the-art regional climate models to simulate cyclone activity in the Arctic is assessed in Akperov et al. (2018) based on an ensemble of 13 simulations from 11 models from the Arctic-CORDEX initiative. Some models employ large-scale spectral nudging techniques. Cyclone characteristics

simulated by the ensemble are compared with the results forced by four reanalyses (ERA-Interim, National Centers for Environmental Prediction-Climate Forecast System Reanalysis, National Aeronautics and Space Administration-Modern-Era Retrospective analysis for Research and Applications Version 2, and Japan Meteorological Agency-Japanese 55-year reanalysis) in winter and summer for 1981–2010 period. In addition, we compare cyclone statistics between ERA-Interim and the Arctic System Reanalysis reanalyses for 2000–2010. Biases in cyclone frequency, intensity, and size over the Arctic are also quantified. Variations in cyclone frequency across the models are partly attributed to the differences in cyclone frequency over land. The variations across the models are largest for small and shallow cyclones for both seasons. A connection between biases in the zonal wind at 200 hPa and cyclone characteristics is found for both seasons. Most models underestimate zonal wind speed in both seasons, which likely leads to underestimation of cyclone mean depth and deep cyclone frequency in the Arctic. In general, the regional climate models are able to represent the spatial distribution of cyclone characteristics in the Arctic but models that employ large-scale spectral nudging show a better agreement with ERA-Interim reanalysis than the rest of the models. Trends also exhibit the benefits of nudging. Models with spectral nudging are able to reproduce the cyclone trends, whereas most of the nonnudged models fail to do so. However, the cyclone characteristics and trends are sensitive to the choice of nudged variables.

In Akperov et al. (2018), estimates of the tropospheric lapse rate γ and an analysis of its connection with the surface air temperature T_s in high latitudes of the Northern Hemisphere for summer and winter are performed using monthly-mean data from the ERAInterim reanalysis (1979–2014). According to the reanalysis data the lapse rate values increase from 4.7 K/km near the pole to 5.3 K/km in subpolar latitudes in winter and from 5.3 to 6.1 K/km in summer. The estimates of $d\gamma/dT_s$ in interannual variability are found positive over the most part of the Arctic from reanalysis data. At the same time, a negative correlation between γ and T_s was found for the Atlantic sector of the Arctic in winter and for the central Arctic in summer. It is also noted regional peculiarities in the connection of lapse rate with Arctic oscillation for winter and summer.

In Chernokulsky et al. (2018), a comprehensive intercomparison of midlatitude storm characteristics is presented. Extratropical storm characteristics were derived from 16 reanalysis-based objective automated algorithms for cyclone identification and tracking from the IMILAST project and from manual method based on an expert inspection of weather charts. The analysis was carried out for the Siberian region (50–80N, 60–110E) for two seasons (winter of 2007/08 and summer of 2008). Most of the automated algorithms show 1.5–3 times

more cyclones and 3–5 times more cyclone tracks in the Siberian region compare to the manual method. The algorithms show a good agreement with the manual method for spatial distribution of cyclones and tracks number with spatial correlation coefficient varies around 0.8–0.9 in summer and around 0.7–0.9 in winter for most of the algorithms. Two ranking measures were used to evaluate similarity of objective algorithms with the manual method.

The paper by Ermakov et al. (2017) is focused on the development of a methodological basis for the authors' approach to the processing of large volumes of satellite radiothermal data, which is known as satellite radiothermovision. A closed scheme for calculating the latent heat flux (and other integral characteristics of the dynamics of geophysical fields) through arbitrary contours (boundaries) has been constructed and mathematically described. The opportunity for working with static, as well as movable and deformable boundaries of arbitrary shape, has been provided. The computational scheme was tested using the example of calculations of the atmospheric advection of the latent heat from the North Atlantics to the Arctic in 2014. Preliminary analysis of the results showed a high potential of the approach when applying it to the study of a wide range of synoptic and climatically significant atmospheric processes of the Earth. Some areas for the further development of the satellite radiothermovision approach are briefly discussed. It is noted that expanding the analysis of the available satellite data to as much data as possible is of considerable importance. Among the immediate prospects is the analysis of large arrays of data already accumulated and processed in terms of the satellite radiothermovision ideology, which are partially presented and continuously updated on a specialized geoportal.

A previously developed approach of satellite radiothermovision was applied by Ermakov (2017) to the analysis of meridional advection of atmospheric latent heat at climatically significant scales (13 years of continuous passive microwave satellite observations). The results are in good agreement with basic understanding of atmospheric latent heat circulation, though some revealed particularities remain to be the subject to further detailed investigation. Further prospects to application of the developed approach to investigation of atmospheric rivers and global tropical cyclogenesis in the context of multiyear climate variations are briefly discussed. An important aspect of the research is that the calculation approach is independent of any estimates from circulation models.

Ermakov (2018) describes the methodical bases and some results of using satellite radiothermovision to study global atmospheric latent heat circulation according to the data of regular satellite radiothermal monitoring. This approach does not use an a priori model of circulation; it implements an objective procedure for the analysis of the dynamics of periodically measured fields of

total precipitable water. The reconstructed directions and the values of the mean-zonal transport velocity, the average position of the thermal equator at ~ 5°N, and the positions of the axis of the intertropical convergence zone over individual oceans are very consistent with the known results of independent observations and numerical modeling. Some problematic aspects of the analysis procedure are discussed.

Komatsu et al. (2018) carried out upper air measurements with radiosondes during the summer over the Arctic Ocean from an icebreaker moving poleward from an ice-free region, through the ice edge, and into a region of thick ice. Rapid warming of the Arctic is a significant environmental issue that occurs not only at the surface but also throughout the troposphere. In addition to the widely accepted mechanisms responsible for the increase of tropospheric warming during the summer over the Arctic, the authors showed a new potentially contributing process to the increase, based on the direct observations and supporting numerical simulations and statistical analyses using a long-term reanalysis dataset. This new process is referred to as "Siberian Atmospheric Rivers (SARs)". Poleward upglides of SARs over cold air domes overlying sea ice provide the upper atmosphere with extra heat via condensation of water vapour. This heating drives increased buoyancy and further strengthens the ascent and heating of the mid-troposphere. This process requires the combination of SARs and sea ice as a land-ocean-atmosphere system, the implication being that large-scale heat and moisture transport from the lower latitudes can remotely amplify the warming of the Arctic troposphere in the summer.

A quasi-geostrophic three-level T63 model of the wintertime atmospheric circulation of the Northern Hemisphere has been applied by Handorf et al. (2017) to investigate the impact of Arctic amplification (increase in surface air temperatures and loss of Arctic sea ice during the last 15 years) on the mid-latitude large-scale atmospheric circulation. The model demonstrates a mid-latitude response to an Arctic diabatic heating anomaly. A clear shift towards a negative phase of the Arctic Oscillation (AO−) during low sea-ice-cover conditions occurs, connected with weakening of mid-latitude westerlies over the Atlantic and colder winters over Northern Eurasia. Compared to reanalysis data, there is no clear model response with respect to the Pacific Ocean and North America.

A two-zone model of the atmospheric circulation over the hemisphere is considered in an article (Kurgansky, 2018) published in the memorial issue of Izvestiya, Atmospheric and Oceanic Physics journal dedicated to the centenary of birth of A.M. Obukhov. The geographic latitude φ of the boundary between the Rossby circulation regime zone at mid and high latitudes and the Hadley circulation regime zone at low latitudes serves as a model variable. The close-

ness between the actual and reference (negative exponential) air-mass distribution over the hemisphere, with respect to Ertel's modified potential vorticity (MPV), is accounted for. The informational entropy of the statistical MPV distribution in the hemispheric atmosphere and the informational entropy of the eddy regime in the basic storm-track zone are used to determine a statistically (climatically) equilibrium value of φ. The question of atmospheric blocking over the hemisphere is considered using the proposed statistical–dynamical model.

Mesoscale processes

An issue of modern "dynamic meso-meteorology" is the study of dynamic processes in the Arctic, particularly with regard to the interaction of the atmosphere with the ice-covered ocean.

In Chechin and Lüpkes (2017) a new quasi-analytical mixed-layer model is formulated describing the evolution of the convective atmospheric boundary layer (ABL) during cold-air outbreaks (CAO) over polar oceans downstream of the marginal sea-ice zones. The new model is superior to previous ones since it predicts not only temperature and mixed-layer height but also the height-averaged horizontal wind components. Results of the mixed-layer model are compared with dropsonde and aircraft observations carried out during several CAOs over the Fram Strait and also with results of a 3D non-hydrostatic (NH3D) model. It is shown that the mixed-layer model reproduces well the observed ABL height, temperature, low-level baroclinicity and its influence on the ABL wind speed. The mixed-layer model underestimates the observed ABL temperature only by about 10%, most likely due to the neglect of condensation and subsidence. The comparison of the mixed-layer and NH3D model results shows good agreement with respect to wind speed including the formation of wind-speed maxima close to the ice edge. It is concluded that baroclinicity within the ABL governs the structure of the wind field while the baroclinicity above the ABL is important in reproducing the wind speed. It is shown that the baroclinicity in the ABL is strongest close to the ice edge and slowly decays further downwind. Analytical solutions demonstrate that the e-folding distance of this decay is the same as for the decay of the difference between the surface temperature of open water and of the mixed-layer temperature. This distance characterizing cold-air mass transformation ranges from 450 to 850 km for high-latitude CAOs.

The interaction between sea ice and atmosphere depends strongly on the near-surface transfer coefficients for momentum and heat. In Lüpkes and Gryanik (2015), a parametrization of these coefficients is developed on the basis of an existing parametrization of drag coefficients for neutral stratification

that accounts for form drag caused by the edges of ice floes and melt ponds. This scheme is extended to better account for the dependence of surface wind on limiting cases of high and low ice concentration and to include near-surface stability effects over open water and ice on form drag. The stability correction is formulated on the basis of stability functions from Monin–Obukhov similarity theory and also using the Louis concept with stability functions depending on the bulk Richardson numbers. Furthermore, a parametrization is proposed that includes the effect of edge-related turbulence also on heat transfer coefficients. The parametrizations are available in different levels of complexity. The lowest level only needs sea ice concentration and surface temperature as input, while the more complex level needs additional sea ice characteristics. An important property of the proposed parametrization is that form drag caused by ice edges depends on the stability over both ice and water which is in contrast to the skin drag over ice. Results of the parametrization show that stability has a large impact on form drag and, thereby, determines the value of sea ice concentration for which the transfer coefficients reach their maxima. Depending on the stratification, these maxima can occur anywhere between ice concentrations of 20 and 80%.

In climate and weather prediction models the near-surface turbulent fluxes of heat and momentum and related transfer coefficients are usually parametrized on the basis of Monin–Obukhov similarity theory (MOST). To avoid iteration, required for the numerical solution of the MOST equations, many models apply parametrizations of the transfer coefficients based on an approach relating these coefficients to the bulk Richardson number Ri_b. However, the parametrizations that are presently used in most climate models are valid only for weaker stability and larger surface roughnesses than those documented during the Surface Heat Budget of the Arctic Ocean campaign (SHEBA). The latter delivered a well-accepted set of turbulence data in the stable surface layer over polar sea-ice. Using stability functions based on the SHEBA data, Gryanik and Lüpkes (2018) solve the MOST equations applying a new semi-analytic approach that results in transfer coefficients as a function of Ri_b and roughness lengths for momentum and heat. It is shown that the new coefficients reproduce the coefficients obtained by the numerical iterative method with a good accuracy in the most relevant range of stability and roughness lengths. For small Ri_b, the new bulk transfer coefficients are similar to the traditional coefficients, but for large Ri_b they are much smaller than currently used coefficients.

Extreme cases of cold-air outbreaks in the Arctic during spring 2013 are identified in Chechin et al. (2015) using MODIS images from Terra and Aqua satellites. Spatial variability of the surface wind speed during considered cases of cold-air outbreaks is quantified using the ERA Interim reanalysis and data

retrieved from the satellite microwave radiometer AMSR2. To explain the observed variability of wind speed in the atmospheric boundary layer (ABL) the contributions of baroclinicity in the ABL and Ekman friction are quantified. For this purpose diagnostic relationships based on the concept of a mixed-layer model are used. It is demonstrated that baroclinic component of the geostrophic wind caused by the horizontal temperature gradients in the ABL over the open water has a strong effect on the spatial variability of wind speed during considered cases of cold-air outbreaks.

Another issue of dynamic meso-meteorology is the study of extreme wind events.

In Smirnova et al. (2015), a new climatology of polar lows over the Nordic and Barents seas for 14 seasons (1995/1996–2008/2009) is presented. For the first time in climatological studies of polar lows an approach based on satellite passive microwave data was adopted for polar low identification. A total of 637 polar lows were found in 14 extended winter seasons by combining total atmospheric water vapor content and sea surface wind speed fields retrieved from Special Sensor Microwave/Imager data. As derived, the polar low activity in the Norwegian and Barents Seas is found to be almost equal, and the main polar low genesis area is located northeastward of the North Cape. For the Barents Sea, a significant correlation is found between the number of polar lows and mean sea ice extent. Individual indicative polar low characteristics (i.e., diameter, lifetime, distance traveled, translation speed, and maximum wind speed) are also presented.

In Verezemskaya and Stepanenko (2016), numerical experiments based on the WRF model were conducted to analyze the structure and evolution of the polar mesoscale cyclone developed over the Kara Sea on September 29-30, 2008. It was found that baroclinic instability in the lower troposphere and convective instability (including that due to the wind-induced surface heat exchange) did not play a significant role. Significant contribution was made by the downward advection of potential vorticity from the upper troposphere and by the conditional instability of second kind. It is demonstrated that if water phase transitions are not taken into account, the mesocyclone intensity is reduced by 7–20% and the time of its development increases by 4 hours. The advection of potential vorticity was not the only process causing the intensification of the lower potential vorticity anomaly associated with cyclonic circulation.

In Akperov et al. (2017), the ability of the reanalyses data (NASA-MERRA, ERA-INTERIM, NCEP-CFSR, ASR) and regional climate model simulations (RCM HIRHAM5) was analyzed to represent polar mesocyclones (PMCs) over European sector of the Arctic (ESA) in comparison with satellite data (STARS project – Sea Surface Temperature and Altimeter Synergy for Improved Forecasting of Polar Lows). The results show that reanalyses can represent up to

65% of concrete observed polar mesocyclones from satellite data for 2002–2008. It is noted that Arctic reanalysis ASR with high spatial resolution reproduces more PMCs than from other reanalyses with a coarser resolution. Noted differences in the characteristics of Arctic mesocyclones from reanalyses data are related both with the model structure and data assimilation methods. RCM HIRHAM reproduces the same number of PMCs as Arctic reanalysis ASR with high spatial distribution. The analysis of the cyclone characteristics and their intra- and interannual variations obtained from a regional climate model simulation for the Arctic (HIRHAM) with spectral nudging in comparison with reanalyses with different spatial resolution (ERA-Interim and ASR) for the period 2000-2009 was carried out in Akperov et al. (2017). It is noted that the cyclones characteristics in the Arctic, especially their spatial distributions, annual and interannual variations from model simulations are generally consistent with those obtained from different reanalyses data, including the Arctic reanalysis (ASR). Differences are noted for the cyclone frequency, which might be related with different spatial resolution and with differences in detecting small cyclones, including polar mesocyclones. Models with a higher spatial resolution and with an adequate description of mesoscale processes in the Arctic are required to reproduce small-scale mesocyclones.

Over the past 60 years, both average daily precipitation intensity and extreme precipitation have increased in many regions. Part of these changes, or even individual events, have been attributed to anthropogenic warming. Over the Black Sea and Mediterranean region, the potential for extreme summertime convective precipitation has grown alongside substantial sea surface temperature increase. A particularly devastating convective event experienced in that region was the July 2012 precipitation extreme near the Black Sea town of Krymsk. Meredith et al. (2015) study the effect of sea surface temperature (SST) increase on convective extremes within the region, taking the Krymsk event as a showcase example. These authors carry out ensemble sensitivity simulations with a convection-permitting atmospheric model and show the crucial role of SST increase in the extremeness of the event. The enhancement of lower tropospheric instability due to the current warmer Black Sea allows deep convection to be triggered, increasing simulated precipitation by more than 300% relative to simulations with SSTs characteristic of the early 1980s. A highly nonlinear precipitation response to incremental SST increase suggests that the Black Sea has exceeded a regional threshold for the intensification of convective extremes. The physical mechanism identified by the authors indicates that Black Sea and Mediterranean coastal regions may face abrupt amplifications of convective precipitation under continued SST increase, and illus-

trates the limitations of thermodynamical bounds for estimating the temperature scaling of convective extremes.

The article by Bykov and Shikhov (2018) is devoted to the evaluation of forecast reliability of mesoscale convective systems (MCS) with hazardous weather events (squalls, large hail and heavy rainfall) using the global and mesoscale atmospheric models data. Two approaches are implemented to perform this evaluation. They are: (i) the forecast based on the instability indices calculated from the GFS and SLAV global atmospheric models output, and (ii) explicit (cloud-resolving) modeling of the deep convection using WRF-ARW and WRFNMM mesoscale models. New instability index is developed for MCS forecasts based on the global atmospheric models output data. This index is based on the Lifted Index (LI) modification. Terra/Aqua MODIS satellite images and ground-based weather station data are used to estimate the reliability of MCS and hazardous weather events forecasts, respectively. It is shown, that the SLAV model forecasts are more reliable in comparison with GFS forecasts, according to comparison of simulated areas of maximum convective instability with satellite-observed MCS position. The estimation of the cloud resolving MCS forecasts by the WRF-ARW and WRF-NMM models shows that the simulated MCS spatial position often did not coincide with the MODIS-observed position. This could be associated with errors in initial conditions (GFS forecast data). Besides, the WRF model does not reproduce the MCS which were formed in the absence of a dynamic (frontal) convection. It should be noted that WRF-NMM model significantly overestimates the convective precipitation intensity and the areas with heavy showers ($\geq$ 30 mm/h). Because of this, the amount of correct forecasts is increasing; however, the number of false alarms is also rising.

In Polnikov et al. (2017), a new Polynomial approximation method has been used for the estimation of the extreme significant wave heights and wind speeds from 33 years of hindcast data for six locations along the Indian coast. These return value estimates are compared with the values obtained from the well-known Generalised extreme value distribution and Generalised Pareto distribution methods. Further, the entire data is subdivided into three decadal time blocks to assess the time variability in model outputs of extreme values of significant wave heights and wind speeds. Although the comparison, in general, is found good, a closer examination of the results reveals that the present method based on polynomial approximation could be preferred for practical applications. The detailed analysis of the Polynomial approximation method, salient features and its fulfilment of consistency condition which overcomes the shortcomings of the other standard extreme value estimation methods are presented and discussed in this paper.

In Polnikov and Pogarskiy (2017) the spectra of long-term series of wind velocity and significant wave height were built in two domains of variability scales: from 1 day to 1 year (D1) and from 1 year to 15 years (D2). Surface wind data from the ERA-Interim reanalysis in the Indian Ocean area for the period of 1979–2015 years, and wave heights simulated with the improved WAM model, were used for this purpose. In order to study the spatial variability of the spectral shapes, spectra of wind speed and wave height were calculated at two sections located along the meridians and three sections located along latitudes with a step of 3°. For the D1 domain, the existence of three ranges of variability scales (R1, R2, and R3) are shown in which both types of spectra have the well-defined and visibly different power-like slopes varying in dependence on the offset from the equator. The Navier–Stokes equations were analyzed in order to design a theoretical interpretation of the spectral shapes features found in the D1 domain. For the D2 domain, no unified system of isolated frequencies has been revealed, which is expected for the entire Indian Ocean. Among the set of selected periods, the most stable one is the variability period of around 5.5 years. Results presented in this work are discussed.

Medium-range Weather Forecasts global reanalysis (ERA-Interim) over the Indian Ocean has been carried out in (Rashmi et al., 2016) by partitioning the Indian Ocean into six zones based on local wind extrema. The trend of mean annual wind speed averaged over each zone shows a significant increase in the equatorial region, the Southern Ocean, and the southern part of the trade winds. This indicates that the Southern Ocean winds and the southeast trade winds are becoming stronger. However, the trend for the Bay of Bengal is negative, which might be caused by a weakening of the monsoon winds and northeast trade winds. Maximum interannual variability occurs in the Arabian Sea due to monsoon activity; a minimum is observed in the subtropical region because of the divergence of winds. Wind speed variations in all zones are weakly correlated with the Dipole Mode Index (DMI). However, the equatorial Indian Ocean, the southern part of the trade winds, and subtropical zones show a relatively strong positive correlation with the Southern Oscillation Index (SOI), indicating that the SOI has a zonal influence on wind speed in the Indian Ocean. Monsoon winds have a decreasing trend in the northern Indian Ocean, indicating monsoon weakening, and an increasing trend in the equatorial region because of enhancement of the westerlies. The negative trend observed during the non-monsoon period could be a result of weakening of the northeast trade winds over the past few decades. The mean flux of kinetic energy of wind (FKEW) reaches a minimum of about 100 Wm^{-2} in the equatorial region and a maximum of about 1500 W in the Southern Ocean. The seasonal variability of

FKEW is large, about 1600 Wm^{-2} along the coast of Somalia in the northern Indian Ocean. The maximum monthly variability of the FKEW field averaged over each zone occurs during boreal summer. During the onset and withdrawal of monsoon, FKEW is as low as 50 Wm^{-2} .The Southern Ocean has a large variation of about 1280 Wm^{-2}, because of strong westerlies throughout the year.

In Kislov et al. (2018), a detailed modeling of meteorological parameters over the last 30 years (1985–2014) has been performed for the Sea of Okhotsk and Sakhalin regions in the frame of the COSMO-CLM regional meso-meteorological non-hydrostatic atmospheric model. The downscaling technology is suggested and achieved with three consequent "nesting domains" (with 13.2-, 6.6-, and 2.2-km grid scales). The COSMO-CLM model reproduces (especially successfully on the 2.2-km grid scale) the extremes of wind velocity observed by meteorological stations well. Synoptic situations accompanied by extreme wind speeds are reproduced in detail.

The wind parameters at the earth's surface and in the free atmosphere can have a significant impact on the progress with space rocket (SR) in the period of the preparation at the launch site, the launch processing and flight. Therefore, the above parameters are reflected in the operational documentation for each SR as critical and are constantly monitored by meteorological services of a spaceport at all stages of preparation and launch of the space rocket, as the cost of transferring one start of a space rocket is quite a significant amount of money. In connection with the construction of the new cosmodrome Vostochny, Amur Oblast should have a more detailed study of the state of the atmosphere in the days with dangerous convective phenomena. For the study by Gorbatenko et al. (2015), a database of thunderstorm days above the meteorological stations in the area of the cosmodrome Vostochny for 1985–2013 was made. It was found that Amur Oblast is characterized by a moderate thunderstorm activity. During the summer every year there are 20–25 days with thunderstorms. An increase in the variability of thunderstorm activity and a tendency to thunderstorm activity increase have been determined. Forecast of such dangerous convective phenomena like thunderstorms, hail, heavy rainfall is based on the analysis of the profiles of atmospheric temperature and humidity, which are recorded by aerological radiosondes. According to the results sensing characteristics of atmospheric instability are calculated: Indexes LIFT SWEET, KIND, TOTL and CAPE. The values of the index assesses the set of temperature and humidity of the atmosphere and wind parameters that are important signs of development of convection. By variability index values probability of dangerous convective phenomena is estimated. The second objective of the present study was to determine the possibility of using these indexes to determine the degree of stability of the atmosphere in the forecast of thunderstorms

over Amur Oblast. According to the upper-air sounding, index values were calculated of atmospheric instability in days with thunderstorms and heavy rain. A comparative analysis of the indexes of atmospheric instability in the days classified as "thunderstorms and rain" and "heavy rain" are presented. The values of the probability of thunderstorms and rain storms without different values of the indexes of atmospheric instability are calculated. An analysis of the differences in the values of the index volatility typical for Amur Oblast and the values obtained for other territories is presented. Discriminant analysis of instability index to separate these two categories of dangerous convective phenomena in the atmosphere is made.

The prediction of thunderstorms is based on the analysis of atmospheric temperature and moisture profiles, which are typically observed with aerological soundings. The problem is that the sounding network is sparse, and soundings are made only every 12 hours. The goal of the study by Gorbatenko et al. (2015) is to find out if the data of radiometer MODIS (Moderate Resolution Imaging Spectroradiometer) for definition of a degree of instability of the atmosphere could be used in the prediction of thunderstorms in Western Siberia. As the characteristic of instability three indices computed on data of satellite and aerological soundings are compared: Lifted Index, TOTL and K Index. Two of the satellite derived instability indices (Lifted Index, TOTL) are well correlated with those derived from aerological soundings. Results of spectroradiometer MODIS sounding allows the spatial position powerful convective cells to determine and the forecast of thunderstorms to improve.

Several papers were devoted to the mountain mesometeorology.

The dependence of orographic disturbances of the atmosphere on properties of the upwind flow is studied by Kozhevnikov et al. (2016) within the semi-analytic approach. Reducing the initial system of equations of hydrothermodynamics to a single equation for an associative stream function makes it possible to consider a class of solutions of a sufficiently general type when the background wind velocity and the Lyra's scale vary with height. It is shown that the dependence of the solution on the indicated factors can be not only strong, but also sufficiently unexpected. In particular, with the monotonic growth in the wind velocity in the troposphere, which corresponds to conditions of a jet stream near the tropopause, disturbances at low and medium heights can acquire an almost resonant and waveguide nature.

In Kozhevnikov et al. (2017), wavy spatial variations in the contents of trace gases are identified using plane measurements of O_3 concentrations in the middle troposphere and the total content (TC) of NO_2 in the atmospheric column from flights above the Subpolar Urals in April 1984. The results of model calculations allow us to relate these variations to mesoscale atmospheric dis-

turbances above the mountains, which are caused by the influence of dynamic relief on the leaked-in flow.

Bora in Novorossiysk (seaport on the Black Sea coast of the Caucasus) is one of the strongest and most prominent downslope windstorms on the territory of Russia, on the north-eastern coast of the Black Sea. Shestakova et al. (2018) evaluate the applicability of the hydraulic and wave hypotheses, which are widely used for downslope winds around the world, to Novorossiysk bora on the basis of observational data, reanalysis, and mesoscale numerical modeling with WRF-ARW. It is shown that mechanism of formation of Novorossiysk bora is essentially mixed, which is expressed in the simultaneous presence of gravity waves breaking and a hydraulic jump, as well as in the significant variability of the contribution of wave processes to the windstorm dynamics. Effectiveness of each mechanism depends on the elevated inversion intensity and mean state critical level height. Most favorable conditions for both mechanisms working together are moderate or weak inversion and high or absent critical level.

Shestakova et al. (2018) present a comprehensive study of the three-dimensional structure of the Novorossiysk bora. The analysis is based on observational data obtained from the Russian Hydrometeorological Service, automatic weather stations, sodar system, microwave temperature profiler and 10-m mast. In addition, WRF-ARW simulations are performed to verify and complement the observations. The data permit us to investigate major features of the flow over mountain ridges during several bora episodes. The qualitative and quantitative characteristics of the Novorossiysk bora were compared with those of other downslope winds, such as the Adriatic bora, the Boulder windstorm, and the Alpine foehn.

The spatial and time variability of the surface wind field during the bora episodes, including the events of January 27 and February 7, 2012, which were accompanied by windstorms on the coast and Markotkhsky ridge downwind slopes, has been analyzed by Shestakova et al. (2015) based on the meteorological parameters observed during the winter expeditions in 2012–2013 to the Novorossiysk–Gelendzhik region. The dependence of the wind velocity on the background atmospheric parameters and incident-flow blocking conditions has been studied for the cases of strong and weak bora. It is assumed that bora is of a wave nature in the considered episodes and the wave drag effect predominated in the observed wind-flow acceleration on a downwind slope. Partial blocking of an incident wind flow by mountains also affects the wind regime in the downwind zone, especially near Gelendzhik, where mountains are higher than in the Novorossiysk region.

Common features of the flow behavior over mountains within the hydraulic jump model are identified in Shestakova and Moiseenko (2018) based on an

analysis of 36 episodes of severe winds in the regions of Novorossiysk, Pevek, and Novaya Zemlya. In all these episodes, the incoming flow is characterized by a strong inversion layer at altitudes of 0.5–1.5 km and, in the case of bora, by a wind profile critical level in the middle troposphere, which creates conditions for a weakened dynamic interaction between the low-level air flowing over mountains and the upper layers of the atmosphere. The windspeed increase on the lee slope is caused by the transition of the incoming flow from the subcritical to supercritical state. In this case, the velocity amplitude increases with increasing inversion intensity. Model estimates of windspeed increase are in good agreement with observations at lee-side weather stations for episodes with a strong elevated inversion.

In Shestakova (2018), the wave drag is considered for downslope windstorms in Novorossiysk, on Novaya Zemlya, and in Pevek. The research is based on the results of numerical simulation with the WRF-ARW model. Special attention is paid to the evaluation of the contribution that wave processes make to the overall dynamics of the phenomenon (based on the ratio of wave and orographic drag) and to the specific features of wave drag for different downslope windstorms.

The WRF-ARW regional atmosphere circulation model has been used by Efimov and Mikhaylova (2017) to reproduce a few episodes of cold intrusion and the Novorossiysk bora accompanied by the formation of the mesoscale cyclonic vortex over the Black sea, which can be clearly observed from satellite images of cloudiness. It has been shown that the vortex development is associated with the specific features of air flow around the northwestern edge of the Caucasus Mountains. We have estimated the vertical vorticity associated with the alongshore horizontal gradient of temperature. We have considered the field structure of wind velocity and temperature of the axisymmetric quasi-two-dimensional vortex generated in the coastal zone and displaced seaward after separating from the coast. With the background northerly wind, the coastal cyclonic circulation is not accompanied by the vortex separation from the coast. The specific feature of the development of the cyclonic vortex is the southeastern wind with velocities of up to 10 m/s in the Caucasus coastal area from Sochi to Sukhum.

The development of the bora in case of strong southeastern wind in the area of Novaya Zemlya in the winter-spring of 2016 is simulated by Efimov and Komarovskaya (2018) using the WRF-ARW numerical atmosphere circulation model with high spatial resolution. The features of wind speed and air temperature fields are considered which define the formation of the intensive near-surface flow, the bora, over the lee western slope of the mountain range. It is demonstrated that the bora development leads to the air temperature rise over

the eastern part of the Barents Sea, to the increased surface heat fluxes, and to the formation of the cloudless zone over the sea westward of Novaya Zemlya. It was found that the main reason for the bora development is the high stability of the atmospheric boundary layer over the Kara Sea. It is shown that in case of western wind the Novaya Zemlya archipelago does not exert considerable influence on the air exchange in the Kara Sea area.

The features of bora formation in the region of Novaya Zemlya surrounded by the Barents and Kara seas, differing in hydrometeorological conditions, are considered in Efimov and Komarovskaya (2018). The annual course of average magnitude of buoyancy frequency estimation at the points of the Barents and Kara seas has been constructed. The necessary conditions of bora development in the winter and summer periods are considered. The value of Froude number Fr is used as the main criterion. The statistics of bora cases made on the basis of joint distributions of values of buoyancy frequency and wind speed is given. Results of numerical simulations using the WRF-ARW model for three (small, intermediate, and large) values of Froude number Fr are given. The features of the formation of bora hydrodynamic characteristics for cases conventionally referred to shallow and deep bora types are considered. Estimations of orographic drag and its separate components are given.

A series of papers is dedicated to the study of tropical cyclones (hurricaines, typhoons) and tornadoes.

Within the framework of the hydromechanical model (HMM), proposed by B.Ya. Shmerlin, a tropical cyclone (TC) motion is defined in (Shmerlin and Shmerlin, 2015) by a large-scale wind field and a TC intensity. The model contains parameters describing TC and its interaction with wind field. The diagnostic, quasi-prognostic and prognostic calculations of TC movement are carried out. Diagnostic and quasi-prognostic calculations mean that an objective analysis of a large scale wind field and an objective analysis of a TC intensity is used during a TC whole lifetime. In case of diagnostic calculations, model parameters (constants for each TC) are defined from the best coincidence between the real and calculated track of a TC during a TC whole lifetime; for quasi-prognostic calculations they are defined during the preliminary “preprognostic” period. Diagnostic calculations show that the HMM rather correctly describes peculiarities of a TC motion. Quasi-prognostic calculations show that model parameters may be rather correctly defined during a preliminary “preprognostic” period. The results of the diagnostic, quasi-prognostic and prognostic calculations are presented.

The results are presented in Novitskii et al. (2016) of computation of trajectory and intensity of two typhoons in 2012 for two groups of parameterization schemes of ocean-atmosphere energy exchange in tropical cyclones (TCs),

boundary and surface layers of TCs, radiation fluxes, microphysics, and convection. The surface layer computations were carried out with and without the relationships that take into account the surface layer cooling due to spray evaporation. It is demonstrated that the accounting of this effect exerts positive influence on the results of TC trajectory modeling at different stages. If there are specific features in TC movement, for example, the loop formation, this improvement may be crucial. The accuracy of the results of computation of TC intensity increases as well.

Satellite radiothermovision is a set of processing techniques applicable for multisource data of radiothermal monitoring of ocean-atmosphere system, which allows creating dynamic description of mesoscale and synoptic atmospheric processes and estimating physically meaningful integral characteristics of the observed processes (like advective flow of the latent heat across a given border). In (Ermakov et al., 2015) this opportunity was used to evaluate the latent heat flux across a set of circular contours, enclosing a tropical cyclone and drifting with it during its evolution. A remarkable interrelation was observed between the calculated magnitude and sign of advective latent flux and the intensity of a tropical cyclone. This interrelation is demonstrated in several examples of hurricanes and tropical cyclones of August, 2000, and typhoons of November, 2013, including super typhoon Haiyan.

In (Ermakov et al., 2017) the satellite radiothermovision methods are further developed for analyzing the evolution of tropical cyclones. The complicated case of Goni and Atsani interacting typhoons is considered. It has been shown that, although their interaction does not explicitly influence the features of the typhoon trajectories, indications of the formation of complex advective fluxes in the lower troposphere can be revealed from both a qualitative analysis of miscellaneous satellite data and a quantitative estimation of latent heat advection. At the same time, in contrast to the previous works, we had to introduce the integration contours of a complex form (differing from a circular one) into the analysis, so that the energy balance of the typhoon system is correctly described. Due to the peculiarity of the considered case of Goni and Atsani twin typhoons, we demonstrated the effectiveness of a simplified approach that uses a composite contour formed by overlapping two circular ones. Generally, as in the cases previously considered, we found the interrelation between the intensification and dissipation of typhoons (tropical cyclones) and the modes of convergent and divergent advection of latent heat with amplitudes sufficient to support the total power of the system.

Chernokulsky et al. (2015) considered the formation conditions of the severe tornado in the South Urals (in the Republic of Bashkortostan) on August 29, 2014. It is noted that the tornado was associated with the supercell, and the

synoptic conditions of its formation corresponded to the type 1 according to the classification proposed by A.I. Snitkovskii in 1987. Estimated are the tornado basic characteristics: the vortex funnel width is 150–200 m, and the maximum wind speed is 65 m/s. It is revealed that the tornado was of EF3 category following the enhanced Fujita scale. Proposed is the simple index of convective instability based on the data of ground-based observations for diagnosing the tornado genesis environments.

A simple index of convective instability (3D-index) is used by Chernokulsky et al. (2017) for analysis of weather and climate processes that favor to the occurrence of severe convective events including tornadoes. The index is based on information on the surface air temperature and humidity. The prognostic ability of the index to reproduce severe convective events (thunderstorms, showers, tornadoes) is analyzed. It is shown that most tornadoes in North Eurasia are characterized by high values of the 3D-index; furthermore, the 3D-index is significantly correlated with the available convective potential energy. Reanalysis data (for recent decades) and global climate model simulations (for the 21st century) show an increase in the frequency of occurrence of favorable for tornado formation meteorological conditions in the regions of Northern Eurasia. The most significant increase is found on the Black Sea coast and in the south of the Far East.

The study by Shikhov and Chernokulsky (2018) presents a novel method of tornado track identification in forested regions in Europe based on remote sensing data. The method enables an objective estimate (i.e. independent of population density and observational networks) of tornado climatology in forested regions. The method is based on the identification of narrow and elongated areas as forest disturbances obtained using Landsat satellite images and Landsat-based Global Forest Change (GFC) data. These areas were subsequently verified with high-resolution satellite images for verification of a tornadic cause of forest damage. Landsat and MODIS satellite images, weather station observations and reanalysis data were additionally involved in order to determine tornado dates. A minimum F-scale tornado intensity was estimated by a Weibull distribution model using information on tornado path lengths and widths. The method is applied to the forested regions of northeast Europe, where 110 tornado tracks were identified between the 2000 and 2014years, 105 of which were previously unreported and discovered for the first time. For some regions, tornado density estimates using the new method is 2–3 times higher than other previously published estimates. The largest number of tornadoes occurred in 2009, and June is the most favourable month for tornado formation (including strong tornadoes and tornado outbreaks). Most identified tornadoes have path length < 10km with maximum and mean widths of approximately 200–300 m

and 100–200 m, respectively. A few tornadoes with long and wide paths were found; four of them likely had F3 minimal intensity.

The 1984 Ivanovo tornado outbreak is one of the most fatal tornado events in Europe with previously unspecified tornado track characteristics. Chernokulsky and Shikhov (2018) used Landsat images to discover tornado-induced forest disturbances and restore actual characteristics of tornadoes during the outbreak. They defined boundaries of tornado-induced windthrows by visual comparison of satellite images and specified them with Normalized Difference Infrared Index. As a result, they confirmed the occurrence of eight tornadoes during the outbreak and determined their location, path width and length. Other tornadoes occurrence during the outbreak was discussed. Fujita-scale intensity of confirmed tornadoes was estimated based on the related literature corpus including previously omitted sources. In addition, information on tornado path lengths and widths was used to estimate minimal tornado intensity for those tornadoes that passed no settlements. In total, the Ivanovo outbreak includes 8–13 tornadoes with F-scale rating mean ranges from 1.8–2.5 and has adjusted Fujita length around 540 km, which makes the outbreak one the strongest in Europe and places it within the upper quartile of U.S. outbreaks. Characteristics of certain tornadoes within the Ivanovo outbreak are exceptional for Russia. The widest tornado path during the Ivanovo outbreak is 1740 m; the longest is from 81.5–85.9 km. With the example of the Ivanovo outbreak, it was shown that existing databases on historical Russian tornadoes tend to overestimate tornado path length (for very long tornadoes) and underestimate maximum tornado path width.

The analysis of the state of the atmosphere, which preceded and accompanied the formation of a tornado in Obninsk (Kaluga region) on May 23, 2013, is made by Novitskii et al. (2015). Meteorological parameters obtained from different sources, in particular the measurements obtained at the High Meteorological Mast in Obninsk, were used. The datasets obtained give a complete image of the 300-m-thick atmospheric boundary layer. Presented also are the computation results for a series of convective indices obtained with the use of the WRF model to describe the situation of 23 May, 2013 in Obninsk. The possibility of long-range forecasting of tornado-like situations on the basis of the approach mentioned is estimated.

An analysis of possible tornado warning has been made by Novitskii et al. (2016). A tornado event on the 29 August 2014 in Bashkiria was analyzed. To calculate the meteorological fields, the model WRF of high spatial and temporal resolution was used. On its basis, indices of convective instability were computed. An analysis of the behavior of the indices made it possible to predict the tornado occurrence with a lead time of up to three days and with an accura-

cy of several hours in time and 200 km in space. Also demonstrated was the possibility of registering and nowcasting tornadoes based on the use of existing software for radar data processing. Also discussed is the possibility of joint use of the information mentioned to create a system of monitoring and forecasting of hazardous weather, including tornadogenesis.

Along with the calculation of convective indices using the WRF model for the analysis and forecasting of tornado-risk situations, involved calculation of vertical velocity field was performed by Novitskii et al. (2018). The results of calculations for the four tornadoes in 2015 are presented. It is shown that the indices values above the threshold to cause the formation of localized intensive convective cell in the vicinity of maximum values of indices and when they reach these values. The possibility of using this result as an additional predictor of occurrence of tornado-like situations is discussed. It confirms the conclusions of the principal possibility for the forecasting of tornado-risk situations with a lead time of up to three days and an accuracy of up to several hours in time and 200 km in space.

Using the WRF-ARW model, Efimov (2017) has conducted a numerical simulation of the atmospheric circulation in the Crimean region for a 30-day period in the summer. The characteristic features of the velocity fields of breeze circulation over Crimea have been identified. The author has reproduced the specific features of the development of breeze as a gravity flow, such as the direct and indirect circulation cells, wave oscillations on the boundary between them associated with the Kelvin–Helmholtz instability, and the formation of the breeze head. The breeze velocities and their diurnal cycle have been estimated. For mountainous regions of the southern coast of Crimea (SCC), it has been shown that the coastal circulation is predominantly contributed by quasi-diurnal oscillations associated with the wind excitation on the mountain slopes. The physical conditions for the development of a strong katabatic wind have been considered. The counter breeze flows in eastern Crimea formed under the influence of the adjacent Black and Azov seas generate an intense air rise in the meeting zone. The related linear cloudiness area is clearly traced on satellite images. Daily hodographs of breeze circulation have been obtained reflecting the local conditions of the shoreline and the configuration of coastal mountains.

Small-scale motions and turbulence in the atmospheric boundary layer

Recent progress of including “lake subroutines” in numerical weather prediction (NWP) models has led to more accurate forecasts. In lake models, one essential parameter is water clarity, parameterized via the light extinction coefficient, K_d, for which a global constant value is usually used. Heiskanen et al.

(2015) used direct eddy covariance fluxes and basic meteorological measurements coupled with lake water temperature and clarity measurements from a boreal lake to estimate the performance of two lake models, LAKE and FLake. These models represent two 1D modeling frameworks broadly used in NWP. The results show that the lake models are very sensitive to changes in K_d when it is lower than 0.5 m^{-1}. The progress of thermal stratification depended strongly on K_d. In dark water simulations the mixed layer was shallower, longwave and turbulent heat losses higher and therefore the average water column temperatures lower than in clear water simulations. Thus, changes in water clarity can also affect the onset of ice cover. The more complex LAKE modelled the seasonal thermocline deepening whereas it remained virtually constant during summer in the FLake model. Both models overestimated the surface water temperatures by about 1°C and latent heat flux by >30%, but the variation in heat storage and sensible heat flux were adequately simulated. Our results suggest that, at least for humic lakes, a lake-specific, but not time-depending, constant value for K_d can be used and that a global mapping of K_d would be most beneficial in regions with relatively clear lakes, e.g. in lakes at high altitudes.

Glazunov and Stepanenko (2015) performed large eddy simulation (LES) runs to calculate flows over heterogeneous surfaces imitating small forest lakes. Regularities in the turbulent exchange of heat and momentum over such objects are examined. A weak sensitivity of turbulence characteristics over a "lake" to thermal stratification is noted. Problems of the representativeness of field eddy covariance measurements of turbulent fluxes over such objects are discussed.

In Glazunov et al. (2016), large-eddy simulation (LES) and Lagrangian stochastic modeling of passive particle dispersion were applied to the scalar flux footprint determination in the stable atmospheric boundary layer (ABL). The sensitivity of the LES results to the spatial resolution and to the parameterizations of small-scale turbulence was investigated. It was shown that the resolved and partially resolved ("subfilter-scale") eddies are mainly responsible for particle dispersion in LES, implying that substantial improvement may be achieved by using recovering of small-scale velocity fluctuations. In LES with the explicit filtering, this recovering consists of the application of the known inverse filter operator. The footprint functions obtained in LES were compared with the functions calculated with the use of first-order single-particle Lagrangian stochastic models (LSMs) and zeroth-order Lagrangian stochastic models – the random displacement models (RDMs). According to the presented LES, the source area and footprints in the stable ABL can be substantially more extended than those predicted by the modern LSMs.

The stochastic ensemble of convective thermals (vortices), forming the fine structure of a turbulent convective boundary layer (CBL), is considered in

(Vulfson and Borodin, 2018). The proposed ensemble model assumes all thermals in the mixed-layer to have the same determinate buoyancies and considers them as solid spheres of variable volumes. The values of radii and vertical velocities of the thermals are assumed random. The motion of the stochastic system of convective vortices is described by the nonlinear Langevin equation with a linear drift coefficient and a random force, whose structure is known for a system of Brownian particles. The probability density of the thermal ensemble in velocity phase space is shown to satisfy an associated K-form of the Fokker–Planck equation with variable coefficients. Maxwell velocity distribution of convective thermals is constructed as a steady-state solution of a simplified Fokker–Planck equation. The obtained Maxwell velocity distribution is shown to give a good approximation of experimental distributions in a turbulent CBL.

In the article by Vulfson and Nikolaev (2017), modifications of integral bubble and jet models including the pressure force are proposed. Exact solutions are found for the modified model of a stationary convective jet from a point source of buoyancy and momentum. The exact solutions are compared against analytical solutions of the integral models for a stationary jet that are based on the approximation of the vertical boundary layer. It is found that the modified integral models of convective jets retain the power-law dependences on the altitude for the vertical velocity and buoyancy obtained in classical models. For a buoyant jet in a neutrally stratified atmosphere, the inclusion of the pressure force increases the amplitude of buoyancy and decreases the amplitude of vertical velocity. The total amplitude change is about 10%. It is shown that in this model there is a dynamic invariant expressing the law of a uniform distribution of the potential and kinetic energy along the jet axis. For a spontaneous jet rising in an unstably stratified atmosphere, the inclusion of the pressure force retains the amplitude of buoyancy and increases the amplitude of vertical velocity by about 15%. It is shown that in the model of a spontaneous jet there is a dynamic invariant expressing the law of a uniform distribution of the available potential and kinetic energy along the jet axis. The results are of interest for the problems of anthropogenic pollution diffusion in the air and water environments and the formulation of models for statistical and stochastic ensembles of thermals in a mass-flux parameterization of turbulent moments.

The Monin–Obukhov similarity theory (MOST) for the convective surface layer distinguishes two limiting cases: a dynamic limit and a free-convection limit. The dynamic limit for the convective surface layer is defined as a flow with a logarithmic profile of wind and a zero buoyancy flux at the underlying surface. The free-convection limit is characterized by a zero wind speed and a positive buoyancy flux at the underlying surface. The limits of the generalized MOST are able to describe the higher order turbulent moments. In the paper by

Vulfson and Nikolayev (2018), it is assumed that the convective surface layer consists of two sublayers: the lower dynamic sublayer adjacent to the surface and the upper forced-convection sublayer. The turbulent moments can be approximated separately for each sublayer. Linear approximations are suggested for the turbulent moments of the vertical velocity and the potential temperature variance in the forced-convection sublayer. The first-order expansion terms of them correspond to the free-convection limits of the MOST under no-wind conditions. The second-order expansion terms describe profiles of the turbulent moments in under convective conditions with a moderate wind. A comparison between the proposed approximations and experimental data strongly suggests that the linear approximation is correct within a forced-convection range.

In Koprov et al. (2015), an experimental measurement of all three components of the velocity and vorticity vectors, as well as the temperature, its gradient, and potential vorticity, has been described using four acoustic anemometers. Anemometers were placed at vertices of a tetrahedron, the horizontal base of which was a rectangular triangle with equal legs, and the upper point was exactly above the top of the right angle. The distance from the tetrahedron surface to its base was 5.5 m, and the lengths of legs and a vertical edge were 5 m. A covariance–correlation matrix for turbulent variations in all measured values has been calculated. In the daytime the helicity horizontal and vertical components are of the order of –0.03 and +0.01 m s^{-2}, respectively. The nighttime signs remain unchanged, but the absolute values are several times smaller. The cospectra and spectral correlation coefficients have been calculated for all helicity components. The time variations in the components of "instantaneous" helicity and potential vorticity are demonstrated.

In August 2014, measurements of the turbulent velocity vorticity, turbulent temperature gradient, turbulent helicity, and turbulent potential vorticity were performed at the Obukhov Institute of Atmospheric Physics testing site in Tsimlyansk under different stratification conditions (Koprov et al., 2018). The measurements were carried out using the technique first used in the Tsimlyansk expedition in 2012. The measuring facility consisted of four three-component acoustic Gill Windmaster anemometers–thermometers placed at the vertices of a rectangular tetrahedron with a base scale of 0.7 m (in contrast to the experiment in 2012, when the base scale was 5 m). The measuring facility was placed on top of a mast with an adjustable height of 3.5, 5, 13.5, and 25 m and was equipped with a rotator. The temperature profile in the 10–600 m layer was continuously recorded by the Kadygrov microwave profiler. The time-series of instantaneous helicity density and average values of the total helicity and its summands were calculated for 12 daytime and 10 daytime 2-hour intervals. The helicity value averaged over 12 day realizations is about 0.2 m/s^2, and the aver-

age cosine of the angle between the velocity and vorticity vectors is close to 0.08 ± 0.03. At night, the helicity is estimated as 0.07 ± 0.03 m/s^2, and the cosine is close to 0.025 ± 0.03. For the abovementioned 12 daytime and 10 daytime 2-hour intervals, the covariance/correlation matrices of temperature components, vorticity, velocity, and temperature gradient are calculated. The off-diagonal terms of the covariance matrix exceed several time by magnitude the diagonal terms. Similar characteristics of a potential vorticity were estimated under the incompressibility approximation. The systematic error due to spatial averaging of the measured quantities is discussed.

The article of Barskov et al. (2017) presents the results of an experimental study of turbulent heat exchange between the surface of a frozen lake surrounded by forest and the atmospheric boundary layer. Heat and momentum fluxes were measured at three levels by an eddy covariance (EC) technique. Additionally, the heat fluxes were estimated by a surface energy balance method using a temperature profile measured in the snow cover and net longwave and shortwave radiation. The results of the measurements show that the eddy covariance fluxes correlate well with those obtained by the surface energy balance method, with a tendency of underestimation. The presence of wind-shear effects at treetop height demonstrated recently in a Large Eddy Simulation was supported in our measurements by the fact that the momentum flux increased with height from the surface. The negative sensible heat flux increased with height most of the time. We suggest that this phenomenon may partially be caused by the high negative heat fluxes above the surface formed when warm advection occurs at altitudes of ~100 m. During the warm advection events, Monin–Obukhov similarity theory (MOST) fails to reproduce the sharp increase of the negative heat flux at the surface layer. Beyond the warm advection events, the MOST calculations agree well with the EC fluxes, however, with some systematic underestimation bias.

In Barskov et al. (2018), micrometeorological measurements in the atmospheric boundary layer (ABL) over a hilly forest terrain have been made on a meteorological tower at several levels from the forest canopy top to a height that exceeds the height of trees almost seven times. A semi-empirical length scale depending on the local topography features and the underlying surface type has been proposed and calculated. This scale has been shown to allow the universal functions of the Monin–Obukhov similarity theory to be corrected for a stable ABL over complex terrain without substantial modification when compared to the universal functions over a homogeneous surface with small roughness elements. This approach can be used to refine the methods for calculating turbulent momentum fluxes from profile measurements over spatially inhomogeneous landscapes.

The observational study by Grachev et al. (2018) compares seasonal variations of surface fluxes (turbulent, radiative, and soil heat) and other ancillary atmospheric/surface/permafrost data based on in-situ measurements made at terrestrial research observatories located near the coast of the Arctic Ocean. Hourly-averaged multiyear data sets collected at Eureka (Nunavut, Canada) and Tiksi (East Siberia, Russia) are analyzed in more detail to elucidate similarities and differences in the seasonal cycles at these two Arctic stations, which are situated at significantly different latitudes (80.0°N and 71.6°N, respectively). While significant gross similarities exist in the annual cycles of various meteorological parameters and fluxes, the differences in latitude, local topography, cloud cover, snowfall, and soil characteristics produce noticeable differences in fluxes and in the structures of the atmospheric boundary layer and upper soil temperature profiles. An important factor is that even though higher latitude sites (in this case Eureka) generally receive less annual incoming solar radiation but more total daily incoming solar radiation throughout the summer months than lower latitude sites (in this case Tiksi). This leads to a counter-intuitive state where the average active layer (or thaw line) is deeper and the topsoil temperature in midsummer are higher in Eureka which is located almost 10o north of Tiksi. The study further highlights the differences in the seasonal and latitudinal variations of the incoming shortwave and net radiation as well as the moderating cloudiness effects that lead to temporal and spatial differences in the structure of the atmospheric boundary layer and the uppermost ground layer. Specifically the warm season (Arctic summer) is shorter and mid-summer amplitude of the surface fluxes near solar noon is generally less in Eureka than in Tiksi. During the dark Polar night and cold seasons (Arctic winter) when the ground is covered with snow and air temperatures are sufficiently below freezing, the near-surface environment is generally stably stratified and the hourly averaged turbulent fluxes are quite small and irregular with on average small downward sensible heat fluxes and upward latent heat and carbon dioxide fluxes. The magnitude of the turbulent fluxes increases rapidly when surface snow disappears and the air temperatures rise above freezing during spring melt and eventually reaches a summer maximum. Throughout the summer months strong upward sensible and latent heat fluxes and downward carbon dioxide (uptake by the surface) are typically observed indicating persistent unstable (convective) stratification. Due to the combined effects of day length and solar zenith angle, the convective boundary layer forms in the High Arctic (e.g., in Eureka) and can reach long-lived quasi-stationary states in summer. During late summer and early autumn all turbulent fluxes rapidly decrease in magnitude when the air temperature decreases and falls below freezing. Unlike Eureka, a pronounced zero-curtain effect consisting of a sustained surface temperature hiatus

at the freezing point is observed in Tiksi during fall due to wetter and/or water saturated soils.

Insufficient knowledge of the atmosphere boundary layer structure and of momentum, heat and moisture exchange between the rough water surface and atmosphere under various background conditions is currently the main obstacle to the proper functioning of the global and regional weather prediction models and models of climate change. The sea surface drag coefficient is one of the main characteristics of the air-sea interaction, included in the wind waves and sea wind prediction models. In the paper by Repina et al. (2015) the sea surface drag coefficient under differing condition in the coastal zone and deep sea was estimated from experimental measurements. The shipboard experimental data confirmed that the drag coefficient levels off as wind speed increases under high wind conditions (wind speed greater 25 m/s) while decreases as wind speed further increases. The characters of air-sea interaction in the coastal zone were investigated. It was documented greater drag coefficient under off-shore wind directions off-shore documented greater wind stress that could explain of the gusty of coastal winds, shoaling waves and development of internal boundary layers with off-shore flow. Also observed drag coefficient values at on-shore wind are greater than deep water values. It is explained that the wind wave state may be related to bottom topography, coastal line and fetch limited condition. Since the deep water surface drag coefficient is likely to underestimate wind stress and thus storm surge near the coast.

Stably stratified turbulent boundary-layer flows over both a waved water surface and a flat smooth surface are investigated by Druzhinin et al. (2015a) through direct numerical simulation (DNS) for the bulk Reynolds numbers, Re, from 15000 to 80000. DNS expose the following basic properties of the flow. A statistically stationary turbulent regime is sustained if the turbulent Reynolds number, Re_L, based on the Obukhov length-scale and friction velocity, is larger than 10^2. At $\mathrm{Re}_L < 10^2$, turbulence over a flat surface degenerates completely, but over a waved surface it survives in the form of residual fluctuations, which are weaker for smaller wave slopes. In the stationary turbulent regime, at $\mathrm{Re}_L > 10^2$, vertical profiles of the mean-flow velocity and temperature have a log–linear shape, as predicted by the Monin-Obukhov similarity theory, with the same empirical dimensionless constants as in laboratory and field experiments. The velocity and temperature roughness lengths, vertical turbulent fluxes of momentum and heat, and root mean square turbulent velocity and temperature fluctuations increase with increasing slope of the surface waves. At the same time, vertical profiles of the mean velocity and temperature keep the self-similar shape predicted by the Monin–Obukhov theory, irrespective of the wave slope. Druzhinin et al. (2015b) have performed DNS of stably stratified flows over both flat and waved surfaces for a wide range of bulk Reynolds numbers

and Richardson numbers and revealed that the same threshold, $\mathrm{Re}_L = 10^2$, holds true over waved surfaces. However, when the surface wave slope is sufficiently steep, the supercritically stratified flow involves wave-induced, 'pre-turbulent' flow patterns, most pronounced in the vicinity of the waved water surface. In the present article, we study basic properties of these motions through DNS and propose a theoretical model of their generation via secondary parametric resonance instability of two-dimensional disturbances induced in the airflow by the surface waves. The study by Druzhinin et al. (2018) is concerned with numerical simulation of momentum, heat, and moisture exchange processes occuring in the marine atmospheric boundary layer. In particular, the influence of sea-spray drops on these processes is investigated. It is shown that drops reduce the mean air velocity and temperature, and increase relative humidity as compared to droplet-free flow.

Influence of the spray generation due to the fragmentation of the "bag-breakup" type on momentum exchange in the atmospheric boundary layer above the sea surface at hurricane winds was investigated by Troitskaya et al. (2017) on the basis of the analysis of the results of laboratory experiments. It was shown that aerodynamic drag is determined by the contribution of three factors: first, the drag of the "bag-breakup" canopies as obstacles; second, acceleration of the spray formed during fragmentation by the air flow; and the third factor is related to the stratification of the near-water atmospheric layer due to the presence of levitated water droplets. Combination of all three factors leads to a non-monotonous dependence of the aerodynamic drag coefficient on wind speed, which confirms the results of the field and laboratory measurements.

Cospectral budgets are used by Li et al. (2015) to link the kinetic and potential energy distributions of turbulent eddies, as measured by their spectra, to macroscopic relations between the turbulent Prandtl number (Pr_t) and atmospheric stability measures such as the stability parameter ζ, the gradient Richardson number R_g, or the flux Richardson number R_f in the atmospheric surface layer. The dependence of Pr_t on ζ, R_g, or R_f is shown to be primarily controlled by the ratio of Kolmogorov and Kolmogorov–Obukhov–Corrsin phenomenological constants and a constant associated with isotropization of turbulent flux production that can be independently determined using rapid distortion theory in homogeneous turbulence. Changes in scaling laws of the vertical velocity and air temperature spectra are also shown to affect the $\mathrm{Pr}_t - \zeta$ (or $\mathrm{Pr}_t - R_g$ or $\mathrm{Pr}_t - R_f$) relation. Results suggest that departure of Pr_t from unity under neutral conditions is induced by dissimilarity between momentum and heat in terms of Rotta constants, isotropization constants, and constants in the flux transfer terms. A maximum flux Richardson number R_{fm} predicted from the cospectral

budgets method (=0.25) is in good agreement with values in the literature, suggesting that R_{fm} may be tied to the collapse of Kolmogorov spectra instead of laminarization of turbulent flows under stable stratification. The linkages between microscale energy distributions of turbulent eddies and macroscopic relations that are principally determined by dimensional considerations or similarity theories suggest that when these scalewise energy distributions of eddies experience a "transition" to other distributions (e.g., when R_f is increased over R_{fm}), dimensional considerations or similarity theories may fail to predict bulk flow properties.

The study by Kurbatskiy and Kurbatskaya (2015) was performed on features of eddy transport of momentum and heat in the lower atmosphere, which includes the planetary boundary layer as well as upper troposphere and lower stratosphere; the study used a three-parametric method for modeling of stratified turbulent flows. A focus was put on analysis of behavior of vertical diffusivities of momentum and heat: data were obtained through direct measurements and through simulation with three-parametric turbulence model with account for effects of internal gravitational waves which support momentum transfer under condition of very stable stratification (while possessing considerable wavy dynamics). It was demonstrated that the profile of vertical diffusivity for momentum, which was calculated using three-parametric turbulence model, is in agreement with data on direct measurements when measured either within a stable stratified planetary boundary layer or beyond this layer, in free atmosphere.

The results of the numerical modeling of turbulent structure of the penetrating convection above the urban heat island with a small aspect ratio in a stably stratified medium at rest are presented in Kurbatskii and Kurbatskaya (2016). The gradient diffusion representations for turbulent momentum and heat fluxes are used, which depend on three parameters – the turbulence kinetic energy, the velocity of its spectral expenditure, and the dispersion of temperature fluctuations. These parameters are found from the closed differential equations of balance in the RANS approach of turbulence description. The distributions of averaged velocity and temperature fields as well as turbulent characteristics agree well with measurement data.

Kurbatskaya and Kurbatskii (2016) examine the parameterizations of the turbulent friction velocity u* for the mathematical model of an urban heat island of a low-aspect-ratio in a calm stably stratified environment with a thermophysically inhomogeneous underlying surface (unstable stratification over a localized surface heat source and stable stratification out of it). The results of u* calculation by Louis and Paulson noniterative algorithms for the quasi-steady circulation over an urban heat island are presented.

An explicit algebraic model of Reynolds stresses and the turbulent heat flux vector for the planetary boundary layer in a neutrally stratified boundary layer of the atmosphere above a homogeneous rough surface is tested by Kurbatskii and Kurbatskay (2017). The version of the algebraic model under consideration is constructed on the physical principles of the RANS (Reynolds-averaged Navier–Stokes) approximation for describing stratified turbulence, it employs three forecasting equations, and a correct reproduction of the main characteristics of a neutral atmospheric boundary layer – the components of the mean wind velocity, the wind turn angle, and the turbulent statistics is shown. Test computations show that the proposed model may be used for goal-oriented investigations of the atmospheric boundary layer.

A recently developed fully explicit algebraic model of Reynolds stress and turbulent heat flux in a thermally stratified planetary atmospheric boundary layer without stratification has been used by Kurbatskii and Kurbatskaya (2018) for a numerical study of the Ekman turbulent boundary layer over a homogeneous rough surface for different dimensionless surface Rossby numbers. A comparative analysis has been conducted for a closure model of the transport term in the prognostic equation of turbulent kinetic energy dissipation including third-order moments. Dependences of the total wind rotation angle on the Rossby number have been obtained. The calculated vertical profiles of mean velocity, turbulent stress, turbulent kinetic energy, surface-friction velocity, and boundary-layer height agree satisfactorily with observational and earlier obtained LES data.

Chkhetiani et al. (2018) consider the assumption postulated by Deusebio and Lindborg (J Fluid Mech 755: 654–671, 2014) that the helicity injected into the Ekman boundary layer undergoes a cascade, with preservation of its sign (right- or alternatively left-handedness), which is a signature of the system rotation, from large to small scales, down to the Kolmogorov microscale of turbulence. At the same time, recent direct field measurements of turbulent helicity in the steppe region of southern Russia near Tsimlyansk Reservoir show the opposite sign of helicity from that expected. A possible explanation for this phenomenon may be the joint action of different scales of atmospheric flows within the boundary layer, including the sea-breeze circulation over the test site. In this regard, we consider a superposition of the classic Ekman spiral solution and Prandtl's jet-like slope-wind profile to describe the planetary boundary-layer wind structure. The latter solution mimics a hydrostatic shallow breeze circulation over a non-uniformly heated surface. A 180°-wide sector on the hodograph plane exists, within which the relative orientation of the Ekman and Prandtl velocity profiles favours the left rotation with height of the resulting wind velocity vector in the lowermost part of the boundary layer. This ex-

plains the negative (left-handed) helicity cascade toward small-scale turbulent motions, which agrees with the direct field measurements of turbulent helicity in Tsimlyansk. A simple turbulent relaxation model is proposed that explains the measured positive values of the relatively minor contribution to turbulent helicity from the vertical components of velocity and vorticity.

In Kurgansky (2018), the combined Rankine vortex model is applied to describe the radial profile of azimuthal velocity in atmospheric dust devils, and a simplified model version is proposed of the turbulent surface boundary layer beneath the Rankine vortex periphery that corresponds to the potential vortex. Based on the results by Burggraf et al. (1971), it is accepted that the radial velocity near the ground in the potential vortex greatly exceeds the azimuthal velocity, which makes tractable the problem of the surface shear stress determination, including the case of the turbulent surface boundary layer. The constructed model explains exceeding the threshold shear velocity for aeolian transport in typical dust-devil vortices both on Earth and on Mars.

Dynamical interaction between the troposphere, middle and high atmosphere

The beginning of research on the interaction between the troposphere and the stratosphere in extratropical latitudes dates back to the mid 1970s (Hines, 1974; Holton and Mass, 1976). However, a deeper understanding of this connection emerged through work (Thompson and Wallace, 1998), where a description was given of the mode of sea level pressure variability in the northern hemisphere in winter, which closely connects the troposphere and the lower stratosphere. This mode is called the Arctic Oscillation (AO), its manifestation on the surface is defined as the first empirical orthogonal function (EOF) – the main mode of pressure variability at sea level north of 20N. Comparing the main component of the EOF and the mean zonal wind at different altitudes, a vertical link is found covering the troposphere and the lower stratosphere. In parallel, downward stratospheric anomalies have been studied using simple and more complex models (Holton and Mass, 1976; Scaife and James, 2000). They constitute a series of stratospheric oscillations without an annual cycle: the alternation of positive and negative anomalies with an appearance very similar to the quasi-biennial oscillation (QBO) but with a shorter period of 50–100 days. The main modes of variability can be characterized as a combination of oscillations of the position of the zonal jet and its stochastic amplification

The variability on the intraseasonal time scales can, at first approximation, be caused by the reddening of the spectrum of random forcing (baroclinic instability). That is, if baroclinic instability is considered as white noise, then the barotropic reaction to such an impact will usually have a red spectrum. Both

friction and non-linear processes tend to suppress long-term correlations and limit spectrum reddening, by whitening a spectrum on long time scales. If stochastic forcing is statistically zonally homogeneous, then the resulting patterns of variability represented by empirical orthogonal functions (EOF) are almost zonally homogeneous with a meridional dipole structure resembling a ring mode. If amplification occurs in storm track zones over the ocean, the resulting structure of variability is localized in zones, resembling the North Atlantic Oscillation (NAO). This suggests that these vibrations and ring modes in the North Atlantic are manifestations of the same phenomenon. Strong interaction between the stratosphere and the troposphere is usually observed in winter. Planetary waves propagating upward, both stationary and non-stationary (of a synoptic time scale), sometimes cause sudden stratospheric warming. On a time scale from month to season, thermal anomalies that are generated as a result of the imbalance of radiation cooling and heating, due to heat fluxes caused by wave dynamics, in the upper stratosphere, propagate downward, affecting the tropospheric circulation. This interaction demonstrates the manifestation of the mode of natural variability, Arctic Oscillations (AO) in the northern hemisphere.

As shown in (Vorobyeva and Volodin, 2018), the first empirical orthogonal function (EOF) of the intra-annual temperature evolution averaged along a circle of latitude in the 0–60 km layer according to a 500-year modeling of a preindustrial climate with the climate model of the Institute of Computational Mathematics (ICM) of the Russian Academy of Sciences, represents temperature anomalies that propagate down from the upper stratosphere during December to April, and a temperature anomaly is preceded meridional heat flow anomaly in a polar upper stratosphere in December.

The dynamic connection between sudden stratospheric warming (SSW) and blocking phenomena in the troposphere is largely associated with vertically propagating planetary waves (PW), which are known to cause SSW through the interaction of the mean flow with waves. In these processes, the role of PWs with zonal wave numbers 1 and 2 is dominant and is especially pronounced during blocking events in the troposphere. In this case, usually episodes of strong blocking over the North Atlantic precede SSW warming.

The paper (Vargin and Volodin, 2016) is devoted to reproducing dynamic processes in the stratosphere of extratropical latitudes, where using the global climate model of the ICM RAS with an upper limit of 0.2 hPa (60 km) for the period from 1979 to 2008 and reanalysis data, the authors analyze changes in temperature, zonal wind, planetary wave activity, heat fluxes in the lower stratosphere, as well as sudden stratospheric warming with the displacement and separation of the polar vortex and the distribution of circulation anomalies in the troposphere

Detailed analysis of the stratospheric-tropospheric dynamic interaction in 5 realizations of the 50-year calculation of the climate model of the ICM RAS, 5th version for the modern climate, presented in (Vargin et al., 2018), makes it possible to formulate a number of important conclusions about the disturbance of the stratospheric polar vortex and its effect on the troposphere, by pointing out the issue of most of the atmospheric general circulation models, which are the basis of climate models, namely a weaker response of the troposphere to disturbances of the stratospheric polar vortex in comparison with observational data.

Specific features of sudden stratospheric warming at the end of January 2017 were considered in (Vargin, 2018), where it was shown that this event led to a significant warming of the Arctic stratosphere, prevented a strong destruction of stratospheric ozone, slowing down the zonal circulation of the stratosphere, which did not recover until spring reconstruction, weakening of the stratospheric polar vortex and changing the phase of the Arctic oscillations from positive to negative with warming in the polar region and cooling in mid-high latitudes, as well as the spread of wave activity flows (due to reflection in the upper stratosphere) in the lower stratosphere and the troposphere over northern Canada. As a result, at the beginning of February 2017, in the upper troposphere, the spread of the wave packet to the east over the North Atlantic intensified, which led to the strengthening of the blocking anticyclone over northwestern Europe and a cooling to the southeast of it, and in the northeast of North America the area of reduced pressure has expanded, which led to a significant cooling and heavy rainfall.

Based on reanalyses, ground-based spectrometric and satellite observations, Vargin and Medvedeva (2015) analyze the change in the general circulation regimes in the stratosphere and troposphere associated with the phenomenon of sudden stratospheric warming in early January 2013. It was discovered, two weeks before the VSP, an increase in wave activity flows from the troposphere to the stratosphere over Eastern Siberia – China. It was shown that a week before the VSP, the wave packet propagating to the east in the upper troposphere could contribute to the strengthening of the anticyclone over the northeastern Atlantic, which during the VSP led to the the stratospheric polar vortex spliting into two parts.

Rossby waves, which propagate upwards from the troposphere, play an important role in the variability of the polar stratosphere. Stratospheric anomalies can, in turn, affect the weather and climate in the troposphere. The mechanism of this connection has received much attention in the last decade, but no consensus has been reached so far. During the weakening of the polar vortex, displacement from the pole (vortex displacement) or separation into two daughter vortex (vortex splitting) can occur, they are known to be mainly associated with

vertically propagating Rossby waves with wave numbers 1 and 2. The structure and evolution of the vortex during these events are also very different and can play an important role in understanding the dynamics of the general circulation in the stratosphere and troposphere.

Winter 2009–2010 in the Arctic stratosphere, as compared with other winter periods, as shown in (Vargin, 2015), is characterized by mainly sudden stratospheric warming (SSW) at the end of January, and this event leads to a significant increase in the temperature of the polar stratosphere and to the reversal of the zonal wind. The main results of (Vargin, 2015) are as follows: (1) unlike other major events of the SSW in recent winters, after the SSW in January 2010, the western stream and the polar vortex did not recover their states that were observed before the SSW until the spring adjustment, resulting in depletion the ozone layer inside the polar vortex throughout the winter has been relatively small over the past 20 years; (2) a distinctive feature of the winter of 2010 was the splitting of the stratospheric polar vortex in December, the splitting of the vortex was accompanied by an increase in temperature of the polar stratosphere and weakening of the westerly winds, splitting occurred when, in addition to the high pressure system over northeast Eurasia and the North Pacific, the tropospheric anticyclone Europe has intensified and spread to the lower stratosphere; (3) analysis of wave activity in the extratropical troposphere showed that two Rossby packets propagated east to the North Atlantic a few days before the vortex splitting, the first wave packet propagated from the subtropics and mid-latitudes of the eastern Pacific over North America, and the second from the northern parts of the Pacific Ocean and these wave flows contributed to the strengthening of the tropospheric anticyclone over Europe and the splitting of the polar stratospheric vortex.

This section focuses on the relationship between the dynamics of Rossby waves, wave breaking, wave activity fluxes and various types of circulation in the stratosphere and troposphere. The Rossby wave breaking (RWB) plays an important role in both horizontal and vertical transport and mixing. For example, in the horizontal direction, RWB makes a significant contribution to the flow of moisture into the Arctic. In the vertical direction, RWB changes the thermal stratification in the vicinity of the tropopause, which leads to an increase in the exchange of mass through the tropopause. The variability associated with RWB, the process of transport and mixing, significantly depends on the type of RWB. There are two fundamentally different types of RWB – anticyclonic wave breaking (AWB) and cyclonic wave breaking (CWB) (Thorncroft et al., 1993). In early September 2002, strong convection processes were observed in south-east Indonesia and south-east Africa. Under conditions of strong divergence of the flow in the upper troposphere, two Rossby wave trains

(RWT) were generated, which spread to the southeast against the background mean flow.

Peters and Vargin (2002) suggested that these wave trains cause an increase in the wave activity of the planetary waves in the upper troposphere / lower stratosphere over Antarctica. Such a change in the structure of planetary waves was diagnosed in September 2002, before the first sudden large warming in the stratosphere occurred in the southern hemisphere. To test the hypothesis, a simplified version of the ECHAM4 model was used. Sensitivity experiments were performed for an average background flux, similar to September 2002, using a Rossby wave generator in the subtropical upper troposphere at two different locations that correspond to the observed regions of flow divergence. As a result, after about 2 weeks of integrating the model using a wave generator, two wave trains (RWT) with propagation to the southeast were discovered, causing an increase in the planetary wave 2 in the upper troposphere and the lower / middle stratosphere. The wave activity flux to the pole turned out to be larger compared with the control run without the use of a wave generator. The simulation results showed that the convergence of the Eliassen-Palm flux causes a slowdown of the mean zonal flow in the stratosphere, but does not change the direction of the wind. Experiments on sensitivity confirm the reliability of these results. The results of the model confirm the hypothesis that the increased activity of planetary waves in the Australian polar region in 2002 is caused by an increase in the subtropical forcing of two RWTs.

Using the winter (November – March) ERA-Interim reanalysis data for geopotential in the troposphere and stratosphere from 1979 to 2016, Guryanov et al. (2018) analyzed wave perturbation spectra with zonal numbers $1 \leq k \leq 10$. At the same time, the contribution of waves propagating to the east (E) and to the west (W), as well as stationary waves (S), was selected. In the troposphere and stratosphere of the tropics, as well as in the upper stratosphere of the entire Northern Hemisphere, an intensification of wave activity was revealed. It turned out that in the tropics and subtropics this is associated with all types of waves (E, W, S), whereas in middle and high latitudes, mainly with stationary waves and waves propagating to the east. In the region of the subtropical tropopause, a general increase in the energy of stationary waves in recent decades has been revealed. In addition, in the troposphere of the tropics and subtropics and in the subtropical lower stratosphere, the energy of waves propagating to the east in the years of El Niño can be one and a half to two times more than in the years of La Nina. The averaged over the spectrum of the zonal wave number for all types of waves (E, W, S) is maximum in the upper troposphere of subtropics. At the same time, the averaged over the spectrum zonal wave number for W and S waves is associated with the Atlantic index between decadal oscillations and changes by 15% in 1979–2016.(on the interdecadal time scale).

The wave-period averaged over the spectrum in the stratosphere is longer than in the troposphere. It is maximal in the middle stratosphere of extratropical latitudes. The relationship between the periods averaged over the spectrum of waves and the activity of sudden stratospheric warmings (SSW) is noted. The sign of this connection depends on the geographic latitude, atmospheric layer and zonal wave number.

A review of the papers dealing with various aspects of stratosphere-troposphere exchange (STE) is presented in Ivanova (2016). The development of STE concepts is described and quantitative estimates of STE obtained by different authors are given. Typical time scales and geographic features of STE are described. Special attention is given to the specific features of STE at extratropical latitudes where active vertical air transport is observed in both directions. The air ascent through the tropopause occurs in the zones of warm conveyor belts, and the air descent takes place in the zones of stratospheric intrusions. Exchange processes in the key region including the upper troposphere and the lowermost stratosphere are described. The mechanisms of large-scale stratospheric intrusions in the systems of tropopause folds or cut-off lows are presented as well as the mechanisms of the mixing of the stratospheric air with the tropospheric one. Specific features of deep stratospheric intrusions are discussed which are based on the analysis of such indicators of stratospheric air as high concentrations of ozone and stratospheric radionuclide 7Be. Some aspects of stratosphere-troposphere energy exchange are considered.

In the northern hemisphere, the stratospheric polar vortex in winter has significant interannual and intraseasonal variability, but, as observations show, this variability increases after large volcanic eruptions (Kodera, 1995; Labitzke and McCormick, 1992). From theoretical considerations it is clear that heating in the lower stratosphere, due to the absorption of radiation by volcanic sulfate aerosols, increases the temperature gradient from the equator to the pole, which, as follows from the equation of thermal wind, leads to strong westerlies. Satellite observations do show warming of the tropical lower stratosphere after volcanic eruptions; therefore, changes in the meridional temperature gradients and zonal flows are physically plausible. The extent to which secondary feedback mechanisms, such as changes in the thickness of the ozone layer or planetary waves propagating upward, affect the intensity of the polar vortex remains uncertain and is the subject of further research.

For example, Zuev et al. (2017), based on reanalysis of ERA-Interim data, studied the effect of heating in the lower tropical stratosphere, due to aerosol from the eruption of the volcano Mt. Merapi in November 2010, on the intensity of the polar vortex in the period February – March 2011. The analysis and assessment of the correlation between volcanic eruptions in the autumn-winter

period and changes in the ozone layer in the Arctic in the next winter-autumn period was also carried out.

Mathematical problems of climate and ecology

Earth system models are complex and represent a large number of processes, resulting in a persistent spread across climate projections for a given future scenario. Owing to different model performances against observations and the lack of independence between models, there is now evidence that giving equal weight to each available model projection is nonoptimal. This Perspective discusses newly developed tools that facilitate a more rapid and comprehensive evaluation of model simulations against observations, process-based emergent constraints that are a promising way to focus evaluation on the observations most relevant to climate projections, and advanced methods for model weighting. These approaches are needed to distil the most credible information on regional climate changes, impacts, and risks for stakeholders and policy-

Volodin et al. (2017) present the fifth generation of the INMCM climate model that is being developed at the Institute of Numerical Mathematics of the Russian Academy of Sciences (INMCM5). The most important changes with respect to the previous version (INMCM4) were made in the atmospheric component of the model. Its vertical resolution was increased to resolve the upper stratosphere and the lower mesosphere. A more sophisticated parameterization of condensation and cloudiness formation was introduced as well. An aerosol module was incorporated into the model. The upgraded oceanic component has a modified dynamical core optimized for better implementation on parallel computers and has two times higher resolution in both horizontal directions. Analysis of the present-day climatology of the INMCM5 (based on the data of historical run for 1979–2005) shows moderate improvements in reproduction of basic circulation characteristics with respect to the previous version. Biases in the near-surface temperature and precipitation are slightly reduced compared with INMCM4 as well as biases in oceanic temperature, salinity and sea surface height. The most notable improvement over INMCM4 is the capability of the new model to reproduce the equatorial stratospheric quasi-biannual oscillation and statistics of sudden stratospheric warmings.

Climate changes observed in 1850–2014 are modeled and analyzed on the basis of seven historical runs with the climate model INM-CM5 under the scenario proposed for the Coupled Model Intercomparison Project Phase 6 (CMIP6) in the article (Volodin and Gritsun, 2018). In all runs global mean surface temperature rises by 0.8K at the end of the experiment (2014) in agreement with the observations. Periods of fast warming in 1920–1940 and 1980–2000 as well as its slowdown in 1950–1975 and 2000–2014 are correctly

reproduced by the ensemble mean. The notable change here with respect to the CMIP5 results is the correct reproduction of the slowdown in global warming in 2000–2014 that we attribute to a change in ocean heat uptake and a more accurate description of the total solar irradiance in the CMIP6 protocol. The model is able to reproduce the correct behavior of global mean temperature in 1980–2014 despite incorrect phases of the Atlantic Multidecadal Oscillation and Pacific Decadal Oscillation indices in the majority of experiments. The Arctic sea ice loss in recent decades is reasonably close to the observations in just one model run; the model underestimates Arctic sea ice loss by a factor of 2.5. The spatial pattern of the model mean surface temperature trend during the last 30 years looks close to the one for the ERA-Interim reanalysis. The model correctly estimates the magnitude of stratospheric cooling.

Thirty models in phase 5 of the Coupled Model Intercomparison Project (CMIP5) are evaluated for their performances in reproducing two summertime atmospheric circulation patterns in the Arctic: the Arctic Oscillation (AO) and Arctic dipole (AD) (Cai et al., 2018). The reference AO and AD are extracted from the ERA-Interim dataset (1979–2016). Model evaluation is conducted during the historical period (1901–2005). Models are ranked by a combined metrics approach based on two pattern correlation coefficients (PCCs) and two explained variances for the AO and AD, respectively. In the projected period (2006–2100), most models produce a positive trend for the AO index and a negative trend for the AD index in summer. The models ranked higher based on the combined metrics ranking show greater consistency and smaller values in the magnitudes of trends of AO and AD than the lower-ranked ones. The projected trends in the AO and AD contribute to a slight increase, if not a decrease, of the air temperature and an acceleration of precipitation increase in the twenty-first century over Arctic Alaska, which is the reverse of over the Barents and Kara Seas. Changes in the AO and AD are relatively minor contributing factors to the projected temperature and precipitation changes in the Arctic, among which the changes in the AD play a bigger role than those in the AO. The summer AO and AD have a stronger impact on the spatial asymmetry of the precipitation field than on the air temperature field.

As noted in the article (Christopher et al., 2018), strong winter warming has dominated recent patterns of climate change along the Arctic Coastal Plain (ACP) of northern Alaska. The full impact of arctic winters may be best manifest by freshwater ice growth and the extent to which abundant shallow ACP lakes freeze solid with bedfast ice by the end of winter. For example, winter conditions of 2016–17 produced record low extents of bedfast ice across the ACP. In addition to high air temperatures, the causes varied from deep snow accumulation on the Barrow Peninsula to high late season rainfall and lake lev-

els farther east on the ACP. In contrast, the previous winter of 2015–16 was also warm, but low snowpack and high winds caused relatively thick lake ice to develop and corresponding high extents of bedfast ice on the ACP. This recent comparison of extreme variation in lake ice responses between two adjacent regions and years in the context of long-term climate and ice records highlights the complexity associated with weather conditions and climate change in the Arctic. Recent observations of maximum ice thickness (MIT) compared to simulated MIT from Weather Research and Forcing (Polar-WRF) model output show greater departure toward thinner ice than predicted by models, underscoring this uncertainty and the need for sustained observations. Lake ice thickness and the extent of bedfast ice not only indicate the impact of arctic winters, but also directly affect sublake permafrost, winter water supply for industry, and overwinter habitat availability. Therefore, tracking freshwater ice responses provides a comprehensive picture of winter, as well as summer, weather conditions and climate change with implications to broader landscape, ecosystem, and resource responses in the Arctic. In this study, authors focus on observations from the two recent winters on the ACP to demonstrate the complex responses among lakes, freshwater ice, and permafrost to winter climate.

New intermediate complexity model (PlaSim-ESM-ICMMG-v.1.0) constructed by coupling the Planet Simulator with ocean and sea-ice models is describe in article (Platov et al., 2017). The results are demonstrated of climate simulation using PlaSim-ICMMG-v.1.0 considering global fields of surface air temperature, precipitation, sea surface temperature, and ocean circulation, and make comparisons with the results obtained using the original PlaSim version. PlaSim-ICMMG-v.1.0 reproduces the main features of the climate system reasonably well and demonstrates that it is useful for climate system modeling. Due to the rapid warming in the Arctic, there are major challenges associated with the mechanisms that regulate the dynamics of weather in the mid-latitudes. The new earth's system model of intermediate complexity PlaSim-ICMMG-v.1.0 can be used to deal with these challenges.

The set of equations for representing the atmosphere's large-scale general circulation in an Earth system model of intermediate complexity (EMIC) are presented and validated in the article (Totz et al., 2018). These dynamical equations have been implemented in Aeolus 1.0, which is a statistical–dynamical atmosphere model (SDAM) and includes radiative transfer and cloud modules. The statistical dynamical approach is computationally efficient and thus enables us to perform climate simulations at multimillennia timescales, which is a prime aim of our model development. Further, this computational efficiency enables us to scan large and high-dimensional parameter space to tune the model parameters, e.g., for sensitivity studies. Here are presented novel equa-

tions for the large-scale zonal mean wind as well as those for planetary waves. Together with synoptic parameterization (as presented by Coumou et al., 2011), these form the mathematical description of the dynamical core of Aeolus 1.0. We optimize the dynamical core parameter values by tuning all relevant dynamical fields to ERA-Interim reanalysis data (1983–2009) forcing the dynamical core with prescribed surface temperature, surface humidity and cumulus cloud fraction. We test the model's performance in reproducing the seasonal cycle and the influence of the El Niño–Southern Oscillation (ENSO). Simulated annealing optimization algorithm, which approximates the global minimum of a high-dimensional function was used. With non-tuned parameter values, the model performs reasonably in terms of its representation of zonal-mean circulation, planetary waves and storm tracks. The simulated annealing optimization improves in particular the model's representation of the Northern Hemisphere jet stream and storm tracks as well as the Hadley circulation. The regions of high azonal wind velocities (planetary waves) are accurately captured for all validation experiments. The zonal-mean zonal wind and the integrated lower troposphere mass flux show good results in particular in the Northern Hemisphere. In the Southern Hemisphere, the model tends to produce too-weak zonal-mean zonal winds and a too-narrow Hadley circulation. We discuss possible reasons for these model biases as well as planned future model improvements and applications.

Krupchatnikov et al. (2018) discuss some aspects of interaction between atmospheric dynamics processes in the Arctic and the mid-latitudes under conditions of global climate change and rapid warming in the Arctic in the lower layer of the troposphere (due to a mechanism of positive feedbacks, enhancement of atmospheric heat and moisture fluxes to the Arctic and heat transfer by currents in the ocean). This is a difficult task, given the fact that the observation of this phenomenon is relatively short. One of the plausible physical hypotheses of the effect of warming in the Arctic on the dynamics of the atmosphere in the mid- and high latitudes is that the reduction of sea ice and snow cover anomalies caused by this warming can lead to changes in the frequency and intensity of the extreme weather events and largescale circulation in the mid-latitudes and in the Arctic region. Polar cyclones, stratospheric vortex, jet streams, North Atlantic oscillations – these objects of atmospheric dynamics are the subject of discussion in this article. The paper also presents the results of a study of the sensitivity of the Arctic Ocean and the sea ice to variability of atmospheric circulation, taking into account the dynamics of the NAO/AO. Special attention is paid to the circulation over the Norwegian and Greenland Seas, which are the area of formation of the initial trajectory of distribution of Atlantic waters in the Arctic Ocean.

The study by (Martynova and Krupchatnikov, 2018) was performed using JSBACH land surface model with atmospheric conditions obtained from INMCM4 modelling results. Vegetation plays a key role in the global climate system via modification of the water and energy balance. Response of different vegetation types to present and projected climatic conditions was assessed for Siberia. A climate change was determined according to the RCP 8.5 scenario. A geographical redistribution of extratropical forest and grass vegetation and weakening of a canopy ability to absorb carbon dioxide from the atmosphere were obtained for climate warming conditions for Siberia. It was established that Eastern Siberia is more sensitive to climate forcing than Western Siberia.

In (Borovko and Krupchatnikov, 2015) responses of the general circulation of the atmosphere to climate changes are simulated with a spectral model. It is shown that as the meridional temperature gradient decreases the Hadley circulation weakens and its boundaries move to the poles. The troposphere height dynamics versus the equilibrium temperature of atmospheric radiation is investigated. A relation between the characteristics determining the baroclinic instability in the atmosphere is obtained. In the lower troposphere, the stratification is determined by radiation-convective processes and baroclinic turbulence. The level at which the thermal stratification regimes change is $\sigma \approx 550$ mbar. Experimental results show that changes in the slope of the isentropic surfaces in the lower troposphere when the stratospheric polar vortex is amplified in the stratosphere are consistent with theoretical estimates.

The results of the study of the connection between abnormally cold weather patterns in winter in Russia at the beginning of the XXI with changes in the sea-ice area in the Arctic are presented in (Semenov and Latif, 2015). The early 21st century was marked by several severe winters over Central Eurasia linked to a blocking anti-cyclone centered south of the Barents Sea. Severe winters in Central Eurasia were frequent in the 1960s when Arctic sea ice cover was anomalously large, and rare in the 1990s featuring considerably less sea ice cover; the 1960s being characterized by a low, the 1990s by a high phase of the North Atlantic Oscillation, the major driver of surface climate variability in Central Eurasia.Weperformed ensemble simulations with an atmospheric general circulation model using a set of multi-year Arctic sea ice climatologies corresponding to different periods during 1966–2012. The atmospheric response to the strongly reduced sea ice cover of 2005–2012 exhibits a statistically significant anti-cyclonic surface pressure anomaly which is similar to that observed. A similar response is found when the strongly positive sea ice cover anomaly of 1966–1969 drives the model. Basically no significant atmospheric circulation response was simulated when the model was forced by the sea ice cover anomaly of 1990–1995. The results suggest that sea ice cover reduction, through a changed atmospheric circulation, considerably contributed to the re-

cent anomalously cold winters in Central Eurasia. Further, a nonlinear atmospheric circulation response to shrinking sea ice cover is suggested that depends on the background sea ice cover.

There were several anomalously cold winter weather regimes in Russia in the early 21st century. These regimes were usually associated with a blocking anticyclone south of the Barents Sea. Numerical simulations with an atmospheric general circulation model (AGCM) using prescribed sea ice concentration (SIC) data for different periods during the last 50 years showed that a rapid sea ice area decline in the Barents Sea in the last decade could bring about the formation of such a blocking anticyclone and cooling over northern Eurasia (Semenov, 2016). The SIC reduction in the former period, from the second half of the 1960s to the first half of the 1990s, results in a weaker response of opposite sign. This suggests a nonlinear atmospheric circulation response to the SIC reduction in the Barents Sea, which has been previously found in the idealized AGCM simulations. An impact of the Barents Sea SIC reduction on the North Atlantic Oscillation (NAO), in particular, on the formation of the anomalously low NAO index, is found. The results indicate an important role that the Barents Sea, a region with the largest variability of the ocean–atmosphere heat exchange in the Arctic in wintertime, plays in generating anomalous weather regimes in Russia.

Possible mechanisms of formation for some significant regional weather and climate anomalies in Russia in the recent years and their link to global climate change and natural quasi-cyclic processes are discussed in (Mokhov and Semenov, 2016). Specifically, extreme Russian heat wave in 2010, Amur flood in 2013 and anomalously cold winters in the recent years are analyzed. All these phenomena are related to formation of long-living blocking anticyclones that are expected in general to be more frequent under global warming. When linking weather and climate extremes to global warming, the effects related to regional and global natural quasi-cyclic processes should be taken into account. They include Atlantic Multidecadal Oscillation, Pacific Decadal Oscillation and El Niño/Southern Oscillation.

Based on observational data on daily mean surface air temperature (SAT) and sea ice concentration (SIC) in the Barents Sea (BS), the characteristics of strong positive and negative winter SAT anomalies in Moscow have been studied by Shukurov and Semenov (2018) in comparison with BS SIC data obtained in 1949–2016. An analysis of surface backward trajectories of air-particle motions has revealed the most probable paths of both cold and warm air invasions into Moscow and located regions that mostly affect strong winter SAT anomalies in Moscow. Atmospheric circulation anomalies that cause strong winter SAT anomalies in Moscow have been revealed. Changes in the

ways of both cold and warm air invasions have been found, as well as an increase in the frequency of blocking anticyclones in 2005–2016 when compared to 1970–1999. The results suggest that a winter SIC decrease in the BS in 2005–2016 affects strong winter SAT anomalies in Moscow due to an increase in the frequency of occurrence of blocking anticyclones to the south of and over the BS.

The influence of the Atlantic Multidecadal Oscillation (AMO) on large-scale atmospheric circulation in the Atlantic region in summer for the period of 1950–2015 is investigated in (Semenov and Cherenkova, 2018). It is shown that the intensification of the summer North Atlantic Oscillation (NAO) with significant changes in sea level pressure anomalies in the main centers of action (over Greenland and the British Isles) occurred while the North Atlantic was cooler. Sea surface temperature anomalies, which are linked to the AMO in the summer season, affect both the NAO index and fluctuations of the centers of action in the Eastern Atlantic/Western Russia (EAWR). The positive (negative) phase of the AMO is characterized by a combination of negative (positive) values of the NAO and EAWR indices. The dominance of the opposite phases of the teleconnection indices in the summer during the warm North Atlantic and in its colder period resulted in differences in the regional climate in Europe.

In the last decades, poleward displacements of elements of the general atmospheric circulation such as the Hadley Cell and storm tracks have been observed. On the basis of results of the numerical modeling of climate dynamics using an idealized model of the climatic system, Martynova and Krupchatnikov (2015) showed that the tendency to the displacement of storm tracks to the poles in the Northern Hemisphere would continue under the conditions of climate warming (according to the RCP 8.5 scenario). The activity of storm tracks and their spatial distribution is not fully restored with the returning climate to the pre-industrial regime. The same can be said about the distribution of heat and moisture fluxes. Study also shows that the tropics are compressed during the period of the warm ENSO phase, causing an offset to the equator of the jet stream, storm tracks, the divergence of the eddy momentum flux and the boundary of the Headley Cell. The calculations performed give an ambiguous picture of the distribution over latitudes of the magnitude of the change in the eddy length scale. Sustained growth of the characteristic wavelength exists only at midlatitudes north of latitude 50°. An increase in the scale of the vortex length is expected to have important consequences. For example, the position of critical latitudes and the associated vortex dissipation depends on the scale of the wavelength; therefore, it can be assumed that this increase will contribute to the jet flow to the pole in middle latitudes. In addition, since longer waves are more able to propagate into the stratosphere, they can lead to increased Bruwer–Dobson circulation.

It has been hypothesised that the Arctic amplification of temperature changes causes a decrease in the northward temperature gradient in the troposphere, thereby enhancing the oscillation of planetary waves leading to extreme weather in mid-latitudes. To test this hypothesis, the response of the atmosphere to Arctic amplification for a projected summer sea-ice-free period using an atmospheric model with prescribed surface boundary conditions from a state-of-the-art Earth system model was studied in the article (Meleshko et al., 2016). Besides a standard global warming simulation, also was conducted a sensitivity experiment with sea ice and sea surface temperature anomalies in the Arctic. There was shown that when global climate warms, enhancement of the northward heat transport provides the major contribution to decrease the northward temperature gradient in the polar troposphere in cold seasons, causing more oscillation of the planetary waves. However, while Arctic amplification significantly enhances near-surface air temperature in the polar region, it is not large enough to invoke an increased oscillation of the planetary waves.

In Kattsov et al. (2017) the problem is stated of quantification of the 21st century climate change projections across Russia detailed in the physical and probability spaces. The obtained projections are to be used for the quantitative description of future climate impacts on the sectors of the Russian economy and, in the end, for developing the federal, sector, and regional plans of adaptation to climate changes. The formulated problem is solved by massive (50 members) ensemble simulations using the high-resolution (the horizontal resolution is 25 km) system of climate models developed in the Voeikov Main Geophysical Observatory.

Studies dealing with impact of the Arctic warming and related sea ice decline on the Northern Hemisphere atmospheric circulation are considered in Meleshko et al. (2018). The causes of occurrence of extremely cold winters over the mid-latitude continents observed in the recent decades against the warming background are discussed. Several conceptions are outlined which explain potential reasons for occurrence of this phenomenon. The paper discusses impacts of the Arctic sea ice loss on the large-scale atmospheric circulation, oscillations of planetary waves. It also discusses issues related to sea ice changes in the Barents and Kara seas and their link to the frequency of extremely cold winters observed in Eurasia and North America, the contribution of internal atmospheric variability to the increasing frequency of cold weather, and the role of the Atlantic Multidecadal Oscillation in the Arctic sea ice reduction.

The abilities of an ensemble of present-day global climate models are analyzed in article (Sporyshev et al., 2018) in the course of modeling of evolution of the Arctic surface temperature over land including spatial consistency between the modeled and observed data. These results are the basis for probabilis-

tic regional prediction of variation in the surface air temperature for the near future (2021–2040).

Polonskii and Kibal'chich (2015) analyzed is the impact that basic spatio-temporal modes in the ocean-atmosphere system of the Northern Hemisphere characterizing interannual variability, produce on the anomalies of surface air temperature in Eastern Europe and the Black Sea countries in winter. It is demonstrated from the data of NCEP reanalysis and standard meteorological observations for 1950–2012 using the composite method that the maximum influence on the anomalies of monthly mean air temperature is exerted by the North Atlantic Oscillation in the northwestern part of the region and by the Scandinavian pattern in its eastern part. Typical anomalies of monthly mean air temperature caused by these modes reach 4–5°C. The effects of East Atlantic and East Atlantic-West Russia patterns prevail in the Black Sea region. Regional monthly mean air temperature anomalies caused by them reach 2–2.5°C. The positive phases of the North Atlantic Oscillation and East Atlantic pattern that describe the intensity of zonal atmospheric circulation are accompanied by the positive anomalies of surface air temperature in the most part of Eastern Europe. The positive phases of the Scandinavian and East Atlantic-West Russia patterns associated with the anticyclonic blocking are accompanied by negative anomalies. Extreme negative anomalies of temperature in January and February are registered most frequently if the negative phase of the East Atlantic pattern coincides with the positive phase of the Scandinavian pattern, and extremely high positive anomalies, at the combination of the positive phase of the East Atlantic pattern and the negative phase of the Scandinavian pattern.

The statistical significance of Global Atmospheric Oscillation (GAO), whose main element is the well-known El Niño–Southern Oscillation in the equatorial Pacific, was assessed from monthly mean atmospheric pressure data at sea level at the nodes of a regular 5×5° grid covering the entire surface of the Earth in the article (Byshev et al., 2016). The data were collected in 1920–2012. It was found that statistically reliable GAO signals cover almost the entire tropical zone and they also appear at mid- and high latitudes of both hemispheres.

Advances in the theory of nonlinear dynamical systems, deterministic or stochastic, as well as advances in the theory of nonlinear partial differential equations, have a profound effect on the modeling and understanding of the dynamics of the atmosphere and the ocean. In the mathematical theory of climate, the idea of simulating fast chaotic atmospheric dynamics using random processes and, therefore, reducing the effective dimension of the entire system goes back to Hasselman (1976), Leith (1975), and Dymnikov (1996).

For E. Lorenz's stochastic system with the right-hand side perturbed by white noise in the article (Klevtsova, 2015) sufficient conditions on the parame-

ters and the right-hand side are obtained for existence of a unique stationary measure. A nonlinear system of partial differential equations of the two-layer quasi-solenoidal Lorentz model of the baroclinic atmosphere on a rotating two-dimensional sphere is considered. The right-hand side of the system is perturbed by white noise. In the article (Klevtsova, 2017) a unique stationary measure for the Markov semigroup defined by the solutions of the Cauchy problem for two-layer quasi-solenoidal Lorenz model of a baroclinic atmosphere on a rotating two-dimensional sphere is considered. The right-hand side of the system is perturbed by white noise. An estimate for the rate of convergence of the distributions of all solutions for a certain class of this system to the unique stationary measure is proposed. A similar result is obtained for the equation of a barotropic atmosphere and the two-dimensional Navier−Stokes (NS) equation. A comparative analysis with some of the available related results is given for the N-S equation.

A virtual research environment aimed at analysis of climate change and its impact on Northern Eurasia based on climatic data archives and dedicated analytics embedded in the web-GIS called “Climate” is presented in Gordov et al. (2018). An extended set of analytical procedures related to the analysis of climatic and meteorological extremes are described. An updated web portal structure is described to facilitate the system use by the general public, regional stakeholders, and decision makers and get the required information without using a tedious registration procedure.

Concluding remarks

In this report, we overviewed the articles belonging to the field of dynamical meteorology, or closely related to it, which are authored or co-authored by Russian scientists and have been published in 2015–2018 in peer-reviewed journals indexed in WoS and/or Scopus databases. The review would not have been possible without participation and support of a large number of Russian scientists, to whom all we are sincerely grateful.

References

1. Akperov M.G., Dembitskaya M.A., Mokhov I.I. Cyclone activity in the Arctic from reanalyses data and regional climate model simulations. Izvestiya Akademii Nauk, Ser. Geograficheskaya. 2017a. No. 6. P. 39–46.

2. Akperov M.G., Mokhov I.I., Dembitskaya M.A. Arctic mesocyclones from satellite data, reanalyses data and model simulations. Sovremennye problemy distantsionnogo zondirovaniya Zemli iz kosmosa. 2017b. V. 14. No. 3. P. 297–304.

3. Akperov M., Mokhov I.I., Dembitskaya M.A., Parfenova M.R. Tropospheric lapse rate and its changes in the Arctic from reanalysis data. Proceedings of SPIE. 2018. Vol. 10833, 108337E.

4. Akperov M., Mokhov I., Rinke A., Dethloff K., Matthes H. Cyclones and their possible changes in the Arctic by the end of the twenty first century from regional climate model simulations. Theor. Appl. Climatol. 2015. Vol. 122. P. 85–96.

5. Akperov M. et al. Cyclone activity in the Arctic from an ensemble of regional climate models (Arctic CORDEX). J. Geophys. Res.: Atmos. 2018. V. 123, No. 5. P. 2537–2554.

6. Barskov K.V., Chernyshev R.V., Stepanenko V.M., Repina I.A., Artamonov A.Y., Guseva S.P., and Gavrikov A.V. Experimental study of heat and momentum exchange between a forest lake and the atmosphere in winter. IOP Conference Series: Earth and Environmental Science. 2017. Vol. 96, No. 1. P. 012003.

7. Barskov K.V., Glazunov A.V., Repina I.A. et al. On the applicability of similarity theory for the stable atmospheric boundary layer over complex terrain. Izvestiya, Atmospheric and Oceanic Physics. 2018. Vol. 54, No. 5. P. 462–471.

8. Bart A.A., Starchenko A.V. Using weather prediction data for simulation of mesoscale atmospheric processes. Proceedings of SPIE. 2015. V. 9680. P. 1–6.

9. Bedritskii A.I., Vil'fand R.M., Kiktev D.B., Rivin G.S. Roshydromet supercomputer technologies for numerical weather prediction. Russ. Meteorol. Hydrol. 2017. V. 42. No. 7. P. 425–434.

10. Borovko I.V., Krupchatnikov V.N. Responces of the Hadley cell and extratropical troposphere stratification to climate changes simulated with a relatively simple general circulation model. Numerical Analysis and Application. 2015. Vol.8, No. 1. P. 23–34.

11. Byshev V.I., Neiman V.G., Romsamov Yu. A., Serykh I.V., Sonechkin D.M. Statistical ignificance and climatic role of the Global Atmospheric Oscillation. Oceanology. 2016. Vol. 56, No. 2, pp. 165–171.

12. Cai L., Alexeev V.A., Walsh J.E., Bhatt U.S. Patterns, impacts, and future projections of summer variability in the Arctic from CMIP5 models. J. Clim. 2018. V. 31. P. 9815–9831.

13. Chechin D.G, Lüpkes C. Boundary-layer development and low-level baroclinicity during high-latitude cold-air outbreaks: A simple model. Boundary-Layer Meteorol. 2017. V. 162. P. 91–116.

14. Chechin D.G., Zabolotskikh E.V., Repina I.A., Shapron B. Influence of baroclinicity in the atmospheric boundary layer and Ekman friction on the surface wind speed during cold-air outbreaks in the Arctic. Izvestiya, Atmos. Oceanic Phys. 2015. V. 51, No. 2. P. 127–137.

15. Chernokulsky A., Akperov M., Podnebesnykh N.V., Mokhov I.I., Objectively and manually identified characteristics of mid-latitude storms: a comparison for Siberian region, Proceedings of SPIE. 2018. V. 10833, 108337D.

16. Chernokulsky A.V., Kurgansky M.V., Mokhov I.I. Analysis of changes in tornadogenesis conditions over Northern Eurasia based on a simple index of atmospheric convective instability. Doklady Earth Sci. 2017. V. 477. Part 2. P. 1504–1509.

17. Chernokulsky A.V., Kurgansky M.V., Zakharchenko D.I., Mokhov I.I. Genesis environments and characteristics of the severe tornado in the South Urals on August 29, 2014. Russ. Meteorol. Hydrol. 2015. V. 40. No. 12. P. 794–799.

18. Chernokulsky A.V., Shikhov A.N. 1984 Ivanovo tornado outbreak: determination of actual tornado tracks with satellite data. Atmospheric Research. 2018, V. 207, P.111–121. DOI: 10.1016/j.atmosres.2018.02.011.

19. Chkhetiani O.G., Kurgansky M.V., Vazaeva N.V. Turbulent helicity in the atmospheric boundary layer. Boundary-Layer Meteorology. 2018. V. 168. No. 3. P. 361–385. DOI: 10.1007/s10546-018-0356-4.

20. Christopher D.A, Benjamin M.J., Engram M., Alexeev V.A., Cai L., Parsekian A., Hinkel K., Bondurant A.C., Creighton A. Contrasting lake ice responses to winter climate indicate future variability and trends on the Alaskan Arctic Coastal Plain. IOP Publishing, Environ. Res. Lett. 2018. V. 13. P. 125001.

21. Druzhinin O.A., Troitskaya Yu.I., Zilitinkevich S.S. Stably stratified airflow over a waved water surface. Part 1: Stationary turbulence regime. First published: 25 September 2015a. DOI: 10.1002/qj.2677.

22. Druzhinin O.A., Troitskaya Yu.I., Zilitinkevich S.S. Stably stratified air-flow over a waved water surface. Part 2: Wave-induced pre-turbulent motions. First published: 25 September 2015b. DOI: 10.1002/qj.2678.

23. Druzhinin O.A., Troitskaya Yu.I., Zilitinkevich S.S. The study of momentum, mass, and heat transfer in a droplet-laden turbulent airflow over a waved water surface by direct numerical simulation. J. Geophys. Res.: Oceans. First published on 06 November 2018. DOI: 10.1029/2018JC014346.

24. Dust Devils. Space Science Series of ISSI. Eds.: Reiss D., Lorenz R., Balme M., Neakease L., Rossi A.P., Spiha A., Zarneski J. Springer, 2017, 426 pp.

25. Dymnikov V.P. Dynamics of the two-dimensional ideal incompressible fluid and Casimirs. Izvestiya, Atmos. Oceanic Phys. 2016, V. 52, No. 4, P. 348–352.

26. Dymnikov V.P., Perezhogin P.A. Systems of hydrodynamic type that approximate two-dimensional ideal fluid equations. Izvestiya, Atmos. Oceanic Phys. 2018, V. 54, No. 3, P. 232–241.

27. Dynamics of Wave and Exchange Processes in the Atmosphere. Eds.: Chkhetiani O.G., Gorbunov M.E., Kulichkov S.N., Repina I.A. Moscow: GEOS, 2017. 508 p. (in Russian)

28. Efimov V.V. Numerical simulation of breeze circulation over the Crimean peninsula. Izvestiya, Atmospheric and Oceanic Physics. 2017. V. 53. No. 1. P. 84–94.

29. Efimov V.V., Komarovskaya O.I. Numerical simulation of the Novaya Zemlya bora. Russ. Meteorol. Hydrol. 2018. V. 43. No. 1. P. 22–28.

30. Efimov V.V., Komarovskaya O.I. Seasonal variability and hydrodynamic regimes of the Novaya Zemlya bora. Izvestiya, Atmos. Oceanic Phys. 2018. V. 54. No. 6. P. 581–593.

31. Efimov V.V., Mikhaylova N.V. The mesoscale atmospheric vortex as a manifestation of the Novorossiysk bora. Izvestiya, Atmos. Oceanic Phys. 2017. V. 53. No. 4. P. 449–458.

32. Ermakov D.M. Investigation of the features of long-term global atmospheric circulation via satellite radiothermovision. Progress In Electromagnetics Research Symposium. Spring (PIERS). 2017. P. 413–418. DOI: 10.1109/PIERS.2017.8261775.

33. Ermakov D.M., Sharkov E.A., Chernushich A.P. Satellite radiothermovision of atmospheric mesoscale processes: case study of tropical cyclones. The International Archives of the Photogrammetry, Remote Sensing and Spatial Information Sciences.

ISPRS Archives. 2015. Vol. XL. No. 7/W3. P. 179–186. DOI: 10.5194/isprsarchives-XL-7-W3-179-2015.

34. Ermakov D.M., Sharkov E.A., Chernushich A.P. Satellite radiothermovision on synoptic and climatically significant scales. Izvestiya, Atmos. Oceanic Phys. 2017. V. 53. No. 9. P. 973–978.

35. Esau I., Tolstykh M., Fadeev R., Shashkin V., Makhnorylova S., Miles V., Melnikov V. Systematic errors in northern Eurasian short-term weather forecasts induced by atmospheric boundary layer thickness. Environ. Res. Lett. 2018. Vol. 13. No. 12. P. 125009.

36. Fomin V.V, Diansky N.A. Calculation of extreme surge in the Taganrog Bay using atmospheric and ocean circulation models of different spatial resolution. Russ. Meteorol. Hydrol. 2018. V. 43, No. 12, P. 843–851.

37. Glazunov A., Rannik Ü., Stepanenko V., Lykosov V., Auvinen M., Vesala T., Mammarella I. Large-eddy simulation and stochastic modeling of Lagrangian particles for footprint determination in the stable boundary layer. Geoscientific Model Development. 2016. V. 9, No. 9. P. 2925–2949.

38. Glazunov A.V., Stepanenko V.M. Large eddy simulation of stratified turbulent flows over heterogeneous landscapes. Izvestiya, Atmos. Oceanic Phys. 2015. V. 51, No. 4. P. 351–361.

39. Gorbatenko V.P., Nechepurenko O.E., Krechetova S.Y., Belikova M.Y. The comparison of atmospheric instability indices retrieved from the data of radio sounding and Modis spectroradiometer on thunderstorm days over West Siberia. Russ. Meteorol. Hydrol. 2015. V. 40. No. 5. P. 289–295.

40. Gorbatenko V.P.; Zolotukhina O.I., Gromnitskaya A. Thermodynamic conditions of hazardous convective phenomena at the Vostochny Cosmodrome. Tomsk State University J. 2015. V. 400. P. 330–336.

41. Gordov E.P., Okladnikov I.G., Riazanova A.A., Titov A.G., Gordova Yu.E. A virtual thematic research environment for analysis of climate change and its consequences for Northern Eurasia: the current state of the art and perspectives. IOP Conf. Series: Earth and Environmental Science. 2018. Vol. 211. P. 012079. DOI: 10.1088/1755-1315/211/1/012079.

42. Grachev A.A., Persson P.O., Uttal T., Akish E.A., Cox C.J., Morris S.M., Fairall C.W., Stone R.S., Lesins G., Makshtas A.P., Repina I.A. Seasonal and latitudinal variations of surface fluxes at two Arctic terrestrial sites. Clim. Dyn. 2018, V. 51. No. 5–6. P. 1793–1818.

43. Gritsun A., Lucarini V. Fluctuations, response, and resonances in a simple atmospheric model. Physica D. 2017.V. 349, pp. 62–76.

44. Gryanik V. Lüpkes C. An efficient non-iterative bulk parametrization of surface fluxes for stable atmospheric conditions over polar sea-ice, Boundary Layer Meteorol. 2018. V. 166, P. 301–325.

45. Guryanov V.V., Eliseev A.V., Mokhov I.I., Perevedentsev Yu.P. Wave activity and its changes in the troposphere and stratosphere of the Northern Hemisphere in winters of 1979–2016. Izvestiya, Atmos. Oceanic Phys. 2018, V. 54, No. 2, P. 114–126.

46. Gushchina D., Dewitte B. Decadal modulation of the relationship between intraseasonal tropical variability and ENSO. Clim. Dyn. 2018. DOI: 10.1007/s00382-018-4235-y.

47. Handorf D., Dethloff K., Erxleben S., Jaiser R., Kurgansky M.V. Arctic-mid-latitude linkages in a nonlinear quasi-geostrophic atmospheric model. Adv. Meteorol. 2017. V. 2017, Article ID 2691368, 9 pages. DOI: 10.1155/2017/2691368.

48. Heiskanen J.J., Mammarella I., Ojala A., Stepanenko V., Erkkilä K.M., Miettinen H., Sandström H., Eugster W., Leppäranta M., Järvinen H., Vesala T., Nordbo A. Effects of water clarity on lake stratification and lake-atmosphere heat exchange. J. Geophys. Res. 2015. V. 120. P. 7412–7428.

49. Horton W., Miura H., Onishchenko O., Couedel L., Arnas C., Escarguel A., Benkadda S., Fedun V. Dust devil dynamics. J. Geophys. Res.: Atmos. 2016. V. 121, P. 7197–7214.

50. Ingel L.Kh. One type of resonance phenomena in the atmosphere and water bodies. Fluid Dyn. 2015a. V. 50. No. 4, P. 494–500.

51. Ingel L.Kh. On the response of a stratified liquid to resonance actions. Techn. Phys., 2015b. V. 60. No. 12, P. 1877–1879.

52. Ingel L.Kh. On the theory of convective jets and thermals in the atmosphere. Izvestiya, Atmos. Oceanic Phys., 2016. V. 52, No. 6, P. 602–605.

53. Ingel L.Kh. Movement of heavy particles in tornadoes. Izvestiya, Atmos. Oceanic Phys., 2017. V. 53, No. 4, P. 413–418.

54. Ingel L.Kh. Generalization of a Prandtl slope flow model with a heavy admixture. J. Appl. Mech. Techn. Phys., 2018a, Vol. 59, No. 5, P. 857–861.

55. Ingel L.Kh. On the theory of slope flows. Journal of Engineering Physics and Thermophysics, 2018b, V. 91, No. 3, P. 641–647.

56. Ingel L.Kh. On calculation of intense descending convection above a “cold spot” on a horizontal surface. J. Engin. Phys. Thermophys. 2018c. V. 91, No. 1. P. 181–184.

57. Ingel L.Kh. Nonlinear dynamics of turbulent thermals in shear flow. Journal of Applied Mechanics and Technical Physics. 2018d. V. 59. No. 2. P. 206–211.

58. Ingel L.Kh., Makosko A.A. On the theory of atmospheric disturbances induced by gravity-field inhomogeneities. Izvestiya, Atmos. Oceanic Phys. 2015. V. 51. No. 4. P. 391–396.

59. Ingel L.Kh., Makosko A.A. Geostrophic flow disturbances generated by inhomogeneities of the gravitational field. Izvestiya, Atmos. Oceanic Physics. 2017. Vol. 53, No. 5, P. 508–515.

60. Ingel L.Kh., Makosko A.A. Generation of the vortex movement in the atmosphere due to gravity inhomogeneities. Izvestiya, Atmos. Oceanic Phys. 2018. Vol. 54, No. 6, P. 536–541.

61. Intense Atmospheric Vortices and their Dynamics. Eds.: Mokhov I.I., Kurgansky M.V., Chkhetiani O.G. Moscow: GEOS, 2018. 482 pp. (in Russian)

62. Ivanova A.R. Stratosphere-troposphere exchange and its specific features at extratropical latitudes. Russian Meteorology and Hydrology. 2016. Vol. 41.No 3. P. 170–185.

63. Jensen A.D., Akperov M.G., Mokhov I.I., Lupo A.R., Sun F. The dynamic character of Northern Hemisphere flow regimes in a near-term climate change projection. Atmosphere. 2018, V. 9. No. 1. P. 27. DOI:10.3390/atmos9010027.

64. Jensen A.D., Lupo A.R., Mokhov I.I., Akperov M.G., Reynolds D.D. Integrated regional enstrophy and block intensity as a measure of Kolmogorov entropy. Atmosphere. 2017. V. 8. No. 12. P. 237. DOI:10.3390/atmos8120237.

65. Kalashnik, M. V. Exact model of a nongeostrophic baroclinic instability. Izvestiya, Atmos. Oceanic Phys. 2015a. V. 51, No. 5. P. 461–471.

66. Kalashnik M.V. Resonant and quasi-resonant excitation of baroclinic waves in the Eady model. Izvestiya, Atmos. Oceanic Phys. 2015b. V. 51, No. 6. P. 576–584.

67. Kalashnik M.V. Resonant excitation of baroclinic waves in the presence of Ekman friction. Izvestiya, Atmos. Oceanic Phys. 2018. V. 54. No. 2. P. 109–113.

68. Kalashnik M.V., Chkhetiani O.G. Generation of gravity waves by singular potential-vorticity disturbances in shear flows. J. Atmos. Sci. 2017. V. 74. P. 293–307.

69. Kalashnik M.V., Chkhetiani O.G., Chagelishvili G.D. New class of edge baroclinic waves and the mechanism of their generation. Izvestiya, Atmos. Oceanic Phys. 2018, V. 54, No. 4, pp 305–312.

70. Kalashnik M.V., Chkhetiani O.G. An analytical approach to determination of optimal perturbation in the Eady model. J. Atmos. Sci. 2018. V. 75. P. 2741–2761.

71. Kalashnik M.V., Khapaev A.A., Chkhetiani O.G. On the cyclone-anticyclone asymmetry in the stability of rotating shear flows. Fluid Dynamics. 2016, Vol. 51, No. 2, pp 167–179.

72. Kalashnik M., Kurgansky M. Nonlinear dynamics of long-wave perturbations of the Kolmogorov flow. Ocean Dyn. 2018. V. 68. P. 1001–1012.

73. Kalashnik M.V., Kurgansky M.V. Hydrodynamic instability of the periodic system of updrafts and downdrafts in the atmosphere. Russ. Meteorol. Hydrol. 2018. V. 43, No. 11, P. 729–736.

74. Kalashnik M.V., Nerushev A.F., Ivangorodskiy R.V. Characteristic scales and horizontal asymmetry of jet streams in the Earth's atmosphere. Izvestiya, Atmos. Oceanic Phys. 2017, V. 53, No. 2, P. 156–163.

75. Kalinin N.A., Shikhov A.N., Bykov A.V. Forecasting mesoscale convective systems in the Urals using the WRF model and remote sensing data. Russ. Meteorol. Hydrol. 2017. V. 42. No. 1. P. 9–18.

76. Kalinin N.A., Shikhov A.N., Sviyazov E.M. Simulation of snow accumulation and the WRF-ARW model. Russ. Meteorol. Hydrol. 2015. V. 40. No. 11, P. 749–757.

77. Kalinin N.A., Vetrov A.L., Pishchal'nikova E.V., Sviyazov E.M., Shikhov A.N. Estimating the accuracy of the very heavy snowfall forecast in the Urals by the WRF model. Russ. Meteorol. Hydrol. 2016. V. 41 No. 3, P. 193–198.

78. Kattsov V.M., Shkolnik I.M., Efimov S.V. Climate change projections in Russian regions: the detailing in physical and probability spaces. Russ. Meteorol. Hydrol. 2017. V. 42. No. 7. P. 452–460.

79. Kiktev D.B., Astakhova E.D., Zaripov R.B., Murav'ev A.V., Smirnov A.V., Tsyrulnikov M. D. FROST-2014 Project and Meteorological Support of the Sochi-2014 Olympics. Russ. Meteorol. Hydrol. 2015. V. 40. No. 8. P. 504–512.

80. Kiktev D., Joe P., Isaac G.A., Montani A., Frogner I.-L., Nurmi P., Bica B., Milbrandt J., Tsyrulnikov M., Astakhova E., Bundel A., Belair S., Pyle M., Muravyev A., Rivin G., Rozinkina I., Paccagnella T., Wang Y., Reid J., Nipen T., Ahn K.-D. FROST-2014: the Sochi Winter Olympics International Project. Bull. Amer. Meteorol. Soc., 2017, V. 98, No. 9. P. 1908–1929.

81. Kislov, A.V., Rivin, G.S., Platonov, V.S., Varentsov, M.I., Rozinkina, I.A., Nikitin, M.A. and Chumakov, M. 2018. Mesoscale Atmospheric Modeling of Extreme Velocities over the Sea of Okhotsk and Sakhalin. Izvestiya, Atmos. Oceanic Phys., V. 54. P. 322–326.

82. Kislov A., Sokolikhina N., Semenov E., Tudrii K. Analyzing the vortex as an integral formation: A case study for the blocking anticyclone of 2010. Russ. Meteorol. Hydrol. 2017. V. 42. P. 222–228.

83. Klevtsova Yu.Yu. The uniqueness of a stationary measure for the stochastic system of the Lorenz model describing a baroclinic atmosphere. Sb. Math. 2015. V. 206, No. 3. P. 421–469.

84. Klevtsova Yu.Yu. On the rate of convergence of the distributions of solutions to the stationary measure for the stochastic system of the Lorenz model describing a baroclinic atmosphere. Sb. Math. 2017. V. 208, No. 7. P. 929–976.

85. Klimova E.G. Application of ensemble Kalman filter in environment data assimilation. IOP Conf. Ser.: Earth Environ. Sci. 2018. V. 211, 012049. DOI: 10.1088/1755-1315/211/1/012049.

86. Komatsu K.K., Alexeev V.A., Repina I.A., Tachibana Y. Poleward upgliding siberian atmospheric rivers over sea ice heat up arctic upper air. Sci. Rep. 2018. V. 8, No. 1. P. 2872–2872.

87. Koprov B.M., Koprov V.M., Kurgansky M.V., Chkhetiani O.G. Helicity and potential vorticity in surface turbulence. Izvestiya, Atmos. Oceanic Phys. 2015. V. 51. No. 6. P. 565–575.

88. Koprov B.M., Koprov V.M., Solenaya O.A., Chkhetiani O.G., Shishov E.A.. Technique and results of measurements of turbulent helicity in a stratified surface layer. Izvestiya, Atmospheric and Oceanic Physics. 2018, Vol. 54, No. 5, pp 446–455.

89. Kozhevnikov V.N., Moiseenko K.B., Volkov, B.I. Flow over mountains with the stream velocity shear. Izvestiya, Atmos. Oceanic Phys. 2016. V. 52. No. 6. P. 587–595.

90. Kozhevnikov V.N., Elansky N.F., Moiseenko K.B. Mountain wave-induced variations of ozone and total nitrogen dioxide contents over the Subpolar Urals. Doklady Earth Sci. 2017. V. 475. No. 2. P. 958–962.

91. Krupchatnikov V., Iakshina D.F., Platov G., Martynova Y., Borovko I. On the interaction of atmospheric dynamics Arctic and midlatitudes under climate change. IOP Conf. Ser.: Earth Environ. Sci. 2018. V. 211. P. 012018. DOI:10.1088/1755-1315/211/1/012018.

92. Kurbatskaya L.I., Kurbatskii A.F. Calculation of the turbulent friction velocity in a mathematical model of an urban heat island in a stably stratified environment. Atmospheric and Oceanic Optics. 2016. V. 29. No. 6. P. 561–564.

93. Kurbatskii A.F., Kurbatskaya L.I. Turbulent circulation above the surface heat source in a stably stratified environment. Thermophys. Aeromech. 2016. V. 23. No. 5. P. 677–692.

94. Kurbatskii A.F., Kurbatskaya L.I. An explicit algebraic model of the planetary boundary layer turbulence: test computation of the neutrally stratified atmospheric boundary layer Thermophys. Aeromech. 2017. V. 24, No. 5, P. 705–717.

95. Kurbatskii A.F., Kurbatskaya L.I. Study of the neutral Ekman flow using an algebraic Reynolds stress model. Izvestiya, Atmos. Oceanic Phys. 2018, V. 54, No. 4, P. 336–343.

96. Kurbatskiy A.F., Kurbatskaya L.I. Features of eddy diffusion of momentum and heat in stably stratified flows of environment. Thermophys. Aeromech. 2015. V. 22, No. 2. P. 163–176.

97. Kurgansky M.V. A simple hydrodynamic model of tornado-like vortices. Izvestiya, Atmospheric and Oceanic Physics, 2015, V. 51, No. 3, P. 292–298.

98. Kurgansky M.V. Helicity in dynamic atmospheric processes. Izvestiya, Atmos. Oceanic Phys. 2017. V. 53. No. 2. P. 127–141.

99. Kurgansky M.V. To the theory of particle lifting by terrestrial and Martian dust devils. Icarus. 2018. V. 300. P. 97–102.

100. Kurgansky M.V. On one estimate of the boundary of the Rossby regime zone in the atmosphere. Izvestiya, Atmos. Oceanic Phys., 2018, V. 54, No. 3, P. 257–264.

101. Kurgansky M.V. On the instability of internal gravity waves propagating at small but finite angles to the vertical. Geophys. Astrophys. Fluid Dyn. 2018. V. 112. No. 4. P. 265–276.

102. Kurgansky M.V., Krupchatnikov V.N. Research in Dynamic Meteorology in Russia in 2011–2014. Izvestiya, Atmos. Oceanic Phys. 2016. V. 52. No. 2. P. 117–131.

103. Kurgansky M.V., Lorenz R.D., Renno N.O., Takemi T., Gu Z., Wei W. Dust devil steady-state structure from a fluid dynamics perspective. Space Sci. Rev. 2016. V. 203. P. 209–244.

104. Kurgansky M.V., Maksimenkov L.O., Khapaev A.A., Chkhetiani O.G. Vertical helicity flux as an index of general atmospheric circulation. Doklady Earth Sci. 2018. V. 479. P. 2. P. 477–481.

105. Levina G.V., Montgomery M.T. When will cyclogenesis commence given a favorable tropical environment?: To the 30th anniversary of the hypothesis on the turbulent vortex dynamo and dedicated to the memory of Soviet-Russian scientist, Professor Semen Samoilovich Moiseev. Procedia IUTAM, 2015, V. 17, P. 59–68.

106. Levina G.V., Zolnikova N.N., Mikhailovskaya, L.A. Cloud-resolving numerical analysis of the process of helicity generation in conditions of tropical cyclogenesis. Sovremennye Problemy Distantsionnogo Zondirovaniya Zemli iz Kosmosa. 2017. V. 14. No. 4. P. 213–222.

107. Li D., Katul G.G., Zilitinkevich S.S. Revisiting the turbulent Prandtl number in an idealized atmospheric surface layer. J. Atmos. Sci. 2015. V. 72. No. 6. P. 2394–2410.

108. Lorenz R.D., Balme M.R., Gu Z., Kahanpää H., Klose M., Kurgansky M.V., Patel M.R., Reiss D., Rossi A. P., Spiga A. History and applications of dust devil studies. Space Sci. Rev. 2016. V. 203. P. 5–37.

109. Lüpkes C., Gryanik, V. M. A stability-dependent parametrization of transfer coefficients for momentum and heat over polar sea ice to be used in climate models. J. Geophys. Res.: Atmos. 2015. V. 120, P. 1–30.

110. Martynova Yu.V., Krupchatnikov V.N. Peculiarities of the dynamics of the general atmospheric circulation in conditions of the global climate change. Izvestiya, Atmos. Oceanic Phys., 2015, V. 51, No. 3, P. 306–317.

111. Martynova Yu.V., Krupchatnikov V.N. Siberian vegetation cover response to projected future climate change. IOP Conf. Series: Earth Environ. Sci. 2018. V. 211. P. 012013.

112. Matveeva T., Gushchina D., Dewitte B. The seasonal relationship between intraseasonal tropical variability and ENSO in CMIP5. Geosci. Mod. Develop. 2018. V. 11. P. 2373–2392.

113. Meleshko V.P., Johannessen O.M., Baidin A.V., Pavlova T.V., Govorkova V.A. Arctic amplification: does it impact the polar jet stream? Tellus Series A – Dyn. Meteorol. Oceanogr. 2016. V. 68. P. 32330. DOI: 10.3402/tellusa.v68.32330.

114. Meleshko V.P., Kattsov V.M., Mirvis V.M., Baidin A.V., Pavlova T.V., Govorkova V.A. Is there a link between Arctic Sea ice loss and increasing frequency of extremely cold winters in Eurasia and North America? Synthesis of current research. Russ. Meteorol. Hydrol. 2018. V. 43. No. 11. P. 743–755.

115. Meredith E.P., Semenov V.A., Maraun D., Park W., Chernokulsky A.V. Crucial role of Black Sea warming in amplifying the 2012 Krymsk precipitation extreme. Nat. Geosci. 2015. V. 8. P. 615–620.

116. Mokhov I.I., Semenov V.A. Weather and climate anomalies in Russian regions related to global climate change. Russ. Meteorol. Hydrol. 2016. V. 41, No. 2. P. 84–92.

117. Mokhov I.I., Akperov M.G., Prokofyeva M.A. Cyclone-anticyclone asymmetry in the atmosphere of the extratropical latitudes of the northern hemisphere. Doklady Earth Sci. 2015. V. 462. № 2. P. 653–657.

118. Nigmatulin R.I. Equations of hydro-and thermodynamics of the atmosphere when inertial forces are small in comparison with gravity. Fluid Dyn. 2018. V. 53, Suppl. 1, P. S121–S130.

119. Novitskii M.A., Pavlyukov Yu.B., Shmerlin B.Ya., Makhnorylova S.V., Serebryannik N.I., Petrichenko S.A., Tereb L.A., Kalmykova O.V. The tornado in Bashkortostan: the potential of analyzing and forecasting tornado-risk conditions. Russ. Meteorol. Hydrol. 2016. V. 41. No. 10. P. 683–690.

120. Novitskii M.A., Petrichenko S.A., Tereb L.A. Evaluation of significance of spray evaporation in the atmospheric surface layer for computing the trajectory and intensity of tropical cyclones. Russ. Meteorol. Hydrol. 2016. V. 41, No. 5, P. 351–357.

121. Novitskii M.A., Shmerlin B.Ya., Petrichenko S.A., Tereb L.A., Kulizhnikova L.K., Kalmykova O.V. Using the indices of convective instability and meteorological parameters for analyzing the tornado-risk conditions in Obninsk on May 23, 2013. Russ. Meteorol. Hydrol. 2015. V. 40. No. 2. P. 79–84.

122. Onishchenko O.G., Pokhotelov O.A., Horton W., Fedun V. "Explosively growing" vortices of unstably stratified atmosphere, J. Geophys. Res. Atmos. 2016. V. 121, P. 11264–11268.

123. Penenko V.V., Tsvetova E.A., Penenko A.V. Development of variational approach for direct and inverse problems of atmospheric hydrothermal dynamics and chemistry. Izvestiya, Atmos. Oceanic Phys. 2015a. V. 51, No. 3, P. 311–319.

124. Penenko V.V., Tsvetova E.A., Penenko A.V. Methods based on the joint use of models and observational data in the framework of variational approach to forecasting weather and atmospheric composition quality. Russ. Meteorol. Hydrol. 2015b. V. 40. No. 6, P. 365–373.

125. Penenko A.V., Penenko V.V., Tsvetova E.A. Sequential data assimilation algorithms for air quality monitoring models based on a weak-constraint variational principle. Numerical Analysis and Applications. 2016. V. 9, No. 4, P. 312–325.

126. Penenko, V.V., Penenko, A.V. & Tsvetova, E.A. Variational approach to the study of processes of geophysical hydro-thermodynamics with assimilation of observation data. J. Appl. Mech. Techn. Phys. 2017. V. 58. No. 5, P. 771–778.

127. Perepelkin V.G., Kulichkov S.N., Chunchuzov I.P., Repina I.A. On experience in recording the voice of the sea in the water area of the black sea. Izvestiya, Atmos. Oceanic Phys. 2015. V. 51, No. 6. P. 639–650.

128. Perezhogin P.A., DymnikovV.P. Modeling of quasi-equilibrium states of a two-dimensional ideal fluid. Doklady Phys. 2017, V. 62, No. 5, P. 248–252.

129. Perezhogin P.A., Dymnikov V.P. Equilibrium states of finite-dimensional approximations of a two-dimensional incompressible inviscid fluid. Russ. J. Nonlin. Dyn. 2017. V. 13, No. 1, P. 55–79.

130. Perezhogin P.A., Glazunov A.V., Mortikov E.V., Dymnikov V.P. Comparison of numerical advection schemes in two-dimensional turbulence simulation. Russ. J. Numerical Analysis Math. Modelling, 2017, V. 32, № 1, P. 47–60.

131. Peters D., Vargin P. Influence of subtropical Rossby wave trains on planetary wave activity over Antarctica in September 2002. Tellus. 2015. V. 67, P. 25875.

132. Platov G., Krupchatnikov V., Martynova Yu., Borovko I., Golubeva E. A new earth's climate system model of intermediate complexity, PlaSim-ICMMG-1.0: description and performance. IOP Conf. Ser.: Earth Environ. Sci. 2017. V. 96. P. 012005. DOI: 10.1088/1755-1315/96/1/012005.

133. Polnikov V.G., Pogarskiy F.A. Spectra of long-term series for wind speed and wave height in the Indian Ocean area. J. Geophys. Res. 2017. V. 122 (1), P. 104–120.

134. Polnikov V.G., Sannasiraj S.A., Satish S., Pogarskii F.A., Sundar V. Estimation of extreme wind speeds and wave heights along the regional waters of India. Ocean Engineering. 2017. V. 146, P. 170–177.

135. Polonskii A.B., Kibal'chich I.A. Circulation indices and thermal regime of Eastern Europe in winter. Russ. Meteorol. Hydrol., 2015. V. 40, No. 1, P. 1–9.

136. Rashmi R., Polnikov V., Pogarskii F., Gomorev I., Samiksha V., Vethamony P. Long-term variability of the wind field over the Indian Ocean based on ERA-Interim reanalysis Atmosphere–Ocean. 2016. Vol. 54. No. 5, pp. 505–518.

137. Repina I.A., Artamonov A.Yu., Varentsov M.I., Kozyrev A.V. Experimental study of the sea surface wind drag coefficient at strong winds. Physical Oceanography, 2015, No. 1, pp. 49–58.

138. Rivin G.S., Rozinkina I.A., Vil'fand R.M., Alferov D.Yu, Astakhova E.D., Blinov D.V., Bundel' A.Yu., Kazakova E.V., Kirsanov A.A., Nikitin M.A., Perov V.L., Surkova G.V., Revokatova A.P., Shatunova M.V., Chumakov M.M.. The COSMO-Ru system of nonhydrostatic mesoscale short-range weather forecasting of the hydrometcenter of Russia: The second stage of implementation and development. Russ. Meteorol. Hydrol. 2015. V. 40. No. 6. P. 400–410.

139. Semenov V.A. Link between anomalously cold winters in Russia and sea ice decline in the Barents Sea. Izvestiya, Atmos. Oceanic Phys. 2016. V. 52, No. 3. P. 225–233.

140. Semenov V.A., Cherenkova E.A. Evaluation of the Atlantic Multidecadal Oscillation impact on large-scale atmospheric circulation in the Atlantic region in summer. Doklady Earth Sci. 2018. V. 478. P. 2. P. 263–267.

141. Semenov V.A. and Latif M. Nonlinear winter atmospheric circulation response to Arctic sea ice concentration anomalies for different periods during 1966–2012. Environ. Res. Lett. 2015. Vol. 10. P. 054020. DOI:10.1088/1748-9326/10/5/054020.

142. Shestakova A.A. Numerical simulation of wave drag during downslope windstorms in different regions of Russia. Russ. Meteorol. Hydrol. 2018. V. 43, No. 3. P. 192–196.

143. Shestakova A.A. Moiseenko K.B. Hydraulic regimes of flow over mountains during severe downslope windstorms: Novorossiysk bora, Novaya Zemlya bora, and Pevek yuzhak. Izvestiya, Atmospheric and Oceanic Physics. 2018, Vol. 54, P. 344–353.

144. Shestakova A.A., Moiseenko K.B., Toropov P.A. Hydrodynamic aspects of the Novorossiysk bora episodes in 2012–2013. Izvestiya, Atmos. Oceanic Phys. 2015. V. 51, No. 5. P. 534–545.

145. Shestakova A.A., Moiseenko K.B., Toropov P.A. Hydraulic and wave aspects of Novorossiysk bora. Pure Appl. Geophys. 2018. V. 175. No. 11. P. 3741–3757.

146. Shestakova A.A., Toropov P.A., Stepanenko V.M., Sergeev D.E., Repina I.A. Observations and modelling of downslope windstorm in Novorossiysk. Dynamics of Atmospheres and Oceans. 2018. Vol. 83, No. September 2018. P. 83–99.

147. Shikhov A.N., Chernokulsky A.V. A satellite-derived climatology of unreported tornadoes in forested regions of northeast Europe. Remote Sens. Environ. 2018, V. 204, P. 553–567.

148. Shmerlin B., Kalashnik M., Shmerlin M. The Formation of Localized atmospheric Vortices of Different Spatial Scales and Ordered Cloud Structures. Discontinuity, Nonlinearity, and Complexity, 2015. V.4. No. 3. P. 313–321.

149. Shmerlin B., Shmerlin M. Application of the hydromechanical model for a description of tropical cyclones motion. Discontinuity, Nonlinearity, and Complexity. 2015. Vol. 4. No. 3. P. 271–279.

150. Shmerlin B.Ya., Shmerlin M.B. Rayleigh Convective Instability in a Cloud Medium. Journal of Experimental and Theoretical Physics. 2017. Vol. 125. No 3. P. 502–517.

151. Shukurov K.A., Semenov V.A. Characteristics of winter surface air temperature anomalies in Moscow in 1970–2016 under conditions of reduced sea ice area in the Barents Sea. Izvestiya, Atmospheric and Oceanic Physics. 2018. Vol. 54, No. 1, pp. 10–24

152. Sitnikov G.I., Starchenko A.V., Terenteva M.V., Barashkova N.D., Volkova M.A., Kuzhevskaia I.A., Kizhner L.I.. Forecast of extreme weather conditions that promote aircraft icing during take-off or landing. Proceedings of SPIE – The International Society for Optical Engineering. 2015. Vol. 9680. P. 1–7.

153. Smirnova J.E., Golubkin P.A., Bobylev L.P., Zabolotskikh E.V., Chapron B. Polar low climatology over the Nordic and Barents seas based on satellite passive microwave data. Geophysical Research Letters. First published: 16 June 2015. DOI: 10.1002/2015GL063865.

154. Sporyshev P.V., Kattsov V.M., Gulev S.K. Changes in surface temperature in the Arctic: accuracy of model reproduction and probabilistic prediction for the near future. Doklady Earth Sci. 2018. V. 479. No. 2. P. 503–506.

155. Starchenko A.V., Danilkin E.A. Large eddy simulation of turbulent flow and of pollutant transport in a street canyon. Proceedings of SPIE. 2015. Vol. 9680. P. 1–6.

156. Starchenko A.V., Bart A.A., Kizhner L.I., Barashkova N.K., Volkova M.A., Zhuravlev G.G., Kuzhevskaia I.V., Terenteva M.V. Analysis of observations and results of numerical modeling of meteorological parameters and atmospheric air pollution under weak wind conditions in the city of Tomsk. Proceedings of SPIE. 2015. Vol. 9680. P. 1–7.

157. Sukhanovskii A., Evgrafova A., Popova E. Horizontal rolls over localized heat source in a cylindrical layer. Physica D: Nonlinear Phenomena. 2016. V. 316. P. 23–33.

158. Sukhanovskii A., Evgrafova A., Popova E. Helicity of convective flows from localized heat source in a rotating layer. Archive of Mechanical Engineering. 2017. Vol. 64. No. 2, pp. 177–188. DOI: 10.1515/meceng-2017-0011.

159. Sukhanovskii A., Evgrafova A., Popova E. Non-axisymmetric structure of the boundary layer of intensive cyclonic vortex. Dyn. Atmos. Oceans. 2017. V. 80. P. 12–28.

160. Sukhanovskii A., Shchapov V., Pavlinov A., Popova E. Laboratory model of tropical cyclone with controlled forcing. J. Phys.: Conference Series. 2018. V. 1128, 012133. DOI: 10.1088/1742-6596/1128/1/012133.

161. Teimurazov A., Sukhanovskii A., Evgrafova A., Stepanov R. Helicity sources in a rotating convection. J. Phys.: Conf. Ser. 2017. V. 899. P. 022017. DOI: 10.1088/1742-6596/899/2/022017.

162. Tolstykh M.A., Geleyn J.-F., Volodin E.M., Bogoslovskii N.N., Vilfand R.M., Kiktev D.B., Krasjuk T.V., Kostrykin S.V., Mizyak V.G., Fadeev R.Yu., Shashkin V.V., Shlyaeva A.V., Ezau I.N., Yurova A.Yu. Development of the multiscale version of the SL-AV global atmosphere model. Russian Meteorology and Hydrology. 2015. Vol. 40, No. 6. P. 374–382.

163. Tolstykh M.A., Fadeev R.Yu., Shashkin V.V., Goyman G.S., Zaripov R.B., Kiktev D.B., Makhnorylova S.V., Mizyak V.G., Rogutov V.S. Multiscale global atmosphere model SL-AV: the results of medium-range weather forecasts. Russ. Meteorol. Hydrol. 2018, V. 43. No. 11. P. 773–779.

164. Tolstykh M., Shashkin V., Fadeev R., Goyman G. Vorticity-divergence semi-Lagrangian global atmospheric model SL-AV20: Dynamical core. Geosci. Model. Dev. 2017. Vol. 10. P. 1961–1983.

165. Totz S., Eliseev A.V., Petri S., Flechsig M., Caesar L., Petoukhov V., Coumou D. The dynamical core of the Aeolus 1.0 statistical–dynamical atmosphere model: validation and parameter optimization. Geosci. Model Dev. 2018. Vol. 11, pp. 665–679.

166. Troitskaya Yu.I., Ermakova O.S., Kandaurov A.A., Kozlov D.S., Sergeev D.A., Zilitinkevich S.S. Non-monotonous dependence of the ocean surface drag coefficient on the hurricane wind speed due to the fragmentation of the ocean-atmosphere interface. Doklady Earth Sci. 2017. V. 477. No. 1. P. 1373–1378.

167. Tsyrulnikov M., Gayfulin D. A limited-area spatio-temporal stochastic pattern generator for simulation of uncertainties in ensemble applications. Meteorologische Zeitschrift. 2017. Vol. 26, No. 5, pp. 549–566. DOI: 10.1127/metz/2017/0815.

168. Turbulence, Atmospheric and Climate Dynamics. Eds.: Golitsyn G.S., Mokhov I.I., Kulichkov S.N., Kurgansky M.V., Repina I.A., Chkhetiani O.G. Moscow: Fizmatkniga. 2018. 586 pp. (in Russian).

169. Vargin P. Stratospheric polar polar vortex splitting in December 2009. Atmosphere-Ocean. 2015. Vol. 53. No. 1, pp. 29–41.

170. Vargin P.N. Stratosphere-troposphere dynamical coupling over boreal extratropics during the sudden stratospheric warming in the Arctic in January–February 2017. Russian Meteorology and Hydrology. 2018. Vol. 43, No. 5, pp 277–287.

171. Vargin P.N., Medvedeva I.V. Study of the temperature and dynamic regime of the extratropical atmosphere of the Northern Hemisphere during a sudden stratospheric warming in the winter of 2012–2013. Izvestiya, Atmospheric and Oceanic Physics. 2015. Vol. 51. No. 1, pp. 20–38

172. Vargin P.N., Volodin E.M. Analysis of the reproduction of dynamic processes in the stratosphere using the climate model of the Institute of Numerical Mathematics. Izvestiya, Atmospheric and Oceanic Physics. 2016. Vol. 52. No. 1, pp 1–15.

173. Vargin P.N., Kostrykin S.V., Volodin E.M. Analysis of simulation of stratosphere-troposphere dynamical coupling with the INM-CM5 climate model. Russian Meteorology and Hydrology. 2018. Vol. 43. No. 11, pp 780–786.

174. Verezemskaya P.S., Stepanenko V.M. Numerical simulation of the structure and evolution of a polar mesocyclone over the Kara Sea. Part 1. Model validation and estimation of instability mechanisms. Russian Meteorology and Hydrology. 2016. Vol. 41. No. 6. P. 425–434.

175. Vil'fand R.M., Kirsanov A.A., Revokatova A.P., Rivin G.S., Surkova G.V. Forecasting the transport and transformation of atmospheric pollutants with the COSMO-ART Model. Russian Meteorology and Hydrology. 2017. Vol. 42, No. 5, pp. 292–298.

176. Volodin E., Gritsun A. Simulation of observed climate changes in 1850–2014 with climate model INM-CM5. Earth Syst. Dynam. 2018. Vol. 9, pp. 1235–1242.

177. Volodin E.M., Galin V.Ya., Gritsun A.S., et al. Mathematical modeling of the Earth system. Ed. Yakovlev N.G. Moscow: MAKS Press, 2016. 328 pp. (in Russian)

178. Volodin E.M., Mortikov E.V., Kostrykin S.V., Galin V.Y., Lykossov V.N., Gritsun A.S., Diansky N.A., Gusev A.V., Iakovlev N.G. Simulation of the present-day climate with the climate model INMCM5.Climate Dynamics. 2017. Vol. 49. No. 11–12. pp. 3715–3734.

179. Vorobyeva V.V., Volodin E.M. Investigation of the structure and predictability of the first mode of stratospheric variability based on the INM RAS climate model. Russian Meteorology and Hydrology. 2018. Vol. 43, No. 11, pp 737–742.

180. Vulfson A.N., Borodin O.O. Brownian ensemble of random-radius buoyancy vortices and Maxwell velocity distribution in a turbulent convective mixed-layer. Physics of Fluids. 2018. Vol. 30. No. 9. P. 095103.

181. Vulfson A.N., Nikolaev P.V. Integral bubble and jet models with pressure forces. Izvestiya, Atmospheric and Oceanic Physics. 2017. V. 53. No. 4. P. 419–427.

182. Vulfson A.N., Nikolaev P.V. Linear approximations of the second turbulent moments of the atmospheric convective surface layer in a forced-convection sublayer. Izvestiya, Atmospheric and Oceanic Physics. 2018. Vol. 54, No. 5. P. 472–479.

183. Yaroshevich M.I., Ingel L.Kh., Lysenko D.A. On seismic manifestations of intensive atmospheric processes. Amer. J. Earth Sci. 2014. V. 1. No 5. P. 99–104.

184. Zahn M., Akperov M., Rinke A., Feser F., Mokhov I.I. Trends of cyclone characteristics in the Arctic and their patterns from different re-analysis data. J. Geophys. Res.: Atmos. 2018. V. 123. No. 5. P. 2737–2751.

185. Zaripov R.B., Martynova Yu.V., Krupchatnikov V.N., Petrov A.P. Atmosphere data assimilation system for the Siberian region with the WRF-ARW model and three-dimensional variational analysis WRF 3D-Var. Meteorology and Hydrology. 2016. Vol. 41, No. 11–12. P. 808–815.

186. Zuev V.V, Zueva N.E, Savelieva E.S. The role of the Mt. Merapi eruption in the 2011 Arctic ozone depletion. Atmos. Environ. 2017. V. 166. P. 327–333.

Middle Atmosphere

A.A. Krivolutsky[1], *A.I. Repnev*[1], *I.A.Mironova*[2],
A.N. Gruzdev[3], *T.I. Tuniyants*[1]
[1] Central Aerological Observatory
alexei.krivolutsky@rambler.ru
[2] Saint Petersburg State University
[3] A.M. Obukhov Institute of Atmospheric Physics RAS

New results obtained during 2015–2018 years demonstrate new numerical atmospheric model developments as well as results of modeling, observations and predictions of ozone and small atmospheric components changes as well as middle atmosphere structure variability. During current years many studies devoted to investigations of sudden stratospheric warming, planetary and gravity waves. Reader can find the details in original paper using the list of references.

A new Chemical Atmospheric Research Model development

A global numerical photochemical model CHARM (Chemical Atmospheric Research Model) was developed at the Laboratory of Atmospheric Chemistry and Dynamics at the Central Aerological Observatory. The article [1] presents the results of three-dimensional numerical modeling of climatological distributions of ozone and other small gas components in the range of 0–90 km. 87 chemical and 40 photochemical reactions were taken into account. The results of the implementation of numerical scenarios of exposure caused by changes in the UV radiation flux of the Sun in the cycle of its activity, as well as due to the destruction of ozone in the polar regions by high-energy particles of cosmic origin, are reported. The amplitudes of variations in UV radiation in various intervals of the spectrum, that characterized 21st and 22nd cycles of solar activity, were used as well as the ionization rates of particles were calculated from data the GOES-10 satellite. To describe the spatial transport of impurities, calculations of global fields of the wind components using the ARM general circulation model were used.

A description of the CHARM-I global numerical photochemical model (Chemical Atmospheric Research Model with Ions) is presented in the paper [2]. In addition to 113 chemical and photochemical reactions, 28 positive ion reactions, 29 negative ion reactions, 9 dissociation and photo-detachment reactions for negative ions and 14 ion recombination reactions were taken into account. As ionizing factors the models include UV-radiation fluxes at the wave-

length Ly-α, as well as galactic cosmic rays. To calculate the concentrations of neutral components, the "chemical families" method was used, and when calculating the charged concentrations, the electroneutrality condition was implicated at each integration step over time. The Prater scheme was used to describe the spatial transfer of a chemically active impurity. The model also makes it possible to take into account the effect of solar flares and particle precipitation on the D region. In [3], a qualitative assessment was made of the possibility of lowering the ozone concentration in the lower part of the D region under the influence of a powerful radio wave (expressed in [4] according to the results of an experiment on the Sura heating facility in March 2009). This estimates suggestion that a conclusion about such an effect on mesospheric ozone is just prematurely. Further experimental and theoretical research is needed. The effect of strong sudden stratospheric warming on the ozone of the middle atmosphere was considered in [5]. The features of changes in the medium-term situation during the mid-winter warming over the past two decades are investigated. The relationships of ozone with planetary waves and the intensity of the polar stratospheric vortex are established. It has been established that relative to the duration of a decrease in the water level in ozone, it cannot be achieved. Such phenomena preceded the development of strong mid-winter stratospheric warming, which expected a significant increase in ozone in January. The amplitude of the waves with n = 1 increased, and the waves with n = 2 increased, and in the center of the polar vortex increased opportunities. These features vary with the scale and extent of stratospheric warming.

Ozone layer: modeling, observations and predictions

A critical analysis of the active methods for the recovery of the ozone layer was carried out in the paper [6]. A critical analysis of various methods for the recovery of the ozone layer is given; emissions of alkane-class gases, destruction of freons by infrared laser radiation and using a microwave discharge, exposure to laser UV radiation and electrical discharge in the atmosphere, using solar radiation and laser infrared radiation shielding ozone-dissociating solar radiation. Optimal from the point of view of efficiency, economic costs and environmental consequences are the use of sources of gamma radiation, electrical discharge in the atmosphere and ultra-high frequencies breakdown.

The analysis of stratospheric O_3 and NO_2 abnormalities was carried out due to sudden stratospheric warming and the stratospheric circumpolar vortex caused by it in early February 2010 and latitudinal shift of the vortex to the European sector in late March 2011 on the eve of the final spring warming. In the first case, the concentration of O_3 in the thickness of the stratosphere was up

to 85% and the NO_2 content doubled; in the second, a decrease in the O_3 concentration by a quarter and the NO_2 content by half compared with the average values for the periods preceding the onset of anomalies. The estimates of the statistical relationship of the stratospheric contents of O_3 and NO_2 with potential vorticity and geopotential were obtained [19].

Analysis of the variability of atmospheric ozone content in different altitudes in the vicinity of St. Petersburg in 2009–2014 made on the basis of a comparison of the results of ground-based measurements at Peterhof atmospheric station, with the results of satellite measurements using the SBUV instrument and the results of numerical simulation. In the model, temperature, wind speed, air humidity and surface pressure were set according to the MERRA reanalysis. Based on a set of measurement results, numerical modeling and reanalysis, the features of seasonal and inter-annual changes in the ozone content in different altitude layers were identified, and the role of photochemical and dynamic factors in variations of the ozone content was estimated [20].

Examples of the total ozone (TO) content recovery from the spectra of outgoing thermal radiation measured with the aid of the IKFS-2 instrument from the "Meteor-M" meteorological satellite No. 2 are given. The method developed by the authors, based on the neural network approach using the TO measurement data using the OMI satellite device, is applied. Comparison of the obtained results with the ground-based measurements of the TO shows from agreement within 2–5% for the global ensemble and within 3–6% for individual latitudinal belts and seasons. Estimates of the measurement errors of the TO at IKFS-2 are close to the measurement errors of the TO using a similar IASI instrument from the MetOp satellite (EUMETSAT) [21].

A review of the observation and study of the ozone layer by Roshydromet institutions, the Russian Academy of Sciences and the Ministry of Education and Science was prepared based on the National Communication of the Russian Federation submitted to the World Meteorological Organization in January 2017. The main modern trends in research and development of ozone layer monitoring abroad and in Russia. Priority measures were proposed to enhance such work in our country [24].

A statistical approach is presented to restore the concentrations of the most important small mesospheric gas components at altitudes of 50–75 km using a photochemical model based on time series of ozone concentration, which was measured during the daytime of one day using a ground-based passive microwave device. Using the model of time series with noise and with the assumption of realistic measurement accuracy in the mesosphere, which is guaranteed by existing ozonometers, the accuracy of restoring unmeasured mesospheric characteristics as a function of the height and length of the time series is investigated [25].

Planetary waves, gravity waves, quasi-biennial oscillations and ozone: modeling, observations and predictions

The influence of planetary waves on the stability of the circumpolar vortex, the temperature of the polar stratosphere, the content of ozone and other gases has been simulated using the global climate-climate model of the lower and middle atmosphere. It was found that the planetary waves propagating from the troposphere to the stratosphere affect the gas composition of the stratosphere of the Arctic and Antarctic in different ways. In the Arctic, the degree of wave activity critically affects the formation of a circumpolar vortex, the appearance of polar stratospheric clouds, halogen activity on their surface and the formation of ozone anomalies. As a rule, at high wave activity, ozone anomalies in the Arctic are not formed, and at low, they can occur. In the Antarctic, wave activity affects the degree of vortex stability and the depth of ozone holes, which are formed at almost any wave activity, and the minimum ozone content depends on whether strong or weak activity is observed in specific years [26].

For a more accurate simulation of stationary planetary waves and atmospheric tides, a three-dimensional (longitude-latitude-height) semi-empirical climate model of water vapor distribution in the troposphere was created using the model of the middle and upper atmosphere (MSVA), which takes into account seasonal changes. Radiation heating and cooling units in MSVA are modified taking into account the dependence of the concentration of water vapor on the longitude. Calculations showed that taking into account the inhomogeneities of the water vapor content along the latitudinal circle leads to a significant dependence of solar heating on longitude, which affects the amplitudes of stationary planetary waves in the stratosphere [27].

Satellite and ground-based measurements of the ozone content in two atmospheric layers (0-25 and 25-60 km) are compared with the data of numerical modeling of the composition of the lower and middle atmosphere for the region of St. Petersburg. Average daily and monthly mean ozone concentrations for 3.5 years were compared (June of 2011th – December of 2014th). In general, agreement is good or satisfactory. Nevertheless, systematic differences in experimental data from model data were found. The model overestimates ozone compared to satellite measurements in the autumn-winter period in a layer of 0–25 km and underestimates in a layer of 25–60 km in the same period. These features are manifested in the average monthly values. The model in some cases demonstrates strong and “high-frequency” ozone oscillations, which are not always recorded in measurements [28].

Using the 3D chemical transfer model (CTM), it was shown that restoring the distribution of atomic oxygen and atomic hydrogen using the chemical ozone equilibrium assumption can lead to large errors below 81–87 km. A simple semi-empirical criterion is given for the practical indication of the lower boundary of the chemical equilibrium region of ozone near the mesopause [29].

The parametrization of the dynamic and thermal effects of orographic gravitational waves (OGW) and quasi-biennial oscillations (QBO) of the zonal wind are introduced into the general circulation model of the middle and upper atmosphere (MIAM). The sensitivity of vertical ozone fluxes to the influence of stationary OGW was studied at different phases of the QBO at altitudes up to 100 km in January. The simulated changes in vertical velocities produce corresponding changes in ozone fluxes caused by the influence of parameterization of the state bodies and the transition from the eastern to the western phase of the QBO. These changes can reach 40-60% in the Northern Hemisphere at the heights of the middle atmosphere [30].

The time series of satellite measurements of total ozone (TO) and ozone in two layers 0–25 and 25–60 km for 2000–2014. compared with the results of numerical simulation using the chemical transport model (CTM) and the EMAC climate model. Daily and average monthly values, short-term periods of its decrease, as well as long-term trends were compared. The statistical characteristics of the three time series (mean, SD, variations, median, asymmetry indices, etc.) are well matched. The EMAS model underestimates the ozone content in all three layers. The mismatch with satellite data is (5 ± 5), (7 ± 7) and (1 ± 4)% for CCA, 0–25 and 25–60 km layers. The mismatches of SBUV and CTM are (0 ± 7), (1 ± 9) and (-2 ± 8)%. Linear long-term trends are close to zero, both in experimental and model data [31].

To restore atomic oxygen from ozone observations in the extended region of the mesopause under sunlight, the assumptions of ozone photochemical equilibrium and ozone loss during photodissociation (excluding destruction by atomic hydrogen) are used. Assumptions verified by 3-D modeling. It was found that ozone is close to photochemical equilibrium at 75–100 km during the day. However, the destruction of ozone by atomic hydrogen cannot be neglected when atomic oxygen is reduced by ozone observations [32].

Observations

For the first time, the total content (OC) of $ClONO_2$ chlorine nitrate was measured using a Bruker IFS-125HR Fourier Spectrometer (FS) in 2009–2012, in Peterhof atmospheric station. The average value of the error is (25 ± 10)%. The results are compared with measurements by similar instruments at NDACC stations, with MIPAS satellite measurements and the EMAC chemical-climatological model. The seasonal course is the same for stations Peterhof,

Kiruna, Eureka with a maximum in February-March. A correlation R = 0.7–0.9 between the MIPAS data, ground-based measurements at Peterhof and the EMAC model was found. On average, the model values are less than both ground-based and satellite measurements [50].

An increase in nightly ozone concentrations in the stratosphere and lower mesosphere by 30–40% compared with daily values at an altitude of 50 km and by 50–80% by 60 km was found. Daily movement not found below 50 km. It is shown that nightly content is experiencing day-to-day changes. The results were compared with the MLS AURA orbital instrument data [51].

In Peterhof in 2009–2012 the ozone content in the troposphere (0–12 km) was measured with an error of ~ 4%, the stratosphere (12–50 km) with an error of ~3%, in layers 10–20 and 20–50 km (3–5%); in layers 12–18, 18–25 and 25–50 km (4–7%). In the seasonal variation in the troposphere and in the 12–18 km layer, a maximum is observed in March and a minimum in November with an amplitude of 30 and 40%, respectively. For a layer of 18–25 km, the maximum occurs in the winter-spring period, the minimum is at the end of summer, the amplitude of the seasonal chord is ~ 20%. The amplitude of changes in the annual variation in the 25–50 km layer is about 30%, with a maximum near the summer solstice and a minimum near the winter solstice. For three years, the increase in the ozone content in this layer amounted to ~10% per year of its average value over the period. The correlation coefficient of terrestrial and satellite measurements of stratospheric ozone is 0.76–0.84. The mean square mismatch of terrestrial and satellite (MLS) measurements is 13.6 and 5% for layers 10–20, 20–50 and 10–50 km, respectively. The correlation coefficient between the two types of measurements is 0.82–0.94 [52].

Ground-based spectrometric measurements revealed a negative anomaly in the stratospheric content of NO_2 in the winter-spring period of 2011 at a number of stations in the Northern Hemisphere. It was accompanied by anomalies of total ozone (TO) and stratospheric temperature and was caused by air transport from the area of the Arctic ozone hole. The analysis of the relation between the variations of the NO_2 OC and the variations in the TO and the temperatures of the Northern and Southern Hemisphere in the winter and spring periods was performed. It is established that it depends on the phase of the quasi-two-year cyclicity of the equatorial stratospheric wind [53].

The climatological model of the lower and middle atmosphere is used to study the sensitivity of the gas composition and temperature of the atmosphere to changes in spectral radiation fluxes in the 11-year cycle based on satellite measurements in the first decade of the 21st century. Model calculations showed that in addition to increasing the spectral flux in the absorption bands of molecular oxygen, leading to an increase in the ozone content, changes in the

flux at long wavelengths are also significant for the composition and temperature of the atmosphere. Changes in the rates of ozone destruction in different catalytic cycles partially compensate each other, while an increase in the destruction rate occurs in the reaction with atomic oxygen and in the nitrogen cycle, and a decrease in the hydrogen and chlorine cycles [54].

At the St. Petersburg State University, Peterhof station, a comparison was made of the data of the global model EMAC with the data of spectrometric measurements of the total (OC) ozone, HNO_3, HCl, NO_2 for 2009–2012. Both daily averages and monthly averages are analyzed. It is shown that the model reproduces the seasonal dependencies of the OC well enough. However several disagreements was identified. So the model for NO_2, HCl, HNO_3 underestimates the values of the OC compared with the experiment (on average by 14% for NO_2, by 22% for HC l and by 36% for HNO3). For the total (OC) ozone, the model gives large values (by an average of 12%) [55].

The article [60] presents the results of the analysis of the phase relationships between the quasi-ten-year variations in the range of 8–13 years of total ozone (TO) at the Aroza station for 1932–2012. and a number of meteorological parameters: monthly mean values of temperature, meridional and zonal components of wind speed and geopotential heights for isobaric surfaces in a layer of 10–925 hPa by Fourier methods, composite and cross-wavelet analysis. Since the beginning of the 24th cycle of solar activity (2008–2010), variations in the TO and meteorological parameters occur approximately in antiphase with variations in solar activity. The periods of maximum temperature growth rate on surfaces of 50–100 hPa approximately correspond to the periods of TOC maxima, and the periods of temperature maxima to the periods of the highest rate of TOC decrease. The moments of the maxima (minima) of the QBOs of the meridional wind speed approximately correspond to the periods of the maximum rate of amplification (attenuation) of the QBO temperature. QBO geopotential heights of isobaric surfaces lag behind the TOC variations by an average of 1.5 years. In general, the periods of variations in the TO and meteorological parameters in the range of 8–13 years are shorter than the period of variations in solar activity [60].

A number of works are devoted to the study of atmospheric circulation [7], planetary and internal gravitational waves, the effect on the composition of the atmosphere [8], and the influence of mesospheric HGV on planetary and tidal waves in the thermosphere [9].

Modeling

The global atmospheric circulation and temperature at altitudes from 0 to 135 km were calculated using the ARM model, taking into account the contribution of solar activity [7]. The ARM model is a development of one of the

versions of the COMMA model, but with a more detailed spatial resolution and more advanced parametrization of radiation sources and heat sinks. At the lower boundary of the model, wave sources of disturbances due to IGW and planetary waves are specified. Global fields of temperature and wind are presented for the average level of solar activity and their changes caused by variations in UV radiation fluxes in the solar activity cycle and solar proton flares.

The effect of planetary waves on the stability of the circumpolar vortex, the temperature of the polar stratosphere, the content of ozone and other gases was simulated using the global climate – climate model of the lower and middle atmospheres [8]. It was found that planetary waves propagating from the troposphere to the stratosphere affect the gas composition of the Arctic and Antarctic in different ways. In the Arctic, the degree of wave activity critically affects the formation of a circumpolar vortex, the appearance of polar stratospheric clouds, halogen activity on their surface and the formation of ozone anomalies. As a rule, at high wave activity, ozone anomalies in the Arctic are not formed, and at low, they can occur. In the Antarctic, wave activity affects the degree of vortex stability and the depth of ozone holes, which are formed during almost any wave activity, and the minimum ozone values depend on whether strong or weak wave activity is observed in specific years.

Planetary and Gravity waves analysis

The influence of mesospheric internal gravity waves (IGWs) on planetary and tidal waves in the thermosphere and ionosphere during the sudden stratospheric warming of 2009 was modeled in [9]. As perturbation sources, local perturbations caused by a planetary wave with a zonal wave number s = 1 and IGW propagating from the perturbation region in the stratosphere are taken into account. It is shown that the inclusion of an additional source of thermospheric perturbations leads to significant changes in the parameters of the thermosphere and ionosphere, including a change in the global structure of the gas component distributions and a shift in the maximum concentrations of atomic oxygen to the low latitudes of the southern hemisphere, an increase in average values, amplitudes of daily and semi-daily variations in ion concentrations in the region F of the ionosphere. These features of changes occurred with minor disturbances of tidal variations in the thermosphere. [9].

These radio meteor measurements of wind in high latitudes of the southern hemisphere (Art. Molodezhnaya, 680 S, 450 E) and at mid latitudes of the northern hemisphere (Art. Obninsk, 550 N, 37 0 E) were analyzed during periods of solar proton events in 1989, 1991, 2000, 2005 and 2012 [10]. In 1989 and 1991 The response to solar proton events was observed simultaneously at

both stations. A consequence of solar proton events is a change in the parameters of the wind regime of the studied region. In the high latitudes of the southern hemisphere, changes in the velocities of the meridional and zonal components of the prevailing wind are observed. The amplitude of the semi-diurnal tide increases in the vicinity of the maximum of the proton flux in the case of powerful solar proton events. The response to them depends on the season. The reaction of the prevailing wind at middle latitudes has the same features as the reaction of the wind at high latitudes. However, a clear response of the amplitude of the tide is not observed. In the summer season, even powerful events (for example, in July 2000) do not cause changes in the wind regime parameters of the mid-latitude region of the mesosphere / lower thermosphere.

The parametrization of normal atmospheric modes (NAM) and orographic gravitational waves (OGWs) are included in the mechanistic model of the general circulation of the middle and upper atmosphere [22]. The numerical experiments of the development of sudden stratospheric warming (SSW) in January-February were carried out using the UK Met Office meteorological information reanalysis data averaged over the years with the eastern phases of the quasi-two-year oscillations (QBO) in 1992–2011. The simulation showed that the amplitudes of the state bodies increase at altitudes greater than 30 km in the Northern Hemisphere after the SSW. The amplitudes of the state bodies have maximum at altitudes of about 50 km, above the North American and European mountain systems before and during the SSW, and also above the Himalayas after warming. At high latitudes of the Northern Hemisphere, significant (up to 50–70%) variations in the amplitudes of stationary planetary waves (SPW) are observed during and after SSW. West-propagating NAMs have local maxima of amplitudes not only in the Northern, but also in the Southern Hemisphere, where waveguides exist for the propagation of these modes. The calculated changes in the amplitudes of SST and NAM correspond to changes in average temperature and wind, Eliassen-Palm flows and the refractive index of the atmosphere for planetary waves during the SSW. The inclusion of the parameterization of the effects of OGW leads to an increase in the amplitudes (up to 30–70%) of almost all SPW before and during SSW and their decrease (to 20–100%) after SSW at middle and high latitudes of the Northern Hemisphere.

To study the variability of the dynamics of the stratosphere and its thermal structure, we used the UK Met Office reanalysis data. The results obtained show that the maximum of the inter-annual variability of the mean zonal flow associated with the FDC was observed at an altitude of about 30 km. It is shown that there is a statistically significant effect of the QBO phase on the extra-tropical stratosphere, the so-called Holton-Tan effect. The results of data analysis show that the conditions in the eastern phase of the FDC are more fa-

vorable for the development of sudden stratospheric warming (SSW). A statistical analysis of 15 strong SSW over the past two decades has been carried out. The results show that in recent years, internal processes associated with nonlinear interaction of stationary planetary waves (SPW) with the average flow play a dominant role. It is shown that the first enhancement of SPW1 in the upper stratosphere occurs due to the amplification of the nonlinear interaction between this wave and the mean flow. This enhancement is accompanied by a subsequent increase in the wave of wave activity from the stratosphere to the troposphere with a further redistribution of wave activity in the horizontal plane. Then the increase in flow from the troposphere to the stratosphere occurs in another area. The second increase in the activity of planetary waves in the stratosphere is accompanied by heating of the polar region and weakening or even reversal of the stratospheric jet flow. Thus, the non-linear wave-wave and medium-wave interaction can play an important role before and during the SSW. It has been shown that the upper stratosphere can be considered as an area where SPW2 is generated during SSW [33].

The recently developed parametrization of stationary orographic gravitational waves (OGW) has been applied in the general circulation model of the middle and upper atmosphere. The mean zonal wind, the amplitudes of stationary planetary waves (SPW) and normal atmospheric modes with periods of 4–16 days at altitudes from the troposphere to the lower thermosphere in January are calculated for the eastern and western phases of the QBO with and without parameterization of stationary OGWs. Taking into account the dynamic and thermal effects of the state body can lead to a significant change (up to 50–90%) of the amplitudes of the SST. The amplitudes of normal atmospheric modes running to the west vary (up to 50–90%) at different altitudes and latitudes of the Northern Hemisphere due to the influence of the state bodies. The transition from the eastern to the western phase of the QBO can change the amplitudes of the PV to +30 -90% at middle and high latitudes. These changes in the PV amplitudes are consistent with the Eliassen-Palma flux distribution and the refractive index at different QBO phases, including our parameterization of stationary OGWs [34].

In [35], it was found that there is a dependence of the transition dates on solar activity in the case of the separation of dates into early and late transitions, the stronger influence of the solar signal is found in the late spring transitions. It was also shown that in conditions of high solar activity, the connection between the transition dates and solar activity is stronger than at low.

The most relevant areas of research in the field of stratosphere-tropospheric interactions and their influence on climate are described in [36].

According to radar measurements of the zonal wind at altitudes of 82–97 km, it was found that in January and especially in February the zonal winds positively correlate with the El Nino index 3. A delay of about a month of the effect of the zonal wind with respect to the variability of the surface temperature of the equatorial sea is noticed. The signal is stronger for high altitudes (above 90 km) and weakens with decreasing altitude. This reflects the fact that during the years of El Nino the western jet streams are weaker. The results can be quantitatively reproduced by numerical experiments with a mechanistic global model of general circulation with a prescribed temperature of the troposphere and the release of latent heat for the conditions of El Niño and La Niña [37].

Planetary-scale waves (PSWs) arising in the troposphere are numerically modeled for heights from the earth up to 300 km. The influence of solar activity (SA) on the amplitudes and phases of the PSWs traveling to the west with zonal wave numbers 1 and 2 and periods of 4–16 days penetrating from the troposphere is calculated. Below 100 km, insignificant differences were obtained in the zonal velocity and amplitude of the PSWs for high and low SA [38].

A numerical simulation of changes in the global atmospheric circulation and the characteristics of stationary planetary waves (SPW) with zonal wave numbers 1–4 has been carried out. To simulate the general circulation and planetary waves at altitudes of 0-300 km, the model of the middle and upper atmosphere (MUAM) was used. Ionospheric conductivities and their latitudinal, longitudinal and temporal dependences are taken into account. Changes in the conditions of propagation and reflection (SPW), caused by the influence of solar activity on the thermosphere, can affect the atmospheric circulation in a wide range of altitudes, including the average atmosphere [39].

Four data series: the UK Met Office, MERRA, JRA-55 and ERA are used to estimate the climatic variability of the zonal mean flow, temperature and stationary planetary waves (SPW 1, SPW 2) at altitudes from the troposphere to the lower mesosphere. Combinations of meteorological fields in the middle of winter are averaged for 11-year intervals 1995–2005 and 2006–2016, and compared with the greatest attention to inter-annual and intra-seasonal variability. The results show that the changes in the mean fields of SPW2 are weaker and the statistical significance of these changes is lower compared to the changes observed in the intra-seasonal variability of these characteristics. All data series show a decrease in the SPW1 amplitudes at high-medium latitudes in the lower stratosphere and the opposite effect in the upper stratosphere. However, there is a statistically significant increase in intra-seasonal variability. UK Met Office data produces stronger changes and increased intra-seasonal variability than other data [40].

Temperature: modeling and observations

The Global Atmospheric Reference Model (GARM), developed in recent years, makes it possible to calculate climatic average monthly temperature, relative pressure and density distributions, as well as zonal and meridional components of wind speed at altitudes of 0–100 km. However, the model does not take into account daily variations, which lead to significant deviations from monthly mean values depending on local time, starting at altitudes of about 60 km and above. The aim of the study is to determine the heights starting from which it is necessary to take into account diurnal variations in atmospheric parameters, to estimate their seasonal and intra-seasonal variability and to discuss possible ways and approaches to take these variations into account in the GARM [41].

The results of sounding a thin layered structure of the wind velocity field in the stratosphere-mesosphere and lower thermosphere using infrasonic waves from ground-based explosions and volcanic eruptions are presented. These results were obtained using a new method of acoustic sounding, based on the phenomenon of scattering, based on the phenomenon of infrasound scattering from anisotropic inhomogeneities of wind speed and temperature in the region of acoustic shadow [59].

Regular nighttime variations in temperature in the region of mid-latitude mesopause by measuring hydroxyl radiation [11], non-zonal structure of the response of the global temperature field to solar activity [12], atmospheric variability by measuring the temperature of the mesopause region [13], and spectral structure of temperature variations in the region of mid-latitude mesopause [14].

According to ground-based spectral measurements in the near infrared region at the Zvenigorod ELISA research station (56N, 37E) during 2000–2013. Average nocturnal changes in the rotational and vibrational temperatures of the OH hydroxyl are obtained, the radiating layer of which is localized at altitudes of the mesopause. Rotational temperature reflects kinetic temperature. The analysis allowed us to determine the characteristics of the first three harmonics of the daily temperature variation, both with and without taking into account the high-altitude oscillations of the radiating layer of OH. For both cases, the second and third harmonics are statistically significant, the amplitudes of which are ~1K, and the phases of their first maxima are near 03:00 and 01:30 local solar time [11].

The results of processing global temperature fields using three reanalysis databases are given: “ERA-20C”, “NOAA-CIRES 20th Century Reanalysis, v2”, “NCEP / NCAR Reanalysis 1”. An analysis of the differences in the average monthly global temperature fields (January and July) between the maxima

and minima of the three cycles of solar activity (21, 22, 23rd cycles) also revealed their non-zonal structure. It is shown that the amplitude of the effect in January in the stratosphere (10 hPa) can be 7–29 K in the northern hemisphere. In July, the effect appears in the southern hemisphere. In the troposphere (500 hPa), a non-zonal temperature response is present in both hemispheres, and the amplitude of the effect is about 5–12K. Thus, the mechanism of the effect of solar activity on the temperature of the atmosphere discovered by numerical simulation is confirmed by processing reanalysis data [12].

For the analysis of atmospheric and ionospheric variability in the region of Eastern Siberia, we used data on the atmospheric temperature (Tm), at altitudes of the mesopause, obtained from spectrometric observations of the OH (6–2) band, 834.0 nm (the maximum of the emission maximum of 87 km), and vertical probing of the maximum electron concentration (N mF2). The period 2008–2015 was analyzed. Seasonal and inter-annual variations in the variability of Tm and NmF2 in different time periods were studied and compared: inter-day variations (T> 24 h), tidal variations (8 h T 24 h), and also with periods of HBV (T <8 h). Possible physical causes of both general features and differences in the behavior of the analyzed parameters are discussed [13].

According to spectral observations of the OH (6–2) 840 nm band at the Torah stations (52 0 N, 1030 E) in 2008–2016. and Zvenigorod (56N, 37E) in 2000–2016 long-term series of midnight temperatures in the mesopause region were obtained. Based on them, the Lomb-Scargle spectra of variations in the period from ~12 days to ~11 years are determined. The dominant oscillations are the first and second harmonics of the annual variation, the amplitudes of which are 23–24 K and 4–7 K, respectively. The remaining variations, the number of which was 16 for st. Torahs and 22 for Art. Zvenigorod, have small amplitudes (0.5-3 K). In addition to the inter-annual oscillations (periods from ~2 to ~11 years) and harmonics of the annual variation (up to its tenth harmonic), oscillations are observed with combination frequencies arising from modulating the harmonics of the annual variation [14].

Sudden Stratospheric Warming

Statistical characteristics of large and small sudden stratospheric warming (SSW) in the Northern Hemisphere for 1958–2015 analyzed according to NCEP-NCAR, ERA 40 and ERA-Interim re-analyses [23]. The dependence of the number of large SSW on the offset circumpolar stratospheric vortex and the number of small SSWs from the quasi-biennial cyclicity phase (QBO) of the equatorial stratospheric wind and the level of solar activity (SA) in the 11-year solar cycle. Large SSW, accompanied by the polar vortex displacement, occur more often with a high level of SA and with the eastern phase of QBO of the

equatorial wind in a layer of 50–40 hPa, and small SSW – vice versa, with a low level of SA and with the western phase of QBO. The analysis of the spatial-temporal dynamics of the polar stratospheric vortex with large SSW is performed, the most probable directions of the vortex displacement as a result of SSW are revealed. The effect of large SSWs on the total content of NO_2 and ozone, as well as on the stratospheric temperature, is analyzed.

According to the reanalysis of meteorological information, a statistical analysis of the dates of sudden stratospheric warming (SSW) in 1958–2014 was performed. Their uneven distribution in the winter months is shown, with maxima in early January, late January – early February, and late February. To explain these patterns, a climatological analysis has been made of changes in the amplitudes and vertical components of the Eliassen-Palma flows created by large-scale planetary waves (PW), average seasonal winds and temperature deviations from their average winter values at high northern latitudes at altitudes from the ground to 3 = 50 km using 20-year (1995–2014) set of daily meteorological information from the UK Met Office database. During more frequent VSP observations, climatological maxima of temperature disturbances, local minima of the westerly winds, as well as local maxima of the amplitudes and fluxes of Eliassen-Palma PV with zone wave number 1 in the high-latitude northern stratosphere were detected. Differences between atmospheric characteristics averaged over the past two decades have been found [42].

The main sudden stratospheric warming (SSW) in early January 2013 led to an increase in the temperature of the polar stratosphere to 60K at an altitude of 44 km, a change in the direction of the zonal wind, separation of the stratospheric polar vortex and a change in the temperature and dynamic regimes in the mesosphere – the lower thermosphere. Using data from re-analyses, ground-based spectrometric and satellite observations, changes in thermodynamic parameters from the troposphere to the lower thermosphere are analyzed related to SSW. Two weeks before the SSW, an increase in wave activity flows from the troposphere to the stratosphere over Eastern Siberia-China was revealed. It was shown that a week before the SSW, the wave chains propagating to the east in the upper troposphere could contribute to the strengthening of the anticyclone over the Northeast Atlantic, which during the SSW led to the division of the stratospheric polar vortex into two parts [49].

The results of a joint analysis of temperature variations in the mesopause region from measurements in 1966–2015 are presented. at the Zvenigorod station of the Institute of Atmospheric Physics RAS and variations in the surface temperature characterizing climatic changes. The marked decrease in temperature in the area of the mesopause in recent decades, in particular in winter, with a tendency its slowdown since the 1980s manifests itself against a general in-

crease in near-surface temperature (Tns) for the Northern Hemisphere, and the Earth as a whole. Revealed a sharp decrease in the temperature of the mesopause in the 1970s and its synchronicity with the climatic shift in climatic features at the surface associated with El Niño phenomena. With significant negative correlation of temperature variations of the mesopause and Tns, according to 56-year observations, the cross-wavelet analysis did not reveal significant coherence of the corresponding most long-term temperature variations. A global climate model was used to assess the possibility of such coherence. According to the calculations for the XX–XXI centuries, to obtain significant coherence of the perennial variations in the temperature of the mesopause, reduced to the same level of solar activity, Tm, and Tns, observations over a century or more are needed [61].

The preliminary results of the space experiment with the IRFS-2 IR probe (Satellite Meteor-M No. 2) showed the high quality of the measured spectra of the outgoing thermal radiation of the atmosphere-surface system and the adequacy of the developed IR radiation models of the atmosphere in the 15 μm absorption band of carbon dioxide used for restore vertical temperature profiles. The spectra of the outgoing radiation, measured with the help of IKFS-2, allow you to restore vertical temperature profiles with errors close to 1K in most of the height range of 0–30 km, except tropospheres and heights of more than 30 km, where these errors are close to 2–3K [62].

According to the ERA-Interim reanalysis, we obtained estimates of changes in temperature, geopotential and its large-scale zonal harmonics, wind speed, potential eddy in the troposphere and stratosphere of the Northern and Southern Hemispheres during the 11-year solar cycle. Estimates are obtained using the multiple linear regression method. The features of the response of these parameters to the solar cycle in certain areas of the atmosphere as a whole for the year and depending on the season are revealed. The results of the analysis indicate the presence of a reliable statistical relationship between large-scale dynamic and thermodynamic processes in the troposphere and stratosphere with an 11-year solar cycle [63].

The dynamic connection of the lower and upper atmospheres through planetary waves (PW) is investigated. A numerical simulation of the SP amplitudes during sudden stratospheric warming (SSW) in January-February was carried out using the general circulation model of the middle and upper atmosphere with initial and boundary conditions typical of the western and eastern phase of the quasi-two-year oscillations (QBO). The changes in the SP amplitudes in the middle atmosphere before, during and after VSP are considered for different phases of the QBO. Near the North Pole, the increase in average temperature during VSP reaches 10–30 K at altitudes of 30–50 km for four pairs of model calculations with the eastern and western phases of the QBO. The amplitudes of

the stationary PW in the middle atmosphere of the Northern Hemisphere can differ by up to 30% during the eastern and western phases of the QBO before and during the VSP. After the VSP event, the amplitudes of the stationary SPs are significantly larger in the western phase of the QBO. The refractive index of the PV and the vectors of the Eliassen-Palma flux (EF) are calculated. The largest fluxes (EF) in the middle atmosphere correspond to the PW with the zonal wave number m = 1. Changes in the amplitudes of PW correspond to inhomogeneities in the global circulation, the refractive index, and the flow formed by a change in the QBO phases. PW can provide an effective mechanism for the interaction and transfer of dynamic changes from local regions of the lower atmosphere to distant regions of the upper atmosphere of both hemispheres [43].

The general temperature structure of the Earth's atmosphere is considered. The conditions for the appearance of different types of atmospheric aerosol in the middle and upper atmosphere: volcanic aerosol, nacreous and silvery clouds are noted. The experimental basis of the work is measurements of the polarization of scattering on volcanic aerosol particles at an angle of about 90° (after the eruption of Rabaul volcano in 2006) and scattering on particles of noctilucent clouds in a wide range of angles in 2014 in middle and northern latitudes. Based on these measurements, an assessment of the particle size characteristics of the aerosol is done [48].

Wave perturbations of the nocturnal emission of the (0,0) O_2 atmospheric band were studied using the mesoscale hydrodynamic model and the zonal-averaged global circulation model [15]. Measurements of hydroxyl radiation served as the basis for studying the regular night course of temperature in the region of mid-latitude mesopause [11]. The O_2 IR band was used as the O_3 tracer in the mesosphere and lower thermosphere [16].

Mesospheric and stratospheric clouds

Features in the area of mesospheric clouds were investigated using data from the CIPS apparatus on the AIM satellite [17].

A unique case of the propagation of an internal gravitational wave that generated a compact and thin layer of noctilucent clouds (NC) at an altitude of 82.7–85.2 km with a horizontal scale characteristic of 65–70 km, observed in the Moscow region at night of July 18–19, 2013, is considered. It lasted about an hour. A model study showed that the wave had a tropospheric source associated with the passage of an occluded front. The wave was probably generated due to a strong horizontal wind shear at an altitude of about 5 km [44].

Atmospheric gravitational waves with very long ridges (450–500 km) and short horizontal wavelengths of about 20 km were observed in silver clouds. Gravitational waves slowly moved in the opposite direction to the background wind, indicating their forced generation outside the mesopause region. Analysis of ray tracing using meteorological reanalysis and empirical atmospheric model data showed that the source of such specific gravity waves was located near the tropopause and could be associated with jet flow at altitudes of 8–10 km [45].

A new mathematical model of global transport of multicomponent gas impurities and aerosol and the formation of polar stratospheric clouds (PSC) in both hemispheres has been built. Two types of PSCs are considered: 1a formation of nitric acid trihydrate particles (NAT), 1b formation of particles of a supercooled three-component H_2SO_4 / HNO_3 / H_2O solution – STS particles (supercooled ternary solutions) For their modeling, new equations have been proposed that describe the variability of components in gas and condensed phases taking into account their thermodynamic properties. The formation of PSC s is considered together with the formation of sulfate aerosol in the upper troposphere and lower stratosphere, taking into account photochemistry, nucleation, condensation-evaporation, and coagulation. Numerical experiments have been carried out to reproduce the space-time variability of PSC in the winter period in both hemispheres [56].

The study of the features of the planetary distribution of ionic eruptions at different levels of magnetic activity is described in [18].

Non-zonal structures of solar activity manifestation in the global temperature field were considered in [12].

The uncertainties in the photolysis rates associated with the variability of the intensity of solar radiation related to the selection of radiation data and to the characteristics of the calculation of photolysis calculations used in global chemical-climatological models are considered. It is shown that the main photolysis reactions responsible for the solar signal in the stratosphere are very sensitive to the spectral distribution of radiation variations. Accordingly, changes in ozone and ozone feedback with temperature substantially depend on the range of radiation data used, which makes it necessary to obtain accurate variations in radiation. It is also shown with the use of eight numbers in photolysis, that in most cases the absolute values of the photolysis rates and their response to the applied changes in radiation agree within 30% [46].

Seasonal and interannual changes in mean monthly values and variances of variations in the nocturnal luminescence of hydroxyl with periods of 0.4–5.4 h are studied. Averaged over 2020–2017. The annual variation of the average monthly temperature near the mesopause has a maximum in winter and a minimum in summer. The average monthly intensities of OH glow, in addition to the winter maximum, have an additional maximum in summer (in June). For

mesoscale variations in the intensity of the OH glow, the spring maximum is shifted to July [47].

A new vertical coupling model development and energetic particle precipitation forcing

A joint model of the troposphere-stratosphere-mesosphere and the D-layer of the ionosphere are presented. The model is based on a three-dimensional model of the general circulation in a hybrid coordinate system. A five-component model is taken as the photochemical model of the lower ionosphere. The role of the thermodynamic characteristics of the neutral atmosphere in the formation of the average state of the D-layer is investigated. Based on preliminary identification of the model from direct measurements, absorption and propagation of radio waves, satisfactory reproduction of the climatic characteristics of the D-layer of the ionosphere was shown [57].

The reproduction of dynamic processes in the stratosphere of extra-tropical latitudes is considered in calculations of the atmospheric block of the global climatological model of the IBM RAS with an upper limit of 0.2 hPa (~60 km) for the period from 1979 to 2008 in comparison with the reanalysis data. Changes in temperature, zonal wind, activity of planetary waves, heat fluxes in the lower stratosphere, as well as sudden stratospheric warming with displacement and separation of the polar vortex and the distribution of circulation anomalies in the troposphere associated with them [58].

Energetic particle precipitation for the fist time was taken into account as solar forcing for the Phase 6 of the Coupled Model Intercomparison Project (CMIP6). Paper [64] shows possibility to retrieve ionization rates in the atmosphere caused by energetic electron precipitation from balloon observations in the polar atmosphere and compares them against ionization rates recommended for the CMIP6. Simulations with 1-D radiative-convective model with interactive neutral and ion chemistry show that the difference of the CMIP6 and balloon-based ionization rate can lead to underestimation of the NO_x enhancement by more than 100% and ozone loss up to 25% in the mesosphere.

References

1. Krivolutsky A.A., T.Yu. Vyushkova, L.A. Cherepanova, A.A. Kukolev, A.I. Repnev, M.V. Banin. Three-dimensional global photochemical model CHARM. Taking into account the contribution of solar activity. Geomagnetism and Aeronomy, 2015, v. 55, No. 1, p. 64–93.

2. Krivolutsky A.A., L.A. Cherepanova, T.Yu. Vyushkova, A.I. Repnev. Three-dimensional global numerical photochemical model CHARM-I. Accounting processes in the field of the ionosphere. Geomagnetism and Aeronomy, 2015, v. 55, No. 4, p. 483–503.

3. Becker S.Z., S.I. Kozlov, S.V. Tasenko. Evaluation of the possibility of lowering the concentration of ozone in the lower part of the D-region under the influence of powerful radio waves. Geomagnetism and Aeronomy, 2016, v. 56, No. 6, p. 796–799.

4. Kulikov Yu.Yu., V.L. Frolov, G.I. Grigoriev et al. The response of the mesospheric ozone to the heating of the lower ionosphere by powerful HF radio emission. Geomagnetism and Aeronomy, 2013, v. 53, No. 1, pp.102–109.

5. Solomonov S.V., E.P. Kropotkin, S.B. Rozanov, A.N. Ignatiev, A.N. Lukin. The effect of strong sudden stratospheric warming on ozone in the middle atmosphere as observed on millimeter waves. Geomagnetism and Aeronomy, 2017, v. 57, No. 3, p. 392–400.

6. Becker S.Z., A.P. Doronin, C.I. Kozlov. Critical analysis of active methods for the recovery of the ozone layer of the Earth. Geomagnetism and Aeronomy, 2017, v. 57, No. 5, p. 676–682.

7. Krivolutsky A.A., L.A. Cherepanova, A.V. Dementieva, A.I. Repnev, A.V. Klyuchnikov. Global atmospheric circulation of Earth at altitudes from 0 to 135 km, calculated using the ARM model. Taking into account the contribution of solar activity. Geomagnetism and Aeronomy, 2015, v. 55, No. 6, p. 808–828.

8. Smyshlyaev S.P., A.I. Pogoreltsev, V.I. Galin, E.A. Drobashevskaya. The influence of wave activity on the gas composition of the stratosphere of polar regions. Geomagnetism and Aeronomy, 2016, v. 56, No. 1, p. 102–116.

9. Karpov I.V., F.S. Bessarab, O.P. Borchevkina, K.A. Artemenko, A.I. Klopov. Modeling of the influence of mesospheric HBV on planetary and tidal waves in the thermosphere and ionosphere during a sudden stratospheric warming in 2009. Geomagnetism and Aeronomy, 2018, v. 58, No.4, p. 526–539.

10. Trifonov A.N., N.A. Makarov, E.G. Merzlyakov. Manifestation of solar proton events in the mesosphere / lower thermosphere according to radio meteor measurements of wind in high and middle latitudes. Geomagnetism and Aeronomy, 2016, v. 56, No. 2, p. 163–177.

11. Perminov V.I., N.N. Peppers. Regular night course of temperature in the region of mid-latitude mesopause as measured by hydroxyl radiation. Geomagnetism and aeronomy, 2016, v. 56, No. 5, p. 657–661.

12. Krivolutsky A.A., A.V. Dementieva. The nonzonal structure of the response of the global temperature field of the Earth's atmosphere to solar activity. Geomagnetism and Aeronomy, 2017, v. 57, №1, p. 116–122.

13. Medvedev I.V., K.G. Ratovsky. Comparative analysis of atmospheric and ionospheric variability from measurements of the temperature of the mesopause region and the maximum of the electron concentration of NmF2. Geomagnetism and Aeronomy, 2017, v. 57, No. 2, p. 236–248.

14. Perminov V.I., A.I. Semenov, I.V. Medvedev, N.N. Pertsev, V.A. Suhodoev. The spectral structure of temperature variations in the region of the mid-latitude mesopause. Geomagnetism and Aeronomy, 2018, v. 58, No. 1, p. 133–140.

15. Poluarshinov M.A., A.N. Belyaev, K.B. Moiseenko, S.Sh. Nikolashishvili. Models of wave disturbances of the nocturnal emission of atmospheric band (0,0) of molecular oxygen. Geomagnetism and Aeronomy, 2015, v. 55, No. 3, p. 386–396.

16. Martyshenko K.V., V.Ya. Yankovsky. IR band 1.27 μm O2 as O3 tracer in the mesosphere and lower thermosphere: correction method. Geomagnetism and aeronomy, 2017, v. 57, No. 2, p. 249–261.

17. Kudabaeva D.A. Stationary longitudinal heterogeneities in the areas of mesospheric clouds according to CIPS / AIM data (June–July). Geomagnetism and aeronomy, 2015, v. 55, No. 6, p. 829–832.

18. Vorobev V.G., O.I. Yagodkina, E.E. Antonov. Features of the planetary distribution of ionic eruptions at different levels of magnetic activity. Geomagnetism and aeronomy, 2015, v. 55, No. 5, p. 611–622.

19. Gruzdev A.N., E.P. Kropotkina, S.I. Solomonov, A.S. Elokhov Winter-spring anomalies of O3 and NO_2 content in the stratosphere over the Moscow region in 2010 and 2011. Physics of the Atmosphere and Ocean, 2017, v. 53, No. 2, p. 223–231.

20. Smyshlyaev S.P., Ya.A. Virolainen, M.A. Motsakov, Yu.M. Timofeev, A.V. Poberovsky, A.V. Polyakov. Interannual and seasonal variations in the ozone content in different altitudes of the atmosphere of St. Petersburg according to observational data and numerical simulation. Physics of the Atmosphere and Ocean, 2017, v. 53, No. 3, p. 343–358.

21. Garkusha A.S., A.V. Polyakov, Yu. M. Timofeev, Ya.A. Virolaynen. Determination of the total ozone content from measurements of the satellite Fourier transform infrared spectrometer. Physics of the Atmosphere and Ocean, 2017, vol. 53, No. 4, p. 433–501.

22. Gavrilov N.M., A.V. Koval, A.I. Pogoreltsev, E.N. Savenkova. Numerical modeling of wave interactions during sudden stratospheric warming. Physics of the Atmosphere and Ocean, 2017, v. 53, No. 6, p. 674–685.

23. Ageeva V.Yu., A.N. Gruzdev A.S. Yelokhov, I.I. Mokhov, N.E. Zueva. Sudden stratospheric warming: statistical characteristics and their effect on the total NO2 and O3 content. Physics of the Atmosphere and Ocean, 2017, v. 53, No. 5, p. 545–555.

24. Zvyagintsev A.M., P.N. Vargin. Russian studies of the ozone layer in the period 2014–2016. Proceedings of the Hydrometeorological Center of Russia, 2017, v. 365, p. 101–117.

25. Nechaev A.A., T.S. Ermakova, V.Yu. Kulikov. Determination of the trace rate of oxygen concentration. Radiophysics and Quantum Electronics, 2016, v. 59, No. 7, p. 547–557.

26. Smyshlyaev S.P., A.I. Pogoreltsev, V.Ya. Galin, E.A. Drobyshevskaya. The influence of wave activity on the gas composition of the stratosphere of polar regions. Geomagnetism and Aeronomy, 2016, v. 56, № 1, p. 102–116.

27. Ermakova T.S., I.A. State, I.N. Fedulina, E.V. Suvorov, A.I. Fire victims. Three-dimensional semi-empirical climate model of water vapor distribution and its use in the radiation block model of the middle and upper atmosphere. Meteorology and Hydrology, 2017, No. 9, p. 75–80.

28. Timofeev Yu.M., Ya.A. Virolainen, S.P. Smyshlyaev, M.A. Motsakov. Ozone over St. Petersburg: comparison of experimental and model data. Optics of the Atmosphere and the Ocean, 2017, v. 30, No. 1, p. 20–24.

29. Belikovich M.Yu., Kulikov M. Grygalashvily, G.R. Sonnemann, T.S. Ermakova, A.A. Nechaev, A.M. Feigin. Ozone chemical equilibrium in the extended mesopause under the night time conditions. Adv. Space Res. 2017. p. 1–7.

30. Gavrilov N.M., A.V. Koval, F.I. Pogoreltsev, E.N. Savenkova. The influence of orografic waves and quasi-biennial oscillations on the ozone flux. Proc. SPIE, 10466, 23 rd Intern. Symp. Atmos. and Ocean Optics: Atmos. Phys. 1046651, 2017, doi: 101117 / 12.2284689.

31. Virolainen Ya.A., Yu.M. Timofeev, S.P. Smyshlyaev, M.A. Motsakov, O. Kirner. The variability of the ozone layer near St. Petersburg according to the SBUV satellite measurements and model calculations (2000–2014). Earth Exploration from Space, 2017, No. 3, p. 3–10.

32. Kulikov M.Y., M.V. Belikovich, M. Grygalashvyly, G.R. Sonnemann, T.S. Ermakova, A.A. Nechaev, A.M. Feigin. Daytime ozone loss term in the mesopause region. Ann. Geophys. 2017, v. 35, p. 1–6.

33. Pogoreltsev A.I., E.N. Savenkova, O.G. Aniskina, T.S.Savenkova, W.Chen, K. Wei. Interannual and interseasonal variability of stratospheric coupling during the winter winter. J. Atmos. Solar Terr. Phys. 2015, v. 136, p. 187–200.

34. Gavrilov N.M., A.V. Koval, A.I. Pogoreltsev, E.N. Savenkova. It is a simulator of phases and orografic gravity wave forcing in the middle atmosphere. Earth, Planets and Space, 2015, v. 67 (86), p. 2–16.

35. Rakushina E.V., A.Yu. Kanukhina, E.N. Savenkova, F.I. Pogoreltsev. Influence of QBO and stratos-heric circulation. J. Atmos. Solar Terr. Physics. 2015, v. 136, p. 231–234.

36. Vargin P.N., E.M. Volodin, A.Yu. Karpechko, A.T. Fire victims. On the stratosphere-tropospheric interactions. VestnikRAN, 2015, v. 85, No. 1, p. 39–46.

37. Jacobi Ch., T. Ermakova, L. Mewes, A.I. Pogoreltsev. El Nino influence on meteor radar at Collm (51.3 N, 13 E). Adv. Radio Sci. 2017, v. 15, p. 199–206.

38. Koval A.V., N.M. Gavrilov, A.I. Pogoreltsev, N.O. Shevchuk. Influence of solar activity on penetration of traveling planetary-scale waves from the troposphere into the thermosphere. J. Geophys. Res.: Space Phys. 2018. v. 123, p. 6888–6903.

39. Koval A.V., N.M. Gavrilov, A.I. Pogoreltsev, N.O. Shevchuk. Propagation of stationary waves at different levels of solar activity. J. Atmos. Solar Terr. Phys. 2018, v. 173, p. 140–149.

40. Rakushina E.V., T.S. Ermakova, A.I. Pogoreltsev. Changes in the mean zonal flow, temperature and planetary waves observed in the Northern Hemisphere mid-winter months during last decades. J. Atmos. Solar-Terr. Phys. 2018, 171,234–240

41. Ermakova E.S., M.A. Motsakov, A.I. Pogoreltsev, A.N. Fomin. Dependence on the season of daily variations of the wind at the heights of the average atmosphere. Proceedings of the Central Research Institute, 2017, v. 135, p. 35–39

42. Savenkova E.N., N.M. Gavrilov, A.I. Pogoreltsev, R.O. Manuylova. Statistical non-uniformity of dates of sudden stratospheric warming in the winter northern hemisphere, Izvestiya, Atmos. Oceanic Phys., 2017, v. 53, No. 3, p. 287–295

43. Koval A.V., N.M. Gavrilov, A.I. Pogoreltsev, E.N. Savenkova. Comparated during the stratospheric phase of the QBO phases. J. Atmos. Solar Terr. Phys. 2018, v. 171, p. 201–209.

44. Dalin P., A. Pogoreltsev, N. Pertsev, V. Perminov, N. Shevchuk, A. Dubietis, M. Zalcik, S. Kulikov, A. Zadorozhny, D. Kudobayeva, A. Solodovnik, G. Salakhutdinov, I. Grigoryeva. Evidence of the formation of noctilucent clouds due to propagation of an isolated gravity wave caused by a tropospheric occluded front. Geophys. Res. Lett. 2015. v. 42, p. 2037–2046.

45. Dalin P., N. Gavrilov, N. Pertsev, V. Perminov, A. Pogoreltsev, M. Shevchuk, A. Dubietis, P. Volger, M. Zalcik, A. Ling, S. Kulikov, A. Zadorozhny, G. Salakhutdinov, I. Grigorieva. A case study of long gravity wave crests in noctilucent clouds and their origin in the upper tropospheric jet stream. J. Geophys. Res.: Atmos., v. 121, p. 14102–14116.

46. Sukhodolov T., E. Rozanov, W.T. Ball, A. Bais, K. Tourpali, A.I. Shapiro, P. Telford, S. Smyshlyaev, B. Fomin, R. Sander, S. Bossay, S. Bekki, M. Marchand, M.P. Chipperfield, S. Dhomse, J.D. Haig, T. Peter, W. Schmutz. Evaluation of simulated photolysis rates and their response to solar irradianct variability. J. Geophys. Res.: Atmos., v. 121, p. 6066–6084.

47. Popov A.A., N.M. Gavrilov, A.B. Andreev, A.I. Fire victims. Interannual changes in the intensity of the mesoscale variations of the hydroxyl nighttime glow in Alma-Ata. Solar-Terr. Phys., 2018, v. 4, No. 2, p. 101–107

48. Ugolnikov O.S., I.A. Maslov, B.V. Kozelov, V.I. Kirillov. The middle and upper atmosphere of the Earth: layers of cold and high clouds. Phys. Auror. Phenom. Proc. XXXIX Ann. Seminar, Apatity, 2016, p.142–145.

49. Vargin P.N., I.V. Medvedeva. Study of the temperature and dynamic regime of the extratropical atmosphere of the Northern Hemisphere during a sudden stratospheric warming period in the winter of 2012–2013. Izvestiya, Atmos. Oceanic Phys., 2015, v. 51, No. 1, p. 20–38.

50. Virolainen Ya.A., Yu.M. Timofeev, A.V. Poberovsky, O. Kirner, M. Höpfner. The content of chlorine nitrate in the atmosphere over St. Petersburg. Izvestiya, Atmos. Oceanic Phys., 2015, v. 51, No. 1, p. 60–68.

51. Ryskin V.G., A.T. Orozobak. Microwave ground-based measurements of diurnal variations of ozone in the upper stratosphere over Kyrgyzstan. Izvestiya, Atmos. Oceanic Phys., 2015, v. 51, No. 1, p. 88–95.

52. Virolainen Ya.A., Yu.M. Timofeev, A.V. Poberovsky, M. Eremenko, G. Dufort. Determination of ozone in different layers of the atmosphere using ground-based Fourier spectrometry. Izvestiya, Atmos. Oceanic Phys., 2015, v. 51, No. 2, p. 191–200.

53. Ageeva V.Yu., A.N. Gruzdev, A.S. Yelokhov, M.V. Grishaev. Winter-spring anomalies of the stratospheric content of NO2 based on the results of ground-based measurements. Izvestiya, Atmos. Oceanic Phys., 2015, v. 51, No. 4, p. 455–463.

54. Smyshlyaev C.P., V.Ya. Galin, P.A. Blakitnaya, A.K. Lemischenko. Investigation of the sensitivity of the composition and temperature of the stratosphere to the variability of the spectral fluxes of solar radiation caused by the 11-year solar cycle. Izvestiya, Atmos. Oceanic Phys., 2016, v. 52, No. 1, p. 19–36.

55. Virolainen Ya.A., Yu.M. Timofeev, A.V. Polyakov, D.V. Ionov, O. Kirner, A.V. Poberovsky, H. Imhasin. Comparison of ground-based measurements of total O_3,, HNO_3, HCl and NO_2 with numerical simulation data. Izvestiya, Atmos. Oceanic Phys., 2016, v. 52, No. 1, p. 64–73.

56. Aloyan A.E., A.N. Ermakov, V.O. Harutyunyan. Simulation of the formation of polar stratospheric clouds, taking into account kinetic and heterogeneous processes. Izvestiya, Atmos. Oceanic Phys., 2015, v. 51, No. 3, p. 276–286.

57. Kulyamin D.V., V.P. Dymnikov. Climate modeling of the lower ionosphere. Izvestiya, Atmos. Oceanic Phys., 2015, v.51, No. 3, p. 317–337.

58. Vargin P.N., E.M. Volodin. Analysis of the reproduction of dynamic processes in the stratosphere by the climate model of the ICM RAS. Izvestiya, Atmos. Oceanic Phys., 2016, v. 52, No. 1, p. 3–18.

59. Chunchuzov I.P., S.N. Kulichkov, O.E. Popov, V.G. Perepelkin, A.P. Vasiliev, A.I. Glushkov, P.P. Firsts. Characteristics of a thin vertical wind structure in the stratosphere and lower thermosphere using infrasonic signals in the region of acoustic shade. Izvestiya, Atmos. Oceanic Phys., 2015, v. 51, No. 1, p. 69–87.

60. Visheratin K.N.. Quasi-ten-year variations in total ozone, wind, temperature, and geopotential height above Arosa Station, Switzerland. Izvestiya, Atmos. Oceanic Phys., 2016, v. 52, No. 1, p. 74–82

61. Mokhov I.I., A.I. Semenov, E.M. Volodin, M.A. Dembitskaya. Cooling in the area of mesopause during global warming according to measurement data and model calculations. Izvestiya, Atmos. Oceanic Phys., 2017, v. 53, No. 4, p. 435–444.

62. Asmus V.V., Yu.M. Timofeev, A.V. Polyakov, A.B. Uspensky, Yu.M. Golovin, F.S. Zavelevich, D.A. Kozlov, A.N. Rublev, A.V. Kukharsky, V.P. Pyatkin, E.V. Rusin. Temperature sounding of the atmosphere according to satellite Fourier transform infrared spectrometer. Izvestiya, Atmos. Oceanic Phys., 2017, v. 53, No. 4, p. 487–492.

63. Gruzdev A.N.. Changes in temperature and atmospheric circulation in the 11-year cycle of solar activity according to reanalysis ERA-INTERIM. Izvestiya, Atmos. Oceanic Phys., 2017, v. 53, No. 4, p. 502–511.

64. Mironova I.A., Artamonov A.A., Bazilevskaya G.A., Rozanov E.V., Kovaltsov G.A., Makhmutov V.S., Mishev A. Karagodin A.V. Ionization of the polar atmosphere by energetic electron precipitation retrieved from balloon measurement. Geophys. Res. Lett., 2019, No. 46, p. 990–996.

Ozone

Elansky N.F.
A.M. Obukhov Institute of Atmospheric Physics RAS

Tropospheric ozone and its precursors

Observations

The Russian network for monitoring the surface concentrations of ozone and its precursors has not changed over the last four years. The background stations mentioned in previous reviews [Elansky, 2016] – the Kislovodsk high-altitude scientific station (KHASS, Institute of Atmospheric Physics-OIAP), Lovozero, Mondy, and Karadag – continued to perform regular measurements. The surface ozone concentration (SOC) was also measured from 300-m towers in Obninsk (Kaluga region, NPO Taifun) and Zotino (Krasnoyarsk region, Obukhov Institute of Atmospheric Physics, Russian Academy of Sciences). All background stations are equipped with network instruments of the same type that are regularly calibrated.

The Tomsk regional network of stations to measure SOCs continued operating. This network includes four stations: two background stations (Fonovyi and Berezorechka), a basic experimental complex (BEC) located in the suburban zone of Tomsk, and an urban tropospheric ozone research (TOR) station. The Fonovyi, BEC, and the TOR station use Russian chemiluminescent ozone analyzers. An ultraviolet ozonometer (TEI 49) is used at the Berezorechka station. At the Fonovyi and BEC, in order to measure the SOC, air samples are taken at heights of 10 and 30 m, which makes it possible to estimate vertical ozone fluxes. At the TOR and Berezorechka stations, air samples are taken at heights of 5 and 10 m, respectively. At all stations, ozone concentrations are continuously measured at an interval of 1 h. Unfortunately, the system for monitoring SOC in urbanized regions is developing slowly.

The state network for monitoring atmospheric pollution, whose stations are located in about 240 Russian cities, does not conduct full-scale SOC measurements. Basically, SOC measurements are occasionally performed at stations that are few in number. Continuous once-per-minute measurements of the surface concentrations of ozone, its precursors (CO, NO, NO_2, and nonmethane hydrocarbons (NMHC)), and other atmospheric components were performed at the monitoring system (about 35 stations) of the Moscow Department of Nature Resources. Regular observations were carried out also in Tomsk, Ulan-Ude, and St.-Petersburg [Elansky, 2016].

Changes in atmospheric composition, ecosystems and climate have given impetus to more active field, marine, and aircraft observations of tropospheric ozone in Russia, which are usually carried out within the frameworks of international programs and projects. Among the most important projects is the tropospheric ozone sounding from board the AN 30 and AN 2 aircraft laboratories (Institute of Atmospheric Optics (IAO), Siberian Branch, Russian Academy of Sciences). The flights were performed in the monitoring regime in a region located to the south of Novosibirsk, and episodic large-scale observations covered the entire Siberian region, including the Arctic. Several research flights aboard the IL 62 aircraft laboratory of the Central Aerological Observatory (CAO) were conducted over northern European Russia in 2015–2018. The transcontinental observations of the composition of the atmosphere over Russia from a mobile railroad laboratory (TROICA experiments) were completed in 2010. However, a large body of data on surface ozone and its precursors are still under treatment and analysis.

The vertical distribution of ozone in the troposphere and lower stratosphere was measured using ozone sondes launched by the CAO and the IAO and a lidar (Tomsk, IAO). This lidar sounding within a height range of 5–16 km was based on the method of differential absorption and scattering at wavelengths of 241/341 nm [23–25]. Satellite ozone data were used in solving many problems. In particular, a station for receiving satellite information continued operating at the IAO.

Instruments and methods for measuring ozone concentrations have been improved. The semiconductor ozone analyzer developed at the Karpov Institute of Physical Chemistry is unique. This compact instrument was compared to standard network gas analyzers and yielded good results. This instrument was regularly used in studying the interaction of ozone with different materials. In particular, fiber filters based on polystyrene and polysulfone as efficient respiratory protective devices against ozone were put into production.

Distribution and variability

The Karadag background station is located on the territory of the T.I. Vyazemskii Karadag Scientific Station – the wildlife preservation of the Russian Academy of Sciences. The APOA 370 (HORIBA) instrument measured surface concentrations of ozone and other atmospheric trace gases. During the whole year, the concentrations of carbon, nitrogen, and sulfur oxides mainly correspond to their small background values. The variability of ozone is close to SOCs over rural areas in southern countries of Western Europe. The daily maximum of SOC is noted within an interval of 14:00–17:00. There are two maxima in the seasonal SOC cycle: basic maximum in July –August and weak-

er maximum in March–April [Lapchenko and Zvyagintsev, 2015; Zvyagintsev et al., 2016, 2017, 2018]. SOC variations are most closely associated with air-temperature variations. The coefficient of correlation between SOC and air temperature was 0.76 in August 2017. The high coefficient of correlation with air humidity (0.71) in February 2017 implies a possible influence of breeze circulation on the ozone behavior. The SOC exceeded the national standard (160 $\mu g/m^3$) in April and May 2016 (181 $\mu g/m^3$) and in August 2018 (195 $\mu g/m^3$). In March 2018, SOC maximum was noted during an anomalous air-temperature drop accompanied by a stratospheric air inflow. In summer, the highest SOCs are caused by an active ozone generation in air plumes with increased concentrations of volatile organic compounds (VOCs) due to heavy traffic during the peak of the holiday season.

The longest (since 1989) SOC observations in Russia have been carried out at the KHASS located at a height of 2070 m (Northern Caucasia). The rapid SOC decrease 1.53±0.14 $ppb \cdot yr^{-1}$ observed from 1989 to 1996 had slowed down by 2006, and, in recent years (up to 2017), the SOC trend has been close to zero. The obtained data series reflect changes that occurred in the industries of the countries of the former Soviet Union in the 1990s and the influence of large-scale atmospheric processes on the long-range transport of ozone and its precursors, vertical mixing, and radiation regime in the troposphere.

Studies of variations in ozone concentrations during the passage of both hot and cold waves over the measurement site have made it possible to obtain the quantitative (not qualitative) air-temperature dependence of SOC. At minimum surface ozone concentration (1999), at 30°C, if the air temperature changes 1°C, the ozone concentration increases by 5 $\mu g/m^3$. At maximum ozone concentration (2001), at the same air temperature, the ozone concentration may increase by almost 25 $\mu g/m^3$per °C. For intermediate periods (1997 and 2010), this increase is on the order of 14 $\mu g/m^3$per °C. An analysis of the cause of such an increase shows that the quadratic character of this dependence is due to a nonlinear increase in reaction constants with respect to air temperature and a quadratic increase in hydrocarbons emitted by vegetation with an increase in air temperature [Belan, 2017]. The relation between air temperature and SOC for the warm season is considered in detail in [Antokhina et al., 2017]. It was found that this relation depends on the character of atmospheric circulation. For the situations under analysis, the correlation of O_3 with air temperature is higher under conditions of well-developed advection and changed air masses. The SOC most noticeably increases when arctic air masses are replaced by subtropical ones. An analysis of circulation processes and the features of photochemical ozone generation, which are characteristic of western Siberia, has made it possible to reveal a significant relation between the snow cover and SOC varia-

tions [Belan et al., 2018]. Multiyear observations of atmospheric gas and aerosol components at the TOR station in the Tomsk region showed that the mean CO_2 and CH_4 concentrations are minimum within an arctic air mass and maximum within a tropical air mass [Antokhina et al., 2018]. On the one hand, this reflects different chemical histories of air masses, and, on the other hand, this is the result of the nonlinear dependence of the rate of ozone generation with an increase in air temperature.

The vertical distribution of ozone during forest fires in Siberia was studied using aircraft sounding data [Antokhin et al., 2018]. It was shown that, under the conditions of high aerosol concentrations, ozone sinks onto aerosol particles. However, despite this ozone sink on aerosol, in individual tropospheric layers, the concentrations of ozone may increase. The presence of such phenomena implies that, even under conditions of attenuated UV solar radiation, the photochemical generation of ozone occurs in the troposphere. In this case, the processes of oxidation of CO and VOCs (that are the products of vegetation combustion at the boundary of smoke plumes) play the main role.

The vertical profiles of the O_3, CO, CO_2, and CH_4 concentrations measured from board an aircraft over the Russian zone of the Arctic and retrieved according to data obtained with an IASI instrument installed aboard the MetOp satellite were compared in [Antokhina et al., 2018b]. It was shown that satellite data overestimate the CH4 and CO_2 concentrations within an atmospheric layer of 0–8 km over the continental Arctic zone and underestimate these concentrations over the ocean. According to satellite data, the excess of the concentration of methane over the continent amounts to 28 ppb in the planetary boundary layer (PBL) and rapidly increases in the middle (182 ppb) and upper (113 ppb) troposphere. The underestimation of its concentration over the ocean amounts to, on average, 37 ppb in the PBL and 73 and 71 ppb in the middle and upper troposphere, respectively. The differences between aircraft and satellite data on CO2 concentrations over the continent in the PBL amount to, on average, 18.2 ppm and may vary from 3.2 to 26.5 ppm. In the free troposphere, these differences decrease, on average, to 10.8 ppm (in this case, the variability range slightly increases – from 0.6 to 25.5 ppm) at a height of 4 km and to 2.8 ppm at a height of 8 km. Over the ocean, the underestimation in amplitude proves to be more significant. The comparisons for CO and O_3 yielded acceptable results.

The vertical profiles of ozone concentrations measured using different methods over the ocean and continent mostly agree with one another. Of 18 profiles under consideration, 16 profiles agree with one another. Disagreements are observed mainly for the middle and upper troposphere. Good agreement was obtained between data obtained with a differential absorption lidar at the Siberian lidar station and profiles retrieved according to satellite (MetOp) data [18].

In [Antokhin et al., 2015], the ratio between the rate of generation of ozone in the PBL and its inflow from the free troposphere was studied for the conditions of Siberia. It was shown that the rate of ozone inflow from the overlying atmospheric layers amounts to 20% of the rate of ozone photochemical formation within the PBL. The vertical profiles of ozone fluxes in the PBL were also calculated on the basis of the k-theory using the approach proposed by Troen and Mahrt. These calculations showed that the maximum of ozone concentrations in the PBL is formed due to photochemical reactions of precursor gases. In [Antokhin et al., 2016], the vertical ozone fluxes in the atmospheric surface layer were calculated using data obtained from gradient measurements (September 2015 – March 2016) from a high-altitude tower located at the Fonovyi ground. Significant diurnal variations in ozone fluxes were noted in September, February, and March. In these months, minimum ozone fluxes were observed at night and maximum ozone fluxes were observed during daylight hours and reached -3.8, -3.2, and -3.4 $\mu g/m^2/(m^2 s)$, respectively. There is no significant diurnal dynamics for October, November, December, and January, and the mean-diurnal variations in ozone fluxes amount to -2.3 ± 0.2, -1.6 ± 0.2, -1.5 ± 0.3, and -0.7 ± 0.3 $\mu g/m^2/(m^2 s)$, respectively.

In the summer months, forest fires affect the radiation regime in western Siberia and the rate of ozone generation. In the summer of 2012, forest fires were the cause of disastrous smoke generation over Tomsk. In [Sklyadneva et al., 2015], the parameters of smoke aerosol were determined, and it was shown that, in the presence of smoky haze (AOT_{500} within 0.53–4.2), the total solar radiation and UV radiation are 45% and 60–65% lower, respectively, than those on days with atmospheric aerosol content that is characteristic of Tomsk.

Airflows over mountains result in the generation of internal gravity waves (IGWs) that (under certain conditions) penetrate into the free troposphere and upper atmospheric layers and affect the atmospheric content and spatial distribution of both gas and aerosol components. In particular, it was shown in [Kozhevnikov et al., 2017] that IGW-induced variations in the O_3 and NO_2 concentration fields may reliably be recorded from the ground or from board an aircraft and, thus, these observational data may serve as a convenient tool for determining lee-wave characteristics.

Ozone and its precursors in cities

Ozone concentrations in the atmospheric surface layer over cities depend on photochemical processes, in which NO, NO_2, CO, and volatile organic compounds (VOCs) have a dominant role. Therefore, measurements of ozone are accompanied by measurements of its precursors. The time variability of the

SOC and its distribution over cities are affected by precursor emissions, meteorological conditions, chemical-transformation processes, precursor transport in the surface layer, and dry and wet deposition. These characteristics of the atmospheric composition and state are monitored in Moscow at the Ecological Station (ES) of the OIAP and Moscow State University (MSU) Meteorological Observatory. Summary results obtained from the 2002–2012 measurements of ozone and its precursors are given in [Elansky et al., 2015]. Changes in the infrastructure of Moscow and, first and foremost, both quantitative and qualitative changes in the system of motor transport were accompanied by an increase in the SOC (1% yr^{-1}) and a decrease in the concentration of NO. The content of NO2 remained almost unchanged. The features of both annual and diurnal variations in the concentrations of O_3, NO, NO_2, CO, and SO_2 are also analyzed. Both synoptic situations and air-mass types strongly affect the air pollution.

Interrelations between atmospheric composition over cities and the PBL thermal structure are studied in [Elansky et al., 2016; Lokoshchenko et al., 2016]. An extensive database obtained from direct measurements of atmospheric composition and air-temperature profiles during the 1995–2010 TROICA experiments was analyzed. Data on temperature, humidity, and surface concentrations of main trace gases (O_3, CO, NO, NO_2, SO_2) in the ambient air over different Russian cities were obtained for different seasons and different times of day. The most significant effect of air-temperature increase was observed in the nighttime in the central parts of large cities (1.9°C); in small towns, the excess of night temperatures is somewhat higher than the average value in average-sized cities because of the low-rise buildings, which leads to greater warming of the surface air layer under nighttime temperature inversions. Such a temperature increase over the central parts of cities is well correlated to changes in the non-organic atmospheric composition.

Atmospheric acoustic sounding is a useful and reliable tool for studying the dynamics of surface air pollution especially within small time intervals [Elansky et al., 2015]. The surface concentrations of ozone, nitrogen and carbon oxides, sulfur dioxide, and others were simultaneously measured at the ES OIAP and the MSU Observatory from 2002 to 2014. Here, two sodars (ECHO-1 since 1988 and MODOS since 2004) continuously operated. Sodar data on temperature stratification have made it possible to explain basic tendencies for variations in O_3, NO, NO_2, CO, SO_2 concentrations especially in the morning during the destruction of elevated inversions. Significant differences between morning and evening maxima and between daytime and nighttime minima during the warm season were shown for the primary products of fuel combustion (NO and CO). These differences are associated with variations in the PBL temperature stratification determined from sodar data. In [Lokoshchenko et al., 2017], this

result was first obtained from measurements during the first year; the statistical significance of these differences was revealed, and the nature of this effect was substantiated in detail in [Lokoshchenko et al., 2016]. The effect of a rapid increase in the surface content of trace gases within a turbulent zone before an increasing cold front was studied using sodar data in [Elansky et al., 2015].

Data on the surface NO, NO_2, CO, SO_2, CH_4, and PM_{10} concentrations measured at 46 stations from 2005 to 2014 in Moscow have been used in studying the features of their time variations and distribution over the city area. [Elansky et al., 2014; 2018; 2019] Both seasonal and interannual variations of pollutant concentrations, as well as their PM_{10} 10-year trends, are closely related with variations in the urban infrastructure and weather conditions. The weekly cycle of the pollutants has been analyzed. The largest amplitude is 18.9±5.6% for NO. For CO, NO_2, and PM_{10}, the amplitudes amount to 9.3±3.2%, 13.6±2.8%, and 10.9±5.5%, respectively. The weekly variations in CH_4 and SO_2 concentrations are not significant for such large-scale territorial averaging.

The emission fluxes of CO, NO_x, SO_2, and CH_4 and their integral emissions from the Moscow megacity have been estimated from multiyear measurements of their surface concentrations and both vertical air-temperature and wind stratifications [Elansky et al., 2018]. During 2005–2014, the annual integral emissions of CO, NO_x, and CH_4 decreased with a rate of -1.9±0.3, -1.7±0.4, and -7.8±3.1%·yr^{-1}, respectively, and that of SO_2 increased with a rate of 3.3±2.3 %·yr^{-1}. The means of integral annual pollutant emissions from Moscow differ slightly from those for other world megacities. Comparison of the calculated emission values with data from the EDGAR v 4.2 global inventory yielded ambiguous results. On the one hand, the CO emission values almost coincided, and, on the other hand, the inventory data for NO_x, SO_2, and CH_4 proved to be significantly higher. It follows from an analysis of contributions made by some sources that the emissions from enterprises of metallurgical and chemical industries are significantly overestimated in this inventory (especially SO_2 emissions during house heating).

Multiyear observational data (obtained at the mobile railroad laboratory in the course of the 1995–2010 TROICA experiments) on the composition and state of the atmosphere were used to study the features of both spatial and temporal variations in the concentrations of trace gases in the surface layer over Russian cities (Elansky et al., 2016). The urban-air characteristics noticeably differ from those obtained at stationary stations. The emission fluxes of NO_x, CO, and CH_4 and their integral emissions from large cities were estimated on the basis of observational data obtained at the mobile laboratory. The values of these emission fluxes reflect the state of urban infrastructure. The integral ur-

ban emissions of CO depend on the city size and vary from 50 Gg yr^{-1} for Yaroslavl to 130 Gg yr^{-1} for Yekaterinburg. For most cities, they agree with the EDGAR v 4.2 data within the limits of experimental error. The agreement is worse for the emissions of NO_x. The EDGAR v 4.2 data on the emissions of CH4 seem to be overestimated.

Results obtained at the Zvenigorod Scientific Station (ZSS) from multiyear measurements of NO_2 and H_2CO concentrations formed the basis for studying the location of their sources using the concentration weighted trajectory (CWT) method [Shukurov et al., 2018]. In the cold season, the main source of anomalously high H_2CO concentrations is Moscow, especially its eastern and southeastern zones with high emissions of anthropogenic H_2CO and VOCs that are the precursors of H_2CO. In the warm season, positive H_2CO anomalies at the ZSS due to Moscow contribution are significantly lower, which may be associated with the fact the lifetime of H_2CO is shorter under the conditions of increased insolation during this season.

The dependence of the time variability of mass aerosol ($PM_{2.5}$) concentration in the surface air layer, which is characteristic of Moscow, on atmospheric parameters, such as concentrations of some trace gases, aerosol optical thickness, surface air temperature, humidity, and wind velocity, was considered in [Gubanova et al., 2018]. The results of an analysis of the 2011–2013 observational data on concentrations of aerosol particles ($PM_{2.5}$) and trace gases SO_2, NH_3, NO_x, CO, O_3 were given. Both diurnal and seasonal variations in the concentrations of aerosols ($PM_{2.5}$) and trace gases were studied, correlations between them were revealed, the variability of the $PM_{2.5}$ concentration depending on concentrations of some gases participating in the formation of atmospheric aerosols and on meteorological parameters was studied. Data on surface aerosol ($PM_{2.5}$) concentrations were compared with data on aerosol optical thickness AOT_{500}. There is evidence in favor of a possibility that superfine particles may be formed of precursor gases in the air basin over Moscow in summer.

Methane (CH_4) is one of the most important greenhouse gases and the source of ozone. Data obtained from measurements of atmospheric methane and its isotopic content over the seas of the Russian Arctic in the summer and fall of 2015 are given in [Skorokhod et al., 2016; Pankratova et al., 2018]. The causes of increased near-water methane concentrations, the highest of which (up to 2050 ppb) were recorded over the waters of the Kara and Laptev seas and the Arkhangelsk seaport region, were studied using the Keeling plot method and inverse numerical simulation. It was shown that the main methane sources within the measurement zone (except regions adjacent to large ports) are both the tundra and marsh ecosystems of Siberia. On the whole, the microbiological sources are responsible for 43% of the total methane variability along the voyage route. The 2013–2014 data obtained from the chamber meas-

urements of methane fluxes in the course of three experiments are given and analyzed in [Ivakhov et al., 2015]. The methane concentration was determined from an analysis of air samples using a gas chromatograph and (in situ) a laser spectrometer. The measurements were performed for 13 different microrelief areas. The mean methane fluxes for wet, dry, and stony tundra amounted to 2,35±2,12 mg/m^2/h, 0,01±0,06 mg/m^2/h, and -0,07±0,05 mg/m^2/h, respectively.

Stratospheric ozone layer

The network including 28 ozonometric stations equipped with M124 filter ozonometers (Voeikov Main Geographical Observatory (MGO)) continues operating in Russia. These ozonometers are calibrated using Dobson spectrophotometer no.108, which regularly participates in intercalibrations. The total ozone content (TOC) data are transmitted to the World Ozone and Ultraviolet Radiation Data Center (WOUDC, www.woudc.org) and the results of an analysis of the current ozone-layer state are regularly published in the journal Russian Meteorology and Hydrology [Zvyagintsev et al., 2015; 2016; 2017; 2018] and in annual reports on the state of environment, which are issued by the Russian Federal Service for Hydrometeorology and Environmental Monitoring (Rosgidromet).

In 2011–2014, the KHASS, Obninsk, and Tomsk stations equipped with Brewer spectrophotometers continued carrying out TOC observations. Data obtained at these stations are also regularly transmitted to the WOUDC. In 2016, these instruments were calibrated using the mobile standard of Brewer spectrophotometer No. 17 [Savinykh et al., 2016; 2018; 2019]. The NO_2 content in a vertical atmospheric column, which is closely related to the TOC and which is necessary for studying variations in the state of the ozone layer, is measured every day at the KHASS, Zvenigorod Scientific Station (ZSS), and in Tomsk. The TOC is regularly measured with an IR Fourier spectrometer (IRFS) at the Peterhof station (59.88°N, 29.83°E) in the vicinity of St. Petersburg [Timofeyev et al., 2018]. It was found that satellite data systematically underestimate TOC when compared to TOC data obtained from ground-based measurements [Ivanova, 2017].

Variations and trends in the total ozone content over the 1979–2014 period are studied using monthly mean data from ERA-Interim TOC reanalysis database in different latitudinal belts and TOMS/SBUV/OMI satellite data [Zvyagintsev et al., 2015]. The authors estimated how TOC variations (averaged over different latitudinal belts and globally) are modulated by Arctic and Antarctic oscillations, quasi-biennial oscillations of zonal wind in the equatorial stratosphere, El Nino – Southern Oscillation, zonal average meridional heat flux

in the lower stratosphere, solar activity (SA), stratospheric content of ozone-depleting substances (ODS), and volcanic aerosol particles. Variations in global TOC can be well described using regression dependence on ODS and SA.

In late January 2016, over the northern Urals and Siberia, total ozone amounts at a level of about 200 DU were recorded for the first time over the entire period of observations since the 1970s, classified as an ozone "mini-hole". In [Nikiforova et al., 2017] possible causes and factors responsible for anomalously low total ozone levels during the winter of 2016 (when compared to a number of previous Arctic winters with severe ozone depletion) were analyzed. Dynamic factors are shown to play a dominating role in the occurrence of the ozone anomaly in late January 2016, and even more significant ozone anomalies in the Arctic are hypothesized to be likely in the future. Anomalous TOC variations in the atmosphere over Russia, which are caused by the anomalous development of large-scale atmospheric processes, are studied in [Ivanova et al., 2017].

The phase relationships during 8–13 years between the longest series of TOC observations at the Arosa station, air temperature, both meridional and zonal components of wind velocity and geopotential heights within a layer of 10–925 hPa are analyzed in [Visheratin et al., 2016a]. It was shown that the phase relationships between quasi-decadal variations (QDVs) in the TOC, meteorological parameters, and the 11-year solar activity (SA) cycle change with time and with height, and, since the beginning of the 24th solar-activity cycle (2008–2010), TOC and some meteorological parameters vary approximately in antiphase with SA. In general, the periods of oscillations of the TOC and meteorological parameters within a range of 8–13 years are shorter than the period of SA oscillations.

Both spatial and temporal variations in the TOC, some meteorological parameters of the lower and middle atmosphere, and phase relations between them were studied using the methods of spectral, cross-wavelet and composite analyses in [Visheratin et al., 2016b,; 2016c; 2017a; 2017b]. Ground-based measurement data were compared with satellite data. Quite interesting is the similarity of the spectral structure of interannual variations for stations located at a considerable distance from each other and separated by high mountains. The phase relations between TOC variations, some parameters of the lower stratosphere, and solar-activity variations were considered for a period of 1979–2015 in the latitudinal zone 90°S–90°N.

In general, the results of comparison of phase relationships show that variations in total ozone and atmospheric parameters are characterized by a shorter variability period than solar-activity variations, which may be due to the interference of oscillations within ranges of 85–105 and 120–140 months presented in most of the considered atmospheric series.

Both space-time and height-time variations in atmospheric ozone under atmospheric-blocking conditions were analyzed using OMI, MLS, AIRS, and MODIS satellite data and ozone sounding data in [Sitnov and Mokhov, 2015, 2016, 2017, 2018]. It was shown that negative TOC anomalies (up to -15%) caused mainly by a quasi-horizontal advection of subtropical ozone-depleted air in the rear of blocking anticyclones and by accompanying tropopause lifting are associated with blocking zones. The most intensive decrease in ozone concentrations was revealed within the tropopause layer (up to 1.25 mg m^{-2} s^{-1} at a level of 200 hPa). The decrease in ozone concentrations in the lower stratosphere under the conditions of an anomalously long atmospheric blocking over European Russia in the summer of 2010 reached 40%. The south-to-north transport of air flows through the tropopause discontinuity is accompanied by the transport of water vapor from the low-latitude troposphere directly to the high-latitude stratosphere. In this case, the decrease in TOC in the blocking zone is partially associated with the photochemical destruction of ozone in the lower stratosphere in catalytic reactions of the hydrogen cycle. Due to such a TOC decrease and slightly cloudy anticyclonic weather conditions, a significant increase was observed in the daily erythemal doze of UV radiation (up to 20%). During the atmospheric blocking over European Russia in summer 2010, the TOC anomalies in the Northern hemisphere were characterized by a clearly pronounced wave structure caused by the effect of the Rossby stationary planetary wave. This wave originated in the vicinity of the Hawaiian Islands, was characterized by a west-to-east increase in its amplitude, and reached its maximum in the blocking zone over European Russia. The TOC wavelength in the Euro-Atlantic region amounted to 5500–6300 km (wavenumber k=4–5). The relation between daily TOC anomalies over European Russia and daily variations in the North Atlantic Oscillation (NAO) index was studied in [Sitnov et al., 2016, 2017]. An extensive spatial region of negative TOC–NAO correlations reaching extremal values up to -0.55 was revealed over northern European Russia. The results of both correlation and cross-wavelet analyses suggest that a high degree of anticorrelation of TOC anomalies over European Russia with the NAO in summer 2010 was caused by coherent variations in TOC and the NAO index during the destruction of the anomalously long summer blocking anticyclone.

Observational TOC data obtained at the Russian Antarctic stations Mirny (66°34 N, 93°01 E), Novolazarevskaya (70º46 S, 11º50 E), and Vostok (78º38 S, 106º52 E) from 1975 to 2017 were given in [Sibir and Radionov, 2018]. The measurements were performed using M-83/M-124 filter ozonometers. Throughout this period, a steady decrease in TOC was observed in spring. In the early 1990s, at the Mirny station, the average TOC values in September

and October decreased by 70–75% when compared to those for 1975–1980. The effect of the ozone hole and its intensity depend on ODS levels, dynamical processes, and temperature variations in the stratosphere. Considering a slow decrease in ODS concentrations, it was found that changes in the size and depth of the ozone hole depend mainly on variations in both thermal and dynamic processes. Due to the destruction of the stratospheric circumpolar vortex in the early spring of 1988, the spring negative anomaly of the TOC was not formed at all. A sharp increase in stratospheric temperature in the spring of 2002 was accompanied by a TOC increase. It led to a reduction in the size of the "ozone hole" and even its division into two parts at the end of September. Since the early 2000s, there has been a tendency to return the TOC to its values observed in the 1970s and to increase its interannual variability when compared to that for the 1990s. Data on TOC and surface aerosol-gas concentrations measured over the Atlantic and Southern oceans from board the research vessels "Akademik Fedorov" and "Akademik Treshnikov" during 2013-2014 are discussed in [Radionov et al., 2015].

A new method of determining TOC from measurements with an IR FS-2 spectrometer was developed and validated [Гаркуша et al., 2017]. This method made it possible to study in detail time variations in the content of ozone during the formation of mini ozone holes over Russia and, using numerical simulation, to determine the basic mechanisms of their formation in winter and spring 2015-2016 [Timofeyev et al., 2018]. Studies of UV irradiance during this period showed that hazardous levels of UV irradiance of the land surface were observed in spring 2016 in Russia.

A number of papers are devoted to studies of changes in stratospheric NO_2 under the influence of various natural factors on the basis of data obtained from ground-based spectrometric measurements. Long-term column NO_2 measurements carried out at the KHASS in 1981–2008 in morning and evening by direct-sun visible radiation at large solar zenith angles. Results of direct-sun measurements were compared with results of simultaneous zenith-sky NO_2 measurements in 1993–1998 and 2000–2008 at the ZSS. For the trend analysis, a multiple linear regression technique is used [Borovski et al., 2016]. The regression model takes into account a linear trend, solar-activity effects, quasi-biennial oscillation, El Nino-Southern Oscillation as well as the influence of the products of the El Chichon (only for Kislovodsk data) and Pinatubo volcanic eruptions. The interannual evolution of the NO_2 column for Kislovodsk is characterized by its general increase in the 1980s followed by its general decrease during the 1990s and 2000s. Large, statistically significant, trends were observed for the two time intervals. The linear trends are about 1.6% and 1.9% per year for the 1981–1989 period and –1.4% and –0.8% per year for the 1990–2008 period for morning and evening data, respectively. The trends for the

whole observational period are about –1.1% and –0.7% per year. The NO_2 trends for the ZSS are negative and equal to –0.38% per year for the whole observational period from 1990 through March 2016. In [Borovski et al., 2016], it was concluded that the stratospheric NO_2 column in the mid-latitude European sector had a negative trend during the past 2.5 decades.

The winter-spring NO_2 anomalies observed in the Northern Hemisphere during winter and spring 2011 were analyzed in [Ageyeva et al., 2015]. They were accompanied by anomalies in total ozone and stratospheric temperature and were caused by the air transport from the region of the Arctic ozone hole. Vertical NO_2 profiles measured at the ZSS showed that the record negative NO_2 anomaly was in part due to the denitrification of the polar stratosphere in the ozone hole region. It was found that, in general, the correlation of NO_2 column in the moderate and high latitudes of the Northern and Southern hemispheres with total ozone and stratospheric temperature in the winter-spring period depends on the phase of the quasi-biennial oscillation (QBO). Both seasonal and latitudinal distributions of the amplitudes of the QBO effects were obtained in [Ageyeva and Gruzdev, 2017]. Differences in the NO_2 diurnal cycles were identified between the westerly and easterly QBO phases.

Results of spectrometric measurements of NO_2 vertical profiles and microwave measurements of O_3 vertical profiles in the Moscow region were used to analyze the anomalies of the species related to the sudden stratospheric warming (SSW) in early February 2010 and to the latitudinal displacement of the vortex towards the European sector in late March 2011 before the final spring warming [Gruzdev et al., 2016; 2017]. In the former case, the O_3 concentration increased up to 85% and the stratospheric NO_2 column increased twice; in the latter case, the O_3 concentration decreased by a quarter and the NO_2 content decreased twice in comparison with the periods preceding the onsets of the anomalies. A strong anticorrelation of stratospheric NO_2 and O_3 with potential vorticity was obtained.

The effects of major and minor SSWs on stratospheric NO_2 and total ozone in 1958–2015 were studied in [Ageyeva et al., 2017] and [Gruzdev et al., 2018]. The dependence of SSWs on the QBO and the 11-year solar cycle was revealed. Strong negative anomalies of NO_2, O_3, and temperature as a result of major SSW are caused by the displacement of the stratospheric circumpolar vortex aside from the pole. Strong positive anomalies are observed more frequently under SSWs accompanied by polar-vortex splitting and are caused by the transport of stratospheric air from the low latitudes. Major SSWs can lead to significant changes in the vertical profile of NO_2. Changes in different stratospheric layers may be opposite to each other when the edge of the polar vortex is over the site of ground-based observations.

The first experimental evidence of the impact of a solar proton event on stratospheric NO_2 was obtained from ground-based spectrometric measurements in the middle and high latitudes of the Northern hemisphere [Ageyeva et al., 2018]. The solar proton event in October 2003 caused the increase in NO_2 in the upper stratosphere by 0.6×1015 cm^{-2}, which accounted for about one-third of the increase in the NO_2 column content.

Developing observation methods

The network of Brewer fully-automatic spectrophotometers has been operating since the early 1980s and is one of the oldest global systems providing ozone data. The available software to control the operation of the Brewer spectrophotometers was developed more than 35 years ago and it should be replaced because of the termination of the operation life of computer platforms for which this software was developed. A new cross-platform software for Brewer spectrophotometers has been developed at the OIAP RAS [Savinykh and Postylyakov, 2018]. This software may be used in computers with current multitasking operating systems (Windows, Linux, macOS) and, at the same time, with one source code.

Improving the DOAS method for determining the integral content (IC) of formaldehyde (H_2CO) in the PBL and studying the features of its time distribution are in progress. The IC of formaldehyde is retrieved from measurements of the UV spectra of scattered solar radiation. In [Post01], a new version of the method used under clear-sky conditions with improved data quality control was developed. This new version took part in international comparison experiments and showed a valid agreement with results obtained in other groups [Borovski et al., 2015]. Time variations in the IC of H_2CO were estimated from observations under clear-sky conditions at the ZSS and IOA (Tomsk) [Postylyakov et al., 2016; Бручковский et al., 2019]. It was shown that there a statistically significant positive dependence of the IC of formaldehyde on air temperature (at the ZSS, the trend amounts to 0.86 10^{15} molec/cm^2 per °C). The observed positive trend is related to an increase in biogenic emissions of isoprene and other volatile organic ozone precursors with increasing air temperature and increasing areas of both forest and peatbog fires. A stable increase in the IC of formaldehyde is observed in air masses arrived at the ZSS from Moscow. Despite a significant distance from Moscow, the formaldehyde IC values observed at the ZSS are, on the whole, 10% higher than those observed in Tomsk.

The method of determining the H_2CO IC, which is used under conditions of heavy clouds, has first been developed [Postylyakov et al., 2015; 2016]. In order to validate this method, its authors compared between mean H_2CO values observed under heavy clouds and under clear sky for different air masses. The

H_2CO values obtained under heavy clouds are systematically higher than those obtained under clear sky; however, this difference is significantly smaller for background air masses than for polluted Moscow air masses. This difference may be associated with photochemical processes of forming and depleting formaldehyde under conditions of different irradiance.

The development of new instruments to perform measurements using the DOAS method is still in progress [Bruchkouski et al., 2016]. Such a new OIAP spectrometer took part in international experiments on comparison of instruments and methods of measuring NO_2 (September 2016, Netherlands) [Borovski et al., 2017]. All in all, 36 spectral instruments presented by 26 scientific groups were compared. In addition, a spectrometer to perform multi-angle measurements using the DOAS method has been developed in cooperation with Belarusian colleagues. The first results obtained with this instrument from measurements of the vertical distribution of aerosol extinction using the MAX-DOAS method at the Progress Antarctic station are given in [Bruchkouski et al., 2016] .

The method of determining the IC of NO_2 in the troposphere with a high spatial resolution (about 2 km) has first been developed at the OIAP RAS [Postylyakov et al., 2017]. The developed approach uses observational data obtained by the operating system of Russian Resurs-P satellites. The possibility of revealing point pollution sources and determining their location has been demonstrated. The algorithms of reconstructing cloud parameters on the basis of simultaneous shooting of the sky with two digital cameras have also been improved [Чуличков et al., 2016]. The new model takes into account the lens distortions of the third- and fifth orders and makes it possible to obtain more accurate estimates of the height of lower cloud boundaries, wind velocity, and wind direction.

Numerical simulation

The CHIMERE and COSMO-ART chemical transport models were used to study variations in anthropogenic pollutions and to verify model calculations of the concentrations of trace gases [Vil'fand et al., 2017; Shalygina et al., 2016; 2017]. The efficiency of regional adaptation of EMEP emissions was determined [Shalygina et al., 2018]. Active applications of simulations and a complex of conducted studies to verify chemical transport models (CHIMERE, COSMO-ART) have formed the basis for the development of a modern technology to regularly calculate the concentrations of CO, NO_x, PM_{10}, O_3, and other trace gases at the Russian Hydrometeorological Research Center; the concentrations of trace gases and aerosols are calculated due to the assimilation of meteorological data of the COSMO system [Rivin et al., 2018].

The methodology to use satellite data on chemically active atmospheric trace gases – nitrogen dioxide and carbon oxide (NO_2 and CO) – has been developed to estimate carbon dioxide (CO_2) emissions associated with fossil-fuel combustion [Konovalov et al. 2016a]. This methodology is based on the inverse simulation of NO_x and CO emissions using a chemical transport model and the estimation of the conversion of NO_x and CO emissions in the CO_2 emission according to available inventory data. The possibility to obtain estimates of total annual anthropogenic CO_2 emissions in a large industrial region with a relative accuracy of about 10% has been demonstrated.

The atmospheric evolution of smoke aerosol, which is important for climate-forming processes, has been studied based on an analysis of both ground-based and satellite measurements of the atmospheric composition under the extreme conditions of the 2010 and 2012 fires in Russia using a chemical transport model [Konovalov et al., 2015; 2016b; 2017; 2018]. The effects of a significant (approximately twofold) increase in the mass concentration of fine-dispersed aerosol and aerosol optical thickness in smoke plumes of natural fires during their mesoscale transport have been revealed. It is shown that these effects may be determined from a set of both physical and chemical processes with participation of semi-volatile organic compounds (SVOCs). Obtained results suggests that it is very important to take into account processes with participation of SVOCs in estimating and forecasting the aerosol impact on climate, including Arctic thermal-balance variations.

A climatic model developed at the Institute of Numerical Mathematics includes an aerosol block describing the evolution of all basic types of aerosols [Volodin and Kostrykin, 2016]. The model aerosol distribution is taken into account in calculating radiation fluxes that affect the atmospheric gas composition and, in particular, ozone content. Numerical experiments using this model have yielded 10-year variations in aerosol characteristics and atmospheric gas composition.

Both spatial and temporal distributions of isoprene and its oxidation products, methyl vinyl ketone and methacrolein in the Far East of Russia were investigated [Safronov et al., 2019]. Measurement data were obtained from board a mobile laboratory that was moving along the Trans-Siberian railway and from WRF CHEM and GEOS CHEM simulations. It was found that the temporal distribution of measured isoprene is in a good agreement with simulation results. The measured concentrations of isoprene, methyl vinyl ketone (MVK) and methacrolein (MACR) demonstrate pronounced diurnal variations, while the average of the MVK+MACR-to-isoprene ratio does not show a clear diurnal cycle. Furthermore, the sum of MVK and MACR is in good correlation with isoprene (R ~0.60–0.86).

The concept of "odd oxygen" is considered and its atmospheric lifetime is evaluated [Larin, 2016]. It is demonstrated that the modern interpretation of this concept precludes obtaining reliable data on the atmospheric lifetime of odd oxygen, which is of fundamental importance in ozonosphere chemistry. An algorithm for correctly assessing the atmospheric lifetime of odd oxygen is presented and relevant estimates for the end of the XX century are made. It is also shown that, if the lifetime of odd oxygen is comparable to or greater than the time of vertical eddy transport, the former should be replaced by a combined lifetime, taking into account the action of both photochemical and dynamic factors.

The chemical composition of the middle atmosphere and its changes in the 21st century are considered by Larin (2017; 2018). The initial data were obtained from the interactive two-dimensional radiation-chemical model SOCRATES, which calculates the height profiles of components with a resolution of 1 km in the latitudinal zone from 85° S to 85° N, with a step of 5°. The initial conditions were taken to be the Intergovernmental Panel on Climate Change (IPCC) RCP 4.5 scenario for June and January of 2000 and 2100 at a latitude of 50° N. It has been shown that for June 2100, the relative change (in %) in the total content of components in the ClO_x, O_x, BrO_x, NO_x, and HO_x families in the stratosphere, in comparison with June 2000, would be –57.5%, +4.0%, –25.7%, –13.9%, and –4.1%, respectively. For January, the corresponding values for ClO_x, O_x, BrO_x, NO_x, and HO_x are –59.1%, +7.3%, –26.2%, –7.1%, and –3.6%, respectively.

A chemical atmospheric research model (CHARM) is described and results of three-dimensional numerical simulation of the climatological distributions of ozone and other atmospheric trace gases within a height range of 0–90 km are given in [Krivolutsky et al., 2015]. Results obtained from numerical calculations of the effects of variations in solar UV radiation fluxes and ozone depletion in polar regions due to high-energy particles of cosmic origin on the composition of the upper atmosphere are also given. In order to describe the spatial transport of chemically active trace gases in the model (Prather's scheme), the global fields of wind-velocity components and air-temperature fields were calculated using an atmospheric research model (ARM) of general circulation.

Conclusions

In 2015–2018, a team of Russian researchers continued to study atmospheric ozone. Noticeable achievements are associated with studying processes that determine the spatiotemporal variability of ozone and its precursors in the atmosphere over northern Eurasia, the Arctic and Antarctic. Because of the reor-

ganization of the Russian Academy of Sciences, many research teams were faced with difficulties in updating instruments and carrying out regular observations. Therefore, more attention was given to analyzing data obtained earlier and developing new methods of observations. The development of new remote-sensing technologies using ground- and satellite-based spectrophotometers should especially be noted. Distributions of the integral content of NO_2 in the atmospheric boundary layer with a resolution of 2×2 km were first obtained from board a Russian satellite. The methods of measuring the atmospheric contents of ozone and some organic compounds according to scattered solar radiation under cloud conditions were developed, which significantly increased the efficiency of monitoring atmospheric composition. Great expectations are associated with an increase in the state support of young professionals in the area of atmospheric investigations.

References

1. Ageev B.G., Gruzdev A.N., Sapozhnikova V.A. Variations in gas components and total pressure in stem and root disc wood of conifer species. Atmos. Oceanic Optics. 2017. V. 30. No. 2. P. 209–215.

2. Ageev B.G., Gruzgev A.N., Ponomarev Yu.N., Sapozhnikova V.A. Variations of residual CO_2 and pressure in conifer woody roots. Atmospheric and Oceanic Optics. 2018. V. 31. No. 2. P. 146–152.

3. Ageyeva V.Yu. and Gruzdev A.N. Seasonal features of quasi-biennial variations of NO_2 stratospheric content derived from ground-based measurements. Izvestiya, Atmos. Oceanic Phys. 2017. V. 53. No. 1. P. 65–75.

4. Ageyeva V.Yu., Gruzdev A. N., Elokhov A.S., Mokhov I.I., Zueva N.E. Sudden stratospheric warmings: Statistical characteristics and influence on NO_2 and O_3 total contents. Izvestiya, Atmos. Oceanic Phys. 2017. V. 53. No. 5. P. 477–456.

5. Ageyeva V.Yu., Gruzdev A.N., Elokhov A.S. Increase in the stratospheric NO_2 content derived from results of ground-based observations after the October 2003 solar proton event // Doklady Earth Sci. 2018. V. 479. P. 539–542.

6. Ageyeva V.Yu., Gruzdev A.N., Elokhov A.S., Grishaev M.Vol. Winter–spring anomalies in the stratospheric content of NO_2 from ground-based measurement results. Izvestiya, Atmos. Oceanic Phys. 2015. V. 51. No. 4. P. 397–404.

7. Antokhin P. N., Antokhina O. Y., Belan B.D. Vertical ozone flux in background area of Tomsk region. 22nd Intern. Symp. Atmospheric and Ocean Optics: Atmospheric Physics, edited by Gennadii G. Matvienko, Oleg A. Romanovskii, Proceedings of SPIE. V. 10035 (SPIE, Bellingham, WA, 2016). 1003–6G.

8. Antokhin P.N., Antokhina O.Yu., Belan B.D. Estimation of the ozone formation rate in the atmospheric boundary layer over a background region of Western Siberia. Proc. of SPIE. 2015. V. 9680. Article CID Number 3Y. 5 p. Doi:10.1117/12.2205688.

9. Antokhin P.N., Arshinova Vol. G., Arshinov M.Yu., Belan B.D., Belan S.B., Davydov D.K., Ivlev G.A., Fofonov A.V., Kozlov A.V., Paris J.-D., Nedelec P., Rasskazchikova T.M., Savkin D.E., Simonenkov D.V., Sklyadneva T.K., Tolmachev G.N. Distribution of trace gases and aerosols in the troposphere over Siberia during wildfires of summer 2012. J. Geophys. Res.: Atmos. 2018. V. 123, No. 4, P. 2285–2297.

10. Antokhina O.Yu., Antokhin P.N., Arshinova V.G., Arshinov M.Yu., Belan B.D., Belan S.B., Davydov D.K., Dudorova N.V., Ivlev G.A., Kozlov A.V., Rasskazchikova T.M., Savkin D.E., Simonenkov D.V., Sklyadneva T.K., Tolmachev G.N., Fofonov A.Vol. Study of air composition in different air masses. Atmospheric and Oceanic Optics. 2019. V. 32, No. 1. P. 72–79.

11. Antokhina O.Yu., Antokhin P.N., Arshinova V.G., Arshinov M.Yu., Belan B.D., Belan S.B., Belov V.V., Gridnev Yu.V., Davydov D.K., Ivlev G.A., Kozlov A.V., Law K.S., Nédélec Ph., Paris J.-D., Rasskazchikova T.M., Savkin D.E., Simonenkov D.V., Sklyadneva T.K., Tolmachev G.N., Fofonov A.V. Comparison of distributions of atmospheric gas admixture concentrations measured by remote and in situ instruments over the Russian sector of the Arctic. Atmospheric and Oceanic Optics. 2018. V. 31, No. 6. P. 626–634.

12. Antokhina O.Yu., Antokhin P.N., Arshinova Vol. G., Arshinov M.Yu., Belan B.D., Belan S.B., Davydov D.K., Ivlev G.A., Kozlov A.V., Nedelec P., Paris J.-D., Rasskazchikova T.M., Savkin D.E., Simonenkov D.V., Sklyadneva T.K., Tolmachev G.N., Fofonov A.Vol. Vertical Distributions of Gaseous and Aerosol Admixtures in Air Over the Russian Arctic. Atmospheric and Oceanic Optics. 2018. V. 31, No. 3. P. 300–310.

13. Antokhina O.Yu., Belan B.D., Savkin D.E., Tolmachev G.N. Dependence of the surface ozone concentration on the air temperature and conditions of atmospheric circulation in Western Siberia in the warm season (May-September). Proc. of SPIE. 2017. V. 10466. Article CID Number 10466 6H [10466–197]. 11 p. DOI: 10.1117/12.2287736

14. Asmi E., Kondratyev V., Brus D., Laurila T., Lihavainen H., Backman J., Vakkari V., Aurela M., Hatakka J., Viisanen Y., Uttal T., Ivakhov V., and Makshtas A. Aerosol size distribution seasonal characteristics measured in Tiksi, Russian Arctic. Atmos. Chem. Phys. 2016. V. 16, No. 3. P. 1271–1287.

15. Belan B.D., Savkin D.E., Tolmachev G.I. Air-Temperature Dependence of the Ozone Generation Rate in the Surface Air Layer. Atmospheric and Oceanic Optics. 2018. V. 31, No. 2. P. 187–196.

16. Belan B.D., Savkin D.E., Tolmachev G.N. Research of relations of snow cover and concentration of ozone in a ground layer of air near Tomsk. Atmospheric and Oceanic Optics. 2018. Vol. 31, No. 8. P. 665–669. (in Russian)

17. Berchet A., Bousquet P., Pison I., Locatelli R., Chevallier F., Paris J.-D., Dlugokencky E.J., Laurila T., Hatakka J., Viisanen Y., Worthy D.E.J., Nisbet E., Fisher R., France J., Lowry D., Ivakhov V., and Hermansen O. Atmospheric constraints on the methane emissions from the East Siberian Shelf. Atmos. Chem. Phys. 2016. V. 16, No. 6. P. 4147–4157.

18. Berezina E.V., Moiseenko K.B., Skorokhod A.I., Elansky N.F., Belikov I.B. Aromatic volatile organic compounds and their role in ground-level ozone formation in Russia. Doklady Earth Sci. 2017. V. 474, No. 1. P. 599–603.

19. Borovski A., Postylyakov O., Elokhov A., Bruchkouski I. Study of different operational modes of the IAP 2-port-DOAS instrument for atmospheric trace gases investigation during CINDI-2 campaign basing on residual noise analysis // Proc. SPIE. 2017. Vol. 10466. 104662Z-9. DOI: 10.1117/12.2285798

20. Borovski A.N., Dzhola A.V., Grechko E.I., Postylyakov O.V., Ivanov V.A., Kanaya Y. Measurements of formaldehyde total content in troposphere using DOAS technique in Moscow Region. Proc. SPIE. 2015. V. 9680. 96804Q-7, DOI: 10.1117/12.2205933.

21. Borovskii A.N., Arabov A.Ya., Golitsyn G.S., Gruzdev A.N., Elansky N.F., Elokhov A.S., Mokhov I.I., Savinyk V.V., Senik I.A., Timazhev A.B. Variations of Total Nitrogen Oxide Content in the Atmosphere over the North Caucasus. Russ. Meteorol. Hydrol. 2016. V. 41, No. 2. P. 93–103.

22. Bruchkouski I., Borovski A., Elokhov A., Postylyakov O. A layout of two-port DOAS system for investigation of atmospheric trace gases based on laboratory spectrograph. Proc. SPIE. 2016. V. 10035. 100353C-9. DOI:10.1117/12.2248634

23. Bruchkouski I.I., Borovski A.N., Dzhola A.V., Elansky N.F., Postylyakov O.V., Bazhenov O.E., RomanovskiI O.A., Sadovnikov S.A., Kanaya Y. Observations of the formaldehyde integral content in the lower troposphere in urban agglomerations of Moscow and Tomsk using DOAS technique. Optika Atmosfery i Okeana. 2019. V. 32. No. 1. P. 11–19 (in Russian).

24. Burlakov V.D., Dolgii S.I., Nevzorov A.A., Nevzorov A.V., Romanovskii O.A. Retrieval of vertical ozone concentration profiles from the data of lidar sensing. Russ. Phys. J. 2015. V. 58, No. 8. P. 1111–1117.

25. Chen L., Zhang M., Zhu J., Skorokhod A. Model analysis of soil dust impacts on the boundary layer meteorology and air quality over East Asia in April 2015. Atmos. Res. 2017. V. 187. P. 42–56.

26. Chen L., Zhang M., Zhu J., Wang Y., Skorokhod A. Modeling Impacts of Urbanization and Urban Heat Island Mitigation on Boundary Layer Meteorology and Air Quality in Beijing Under Different Weather Conditions. J. Geophys. Res.: Atmos. 2018. V. 123, No. 8. P. 4323–4344.

27. Chulichkov A.I., Andreev M.S., Golitsyn G.S., Elansky N.F., Medvedev A.P., Postylyakov O.Vol. On Cloud Bottom Boundary Determination By Digital Stereo Photography From The Earth's Surface. Atmospheric and Oceanic Optics. 2017. V. 30, No. 2. P. 184–190.

28. Chulichkov A.I., Nikitin S.V., Emilenko A.S., Medvedev A.P., Postylyakov O.Vol. Selection of optical model of stereophotography experiment for determination the cloud base height as a problem of testing of statistical hypotheses. Proc. SPIE. 2017. Vol. 10424. 1042411-11. DOI: 10.1117/12.2279553

29. Davydov D.K., Belan B.D., Antokhin P.N., Antokhina O.Yu., Antonovich V.V., Arshinova V.G., Arshinov M.Yu., Akhlestin A.Yu., Belan S.B., Dudorova N.V., Ivlev G.A., Kozlov A.V., Pestunov D.A., Rasskazchikova T.M., Savkin D.E., Simonenkov D.V., Sklyadneva T.K., Tolmachev G.N., Fazliev A.Z., Fofonov A.Vol. Monitoring of atmospheric parameters: 25 years of the IOA SB RAS TOR station. Atmospheric and Oceanic Optics. 2018. V. 31, No. 10. P. 845–853. (in Russian).

30. Dolgii S.I., Nevzorov A.A., Nevzorov A.V., Romanovskii O.A., Kharchenko O.V. Lidar differential absorption system for measuring ozone in the upper troposphere-stratosphere. J. Appl Spectrosc, 2019. DOI: https://doi.org/10.1007/s10812-019-00767-8.

31. Dolgii S.I., Nevzorov A.A., Nevzorov A.V., Makeev A.P., Romanovskii O.A., Kharchenko O.V. Lidar complex for measurement of vertical ozone distribution in the upper troposphere-stratosphere. Atmospheric and Oceanic Optics. 2018. V. 31, No. 6, P. 1–7.

32. Dolgii S.I., Nevzorov A.A., Nevzorov A.V., Romanovskii O.A. and Kharchenko O.Vol. Intercomparison of ozone vertical profile measurements by differential absorption lidar and IASI/MetOp satellite in the upper troposphere–lower stratosphere. Remote Sensing. 2017. V. 9, No. 5. P. 447. DOI:10.3390/rs9050447.

33. Dorokhov V., Yushkov V., Makshtas A., Ivlev G., Tereb N., Savinykh V., Shepelev D., Nakajima H., McElroy C.T., Tarasick D., Goutail F., Pommereau J.-P., Pazmino A. Brewer, SAOZ and ozonesonde observations in Siberia. Atmos.-Ocean. 2015. V. 53, No. 1. P. 14–18.

34. Dorokhov V., Yushkov V., Makshtas A., Ivlev G., Tereb N., Savinykh V., Shepelev D., Nakajima H., McElroy C.T., Tarasick D., Goutail F., Pommereau J.-P., Pazmino A. Brewer, SAOZ and ozonesonde observations in Siberia. Atmos.-Ocean. 2015. V. 53. No. 1. P. 14–18.

35. Elansky N.F. Russian Studies of Atmospheric Ozone in 2011–2014. Izvestiya, Atmospheric and Oceanic Physics. 2016. V. 52, No. 2. P. 132–146.

36. Elansky N.F., Lavrova O.V., Skorokhod A.I., Belikov I.B. Trace gases in the atmosphere over Russian cities. Atmos. Environ. 2016. V. 143. P. 108–119. Elansky N.F., Lokoshchenko M.A., Trifanova A.V., Belikov I.B., and Skorokhod A.I. On Contents of Trace Gases in the Atmospheric Surface Layer over Moscow. Izvestiya, Atmos. Oceanic Phys. 2015. V. 51, No. 1. P. 30–41.

37. Elansky, N.F., Ponomarev, N.A., Verevkin, Y.M. Air quality and pollutant emissions in the Moscow megacity in 2005–2014. Atmos. Environ. 2018. V. 175. P. 154–164.

38. Elansky N.F., R.D. Kouznetsov, Y.M. Verevkin, N.A. Ponomarev, V.S. Rakitin, A.V. Shilkin, E.G. Semutnikova, P.V. Zakharova. Time variations in the concentration of pollutants in the atmosphere over Moscow and estimation of their emissions. Turbulence, Atmosphere and Climate. Dynamics. IOP Conf. Series: Earth and Environmental Science 231 (2019) 012014. IOP Publishing. doi:10.1088/1755-1315/231/1/012014.

39. Garkusha A.S., Polyakov A.V., Timofeev Y.M., Virolainen Y.A. Determination of the total ozone content from data of satellite ir Fourier-spectrometer. Izvestiya. Atmospheric and Oceanic Physics. 2017. Vol. 53, No. 4. P. 433–440.

40. Golitsyn G.S., Grechko E.I., Wang Gengchen, Wang Pucai, Dzhola A.V., Emilenko A.S., Kopeikin V.M., Rakitin V.S., Safronov A.N., Fokeeva E.Vol. Studying the pollution of Moscow and Beijing atmospheres with carbon monoxide and aerosol. Izvestiya, Atmospheric and Oceanic Physics. 2015. Vol. 51. Issue 1. PP. 1–11.

41. Gruzdev A.N. and Isakov A.A. On the nature of long-period variations in mass concentration of near-ground aerosol. Atmos. Oceanic Optics. 2016. Vol. 29. No. 1. P. 73–78.

42. Gruzdev A.N., Kropotkina E.P., Solomonov S.V., Elokhov A.S. Anomalies of the ozone and nitrogen dioxide contents in the stratosphere over Moscow region as a manifestation of the dynamics of the stratospheric polar vortex. Doklady Earth Sciences. 2016. Vol. 468. Pt. 2. P. 602–606.

43. Gubanova D.P., Belikov I.B, Elansky N.Ph., Skorokhod A.I., Chubarova N.E. Variations in PM2.5 Surface Concentration in Moscow according to Observations at MSU Meteorological Observatory. Atmospheric and Oceanic Optics. 2018. Vol. 31, No. 3. P. 290–299. Han X., Zhang M., Skorokhod A., Kou X. Modeling dry deposition of reactive nitrogen in China with RAMS-CMAQ. Atmospheric Environment. 2017. V. 166. P. 47–61.

44. Ionov D.V., Poberovskii A.V., Ionov D.V. Spectroscopic Remote Sensing of NO2 Levels in Urban Air. Journal of Applied Spectroscopy. 2017. Vol. 84, No. 1. P. 109–113.

45. Ionov D.V., Poberovskii A.Vol. Integral emission of nitrogen oxides from the territory of St. Petersburg based on the data of mobile measurements and numerical simulation results. Izvestiya. Atmospheric and Oceanic Physics. 2017. Vol. 53, No. 2. P. 204–212. Ionov D.V., Timofeyev Y.M., Poberovskii A.Vol. Spectroscopic measurements of O3 and NO2 atmospheric content: correction of ground-based method and comparison with satellite data. Atmospheric and Oceanic Optics. 2015. Vol. 28, No. 6. P. 526–532.

46. Ivanov V., Borovski A., Postylyakov O. First comparison of formaldehyde integral contents in ABL retrieved during clear-sky and overcast conditions by ZDOAS technique. Proc. SPIE. 2017. Vol. 10424. 104240O-9. DOI: 10.1117/12.2278235.

47. Ivanova N.S., Kuznetsova I.N., K.A. Sumerova. Anomalies of atmospheric ozone in February-March, 2018. Proceedings of the Hydrometcentre of Russia. 2018. Vol. 370. P. 36–47. ISSN 2618-9631.

48. Ivanova N.S. Comparison of surface and satellite measurements of total ozone. Proc. of the Hydrometcentre of Russia. 2017. V. 365. P. 94–100. ISSN 2618-9631.

49. Ivanova N.S. The empirical model for calculating the UV index. Proc. of the Hydrometcentre of Russia. 2017. Vol. 365. P. 119–127. ISSN 2618-9631.

50. Khuriganova O., Obolkin V., Akimoto H., Ohizumi T., Khodzher T., Potemkin V. and Golobokova L. Long-Term Dynamics of Ozone in Surface Atmosphere at Remote Mountain, Rural and Urban Sites of South-East Siberia, Russia. Open Access Library J. 2016. 3: e2578. DOI: http://dx.doi.org/10.4236/oalib.1102578

51. Konovalov I.B., Beekmann M., Berezin E.V., Formenti P., Andreae M.O. Probing into the aging dynamics of biomass burning aerosol by using satellite measurements of aerosol optical depth and carbon monoxide. Atmos. Chem. Phys. 2017. Vol. 17. P. 4513–4537.

52. Konovalov I.B., Beekmann M., Berezin E.V., Petetin H., Mielonen T., Kuznetsova I.N., Andreae M.O. The role of semi-volatile organic compounds in the mesoscale evolution of biomass burning aerosol: a modeling case study of the 2010 mega-fire event in Russia. Atmos. Chem. Phys. 2015. Vol. 15. P. 13269–13297.

53. Konovalov I.B., Berezin E.V., Beekmann M. Effect of photochemical self-action of carbon-containing aerosol: wildfires. Izv. Atmos. Oceanic Phys. 2016b. Vol. 52. P. 263–270.

54. Konovalov I.B., Berezin E.V., Beekmann M., Petetin H., Mielonen T., Kuznetsova I.N., Andreae M.O. The role of semi-volatile organic compounds in the mesoscale evolution of biomass burning aerosol: a modeling case study of the 2010 mega-fire event in Russia. Atmos. Chem. Phys. 2015. Vol. 15, No. 23. P. 13269–13297.

55. Konovalov I.B., Berezin E.V., Ciais P., Broquet G., Zhuravlev R.V., Janssens-Maenhout G. Estimation of fossil-fuel CO_2 emissions using satellite measurements of "proxy" species // Atmos. Chem. Phys. 2016a. Vol. 16. P. 13509–13540.

56. Konovalov I.B., Lvova D.A., Beekmann M. Estimation of the elemental to organic carbon ratio in biomass burning aerosol using AERONET retrievals. Atmosphere. 2017. V. 8. 122, DOI: 10.3390/atmos8070122.

57. Konovalov I.B., Lvova D.A., Beekmann M., Jethva H., Mikhailov E.F., Paris J.-D., Belan B.D., Kozlov V.S., Ciais P., Andreae M.O. Estimation of black carbon emissions from Siberian fires using satellite observations of absorption and extinction optical depths. Atmos. Chem. Phys. 2018. V. 18. P. 14889–14924.

58. Korshunov V.A., Zubachev D.S. Temporal Variations in the Vertical Distribution of Stratospheric Ozone over Obninsk from Lidar Data. Russ. Meteorol. Hydrol. 2018. V. 43, No.3. P. 168–177.

59. Kozhevnikov V.N. Elansky N.F., Moiseenko K.B. Mountain wave-induced variations of ozone and total nitrogen dioxide contents over the Subpolar Urals. Doklady Earth Sci. 2017. V. 475, No. 2. P. 958–962.

60. Lappalainen, H.K., Kerminen, V.-M., Petäjä, T., Kurten, T., Baklanov, A., Shvidenko, A., Bäck, J., Vihma, T., Alekseychik, P., Arnold, S., Arshinov, M., Asmi, E., Belan, B., Bobylev, L., Chalov, S., Cheng, Y., Chubarova, N., de Leeuw, G., Ding, A., Dobrolyubov, S., Dubtsov, S., Dyukarev, E., Elansky, N., Eleftheriadis, K., Esau, I., Filatov, N., Flint, M., Fu, C., Glezer, O., Gliko, A., Heimann, M., Holtslag, A. A.M., Hõrrak, U., Janhunen, J., Juhola, S., Järvi, L., Järvinen, H., Kanukhina, A., Konstantinov, P., Kotlyakov, V., Kieloaho, A.-J., Komarov, A. S., Kujansuu, J., Kukkonen, I., Kyrö, E., Laaksonen, A., Laurila, T., Lihavainen, H., Lisitzin, A., Mahura, A., Makshtas, A., Mareev, E., Mazon, S., Matishov, D., Melnikov, V., Mikhailov, E., Moisseev, D., Nigmatulin, R., Noe, S. M., Ojala, A., Pihlatie, M., Popovicheva, O., Pumpanen, J., Regerand, T., Repina, I., Shcherbinin, A., Shevchenko, V., Sipilä, M., Skorokhod, A., Spracklen, D. V., Su, H., Subetto, D. A., Sun, J., Terzhevik, A. Y., Timofeyev, Y., Troitskaya, Y., Tynkkynen, V.-P., Kharuk, Vol. I., Zaytseva, N., Zhang, J., Viisanen, Y., Vesala, T., Hari, P., Hansson, H. C., Matvienko, G. G., Kasimov, N. S., Guo, H., Bondur, V., Zilitinkevich, S., and Kulmala, M.: Pan-Eurasian Experiment (PEEX): Towards holistic understanding of the feedbacks and interactions in the land–atmosphere–ocean–society continuum in the Northern Eurasian region. Atmos. Chem. Phys. 2016. V. 16, No. 22. P. 14421–14461.

61. Larin I.K. Odd Oxygen and its Atmospheric Lifetime // Russian Journal of Physical Chemistry B. 2017. V. 11. No. 2. P. 375–379.

62. Larin I.K. On the reovery of the ozone layer in the Northern Hemisphere in the XXI century. Russ. J. Phys. Chem. B. 2015. V. 9. No. 1. P. 157–162.

63. Larin I.K. The chemical composition of the middle atmosphere and its change in the XXI century. Russ. J. Phys. Chem. B. 2018. V. 12. No. 6. P. 1–5.

64. Larin I.K. Contribution of O_X, HO_X, NO_X, ClO_X, and BrO_X cycles to the destruction of stratospheric ozone in the 21st century. Russ. J. Phys. Chem. B. 2017. V. 11. No. 1. P. 189–194.

65. Larin I.K. Unresolved problems in the chemistry of the middle atmosphere. Russ. J. Phys. Chem. B. 2018. V. 12. No. 4. P. 791–796.

66. Makukhin V.L., Obolkin V.A., Potemkin V.L., Latysheva I.V., Khodzher T.V. Estimation of minor gaseous admixtures spatial distribution over the Lake Baikal water area in summer period by the use of field measurements and mathematical simulation. J. “Izvestia Irkutskogo Gosudarstvennogo Universiteta” (“The Bulletin of Irkutsk State University”). Ser. “Nauki o Zemle” (Ser. “Earth Sciences”). 2016. V. 18. P. 69–80. (in Russian).

67. Moiseenko K.B., Shtabkin Yu.A., Berezina E.V., Skorokhod A.I. Regional photochemical surface-ozone sources in Europe and Western Siberia. Izvestiya, Atmos. Oceanic Phys. 2018. V. 54, No. 6. P. 545–557.

68. Nahaev M.I., Berezin E.V., Shalygina I.Yu., Kuznetsova I.N., Konovalov I.B., Blinov D.V., Lesina E.A. Pilot calculations of PM_{10} and CO concentrations with com-

plex models CHIMERE and COSMO-Ru7**.** Atmospheric and Oceanic Optics. 2015. V. 28, No. 6. P. 569–578.

69. Nevzorov A.A., Burlakov V.D., Dolgii S.I., Nevzorov A.V., RomanovskiI O.A., Kharchenko O.V., Gridnev Yu.Vol. Comparison of lidar and satellite measurements of vertical ozone profiles using data received in 2015 // Atmospheric and Oceanic Optics. 2016. V. 29, No. 8. P. 703–708 (in Russian).

70. Nikiforova M.P., Zvyagintsev A.M., Vargin P.N., Ivanova N.S., Lukyanov A.N., Kuznetsova I.N. Anomalously low total ozone levels over the Northern Urals and Siberia in late January 2016. Atmospheric and oceanic optics. 2017. V. 30, No. 3. P. 255–262.

71. Nikiforova M.P., Vargin P.N., Zvyagintsev A.M. Ozone Anomalies over Russia in Winter and Spring of 2015/2016. Russ. Meteorol. Hydrol. 2019. V. 44, No. 1. P. 36–49. (in Russian).

72. Obolkin V., Khodzher T., Sorokovikova L., Tomberg I., Netsvetaeva O. & Golobokova L. Effect of long-range transport of sulphur and nitrogen oxides from large coal power plants on acidification of river waters in the Baikal region, East Siberia. Intern. J. Environ. Studies. 2016. V. 73, No. 3. P. 452–461.

73. Obolkin V.A., Maysyuk E.P., Ivanova I.Yu., Khodzher T.V. Nitrogen oxides in the atmosphere of coastal areas of Lake Baikal: sources and possible impact on the ecosystem of the lake. Proc. of SPIE. 2018. V. 10833. 108336. DOI:10.1117/12.2505770

74. Obolkin V.A., Potemkin V.L., Makukhin V.L., Khodzher T.V., and Chipanina E.V. Long-range transport of plumes of atmospheric emissions from regional coal power plants to the South Baikal water basin. Atmospheric and Oceanic Optics. 2017. V. 30, No. 4. P. 360–365.

75. Pankratova N., Skorokhod A., Belikov I., Elansky N., Rakitin V., Shtabkin Y., Berezina E. Evidence of atmospheric response to methane emissions from the East Siberian Arctic shelf. Geography, Environment, Sustainability. 2018. V. 11, No. 1. P. 85–92.

76. Postylyakov O. Borovski A., Ivanov V.. On determination of formaldehyde content in atmospheric boundary layer for overcast using DOAS technique. Proc. SPIE, 2015, V. 9680, 96804O–10, doi: 10.1117/12.2205925.

77. Postylyakov O.V., Borovski A.N., Ivanov V.A., Dzhola A.V., Elokhov A.S., Grechko E.I., Kanaya Y. Formaldehyde integral content in troposphere of Moscow Region: preliminary results of 6 years of measurements using DOAS technique. Proc. SPIE. 2016. V. 10035. 100353A-8. DOI:10.1117/12.2248630

78. Postylyakov O.V., Borovski A.N., Makarenkov A.A. First experiment on retrieval of tropospheric NO_2 over polluted areas with 2.4-km spatial resolution basing on satellite spectral measurements. Proc. SPIE. 2017. Vol. 10466. 104662Y-8. DOI: 10.1117/12.2285794

79. Radionov V.F., Kabanov D.M., Polkin V.V., Savkin D.E., Sakerin S.M., Sibir E.E. Variability of characteristics of aerosol and gas composition of the atmosphere along the routes of RVs “Akademik Fedorov” and “Akademik Treshnikov” in period of 59th Russian Antarctic expedition. Problemy Arktiki i Antarktiki. Arctic and Antarctic Research. 2015, V. 106. No. 4. P. 5–19. (in Russian). http://www.aari.ru /misc/publicat/paa/PAA-106/PAA-106_Page_05–19.pdf

80. Rakitin V.S., Elansky N.F., Pankratova N.V., Skorokhod A.I., Dzhola A.V., Shtabkin Yu.A., Wan P., Wan G., Vasilieva A.V., Makarova M.V., Grechko E.I. Study of trends of total CO and CH4 contents over Eurasia through analysis of ground-based

and satellite spectroscopic measurements. Atmospheric and Oceanic Optics. 2017. V. 30, No. 6. P. 517–526.

81. Rakitin V.S., Elansky N.F., Wang P., Wang G., Pankratova N.V., Shtabkin Yu.A., Skorokhod A.I., Safronov A.N., Makarova M.V., Grechko E.I. Changes in trends of atmospheric composition over urban and background regions of Eurasia: Estimates based on spectroscopic observations. Geography, Environment, Sustainability. 2018. V.11, No. 2, P. 84–96.

82. Rakitin V.S., Shtabkin Yu.A., Elansky N.F., Pankratova N.V., Skorokhod A.I., Grechko E.I., Safronov A.N. Comparison results of satellite and ground-based spectroscopic measurements of CO, CH4, and CO2 total contents. Atmospheric and Oceanic Optics. 2015. V. 28, No. 6. P. 533–542.

83. Rivin G.S., Rozinkina I.A., Vilfand R.M., Astakhova E.D., Blinov D.V., Kirsanov A.A., Kuzmina E.V., Olchev A.V.3, Surkova G.V., Shatunova M.V., Chubarova N.E., Chumakov M.M., Alferov D.Yu., Bundel A.Yu., Kopeikin V.V., Nikitin M.A., Poliukhov A.A., Revokatova A.P., Tatarinovich E.V., Churyulin E.Vol. COSMO-Ru: operational mesoscale numerical weather prediction system of the Hydrometcenter of Russia. Current status and recent developments. Research Activities in Atmospheric and Oceanic Modelling. 2018. V. 18, No. 15. P. 5.11–5.12.

84. Rubinshtein K.G., Safronov A.N., Pripachkin D.A., Ignatov R.Yu., Emelina S.V., Nabokova E.V., Kurbatova M.M., Blagodatskikh D.V., Arutyunyan R.V., Sorokovikova O.S., and Semenov V.N. Comparison of the results of 85Kr transport modeling with the ACURATE field experiment data. Russ. Meteorol. Hydrol. 2017. V. 42. No. 3. P. 168B180, DOI:10.3103/S1068373917030049

85. Safatov A.S., Agafonov A.P., Arshinov M.Yu., Baklanov A.M., Belan B.D., Buryak G.A., Fofonov A.V., Generalov V.M., Kozlov A.S., Lapteva N.A., Malyshkin S.B., Marchenko Yu.V., Olkin S.E., Reznikova I.K., Sergeev A.N., Simonenkov D.V., Ternovoi V.A., Tumanov Yu.V., Shmargunov V.P. Complex assessment of atmospheric air quality in the city of Gelendzhik. Atmospheric and Oceanic Optics. 2018. V. 31, No. 5, P. 519–531.

86. Safronov A.N., Elansky N.F., Skorokhod A.I. Detection of atmospheric pollution sources by using cross-plume scanning method and mobile railway laboratory. Geography, Environment, Sustainability. 2018. V.11. No. 3. P. 71–82.

87. Savinykh V.V., Borovski A.N., Postylyakov, O.V., Dormidontov, D.Vol. Cross-platform software to continue long-term observations with the Brewer spectrophotometer in the face of changing computer platforms: Implementing the Model-View architecture. Proc. SPIE. 2018. Vol. 10833. 1083363. P. 1–9. DOI: 10.1117/12.2504611.

88. Savinykh V.V., Postylyakov O.Vol. Implementing the Model/View architecture in software of Brewer Network Spectrophotometer for long-term monitoring of UV radiation and ozone atmospheric content. IOP Conf. Ser.: Earth Environ. Sci. 2019. V. 231. 012045. DOI: 10.1088/1755-1315/231/1/012045

89. Savinykh V.V., Postylyakov O.V. On development of cross-platform software to continue long-term observations with the Brewer Ozone Spectrophotometer. Proc. SPIE. 2018. Remote Sensing of Clouds and the Atmosphere XXIII. Vol. 10786. 107860V-12. DOI: 10.1117/12.2515121.

90. Savinykh V.V., Skornyakov Vol. Yu. New cross-platform control software for Brewer spectrophotometer // Proc. SPIE. 2016. Vol. 10035. 100355P. P. 1–6. DOI: 10.1117/12.2248536.

91. Shalygina I.Yu., Kuznetsova I.N., Nahaev M.I., Konovalov I.B., Berezin E.Vol. Diurnal cycle of air pollutants on measurements and calculations of chemical transport model. Proc. of the Hydrometcentre of Russia. 2016. V. 360. P. 149–167.

92. Shalygina I.Yu., Nahaev M.I., Kuznetsova I.N., Berezin E.V., Konovalov I.B., Blinov D.V., Kirsanov A.A. Comparison of the ground concentration of the polluting substances calculated by means of CTM with data of measurements in the Moscow region**.** Atmospheric and Oceanic Optics. 2017. V. 30, No. 1. P. 53–59.

93. Shalygina I.Yu., Nahaev M.I., Kuznetsova I.N., Konovalov I.B., Zakharova P.Vol. Regional adaptation of the EMEP emission calculations for chemical transport CHIMERE model. Proc. of the Hydrometcentre of Russia. 2018. V. 369. P. 33–45.

94. Shtabkin Y.A., Moiseenko K.B., Skorokhod A.I., Vasileva A.V., Heimann M. Sources of and variations in tropospheric CO in Central Siberia: Numerical experiments and observations at the Zotino Tall Tower Observatory. Izvestiya, Atmos. Oceanic Phys. 2016. V. 52, No. 1. P. 45–56.

95. Shukurov K.A., Borovski A.N., Postylyakov O.V., Dzhola A.V., Grechko E.I., Kanaya Y. Potential sources of tropospheric nitrogen dioxide for Western Moscow Region, Russia. Proc. SPIE. 2018. V. 10833. P. 108337N-7. DOI: 10.1117/12.2504138

96. Sibir E.E., Radionov V.F. Total ozone variations at Russian Antarctic stations. results of long-term observations. Problemy Arktiki i Antarktiki. Arctic and Antarctic Research. 2018. Vol. 64, No. 3. P. 250–261. (in Russian). http://www.aari.ru/misc/publicat/paa/PAA-64/PAA_64_250-261.pdf

97. Sitnov S.A., Mokhov I.I. Ozone mini-hole formation under prolonged blocking anticyclone conditions in the atmosphere over European Russia in summer 2010. Doklady Earth Sci. 2015. V. 460. P. 1. P. 41–45.

98. Sitnov S.A., Mokhov I.I. Satellite-derived peculiarities of total ozone field under atmospheric blocking conditions over the European part of Russia in summer 2010. Russ. Meteorol. Hydrol. 2016. V. 41. No. 1. P. 28–36.

99. Sitnov S.A., Mokhov I.I. Spatial distribution of total column ozone and total column water vapor over European Russia during the spring and summer atmospheric blocks in 2010. Proc. of SPIE. 2015. Vol. 9680. No. 968059. P. 1–6. DOI: 10.1117/12.2197503.

100. Sitnov S.A., Mokhov I.I. Variations in atmospheric composition over Northern Eurasia regions under weather and climate anomalies associated with atmospheric blocking events // IOP Conf. Series: Earth Environ. Sci. 2019. V. 231. 012049.

101. Sitnov S.A., Mokhov I.I. Vortex activity and the anomalies of atmospheric composition // In “Intense atmospheric vortices and their dynamics”. Eds. I.I. Mokhov, M.Vol. Kurgansky, O.G. Chkhetiani. Moscow: GEOS, 2018. 482 p. (in Russian).

102. Sitnov S.A., Mokhov I.I., Bezverkhny V.A. Connections of precipitable water vapor and total ozone anomalies over European Russia with the North Atlantic Oscillation: specific features of summer 2010. Izvestiya. Atmos. Oceanic Phys. 2017. V. 53. No. 9. P. 885–893.

103. Sitnov S.A., Mokhov I.I., Bezverkhny V.A. Analysis of the connections between total column ozone and precipitable water vapor over European Russia with the North Atlantic Oscillation in the summer of 2010. Atmospheric and Oceanic Optics. 2016. V. 29. No. 6. P. 457–461 (in Russian).

104. Sitnov S.A., Mokhov I.I., Lupo A.R. Ozone, water vapor, and temperature anomalies associated with atmospheric blocking events over Eastern Europe in spring – summer 2010. Atmos. Environ. 2017. V. 164. P. 180–194.

105. Sklyadneva T.K., Ivlev G.A., Belan B.D., Arshinov M.Yu., Simonenkov D.Vol. The radiation regime of Tomsk in conditions of a smoky haze. Atmospheric and Oceanic Optics. 2015. V. 28, No. 3. P. 215–222. (in Russian).

106. Skorokhod A.I., Berezina E.V., Moiseenko K.B., Elansky N.F., Belikov I.B. Benzene and Toluene in the surface air of North Eurasia from TROICA-12 campaign along the Trans-Siberian railway. Atmos. Chem. Phys. 2017. Vol. 17, No. 8. P. 5501–5514.

107. Skorokhod A.I., Elansky N.F., Safronov A.N., Eremina I.D., Pankratova N.V., and Chubarova N.E. The Impact of the April 2010 Eyjafjallajokull Eruption on the Atmosphere Composition in Moscow. J. Volcanol. Seismol. 2016. V. 10. No. 4. P. 263–274.

108. Skorokhod A.I., Pankratova N.V., Belikov I.B., Golitsyn G.S., Thompson R.L., Novigatsky A.N. Observations of atmospheric methane and its stable isotope ratio (δ13C) over the Russian Arctic seas from ship cruises in the summer and autumn of 2015. Doklady Earth Sci. 2016. V. 470, No. 2. P. 1081–1085.

109. Timofeyev Y.M., Smyshlyaev S.P., Virolainen Y.A., Garkusha A.S., Polyakov A.V., Motsakov M.A., and Kirner O. Case study of ozone anomalies over northern Russia in the 2015/2016 winter: Measurements and numerical modeling. Ann. Geophys. 2018. V. 36, No. 6. P. 1495–1505.

110. Trifonova-Yakovleva A.M., Gromov S.A., Gromov S.S., Khodzher T.V., Potemkin V.L., Obolkin V.A. On the possibility of using the GOME-2 high resolution ozone profiles for assessment of near-surface ozone concentrations. Sovremennye problemy distantsionnogo zondirovaniya Zemli iz kosmosa. 2017. V. 14. № 5. P. 239–247. (in Russian).

111. Uttal T. et al. International Arctic Systems for Observing the Atmosphere: An International Polar Year Legacy Consortium. Bull. Am. Meteorol. Soc. 2016. V. 97, No. 6. P. 1033–1056.

112. Vargin P. Stratosphere-troposphere dynamical coupling over boreal extratropics during sudden stratospheric warming in Arctic in January-February 2017. Russ. Meteorol. Hydrol. 2018. V. 43, No. 5. P. 277–287.

113. Vargin P.N., Kirushov B.M. Major sudden stratospheric warming in February 2018 and its impacts on troposphere, mesosphere and ozone layer. Russ. Meteorol. Hydrol. 2019. V. 44, No. 2. P. 41–56. (in Russian).

114. Vasileva A., Moiseenko K., Skorokhod A., Belikov I., Kopeikin V., Lavrova O. Emission ratios of trace gases and particles for Siberian forest fires on the basis of mobile ground observations. Atmos. Chem. Phys. 2017. V. 17. P. 12303–12325.

115. Vil'fand R.M., Kirsanov A.A., Revokatova A.P., Rivin G.S., Surkova G.Vol. Forecasting the Transport and Transformation of Atmospheric Pollutants with the COSMO-ART Model. Russ. Meteorol. Hydrol. 2017. No. 5. P. 292–298.

116. Virolainen Y.A., Timofeev Y.M., Poberovskii A.V., Eremenko M., Dufour G. Evaluation of ozone content in different atmospheric layers using ground-based fourier transform spectrometry. Izvestiya. Atmos. Oceanic Phys. 2015. V. 51, No. 2. P. 167–176.

117. Visheratin K.N. Quasidecadal variations in total ozone content, wind velocity, temperature, and geopotential height over the Arosa Station (Switzerland). Izvestiya, Atmos. Oceanic Phys. 2016a. V. 52. No. 1. P. 66–73.

118. Visheratin K.N. Spatio-temporal variability of the phase of total ozone quasi-decennial oscillations. Izvestiya, Atmos. Oceanic Phys. 2017a. V. 53. No. 9. P. 904–910.

119. Visheratin K.N., Kalashnik M.Vol. Quasidecadal variations of lower stratosphere meteorological parameters and total ozone global fields based on satellite data. Izvestiya, Atmos. Oceanic Phys. 2018. V. 54. No. 9. P. 1068–1075.

120. Visheratin K.N., Kuznetzov V.Vol. Basic characteristics of total ozone global field variability from merged databases comparison. Sovremennye problemy distantsionnogo zondirovaniya Zemli iz kosmosa. 2016b. V. 13. № 3. P. 165–172. (in Russian).

121. Visheratin K.N., Nerushev A.F., Orozaliev M.D., Zheng X., Sun S., Liu L. Temporal variability of total ozone in the Asian region inferred from ground-based and satellite measurement data. Izvestiya, Atmos. Oceanic Phys. 2017b. V. 53. No. 9, P. 894–903.

122. Wang P., Elansky N.F., Timofeev Yu.M., Wang G., Golitsyn G.S., Makarova M.V., Rakitin V.S., Shtabkin Yu.A., Skorokhod A.I., Grechko E.I., Fokeeva E.V., Safronov A.N., Ran L., Wang T. Long-term trends of carbon monoxide total columnar amount in urban areas and background regions: ground- and satellite-based spectroscopic measurements. Adv. Atmos. Sci. 2018. V. 35, No. 7. P. 785–795.

123. Zerefos C.S., Eleftheratos K., Kapsomenakis J., Solomos S., Inness A., Balis D., Redondas A., Eskes H., Allaart M., Amiridis V., Dahlback A., De Bock V., Diémoz H., Engelmann R., Eriksen P., Fioletov V., Gröbner J., Heikkilä A., Petropavlovskikh I., Jarosławski J., Josefsson W., Karppinen T., Köhler U., Meleti C., Repapis C., Rimmer J., Savinykh V., Shirotov V., Siani A.M., Smedley A.R.D., Stanek M., Stübi R. Detecting volcanic sulfur dioxide plumes in the Northern Hemisphere using the Brewer spectrophotometers, other networks, and satellite observations. Atmos. Chem. Phys. 2017. V. 17, No. 1. P. 551–574.

124. Zubachev D.S., Korshunov V.A., Tereb N.V. Concentration of Stratospheric Ozone Derived from Lidar, Satellite, and Surface Observations. Russ. Meteorol. Hydrol. 2018. V. 43, No. 7. P. 488–493.

125. Zvyagintsev A.M., Ivanova N.S., Kruchenitskii G.M., Kuznetsova I.N., Lapchenko V.A. Ozone content over the Russian Federation in 2014. Russ. Meteorol. Hydrol. 2015. V. 40, No. 2. P. 141–145.

126. Zvyagintsev A.M., Ivanova N.S., Kruchenitskii G.M., Kuznetsova I.N., Lapchenko V.A. Ozone content over The Russian Federation in 2015. Russ. Meteorol. Hydrol. 2016. V. 41, No. 2. P. 151–156.

127. Zvyagintsev A.M., Ivanova N.S., Kruchenitskii G.M., Kuznetsova I.N., Lapchenko V.A. Ozone content over the Russian Federation in 2017. Russ. Meteorol. Hydrol. 2018. V. 43, No. 2. P. 138–144.

128. Zvyagintsev A.M., Vargin P.N., Peshin S. Total Ozone Variations and Trends during the Period 1979–2014. Atmospheric and Oceanic Optics. 2015. V. 28, No. 6. P. 575–584.

Planetary Atmospheres

O.I. Korablev
Space Research Institute RAS
korab@iki.rssi.ru

Introduction

The 2019 Russian national report on meteorology and atmospheric sciences include studies of planetary atmospheres performed in 2015–2018. Like before [1], a considerable share of findings follows from the analysis of data obtained by the European *Mars Express* and *Venus Express* spacecraft equipped with instruments with Russian participation. The *Mars Express* spacecraft has been operating in Martian orbit for more than 15 years and continues observations. Several works summarizing the long-term observations were published upon ten years of *Mars Express* successful operations. The *Venus Express* spacecraft completed its science observations in 2014, after almost nine years of successful work. The three years of 2015–2018 was the time to summarize the long series of observations acquired, and to publish the results of three coordinated workgroups dedicated to Venus atmosphere and held in the International Space Science Institute (ISSI) in Bern in 2013–2014. The success of *Venus Express* to a large extent promoted the completion of the new Venus III book, and the associated series of papers in Space Science Reviews journal [2]. Finally, the progress of planetary atmospheric science in Russia was boosted by the creation of a dedicated laboratory 'Terrestrial Planets and habitable exo-planets: Past, Present and Future' headed by J.-L. Bertaux in Space Research Institute (IKI) ('Megagrant' 2017–2019).

The resent report is based on the results of works related to neutral planetary atmospheres and planetary climates, published in the peer-reviewed literature. The report follows the repartition by planets, including, where appropriate, a brief account for ongoing or future experiments with Russian involvement.

Venus

Composition of the atmosphere

The results of ISSI International Team dedicated to sulfur dioxide (SO_2) in the atmosphere ('SO_2 variability in the Venus atmosphere' led by A.C. Vandaele and O. Korablev) were published in 2017 [3, 4]. The core measurements used are from SPICAV/SOIR experiment operated onboard *Venus Express*, though these review papers account for all data sources available to date. SO_2 is

a crirical element of the sulfur cycle on Venus, closely linked to the global-scale cloud and haze layers, which are composed primarily of concentrated sulfuric acid. Sulfur oxide observations provide, therefore, valuable insight into the ongoing chemical evolution of Venus' atmosphere, atmospheric dynamics, and possible volcanism. Recent observations of sulfur-containing species (SO_2, SO, OCS, and H_2SO_4) in Venus' mesosphere have generated controversies, revealing unexpected spatial patterns and spatial/temporal variability, in particular between spaceborne and Earth-based observations, and that have not been satisfactorily explained by models. Paper [3] puts focus on the vertical distribution of SO_2 (see also [5]). The most noticeable feature of the vertical profile of the SO_2 abundance in the Venus atmosphere is the inversion layer located at 70–75 km, with VMRs increasing above. Observations suggest that at least one other significant sulfur reservoir (in addition to SO_2 and SO) must be present throughout the 70–100 km altitude region to explain the inversion. No photochemical model has an explanation for this behavior. GCM modelling indicates that dynamics may play an essential role in generating an inflection point at 75 km altitude but does not provide a definitive explanation of the source of the inflection at all local times or latitudes. Paper [4] addresses the horizontal and temporal variability of SO_2, observed from *Venus Express*, ground-based facilities, and the *Hubble Space Telescope* both on short-term and short-scale.

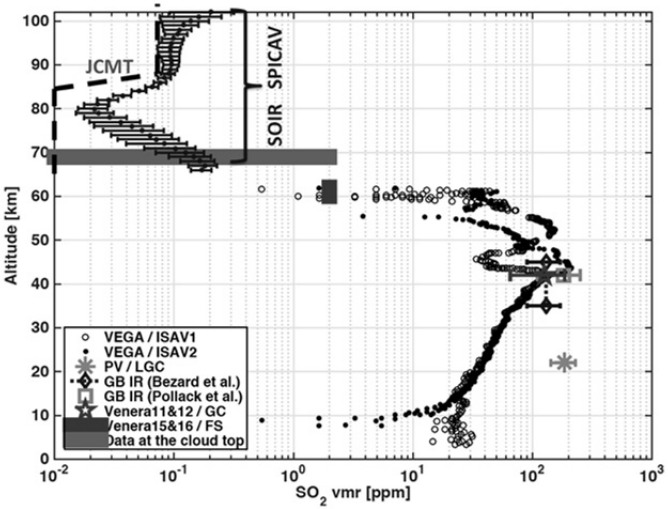

Figure 1. Vertical distribution of SO_2 VMR in the Venus atmosphere (compilation of all available datasets; see [2] for references).
Figure credit: Belyaev D.A. (presented at 6MS3 symposium, IKI, Moscow 5–9 Oct 2015)

The observed long-term trends show a succession of rapid increases followed by slow decreases in the SO_2 abundance at the cloud tops level, implying that the transport of air from lower altitudes plays an important role. The origins of the larger amplitude short-scale, short-term variability observed at the cloud tops are uncertain but are likely connected to variations in vertical transport of SO_2 or variations in the abundance and production and loss of H_2O, H_2SO_4, and S_x.

The atmosphere of Venus is almost deprived of water vapor, while its presence in trace quantities plays a crucial role in the overall radiative balance of the planet. The H_2O content above clouds has been retrieved for the complete *Venus Express* dataset from 2006 to 2014 obtained by SPICAV VIS-IR spectrometer, which measured the H_2O abundance in the reflected sunlight by 1.38-μm band absorption. The water lines form at altitudes of 59–66 km. The retrieved H_2O mixing ratio is ≈6 ppm at low latitudes, 5.5 ppm at mid-latitude, and increasing to 7 ppm at high latitudes in both hemispheres. Observed variations of water vapor within a factor of 2–3 on the short timescale appreciably exceed individual measurement errors and could be explained as a real variation of the mixing ratio or/and variations of the cloud opacity. The maximum of water at lower latitudes supports possible convection and injection of water from lower atmospheric layers [6]. The vertical gradient of water inside the clouds well correlates with the increase of water column and lowered clouds near the poles (cloud top altitude retrieved from the CO_2 1.4–1.6-μm absorptions). No prominent long-term variations of water vapor or the cloud top altitude during the 8.5 years of observation, nor a local time dependence was detected. SPICAV H_2O mixing ratios are generally higher than those obtained in the 2.56-μm band from VIRTIS-H data [7].

A one-dimensional model of the Venus clouds [8] was updated thermodynamic parameters and reduced photochemical production of sulfuric acid. It was used to model vertical profiles of H_2O and H_2SO_4 vapors and sulfuric acid concentration. For the global-mean conditions, the model predicts a lower cloud boundary (LCB) at 47.5 km, H_2SO_4 peak abundance of 7.5 ppm at the LCB, and H_2O mixing ratios of 7 ppm at 62 km and 3.5 ppm above 67 km. A reasonable agreement between these results and observations is found except for the sulfuric acid concentration in the lower clouds [9]. The photochemical model of Venus atmosphere at 47–112 km [10] was updated by new S_2O_2 data and densities of H_2O, OCS, and H_2 [11]. Variations of sulfur species may be induced by minor changes in atmospheric dynamics, and do not require volcanism to explain them. The S_2O_2 abundance found in the model is too low to be responsible for the near-UV absorption.

An upper limit on HBr in Venus' atmosphere is established from ground-based observations. The strongest line of HBr at 2605.8 cm^{-1} was observed using the NASA IRTF and a high-resolution long-slit spectrograph CSHELL with resolving power of 4×10^4. Averaging of 101 spectra of Venus resulted in the upper limit to HBr mixing ratio at the cloud tops of Venus of ~1 ppb [12]. This limit refers to 78 km. A simplified version of the bromine photochemistry is included in the photochemical model [10]. Modeling shows that the bromine chemistry may be active on Venus even under the observed upper limit. However, if a Cl/Br ratio in the Venus atmosphere is similar to that in the Solar System, then HBr is ≈1 ppb in the lower atmosphere, and the bromine chemistry is insignificant.

Aerosols

Several studies are dedicated to the composition of the Venus clouds, in particular to the unknown UV absorber. The phenomenon of glory produced from scattering by spherical particles is often present in the images of Venus taken at small phase angles. Comparison of the phase profiles of glories observed on the cloud top (70–90 km altitude) by the *Venus Monitoring Camera* (*Venus Express*) and the light-scattering characteristics of sulfuric acid droplets, containing admixtures with higher refractive index, helps to select candidates for the so-called unknown UV absorber responsible for contrasts observed at 0.365 μm in the upper Venus clouds. It was found that the frequently considered sulfur is not a plausible candidate since it is not wetted by sulfuric acid. Sulfur particles adhere to the H_2SO_4 droplets, but not enveloped by them. Scattering at such droplets with sulfur blobs would distort or blur the characteristic glory pattern completely. Other candidate UV absorbers, such as, e.g., iron chloride, can be readily embedded into the H_2SO_4 droplets, and are therefore compliant with the observations of glory [13–17]. More systematic observations of the glory by SPICAV IR spectropolarimeter (*Venus Express*) in the near-IR range (0.65–1.7 μm) confirms that the spherical particles constitute most of the cloud layer on the planet [18].

The presence of the iron chloride $FeCl_3$ in the middle and lower clouds is considered in ref. [19]. Iron chloride in the Venus clouds is under discussion for three decades. $FeCl_3$ in the Venus clouds was observed by the direct X-ray fluorescent spectroscopy. It agrees with the near UV and blue reflectivity of Venus, explains the altitude profiles of the mode one aerosol in the middle and lower cloud layers, and explains the decrease in the near-UV absorption below 60 km. Also, the delivery of $FeCl_3$ into the upper cloud layer and the production of sulfuric acid are just in a proportion of 1:100 by mass that is required to fit the observed near-UV albedo, and the mode 1 and 2 particle sizes fit this propor-

tion as well. The inferred mixing ratio of Fe_2Cl_6 in the atmosphere is 17 ppbv, and the $FeCl_3$ mole fraction in the surface rocks is 19 ppbv.

Another near-UV absorber candidate, a sulfur aerosol is considered in ref. [20]. The photochemical model [10] predicts sulfur aerosol as a product of the OCS photolysis at 55–60 km. The calculated mass loading is much smaller than that of the mode one particles in the upper cloud layer. The chemical kinetic modelling [21] results in a constant mixing ratio of 20 ppm for OCS + XSX, and the S_8 mixing ratio of 2.5 ppm at ~47 km. This abundance, ~10% of the total mass loading in the lower cloud layer, limits the calculated profile of the sulfur aerosol at the lower boundary of modes 2 and 3. The S_8 abundance is therefore too small at the cloud tops, and the sulfur aerosol cannot be the near UV absorber. Also its profile disagrees with the profile of the absorber, as observed by Venera 14.

Ref [6] provided an estimation of the cloud top altitude from SPICAV IR/*Venus Express* nadir measurements of the CO_2 bands. The altitude where the nadir aerosol optical depth at 1.48 μm equals unity, varies from 68 to 73 km at 40°S to 40°N with an average of 70.2±0.8 km, assuming the aerosol scale height of 4 km (see below). In high northern latitudes, the cloud top is lowered to 62–68 km.

The upper cloud layer of Venus is crucial for the radiative energy balance of the mesosphere. The radiative forcing variations due to clouds of the Venus mesosphere, revealing substantial variability with latitude, was studied using *Venus Express* radio occultations and a 1-D radiative transfer model [22]. The cloud top altitude effectively controls outgoing thermal fluxes. Sharp cloud top boundary can produce a pronounced peak of both solar heating and thermal cooling, suggesting a radiative origin of temperature inversions in the cold collar. Considerable diurnal variation of net forcing at low latitudes can explain convective cells observed in UV images. Latitudinal contrasts in the radiative forcing in the mesosphere can drive meridional Hadley-type circulation with meridional winds of few m/s and vertical motions with speed of few cm/s.

The vertical structure and properties of the upper cloud layer were studied using solar occultation observations at the limb of Venus by SPICAV IR spectrometer. The occultation data were analyzed throughout the mission (May 2006 to November 2014). Vertical profiles of atmospheric extinction obtained at ten near-IR wavelengths (in the range of 0.65–1.7 μm) at altitudes 70–95 km allow deriving microphysical properties of the mesospheric haze. The haze top is higher near the equator than near the pole. The aerosol scale height in the upper haze is 3.3±0.7 km. Detached haze layers were often observed at 70–90 km. The properties of aerosol particles retrieved from the occultation data are consistent with single-mode or bimodal distribution. With the H_2SO_4

refraction index, particles sizes are found as 0.12 μm and 0.84 μm for the bimodal distribution, or ~0.5 μm, for a single mode. The particle radii vary on the time scale of several months; also, they are 1.5–2 times smaller in the polar regions [23, 24].

Already mentioned polarization data from the SPICAV IR (0.65–1.7 μm) nadir observations were analyzed for the period between 2006 and 2010, the data covering mostly the northern hemisphere [18]. The degree of polarization measured on a few test orbits agrees with previous observations from the ground and *Pioneer Venus*. Mean value of effective radius $r_{\text{eff}} \approx 1$ μm with a narrow distribution (effective variance $v_{\text{eff}} \approx 0.07$) was retrieved, and refractive index of 1.42 at 1 μm. Comparing to SPICAV occultation data one may conclude that the polarimetric measurements in the IR are most sensitive to the larger mode. Global observations show significant polarization patterns. A sharp increase towards positive polarization with increasing latitude, confirms smaller, sub-micron sized haze particles in the polar areas. Also, the optical depth of this sub-micron haze doubles at higher latitudes. A more systematic approach to rich corpus of SPICAV polarization data, than presented in this 2015 paper can be expected, allowing to make a long-term survey of the cloud and haze parameters, especially when comparing to results by Pioneer Venus [25].

A chapter for the *Venus III* book and an article reviewing the clouds and hazes on Venus was published [26].

Atmospheric structure and dynamics

The thermal structure of Venus upper atmosphere (90–140 km) was investigated using SPICAV *UV/Venus Express* stellar occultations [27]. The nightside (18:00–06:00 h local time) CO_2 local density, and temperature profiles are available with vertical resolution of 7 km in both the southern and the northern hemispheres. A permanent layer of warm air is observed at the mesopause (90–100 km). With increasing altitude the temperature decreases, reaching a minimum at ~125 km. Local time variations dominate the structure of Venus atmosphere at these altitudes: temperatures increase by 20 K on the morning side compared to the evening side. The homopause height varies between 119 km on the evening side and 138 km on the morning side.

A review of up-to-date observations of the thermal structure of the Venus atmosphere, in particular comparing the *Venus Express* and ground-based observations, and the update for the Venus International Reference Atmosphere (VIRA) was published [28]. The *Venus Express* observations have considerably increased our knowledge of the Venus atmospheric thermal structure above ~40 km and provided new information above 100 km. The contribution of the new *Venus Express* data to VIRA is also considered in refs. [22, 29].

Advancements in the field of molecular absorption at high pressure (a non-exhaustive list of references is [30–35]) led to improved understanding the to the radiation transfer in the Venus' atmosphere and updates for spectroscopic databases [36, 37].

A corpus of Venus images collected by *Venus Monitoring Camera* (VMC) though the lifetime of *Venus Express* mission in the UV and near-IR ranges was used to track visible motions of clouds to infer winds and the superrotation rate at the cloud level [38–40]. The cloud top altitude in low latitudes is seen in the UV at ≈67 km, and the middle and lower cloud level (49–57 km) is observed in the near-IR. The mean retrograde zonal wind speed at these levels is about 90 m/s, and 68–70 m/s, respectively. A maximum of wind speed of about 100 m/s is observed at the cloud tops at 40–50°S, decreasing with latitude poleward of 50°S. The mean poleward meridional wind slowly varies from zero value at the equator to about 10 m/s at 50°S and then back to zero at the pole. The mean meridional speed within the clouds has a positive sign at 5–65°S suggesting equatorward flow. Together with the poleward flow at the cloud tops, it indicates the presence of a closed Hadley cell at 55–65 km.

A correlation between the zonal low-latitude wind pattern and the underlying topography of Aphrodite Terra is found [41], and interpreted as a result of stationary gravity waves produced at the ground level near the mountains. A long term trend (2006–2012) of the zonal wind speed at low latitudes suggested earlier [38] is not confirmed [40, 41]. The variability in the retrieved wind speed is explained by the observational selection, associated with the influence from the surface topography.

The Venus circulation was also studied in the mesosphere region (90–110 km) using tracking of the singlet oxygen $O_2(a^1\Delta_g)$ 1.27 μm nightglow [42]. The images of the nightglow were obtained by VIRTIS-M on *Venus Express* over the course of ≥2 years, covering the nightside southern hemisphere of the planet. Two opposite flows from terminators to midnight are observed. The eastward wind (from the morning side) exceeds the westward (evening) by 20–30 m/s, and the two streams meet at ≈22.5 h. Surprisingly the influence of underlying topography was suggested as well: above mountain regions, flows tend to behave as if they encounter an obstacle, sometimes shifted by several degrees. Therefore the stationary gravity waves, emerging from the surface can reach such altitudes. Instances of circular motion were discovered, encompassing areas of 1,500–4,000 km. The mean horizontal circulation at about 100 km does represent neither superrotation, nor subsolar-to-antisolar circulation, nor a superposition of the two. Both the zonal and the meridional components of the motion have different magnitudes and direction before and after midnight.

Interestingly, the influence of the surface on the circulation is confirmed by the general circulation modeling, though the effect is only apparent above 80 km [43]. Review papers on superrotation and turbulence in the atmosphere of Venus are published [44, 45].

Future Venus missions

Despite the tremendous progress that has been made in recent years and the success of *Venus Express* and *Akatsuki* orbiters, many fundamental questions remain concerning Venus' history, evolution, and current geologic and atmospheric processes. Among the approaches to prioritizing these questions, a joint science definition team between Russia and the United States is working since 2015 to formulate the science priorities for a new Venus space mission, *Venera-D*. It is planned that the mission will include an instrumented orbiter and *in situ* elements, including a classical *VeGa*-type lander, long term survival elements on the surface of Venus, and an element, permitting controlled aerial mobility [46]. Supportive studies related to the atmosphere included thermal protection systems for Venus landers [47] and an estimate the visibility of Venus' surface through clouds at the nightside [48]. As of 2019, the practical implementation of this mission is been considered by funding agencies, Roscosmos and NASA.

Mars

Atmospheric chemistry

The SPICAM experiment onboard *Mars Express* has accumulated since 2004 a wealth of observations permitting a detailed characterization of the atmospheric composition and activity from the near-surface up to above the exosphere. The SPICAM climatology is one of the longest assembled to date by an instrument in orbit around Mars, offering the opportunity to study the fate of major volatile species in the Martian atmosphere over a multi-(Mars)year (MY) timeframe. With his dual ultraviolet (UV)-near Infrared channels, SPICAM observes a variety of atmospheric gases, from abundant (CO_2) to trace species (H_2O, O_3) [49-51]. Long-term observations of atmospheric water vapor [51], airglows [52], ozone, clouds and dust, carbon dioxide, exospheric hydrogen [51] cover the MY27–MY31 period (Figure 2). The monitoring of UV-derived species was stopped at the end of 2014 (MY30) due to failure of the UV channel, while the IR channel continues to observe. An SO_2 detection attempt was undertaken but proved unsuccessful: with an upper limit higher than previously published.

One particular conclusion stemming from long-term SPICAM observations concerns an efficient mass transfer between the lower and the upper atmospher-

ic reservoirs. This is best illustrated by water and hydrogen, SPICAM monitored both species in their respective atmospheric reservoir. Coupling between the two appear to occur on seasonal timescales, much shorter than theoretical predictions (see below).

SPICAM data on molecular oxygen singlet delta emission was compared to the height profiles of atomic oxygen resulting from 1-D modeling the chemical composition of the martian atmosphere [52].

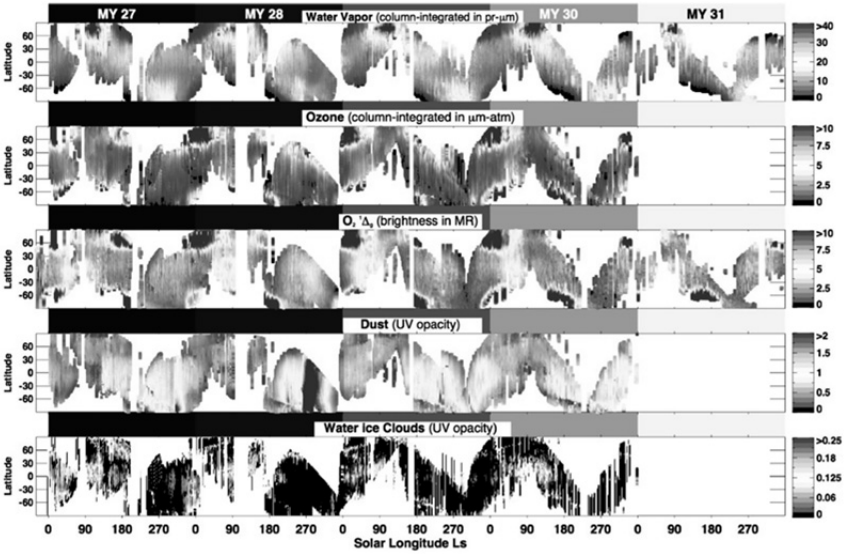

Figure 2. A compilation of five Martian years of observations by SPICAM in a nadir-looking mode [51]. The chart displays zonally averaged values as a function of solar longitude (Ls) of the retrieved (from top to bottom) water vapor, ozone, molecular oxygen singlet delta daytime emission in the near infrared, and dust as well as water ice opacity at 250 nm

CO variations on Mars were studied by means of ground-based spatially-resolved high-resolution spectroscopy [53]. Earlier results have been improved using the ^{13}CO and CO_2 lines with low temperature dependence, and good knowledge of spectroscopy. The $^{13}CO/CO$ ratio of 1.023 times terrestrial was calculated using the ratio of $^{13}CO_2/CO_2$=1.046 measured by *MSL Curiosity*, with an account for isotope fractionation in the CO_2 photolysis, and in the reaction between CO and OH. The observations extended over the maximum of CO in the southern hemisphere during the northern summer. The enrichment of incondensable gases by condensation of CO_2 in the southern polar regions is

found mostly confined to high latitudes, in agreement with the Mars Climate Database model predictions, but contradicting other observations, showing larger latitudinal gradients and seasonal variations. The retrieved global mean CO abundance is 700 ppm on Mars, smaller than many recent results by a factor of ≈1.4. The issue of the CO_2 isotopologues measured by *MSL Curiosity* was as well addressed in ref. [54].

The mixing ratios of N_2, Ar, O_2, and CO precisely measured by the *MSL Curiosity* quadrupole mass spectrometer were corrected for the seasonal variations of the atmospheric pressure to reproduce annual mean mixing ratios on Mars [55]. The corrections are made using the pressure measurements for the first year of the *Viking Landers* 1 and 2 and the Mars Climate Database. The resulting annual mean mixing ratios of (1.83±0.03)% for N_2, (1.86±0.02)% for Ar, $(1.56\pm0.06)10^{-3}$ for O_2, and 673±2.6 ppm for CO are found.

A review of the current understanding of the Mars' atmospheric photochemistry is presented as the *Atmosphere and Climate of Mars* book chapter [56].

Water cycle and escape

Better characterization of the water cycle progressively leads to an understanding that water in the neutral lower atmosphere is connected to the hydrogen corona and loss of water from Mars. We therefore considered these issues together.

The current status of understanding of the Mars' water cycle is presented in the *Atmosphere and Climate of Mars* book [57]. Multi-Mars-year climatology of atmospheric water vapor is given in ref. [49]. A new hydrological cycle scheme was implemented into the Max Planck Institute Martian general circulation model (Martian Atmosphere Observation and Modeling, MAOAM) [58, 59]. The new scheme includes more accurate parameterization of microphysical processes between water vapor and ice clouds, including processes of saturation, nucleation, particle growth, sublimation, and sedimentation under the assumption of variable size distribution. Simulations of annual variations, horizontal and vertical distribution of water vapour and ice clouds are compared to available observations. In particular, monomodal and bimodal distributions of ice condensation nuclei were studied.

Observations of the Martian hydrogen corona in the UV H Ly-alpha emission by HST and SPICAM/*Mars Express* [51] show changes with Martian season, significantly increasing in perihelion (see also [60]). A difference by order of magnitude occurred over a few months in 2007 (MY28) coincident with a global dust storm. The observed increase of Ly-alpha suggests that the increased dust loading incites water vapor from the lower atmosphere to reach higher altitudes. Over there the water is photo-dissociated by sunlight, provid-

ing a source of hydrogen for the upper atmosphere. SPICAM IR occultation profiles were used to study the water vapor vertical distribution during the 2007 global dust storm [61]. In the Northern hemisphere at Ls = 268°–285° the H_2O density increased by order of magnitude at 60–80 km. During the dust storm, the profiles extended up to 80 km, with an H_2O density exceeding 10^{10} molecules cm^{-3} (volume mixing ratio ≥200 ppm). The largest H_2O densities observed above 60°N, over Ls = 269°–275°, do not directly correlate with the aerosol loading. This increase likely relates to the downwelling branch of the meridional circulation transporting water from the Southern hemisphere to high northern latitudes, intensified during the dust storm. A comparison with a quiet Mars year MY32, when the H_2O content in the Northern hemisphere did not exceed 2×10^{10} molecules cm^{-3} and 50 ppm at 60 km, showed that the global dust storm was a unique event. In the Southern hemisphere the increase of water during the storm was milder (a factor of 4–5), and a comparable increase (a factor of 2–3) was also observed during MY32, suggesting seasonal repeatability. The observed amount of water at high altitudes in both hemispheres can produce a substantial increase in the H escape rate on a timescale of weeks. More observations and modelling is needed to separate the seasonal and the dust storm contributions to the hydrogen escape.

Results of ground-based high-resolution spectroscopy observations of the HDO/H_2O ratio in the martian atmosphere conducted at NASA IRTF in 2007–2014 published in ref. [62]. The observations are difficult because telluric water exceeds the martian water by two orders of magnitude even under excellent conditions at Mauna Kea (Hawaii, elevation 4.2 km). The HDO and H_2O lines of comparable equivalent widths were observed at close wavenumbers of 2722 and 2994 cm^{-1}, minimizing effects of aerosol absorption and scattering in the resulting HDO/H_2O ratios. The ratios found from four observations are flat in broad latitude ranges, as predicted by the GCM model. Two other observations depart from the model predictions, showing a strong correlation between HDO/H_2O and temperature at ≈7 km above the surface. The observed global-mean HDO/H_2O ratio is 4.6±0.7 times the terrestrial ratio; the ratio in the vapour released from the north polar cap is 6.2±1.4. The ratio in the north polar cap ice inferred using the GCM estimate is 7.1±1.6.

Upper neutral atmosphere

An improved physical model and the calculation method for the radiative transfer problem under nonlocal thermodynamic equilibrium (NLTE) conditions published in refs. [63, 64]. Vibrational states in the CO_2 and CO molecular bands in the near-infrared (NIR) wavelength range (~1–5 μm) in the daytime atmosphere of Mars, and their population are considered.

Though the Martian mesosphere and thermosphere, the region above about 60 km, is not the primary target of the *ExoMars* 2016 mission, the *Trace Gas Orbiter* (TGO), can explore it and address many interesting issues [65].

ExoMars mission

A significant advancement in the understanding Mars atmosphere, climate, and meteorology are expected from ExoMars mission (ESA and Roscosmos). The firsts part of the mission, the *Trace Gas Orbiter* (TGO) launched by Russian *Proton* in 2016, has reached final science orbit in March 2018, and performing full-scale science observations from April 21, 2018. The orbit of the spacecraft is specifically designed for atmospheric and climate studies: it is optimized for solar occultations, permitting the most sensitive survey for trace gases in the atmosphere, while nadir tracks allow observing at variable local time. A full local time turnover requires 60 days. Two out of four instruments of the satellite, the Russian ACS [66, 67] and the European NOMAD [68–70], are designed for measuring the small atmospheric constituents and monitoring the basic climate parameters. The two instruments performed a survey of the trace components and observed the global dust storm of 2018 (the event 2018A), and a regional dust storm at the beginning of 2019. No findings of these experiments were published in 2018 yet.

The *ExoMars* 2020, the second part of the mission will carry a series of instruments for meteorological and atmospheric studies on a stationary landing platform with a lifetime of no less than a year [71]. A full-scale meteorological package, using the heritage of previous missions [72] is under development. Measurements of the atmospheric profile during the descent of the landing vehicle are also planned. The *ExoMars* 2020 rover [73] also carries some instruments, which can deliver meteorological information [74].

Other planets

A few studies related to the atmospheres of other planets include the analysis of JUNO mission data [75], interpretation of the *New Horizons* observations [76], and photochemical modelling of the Titan atmosphere [77].

References

1. Korablev O.I. (2016), Studies of planetary atmospheres in Russia (2011–2014), Izvestiya, Atmos. Oceanic Phys., 52, 483–496.

2. Bézard B., C.T. Russell, T. Satoh, S.E. Smrekar, C.F. Wilson (2018), Editorial: Topical Collection on Venus, Space Science Reviews, 214(8), 128, doi:10.1007/s11214-018-0564-8.

3. Vandaele A.C. et al. (2017), Sulfur dioxide in the Venus atmosphere: I. Vertical distribution and variability, Icarus, 295, 16–33.

4. Vandaele A.C., et al. (2017), Sulfur dioxide in the Venus Atmosphere: II. Spatial and temporal variability, Icarus, 295, 1–15, doi:10.1016/j.icarus.2017.05.001.

5. Belyaev D.A., D.G. Evdokimova, F. Montmessin, J.L. Bertaux, O.I. Korablev, A.A. Fedorova, E. Marcq, L. Soret, M.S. Luginin (2017), Night side distribution of SO_2 content in Venus' upper mesosphere, Icarus, 294, 58–71.

6. Fedorova A., E. Marcq, M. Luginin, O. Korablev, J.-L. Bertaux, F. Montmessin (2016), Variations of water vapor and cloud top altitude in the Venus' mesosphere from SPICAV/VEx observations, Icarus, 275, 143–162.

7. Cottini V., N.I. Ignatiev, G. Piccioni, P. Drossart (2015), Water vapor near Venus cloud tops from VIRTIS-H/Venus express observations 2006–2011, Planetary and Space Science, 113, 219–225.

8. Krasnopolsky V., J. Pollack (1994), H_2O-H_2SO_4 system in Venus clouds and OCS, CO, and H2SO4 profiles in Venus tropospher, Icarus, 109(1), 58–78.

9. Krasnopolsky V.A. (2015), Vertical profiles of H_2O, H_2SO_4, and sulfuric acid concentration at 45–75 km on Venus, Icarus, 252, 327–333.

10. Krasnopolsky V.A. (2012), A photochemical model for the Venus atmosphere at 47–112 km, Icarus, 218, 230–246.

11. Krasnopolsky V.A. (2018), Disulfur dioxide and its near-UV absorption in the photochemical model of Venus atmosphere, Icarus, 299, 294–299.

12. Krasnopolsky V.A., D.A. Belyaev (2017), Search for HBr and bromine photochemistry on Venus, Icarus, 293, 114–118.

13. Petrova E.V. (2018), Glory on Venus and selection among the unknown UV absorbers, Icarus, 306, 163–170.

14. Markiewicz W.J., E.V. Petrova, O.S. Shalygina (2018), Aerosol properties in the upper clouds of Venus from glory observations by the Venus Monitoring Camera (Venus Express mission), Icarus, 299, 272–293.

15. Petrova, E. V., O. S. Shalygina, and W. J. Markiewicz (2015), The VMC/VEx photometry at small phase angles: Glory and the physical properties of particles in the upper cloud layer of Venus, Planetary and Space Science, 113, 120–134.

16. Shalygina O.S., E.V. Petrova, W.J. Markiewicz, N.I. Ignatiev, E.V. Shalygin (2015), Optical properties of the Venus upper clouds from the data obtained by Venus Monitoring Camera on-board the Venus Express, Planetary and Space Science, 113, 135–158.

17. Petrova E.V., O.S. Shalygina, W.J. Markiewicz (2015), UV contrasts and microphysical properties of the upper clouds of Venus from the UV and NIR VMC/VEx images, Icarus, 260, 190–204.

18. Rossi L., E. Marcq, F. Montmessin, A. Fedorova, D. Stam, J.-L. Bertaux, O. Korablev (2015), Preliminary study of Venus cloud layers with polarimetric data from SPICAV/VEx, Planetary and Space Science, 113, 159–168.

19. Krasnopolsky V.A. (2017), On the iron chloride aerosol in the clouds of Venus, *Icarus*, *286*, 134–137.

20. Krasnopolsky V.A. (2016), Sulfur aerosol in the clouds of Venus, Icarus, 274, 33–36.

21. Krasnopolsky V.A. (2013), S3 and S4 abundances and improved chemical kinetic model for the lower atmosphere of Venus, Icarus, 225, 570–580.

22. Lee Y.J., D.V. Titov, N.I. Ignatiev, S. Tellmann, M. Pätzold, G. Piccioni (2015), The radiative forcing variability caused by the changes of the upper cloud vertical structure in the Venus mesosphere, Planetary and Space Science, 113, 298–308.

23. Luginin M., A. Fedorova, D. Belyaev, F. Montmessin, V. Wilquet, O. Korablev, J.-L. Bertaux, A. C. Vandaele (2016), Aerosol properties in the upper haze of Venus from SPICAV IR data, Icarus, 277, 154–170.

24. Luginin M., A. Fedorova, D. Belyaev, F. Montmessin, O. Korablev, J.-L. Bertaux (2018), Scale heights and detached haze layers in the mesosphere of Venus from SPICAV IR data, Icarus, 311, 87–104.

25. Esposito L.W. (1984), Sulfur dioxide – Episodic injection shows evidence for active Venus volcanism, Science, 223, 1072–1074.

26. Titov D.V., N.I. Ignatiev, K. McGouldrick, V. Wilquet, C.F. Wilson (2018), Clouds and Hazes of Venus, Space Science Reviews, 214(8), 126, doi:10.1007/s11214-018-0552-z.

27. Piccialli A., F. Montmessin, D. Belyaev, A. Mahieux, A. Fedorova, E. Marcq, J.-L. Bertaux, S. Tellmann, A.C. Vandaele, O. Korablev (2015), Thermal structure of Venus nightside upper atmosphere measured by stellar occultations with SPICAV/Venus Express, Planetary and Space Science, 113, 321–335.

28. Limaye S.S. et al. (2017), The thermal structure of the Venus atmosphere: Intercomparison of Venus Express and ground based observations of vertical temperature and density profiles, Icarus, 294, 124–155.

29. Vandaele A.C. et al. (2016), Contribution from SOIR/VEX to the updated Venus International Reference Atmosphere (VIRA), Advances in Space Research, 57, 443–458.

30. Fedorova A., B. Bézard, J.-L. Bertaux, O. Korablev, C. Wilson (2015), The CO_2 continuum absorption in the 1.10- and 1.18-μm windows on Venus from Maxwell Montes transits by SPICAV IR onboard Venus express, Planetary and Space Science, 113, 66–77.

31. Ignat'ev N.I., I.V. Mingalev, A.V. Rodin, E.A. Fedotova (2015), A new version of the discrete ordinate method for the calculation of the intrinsic radiation in horizontally homogeneous atmospheres, Computational Mathematics and Mathematical Physics, 55, 1713–1726.

32. Mondelain D., A. Campargue, P. Cermak, R.R. Gamache, S. Kassi, S.A. Tashkun, H. Tran (2017), The CO_2 absorption continuum by high pressure CRDS in the 1.74 mu m window, J. Quantitative Spectrosc. Radiat.Transfer, 203, 530–537.

33. Vasilchenko S., M. Konefal, D. Mondelain, S. Kassi, P. Čermák, S.A. Tashkun, V.I. Perevalov, A. Campargue (2016), The CO2 absorption spectrum in the 2.3 μm transparency window by high sensitivity CRDS: (I) Rovibrational lines, J. Quantitative Spectrosc. Radiat. Transfer, 184, 233–240.

34. Gamache R.R. et al. (2017), Total internal partition sums for 166 isotopologues of 51 molecules important in planetary atmospheres: Application to HITRAN2016 and beyond, J. Quantitative Spectrosc. Radiat. Transfer, 203, 70–87.

35. Lavrentieva N.N., B.A. Voronin, A.A. Fedorova (2015), H-2O-16 line list for the study of atmospheres of Venus and Mars, Optics and Spectroscopy, 118(1), 11–18.

36. Gordon I.E. et al. (2017), The HITRAN2016 molecular spectroscopic database, J. Quantitative Spectrosc. Radiative Transfer, 203, 3–69.

37. Tashkun S.A., V.I. Perevalov, R.R. Gamache, J. Lamouroux (2019), CDSD-296, high-resolution carbon dioxide spectroscopic databank: An update, J. Quantitative Spectrosc. Radiat. Transfer, 228, 124–131.

38. Khatuntsev I.V., M.V. Patsaeva, D.V. Titov, N.I. Ignatiev, A.V. Turin, S.S. Limaye, W.J. Markiewicz, M. Almeida, T. Roatsch, R. Moissl (2013), Cloud level winds from the Venus Express Monitoring Camera imaging, Icarus, 226, 140–158.

39. Patsaeva M.V., I.V. Khatuntsev, D.V. Patsaev, D.V. Titov, N.I. Ignatiev, W.J. Markiewicz, A.V. Rodin (2015), The relationship between mesoscale circulation and cloud morphology at the upper cloud level of Venus from VMC/Venus Express, Planetary and Space Science, 113, 100–108.

40. Khatuntsev I.V., M.V. Patsaeva, D.V. Titov, N.I. Ignatiev, A.V. Turin, A.A. Fedorova, W.J. Markiewicz (2017), Winds in the middle cloud deck from the near-IR imaging by the Venus Monitoring Camera onboard Venus Express, J. Geophys. Res.-Planets, 122(11), 2312–2327.

41. Bertaux J.-L., I.V. Khatuntsev, A. Hauchecorne, W.J. Markiewicz, E. Marcq, S. Lebonnois, M. Patsaeva, A. Turin, A. Fedorova (2016), Influence of Venus topography on the zonal wind and UV albedo at cloud top level: The role of stationary gravity waves, J. Geophys. Res.: Planets, 121, 1087–1101.

42. Gorinov D.A., I.V. Khatuntsev, L.V. Zasova, A.V. Turin, G. Piccioni (2018), Circulation of venusian atmosphere at 90–110 km based on apparent motions of the O_2 1.27 μm nightglow from VIRTIS-M (Venus Express) data, Geophys. Res. Lett., 45(5), 2554–2562.

43. Mingalev I.V., A.V. Rodin, K.G. Orlov (2015), Numerical simulations of the global circulation of the atmosphere of Venus: Effects of surface relief and solar radiation heating, Solar System Research, 49, 24–42.

44. Cirilo-Lombardo D.J., M. Mayochi, F.O. Minotti, C.D. Vigh (2018), About superrotation in Venus, Solar System Research, 52, 223–233.

45. Izakov M.N. (2016), Turbulence, superrotation, and general circulation models of the atmosphere of Venus, Solar System Research, 50, 301–315.

46. Ekonomov A.P., L.V. Ksanfomality (2018), On the thermal protection systems of landers for Venus Exploration, Solar System Research, 52, 37–43.

47. Ekonomov A.P. (2015), Resolving the surface details on Venus in the balloon- or lander-borne images with a computer modeling method, Solar System Research, 49, 110–113.

48. Glaze L.S., C.F. Wilson, L.V. Zasova, M. Nakamura, S. Limaye (2018), Future of Venus research and exploration, Space Science Reviews, 214 (5), 89.

49. Trokhimovskiy A., A. Fedorova, O. Korablev, F. Montmessin, J.-L. Bertaux, A. Rodin, M. D. Smith (2015), Mars' water vapor mapping by the SPICAM IR spectrometer: Five martian years of observations, Icarus, 251(0), 50–64.

50. Guslyakova S., A. Fedorova, F. Lefèvre, O. Korablev, F. Montmessin, A. Trokhimovskiy, J.L. Bertaux (2016), Long-term nadir observations of the O2 dayglow by SPICAM IR, Planetary and Space Science, 122, 1–12.

51. Montmessin F. et al. (2017), SPICAM on Mars Express: A 10 year in-depth survey of the Martian atmosphere, Icarus, 297, 195–216.

52. Kulikov Y.N. (2018), Modeling the chemical composition of the martian atmosphere. Preliminary results of comparing the height profile of atomic oxygen with the observational data by the SPICAM spectrometer, Proc. of the Kola Scientific Center of the Russian Academy of Science (Geophysics), 9(5), 202–216.

53. Krasnopolsky V.A. (2015), Variations of carbon monoxide in the martian lower atmosphere, Icarus, 253, 149–155.

54. Shved G.M. (2016), On the abundances of carbon dioxide isotopologues in the atmospheres of mars and earth, Solar System Research, 50, 161–164.

55. Krasnopolsky V.A. (2017), Annual mean mixing ratios of N-2, Ar, O-2, and CO in the martian atmosphere, Planetary and Space Science, 144, 71–73.

56. Lefèvre F., V. Krasnopolsky, R.T. Clancy, F. Forget, M.D. Smith, R.W. Zurek (2017), Atmospheric Photochemistry, in The Atmosphere and Climate of Mars, ed. by R. M. Haberle, pp. 374–404, Cambridge UP.

57. Montmessin F., M.D. Smith, Y. Langevin, M.T. Mellon, A. Fedorova, R.M. Haberle, R. T. Clancy, F. Forget, M.D. Smith, R.W. Zurek (2017), The Water Cycle, in Atmosphere and Climate of Mars, pp. 338–373, Cambridge UP.

58. Shaposhnikov D.S., A.V. Rodin, A.S. Medvedev (2016), The water cycle in the general circulation model of the martian atmosphere, Solar System Research, 50(2), 90–101.

59. Shaposhnikov D.S., A.V. Rodin, A.S. Medvedev, A.A. Fedorova, T. Kuroda, P. Hartogh (2018), Modeling the Hydrological Cycle in the Atmosphere of Mars: Influence of a Bimodal Size Distribution of Aerosol Nucleation Particles, Journal of Geophysical Research-Planets, 123(2), 508–526.

60. Krasnopolsky V.A. (2017), On the hydrogen escape from Mars: Comments to "Variability of the hydrogen in the martian upper atmosphere as simulated by a 3D atmosphere-exosphere coupling" by J.Y. Chaufray et al. (2015, Icarus 245, 282–294), Icarus, 281, 262–263

61. Fedorova A., J.-L. Bertaux, D. Betsis, F. Montmessin, O. Korablev, L. Maltagliati, J. Clarke (2018), Water vapor in the middle atmosphere of Mars during the 2007 global dust storm, Icarus, 300, 440–457.

62. Krasnopolsky V.A. (2015), Variations of the HDO/H2O ratio in the martian atmosphere and loss of water from Mars, Icarus, 257, 377–386.

63. Ogibalov V.P., G.M. Shved (2016), An improved model of radiative transfer for the NLTE problem in the NIR bands of CO2 and CO molecules in the daytime atmosphere of Mars. 1. Input data and calculation method, Solar System Research, 50, 316–328.

64. Ogibalov V.P., G.M. Shved (2017), An improved model of radiative transfer for the NLTE problem in the NIR bands of CO_2 and CO molecules in the daytime atmosphere of Mars. 2. Population of vibrational states, Solar System Research, 51, 373–385.

65. Lopez-Valverde M.A. et al. (2018), Investigations of the Mars upper atmosphere with ExoMars Trace Gas Orbiter, Space Science Reviews, 214(1), doi:10.1007/s11214-017-0463-4.

66. Korablev O.I., F. Montmessin, A.A. Fedorova, N.I. Ignatiev, A.V. Shakun, A.V. Trokhimovskiy, A.V. Grigoriev, K.A. Anufreichik, T.O. Kozlova (2015), ACS experiment for atmospheric studies on "ExoMars-2016" Orbiter, Solar System Research, 49(7), 529–537.

67. Korablev O. et al. (2018), The Atmospheric Chemistry Suite (ACS) of Three Spectrometers for the ExoMars 2016 Trace Gas Orbiter, Space Science Reviews, 214, 7.

68. Vandaele A.C. et al. (2015), Science objectives and performances of NOMAD, a spectrometer suite for the ExoMars TGO mission, Planetary and Space Science, 119, 233–249.

69. Robert S. et al. (2016), Expected performances of the NOMAD/ExoMars instrument, Planetary and Space Science, 124, 94–104.

70. Vandaele A.C. et al. (2018), NOMAD, an Integrated Suite of Three Spectrometers for the ExoMars Trace Gas Mission: Technical Description, Science Objectives and Expected Performance, Space Science Reviews, 214.

71. Zelenyi L.M., O.I. Korablev, D.S. Rodionov, B.S. Novikov, K.I. Marchenkov, O.N. Andreev, E.V. Larionov (2015), Scientific objectives of the scientific equipment of the landing platform of the ExoMars-2018 mission, Solar System Research, 49, 509–517.

72. Harri A.-M. et al. (2017), The MetNet vehicle: a lander to deploy environmental stations for local and global investigations of Mars, Geoscientific Instrumentation Methods and Data Systems, 6(1), 103–124.

73. Vago J.L. et al. (2017), Habitability on early Mars and the search for biosignatures with the ExoMars Rover, Astrobiology, 17, 471–510.

74. Korablev O.I. et al. (2017), Infrared spectrometer for ExoMars: A mast-mounted Instrument for the Rover, Astrobiology, 17, 542–564.

75. Grassi D. et al. (2017), Analysis of IR-bright regions of Jupiter in JIRAM-Juno data: Methods and validation of algorithms, J. Quantitative Spectrosc. Radiat. Transfer, 202, 200–209.

76. Krasnopolsky V.A. (2016), Isotopic ratio of nitrogen on Titan: Photochemical interpretation, Planetary and Space Science, 134, 61–63.

77. Krasnopolsky V.A. (2018), Some problems in interpretation of the New Horizons observations of Pluto's atmosphere, Icarus, 301, 152–154.

Polar Meteorology

A.V. Klepikov, A.I. Danilov
Arctic and Antarctic Research Institute
klep@aari.ru

This section is a review of the results of Russian polar studies performed in 2015–2018. It is based on material prepared by the Commission on Polar Meteorology of the National Geophysical Committee, Russian Academy of Sciences, and included in the National Report on Meteorology and Atmospheric Sciences to the XXVII General Assembly of the International Union of Geodesy and Geophysics, Montreal, Canada, July 8–18, 2019.

Arctic meteorology studies

The Arctic regions are characterized by the strongest and fastest climatic changes. The warming rate in the Arctic in recent decades has been significantly greater than global warming rate. The substantial Arctic amplification, which characterizes the degree of sharper climate changes at high latitudes compared to lower ones, is due to a number of factors. The Arctic amplification is influenced by the dependence of thermal radiation and albedo on temperature, changes in the vertical temperature stratification of the atmosphere, meridional heat transfer, and the content of water vapor and clouds in the atmosphere. The most significant changes in recent decades are associated with a very rapid decrease in the ice cover of the Arctic Ocean, especially at the end of summer. These changes indicate a possible future absence of sea ice in the Arctic Ocean in the summer and autumn months already in the first half of the 21st century. The change in the distribution of sea ice in the Arctic is of great importance in connection with the development of Arctic marine transport systems and the shelf exploration. All these problems are described in the review [1]. Results of the Arctic climate and cryosphere studies in the Arctic and Antarctic Research Institute, St.Petersburg, are described in comprehensive reviews [2, 3].

The paper [4] presents the evaluation of climate change in the Arctic during the development of the global warming, and considers the role of various factors in the Arctic amplification of changes. It is shown that the increase of surface air temperature began in the 1990‘s and reached its maximum in 2012. Rapid reduction of the Arctic sea ice cover at the end of the summer period occurred concurrently and reached the deepest minimum in September 2012. The changes of summer air temperature in the marine Arctic and sea ice extent in September correlate with the coefficient equals to -0,93 for 1980–2014.

Quadratic and linear models of relationships between the summer air temperature and sea ice extent indicate the period 2029–2037 as that of September ice disappearance. The inflow of warm and salty Atlantic water and displacement of its limits distribution in the sub-Atlantic Arctic, especially significant in the Barents Sea, affect changes of the winter sea ice extent. It is shown that the greatest contribution to amplified warming of the Arctic climate is that of the poleward atmospheric heat transport. This transport accounts for almost 90% of the trend in average temperature in the Arctic, most of the trend of average temperature in the Northern Hemisphere and more than half of the global mean temperature trend from 1969–2008 [4].

In [5] it has been hypothesised the Arctic amplification of temperature changes causes a decrease in the northward temperature gradient in the troposphere, thereby enhancing the oscillation of planetary waves leading to extreme mid-latitudes weather. To test the hypothesis, we study the response of the atmosphere to Arctic amplification for a projected summer sea-ice-free period using an atmospheric model with prescribed surface boundary conditions from a state-of-the-art Earth system model. Besides a standard global warming simulation, we also conducted a sensitivity experiment with sea ice and sea surface temperature anomalies in the Arctic. We show that when global climate warms, enhancement of the northward heat transport provides the major contribution to decrease the northward temperature gradient in the polar troposphere in cold seasons, causing more oscillation of the planetary waves. However, while Arctic amplification significantly enhances near-surface air temperature in the polar region, it is not large enough to invoke an increased oscillation of the planetary waves [5].

Possible mechanisms for the formation of significant weather-climatic anomalies in the Russian territory in recent years and their connection with global climate change and natural quasi-cyclic processes are discussed in [6]. Extreme heat of 2010, floods of the Amur river in 2013, and abnormally cold winters associated with the long-lived blocking anticyclones, for which, with continued global warming, a general increase in repeatability is analyzed. To determine the connection of such events with global warming, it is necessary to take into account the effects of regionally and globally significant natural quasi-cyclic processes, including the Atlantic long-period oscillation, the Pacific decade oscillation and the ENSO [6].

An assessment of the relationship between changes of sea ice extent and Arctic climate is presented in [7]. Increase of surface air temperature (SAT) in the marine Arctic shows a good relationship with reduction of sea ice extent (SIE) in summer. A strong correlation (a coefficient equal to -0.93) was found between the summer SAT in the marine Arctic and satellite-derived 1980–2014

September sea ice index (the average of SIE in the Arctic since 1978, in millions of km^2). Based on this finding, anomalies of Arctic September SIE were reconstructed from the beginning of 20th century using a linear regression relationship. This reconstructed SIE shows a substantial decrease in the 1930–1940s with a minimum occurring in 1936, which, however, is only a half of the decline in 2012. The strong relationship between the summer SAT and September SIE was used to assess the onset of summer sea ice disappearance in the Arctic Ocean. According to the estimates made with a simple regression model, we can expect a seasonally ice-free Arctic Ocean as early as in the mid-2030s. An impact of the inflow of warm and salty Atlantic water (AW) on winter SIE was evaluated as an example for the Barents Sea. This evaluation reveals a coherent spatial pattern of the AW spreading, presented by surface salinity distribution, and the position of sea ice edge, and significant correlation between the inflow of the AW and maximal sea ice extent [7].

Recently published articles on some issues of the evolution of Arctic sea ice cover are reviewed in [8]. It is shown the high correlation between the increasing of surface air temperature and shrinking of the ice cover in summer. Based on this, anomalies of the September ice extent have been retrieved from 1900. They show a significant decrease in the 1930–1940s, which is almost twice as low as in 2007–2012. The influence of fluctuations in the flow of warm and salty Atlantic water is noted in variations in the winter maximum of the sea ice extent in the Barents Sea. An accelerated positive trend has been ascertained for the air temperature in late autumn – early winter in 1993–2012 due to increase in the open water area in late summer. Inherent regularities of the variability of ice covered area made it possible to develop a prediction of the monthly values of sea ice extent with lead time from 6 months to 2 years [8].

Influence of anomalies of the sea surface temperature (SST) in low latitudes of the North Atlantic on the sea ice cover and the surface air temperature in the Arctic is discussed in [9, 10]. Data on the SST in the Atlantic Ocean from the HadISST, series of the water temperature on the section along the Kola meridian together with mean monthly data on sea ice extent and air surface temperature in the Arctic Ocean and the Northern hemisphere were analyzed. Cross-correlation analysis was applied to determine the maximum correlation coefficients between the SST anomalies, climate characteristics and their corresponding delays within time limits of 33 to 38 months. Existence of intimate link had been found between changes of the Atlantic SST in low latitudes and the sea ice extent in the Arctic with correlation coefficients up to 0.90 and delays up to 3 years. A mechanism of formation of the remote influence of low-latitude SST anomalies on the sea ice anomalies in the Arctic Ocean is proposed [9, 10].

There are different points of view on the role of the atmospheric heat and moisture transport in increasing summer warming in the Arctic, which are often

based on the analysis of average annual data. In [11, 12] the analysis of summer atmospheric transport, their influence on air temperature and water vapor content in the atmosphere, trends in multi-year transport changes is considered. It is noted the important role of moisture inflows from the Arctic Ocean in the summer season and their influence on the growth of long-wave radiation and amplification of sea ice shrinking.

A lag between temperature and atmospheric CO_2 concentration based on a simple coupled model of climate and the carbon cycle is considered in [13]. It is shown that the lag in changes in carbon dioxide concentration in the atmosphere relative to changes in global surface temperature, obtained from paleoreconstructions, is reproduced in the framework of generally accepted climate models and does not contradict the conclusions about the key role of the anthropogenic greenhouse effect in current climate change. It was found that the dependence of the solubility of CO_2 in the ocean on temperature does not fundamentally change the mutual delay between CO_2 concentration in the atmosphere and global surface temperature under external influence on the system [13].

Projections of the surface air temperature, precipitation and evaporation in the Arctic through the 21st century using an ensemble of CMIP5 climate models are analyzed in [14, 15]. The projections are shown for three scenarios of radiative forcing of the climate system: RCP2.6, RCP4.5 and RCP8.5. A comparison is undertaken with CMIP3 projections under SRES scenarios.

In [16] the investigation is made of interconnections amongst climatic processes in the North Atlantic and Arctic. It is shown that ice melting in the Arctic in 70's-90's of the 20th century is connected with climate variability in the North Atlantic well presented in the indexes of multidecadal oscillation and intensity of Atlantic meridional overturning circulation. As well, the latter reflects climatic changes in the heat and fresh water fluxes from the North Atlantic surface to the mid-latitude atmosphere. The physicostatistical scenario of climate change (the combined scenario) based on composition of the so-called "greenhouse" (external forcing) and "cyclic" (internal variability of climatic system) effects. The numerical simulations were performed with the ocean general circulation model for retrospective and prognostic reconstruction of thermohaline circulation and sea ice in the North Atlantic and Arctic Oceans. Due to analysis of the simulation results and investigation of their cyclic properties the authors find a new approach to description of climatic variability of the Arctic and the Northern Sea Route. This approach lets one describe temperature growth concerned with both greenhouse gas emission and climate variability (particularly, the observed cooling in 1950–1970 years). The proposed combined scenario of the climatic change presents the possible cooling in the Arctic and the corresponding decrease of the shipping season in the Northern Sea

Route for the next 10–20 years. The aim of the research is to estimate how much the North Atlantic variability influences Eurasia climate variations, in order to allow for them by the following forecasting.

The effects of Atlantic water inflow on the climate variability in the Barents Sea are studied in [17]. Initial data are the series of water temperature at the Kola meridian cross-section, monthly values of ice extent, air temperature at the stations, sea level pressure from the reanalysis data, and sea surface temperature. The methods of multivariate correlation, spectral, and factor analysis and EOF decomposition are used. It was found that variations in the Atlantic water inflow define the main part of interannual variability of sea ice extent, water temperature, and air temperature in the Barents Sea in the cold season. The influence of regional atmospheric circulation on the interannual variability of these parameters is small. The effects that water temperature anomalies in the area of Newfoundland and in the equatorial part of the North Atlantic have on climate parameters in the Barents Sea are discovered. The response of these parameters lags behind the respective anomalies by 9–58 months. The high correlation between them makes it possible to develop the method of statistical forecasting of sea ice extent and water temperature in the Barents Sea with the lead time up to 4 years.

In [18] advancing polar prediction capabilities on daily to seasonal time scales are considered. The polar regions have been attracting more and more attention in recent years, fuelled by the perceptible impacts of anthropogenic climate change. Polar climate change provides new opportunities, such as shorter shipping routes between Europe and East Asia, but also new risks such as the potential for industrial accidents or emergencies in ice-covered seas. It is argued that environmental prediction systems for the polar regions are less developed than elsewhere. There are many reasons for this situation, including the polar regions being (historically) lower priority, with less in situ observations, and with numerous local physical processes that are less well-represented by models. By contrasting the relative importance of different physical processes in polar and lower latitudes, the need for a dedicated polar prediction effort is illustrated. Research priorities are identified that will help to advance environmental polar prediction capabilities. Examples include an improvement of the polar observing system; the use of coupled atmosphere-sea ice-ocean models, even for short-term prediction; and insight into polar-lower latitude linkages and their role for forecasting. Given the enormity of some of the challenges ahead, in a harsh and remote environment such as the polar regions, it is argued that rapid progress will only be possible with a coordinated international effort. More specifically, it is proposed to hold a Year of Polar Prediction (YOPP) from mid-2017 to mid-2019 in which the international research and operational forecasting community will work together with stakeholders in a period of in-

tensive observing, modelling, prediction, verification, user-engagement and educational activities.

In [19] the influence of global warming and the rapid reduction of sea ice in the Arctic (up to the formation of ice-free conditions in the Arctic Ocean during the summer period) on the hydrological regime in northern Eurasia is considered. Ensemble calculations of climate were made and changes in atmospheric moisture circulation and water balance were estimated at large watersheds after the disappearance of long-term sea ice in the Arctic. On the example of large watersheds of the Siberian rivers, significant changes in the hydrological regime are shown, which are especially evident during the period of intensive snow melting in spring and early summer. It has been established that an increase in the frequency of spring floods in the river watersheds adjacent to the Arctic Ocean is expected. It is shown that the reduction of the ice cover of the Arctic Ocean does not have a significant effect on changes in the hydrological cycle in Northern Eurasia, in contrast to global warming.

In [20] climate change simulation based on 30-member ensemble of Voeikov Main Geophysical Observatory RCM (resolution 25 km) for Northern Eurasia is used to drive hydrological model CaMa-Flood. Using this modeling framework, we evaluate the uncertainties in the future projection of the peak river discharge and flood hazard by 2050–2059 relative to 1990–1999 under IPCC RCP8.5 scenario. Large ensemble size, along with reasonably high modeling resolution, allows one to efficiently sample natural climate variability and increase our ability to predict future changes in the hydrological extremes. It has been shown that the annual maximum river discharge can almost double by the mid-XXI century in the outlets of major Siberian rivers. In the western regions, there is a weak signal in the river discharge and flood hazard, hardly discernible above climate variability. Annual maximum flood area is projected to increase across Siberia mostly by 2–5% relative to the baseline period. A contribution of natural climate variability at different temporal scales to the uncertainty of ensemble prediction is discussed. The analysis shows that there expected considerable changes in the extreme river discharge probability at locations of the key hydropower facilities. This suggests the extensive studies are required to develop recommendations for maintaining regional energy security.

A long-term climatology of cloudiness over the Norwegian, Barents and Kara Seas (NBK) based on visual surface observations is presented in [21]. Annual mean total cloud cover (TCC) over the NBK is almost equal over solid-ice (SI) and open-water (OW) parts of NBK (73B±3% and 76B±2% respectively). In general, TCC has higher intra- and inter-annual variability over SI than over OW. A decrease of TCC in the middle of the 20th century and an increase in the last few decades was found at individual stations and for the NBK as a

whole. In most cases these changes are statistically significant with magnitudes exceeding the data uncertainty that is associated with the surface observations. The most pronounced trends are observed in autumn when the largest changes to the sea-ice concentration (SIC) occur. TCC over SI correlates significantly with SIC in the Barents Sea, with a statistically significant correlation coefficient between annual TCC and SIC. Cloudiness over OW shows non-significant correlation with SIC. An overall increase in the frequency of broken and scattered cloud conditions, and a decrease in the frequency of overcast and cloudless conditions were found over OW. These changes are statistically significant and likely to be connected with the long-term changes of morphological types.

The observational study [22] compares seasonal variations of surface fluxes (turbulent, radiative, and soil heat) and other ancillary atmospheric/surface/permafrost data based on in-situ measurements made at terrestrial research observatories located near the coast of the Arctic Ocean. Hourly-averaged multi-year data sets collected at Eureka (Nunavut, Canada) and Tiksi (East Siberia, Russia) are analyzed in more detail to elucidate similarities and differences in the seasonal cycles at these two Arctic stations, which are situated at significantly different latitudes (80.0°N and 71.6°N, respectively). While significant gross similarities exist in the annual cycles of various meteorological parameters and fluxes, the differences in latitude, local topography, cloud cover, snowfall, and soil characteristics produce noticeable differences in fluxes and in the structures of the atmospheric boundary layer and upper soil temperature profiles. An important factor is that even though higher latitude sites (in this case Eureka) generally receive less annual incoming solar radiation but more total daily incoming solar radiation throughout the summer months than lower latitude sites (in this case Tiksi). This leads to a counter-intuitive state where the average active layer (or thaw line) is deeper and the topsoil temperature in mid-summer are higher in Eureka which is located almost 10° north of Tiksi. The study highlights the differences in the seasonal and latitudinal variations of the incoming shortwave and net radiation as well as the moderating cloudiness effects that lead to temporal and spatial differences in the structure of the atmospheric boundary layer and the uppermost ground layer. Specifically the warm season is shorter and mid-summer amplitude of the surface fluxes near solar noon is generally less in Eureka than in Tiksi. During the dark Polar night and cold seasons when the ground is covered with snow and air temperatures are sufficiently below freezing, the near-surface environment is generally stably stratified and the hourly averaged turbulent fluxes are quite small and irregular with on average small downward sensible heat fluxes and upward latent heat and carbon dioxide fluxes. The magnitude of the turbulent fluxes increases rapidly when surface snow disappears and the air temperatures rise above freezing

during spring melt and eventually reaches a summer maximum. Throughout the summer months strong upward sensible and latent heat fluxes and downward carbon dioxide (uptake by the surface) are typically observed indicating persistent unstable (convective) stratification. Due to the combined effects of day length and solar zenith angle, the convective boundary layer forms in the High Arctic and can reach long-lived quasi-stationary states in summer. During late summer and early autumn all turbulent fluxes rapidly decrease in magnitude when the air temperature decreases and falls below freezing. Unlike Eureka, a pronounced zero-curtain effect consisting of a sustained surface temperature hiatus at the freezing point is observed in Tiksi during fall due to wetter and/or water saturated soils.

In [23] the modern climate of atmospheric surface layer in the Northern Yakutia and, in particular, in Tiksi. Climatic characteristics of minimal and maximal air temperatures are estimated with data of standard meteorological measurements collected at 22 marine and continental weather stations in 1978–2010 and in Tiksi during 1936–2015. The basic parameters of extremes, maps of its spatial distribution, and trends are presented. Synoptic conditions of storms and sharp temperature changes are investigated.

Results of comparative analysis of Russian and Norwegian precipitation gauges measurements in Barentsburg, Western Spitsbergen, is discussed in [24]. Results of albedo measurements of snowglacier surface of Svalbard on example of Aldegonda glacier (Greenfjorden Bay) and surrounding area of Russian settlement Barentsburg, obtained in recent years including field phase of IPY 2007-2008 are discussed in [25, 26]. The spatial and temporal variability of the albedo and its relationship to surface contamination is analyzed.

Data on spectral composition of shortwave radiation that is reflected from snow and penetrates deep into the snow cover obtained near the Barentsburg settlement (Svalbard) are discussed in [27]. Measurements were made by the use of the spectral radiometer TriOS Ramses within the wavelength range of 280–950 nm. The results will allow more proper taking account of the anthropogenic pollution effects on the radiative properties of snow cover under conditions of industrial activity related to the coal extraction and burning in Barentsburg.

Episodic emissions of methane with the concentration of 4 ppm to the lower atmosphere near the continental slope of the Arctic Ocean are considered in [28, 29]. It is revealed that such methane emissions can be associated with the erosion of sediments containing gas hydrates, for example, as a result of the effects of mudflows caused by the instability of slope currents as well as by the geologic activity in the zone of significant depth drops. The high background concentration of methane is registered in the central part of the Arctic Ocean that is probably provoked by biologic activity within sea ice and on its bottom.

In [30] changing the boundaries of the permafrost layer and the zone of stability of methane hydrates on the Arctic shelf of Eurasia in 1950–2100 is considered using the bottom sediment model and the Arctic Ocean model. The thermal condition of the soils of the Yamal Peninsula and adjacent regions for the last 90000 years has been calculated in [31, 32]. According to the results obtained in climate conditions of maximum glaciation about 90 000 years ago, the depth of the upper boundary of the stability zone of methane hydrates in this region could reach the surface. The estimates of the influence of modern climatic changes on the strength of frozen rocks and the stability of relict methane hydrates of the Yamal Peninsula are obtained. The formation of craters after gas emissions in Yamal may be associated with the destabilization of relict methane hydrates as a result of an increase in near-surface temperature in recent years.

In [33] stability estimates for the continental permafrost methanhydrates of the regions of Northern Eurasia and North America with the risk of gas emissions into the atmosphere as a result of possible dissociation of gas hydrates in the Holocene optimum and under current climatic conditions are obtained using an ensemble of model calculations of the thermal regime of permafrost soils and paleo-reconstructions.

The results of modeling changes in the thermal regime of permafrost soils with the assessment of thermobaric conditions of formation, stability and dissociation of gas hydrates on the Yamal Peninsula, taking into account the formation and degradation of glaciation, transgression of the sea and various geothermal flows are presented in [34].

The relationship between regional anomalies of methane in the atmosphere and temperature anomalies at the surface in the north of Western Siberia, in particular, on the Yamal Peninsula in the summer of 2016, was analyzed in [35]. Quantitative estimates of regional anomalies, trends and sensitivity of changes in atmospheric methane to changes in near-surface temperature on the daily and interannual scale were obtained. The features of the large-scale atmospheric circulation that contributed to the formation of the anomalous temperature regime over the north of Western Siberia with an increase in the regional content of methane in the atmosphere are noted.

The quantitative estimates of the contribution of the radiative forcing of greenhouse gases and the Atlantic multi-ten-year oscillation to the trends of global near-surface temperature and near-surface temperature in different latitudinal zones are presented in [36].

Characteristics of cyclones (frequency, intensity and size) and their changes in the Arctic region in a warmer climate have been analyzed in [37] with the use of the HIRHAM regional climate model simulations with SRES-A1B anthropogenic scenario for the twenty first century. The focus was on cyclones for

the warm (April–September) and cold (October–March) seasons. The present-day cyclonic characteristics from HIRHAM simulations are in general agreement with those from ERA–40 reanalysis data. Differences noted for the frequency of cyclones are related with different spatial resolution in the model simulations and reanalysis data. Potential future changes in cyclone characteristics at the end of the twenty first century have been analyzed. According to the model simulations, the frequency of cyclones is increasing in warm seasons and decreasing in cold seasons for a warmer climate in the twenty first century.

The ability of the reanalyses data (NASA-MERRA, ERA-INTERIM, NCEP-CFSR, ASR) and regional climate model simulations (RCM HIRHAM5) to represent polar mesocyclones (PMCs) over European sector of the Arctic (ESA) in comparison with satellite data is estimated in [38]. Results show that reanalyses can represent up to 65% of concrete observed polar mesocyclones from satellite data for 2002−2008. It is noted that Arctic reanalysis ASR with high spatial resolution reproduces more PMCs than from other reanalyses with a coarser resolution. Noted differences in the characteristics of Arctic mesocyclones from reanalyses data are related both with the model structure and data assimilation methods. RCM HIRHAM reproduces the same number of PMCs as Arctic reanalysis ASR with high spatial distribution. Models with a higher spatial resolution and with an adequate description of mesoscale processes in the Arctic are required to reproduce small-scale mesocyclones.

In [39] the analysis of the characteristics of Arctic cyclones and their intra- and interannual variations obtained by calculations with a regional climate model for the Arctic region (HIRHAM) with spectral attraction (spectral nudging) was carried out in comparison with reanalyses with different spatial resolution (ERA-Interim and ASR) for the period 2000–2009. It is noted that the characteristics of Arctic cyclones, the features of their spatial distributions, annual variation and interannual variations according to model calculations are generally consistent with the data of reanalyses, including ASR. The differences noted for the repeatability of Arctic cyclones are associated, in particular, with different spatial resolution of the data and differences in the detection of small cyclones, including polar mesocyclones. To reproduce small polar mesocyclones, models with higher spatial resolution and with an adequate description of mesoscale processes in the Arctic region are needed.

The ability of state-of-the-art regional climate models to simulate cyclone activity in the Arctic is assessed in [40] based on an ensemble of 13 simulations from 11 models from the Arctic-CORDEX initiative. Some models employ large-scale spectral nudging techniques. Cyclone characteristics simulated by the ensemble are compared with the results forced by four reanalyses (ERA-Interim, NCEP Climate Forecast System Reanalysis, NASA Modern-Era Ret-

rospective analysis for Research and Applications Version 2, and Japan Meteorological Agency-Japanese 55-year reanalysis) in winter and summer for 1981–2010. Cyclone statistics between ERA-Interim and the ASR reanalyses for 2000–2010 have been compared. Biases in cyclone frequency, intensity, and size over the Arctic are also quantified. Variations in cyclone frequency across the models are partly attributed to the differences in cyclone frequency over land. The variations across the models are largest for small and shallow cyclones for both seasons. A connection between biases in the zonal wind at 200 hPa and cyclone characteristics is found for both seasons. Most models underestimate zonal wind speed in both seasons, which likely leads to underestimation of cyclone mean depth and deep cyclone frequency in the Arctic. In general, the regional climate models are able to represent the spatial distribution of cyclone characteristics in the Arctic but models that employ large-scale spectral nudging show a better agreement with ERA-Interim reanalysis than the rest of the models. Trends also exhibit the benefits of nudging. Models with spectral nudging are able to reproduce the cyclone trends, whereas most of the nonnudged models fail to do so. However, the cyclone characteristics and trends are sensitive to the choice of nudged variables.

In [41] cyclones in the Arctic are detected and tracked in four different reanalysis data sets from 1981 to 2010. In great detail the spatial and seasonal patterns of changes are scrutinized with regards to their frequencies, depths, and sizes. Common spatial patterns for their occurrences, with centers of main activity over the seas in winter, and more activity over land and over the North Pole in summer have been found. The deep cyclones are more frequent in winter, and the number of weak cyclones peaks in summer. Good agreement of our tracking results across the different reanalyses was obtained. Regarding the frequency changes, strong decreases in the Barents Sea and along the Russian coast toward the North Pole and increases over most of the central Arctic Ocean and toward the Pacific in winter. Areas of increasing and decreasing frequencies are of similar size in winter. In summer there is a longish region of increase from the Laptev Sea toward Greenland, over the Canadian archipelago, and over some smaller regions west of Novaya Zemlya and over the Russia. The larger part of the Arctic experiences a frequency decrease. All summer changes are found statistically unrelated to the winter patterns. The frequency changes are found unrelated to changes in cyclone depth and size. There is generally good agreement across the different reanalyses in the spatial patterns of the trend sign. The magnitudes of changes in a particular region may strongly differ across the data.

The results of expedition measurements of the set of physical-chemical characteristics of atmospheric aerosol in areas of the Arctic and Far East seas during summer 2013 is presented in [42]. The specific features of spatial distri-

bution and time variations of aerosol optical depth (AOD) of the atmosphere in the wavelength range of 0.34–2.14 μm and boundary layer height, aerosol and black carbon mass concentrations, and disperse and chemical composition of aerosol are discussed. Over the Arctic Ocean there is a decrease in aerosol and black carbon concentrations in a northeastern direction: higher values were observed in the region of Spitsbergen and near the Kola Peninsula; and minimum values were observed at northern margins of the Laptev Sea. Average AOD (0.5 μm) values in this remote region were 0.03; the aerosol and black carbon mass concentrations were 875 and 22 ng m^{-3}, respectively. The spatial distributions of most aerosol characteristics over Far East seas show their latitudinal decrease in the northern direction. From the Japan Sea to the Chukchi Sea, the aerosol number concentration decreased on average from 23.7 to 2.5 cm^{-3}, the black carbon mass concentration decreased from 150 to 50 ng m^{-3}, and AOD decreased from 0.19 to 0.03. Variations in the boundary layer height, measured by ship-based lidar: the average value was 520 m, and the maximal value was 1200 m. In latitudinal distribution of the boundary layer height, there is a characteristic minimum at a latitude of ~ 55° N. For water basins of eight seas, the authors present the chemical compositions of the water-soluble aerosol fraction (ions, elements) and small gas-phase species, as well as estimates of their vertical fluxes. It is shown that substances are mainly (75–89%) supplied from the atmosphere to the sea surface together with gas-phase species. The deposited ions account for from 11 to 24.5%, and trace elements account for 0.2–0.4% of the total sum of water-soluble components. The average vertical fluxes of aerosol substance are a factor of 4–7 larger in the Japan Sea than in the water basins of Arctic seas [42].

Results of atmospheric aerosol optical depth measurements on Spitsbergen Archipelago in 2011–2016 are presented in [43]. The results of comparison of the average physical-chemical aerosol characteristics in the Barentsburg (Spitsbergen Archipelago) and over the Barents Sea are discussed in [44]. A small (less than 0.02) excess of the atmospheric aerosol optical depth in the island area over the maritime region is noted. The aerosol microphysical characteristics differ stronger in the surface layer: the black carbon concentrations are 4 times larger in Barentsburg, and particle concentrations are 2,4 times larger over the Barents Sea. The absolute concentrations of ions in the atmosphere of Barentsburg are smaller than over sea. However, with respect to the relative content, Na^+, Cl^- and NH_4^+, SO_4^{2-} ions predominate in both regions, indicating equivalent contributions of continental and maritime sources.

Four years of continuous aerosol number size distribution measurements in Tiksi, are analyzed in [45]. Particle size distributions were measured with a differential mobility particle sizer (in the diameter range of 7–500 nm) and with

an aerodynamic particle sizer (in the diameter range of 0.5–10 μm). Source region effects on particle modal features and number, and mass concentrations are presented for different seasons. The monthly median total aerosol number concentration in Tiksi ranges from 184 cm^{-3} in November to 724 cm^{-3} in July, with a local maximum in March of 481 cm^{-3}. The total mass concentration has a distinct maximum in February–March of 1.72–2.38 μgm^{-3} and two minimums in June (0.42 μgm^{-3}) and in September–October (0.36–0.57 μgm^{-3}). These seasonal cycles in number and mass concentrations are related to isolated processes and phenomena such as Arctic haze in early spring, which increases accumulation and coarse-mode numbers, and secondary particle formation in spring and summer, which affects the nucleation and Aitken mode particle concentrations. Secondary particle formation was frequently observed in Tiksi and was shown to be slightly more common in marine, in comparison to continental, air flows. Particle formation rates were the highest in spring, while the particle growth rates peaked in summer. These results suggest two different origins for secondary particles, anthropogenic pollution being the important source in spring and biogenic emissions being significant in summer. The impact of temperature-dependent natural emissions on aerosol and cloud condensation nuclei numbers was significant: the increase in both the particle mass and the CCN (cloud condensation nuclei) number with temperature was found to be higher than in any previous study done over the boreal forest region. In addition to the precursor emissions of biogenic volatile organic compounds, the frequent Siberian forest fires, although far away, are suggested to play a role in Arctic aerosol composition during the warmest months. Five fire events were isolated based on clustering analysis, and the particle mass and CCN number were shown to be somewhat affected by these events. In addition, during calm and cold months, aerosol concentrations were occasionally increased by local aerosol sources in trapping inversions [45].

The results of the atmospheric sea surface layer aerosol composition studies executed during expedition “Sever-2015” on the route from Arkhangelsk to the Severnaya Zemlya archipelago from October 9 to 26, 2015 are presented in [46]. The data about mass concentration of black carbon obtained with high spatial-temporal resolution in the White, Barents and Kara Seas showed its significant variability: from background values about 20 ng/m^3 to values of more than 1000 ng/m^3 during periods of air mass transfer from the continent. Cluster analysis of the microstructure of natural arctic aerosols gave possibility to identify the dominant groups of particles of sea salt and calcium sulfate. In case the increase of black carbon up to 250 ng/m^3 the groups of carbon-containing aerosols and particles rich in sulfur, characteristic for emissions from the combustion of natural fuel were revealed.

Estimates of the duration of the navigation period and its changes in 1980–2013 were obtained in [47]. For the Northern Sea Route (NSR) based on satellite data on sea ice concentration in the Arctic Ocean. The ability of modern climate models to reproduce the current regime of sea ice in the Arctic and its changes in comparison with satellite data has been evaluated. The model estimates of the possible prospects of the NSR in the XXI century are made. New model estimates of changes in the duration of the navigation period for the NSR in the XXI century have been presented in [48].

Transit navigation through Northern Sea Route from satellite data and CMIP5 simulations is considered in [49]. Rapid Arctic sea ice decline over the last few decades opens new perspectives for Arctic marine navigation. Both satellite data and CMIP5 ensemble of climate models were used to estimate the NSR transit window allowing intercontinental navigation between Atlantic and Pacific regions. New approach to calculate start and end dates of the navigation season along the NSR was introduced. We show that modern climate models are able to reproduce the mean time of the NSR transit window and its trend over the last few decades. The selected models demonstrate that the rate of increase of the NSR navigation season will slow down over the next few decades with the RCP4.5 scenario. By the end of the 21st century ensemble-mean estimates show an increase of the NSR transit window by about 4 and 6.5 months according to RCP4.5 and 8.5, respectively. Estimated trends for the end date of the navigation season are found to be stronger compared to those for the start date [49].

Variations in the duration of the navigation period along the NSR based on simulations with an ensemble of climatic models are presented in [50]. Due to the rather large uncertainty in the sensitivity of sea ice characteristics in the Arctic Ocean to climate change in modern climate models, it is necessary to use analysis methods that take into account the uncertainty of the results of numerical calculations with such models, as well as the uncertainty of observational data. The purpose of this work was to analyze changes in the duration of navigation period at the NSR according to calculations with climate models of the CMIP5 ensemble (CoupledModelsIntercomparisonProject, phase 5) using Bayesian statistics. It was obtained that under the scenarios of anthropogenic effects of RCP 4.5 and 8.5, the expected duration of navigation period at the NSR will be 2–3 months in the middle of the XXI century and 3–6 months at its end.

The article [51] presents an analysis of the impacts of climate change on the natural and economic systems of the Arctic and the existing methods for assessing climatic risks. Based on the analysis of the impact of climate change on natural and economic systems and the Arctic population, a register of risks due to climate change has been formed. A conceptual model for assessing the impact of climate change on various systems is proposed. The main problems in

the identification of climatic risks in the Arctic are identified. Indicators of climate change were selected: the surface air temperature; sea ice extent and the frequency of extreme hydrometeorological phenomena that affect economic activity in the marine Arctic and its sub-regions. The assessment methodology of natural and economic systems vulnerabilities in the marine part of Russian Arctic, including susceptibility to impacts, sensitivity and adaptive potential, is considered. These are the key factors on the basis of which the systems vulnerability to climate change is determined, as well as the information support of the processes of assessment and reduction of the consequences of climate threats. The algorithm of the developed methodology for determining of vulnerability includes a sequence of 7 steps [51].

Antarctic meteorology studies

In the Antarctic, most of the Russian meteorological and climate studies ares associated with paleoclimate and atmospheric aerosols.

An important share of paleoclimatic information is buried within the lowermost layers of deep ice cores. Because improving our records further back in time is one of the main challenges in the near future, it is essential to judge how deep these records remain unaltered, since the proximity of the bedrock is likely to interfere both with the recorded temporal sequence and the ice properties. In [52] a multiparametric study (δD-$\delta^{18}O$ice, $\delta^{18}O$atm, total air content, CO_2, CH_4, N_2O, dust, high-resolution chemistry, ice texture) of the bottom 60 m of the EPICA (European Project for Ice Coring in Antarctica) Dome C ice core from central Antarctica, is presented. These bottom layers were subdivided into two distinct facies: the lower 12 m showing visible solid inclusions (basal dispersed ice facies) and the upper 48 m, which we will refer to as the "basal clean ice facies". Some of the data are consistent with a pristine paleoclimatic signal, others show clear anomalies. It is demonstrated that neither large-scale bottom refreezing of subglacial water, nor mixing (be it internal or with a local basal end term from a previous/initial ice sheet configuration) can explain the observed bottom-ice properties. It is concluded that the paleoclimatic signal is only marginally affected in terms of global ice properties at the bottom of EPICA Dome C, but that the timescale was considerably distorted by mechanical stretching of MIS20 due to the increasing influence of the subglacial topography, a process that might have started well above the bottom ice. A clear paleoclimatic signal can therefore not be inferred from the deeper part of the EPICA Dome C ice core. The work suggests that the existence of a flat monotonic ice–bedrock interface, extending for several times the ice thickness, would be a crucial factor in choosing a future "oldest ice" drilling location in Antarctica [52].

Marine records indicate a dramatic change in the predominant periodicity of climate variability, from about 40 ka to about 100 ka around one million years ago. The reason for this major climatic shift, called the Mid-Pleistocene Transition (MPT), remains unknown and is of great interest to the climate scientist. Could the core of the oldest meteoric ice bedded at Vostok between 3310 and 3539 m, which has experienced severe deformation, nevertheless be useful in deciphering some of the aspects of the MPT enigma? Reflecting upon this question and considering the available data from the disturbed section of the ice core, the authors of [53] feel impelled to propose a new project focused on the oldest Vostok meteoric ice, which could be named the Vostok Oldest Ice Challenge (VOICE).

The loss and alteration of past atmospheric information from air trapping mechanisms under low-accumulation conditions through continuous CH_4 (and CO) measurements are investigated in [54]. Methane concentration changes were measured over the Dansgaard–Oeschger event 17 (DO-17, ~60 000yr BP) in the Antarctic Vostok 4G-2 ice core. Measurements were performed using continuous-flow analysis combined with laser spectroscopy. The results highlight many anomalous layers at the centimeter scale that are unevenly distributed along the ice core. The anomalous methane mixing ratios differ from those in the immediate surrounding layers by up to 50 ppbv. This phenomenon can be theoretically reproduced by a simple layered trapping model, creating very localized gas age scale inversions. A method for cleaning the record of anomalous values that aims at minimizing the bias in the overall signal is proposed. Once the layered-trapping-induced anomalies are removed from the record, DO-17 appears to be smoother than its equivalent record from the high-accumulation WAIS Divide ice core. This is expected due to the slower sinking and densification speeds of firn layers at lower accumulation. However, the degree of smoothing appears surprisingly similar between modern and DO-17 conditions at Vostok. This suggests that glacial records of trace gases from low-accumulation sites in the East Antarctic plateau can provide a better time resolution of past atmospheric composition changes than previously expected [54].

The results of detailed isotopic studies of ice core samples from the Vostok station (East Antarctica) related to the MIS-11 era (the 11th sea isotope stage, i.e. 370–440 thousand years ago) are presented in [55]. Reconstruction of paleoclimatic conditions in this period of time was performed using the method of interpretation of the results of isotopic studies of ice which is based on the joint analysis of three independent parameters: δD, d-excess, 17O-excess. The isotopic composition (δD) and the deuterium excess depend on the following three meteorological parameters – the condensation temperature near the Vostok station, relative humidity, and the sea surface temperature at the source of

moisture, whereas 17O-excess depends only on the first two parameters. Accordingly, the proposed method of interpretation allows reconstructing the paleoclimatic conditions (the condensation temperature and surface air temperature at the Vostok station; sea surface temperature and relative humidity above the ocean) in two different regions in past epochs. For the first time, data on minor fluctuations in the relative humidity of the air in the moisture source throughout the MIS-11 era were obtained. The results obtained on the basis of isotopic analysis of ice cores from stations Vostok and Concordia indicated that in the optimum MIS-11 the air temperature was 4°C higher, and in the Termination V – 8°C lower than the present-day values. The similarity of data between the marine columns DSDP 94-607 (North Atlantic), ODP 177-1090 (South Ocean) and results of [55] points to the global nature of changes in the sea surface temperature during the MIS-11 era.

One of the key priority tasks for the international Antarctic community is drilling and studying old Antarctic ice with age exceeding 1 million years in order to investigate possible reasons for the Mid-Pleistocene Transition. During the 2017–2018 austral season at Vostok station the authors of [56] carried out microscopic study of geometrical properties of the crystalline inclusions of air hydrates in ice core samples from boreholes 5G-3 (Vostok) and DC2 (EPICA DC) in depth intervals where the age of the ice exceeded 400,000 years. The obtained data confirmed the existence of a robust linear relationship between the mean radius of the hydrates and the age of the ice in the bottom part of the East Antarctic ice sheet, and will be useful for further development of the new dating technique based on the phenomena of hydrate growth in polar ice. Preliminary, the age of the atmospheric ice bedded at Vostok at a depth of 3538 m, inferred from the data on the size of the hydrates, amounts to 1.3 million years. The existence of ice older than 1 million years in the vicinity of Vostok implies that in the area of Ridge B, where the ice flow line which passes through Vostok Station originates, even older ice, with undisturbed stratigraphy, may exist. It would be desirable therefore to carry out a glacio-geophysical traverse to Ridge B in order to implement a detailed study of Dome B area aimed at identifying the most suitable site for a new deep drilling of the Antarctic ice sheet.

In [57] for the first time on the base of reliable field data the maps of accumulation rate, isotopic composition and density of the snow were prepared for the Indian ocean sector of East Antarctica and particularly for the vicinity of subglacial lake Vostok. The area of minimum values of the isotopic composition and accumulation of the snow was found. It was shown that in Central Antarctica the distribution of glaciological and climatic characteristics does not obey well the rules of latitudinal and altitudinal zonality and is predominantly controlled by distance to the moisture source. The complicated interconnection between snow isotopic composition and surface air temperature in Central Ant-

arctica was depicted. It was demonstrated that the surface of the glacier above subglacial lakes presents a unique locality with special meteorological and glaciological conditions.

The temperature and snow accumulation rate anomaly over the past 350 years have been reconstructed in [58] based on isotopic composition of shallow ice cores and snow pits samples as well as glaciological observations in pits and at stake farms located in Indian Ocean sector of East Antarctica. The relationship of temporal variability of isotopic composition of precipitation and surface air temperature in ensemble with sea surface temperature has been analyzed. The fingerprints of Little Ice Age and climatic shift 1970s have been defined.

In 2011–2015, during five summer seasons and two winter seasons of Russian Antarctic Expedition at Vostok Station (Antarctica) direct measurements of snow sublimation were conducted [59]. The sublimation rate depends on two parameters: surface air temperature and wind speed. During the cold period of year (March–October with the average day air temperature below –45°C) the sublimation rate is near zero, or even condensation of water vapor on the snow surface occurs (in total up to 0.2 mm w.e.). The total sublimation during the warm period of year (November – February) is about 2.3 mm w.e. However, this value does not take into account the sublimation of the snow particles during the wind-driven snow transport. With this factor, total sublimation could be 4–5 mm w.e. Taking into account the present-day snow accumulation rate at Vostok, 23 mm w.e./year, there was estimated the annual precipitation amount in this area is about 25–28 mm w.e.

The results of glaciological investigations in the megadune area located 30 km to the east of Vostok Station are presented in [60]. Snow accumulation rate and isotope content (δD, $\delta^{18}O$ and $\delta^{17}O$) were measured along the 2 km profile across the megadune ridge accompanied by precise GPS altitude measurements and ground penetrating radar survey. It is shown that the spatial variability of snow accumulation and isotope content covaries with the surface slope. The accumulation rate regularly changes by 1 order of magnitude within the distance < 1 km, with the reduced accumulation at the leeward slope of the dune and increased accumulation in the hollow between the dunes. At the same time, the accumulation rate averaged over the length of a dune wave (22 mm w.e.) corresponds well with the value obtained at Vostok Station, which suggests no additional wind-driven snow sublimation in the megadunes compared to the surrounding plateau. The snow isotopic composition is in negative correlation with the snow accumulation. From the analyses the authors conclude that the spatial variability of the snow isotopic composition in the megadune area could be explained by post-depositional snow modifications.

To better understand how the climatic signal is passed from the precipitation to the snow, authors of [61] present results from varied snow samples from East Antarctica. In [62] isotopic composition (δD) data from six sites in Princess Elizabeth Land have been used in order to reconstruct air temperature variability in this sector of East Antarctica over the last 350 years. Surface studies of water isotopes in Antarctica for quantitative interpretation of deep ice core data is presented in [63].

Using new high-resolution 10Be measurements in the different ice cores, together with previously published data, an improved synchronization between Greenland and Antarctic ice cores during the Laschamp geomagnetic excursion ~41 kyr ago is presented in [64].

In [65] the authors build an enlarged database of ice core water stable isotope records from Antarctica, consisting of 112 records, to reconstruct Antarctic climate variability at regional and continental scales over the last 2,000 years. New reconstructions confirm a significant cooling trend from 0 to 1900 CE across all Antarctic regions where records extend back into the 1st millennium, with the exception of the Wilkes Land coast and Weddell Sea coast regions. Within this long-term cooling trend from 0 to 1900 CE, it was found that the warmest period occurs between 300 and 1000 CE, and the coldest interval occurs from 1200 to 1900 CE. Since 1900 CE, significant warming trends are identified for the West Antarctic Ice Sheet, the Dronning Maud Land coast and the Antarctic Peninsula regions, and these trends are robust across the distribution of records that contribute to the unweighted isotopic composites and also significant in the weighted temperature reconstructions. Only for the Antarctic Peninsula is this most recent century-scale trend unusual in the context of natural variability over the last 2000 years [65].

Antarctic snow accumulation variability at the regional scale over the past 1000 years is presented in [66]. A total of 79 ice core snow accumulation records were gathered and assigned to seven geographical regions, separating the high-accumulation coastal zones below 2000m of elevation from the dry central Antarctic Plateau. The regional composites of annual snow accumulation were evaluated against modelled surface mass balance (SMB) from RACMO2.3p2 and precipitation from ERA-Interim reanalysis. With the exception of the Weddell Sea coast, the low-elevation composites capture the regional precipitation and SMB variability as defined by the models. The central Antarctic sites lack coherency and either do not represent regional precipitation or indicate the model inability to capture relevant precipitation processes in the cold, dry central plateau. Study emphasizes the importance of low-elevation coastal zones, which have been under-represented in previous investigations of temporal snow accumulation.

Authors of [67] considered variations of snow accumulation rate in Central Antarctica over the last 250 years to compare the present-day data of instrumental observations of the air temperature and snow accumulation rate performed in Central Antarctica (the Vostok station) with the reconstructed paleogeographic data on a variability of these parameters in the past. The Vostok station is shown to be differing from other East Antarctic stations due to relatively higher rate of warming (1.6°C per 100 years) since 1958. A statistically significant relationship between the rate of snow accumulation and air was found.

Reproducible climate reconstructions of the Common Era are key to placing industrial-era warming into the context of natural climatic variability. In [68] a community-sourced database of temperature-sensitive proxy records from the PAGES2k initiative is presented. The database gathers 692 records from 648 locations, including all continental regions and major ocean basins. The records are from trees, ice, sediment, corals, speleothems, documentary evidence, and other archives. They range in length from 50 to 2000 years, with a median of 547 years, while temporal resolution ranges from biweekly to centennial. Nearly half of the proxy time series are significantly correlated with HadCRUT4.2 surface temperature over the period 1850–2014. Global temperature composites show a remarkable degree of coherence between high- and low-resolution archives, with broadly similar patterns across archive types, terrestrial versus marine locations, and screening criteria. The database is suited to investigations of global and regional temperature variability over the Common Era.

Better assessing the dynamic of stratosphere-troposphere exchange is a key point to improve our understanding of the climate dynamic in the East Antarctica Plateau, a region where stratospheric inputs are expected to be important. Although tritium (3H or T), a nuclide naturally produced mainly in the stratosphere and rapidly entering the water cycle as HTO, seems a first-rate tracer to study these processes, tritium data are very sparse in this region. The first high resolution measurements of tritium concentration over the last 50 years in three snow pits drilled at the Vostok station is presented in [69]. Natural variability of the tritium records reveals two prominent frequencies, one at about 10 years (to be related to the solar Schwabe cycles) and the other one at a shorter periodicity: despite dating uncertainty at this short-scale, a good correlation is observed between 3H and Na^+ and an anti-correlation between 3H and $\delta^{18}O$ measured on an individual pit. The outputs from the LMDZ Atmospheric General Circulation Model including stable water isotopes and tritium show the same 3H-$\delta^{18}O$ anti correlation and allow further investigation on the associated mechanism. At the interannual scale, the modelled 3H variability matches well with the Southern Annular Mode index. At the seasonal scale the modelled stratospheric tritium inputs in the troposphere are favored in winter cold and dry conditions.

Chemical composition of aerosol in the atmospheric surface layer of the East Antarctica coastal zone is analyzed in [70]. The aerosol samples were taken in 2006–2015 in the 200-km band of the sea-shore zone along routes of the research vessels of the Russian Antarctic Expedition as well as on territories of the Russian stations Molodezhnaya and Mirny. The results obtained did show the wide range of the aerosol concentrations and a certain variability of their chemical composition. The elemental composition of solid aerosols was analyzed. The largest concentrations were determined for Zn, Al and Fe.

In [71] the 12-year aerosol studies along the route of the Russian Antarctic Expeditions in the East Atlantic and the Southern Ocean are summarized. The authors analyzed the spatial distribution (with 5° step in latitude), seasonal (November/April) variations, and interrelations of aerosol optical and microphysical characteristics. It is shown that the latitudinally average variations in aerosol parameters in the East Atlantic exceed one order of magnitude. The lowest values are observed near Antarctica: aerosol optical depth (0.5 μm) varies from 0.02 to 0.5, number concentrations of small particles (d = 0.4–1 μm) vary in the range 0.8–19 cm^{-3}, concentrations of large (d > 1 μm) particles vary in the range 0.04–2.2 cm^{-3}, and aerosol and black carbon mass concentrations vary in ranges 0.5–14 $\mu g/m^3$ and 0.026–0.7 $\mu g/m^3$.

Based on long-term (2004–2016) expedition studies, statistical generalization and zoning of physical-chemical aerosol characteristics in the Eastern Atlantic (from English Channel to Antarctica) are performed in [71]. For six latitudinal zones of the Atlantic and Southern Oceans (> 45°N; 20°–45°N; 0°–20°N; 0°–20°S; 20°–55°S; > 55°S) the average values of the main aerosol characteristics are calculated, i.e., atmospheric AOD, fine and coarse AOD components, particle number concentrations, and mass concentrations of aerosol, black carbon, and water-soluble ions (Na^+, Mg^{2+}, Cl^-, K^+, Ca^{2+}, NH_4^+, NO_3^-, SO_4^{2-}), as well as of gas admixtures (SO_2, HCl, HNO_3, NH_3). It is shown that the zonal variability range of optical and microphysical aerosol characteristics is about an order of magnitude: the largest (minimal) average values are observed in the tropical zone (Southern Ocean). The zonal differences (a factor of 1.3 to 4.3) in concentrations of ions and gas admixtures are much smaller and comparable to synoptic variations. The concentrations of "marine" ions are maximal over the Southern Atlantic, and of "continental" ions, in the Northern hemisphere, in tropical and subtropical zones; the concentrations of all ions are minimal over the Southern Ocean.

References

1. Mokhov I.I. Modern climate change in the Arctic. Bulletin of the Russian Academy of Sciences. 2015, 85, No. 5–6, 478–484. (In Russian).

2. Alekseev G.V., Bolshiyanov D.Y., Radionov V.F., Frolov S.V. 95 years of climate and cryosphere studies of the Arctic in the Arctic and Antarctic Research Institute. Ice and Snow. 2015, 55(4):127–140. DOI: 10.15356/2076-6734-2015-4-127-140. (In Russian).

3. Alekseev G.V., Radionov V.F., Smolyanitsky V.M., Filchuk K.V. Results and prospects of the climate studies and climate service in the Arctic. Problemy Arktiki i Antarktiki. Arctic and Antarctic Research. 2018, 64, 3: 262–269. DOI: 10.30758/0555-2648-2018-64-3-262-269. (In Russian).

4. Alekseyev G. V. Development and amplification of global warming in the Arctic. Fundamental and applied climatology. 2015, No. 1, 11–26. (In Russian).

5. Meleshko V. P., O. M. Johannessen, A. V. Baidin, T. V. Pavlova, V. A. Govorkova, 2016: Arctic amplification: does it impact the polar jet stream? Tellus A. 2016, 68:1, 32330, DOI: 10.3402/tellusa.v68.32330.

6. Mokhov I.I., Semenov V.A. Weather and Climate Anomalies in Russian Regions Related to Global Climate Change. Russian Meteorology and Hydrology. 2016, 41, No. 2, 84–92.

7. Alekseev, G., Glok, N. and Smirnov, A. On assessment of the relationship between changes of sea ice extent and climate in the Arctic. Int. J. Climatol. 2015; 36(9). DOI:10.1002/joc.4550.

8. Alekseev G.V., Aleksandrov E.I., Glok N.I., Ivanov N.E., Smolyanitsky V.M., Kharlanenkova N.E., and Yulin A.V. Arctic Sea Ice Cover in Connection with Climate Change. Izvestiya. Atmospheric and Oceanic Physics. 2015, 51, No. 9, 889–902. DOI: 10.1134/S0001433815090029. (In Russian).

9. Alekseev G.V., Kuzmina S.I., Glock N.I. The influence of ocean temperature anomalies at low latitudes on the atmospheric heat transfer to the Arctic. Fundamental and applied climatology. 2017, No. 1, 106–123. (In Russian).

10. Alekseev G.V., Kuzmina S.I., Glok N.I., Vyazilova A.E., Ivanov N.E., Smirnov A.V. The influence of the Atlantic on warming and shrinking sea ice cover in the Arctic. Ice and Snow. 2017, 57 (3), 381–390. DOI: 10.15356/2076-6734-2017-3-381-390 (In Russian).

11. Alekseev G.V., Kuzmina S.I., Urazgildeeva A.V., Bobylev L.P. Influence of atmospheric heat and moisture transfers on the increase of warming in the Arctic during the winter period. Fundamental and applied climatology. 2016, No. 1, 43–63. (In Russian).

12. Alekseev G.V., Kuzmina S.I., Urazgildeeva A.V., Bobylev L.P. N.V. Gnatuk Influence of the atmospheric heat and moisture transport on summer warming in the Arctic. Problems of Arctic and Antarctic. 2017, No.3 (113), 67–77. (in Russian)

13. Muryshev K.E., Eliseev A.V., Mokhov I.I., Timazhev A.V. A lag between temperature and atmospheric CO_2 concentration based on a simple coupled model of climate and the carbon cycle. Doklady Earth Sciences. 2015, 463, No. 2, 863–867. (In Russian)

14. Kattsov V.M., Pavlova T.V. Expected Arctic surface air temperature changes through the 21st century: projections with ensembles of global climate models (CMIP5 and CMIP3). Proceedings MGO. 2015, 579, 7−21. (In Russian).

15. Pavlova T.V., Kattsov V.M. Expected Arctic precipitation and evaporation changes through the 21st century: projections with ensembles of global climate models (CMIP5). Proceedings MGO. 2015, 579, 22–34. (In Russian)

16. Panin G., Vyruchalkina T., Solomonova I., Gusev A., Diansky N. Assessment of climatic changes in the Arctic in the 21st century based on the combined forecast. Arctic: Ecology and Economy. 2017, No. 2 (26), 35–52. DOI:10.25283/2223-4594-2017-2-35-52. (In Russian).

17. Alekseev G.V., Glok N.I., Smirnov A.V., Vyazilova A.E. The Influence of the North Atlantic on Climate Variations in the Barents Sea and Their Predictability. Russian Meteorology and Hydrology. 2016, 41, No. 8, 544–558. DOI: 10.3103/S1068373916080045.

18. Jung T., N.D. Gordon, P. Bauer, D.H. Bromwich, M. Chevallier, J. Day, J. Dawson, F. Doblas-Reyes, C. Fairall, H.F. Goessling, M. Holland, J. Inoue, T. Iversen, S. Klebe, P. Lemke, M. Losch, A. Makshtas, B. Mills, P. Nurmi, D. Perovich, P. Reid, I.A. Renfrew, G. Smith, G. Svensson, M. Tolstykh, Q. Yang, Advancing polar prediction capabilities on daily to seasonal time scales. Bulletin of the American Meteorological Society. 2016, 97, No. 9, 1631–1647. DOI: 10.1175/BAMS-D-14-00246.1.

19. Meleshko V.P., V.M. Kattsov, A.V. Baydin, T.V. Pavlova, V.A. Govorkova., 2016: Expected changes in the hydrological regime in Northern Eurasia as a result of the disappearance of long-term sea ice in the Arctic. Russian Meteorology and Hydrology. 2016, 41, No. 11, 5–21.

20. Shkolnik, I., Pavlova, T., Efimov, S., Zhuravlev, S. Future changes in peak river flows across Northern Eurasia as inferred from an ensemble of regional climate projections under the IPCC RCP8.5 scenario. Climate Dynamics. 2018, 50, 1–2, 215–230. Doi: 10.1007/s00382-017-3600-6.

21. Chernokulsky A.V., Esau I., Bulygina O.N., Davy R., Mokhov I.I., Outten S., Semenov A.V. Climatology and interannual variability of cloudiness in the Atlantic Arctic from surface observations since the late nineteenth century. J. Climate. 2017, 30, 2103–2120. DOI: 10.1175/JCLI-D-16-0329.1

22. Grachev A.A., Persson P.O.G., Uttal T., Akish E.A., Cox C.J., Morris S.M., Fairall C.W., Stone R.S., Lesins G., Makshtas A.P., Repina I.A.. Seasonal and latitudinal variations of surface fluxes at two Arctic terrestrial sites. Climate Dynamics. 2018, 51(5–6), 1793–1818. DOI: 10.1007/s00382-017-3983-4

23. Ivanov N.E., Makshtas A.P. Characteristics of climate variability in the Northern Yakutia – extremes of air temperature. Problems Arctic and Antarctic. 2017, No. 112 (2), 50–69. (In Russian).

24. Urazgildeeva, A. V., Sviashchennikov, P. N., Ivanov, B. V., Isaksen, K., Førland, E. J., Brækkan, R. Comparative analysis of Russian and Norwegian precipitation gauges measurements in Barentsburg, Western Spitsbergen. Czech Polar Reports. 2017, No. 7(1). DOI: 10.5817/CPR2017-1-5.

25. Ivanov B.V., Svyashchennikov P.N. Albedo of the snow-glacial surface of the Svalbard archipelago. Earth Research from Space. 2015, No. 4, 88–93. DOI: 10.7868 / S0205961415040041 (In Russian).

26. Ivanov B.V., Svyashchennikov P.N. Albedo of the snow-glacier surface of Svalbard. Atmosphere and Oceanic Physics, Issue of RAS. 2015, 51, No.9, 943–948. DOI: 10.1134/S0001433815090108.

27. Svyashchennikov P.N., A.V. Urazgildeeva, Y.N. Kurochkin, B.V. Ivanov, K.V. Chistyakov, D. Divin, S. Hudson. Spectral composition of shortwave radiation reflected and deep penetrating into snow near the Barentsburg settlement (Svalbard). Ice and Snow. 2015, 55 (3), 67–72. DOI: 10.15356/2076-6734-2017-3-381-390 (In Russian).

28. Nagurny A.P., Makshtas A.P., Makarov A.S. Methane in arctic atmospheric surface layer. Problems Arctic and Antarctic. 2015, No. 2 (104), 33–43. (In Russian).

29. Nagurny A.P., Makshtas A.P. Concentration of methane in atmospheric boundary layer by data of measurements on drifting ice stations "North Pole-36" and "North Pole 39". Russian Meteorology and Hydrology, 2016, 41, No. 3, 199–204.

30. Eliseev A.V., Malakhov V.V., Arzhanov M.M., Golubeva E.N., Denisov S.N., Mokhov I.I. Changing the boundaries of the permafrost layer and the zone of stability of methane hydrates on the Arctic shelf of Eurasia in 1950–2100. Doklady Earth Sciences. 2015, 465, No. 5, 598–603. (In Russian)

31. Arzhanov M.M., Mokhov I.I., Denisov S.N. Destabilization of relict gas hydrates with observed regional climate change. Arctic: Ecology and Economics. 2016, No. 4 (24), 46–51. (In Russian).

32. Arzhanov M.M, Mokhov I.I., Denisov S.N. The impact of regional climate change on the stability of relict gas hydrates. Doklady Earth Sciences. 2016, 468, No. 5, 572–574. (In Russian).

33. Arzhanov M.M., Mokhov I.I. Estimates of the degree of stability of continental relict methanhydrates in the Holocene optimum and under current climatic conditions. Doklady Earth Sciences. 2017, 476, No. 4, 456–460. (In Russian).

34. Arzhanov M.M., Malakhova V.V., Mokhov I.I. The conditions of formation and dissociation of methane hydrates over the past 130 thousand years according to model calculations. Doklady Earth Sciences. 2018, 480, No. 6, 725–729. DOI: 10.7868 / S0869565218180202. (In Russian).

35. Sitnov S.A., Mokhov I.I. Anomalies of methane content in the atmosphere over northern Eurasia in the summer of 2016. Doklady Earth Sciences. 2018, 480, No. 2, 223–228. (In Russian).

36. Mokhov I.I., Smirnov D.A. Contribution of radiation effects of greenhouse gases and Atlantic multi-ten-year oscillation to trends in surface temperature. Russian Meteorology and Hydrology. 2018, No. 9, 5–13

37. Akperov M., I Mokhov, A Rinke, K Dethloff, H Matthes. Cyclones and their possible changes in the Arctic by the end of the twenty first century from regional climate model simulations. Theor. Appl. Climatol. 2015, 122 (1–2), 85–96.

38. Akperov M.G., I.I. Mokhov, M.A. Dembickaya Arctic mesocyclones from satellite data, reanalyses data and model simulations. Modern problems of remote sensing of the Earth from space. 2017, 14, No.3, 297–304. DOI: 10.21046/2070-7401-2017-14-3-297-304. (In Russian).

39. Akperov M.G., Dembitskaya M.A., Mokhov I.I. Cyclone activity in the Arctic from reanalyses data and regional climate model simulations. Izvestiya Rossiiskoi Akademii Nauk. Seriya Geograficheskaya. 2017, 6, 39–46. (In Russian) DOI: 10.7868/S0373244417060044. (In Russian).

40. Akperov M., Rinke A., Mokhov I., Matthes H., Semenov V. and the Arctic Cordex Team. Cyclone activity in the Arctic from an ensemble of regional climate models (Arctic CORDEX). J. Geophys. Res.: Atmos. 2018, 123, 2537–2554. DOI: 10.1002/2017JD027703.

41. Zahn M., Akperov M., Rinke A., Feser F., Mokhov I.I. Trends of cyclone characteristics in the Arctic and their patterns from different re-analysis data. J. Geophys. Res.: Atmos. 2018, 123. DOI: 10.1002/2017JD027439.

42. Sakerin S.M., Bobrikov A.A., Bukin O.A., Golobokova L.P., Pol'kin Vas.V., Pol'kin Vik.V., Shmirko K.A., Kabanov D.M., Khodzher T.V., Onischuk N.A., Pavlov A.N., Potemkin V.L., Radionov V.F. On measurements of aerosol–gas composition of the atmosphere during two expeditions in 2013 along Northern Sea Route. Atmos. Chem. Phys., 2015, 15, 12413–12443, DOI:10.5194/acp-15-12413-2015.

43. Sakerin S.M., Kabanov D.M., Radionov V.F., Chernov D.G., Turchinovich Yu.S., Lubo-Lesnichenko K.E., Prakhov A.N. Generalization of results of atmospheric aerosol optical depth measurements on Spitsbergen Archipelago in 2011–2016. Optika Atmosfery i Okeana. 2018, 31, No. 2, 163–170. DOI: 10.1134/S1024856018020112. (In Russian).

44. Sakerin S.M., Golobokova L.P., Kabanov D.M., Kozlov V.S., Pol'kin V.V., Radionov V.F., Chernov D.G. Comparison of average aerosol characteristics in the neighboring Arctic regions. Optika Atmosfery i Okeana. 2018, 31, No. 8, 640–646. (in Russian).

45. Asmi, E., Kondratyev, V., Brus, D., Laurila, T., Lihavainen, H., Backman, J., Vakkari, V., Aurela, M., Hatakka, J., Viisanen, Y., Uttal, T., Ivakhov, V., and Makshtas, A.: Aerosol size distribution seasonal characteristics measured in Tiksi, Russian Arctic, Atmos. Chem. Phys., 16, 1271–1287. DOI: 10.5194/acp-16-1271-2016, 2016.

46. Popovicheva O.B., A.P. Makshtas, V.V. Movchan, N.M. Persiantseva, M.A. Timofeev, N.M. Sitnikov Aerosol component of the atmospheric surface layer according observations of the expedition "North-2015", Problems of Arctic and Antarctic, 2017, No.4 (114), 57–65. (In Russian).

47. Mokhov I.I., Khon V.C. The duration of the navigation period and its changes for the Northern Sea Route: model estimates. Arctic: Ecology and Economics, 2015, No. 2(18), 88–95. (In Russian).

48. Mokhov I.I., Khon V.C., Prokofyeva M.A. New model estimates of changes in the duration of the navigation period for the Northern Sea Route in the XXI century. Doklady Earth Sciences. 2016, 468, No. 6, 699–704. (In Russian)

49. Khon V.C., Mokhov I.I., Semenov V.A. Transit navigation through Northern Sea Route from satellite data and CMIP5 simulations. Environ. Res. Lett. 2017, 12, 024010.

50. Kibanova, O.V., A.V. Eliseev, I.I. Mokhov, V.C. Khon, 2018: Variations in the duration of the navigation period along the Northern Sea Route in the 21st century based on simulations with an ensemble of climatic models: Bayesian estimates. Doklady Earth Sciences, 2018, 481, No. 1, 223–228, DOI: 10.1134/S1028334X18070073. (In Russian)

51. Soldatenko S.A., G.V. Alekseev, N.E. Ivanov, A.E. Vyazilova, N.E. Kharlanenkova.On Assessment of Climatic Risks and Vulnerability of Natural and Economic Systems in the Sea Zone of the Russian Arctic. Problemy Arktiki i Antarktiki. Arctic and Antarctic Research. 2018, 64 (1): 55–70. DOI: 10.30758/0555-2648-2018-64-1-55-70. (In Russian).

52. Tison J.-L., M. de Angelis, G. Littot, E. Wolff, H. Fischer, M. Hansson, M. Bigler, R. Udisti, A. Wegner, J. Jouzel, B. Stenni, S. Johnsen, V. Masson-Delmotte, A. Landais, V. Lipenkov, L. Loulergue, J.-M. Barnola, J.-R. Petit, B. Delmonte, G. Dreyfus, D. Dahl-Jensen, G. Durand, B. Bereiter, A. Schilt, R. Spahni, K. Pol, R. Lorrain, R. Souchez, and D. Samyn. Retrieving the paleoclimatic signal from the deeper part of the EPICA Dome C ice core. The Cryosphere. 2015, 9, 1633–1648. DOI:10.5194/tc-9-1633-2015.

53. Lipenkov V.Y., Raynaud D. The Mid-Pleistocene Transition and the Vostok Oldest Ice Challenge. Ice and Snow. 2015, 55(4):95–106. DOI:10.15356/2076-6734-2015-4-95-106. (In Russian).

54. Fourteau K., Faïn X., Martinerie P., Landais A., Ekaykin A.A., Lipenkov V.Ya., Chappellaz J. Analytical constraints on layered gas trapping and smoothing of atmospheric variability in ice under low-accumulation conditions. Climate of the Past, 2017, 13, 1815–1830. DOI: 10.5194/cp-13-1815-2017.

55. Veres A.N., Ekaykin A.A., Vladimirova D.O., Kozachek A.V., Lipenkov V.Ya., Skakun A.A. Climatic variability in the era of MIS-11 (370–440 ka BP) according to isotope composition (δD, $\delta^{18}O$, $\delta^{17}O$) of ice from the Vostok station cores. Led i Sneg. Ice and Snow. 2018. 58 (2): 149–158. DOI: 10.15356/2076-6734-2018-2-149-158. (In Russian).

56. Lipenkov V.Ya., Ekaykin A.A. Hunting for Antarctica's oldest ice. Led i Sneg. Ice and Snow. 2018, 58 (2): 255–260. DOI: 10.15356/2076-6734-2018-2-255-260. (In Russian).

57. Vladimirova D.O., Ekaykin A.A., Lipenkov V.Ya., Popov S.V., Shibaev Yu.A. Spatial variability of the accumulation rate and isotopic composition of the snow in Indian ocean sector of East Antarctica including the vicinity of subglacial lake Vostok. Problems of Arctic and Antarctic. 2015, No.1 (103), 69–86. (In Russian).

58. Vladimirova D.O., Ekaykin A.A., Lipenkov V.Y. The variability of climate in Indian Ocean sector of East Antarctica over the past 350 years. Ice and Snow. 2015, 55(4): 5–18. DOI:10.15356/2076-6734-2015-4-5-18. (In Russian).

59. Ekaykin A.A., Zarovchatskiy V.A., Lipenkov V.Ya. Measurements of snow sublimation rate at Vostok station (Antarctica). Problems of Arctic and Antarctic. 2015, No.4 (106), 20–25. (in Russian).

60. Ekaykin A., Eberlein L., Lipenkov V., Popov S., Scheinert M., Schröder L., Turkeev A. Non-climatic signal in ice core records: lessons from Antarctic mega-dunes. The Cryosphere. 2016, 10, 1217–1227. DOI: 10.5194/tc-10-1217-2016.

61. Touzeau A., Landais A., Stenni B., Uemura R., Fukui K., Fujita S., Guilbaud S., Ekaykin A. Acquisition of isotopic composition for surface snow in East Antarctica and the links to climatic parameters. The Cryosphere. 2016, 10, 1–16. DOI:10.5194/tc-10-1-2016.

62. Ekaykin A.A., Vladimirova D.O., LipenkovV.Ya, Masson-Delmotte V. Climatic variability in Princess Elizabeth Land (East Antarctica) over the last 350 years. Climate of the Past. 2017, 13, 61–71. DOI:10.5194/cp-13-61-2017.

63. Landais A., Casado M., Prie F., Magand O., Arnaud L., Ekaykin A., Petit J.R., Picard G., Fily M., Minster B., Touzeau A., Goursaud S., Masson-Delmotte V., Jouzel J., Orsi A. Surface studies of water isotopes in Antarctica for quantitative interpretation of deep ice core data. Comptes Rendus Geoscience. 2017, 349, 139–150. DOI: 10.1016/j.crte.2017.05.003.

64. Raisbeck G.M., Cauquoin A., Jouzel J., Landais A., Petit J.R., Lipenkov V.Y., Beer J., Synal H.-A., Oerter H., Johnsen S.J., Steffensen J.P., Svensson A., Yiou F. An improved north–south synchronization of ice core records around the 41 kyr 10Be peak. Climate of the Past. 2017, 13, 217–229. DOI:10.5194/cp-13-217-2017.

65. Stenni B., Curran M.A. J., Abram N.J., Orsi A., Goursaud S., Masson-Delmotte V., Neukom R., Goosse H., Divine D., van Ommen T., Steig E.J., Dixon D.A., Thom-

as E.R., Bertler N.A.N., Isaksson E., Ekaykin A., Frezzotti M., Werner M. Antarctic climate variability at regional and continental scales over the last 2,000 years. Climate of the Past. 2017. Vol. 13. P. 1609–1634. DOI: 10.5194/cp-2017-402017.

66. Thomas E.R., van Wessem J.M., Roberts J., Isaksson E., Schlosser E., Fudge T., Vallelonga P., Medley B., Lenaerts J., Bertler N., van den Broeke M.R., Dixon D.A., Frezzotti M., Stenni B., Curran M., Ekaykin A.A. Regional Antarctic snow accumulation over the past 1000 years. Climate of the Past. 2017, 13, 1491–1513. DOI: 10.5194/cp-13-1491-2017.

67. Ekaykin A.A., Vladimirova D.O., Lipenkov V.Y. Variations of snow accumulation rate in Central Antarctica over the last 250 years. Ice and Snow. 2017, 57(1):5-9. DOI:10.15356/2076-6734-2017-1-5-9. (In Russian).

68. PAGES2k Consortium (including Ekaykin A., Vladimirova D.). A global multiproxy database for temperature reconstructions of the Common Era. Sci. Data. 2017. DOI: 4:17008810.1038/sdata.2017.88

69. Fourré E., Landais A., Cauquoin A., Jean-Baptiste P., Lipenkov V., Petit J.-R. Tritium Records to Trace Stratospheric Moisture Inputs in Antarctica. J. Geophys. Res. (Atmospheres). 2018, 123 (6), 3009–3018. DOI: 10.1002/2018JD028304.

70. Golobokova L.P., Polkin V.V., Onischuk N.A., Khuriganova O.I., Tikhomirov A.B., Terpugova S.A., Polkin V.V., Turchinovich U.S., Radionov V.F. Chemical composition of aerosol in the atmospheric surface layer of the East Antarctica coastal zone. Ice and Snow. 2016, 56(2), 177–188. DOI: 10.15356/2076-6734-2016-2-177-188. (In Russian).

71. Sakerin S.M., Golobokova L.P., Kabanov D.M., Pol'kin V.V., Radionov V.F. Zonal distribution of aerosol physical-chemical characteristics in the Eastern Atlantic. Optika Atmosfery i Okeana. 2018, 31. No. 4, 303–312. (In Russian).

Научное издание

НАЦИОНАЛЬНЫЙ ОТЧЕТ РОССИИ ПО МЕТЕОРОЛОГИИ И АТМОСФЕРНЫМ НАУКАМ В 2015–2018 гг.

XXVII Генеральная Ассамблея
Международного союза геодезии и геофизики,
Монреаль, Канада, 8–18 июля 2019 г.

На английском языке

Под редакцией:
И.И. Мохова, А.А. Криволуцкого

Подготовка оригинал-макета:
Издательство «МАКС Пресс»
Главный редактор: *Е.М. Бугачева*
Компьютерная верстка: *Н.С. Давыдова*

Подписано в печать 26.06.2019 г.
Формат 60x90 1/16. Усл.печ.л. 20,75. Тираж 100 экз. Заказ 152.
Издательство ООО “МАКС Пресс”
Лицензия ИД N 00510 от 01.12.99 г.
119992, ГСП-2, Москва, Ленинские горы, МГУ им. М.В. Ломоносова,
2-й учебный корпус, 527 к.
Тел. 8(495)939-3890/91. Тел./Факс 8(495)939-3891.

Отпечатано в полном соответствии с качеством
предоставленных материалов в ООО «Фотоэксперт»
115201, г. Москва, ул. Котляковская, д.3, стр. 13.